Journal of METALS

OCTOBER 1957

TRANSACTIONS SECTION

VOL. 9, NO. 10, IN TWO SECTIONS—SECTION TWO

Tensile Deformation of Aluminum as a Function of Temperature, Strain Rate, and Grain Size R. P. Carreker, Jr. and W. R. Hibbard, Jr.	1157
Cross-Rolling and Annealing Textures In High-Purity Iron H. Hu	1164
Effects of Crystal Orientation, Temperature, and Molten Zone Thickness in Temperature-Gradient Zone-Melting J. H. Wernick	1169
Formation of Intermetallic Layers in Diffusion Couples L. S. Castleman and L. L. Seigle	1173
Preparation and Diffraction Data of Ba-Al Alloys D. K. Das and Douglas T. Pitman	1175
Stability of AISI Alloy Steels A. B. Wilder, E. F. Ketterer, and D. B. Collyer	1176
Creep of Al-Cu Alloys During Age Hardening E. E. Underwood	1182
Investigation of the Nickel-Rich Portion of the System Ni-Zr E. Smith and R. W. Guard	1189
Transformation Kinetics and Mechanical Properties of Zr-Mo Alloys R. F. Domagala, D. W. Levinson, and D. J. McPherson	1191
Copper-Silica and Copper-Alumina Alloys of High Temperature Interest K. M. Zwilsky and N. J. Grant	1197
Some Characteristics of the Martensite Transformation of Cu-Al-Ni Alloys C. W. Chen	1202
Approximate Method of Calculations Using Concentration-Dependent Diffusion Coefficients A. G. Guy, M. Golomb, and A. S. Yue	1204
Diffusion of the Elements of the IB and IIB Subgroups in Silver A. Sawatzky and F. E. Jaumot, Jr.	1207
Investigation of Grain Boundary Phase in Stainless Steel C. C. Clark, J. R. Mihalisin, and K. G. Carroll	1210
Elastic Properties of Yttrium and Eleven of the Rare Earth Elements J. F. Smith, C. E. Carlson, and F. H. Spedding	1212
Mechanism of Precipitation in a Cu-2.5 Pct Fe Alloy J. B. Newkirk	1214
Some Observations on 885°F Embrittlement G. F. Tisinai and C. H. Samans	1221
Phase Transformation in Hypoeutectoid Ti-Cr Alloys H. I. Aaronson, W. B. Triplett, and G. M. Andes	1227
The Uranium-Silicon Epsilon Phase S. Isserow	1237

Table of Contents Continued

Misfit Strain Energy in the Au-Cu System — R. Hultgren — 1240

Temperature Dependence of the Tensile Properties of Vanadium — J. W. Pugh — 1243

Sand Cast Magnesium Rare Earth Metal-Zirconium Alloys — T. E. Leontis and D. H. Feisel — 1245

Grain Boundary Deformation in Fine-Grained Electrolytic Magnesium — S. L. Couling and C. S. Roberts — 1252

The Nature of the Nickel-Chromium System — R. O. Williams — 1257

The Effect of Heat Treatment on the Hardness and Microstructure Of Uranium-Titanium Alloys — D. L. Douglass and L. L. Marsh, Jr. — 1260

Growth of Iron Alloy Single Crystals From the Melt — R. C. Hall — 1267

CsCl-Type Ordered Structures in Binary Alloys of Transition Elements — T. V. Philip and Paul A. Beck — 1269

The Notch Tensile Properties of Selected Titanium Alloys — E. P. Klier and N. J. Feola — 1271

Cylindrical Carbide Particles — J. H. Westbrook — 1277

The Distribution of Boron in Gamma Iron Grains — R. M. Goldhoff, R. Spenser, and J. W. Spretnak — 1278

Crystallographic Angles for Manganese Bismuthide — W. J. Romanow — 1284

Some Internal Friction Studies in Columbium — R. W. Powers and M. V. Doyle — 1285

Discussion—Iron & Steel Division — 1288

Discussion—Extractive Metallurgy Division — 1292

Discussion—Institute of Metals Division — 1295

The Transactions papers appearing in JOURNAL OF METALS during 1957 will subsequently appear in *AIME Transactions* Volume 209, and may be permanently referenced to that volume.

Tensile Deformation of Aluminum as a Function Of Temperature, Strain Rate, and Grain Size

True stress, true strain data are presented for two lots of high-purity aluminum annealed to produce several different grain sizes from each lot. The testing temperature range 20° to 873°K (0.021 to 0.94 T/T_m) was explored and the effect of strain rate was measured at 77° and 300°K.

by R. P. Carreker, Jr., and W. R. Hibbard, Jr.

ONE of a series, this report is concerned with the experimental documentation of the deformation behavior of pure metals over a wide range of temperature. Previous reports in the series describe the creep behavior of platinum[1] and aluminum[2] and the tensile behavior of copper,[3] silver,[4] and molybdenum.[5] Subsequent reports will describe the creep behavior of copper and silver and the tensile behavior of platinum, thus providing extensive creep and tensile data on four face-centered-cubic metals tested under comparable conditions.

Material

Two lots of high-purity aluminum were used in this investigation. One lot, designated *AC*, was obtained direct from the Aluminum Co. of America as high-purity aluminum in *notch-bar* form. A typical analysis of this type of aluminum is 0.006 pct Si, 0.015 pct Cu, 0.006 pct Fe, and 99.975 pct Al. Lot *BS* was obtained from J. I. Hoffman of the Bureau of Standards as a portion of the *Aluminum A* described in his report of the redetermination of the atomic weight of aluminum.[6] Lot *BS* originated with the Aluminum Co. of America also, and was received in the standard notch-bar form. A detailed chemical and spectroscopic analysis of lot *BS* has been published.[6] Principal impurities were 0.006 pct Si, 0.003 pct Fe, 0.002 pct Cu, and >99.987 pct Al.

Samples were processed identically by room-temperature swaging and drawing to 0.030 in. diam wires from approximately ½ in. diam rods that were machined from the notch-bar pigs. Samples were cut from the cold-drawn wire, placed in a grooved graphite block in groups of thirteen, and annealed in air for 1 hr at each of several temperatures, with the results shown in Table I. The two lots of aluminum responded quite differently to annealing, the behavior of aluminum *AC* suggesting that its grain growth was controlled by impurities. The recrystallization texture of aluminum of similar purity comparably treated has been reported as predominantly <111> fiber with some <100> fiber present.[7]

Testing Procedure

The testing procedure and method of analyzing the data have been described previously.[2,3] Annealed specimens of 5 in. gage length were tested in an Instron tensile testing machine at a constant head motion corresponding to a strain rate of 0.04 min^{-1} at a number of temperatures. Instantaneous tenfold rate changes were employed in some tests to deter-

R. P. CARREKER, JR., Junior Member AIME, and W. R. HIBBARD, JR., Member AIME, are associated with General Electric Co., Schenectady.

TP 4129E. Manuscript, June 15, 1955. New York Meeting, February 1956.

Copyright 1957 by American Institute of Mining, Metallurgical, and Petroleum Engineers, Inc. Printed in U. S. A.

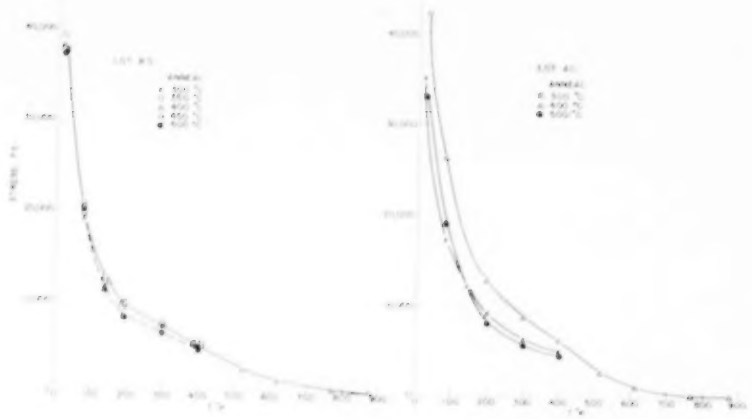

Fig. 1—Tensile strength of two lots of aluminum as a function of temperature and grain size.

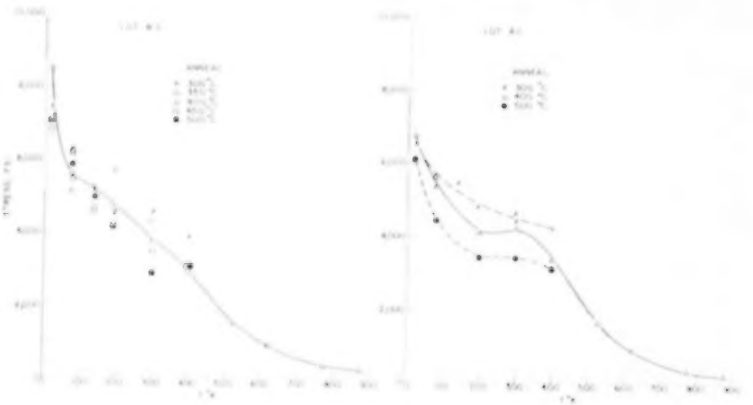

Fig. 2—Yield strength (σ at ϵ = 0.005) of two lots of aluminum as a function of temperature and grain size.

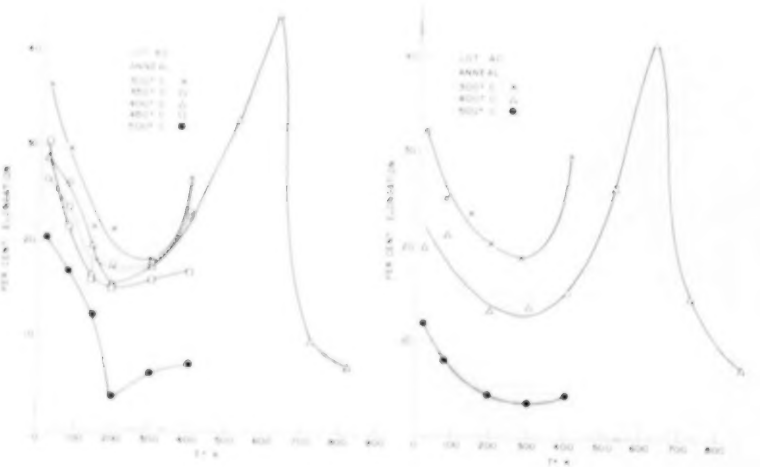

Fig. 3—Percentage elongation of two lots of aluminum as a function of temperature and grain size.

mine the strain-rate sensitivity. The symbol σ is used to indicate true stress and ϵ to indicate true strain, defined by

$$\sigma = \frac{P}{A} = \frac{P}{A_0}\left(1 + \frac{\Delta l}{L_0}\right)$$

and

$$\epsilon = \int \frac{dl}{l} = \ln\left(1 + \frac{\Delta l}{L_0}\right)$$

where P equals load; A, area; and l, length. The subscript zero refers to initial values; all other symbols refer to instantaneous values.

Effect of Temperature

Figs. 1 to 3 show the effect of temperature on the tensile strength, the yield strength, and the percentage of elongation for the two lots of aluminum annealed at several different temperatures. Note that grain size (or annealing temperature) has a pronounced effect on the yield and tensile strengths of aluminum *AC*, but has a comparatively slight effect

on the yield strength of aluminum *BS* and a negligible effect on its tensile strength. The virtual independence of the tensile strength on grain size (or annealing temperature) is consistent with the behavior of 99.999 pct Cu.[3]

Fig. 4 shows a typical family of true stress-true strain curves for aluminum *BS* tested at several temperatures. Fig. 5 is a logarithmic plot of the same data. A straight line on such coordinates implies a stress-strain relationship of the form $\sigma = K\epsilon^m$. The data of Fig. 5 do not conform to that relationship over the entire range of strain but, in the range $\epsilon = 0.01$ to 0.10, they approximate the relationship sufficiently well for m at $\epsilon = 0.10$ to be a quantitative measure of strain hardening. Values of the strain-hardening exponent, m, are plotted as a function of temperature in Fig. 6. As would be expected, strain hardening decreases with increasing temperature. However, the shape of the curve is quite different from the approximately linear dependence observed for copper[3] and silver.[4]

Fig. 7 is a composite plot of tensile strength as a function of temperature, including all comparable data from the literature and data on both *BS* and *AC* aluminum from the present report. A 10 pct scatter band includes all data, except a portion of Inokuty's[5] in the region where impurities have their maximum effect. The consistency of the tensile strength of nominally pure metals in the annealed condition, regardless of the details of testing procedures, minor impurities, grain size, and metallurgical history, has been noted in previous reports on copper[3] and silver.[4]

The scatter bands for these face-centered-cubic metals are compared in Fig. 8 on a reduced temperature scale. The behavior of copper and silver are strikingly similar. The reduced temperature scale normalizes the shape of all three—copper, silver, and aluminum—curves above $T/T_m = 0.2$, but the tensile strength values do not coincide. A second shift, along the stress axis, would be necessary to make them superpose; the degree and direction of the stress axis shift apparently are proportional to the melting point of the metal. The large increase in tensile strength of aluminum below $T/T_m = 0.2$ is not shown by copper or silver. It is similar to the temperature dependence of the tensile strength of body-centered-cubic metals, in which impurities exert a strong influence.[5,12]

Fig. 9 is a plot of the true flow stress at several arbitrary strains as a function of temperature for

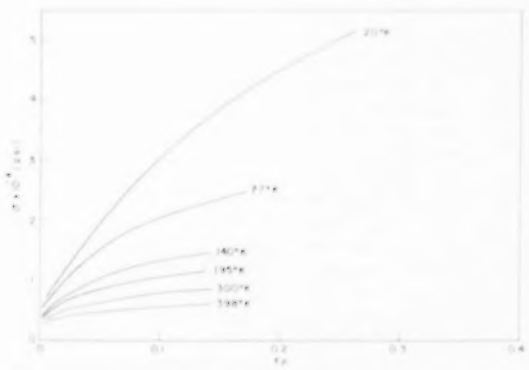

Fig. 4—Typical family of true stress-true strain curves for annealed aluminum at several temperatures. Aluminum *BS*, annealed 1 hr at 450°C; average grain diam, 0.065 mm.

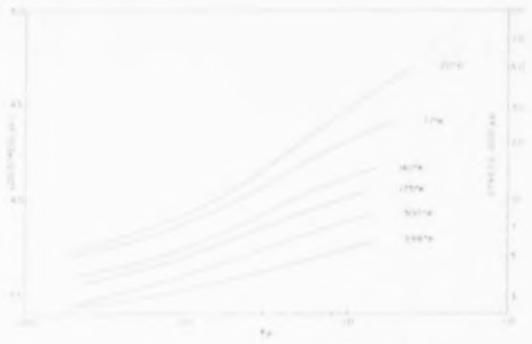

Fig. 5—Logarithmic plot of the data in Fig. 4.

both the *BS* and *AC* lots after 400°C anneals. The shapes of these curves in the region below 400°K are indicative of strain aging.

Effect of Strain Rate

The use of the rate-change test to determine rate sensitivity has been described.[3] Briefly, a specimen is strained to a prescribed nominal strain (in this case $\epsilon = 0.09$) at a standard strain rate; at that strain the strain rate is changed suddenly to a new value and the test continued to a prescribed strain (in this case $\epsilon = 0.11$), whereupon the strain rate is changed suddenly to the standard rate. In these tests the strain rates employed were 0.04, 0.004, and 0.04 min^{-1}. At constant strain and temperature, strain rate is known to affect the flow stress through the relation $\sigma = K'\dot{\epsilon}^n$. Under the conditions of these tests, the strain-rate exponent, n, is given by the difference in the logarithm of the flow stress at the two rates. Typical rate-change tests are shown in Fig. 10. The strain-rate exponent, n, of the expression $\sigma = K'\dot{\epsilon}^n$, was determined at 77°K and 300°C on samples representing each annealing treatment of both *AC* and *BS* aluminum. The strain-rate sensitivity was the same for all annealing treatments in both lots, within the accuracy of the measurements. The n values obtained were: at 77°K, n was equal to 0.010 ± 0.001; at 300°K, n was equal to 0.005 ± 0.001. It is somewhat surprising to find the larger rate sensitivity at the lower temperature. The rate sensitivities of both copper and silver were observed to increase linearly with increasing temperature.[3,4] However, Lubahn[12] has noted that rate sensitivities of materials known to undergo strain aging pass through minima when plotted as a function of temperature. For example, 61S aluminum alloy has a minimum in rate sensitivity at approximately 273°K. Strain aging effects are usually considered to be associated with soluble impurities. It appears that there is some manifestation of strain aging, even in this relatively pure aluminum.

Discontinuous Yielding

A qualitative difference between the two lots of aluminum was apparent in their initial yielding behavior. Aluminum *AC* had definite yield points at 195°K and below when annealed at 300°C, whereas aluminum *BS* did not have such yield points. The effect was noted in *AC* aluminum annealed at 300°C, not in *AC* aluminum annealed at 400° and 500°C. Figs. 11 and 12 show tracings of the autographic load-elongation records. It should be mentioned that the testing machine used was relatively stiff and utilized a weigh-bar mounting a resistance-wire

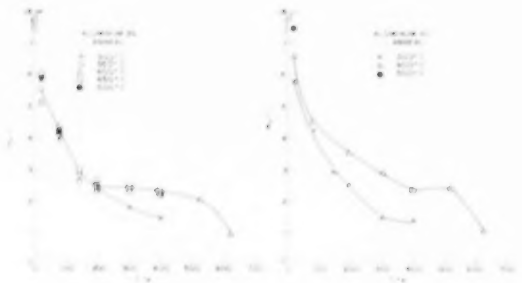

Fig. 6—Strain hardening exponent, m, at a strain of 0.1, as a function of temperature for several grain sizes.

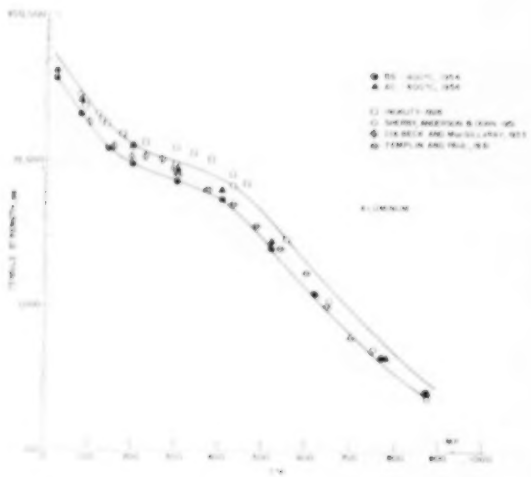

Fig. 7—Composite plot of literature data on tensile strength of aluminum as a function of temperature.

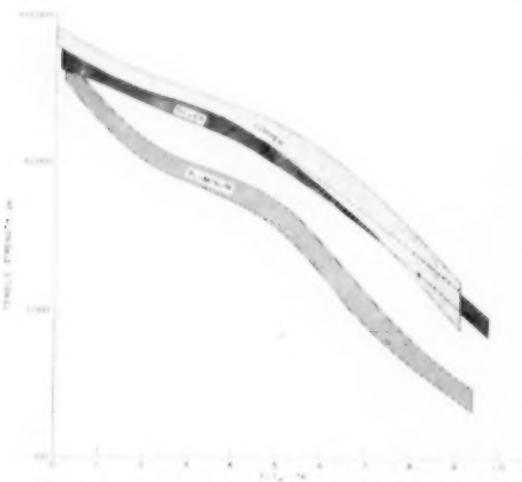

Fig. 8—Comparison of tensile strength of copper, silver, and aluminum on a reduced temperature scale.

strain gage whose output was recorded by a short-response time recorder. Such a system is sensitive to the rapid fluctuations in load that accompany discontinuous yielding.

Yield points are not commonly observed in nominally pure face-centered-cubic materials; the effect is usually associated with body-centered-cubic metals containing interstitial impurities.[15] Smallman, Williamson, and Ardley[16] have recently described yield points observed in careful tests of aluminum alloy single crystals.

The same general mechanism that is widely accepted as the explanation of yield points in body-centered-cubic metals, namely, the pinning of dislocations by impurities through their mutual interaction, can apply to face-centered-cubic metals. The question is one of degree. The difference in the yielding behavior of the two lots of aluminum is presumably due to a difference in impurity content. It is somewhat surprising that a 300°C anneal should produce a yield point when higher temperature anneals did not, since the yield-point phenomenon is considered to be due to soluble impurities. However, it is commonly observed that the magnitude of the yield-point phenomenon in Fe-C alloys decreases with increasing grain size.

Effect of Grain Size

The annealing treatments resulted in a range of grain size from 0.027 to 0.105 mm average diam for *BS* aluminum and from 0.021 to 0.143 mm for *AC* aluminum. Fig. 13 shows the effect of grain size on the flow stress at selected strains for *BS* aluminum at 20° and 300°K. At 300°K, the grain size dependence of the flow stress is similar to that previously reported for copper[2] and for silver,[4] being most pronounced at small strains and insensitive to grain size at strains of the order of 0.05. At 20°K, the flow stress is not a rational function of grain size. Examination of the data shows that the systematic grain size dependence observed at 300°K is the exception, rather than the rule, in these experiments. The derived values of the strain hardening exponent, m, and the strain-rate exponent, n, are independent of grain size. Both these quantities were observed to depend on grain size in the cases of copper[2] and silver.[4] Presumably, the effects of grain size are obscured by experimental scatter and aging effects in the present experiments.

Discussion

Aluminum has been the subject of much research in recent years, due in no small part to its suitability for interesting experimental techniques. A large body of experimental observations is now available in the literature, including descriptions of the slip process details, substructure formation and growth, annealing characteristics, and thermodynamic properties. So much information about aluminum is available that it has often been used as the epitome of the important face-centered-cubic class of metals. However, the most striking general conclusion to be drawn from the present research is that aluminum is atypical when its mechanical properties are compared with copper and silver.

Many of the features of the influence of temperature on the mechanical properties of aluminum described above suggest that the small concentration of impurities present produced important effects. Recall the following observations:

1) Distinct yield points, of the type usually associated with body-centered-cubic metals containing interstitial impurities, were observed in this relatively high purity, face-centered-cubic metal. The yield points were evident in fine-grained specimens tested at low temperatures.

2) The shape of the strain hardening vs temperature curve, which rises markedly below room temperature and is virtually flat in the range 200° to 500°K, is decidedly different from the approximately linear temperature dependence observed for copper and silver. It seems evident that some recovery process occurs in aluminum at temperatures well below room temperature to an extent that does not occur in copper or silver at the same or even much higher homologous temperatures. This observation brings to mind the evidence of low-temperature polygonization in aluminum.[14] It also suggests that measurements of changes in electrical resistivity[15] or stored energy[16] during annealing should be performed on aluminum deformed at very low temperatures. Comparison should be made with copper.

3) The shapes of the flow stress vs temperature and the tensile strength vs temperature curves are similar to such data on body-centered-cubic metals, in which impurities interact with dislocations to inhibit slip, with resultant yield-point and strain-aging phenomena.

4) The apparent anomaly in the effect of temperature on strain-rate sensitivity, the rate effect at 77°K being several times greater than that at room temperature, is typical of metals in which strain-aging effects are found.[18]

Much of our current understanding of yield points and strain-aging effects is due to Cottrell and collaborators,[17-20] who have considered in detail the *pinning* of dislocations by impurities. Solute atoms

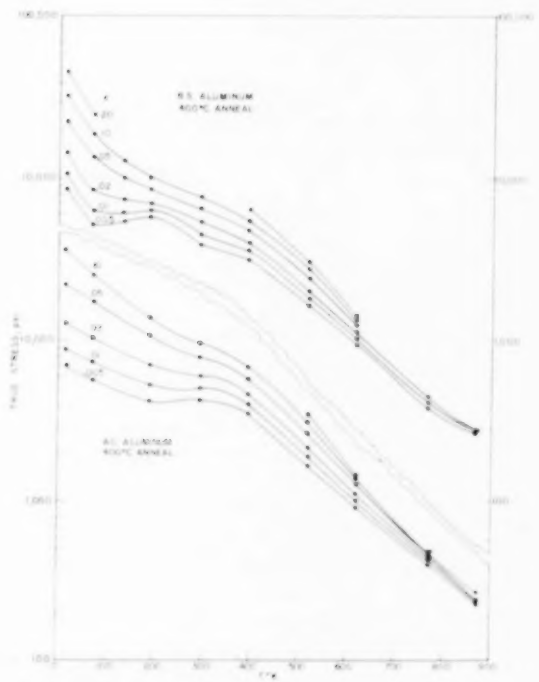

Fig. 9—True flow stress at several strains for two lots of aluminum as a function of temperature.

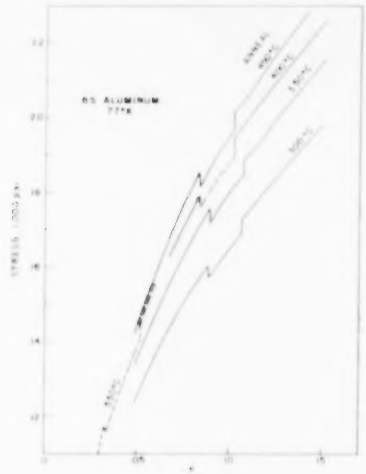

Fig. 10—Typical rate-change tests.

having appreciable misfit in the lattice condense into dislocations because of an elastic interaction with them. Interstitial solute atoms such as carbon and nitrogen produce nonspherically symmetrical distortions in body-centered-cubic and hexagonal-close-packed metals, distortions that interact with both edge and screw dislocations. Substitutional solute atoms in face-centered-cubic metals produce only spherically symmetrical distortions which can interact only with edge dislocations. However, Cottrell[20] has pointed out that the dissociation of dislocations in face-centered-cubic metals into partial dislocations, as discussed by Heidenreich and Shockley,[21] always leads to some edge-type component which can be anchored by substitutional impurities. Since the two partial dislocations are elastically bound to one another, the whole dislocation may be pinned by impurities. Thus, face-centered-cubic metals can be expected to have yield points, but to a much less pronounced degree than body-centered-cubic metals.

Suzuki[17] pointed out that the *fault* or ribbon-like region between two partial dislocations is a region that is crystallographically equivalent to a layer of hexagonal-close-packed structure of two atomic planes in thickness. As such, it is characterized by an interfacial free energy, twice that of a coherent twin boundary, and possesses a solubility for a particular impurity that is different from the surrounding crystal. There is thus a driving force for the segregation of impurities to the fault between partial dislocations. Segregation of impurities to the fault inhibits separation of the dislocation ribbon from the impurity concentration. Thus, the Suzuki concept also leads to the prediction of yield points in face-centered-cubic metals. Note that both concepts lead to the impurity pinning of a ribbon-like dislocation configuration in face-centered-cubic metals as contrasted to the pinning of a single-line dislocation in body-centered-cubic crystals. The question remains as to why aluminum should show the effects of impurities interacting with dislocations to a much greater extent than, say, copper.

Fullman[16] has measured the ratios of the interfacial free energies of coherent twin boundaries to that of grain boundaries in both aluminum and copper, the values being 0.21 ± 0.05 Al, and 0.036 ± 0.006 Cu. Suzuki[17] gives the approximate width, l_s,

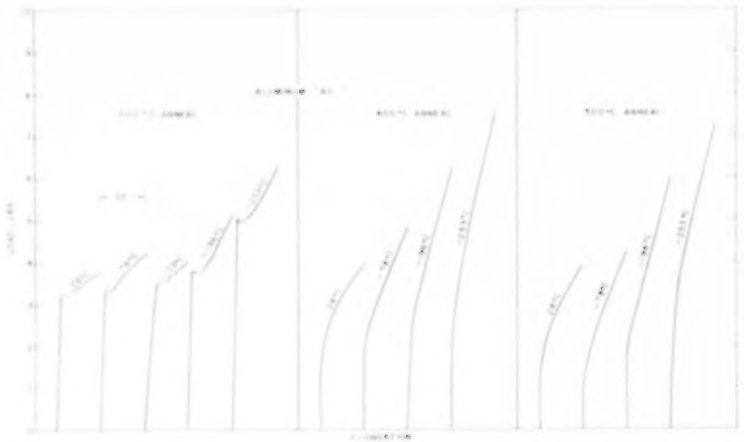

Fig. 11—Load-elongation records showing the initial yielding of aluminum *AC*.

of an extended dislocation fault in metal *A* to be

$$l_A = l_{Cu} \frac{\alpha'_{Cu}\,\mu_A}{\alpha'_A\,\mu_{Cu}}$$

where α' is the coherent twin boundary energy, and μ is the shear modulus. Suzuki gives l_{Cu} as approximately 50A. The μ_{Al}/μ_{Cu} is approximately ½. In the absence of an absolute measurement of the grain boundary energy of aluminum, we may take $\alpha^b_{Cu}/\alpha^b_{Al} = \Delta H_{Cu}^{twin}/\Delta H_{Al}^{twin} = 50/94 = ½$. Appropriate values may then be substituted in Suzuki's equation to give the width of the extended dislocation fault in aluminum as follows

$$l_{Al} = l_{Cu}\left[\frac{\alpha'_{Cu}/\alpha^b_{Cu}}{\alpha'_{Al}/\alpha^b_{Al}}\right]\left(\frac{\Delta H'_{Cu}}{\Delta H'_{Al}}\right)\left(\frac{\mu_{Al}}{\mu_{Cu}}\right)$$

$$l_{Al} = 50\left(\frac{0.036}{0.21}\right)\left(\frac{1}{2}\right)\left(\frac{1}{2}\right)\text{A}$$

$$l_{Al} = 2\text{A}.$$

Admitting the crude approximation, it seems evident that the faults between dissociated dislocations in aluminum are quite narrow and might better be likened to a fine than to a ribbon. Impurity pinning in aluminum would then be expected to be characterized by a relatively strong, narrow interaction in contrast to the weaker and broader interaction in copper. The impurity interaction in aluminum would then be of similar form to, but of much less strength than, the interaction caused by interstitial impurities in body-centered-cubic metals. Thus, aluminum should exhibit a propensity for yield points and strain-aging phenomena intermediate to iron and copper.

A comparison of the temperature dependence of the yield strength or tensile strength of copper and aluminum is consistent with such an argument. As discussed by Suzuki,[17] thermal fluctuations do not markedly affect the critical shear stress of an extended dislocation pinned by a heterogeneous distribution of solute atoms. On the other hand, thermal fluctuations will markedly affect the critical shear stress of a dislocation pinned by a strong, narrow impurity interaction. Thus, the yield strength and tensile strength of aluminum are noted to rise markedly with temperature as the temperature is decreased below $T/T_m = 0.2$, as compared to the moderate increase in strength observed for copper.

Table I. Annealing Results

Annealing Temperature, °C	Average Grain Diam, Mm	
	BS	*AC*
300	0.027	0.021
350	0.039	—
400	0.046	0.118
450	0.065	—
500	0.105	0.143

Summary

Constant strain-rate tensile tests have been performed on polycrystalline wires of two lots of high-purity aluminum designated *AC* and *BS*. Tests were made of five groups of *BS* specimens annealed at 300°, 350°, 400°, 450°, and 500°C, and three groups of *AC* specimens annealed at 300°, 400°, and 500°C. The annealing treatments produced a range of grain sizes extending from 0.02 to 0.14 mm average grain diam. The specimens were tested at a strain rate of 0.04 min^{-1} over the range 20° to 873°K (0.021 to 0.94 T/T_m). The data were analyzed to determine the effect of temperature on the flow stress at selected strains, tensile strength, yield strength, and strain hardening. Rate-change tests were used to measure the strain-rate sensitivity at 77° and 300°K.

It is concluded that:

1) The flow curves of aluminum are generally regular over the range 0.021 to 0.94 of the absolute melting temperature. Some discontinuous yielding was observed in one lot of aluminum at 195°K and below.

2) The yield strength, tensile strength, and true flow stress at arbitrary strains extrapolate to finite values at the absolute zero of temperature.

3) Strain hardening, as measured by the strain-hardening exponent *m*, increases markedly with decreasing temperature in the region below 200°K and is virtually constant in the region 200° to 550°K. This temperature dependence is qualitatively different from that previously observed for copper and silver, both of which showed approximately linear temperature dependence until annealing temperatures were approached.

4) Complexities in the shapes of flow stress vs temperature curves suggest strain aging effects were operative in these relatively high-purity aluminum samples.

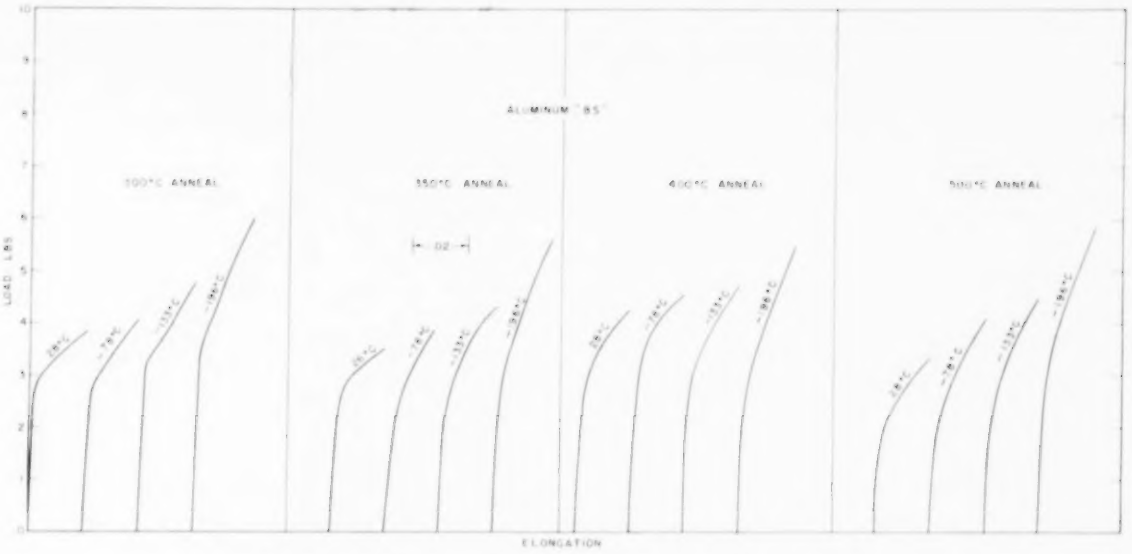

Fig. 12—Load-elongation records showing the initial yielding of aluminum BS.

5) The effects of grain size, within the 0.02 to 0.14 mm average diam obtained in this investigation, were masked by specimen scatter and side effects, so that no systematic trends were established.

6) The strain-rate sensitivity at 300°K was found to be less than at 78°K, an anomaly that is usually associated with strain aging.

7) As in the case of copper and silver, the tensile strength vs temperature relation for aluminum is influenced but slightly by variations in specimen history. However, the temperature dependence of the tensile strength of aluminum is qualitatively different from copper and silver below a homologous temperature of 0.2 in that the tensile strength of aluminum increases much more rapidly with decreasing temperature.

8) The differences in the behavior of aluminum and copper are ascribed to a deduced difference in the width of the extended dislocation fault in these two face-centered-cubic metals.

Acknowledgments

The authors are indebted to J. I. Hoffman of the Bureau of Standards for his contribution of high-purity aluminum, R. L. Fullman for helpful discussion, and E. A. Smith for his careful work in performing the tests. The work on which this report is based was supported by the Aeronautical Research Laboratory, Wright Air Development Center, under Contract No. AF 33 (616)-2120.

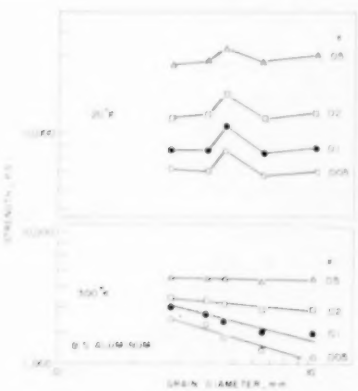

Fig. 13—Effect of grain size on the flow stress of aluminum at arbitrary strains.

References

[1] R. P. Carreker, Jr.: Plastic Flow of Platinum Wires. *Journal of Applied Physics*, 1950, vol. 21, p. 1289.

[2] R. W. Guard and W. R. Hibbard, Jr.: Tensile Creep of High-Purity Aluminum. *AIME Trans.*, 1956, vol. 203, p. 195; JOURNAL OF METALS, February 1956.

[3] R. P. Carreker, Jr. and W. R. Hibbard, Jr.: Tensile Deformation of High-Purity Copper as a Function of Temperature, Strain Rate and Grain Size. *Acta Metallurgica*, 1953, vol. 1, p. 654.

[4] R. P. Carreker, Jr.: Tensile Deformation of Silver as a Function of Temperature, Strain Rate and Grain Size. *AIME Trans.*, 1957, vol. 200, p. 112; JOURNAL OF METALS, January 1957.

[5] R. P. Carreker, Jr. and R. W. Guard: Tensile Deformation of Molybdenum as a Function of Temperature, Strain Rate and Grain Size. *AIME Trans.*, 1956, vol. 206, p. 178; JOURNAL OF METALS, February 1956.

[6] J. I. Hoffman and G. E. F. Lundell: Redetermination of the Atomic Weight of Aluminum. *Journal of Research* National Bureau of Standards, 1937, vol. 18, p. RP957.

[7] W. R. Hibbard, Jr.: Deformation Texture of Drawn Face-Centered-Cubic Metal Wires. *Journal* Institute of Metals, 1950, vol. 77, p. 581.

[8] T. Inokuty: On the Thermal Brittleness in Metals. *Science Reports* Tohoku Imperial University, 1928, vol. 17, p. 817.

[9] O. D. Sherby, R. A. Anderson, and J. E. Dorn: Effect of Alloying Elements on the Elevated-Temperature Plastic Properties of Alpha Solid Solutions of Aluminum. *AIME Trans.*, 1951, vol. 191, pp. 643-652; JOURNAL OF METALS, May 1951.

[10] E. W. Colbeck and W. E. MacGillivray: The Mechanical Properties of Metals at Low Temperatures (Nonferrous). *Trans.* Institute of Chemical Engineering, London, 1933, vol. 11, p. 107.

[11] R. L. Templin and D. A. Paul: The Mechanical Properties of Aluminum and Magnesium Alloys at Elevated Temperatures. *Symposium of Effect of Temperature on Metals*, p. 290. ASTM and ASME, Philadelphia, 1931.

[12] A. H. Cottrell and B. A. Bilby: Dislocation Theory of Yielding and Strain Aging of Iron. *Proceedings* Physical Soc., London, 1949, vol. 62A, pp. 49-62.

[13] J. D. Lubahn: Strain Aging Effects. *ASM Trans.*, 1952, vol. 44, pp. 643-660.

[14] R. D. Heidenreich: Electron Transmission Through Thin Metal Sections with Application of Self Recovery in Cold-Worked Aluminum. *Technical Journal* Bell System, 1951, vol. 30, pp. 867-887.

[15] T. Broom: *Philosophical Magazine*, 1954, vol. 3, No. 9, p. 26.

[16] A. W. Overhauser: Stored Energy Measurements in Irradiated Copper. *Physical Review*, 1954, vol. 94, No. 6, p. 1551.

[17] H. Suzuki: Chemical Interaction of Solute Atoms with Dislocations. *Science Reports* Research Institute, Tohoku University, 1952, vol. 4A, p. 455.

[18] R. L. Fullman: Formation of Annealing Twins During Grain Growth. *Journal of Applied Physics*, 1950, vol. 2, p. 1069.

[19] R. E. Smallman, G. K. Williamson, and G. Ardley: Yield Points in Aluminum Alloy Single Crystals. *Acta Metallurgica*, 1953, vol. 1, No. 2, p. 126.

[20] A. H. Cottrell: *Dislocations and Plastic Flow in Crystals*, p. 133. Oxford Press, Oxford, 1953.

[21] R. D. Heidenreich and W. Shockley: *Report on the Strength of Solids* Physical Soc., London, 1948, vol. 57, p. 57.

Discussion of this paper sent (2 copies) to AIME by Sept. 1, 1957 will appear in AIME *Transactions* Vol. 212, 1958, and in JOURNAL OF METALS, April 1958.

Cross-Rolling and Annealing Textures In High-Purity Iron

The deformation and annealing textures of cross-rolled high-purity iron specimens were determined by use of an X-ray Geiger counter spectrometer. The deformation texture was predominantly (100) [011], plus minor texture components of the (111) [110] or the (111) [112] type. In a partially recrystallized specimen, the minor deformation texture components were replaced by new orientations, while the (100) [011] main deformation texture was retained. A rather complex and widely scattered texture was developed in the completely recrystallized specimen. This recrystallization texture could be derived from the deformation texture components by rotations around (110) poles. The difference in the tendency for recrystallization among different deformation texture components may serve as an important factor in the formation of annealing textures.

by Hsun Hu

NOT much data are available in the literature on textures in cross-rolled metal sheets. Among the body-centered-cubic metals, a few investigators have studied the preferred orientations developed in cross-rolled and in subsequently annealed molybdenum specimens.[1-4] Semchyshen and Timmons[5] constructed complete pole figures for the cross-rolled and subsequently annealed arc-cast molybdenum. They used the conventional photographic method. Similar data on cross-rolled iron are still lacking. In view of the fundamental importance of iron as a basic metal for magnetic alloys and many industrial steels, the present investigation was undertaken in an attempt to understand more about its properties. The material selected for the present work was of high purity, and the textures were determined by the Geiger counter spectrometer technique, which permits the construction of quantitative pole figures.

H. HU, Member AIME, is with the Westinghouse Research Laboratories, Churchill Boro, Pittsburgh.

TP 4473E. Manuscript, Sept. 10, 1956. New Orleans Meeting, February 1957.

Experimental Procedure

The material used for this investigation was NRC (National Research Corp.) high-purity, gas-free iron. The total gas content ($N_2 + O_2 + H_2$) given was less than 0.026 pct, and the carbon content, less than 0.005 pct. Spectrographic analysis of a 2 in. cast ingot showed the percentage of metallic impurities as 0.0004 pct Cu, 0.0002 pct Mg, 0.001 pct Mn, 0.01 pct Ni, and 0.006 pct Si.

A 1 in. thick slice was cut off from the 2 in. cast ingot. It was hot-forged at 850°C to destroy most of the cast structure. Surface scale was removed by milling the forged piece to a size 2 in. long, 1½ in. wide, and ¾ in. thick. After normalizing at 915°C for 15 min, the piece was alternately cold-rolled 40 pct and annealed at 750°C in hydrogen to a final thickness of 0.165 in., with a resulting uniform grain size of 0.1 mm.

Final rolling was performed in such a manner that the sheet was turned 90° between each successive pass to a final thickness of 0.008 in. This corresponded to a total reduction in thickness of 95 pct. The amount of reduction in each pass was about 0.005 in. Specimens were cut from the central portion, 5 x 5 in. in area, of the rolled sheet. The cut edges on each specimen were removed by etching in a nitric acid solution before the specimen was heat-treated. Annealing of the specimens was done in a laboratory tube furnace with a hydrogen, or an argon, atmosphere. Specimens were quenched after annealing for 15 min at various temperatures within the range of 350° to 850°C. Hardness measurements were made on a Vickers hardness tester with 1 kg load. For each specimen the Vickers hardness number was taken from the average of ten measurements at different areas of the specimen.

A Norelco X-ray Geiger counter spectrometer with molybdenum radiation was used for texture determinations. Prior to X-ray exposure, the specimen was etched to a uniform thickness of 0.0015 in. in a solution of phosphoric acid-nitric acid mixture. Only the transmission method[4] was used. Intensity measurements were taken at 5° intervals of the azimuthal angle, and at 5° or 10° intervals of the radial angle on a pole figure projection. In high intensity areas, intensity measurements were taken at closer intervals when detailed information was needed. Since no integration device was available at the time that this work was carried out, and the intensity data obtained from the specimen annealed at a higher temperature showed some degree of scatter, duplicate pole figures were determined from identically heat-treated specimens. High intensity areas of such a pole figure were also checked by taking several integrated transmission Laue photographs to assure their certainty. Only the reflections from the {110} planes were recorded. After making appropriate corrections for background intensity, the pole figures were constructed by plotting the intensity data as a series of contour lines, with intensities expressed in multiples of the random intensity measured from a carbonyl iron powder specimen. The texture of the as-rolled specimen was actually determined without using a zirconium filter; others were determined with filtered radiation. The pole figures of the annealed specimens were arbitrarily symmetrized.

Experimental Results

Fig. 1 is the (110) pole figure of the as-rolled specimen. The texture consists predominantly of the (100)[011] type orientation, i.e., the (100) plane is parallel to the rolling plane and the [011] and $[01\bar{1}]$ directions are parallel to the two mutually perpendicular rolling directions. The four secondary intensity areas near the center of the (110) pole figure and the rotary spread along the periphery can well be accounted for by the (111)[110] or the $(111)[11\bar{2}]$ type orientations, plus a partial [111] fiber texture, spread mainly between them. These were also confirmed by examining the (200) reflections from Laue photographs. The microstructures of the as-rolled and of the annealed specimens are shown in Fig. 2.

The change in hardness upon annealing is shown in Fig. 3. The initial decrease in hardness which occurred during annealing at low temperatures indicates that recovery has taken place to an appre-

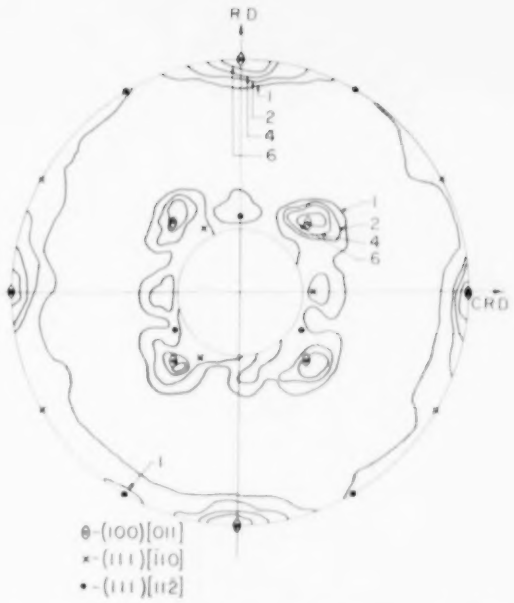

Fig. 1—(110) pole figure of the 95 pct cross-rolled high-purity iron. Intensities are expressed as multiples of random intensity of a carbonyl iron powder specimen.

ciable extent before recrystallization in its classical sense has begun. The microstructure of a partially recrystallized specimen, which was annealed 15 min at 550°C, is shown in Fig. 2b. It consists of clusters of recrystallized grains and areas in which the grains are outlined by light-etching, low angle boundaries. These grains with low angle boundaries were apparently formed by the so-called *recrystallization in situ* or *polygonization* process, which results in very slight orientation difference from the deformed matrix. It is interesting to note that there are no, or very few, new grains formed in these areas.

As shown in Fig. 4, the texture developed in the partially recrystallized specimen has undergone very little change as compared with that of the deformed specimen, except that most of the (111)[110] or the $(111)[11\bar{2}]$ texture components have disappeared. In addition to the retained (100)[011] main texture, there are a few scattered new orientations present, which apparently have been derived from the recrystallized grains.

The texture developed in the completely recrystallized specimen (annealed 15 min at 675°C) showed considerable scatter in orientation. Since the X-ray beam was 2 x 5 sq mm in area, the total number of grains exposed to the X-rays was nearly 4,000, so that this orientation scatter is not likely to be due to inadequate sample. The reliability of the texture data was also checked by actually determining two individual pole figures from two identically annealed specimens. Their essential features were very much the same. Therefore, the recrystallization texture as shown in Fig. 5 should be representative.

Discussion of Results

The cross-rolling texture of iron obtained in the present investigation is similar to that of molybdenum as obtained by Custers and Riemersma,[5] and

Fig. 2—Microstructures of high-purity iron specimens. Electrolytically polished, and etched with 2 pct Nital. a) LEFT: as-rolled, total reduction in thickness 95 pct; b) CENTER: annealed 15 min at 550°C (partially recrystallized); and c) RIGHT: annealed 15 min at 675°C (completely recrystallized). X100. Reduced approximately 45 pct for reproduction.

by Semchyshen and Timmons.[5] These investigators have reported a predominant (100)[011] orientation plus a continuous rotation around the [111] direction, normal to the rolling plane. Semchyshen and Timmons[5] have assigned the ideal orientations of (111)[110] and (111)[112] to these continuous rotary orientations. The present results show that this rotary orientation spread is not uniform. It may best be described as a partial [111] fiber texture, spreading mainly between the (111)[110] and the (111)[112] orientations. In fact, when putting these two orientations 90° from each other, the mode of cross-rolling operation actually makes them indistinguishable.

In the partially recrystallized specimen, the retention of the (100)[011] main deformation texture is evident. Compare Fig. 4 with Fig. 1. Similar observations of the strong retainment of the (100)[011] texture were recently reported by Wiener and Corcoran[7] in the recrystallization of straight-rolled Si-Fe specimens. The strong retainment of the (100)[011] main texture, together with the early disappearance of the minor texture components of the (111)[110] or the (111)[112] type, and the addition of some new orientations, as seen from Fig. 4, are instructive. These experimental results indicate that while most of the deformed material in the (111)[110] or the (111)[112] orientation is replaced by recrystallized grains having new orientations, other portions of the deformed matrix in the (100)[011] orientation have mainly undergone *recrystallization in situ* or *polygonization*, with no or very few grains of new orientations formed. These facts are further proved by examining the microstructure of the specimen, Fig. 2b. Therefore, it may be stated that differently oriented regions in the deformed matrix respond to thermal treatment differently. These findings are in essential agreement with the observations of Dunn and Koh[8,9] on Si-Fe single crystals. Their results showed that the tendency for recrystallization can be greatly different in crystals with different deformation textures. The present results also add support to the observations of Liu and Hibbard[10] that the recrystallization temperature may be texture dependent.

Fig. 5 shows the texture of the completely recrystallized specimen, which is apparently different from the recrystallization texture of cross-rolled molybdenum, although the cross-rolling textures of both metals are quite similar. In molybdenum, the cross-rolling texture is retained and somewhat sharpened after complete recrystallization.[11] However, in iron an entirely different texture is developed. As seen from Fig. 5, the texture is rather complex, and has considerable scatter in orientation. An exact analysis of all the individual orientation components in such a widely scattered texture appears quite impractical. However, it was found that rotations of 25° in both clockwise and counter-clockwise directions around each of the (110) poles of the (111)[$\bar{1}$10] or the (111)[11$\bar{2}$] orientation components of the deformation texture seem to fit most of the intensity areas fairly well.* Fig. 6 shows

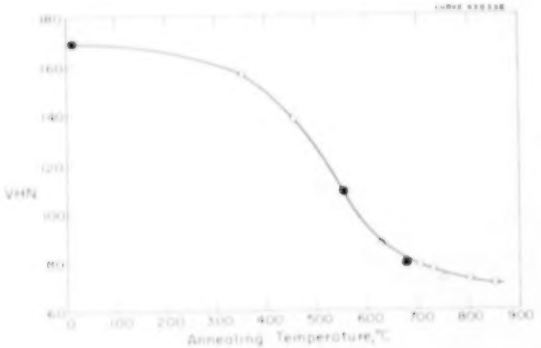

Fig. 3—Vickers hardness vs annealing temperature. Applied load: 1 kg; annealing time: 15 min at temperature. Textures were determined for those specimens marked with solid dots.

* No attempt was made in this paper to analyze the selection of ⟨110⟩ poles as rotation axes. It seems that orientations resulting from rotations around poles 4, 5, and 6 fall on high intensity areas more markedly than those from rotations around other ⟨110⟩ poles, Fig. 6.

such rotations around the (110) poles of the (111)[112] orientation.

On further study of the orientation relationships between the recrystallization texture and the deformation texture components, it was found that some of the resulting orientations derived from the [110] rotations of the minor deformation texture components can also be obtained by similar rotations from the (100)[011] main deformation texture. Fig. 7 shows the rotations of 30° in both clockwise and counter-clockwise directions around the (110) pole at the cross-rolling direction of the (100)[011] orientation. The resulting orientation, as shown by the small circles of 5° radius, coincides exactly with the orientation derived from the 25° rotations around the same (110) pole, but is derived from the (111)[110] or the (111)[112] orientation (small circles numbered 1 in Fig. 6). The minor de-

formation texture components actually consist of a partial [111] fiber texture, spreading mainly between the (111)[110] and (111)[112] orientations. Therefore, rotations around each of the peripheral (110) poles of either of these two orientations (such as poles 1, 2, and 3 in Fig. 6) are practically equivalent. This will bring many poles, away from the peripheral region in Fig. 6, coincident with those derived by the [110] rotations from the (100)[011] orientation. However, the high intensity areas near the periphery of the pole figure of the completely recrystallized specimen, Fig. 5, cannot be very well accounted for by the rotations from the (100)[011] orientation.

The above analysis that the recrystallization texture can be uniquely derived from the [110] rotations of the (111)[110] or the (111)[112] *minor* deformation texture components immediately raises a question about what has happened to the (100)[011] *main* deformation texture. Early results indicated that this main deformation texture material had hardly recrystallized, while the minor deformation texture components were completely replaced by recrystallized grains, Figs. 2b and 4. Thus, upon further annealing toward complete recrystallization, the main deformation texture material may either recrystallize in the normal manner, but at a much later stage of annealing, or never reach complete recrystallization before being absorbed by the recrystallized grains formed much earlier from the minor deformation texture matrix. However, there is considerable evidence to suggest that the latter is what occurs in practice.

First, the new orientations developed in the partially recrystallized specimen are very similar in nature to the features of the recrystallization texture. This is particularly obvious when comparing the high intensity areas near the periphery of the two pole figures, Figs. 4 and 5. These new orientations were first formed in the partially recrystallized specimen at the expense of *only* the minor deformation texture components, and gained intensity in the completely recrystallized specimen at the expense of the main deformation texture.

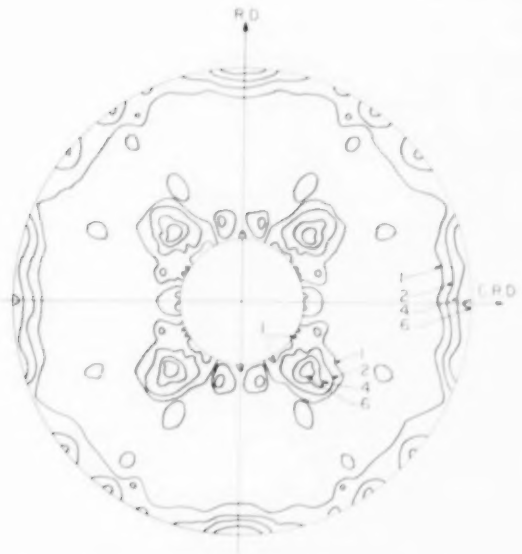

Fig. 4—(110) pole figure of the partially recrystallized specimen (annealed 15 min at 550°C). Intensities are expressed as multiples of random intensity of a carbonyl iron powder specimen.

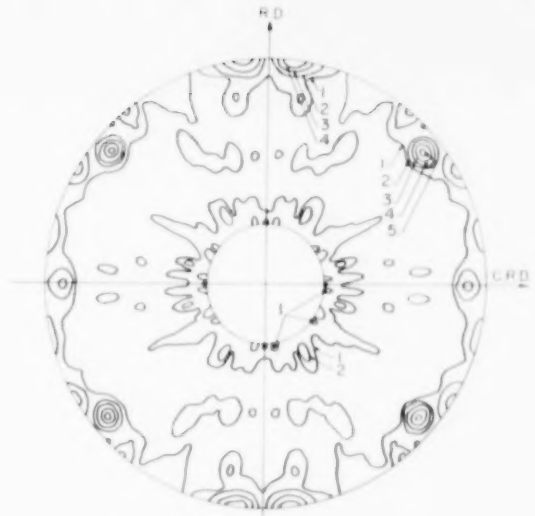

Fig. 5—(110) pole figure of the completely recrystallized specimen (annealed 15 min at 675°C). Intensities are expressed as multiples of random intensity of a carbonyl iron powder specimen.

Secondly, these high intensity areas near the periphery of the pole figures can be derived by [110] rotations from the (111)[110] or the (111) [112] minor deformation texture components, but not as well by similar rotations from the (100)[011] main deformation texture. The fact that some of the orientations in the recrystallization texture were found similarly related to both minor and main deformation texture components can probably be postulated as a favorable condition for the growth of the early recrystallized grains into the main deformation texture matrix.

Thirdly, the microstructure of the annealed specimens shows that there is considerable grain growth from the partially recrystallized state to the completely recrystallized state, and that the grain size distribution in the completely recrystallized specimen is fairly uniform, Fig. 2b and c.

Lastly, as seen from Fig. 2c, some of the light-etching low angle boundary areas are still visible, although the X-ray intensities of the retained (100)[011] main deformation texture are too low to be shown in the pole figure, Fig. 5. In this respect, Wiener and Corcoran[7] have reported different recrystallization textures obtained from different annealing temperatures (925°C vs 650°C) in Si-Fe specimens with essentially similar deformation texture components as in the present case. They observed no evidence of the light-etching low angle boundary areas in the high-temperature annealed specimen, but in the low-temperature annealed specimens, such light-etching areas were always present, although the grain size was virtually equal to that in the high-temperature annealed specimen.

In the light of the present results, the formation of a different recrystallization texture at a higher an-

Fig. 6—(110) pole positions as derived from rotations of 25° in both clockwise and counter-clockwise directions around each of the (110) poles of the (111) [112] orientation. Poles, and rotations around each pole, are numbered correspondingly. Small circles are drawn with a radius of 5°. Crosses refer to (111) [110]; solid dots, (111) [112]; arrows indicate the directions of rotations.

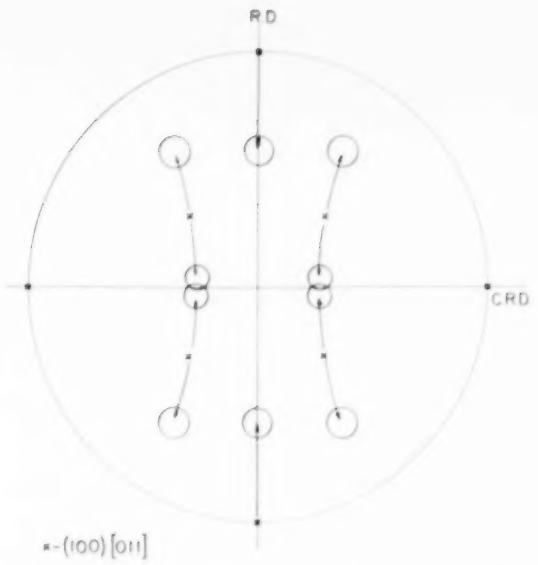

Fig. 7—(110) pole positions as derived from rotations of 30° in both clockwise and counter-clockwise directions around the (110) pole at cross-rolling direction of the (100) [011] orientation, indicated by crosses. Small circles are drawn with a radius of 5°. They coincide exactly with those small circles marked with number 1 in Fig. 6.

nealing temperature may perhaps be qualitatively explained on the same basis, for at low annealing temperatures, only certain texture components in the deformed matrix are active, while at high annealing temperatures, all the deformation texture components may recrystallize almost simultaneously, particularly at high heating rates. The present results add further support to the oriented growth theory for the formation of annealing textures. Merlini and Beck[11, 12] have pointed out the complexities in the prediction of an annealing texture in a complex deformed matrix. It seems that the potentiality for recrystallization of each texture component is an important factor. As in the present case, the effect of a minor texture component seems to have played a determining role in the formation of an annealing texture, since the main deformation texture has a much smaller tendency to recrystallize than the minor texture components.

Summary

1) The cross-rolling texture of high-purity iron was found to be similar to that of molybdenum, i.e., the texture is predominantly (100)[011], plus minor texture components of the (111)[110] or the (111)[112] type.

2) The minor texture components of the (111)[110] or (111)[112] type exhibited a greater tendency for recrystallization than the (100) [011] main texture.

3) The texture developed after complete recrystallization could be described as rotations around each of the (110) poles of the minor texture components, the (111)[$\bar{1}$10] or the (111)[112] type.

4) The difference in the tendency for recrystallization among texture components in a deformed matrix may play an important role in the formation of an annealing texture. It may be expected that this effect would be particularly notable when there is a remarkable difference in the tendency for recrystallization among different deformation texture components.

5) The formation of a different recrystallization texture from a higher temperature anneal, particularly at high heating rates, may be qualitatively explained on the same basis.

Acknowledgments

The author wishes to thank George Wiener for his helpful discussions and critical reading of the manuscript. Thanks are due to Mrs. Sally Smudski for the X-ray pole figure work, and to Roy Anderson for preparing the micrographs. The material used in this investigation was originally furnished and processed by The Institute for the Study of Metals, University of Chicago. Appreciation is hereby extended.

References

[1] C. J. Smithells and C. E. Ransley: *Journal* Institute of Metals, 1937, vol. 60, p. 172.
[2] C. E. Ransley and H. P. Rooksby: *Journal* Institute of Metals, 1938, vol. 62, p. 205.
[3] J. H. F. Custers and J. C. Riemersma: *Physica*, 1946, vol. 12, p. 195.
[4] M. J. Druyvesteyn: *Physica*, 1941, vol. 8, p. 439.
[5] M. Semchyshen and G. A. Timmons: *AIME Trans.*, 1952, vol. 194, p. 279; Journal of Metals, March 1952.
[6] B. F. Decker, E. T. Asp, and D. Harker: *Journal of Applied Physics*, 1948, vol. 19, p. 388.
[7] G. Wiener and R. Corcoran: *AIME Trans.*, 1956, vol. 206, p. 901; Journal of Metals, August 1956.
[8] P. K. Koh and C. G. Dunn: *AIME Trans.*, 1955, vol. 203, p. 401; Journal of Metals, January 1955.
[9] C. G. Dunn and P. K. Koh: *AIME Trans.*, 1956, vol. 206, p. 1017; Journal of Metals, August 1956.
[10] Y. C. Liu and W. R. Hibbard, Jr.: *AIME Trans.*, 1955, vol. 203, p. 381; Journal of Metals, February 1955.
[11] A. Merlini and P. A. Beck: *AIME Trans.*, 1955, vol. 203, p. 385; Journal of Metals, February 1955.
[12] A. Merlini and P. A. Beck: *AIME Trans.*, 1955, vol. 203, p. 1269; Journal of Metals, November 1955.

Discussion of this paper sent (2 copies) to AIME by Sept. 1, 1957 will appear in AIME *Transactions* Vol. 212, 1958, and in Journal of Metals, April 1958.

Effects of Crystal Orientation, Temperature, and Molten Zone Thickness in Temperature-Gradient Zone-Melting

A strong orientation effect has been found for molten aluminum-rich wire zones traversing single crystals of germanium. If the intersection of a {111} plane with the plane of wire-travel is oblique to the wire, the wire breaks into segments that lie parallel to the line of intersection. However, if the line of intersection is perpendicular or parallel to the wire, the wire remains straight. This crystalline anisotrophy has been utilized to make highly parallel *npn* junctions using aluminum-rich wire zones in germanium. The rate of zone movement increases unusually rapidly with temperature and with diameter of the wire zone. These findings suggest that the rate-controlling factor in these experiments is not diffusion in the liquid zone, but the solution rate at the hotter interface. Diffusion may become the limiting process at higher temperatures and lower temperature gradients.

by J. H. Wernick

IN temperature-gradient zone-melting[1] a molten zone is moved through a solid or across a solid surface by the establishment of a temperature gradient. This technique has both practical and fundamental aspects. One practical application is to make *p-n* junctions for semiconductive devices, particularly for devices in which the junctions are desired within the semiconductor. From a fundamental point of view, the technique is being investigated as a method for determining diffusivities in liquid alloys, and preliminary diffusivity results have been reported by the writer.[2]

In this paper, the effects of crystal orientation, temperature, and molten zone thickness in temperature-gradient zone-melting, and the bearing of these effects on diffusivity measurements and *n-p-n* junction formation are discussed.

J. H. WERNICK, Associate Member AIME, is associated with Bell Telephone Laboratories Inc., Murray Hill, N. J.

TP 4476E. Manuscript, Oct. 25, 1956. New York Meeting, February 1956.

Experimental Procedure

An effect of crystal orientation was noted in early experiments. To facilitate its study, movements of wire zones across a surface, rather than through the body of a single crystal, were observed for various surface planes and travel directions. The experimental setup is illustrated in Fig. 1. The graphite end-section for the high temperature heater has an apron about 1/16 in. above the upper surface of the crystal. This apron insures that the surface temperature of the block is equal to or greater than the temperature within the block at every point. Thus, the zone does not penetrate the block and convection in the liquid is minimized. The experimental setup for the movement of molten zones through a block is shown in Fig. 2.

The temperature gradient in the solid was determined by two thermocouples in a germanium test block, close to the hottest and coldest surfaces. It was assumed that the thermal diffusivity was constant in the temperature range in question. Temperature gradients so determined were assumed to be the same as those which existed in the liquid zone.

Effects of Crystal Orientation On the Movement of A Molten Zone Across a Surface

It was found that if the starting 3 mil Al solvent wire lies in a (111) plane in a [112] direction and if it travels in a [110] direction, that is, the direction of the temperature gradient, the molten wire zone moves so that it will lie in a [101] or [011] direction. Usually, the molten zone breaks up and the segments move so that they will lie along <110> directions, as shown in Fig. 3. If the starting wire lies in a (111) plane in a [$\bar{1}$10] direction and if its travel direction is [11$\bar{2}$], the wire breaks up and each segment travels as a unit, all points advancing at the same rate. However, the area over which each segment moved is bounded by <110> directions. In one case, shown in Fig. 4, the wire did not break up, but it moved over an area bounded by <110> directions. The frozen wire-zone is at the top of the swept area. If the starting wire lies in a (001) plane in a [010] direction and if its travel direction is [100], it breaks up and each segment becomes confined to a region bounded on two sides by <110> directions. This case is illustrated in Fig. 5.

These results indicated that an originally straight molten zone tends not to cross oblique <110> directions on a surface over which movement is occurring, but moves so as to lie in <110> directions or to be confined to regions bounded by <110> directions. This direction apparently is a barrier or a stable direction for wires in {111} and {100} planes.

Additional experiments were performed to learn more concerning this orientation effect. For example, it was found that, if the starting wire lies in a

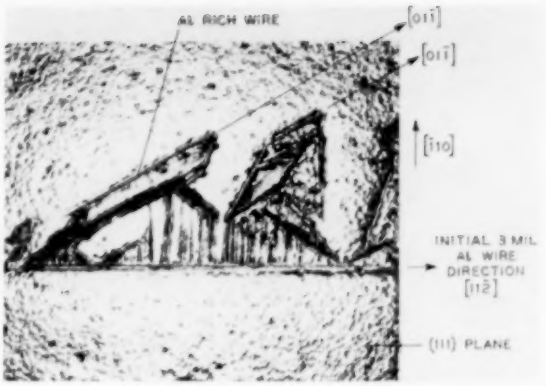

Fig. 3—Three mil Al wire on (111) plane in [112] direction. Etch: 3 parts HF, 5 parts HNO_3, 3 parts CH_3COOH. X15. Reduced approximately 45 pct for reproduction.

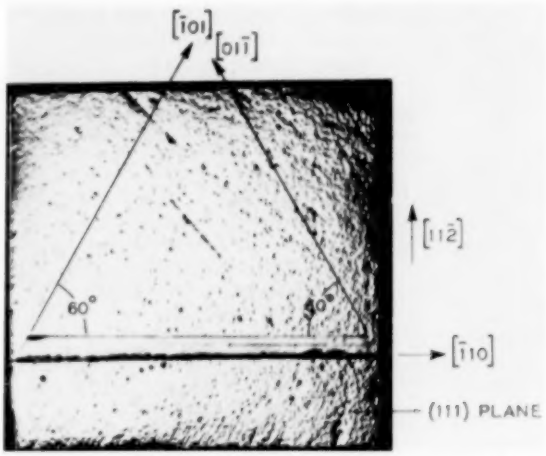

Fig. 4—Three mil Al wire across (111) surface. Unetched. X7.5. Reduced approximately 30 pct for reproduction.

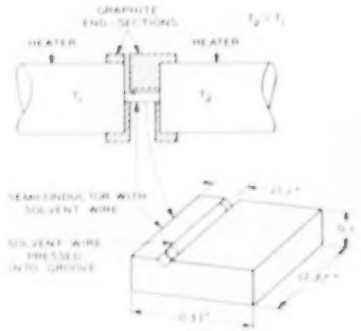

Fig. 1—Experimental setup for movement of molten zones across germanium surface.

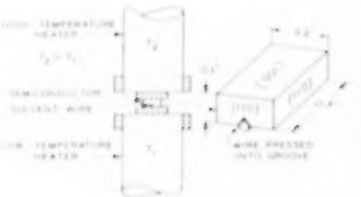

Fig. 2—Experimental setup for movement of molten zones through germanium.

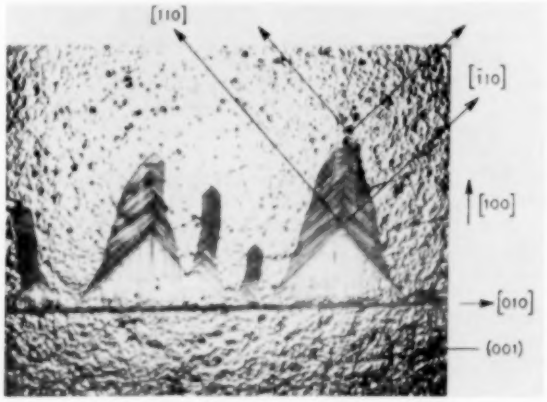

Fig. 5—Three mil Al wire across (001) surface. Unetched. X15. Reduced approximately 45 pct for reproduction.

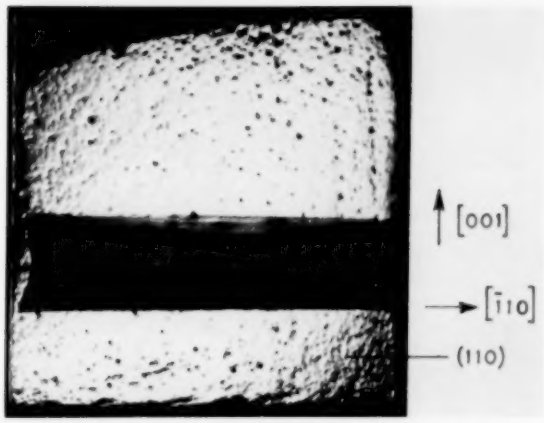

Fig. 6—Three mil Al wire across (110) surface. Unetched. X7.5. Reduced approximately 25 pct for reproduction.

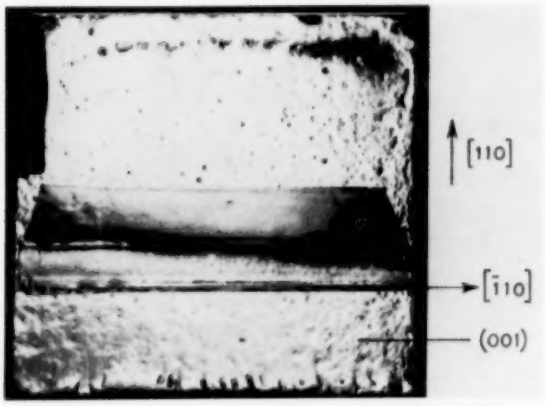

Fig. 7—Three mil Al wire across (001) surface. Unetched. X7.5 Reduced approximately 20 pct for reproduction.

(110) plane in a [001] direction and if its travel direction is [110], the wire breaks up and each segment becomes confined to a region bounded on two sides by <112> directions, i.e., the 35° oblique intersections of the {111} planes on the (110) plane. If the starting wire lies in a (110) plane in a [110] direction and if its travel direction is [001], the wire travels as a unit, all points advancing at the same rate, and remains extremely straight. This case is illustrated in Fig. 6. The left side of the swept area would be expected to be an oblique <112> direction 55° to the original wire direction. This type of movement, analogous to the case shown in Fig. 4, was not observed. If the starting wire lies in a (001) plane in a [110] direction and if its travel direction is [110], the wire travels as a unit, all points advancing at the same rate. This case is illustrated in Fig. 7. The intersections of the {111} planes, i.e., the <110> directions, are perpendicular and parallel to the wire. Thus, it appears that the intersecting {111} planes impede zone movement and give rise to the above orientation effect.

The temperature-gradient employed for the above experiments was approximately 31°C per cm at a mean temperature of 667°C. Similar results were obtained for temperature gradients of approximately 15°C per cm, 8°C per cm, and 4°C per cm. The last gradient corresponds to a temperature change of 0.03°C in 3 mil.

To see if the above orientation results were due to convection effects, the setup shown in Fig. 1 was rotated 180° so as to have the molten zone move on the lower surface of the block. Surface tension prevented the molten zone from falling off the surface. The same orientation results were obtained.

The surface results apply to the movement of a wire zone *through* a block, as shown by the following results. If the wire direction is <110>, and the direction of temperature gradient <001>, as shown in Fig. 2, the variation in penetration from section to section for a given specimen was considerably less than that observed previously,[2] and amounted to less than 11 pct.

Effect of Temperature and Zone Diameter On the Rate of Movement

The rate of movement of Ge-Al wire zones increased rapidly with temperature for a temperature-gradient of 31°C per cm. This information is shown in Fig. 8. To show this effect in another way, 3 mil Al wires were placed at different positions along a 31°C per cm temperature gradient on a block of germanium. The hotter the zone the higher was the mean rate of movement. This result is shown in Fig. 9, together with the mean rates of movement at the end of the run. The temperature difference across the block was 28.5°C. The large change in the rate of movement for such small change in temperature cannot be accounted for by the change of diffusivity with temperature in the liquid zone. This statement is based on data for diffusion in liquid Pb-Bi alloys[5] and the low activation energies required for diffusion in other liquids.[4] The activation energy required for diffusion in liquids is, on the average, a few kilocalories per mol. The Ge-Al preliminary data reported earlier[2] gave an activation energy (based on two mean temperatures) of 31,000 cal per mol. Hence, an explanation other than the temperature coefficient of diffusivity must be sought.

The penetration rate of a Ge-Al wire zone increases with increasing diameter of the aluminum solvent wire for a temperature-gradient of 114°C per cm at a mean temperature of 667°C. The data are shown in Fig. 10. The experimental setup is illustrated in Fig. 2.

Discussion

The orientation, temperature, and zone diameter effects can be explained by assuming that the higher temperature portion of the molten zone is not satur-

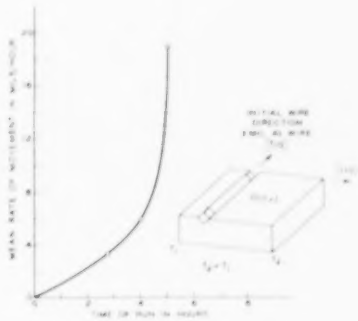

Fig. 8—Mean rate of movement at end of run vs time of run. Temperature gradient, 31° per cm.

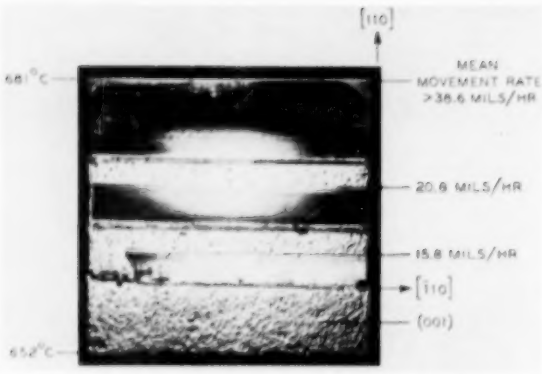

Fig. 9—Three mil Al wires across (001) surface. Unetched. X7.5. Reduced approximately 45 pct for reproduction.

ated. Temperature-gradient zone-melting can be considered as three consecutive processes:

Solution (high temperature interface) → Diffusion → Precipitation (low temperature interface).

If it is assumed that diffusion occurs more rapidly than solution, then ΔC, the concentration difference in the molten zone, never reaches the value corresponding to ΔT along the liquidus curve, Fig. 11; and hence the solution does not attain saturation at the hotter interface. This nonsaturated solution can differentiate between atomic planes having different solution rates. Results obtained in the fabrication of semiconductor devices by alloying indicate that the solution rate is lowest for (111) planes. The (111) plane can be considered to be the most *stable*, and the <110> directions, being the intersections of the {111} planes on a given (111) and (100) plane, the most *stable* directions. It would appear in general that an originally straight wire zone tends not to cross directions which are the intersections of {111} planes and the plane of wire movement.

The large temperature effect on the rate of zone movement suggests that the rate of the limiting step changes rapidly with temperature; i.e., has a high activation energy. It is known that the solution rate can change rapidly with small changes in temperature.[5] As the zone moves to higher temperatures, the solution rate increases, thereby increasing the concentration gradient in the zone, as shown in Fig. 11. The increased concentration gradient gives rise to an increase in the flux of solute and consequent increase in the rate of movement. Therefore, the rate of movement is determined by the rate of solution and its subsequent effect on the concentration gradient. For the diffusion process to be the overall rate determining step, the rate of solution must be large in comparison to the rate of diffusion. This condition should be obtained at higher temperatures and lower temperature gradients.

One of the reasons travel rate increases with wire diameter may be that an increase in the diameter of the starting wire results in an increase in the diameter of the molten zone. The high temperature interface of a thick zone will be at a higher temperature at a given time and the solution rate will be greater than for a thin zone. However, it is felt that this alone cannot completely account for nearly a two fold increase in rate in going from a 2 to 3 mil starting wire. When the penetrations shown on Fig. 10 are expressed in terms of penetration per unit radius of starting wire, a roughly constant value is obtained. For 2, 3, and 5 mil wires, the penetrations are 25, 30, and 24 mil per mil, respectively. A larger high temperature interface area will result in a greater amount of solution at a given time and possibly a greater ΔC. However, when the rates are expressed on the basis of radius of curvature or interfacial area, the same penetration rate should be obtained if the solution rate is the limiting process. This appears to be the case.

The use of the diffusion equation, $F = -D\frac{dc}{dx}$, as an approximate rate equation for this process in the temperature region where diffusion in the liquid zone is not the limiting step is valid if the D values are regarded as rate constants for the overall process. The preliminary D values obtained by use of this technique are of the right order of magnitude for diffusion in liquids, namely, 10^{-5} sq cm per sec. For the rate constant to be a true diffusion coefficient at a given temperature, diffusion must be established for the system in question as the rate limiting process. When this is the case, it is believed that the orientation, zone thickness, and large temperature effects reported here will not be observed. It may well be, for some systems, that diffusion will be the limiting process over the complete liquidus temperature range.

Convection Effects

For the movement of Ge-Al molten zones through germanium, it was observed that convection occurs if the original wire diameter is 5 mil and above. If the low temperature heater was above the high temperature heater for a starting 5 mil Al wire through germanium, an average penetration of 102 mil was obtained in 50 min. If the high temperature heater was above the low temperature heater, an average penetration of 60 mil was obtained in 50 min. No such effect was observed for 3 mil and 2 mil diam

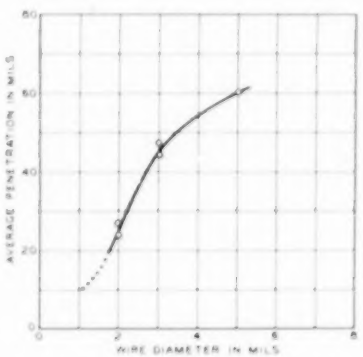

Fig. 10—Average penetration in 50 min vs starting wire diameter for aluminum wires through germanium.

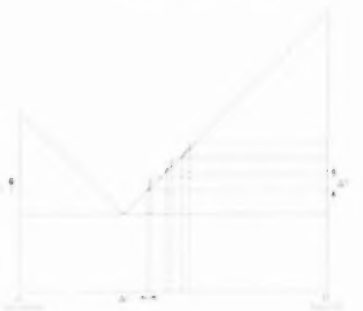

Fig. 11—Diagram illustrating change in concentration gradient across zone with increasing temperature.

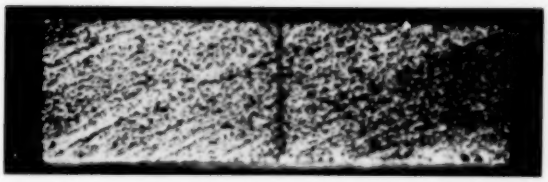

Fig. 12—n-p-n type. Transverse section of *n*-germanium block through which a 3 mil Al wire was moved by temperature-gradient zone-melting. Etch: 1 part HF, 1 part 30 pct H_2O_2, and 4 parts H_2O. X9.

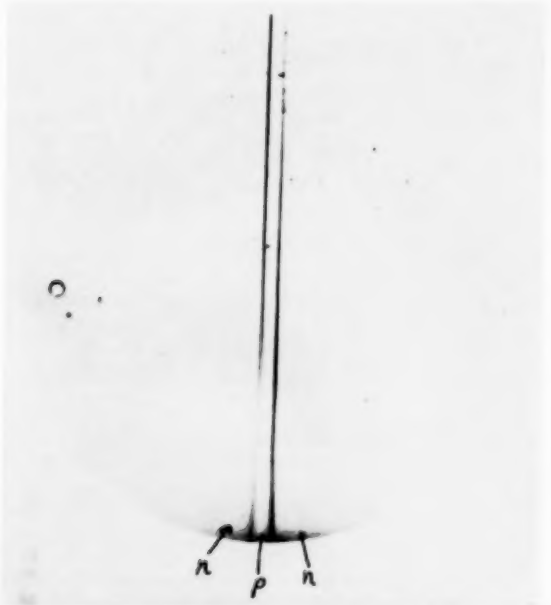

Fig. 13—Transverse section of *n*-germanium block through which a vapor plated aluminum strip was moved by temperature-gradient zone-melting. Specimen held at 500°C during plating. Etched. X500. Reduced approximately 25 pct for reproduction.

wires. The temperature gradient employed was 114°C per cm and corresponds to a temperature change of 1.5°C over 5 mil.

n-p-n Structures

From the preceding, it is apparent that for these systems there are two orientations for which a molten wire zone moves as a unit in the direction of the temperature gradient. They are:

1) a, wire in (110) plane in $<\bar{1}10>$ direction; and b, direction of temperature gradient $<001>$.

2) a, wire in (001) plane in $<\bar{1}10>$ direction; and b, direction of temperature gradient $<110>$.

Using orientation 2, the *n*-*p*-*n* structures shown in Figs. 12 and 13 were obtained. Molten Ge-Al wire zones were moved through *n*-germanium blocks. The photographs show transverse sections. The *n*-*p*-*n* shown in Fig. 13 was produced from a vapor deposited aluminum strip, 6 mil wide and 0.5 mil thick. Plating was done at a temperature estimated to be about 500°C. The average thickness of the *p*-layer is 0.3 mil. Surface tension appeared to cause the original 6 mil wide aluminum strip to form a wire of much smaller width. From a useful device point of view, the above *p*-layers are saturated with aluminum and therefore are too heavily doped for conventional *n*-*p*-*n* configurations.

Acknowledgments

Thanks are due to W. G. Pfann for his help and interest in this research. Thanks are also due to H. Reiss for helpful discussion; to J. J. Gillich for experimental assistance; and to J. Jaworski for several macrographs.

References

[1] W. G. Pfann: Temperature Gradient Zone Melting. *AIME Trans.*, 1955, vol. 203, p. 961; Journal of Metals, September 1955.

[2] J. H. Wernick: Determination of Diffusivities in Liquid Metals by Means of Temperature Gradient Zone Melting. *Journal of Chemical Physics*, 1956, vol. 25, No. 1, p. 47.

[3] R. E. Grace and G. Derge: Diffusion in Liquid Lead-Bismuth Alloys. *AIME Trans.*, 1955, vol. 203, p. 839; Journal of Metals, July 1955.

[4] W. Jost: *Diffusion in Solids, Liquids, Gases*. Academic Press Inc., New York, 1952.

[5] C. M. Craighead, E. W. Cawthorne, and R. I. Jaffee: Solution Rate of Solid Al in Molten Al-Si Alloys. *AIME Trans.*, 1955, vol. 203, pp. 81-87; Journal of Metals, January 1955.

Discussion of this paper sent (2 copies) to AIME by Sept. 1, 1957 will appear in AIME *Transactions* Vol. 212, 1958, and in Journal of Metals, April 1958.

Technical Note

Formation of Intermetallic Layers in Diffusion Couples

by L. S. Castleman and L. L. Seigle

IN a recently reported investigation, J. B. Clark and F. N. Rhines[1] used a diffusion couple technique to determine the number of intermetallic phases which should be present in the Al-Mg equilibrium phase diagram. Their method was an application of the following generally accepted principle. If a diffusion couple made up of two metals is annealed at a given temperature for a long time, all the phases of the binary system which exist under equilibrium conditions at the diffusion temperature will form intermetallic layers. It is important that the diffusion temperature be high enough and the diffusion time be long enough to permit the nucleation of all thermodynamically stable phases at the interface of the couples and their growth to observable thicknesses. These simple time-temperature criteria are at times difficult to satisfy, and it is the purpose of this note to point out a situation in which this is the case.

The authors are currently studying diffusion bonding in the Al-Ni system.[2] It is well established

L. S. CASTLEMAN, Associate Member AIME, and L. L. SEIGLE, Member AIME, are associated with Sylvania Electric Products Inc., Bayside, N. Y.

TN 423E. Manuscript, Mar. 19, 1957.

Fig. 1—Al-Ni couple diffused at 600°C for 96 hr under a pressure of 5 tsi. Unetched. X100. Reduced approximately 25 pct for reproduction.

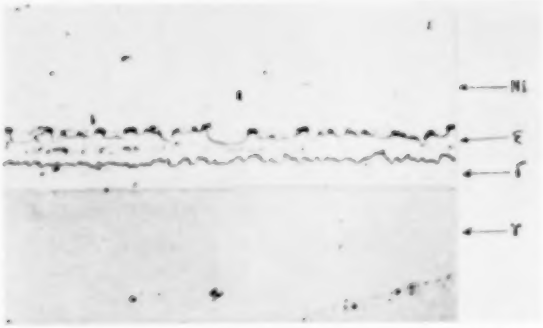

Fig. 2—γ-Ni couple diffused at 900°C for 24 hr. Sample etched in H_2SO_4-H_3PO_4-HNO_3 solution. X350. Reduced approximately 25 pct for reproduction.

that four intermetallic phases occur, which are designated β ($NiAl_3$), γ (Ni_2Al_3), δ (NiAl), and ϵ (Ni_2Al). Diffusional bonding between aluminum and nickel is limited to temperatures below the eutectic, which occurs at 640°C. Previous investigators[1] had concluded that only two phases, the β and γ phases, formed in diffusion couples annealed at 600°C and below for times of the order of minutes. This result seemed to be confirmed by the initial experiments of the present investigators, who extended the times to a few hundred hours, Fig. 1. As part of a study of intermediate layer formation above the eutectic temperature, a few γ-Ni diffusion couples were prepared and annealed for 24 hr at 800°, 900°, and 1050°C, Fig. 2. Significantly, both the δ and ϵ phases were found in these diffusion couples, in layers of approximately equal thicknesses. The data for the δ phase are summarized in Table I.

If ln K is plotted vs $1/T$, where T is the absolute temperature, a reasonably good straight line is obtained which can be used to extrapolate the data to lower temperatures. In addition, if it is assumed that the δ layer grows parabolically with time, it becomes possible to determine the times and temperatures needed to grow a layer of δ (or ϵ) phase of constant thickness. A series of such plots is shown in Fig. 3, in which three curves have been drawn to show the *iso-thickness* lines for the δ phase (the curves can be shown to be hyperbolas); the lines have been drawn for thicknesses of 0.1, 1.0, and 2.0 μ. In the work on the Al-Ni alloy system, it has proven difficult to determine unequivocally by optical methods the presence of a phase whose thickness is less than 1 to 2 μ. Consequently, it was surmised that the *missing* phases in the Al-Ni couples diffused below the eutectic temperature might actually have been present as undetectably thin layers. This hypothesis was confirmed by diffusion of an additional Al-Ni specimen for 340 hr at 600°C. Careful examination of the Al-Ni interface at high magnification revealed the δ and ϵ layers in thicknesses of 2 μ or less. For diffusion temperatures below 600°C, these layers would evidently not grow to sufficient thickness in any reasonable time to be detected by ordinary metallographic examination.

Table I. NiAl (δ) Phase Thickness in Diffusion Layer

Couple	Temperature, °C	Time t, Hr	Thickness x (Mm)	K,* Sq Mm per Hr
γ-Ni	800	24	0.0035	5.1×10^{-4}
γ-Ni	900	24	0.018	1.4×10^{-3}
γ-Ni	1050	24	0.112	5.0×10^{-2}

* K is defined by the relation $x^2 = Kt$.

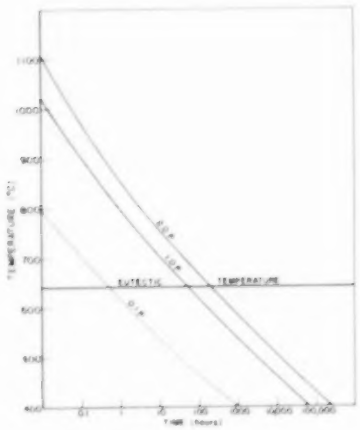

Fig. 3—Thickness of NiAl (δ) phase as a function of diffusion temperature and time.

The existence of a eutectic in the Al-Ni system at 640°C precludes the use of Al-Ni diffusion couples above this temperature. Below 640° the high melting intermediate phases grow very slowly. In general, therefore, it appears that caution should be exercised in applying the diffusion couple technique to systems in which low melting components are found in conjunction with high melting compounds. Under these conditions, inferences concerning the number of phases present in the equilibrium diagram drawn from studies of intermediate layer formation should be accepted with reservations until corroborated by independent tests.

Acknowledgments

The authors would like to acknowledge the able assistance of J. J. Gitto in performing the above experiments. This work was supported by the Atomic Energy Commission under Contract No. AT-30-1 GEN-366.

References

[1] J. B. Clark and F. N. Rhines: Aluminum-Magnesium Equilibrium Diagram. *AIME Trans.*, 1957, vol. 209, pp. 6-7; Journal of Metals, January 1957.

[2] L. S. Castleman and L. L. Seigle: Fundamentals of Diffusional Bonding—I. First Annual Progress Report, 1955-1956, SEP 227, pp. 1-37.

[3] S. Storchheim, J. L. Zambrow, and H. H. Hausner: Solid State Bonding of Aluminum to Nickel. *AIME Trans.*, 1954, vol. 200, pp. 269-274; Journal of Metals, February 1954.

Technical Note

Preparation and Diffraction Data of Ba-Al Alloys

by Dilip K. Das and Douglas T. Pitman

ONE of the major uses of barium in metallic form is as a getter material in vacuum tubes. Because of the high chemical reactivity of the metal, Ba-Al alloys are extensively used. Numerous methods for the preparation of Ba-Al alloys have been published, a few of which[1-4] are cited here. Most of these methods were found to be quite elaborate, involving the reduction of BaO, and not too well adapted for the close control of the final composition of small amounts of alloys prepared for laboratory use. A simple laboratory method for the preparation of Ba-Al alloys in small batches starting from pure metals was devised, so that it was possible to control the desired compositions to within 1 pct.

The pertinent features of the alloy system Ba-Al[5] are 1) an intermediate compound $BaAl_4$, with the melting point of 1050°C, and 2) a eutectic between aluminum and $BaAl_4$ at 98 pct Al.

The accompanying sketch shows the experimental arrangement for the preparation of the alloys. Weighed amounts of aluminum and barium were placed in an alumina and a stainless steel crucible, respectively. According to the supplier's specification, the purity of the metals used in the alloys is as follows: a) aluminum rods—99.9 pct Al, and b) barium rods—99.5 pct Ba. The stainless steel crucible, tapered at the bottom and having a 1/16 in. diam hole, rested on top of the alumina crucible. The assembly was placed inside a graphite sleeve which rested on a refractory platform. The platform moved the assembly up and down through the field of a radio frequency coil. A glass bell jar was placed between the crucible assembly and the radio frequency coil to maintain a steady flow of helium around the melt. A small window was cut out on the wall of the alumina crucible to observe the progress of the reaction and to record the temperature with an optical pyrometer.

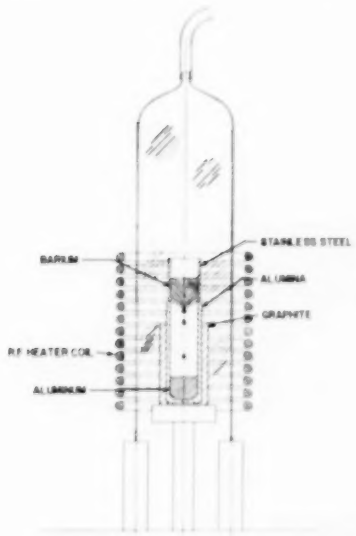

Fig. 1—Experimental arrangement for the preparation of $BaAl_4$.

The platform was first raised high enough to move the barium out of the radio frequency coil field in order to allow only the aluminum to melt. The assembly was then lowered so that the barium began to melt and flow out through the small orifice into the molten aluminum. In order to keep the violence of the exothermic reaction under control, the rate of flow of barium was carefully regulated by raising or lowering the crucible assembly.

All the samples prepared by this technique were examined by a Norelco X-ray diffractometer using CuK_α radiation. The diffraction specimens were prepared by placing the finely powdered samples in flat specimen holders. The Ba-Al alloys prepared with a high barium content were found to consist mainly of $BaAl_4$. The structure of $BaAl_4$ has previously been reported by Alberti and Andress.[6] They found that $BaAl_4$ was body-centered-tetragonal with an $a_o = b_o = 4.530$A and $c_o = 11.14$A.

An alloy whose composition was found by chemical analysis to be almost 100 pct $BaAl_4$, was used to determine the relative intensities. The *d*-spacings were obtained from the same alloy to which a small amount of tungsten had been added as a calibrating material. Accurate values for a_o and c_o were calculated according to the method proposed by Taylor and Floyd.[7] The calculated values are: $a_o = b_o = 4.566$A and $c_o = 11.250$A. The measured *d*-values for $BaAl_4$ are shown in Table I along with relative peak intensities above background and *hkl* indices.

Table I. Powder Diffraction Data of $BaAl_4$

hkl	*d*, A	*I*	*hkl*	*d*, A	*I*
002	5.60	0.61	206	1.442	0.06
101	4.23	0.74	310	1.435	0.05
110	3.228	0.34	008	1.408	0.13
103	2.902	0.78	224	1.405	0.09
004	2.815	0.66	312	1.396	0.17
112	2.804	1.00	118	1.289	0.05
200	2.282	0.47	217	1.263	0.10
114	2.117	0.11	321	1.258	0.08
202	2.112	0.02	226	1.223	0.02
105	2.023	0.37	109	1.206	0.01
211	2.009	0.20	323	1.198	0.11
006	1.874	0.03	208		
213	1.794	0.40	316	1.144	0.06
204	1.774	0.15	400	1.141	0.05
116	1.624	0.16	0010	1.125	0.01
220	1.615	0.10	402	1.119	0.01
222	1.551	0.03	307	1.103	0.06
107	1.512	0.19	325		
215			411	1.076	0.01
301			330		

Acknowledgment

The authors are grateful to L. J. Cronin, the head of the Techniques Dept., for suggesting the problem and for his constant interest.

References

[1] Froges and Camargue: German Patent No. 809107, 1951. French Patent No. 935324, 1949.
[2] E. Bonnier: *Annales de physique*, 1953, vol. 8, pp. 259-312.
[3] M. Orman and E. Zembela: *Proc.* Institute of Metals, 1952, vol. 4, pp. 437-445.
[4] E. Fujita and H. Yokomizo: *Reports Gov.* Chemical Industrial Research Institute, Tokyo, 1952, vol. 47, pp. 291-297.
[5] E. Alberti: *Ztsch. für Metallkunde*, 1934, vol. 26, p. 6.
[6] E. Alberti and K. R. Andress: *Ztsch. für Metallkunde*, 1935, vol. 27, p. 126.
[7] A. Taylor and R. W. Floyd: *Acta Crystallographica*, 1950, vol. 3, p. 285.

D. K. DAS, Associate Member AIME, and D. T. PITMAN are associated with Techniques Dept., Microwave and Power Tube Operations, Raytheon Manufacturing Co., Waltham, Mass.
TN 402E. Manuscript, Oct. 8, 1956.

Stability of AISI Alloy Steels

Typical AISI alloy steels which are used extensively in the automotive industry were investigated. These steels were studied in order to provide a comparison with the steels now used for piping and elevated temperature service. The results indicate that the Cr-Mo steels now employed for piping are satisfactory in comparison with the AISI alloy steels. The steels were exposed at 900° and 1050° and, in several instances, 1200°F. They were either normalized or annealed before exposure and, in general, two carbon levels were investigated. The microstructure was observed after 34,000 hr exposure. Tensile and creep rupture properties were determined after 10,000 hr exposure. Graphite was observed in the Ni-Mo steels, but not in the chromium bearing steels, which were the most structurally stable of the AISI steels investigated. A slight decrease in tensile strength in the various steels was observed after exposure. The creep rupture strength of the nickel steels was similar to plain carbon steels, but the steels containing molybdenum or vanadium had a higher creep rupture strength.

by A. B. Wilder, E. F. Ketterer, and D. B. Collyer

AISI constructional alloy steels are a series of steels in which a numbering system signifies the chemical composition limits. SAE (Society of Automotive Engineers) and AISI (American Iron and Steel Institute) use basically the same numbering system. The steels contain, in part, alloy additions of chromium, molybdenum, nickel, and vanadium. They are used widely in the automotive industry but have not been adopted for high temperature service.

The purpose of this investigation was to study changes in microstructure observed in typical AISI constructional alloy steels in the welded and unwelded conditions after exposure for 34,000 hr at 900° and 1050° and, in several instances, 1200°F. The tensile and creep rupture properties after exposure for 10,000 hr were also evaluated. The investigation is a continuation of the work previously discussed.

Little was known concerning the existence of graphite in medium or low carbon steels before 1943. It is important to note that continued exposure at elevated temperature is required in order to develop graphite in steels. Interest in the presence of graphite in steel, and also in changes in the properties of steels after long service at elevated temperatures, developed after 1943 when a failure of a welded joint of high temperature piping was associated with the graphitization of a relatively low carbon content steel with 0.50 pct Mo.[1,2]

Numerous investigations have beeen made in recent years studying the relationship of this type of failure to changes in properties. Attempts have been made to evaluate the performance of a number of steels, particularly in the heat-affected zone of welds. It was the unfortunate failure of a weld-heated zone in high temperature piping in the steam-power industry which focused attention upon possible failures, and upon the need for improved steels for high temperature piping service.

Investigation by the National Tube Div., U. S. Steel Corp., Lorain Works, has included a wide variety of steels in an attempt to learn the effects of numerous factors and elements upon the long time performance of steels, although many of the compositions studied will never be used at elevated temperatures.[1-3] Included were the well established AISI steel series, which offered opportunity to test moderately high carbon content steels as well as observe the effect of nickel, chromium, molybdenum, etc., upon the properties of these well known steels.

The properties of the AISI steels were also studied for comparison with the previously reported properties of the Cr-Mo steels, now used by the steam-power industry.[3,4]

Materials and Testing Procedure

The AISI alloy steels in Table I were exposed for 10,000 and 34,000 hr at 900°, 1050°, and 1200°F.

A. B. WILDER, Member AIME, is Chief Metallurgist, National Tube Div., U. S. Steel Corp., Pittsburgh. E. F. KETTERER and D. B. COLLYER, Members AIME, are Chief Metallurgist and Metallurgist, respectively, National Tube Div., Lorain Works, Lorain, Ohio.

TP 4503E. Manuscript, June 23, 1955. Philadelphia Meeting, October 1955.

Table I. Types of Steel, Heat Treatment, and Welding Electrodes

AISI Designation	Type	Chemical Composition*						Heat Treatment Prior to Exposure, 1650°F†	Welding Electrode Employed
		C	Mn	Ni	Cr	Mo	V		
2320	Ni	0.20	0.70	3.70	0.03	0.002		*N*	E7020
2517	Ni	0.14	0.41	5.18	0.08	0.003		*N*	E7020
3115	Ni-Cr	0.16	0.49	1.20	0.61	0.050		*N*	E7020
3130	Ni-Cr	0.31	0.71	1.44	0.74	0.005		*A*	E7020
3316	Ni-Cr	0.16	0.44	3.30	1.48	0.006		*N*	E7020
4115	Cr-Mo	0.21	0.83	0.05	0.49	0.26		*N*	E7010
4140	Cr-Mo	0.38	0.75	0.03	0.94	0.20		*A*	E7010
4317	Ni-Cr-Mo	0.18	0.48	1.79	0.41	0.23		*N*	E7020
4337	Ni-Cr-Mo	0.36	0.70	1.91	0.86	0.30		*A*	E7020
8625	Ni-Cr-Mo	0.24	0.72	0.45	0.50	0.20		*N*	E7020
8630	Ni-Cr-Mo	0.29	0.83	0.64	0.56	0.20		*A*	E7020
4615	Ni-Mo	0.16	0.58	1.87	0.12	0.27		*N*	E7020
4640	Ni-Mo	0.38	0.67	1.66	0.04	0.26		*A*	E7020
4815	Ni-Mo	0.19	0.63	3.56	0.16	0.23		*N*	E7020
6120	Cr-V	0.20	0.51	0.06	1.00	0.016	0.17	*N*	E7020
6145	Cr-V	0.49	0.85	0.05	1.07	0.007	0.19	*A*	Type 502

* Other elements included between 0.008 and 0.031 pct P, 0.011 to 0.030 pct S, and 0.17 to 0.32 pct Si.
† *N* refers to normalized, air cool; *A*, annealed, furnace cool.

The steels were forged to 1x1 in. bars. All of the steels after carburizing at 1700°F had a fine grain size.

The graphitization chart[5] employed in this investigation contains designations *A*, *B*, *C*, etc. (*A* being the smallest size particle) which are used with a prefix. A rating of 10*C*, for example, indicates ten particles of dispersed graphite with an average size *C* in a representative 4x5 in. field at X500.

A weld bead for graphitization studies was deposited with automatic welding equipment at the U.S. Steel Corp. Fundamental Research Laboratory using a ⅛ in. diam coated electrode with 100 amp at 24 volts and an arc travel speed of 10 in. per min. No preheating or postheating was employed. The type of welding electrodes employed in this investigation is shown in Table I. The results with weld beads are not always strictly comparable to commercial welding conditions. However, the automatic weld beads used in this investigation provided uniform conditions for the experimental work. Specimens containing portions of the bead welds were microscopically examined after 34,000 hr exposure at 900° and 1050°F. The samples exposed at 1200°F were not examined due to the large amount of oxidation and decarburization.

The type of specimen used for tensile and creep rupture testing is shown in Fig. 1. Standard procedure for creep rupture testing was followed.[6] The tensile and creep rupture tests were conducted before exposure and after 10,000 hr exposure at 900°, 1050°, and, in several instances, after exposure at 1200°F. The creep rupture tests were performed at the exposure temperatures and were of sufficient duration for actual determination of the 1000 hr properties. The tensile tests were at ambient temperatures.

Microstructure

Specimens containing the small weld bead were examined microscopically after 34,000 hr exposure and compared with the microstructures of the same group of AISI steels after only 10,000 hr exposure at 900° and 1050°F.[4] In general, there was very little change in microstructure between 10,000 and 34,000 hr exposure.

Fig. 1—Diagram of test specimen.

Graphite in Weld Metal—A small amount of graphite was found in the bead weld metal and weld heat-affected zone of AISI Grade 4640 steel after 34,000 hr exposure at 1050°F. A ⅛ in. diam *E*7020 coated electrode was employed, with no preheat or postheat. The appearance of one of the graphite nodules in the weld metal is illustrated in Fig. 2. The graphite rating is 0.04*G*.

A number of dark gray particles, too small to identify, were visible in the deposited weld metal in several of the higher carbon steels, for example, the AISI 4140 and AISI 4337 steels after 34,000 hr exposure. In the AISI 4140 and AISI 4337 welds, the small dark particles were visible along the boundaries of columnar structure areas after 900°F exposure. Particles in the columnar boundaries after 1050°F exposure appeared to be small, light colored carbides.

Nickel Steels—The AISI 2320 and AISI 2517 nickel steels exhibited slightly greater spheroidization and graphitization after 34,000 hr exposure than was visible after the 10,000 hr exposure, particularly in the weld heat-affected zones. After 34,000 hr exposure at 900°F the structure of the parent metal of both steels was still similar to that visible after 10,000 hr exposure, and is illustrated in Fig. 3a. After 34,000 hr exposure at 1050°F the structure of both steels was similar to Fig. 3b, except that AISI 2517 steel contained small carbides.

The greatest change in the nickel steels occurred in the weld heat-affected zone. At 900°F the weld-heated zone of steel AISI 2320 resembled that of AISI 4640 in Fig. 5, and this same zone of steel AISI 2517 resembled AISI 8625 in Fig. 4. At 1050°F the weld heat-affected zone of both steels was similar to AISI 4640, Fig. 5, except that the ferrite areas were considerably coarser.

With regard to the subcritical growth of ferrite areas at 1050°F in portions of the weld heat-affected zones of the parent metal, this condition has been observed previously.[4] The phenomenon of growth in this area may be associated with welding stresses. The growth of the ferrite areas in the plain carbon steels[7] did not show any appreciable increase between the 10,000 hr exposure and the 34,000

Table II. Graphite Rating of Steels; 34,000 Hr Exposure

AISI Designation	Type	900°F 1*	900°F 2†	900°F 3‡	900°F 4§	1050°F 1*	1050°F 2†	1050°F 3‡	1050°F 4§
2320	Ni	0	30*C*	200*B*	0.5*G*	1*D*	40*D*	100*D*	0.2*K*
2517	Ni	0	0	0	1*E*	0	0	0.1*K*	0.3*J*
3115	Ni-Cr	0	0	0	0	0	0	0	0
3130	Ni-Cr	0	0	0	0	0	0	0	0
3316	Ni-Cr	0	0	0	0	0	0	0	0
4115	Cr-Mo	0	0	0	0	0	0	0	0
4140	Cr-Mo	0	0	0	0	0	0	0	0
4317	Ni-Cr-Mo	0	0	0	0	0	0	0	0
4337	Ni-Cr-Mo	0	0	0	0	0	0	0	0
8625	Ni-Cr-Mo	0	0	0	0	0	0	0	0
8630	Ni-Cr-Mo	0	0	0	0	0	0	0	0
4615	Ni-Mo	0	0	#	#	0	20*A*	50*A*	10*B*
4640*	Ni-Mo	4*B*	20*D*	40*B*	1*F*	1*E*	8*F*	20*E*	0.5*K*
4815	Ni-Mo	0	0	0	0	0	0	12*C*	5*C*
6120	Cr-V	0	0	0	0	0	0	0	0
6145	Cr-V	0	0	0	0	0	0	0	0

* 1 refers to heated zone immediately beneath weld metal.
† 2 refers to heated zone beneath Zone 1.
‡ 3 refers to area near boundary of heat-affected zone.
§ 4 refers to parent metal.
# Very small dark gray particles, unidentified.
* Graphite rating at 1050°F for deposited weld metal equals 0.04*G*.

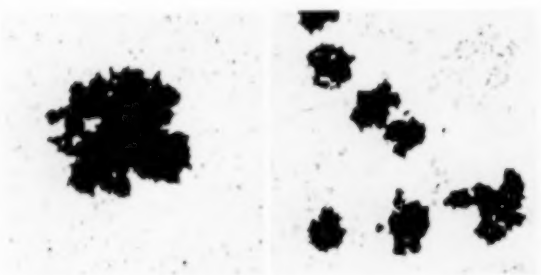

Fig. 2—Stability of AISI alloy steels, showing structures visible in bead weld of AISI Grade 4640 steel exposed 34,000 hr at 1050°F. Picral-nital Etch. a) LEFT: Graphite in *E*7020 deposited weld metal. b) RIGHT: Graphite in weld heat-affected zone. X1000. Reduced approximately 45 pct for reproduction.

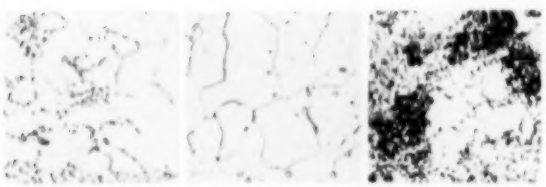

a) AISI 2517, 900°F b) AISI 2517, 1050°F c) AISI 4337, 900°F

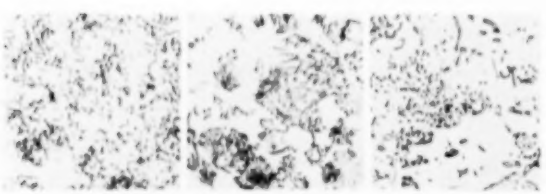

d) AISI 4337, 1050°F e) AISI 8630, 900°F f) AISI 8630, 1050°F

Fig. 3—Parent metal structures after 34,000 hr exposure. Picral-nital Etch. X1000. Reduced approximately 45 pct for reproduction.

hr exposure interval. The growth of the ferrite in the nickel steels is also believed to be virtually completed during 10,000 hr exposure.

Samples of each of the nickel steels contained more graphite in the parent metal and the weld heat-affected zone after 34,000 hr exposure at 900° and 1050°F than previously found after 10,000 hr exposure.[1] AISI 2517 steel, which did not contain graphite after 10,000 hr exposure at 900°F, contained a small amount of graphite in the parent metal after 34,000 hr. The graphite ratings are shown in Table II. The reason for the absence of graphite in the weld heat-affected zone of the 900°F sample of AISI 2517 steel is not clear.

Ni-Cr Steels—The Ni-Cr steels continued to exhibit a relatively stable microstructure. After exposure for 34,000 hr at 900°F AISI 3115, 3130, and 3316 steels were similar to the steels after 10,000 hr exposure and resembled Fig. 3e. After exposure for 34,000 hr at 1050°F the Ni-Cr steels were spheroidized somewhat more than after the 10,000 hr exposure. The AISI 3115 steel was similar to Fig. 3a, the AISI 3130 steel resembled Fig. 3f, and the AISI 3316 steel was similar to Fig. 3d.

The structure of the weld heat-affected zones of these steels after exposure for 34,000 hr at 900°F was similar to AISI 8625 in Fig. 4. After exposure for 34,000 hr at 1050°F the weld-heated zone of AISI 3115 steel was similar to AISI 4115 in Fig. 4a, and AISI 3130 and 3316 steels were similar to AISI 8625 in Fig. 4.

The Ni-Cr steels contained no evidence of graphite in the parent metal or weld heat-affected zones after exposure.

Cr-Mo Steels—Steels AISI 4115 and 4140 continued to be relatively stable after prolonged exposure, but additional spheroidization was observed, particularly in the samples exposed at 1050°F. After 34,000 hr exposure at 900°F the Cr-Mo steels were still structurally stable and were similar in appearance to Fig. 3e. After similar exposure at 1050°F the AISI 4115 steel resembled Fig. 3d, and the AISI 4140 steel was similar to Fig. 3f. In the weld-heated zone the structure of the two steels did not change to any great extent since the previous examination. After 34,000 hr exposure at 900°F the structure of the AISI 4115 steel is illustrated in Fig. 4, while the AISI 4140 steel resembled the AISI 8625 steel in Fig. 4. After 34,000 hr exposure at 1050°F the AISI

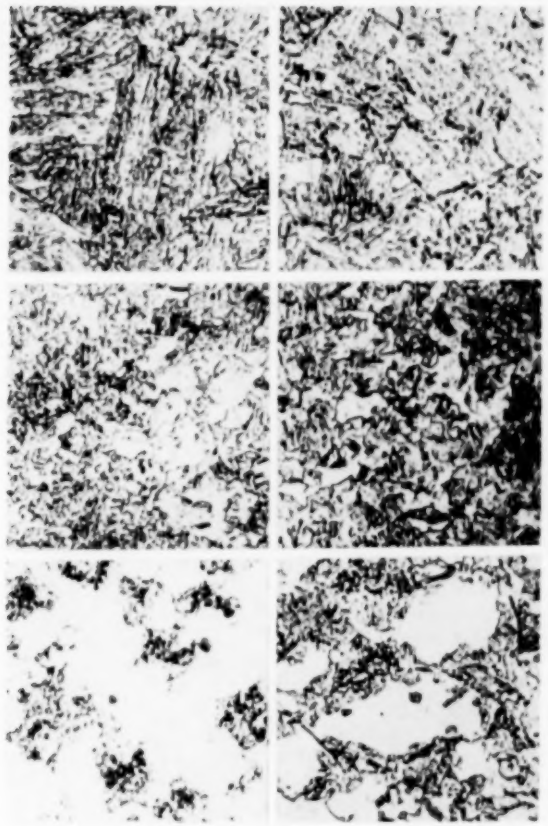

Fig. 4—Structural changes in weld heat-affected zones of AISI 4115 (left) and 8625 (right hand micrographs) steels after 34,000 hr exposure at 900°F. Picral-nital etch. TOP ROW: weld metal; CENTER ROW: weld heat-affected zone; and BOTTOM ROW: parent metal. X1000. Reduced approximately 20 pct for reproduction.

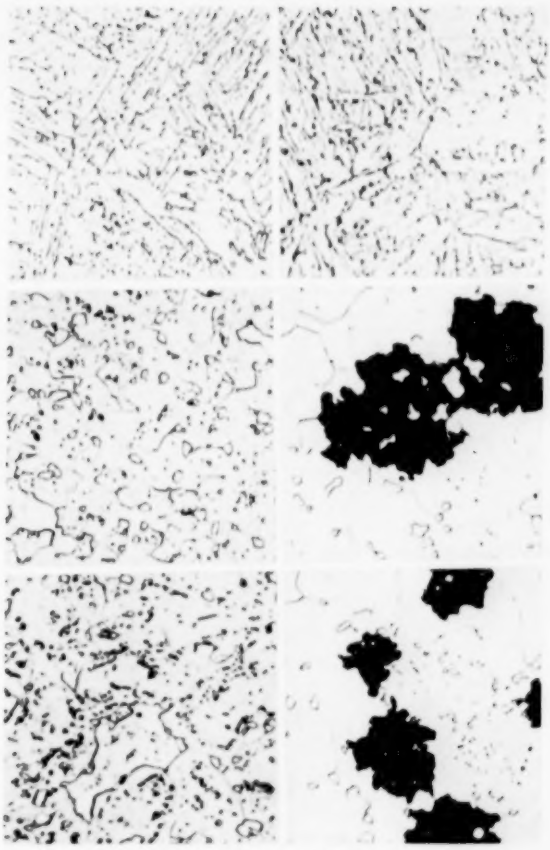

Fig. 5—Structural changes in weld heat-affected zones of AISI 8625 (left) and 4640 (right hand micrographs) steels after 34,000 hr exposure at 1050°F. Picral-nital etch. TOP ROW: weld metal; CENTER ROW: weld heat-affected zone; and BOTTOM ROW: parent metal. X1000. Reduced approximately 20 pct for reproduction.

4115 steel compared with AISI 8625 in Fig. 5, and the AISI 4140 steel with AISI 8625 in Fig. 4. Graphite was not observed.

Ni-Cr-Mo Steels—The Ni-Cr-Mo AISI steels, 4317, 4337, 8625, and 8630, changed considerably during early exposure but appear to have changed very little during the exposure interval from 10,000 hr to 34,000 hr. After exposure for 34,000 hr at 900°F, steels 4317, 8625, and 8630 remained essentially the same in appearance and were similar to Fig. 3e. After the same exposure at 1050°F some changes were observed in the microstructure of these steels which resembled Fig. 3f. The structure of the AISI 8630 steel exposed at 900°F is illustrated in Fig. 3e, and at 1050°F in Fig. 3f. The AISI 4337 steel was not changed after 34,000 hr at 900° but showed additional spheroidization after exposure at 1050°F. Figs. 3c and 3d illustrate the structures of this steel after 34,000 hr exposure at 900° and 1050°F.

The weld-heated zones after exposure at 900°F were essentially unchanged and resembled AISI 8625 in Fig. 4, but slightly more spheroidization was observed in the material exposed at 1050°F with the structures resembling AISI 8625 in Fig. 5. Graphite was not observed in these steels.

Ni-Mo Steels—These steels showed a change in microstructure during early exposure intervals, but do not appear to have changed materially between the 10,000 hr and the 34,000 hr exposure periods. The AISI 4615 steel contained 0.12 pct residual chromium, the AISI 4815 steel contained 0.16 pct residual chromium, and the AISI 4640 steel contained only 0.04 pct residual chromium. After exposure for 34,000 hr at 900°F the AISI 4615 steel resembled Fig. 3a; the AISI 4640 steel, Fig. 3f; and the AISI 4815 steel, Fig. 3d. After exposure at 1050°F the AISI 4615 steel resembled Fig. 3b; the AISI 4640 steel, Fig. 3f; and the AISI 4815 steel, Fig. 3d.

The weld-heated zones of all these steels were similar to AISI 8625 in Fig.4 after 900°F exposure. After exposure at 1050°F the AISI 4615 steel resembled AISI 8625 in Fig. 5. The AISI 4815 steel was similar in appearance to the AISI 4640 steel after 34,000 hr at 1050°F, as illustrated in Fig. 5.

All three steels displayed evidence of graphitization, as shown in Table II. The AISI 4615 steel graphitized considerably at 1050°F. However, graphitization at 900°F was questionable. In the 900°F specimen after 34,000 hr exposure a number of dark gray particles too small to be identified could

Table III. Tensile Properties Before and After 10,000 Hr Exposure at 1200°F

AISI Grade	Yield Strength, 1000 Psi		Tensile Strength, 1000 Psi		Elongation, Pct In 1 In.		Reduction of Area, Pct	
	Before Exposure	After Exposure	Before Exposure	After Exposure	Before Exposure	After Exposure	Before Exposure	After Exposure
2320	65	50	86	61	33	42	67	80
2517	59	55	82	71	34	39	68	83
3316	92	61	147	76	21	38	54	82
4815	75	39	106	58	24	44	63	85

Table IV. Creep Rupture Strength Before and After 10,000 Hr Exposure at 900°, 1050°, and 1200°F

Exposure and Testing Temperature, °F	Stress for Rupture, 1000 Psi			
	1000 Hr		10,000 Hr‡	
	Before*	After†	Before*	After†
		AISI 2320		
900	15.9	15.9	11.0	11.8
1050	5.7	5.6	3.5	3.6
1200	1.7	2.4	0.8	1.5
		AISI 3115		
900	26.1	25.9	21.5	21.5
1050	9.8	9.4	6.9	6.8
		AISI 3316		
900	29.2	22.3	17.5	16.0
1050	9.4	9.3	5.3	6.4
1200	3.1	2.7	1.4	1.3
		AISI 4115		
900	44.5	42.0	39.5	38.0
1050	13.3	10.2	8.0	7.4
		AISI 4317		
900	45.1	38.0	41.0	34.0
1050	13.1	9.1	8.6	6.3
		AISI 4615		
900	43.0	38.5	40.0	35.0
1050	12.2	11.1	7.6	8.3
		AISI 6120		
900	42.5	41.5	36.0	37.0
1050	17.5	13.7	11.4	10.2
		AISI 8625		
900	38.8	38.0	33.0	33.0
1050	12.0	9.6	7.6	6.9
		AISI 2517		
900	16.0	15.9	11.3	11.4
1050	6.3	5.7	4.0	3.7
1200	1.8	1.8	0.7	0.8
		AISI 3130		
900	22.0	22.6	16.0	16.9
1050	8.1	8.2	5.0	5.6
		AISI 4815		
900	40.5	39.0	42.8	30.5
1050	11.8	11.8	6.3	8.3
1200	2.9	3.1	1.2	1.8
		AISI 4140		
900	49.0	41.0	32.5	36.0
1050	16.2	14.5	11.6	10.4
		AISI 4337		
900	31.9	29.2	24.2	22.0
1050	10.4	9.0	6.2	6.2
		AISI 4640		
900	34.0	29.0	28.9	23.2
1050	10.9	9.0	6.6	6.6
		AISI 6145		
900	30.0	29.6	24.5	23.5
1050	13.5	12.1	8.9	8.7
		AISI 8630		
900	36.5	35.0	31.0	30.0
1050	13.3	11.0	8.5	7.7

* Material creep rupture tested before 10,000 hr exposure.
† Material creep rupture tested after 10,000 hr exposure without stress.
‡ Values obtained by extrapolation.

be seen in the parent metal and in the weld-heated zone. The AISI 4815 steel graphitized only after exposure at 1050°F. A large amount of graphitization was observed in the AISI 4640 steel at 900° and 1050°F in the weld-heated zones and parent metal. The micrograph in Fig. 2 illustrates the degree of graphitization in the weld heat-affected zone of AISI 4640 steel after 34,000 hr exposure at 1050°F. Graphitization in the deposited weld metal occurred in this specimen.

Cr-V Steels—AISI steels 6120 and 6145 remained relatively stable microstructurally after 34,000 hr exposure. Both steels had an appearance similar to Fig. 3e after exposure at 900°F. At 1050°F the AISI 6120 steel resembled Fig. 3d; and the AISI 6145 steel, Fig. 3c. The weld-heated zones of these steels were similar to AISI 4115 in Fig. 4 at 900°F and AISI 8625 in Fig. 5 at 1050°F. Graphitization was not observed in these steels.

Tensile Properties

In general, there was a slight decrease in the yield strength and tensile strength of the various steels after 10,000 hr exposure at 900°, and the decrease was more noticeable after exposure at 1050°F. An appreciable decrease was observed in the yield strength and tensile strength of the steels exposed at 1200°F, see Table III. The elongation in the tensile test was not changed appreciably by exposure at 900° and 1050°F, but the reduction of area was increased in several steels. The ductility properties were appreciably increased in the steels exposed at 1200°F. The tensile properties for the steels are shown in Fig. 6 for the 900° and 1050°F exposure temperatures.

Creep Rupture Properties

The creep rupture strength of the nickel steels in Table IV is similar to that of plain carbon steels and showed no appreciable change after exposure at 900° to 1200°F. Two levels of nickel did not influence the creep rupture properties, but the addition of chromium to steel containing nickel appreciably increased the creep rupture strength. These properties were not changed to any great extent by exposure at 900° and 1050°F.

In the steels of Table IV containing molybdenum or vanadium, the creep rupture properties were higher than the nickel and Cr-Ni steels. The steels containing higher levels of carbon had lower creep rupture properties than the lower carbon alloy steels. The creep rupture strength was slightly decreased due to exposure at 900° and 1050°F.

The ductility in Fig. 7 before or after exposure was greater at 1050° than at 900°F. The ductility after exposure at either temperature was greater in general than the ductility before exposure. The ductility level of some of the steels was low, particularly at 900°F.

Conclusions

1) Evidence that *E*7020 weld metal may graphitize when deposited on AISI 4640 Ni-Mo steel was observed after exposure for 34,000 hr at 1050°F.

2) The AISI 2320 and 2517 nickel steels and the AISI 4640 Ni-Mo steel graphitized at 900° and 1050°F during 34,000 hr exposure. The AISI 4615 and 4815 Ni-Mo steels with residual chromium graphitized at 1050°F during 34,000 hr exposure. Nickel is not effective in preventing graphitization.

3) The chromium bearing AISI steels did not graphitize after 34,000 hr exposure at 900° or

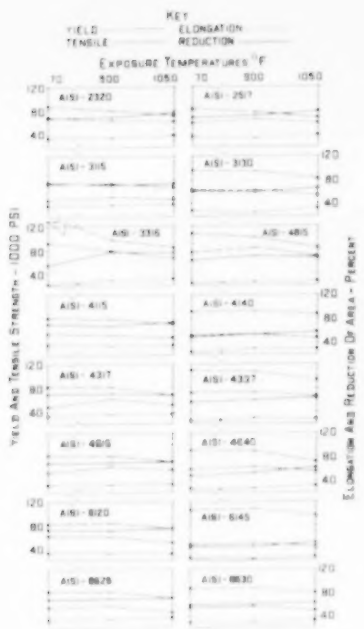

Fig. 6—Tensile properties before and after 10,000 hr exposure.

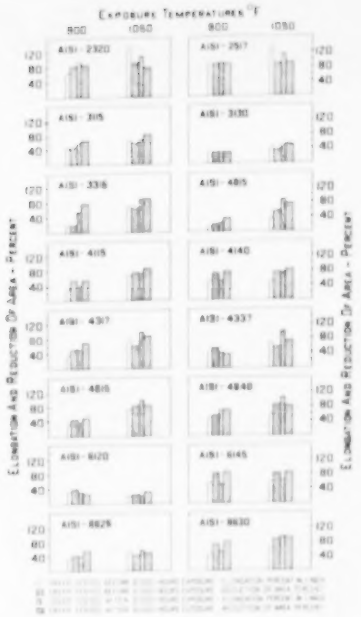

Fig. 7—Creep rupture elongation and ductility.

1050°F, although some of the steels contained appreciable amounts of aluminum, relatively high levels of carbon, and nickel.

4) The chromium bearing AISI steels appear to be more stable structurally than the other AISI steels.

5) A slight decrease in the yield strength and tensile strength was observed in the AISI steels after 10,000 hr exposure at 900° and 1050°F.

6) The creep rupture properties of nickel steels were similar to those of plain carbon steels. The addition of chromium to steel containing nickel increased the creep rupture strength.

7) The creep rupture properties of molybdenum or vanadium steels were higher than those of the nickel and Cr-Ni steels. The steels containing higher levels of carbon had lower creep rupture properties than the lower carbon alloys.

8) The ductility after exposure at 900° or 1050°F was greater than the ductility before exposure.

9) The powerful effect of chromium is further shown and suggests that the Cr-Mo steels now employed as piping materials for elevated temperature service appear satisfactory for acceptable performance in comparison with the AISI steels.

Acknowledgments

The authors wish to express their appreciation for the assistance received from the management and operating personnel of National Tube Div., U. S. Steel Corp. They are particularly indebted to D. T Boughner and J. B. Adamczyk of the National Tube Div. Research Laboratory for the tensile and creep rupture data.

References

[1] A. B. Wilder and J. O. Light: Stability of AISI Alloy Steels at Elevated Temperatures. *ASM Trans.*, 1950, vol. 42, pp. 917-934.

[2] D. B. Collyer and J. O. Light: Graphitization Rating Chart. *Metal Progress*, 1949, vol. 55, p. 664-B.

[3] *Steels for Elevated Temperature Service*. U. S. Steel Corp. Pittsburgh, 1949.

[4] A. B. Wilder and J. D. Tyson: Graphitization of Steel at Elevated Temperatures. *ASM Trans.*, 1948, vol. 40, p. 233.

[5] A. B. Wilder, E. F. Ketterer, and D. B. Collyer: Creep Rupture Properties and Structural Changes in Carbon and Low Alloy Steels. *AIME Trans.*, 1954, vol. 200, p. 784; JOURNAL OF METALS, June 1954.

[6] A. B. Wilder and J. O. Light: Stability of Steels at Elevated Temperatures. *ASM Trans.*, 1949, vol. 41, pp. 141-166.

[7] A. B. Wilder and J. O. Light: Long-Time Elevated Temperature Test of Chromium-Molybdenum Steels. *ASM Trans.*, 1951, vol. 43, p. 323.

[8] R. W. Emerson: Carbide Instability of Carbon-Molybdenum Steel Piping. *ASME Trans.*, 1944, vol. 66, p. 5.

[9] R. W. Emerson and M. Morrow: Further Observation of Graphitization in Aluminum Killed Carbon-Molybdenum Steel Steam Piping. *ASME Trans.*, 1946, vol. 68, No. 6, p. 597.

Discussion of this paper sent (2 copies) to AIME by Dec. 1, 1957 will appear in AIME *Transactions* Vol. 212, 1958, and in JOURNAL OF METALS, April 1958.

Authors' Corrections

"Structure of the Transition Phase Omega in Ti-Cr Alloys" by A. E. Austin and J. R. Doig, *AIME Trans.*, 1957, vol. 209, p. 27; JOURNAL OF METALS, January 1957.

The last sentence of the abstract should read "The hardness appears to be caused by strain in the β-matrix produced by concurrent enrichment of alloy content in the β-phase", rather than in the ω-phase as was printed.

"Some Properties of Certain High-Conductivity Copper-Base Alloys" by Webster Hodge, *AIME Trans.*, 1957, vol. 209, p. 408; JOURNAL OF METALS, April 1957.

The statement under *Softening Temperature and Electrical Conductivity* that "the addition to copper of zirconium in amounts less than 0.12 pct had little effect on the softening temperature" is incorrect. Subsequent research has shown that additions of zirconium in amounts as small as 0.02 pct have a notable effect on raising the softening temperature of cold-worked copper.

Creep of Al-Cu Alloys During Age Hardening

High purity polycrystalline alloys of aluminum with 1 to 4 pct Cu were tested in creep over a temperature range of 200° to 540°C. Hardness, X-ray, and tensile data supplemented the creep results. Starting with alloys in the quenched, single-phase condition, creep tests were performed both within the single-phase and two-phase region of the equilibrium diagram. Aging under stress was initiated by enclosing the specimen with the hot furnace at the same time that the load was applied. The effects of aging on the minimum creep rate were determined by comparison of two types of creep curves: 1) the curves obtained when creep is accompanied by aging, and 2) the curves obtained under identical circumstances but without aging. The first curves were determined experimentally, while the second were obtained by extrapolation of the high-temperature single-phase creep data into the two-phase field. At the intermediate stresses, precipitation resulted in stronger alloys. Inversions in the relative strengths of the two-phase and single-phase alloys were predicted at the higher and lower stresses, whereby the single-phase alloys became stronger than the two-phase alloys. Low stress (high temperature) inversions have been reported by other investigators.

by Ervin E. Underwood

IT has been recognized for many years that dispersed particles have great value in raising the creep resistance of metallic alloys. In fact, some of the most successful high-temperature alloys owe their superiority to this factor above all others. A recent observation by Glen[1] indicates that even better high-temperature resistance to deformation results in alloys capable of two successive precipitation reactions.

The ramifications of this finding are of great interest. Unfortunately, our understanding of the reasons for such notable improvements has not kept pace with technical developments. In an effort to uncover some of the basic facts governing strengthening by particles, a program was initiated at the Battelle Memorial Institute with the primary goal of comparing creep strengths in single-phase and two-phase (precipitating) alloys.

The effects of precipitation from solid solution on the creep properties of alloys are generally such that the resistance to creep is increased. However, if alloys are heat treated to different degrees of hardness before creep testing, it is often found that those possessing the maximum hardness initially do not necessarily have the maximum creep resistance. Depending on the stresses and temperatures involved other structures may prove more desirable. Considerations of the above nature indicate the importance of defining the initial state of the alloy. Here, it was decided to start with quenched single-phase alloys in which precipitation and creep deformation proceed concurrently.

E. E. UNDERWOOD, Member AIME, is Assistant Division Consultant, Battelle Memorial Institute, Columbus, Ohio.

TP 4477E. Manuscript, Sept. 17, 1956. New Orleans Meeting, February 1957.

Equipment and Experimental Procedures

Preparation of the Specimens—Four 25 lb ingots were prepared from 99.999 pct Cu and 99.996 pct Al to compositions of 1, 2, 3, and 4 wt pct Cu. Spectrographic and chemical analyses are listed in Table I. After heat treatments and intermediate reductions, the alloys were cold rolled to $\frac{1}{8}$ in. thick sheet. The final cold reductions amounted to 50, 40, 20, and 10 pct for the 1, 2, 3, and 4 pct Cu alloys, respectively.

The specimens for creep testing were machined into tensile flats 7 in. long, $\frac{3}{4}$ in. wide (at the shoulders), and $\frac{1}{8}$ in. thick. The reduced sections were $\frac{1}{4}$ in. wide and $2\frac{1}{2}$ in. long. After heat treatments at 540°C to an ASTM grain size of 1 ±1, the specimens were quenched into water at room temperature, then electropolished in a glacial acetic acid and perchloric acid solution. The gage marks were Knoop impressions placed 2 in. apart on the reduced sections. Blanks of 1 x 1 in. were cut from the same sheets for the age hardening runs and were given the same grain size heat treatments. The specimens and blanks were stored in a refrigerator at —40°C until needed for testing.

Creep Measurements—Creep tests were conducted in a constant temperature room which was maintained at 26° ±1°C. A split-type, hinged, vertical-tube furnace was mounted on a horizontal track so that the specimen could be enclosed suddenly. Thus, it took about 15 min for the specimen to come within 5°C of the test temperature. The temperature variation along the specimen was controlled to about

½°C by an auxiliary heating coil, while the furnace temperature was controlled within ±2°C.

The surface of the specimen and the gage marks were observed through narrow slit windows at a magnification of 20 times. A microscope, mounted on a vertical 4 in. micrometer slide, permitted the distance between the two gage marks to be measured with a sensitivity of about 50 μin. Direct loading was used so that the specimen could be unloaded quickly and quenched into water at 26°C after a selected amount of creep.

X-Ray Technique—The X-ray examination was of a simple back-reflection type used previously.[5] Diffraction patterns were obtained from the reduced sections of the specimens using filtered cobalt radiation.

Hardness Data—Vickers diamond hardness numbers were obtained from the 1 x 1 in. blanks, and from the reduced sections and shoulders of the creep specimens. The blanks were aged in salt pots at temperatures ranging from 200° to 400°C, and were quenched periodically in water at room temperature. The average of five impressions was used to plot the hardness-time curves. Hardnesses were measured at the shoulders and reduced sections of the creep specimens after the creep test.

Tensile Tests—Tensile tests of specimens crept to various strains were conducted at constant strain rates of about 0.0078 or 0.0108 per min and at temperatures between 26° and 300°C. The tests were usually discontinued shortly after the maximum load was detected.

Experimental Results and Their Evaluation

Creep Tests—In attempting a comparison of creep strengths in single-phase and two-phase alloys, it is necessary to identify the effects of age hardening on creep. The procedure devised for this purpose was that of interrupting the creep run at selected times by quenching the specimens from the furnace. First, the entire creep curve was delineated. Then, additional specimens were tested, under the same conditions of stress and temperature, but for successively shorter times. Thus, several specimens, representative of as many points along the creep curve, were available for other measurements.

The conditions of the creep tests are given in Table II. In general, the temperature dependence of creep was obtained with the 2 pct Cu alloys, and the compositional dependence of creep was determined at 300°C. There is some spread among the creep curves belonging to the same stress and temperature group. The deviations do not appear to be greater than those normally encountered, even in view of the unusual experimental requirements of this investigation. A few creep curves were not used because of excessive deviation from the average curve. However, in some cases, these specimens have yielded data useful in other connections.

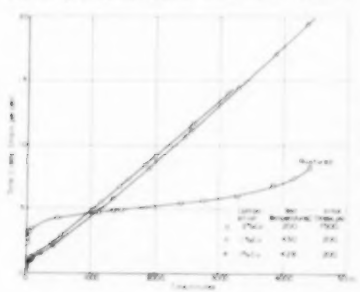

Fig. 1—Representative creep curves of single-phase or aging Al-Cu alloys.

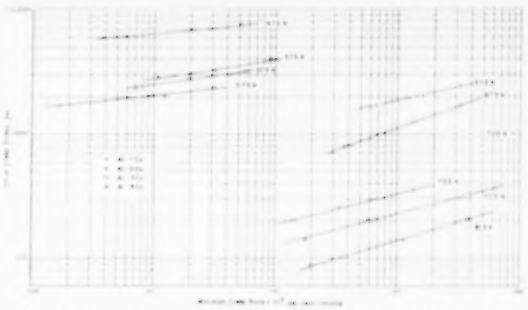

Fig. 2—Initial creep stress vs minimum creep rate for single-phase or aging Al-Cu alloy.

The shoulders and reduced sections of the creep specimens were selected as likely spots to study the effects of strain on age hardening. It was hoped that the shoulders would be elastically strained and that the reduced sections would be plastically strained. To verify this, a fine square grid of 20 lines to the inch was applied photographically to two electropolished specimens before creep testing. The residual creep strain, measured at room temperature, amounted to about 0.2 pct in the shoulders. It appears that the deformation there is not entirely elastic. The grid deteriorated at higher temperatures, so the deformation resulting from creep above 200°C was not determined.

Typical creep curves have been plotted to linear strain and time scales in Fig. 1 to illustrate the variations encountered under widely differing creep conditions. The 200°C curve is typical of those obtained at the lower temperatures and under relatively high stresses. It should be noted that this curve represents creep in an alloy in which aging is proceeding concurrently with deformation. It has the appearance of a normal creep curve. The other two curves were obtained from creep tests in the single-phase region. The alloys were tested under almost identical conditions except for one important difference. In one case (the upper curve) the specimen was allowed to come to temperature *before* the load was applied. This procedure was followed only at temperatures within the single-phase field. In the other case (the lower curve), the hot furnace was placed around the specimen at the same time the load was applied. This was the normal procedure when the specimen was to be tested at a temperature within the two-phase region. The difference in experimental techniques does not appear to give noticeably different results except at the very short times. The magnitude of this early difference for all alloys was usually much less than 1 pct strain, and this only at the shorter times.

The consistency of the creep data is indicated in Fig. 2, where the logarithm of the stress is plotted

Table I. Spectrographic and Chemical Analyses of Al-Cu Alloys

Nominal Composition, Pct	Chemical Analysis, Wt Pct Cu	Spectrographic Analysis, Ppm			
		Si*	Fe	Pb	Mg
1	0.99	20	20	<10†	1.0
2	1.95	20	<20†	†	1.0
3	2.96	20	<20†	†	1.0
4	3.97	20	<20†	20	1.0

* Silicon pickup possible from the electrode.
† Not detected.

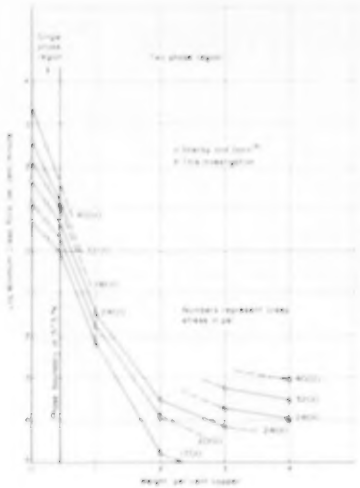

Fig. 3—Effect of stress on the minimum creep rate of single-phase and aging Al-Cu alloys at a temperature of 573°K.

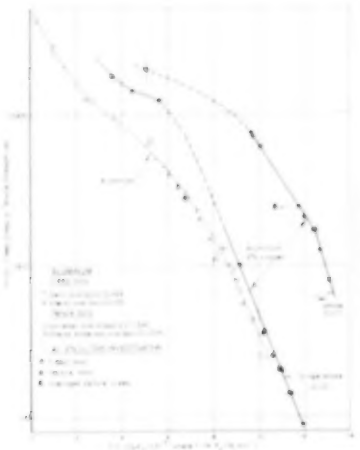

Fig. 4—Correlation of creep and tensile data for aluminum and Al-2 pct Cu alloys.

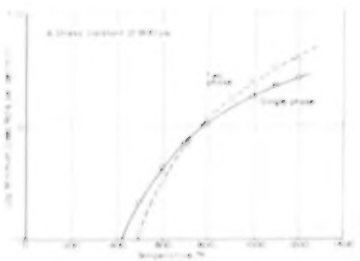

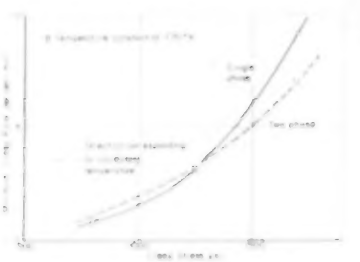

Fig. 5—Calculated minimum creep rates for single and two-phase alloys of Al-2 pct Cu.

vs the logarithm of the minimum creep rate. These data points and extrapolated values are utilized later in the paper since the minimum creep rate is used as an index of the creep strength. The variation in the slopes of these lines with temperature approximates qualitatively the behavior observed in other creep studies.[4,5]

An informative series of curves appears in Fig. 3 as a result of plotting minimum creep rates at 573°K against the composition. Dorn's data[7] were used to fill in the single-phase area, while the remaining two-phase data represent minimum creep rates of aging Al-Cu alloys. The maximum rate of improvement in creep strengths occurs between 1 and 2 pct Cu. This fact gains additional significance when associated with the results of a kinetic analysis of age hardening,[1] where it is shown that a marked retardation of rate of age hardening occurs at the same compositions (1 to 2 pct Cu) and temperature (573°K). Returning to Fig. 3, it is apparent that relatively little additional creep resistance is gained by increasing the copper content from 2 to 4 pct.

Low-magnification examinations were made of the surface deformation markings on Al-Cu specimens crept to various strains at various temperatures. It was found that the sequence of changes and the specific manifestations of deformation (slip-bands, folds, grain rotation, grain boundary migration, etc.) are much the same as in creep of high-purity aluminum. The application of stress to the aging alloys was found to give considerably widened and numerous bands of the *light phenomenon* at the grain boundaries. Furthermore, platelets re-precipitating within these regions appeared to assume a new orientation.

A major goal of this investigation is the determination and evaluation of the effects of age hardening on creep. To accomplish this goal, a comparison was made of the following two types of creep curves: 1) the curves obtained when creep is accompanied by aging, and 2) the curves obtained under identical circumstances, but without aging. Obviously, both curves cannot be determined experimentally. Therefore, it was proposed to extrapolate the high-temperature single-phase creep data into the two-phase field. The latter data would be representative of creep without aging, while the corresponding creep plus aging curves could be obtained experimentally.

The value of such a comparison depends greatly on the accuracy of the extrapolated data. For this purpose an extrapolation is desired capable of handling stress and temperature changes plus one other creep variable, such as strain or minimum creep rate. Two relatively simple functions have emerged lately which relate creep stress to the temperature and minimum creep rate. One of these functions, the Larson-Miller[8] parameter, P, has the form

$$P = T\,(C - \log \dot{\epsilon}_s) \qquad [1]$$

where T is the absolute temperature, $\dot{\epsilon}_s$ is the minimum creep rate, and C is a material constant. This parameter has been used extensively to relate and correlate both creep and tensile data.[9,10] Although the exact shape of the stress vs P plot is not specified, the curves have qualitatively the same shape.[11] These findings give increased confidence in judging the probable usefulness of an extrapolated curve.

Another expression which relates the stress to a function of temperature and strain rate has been

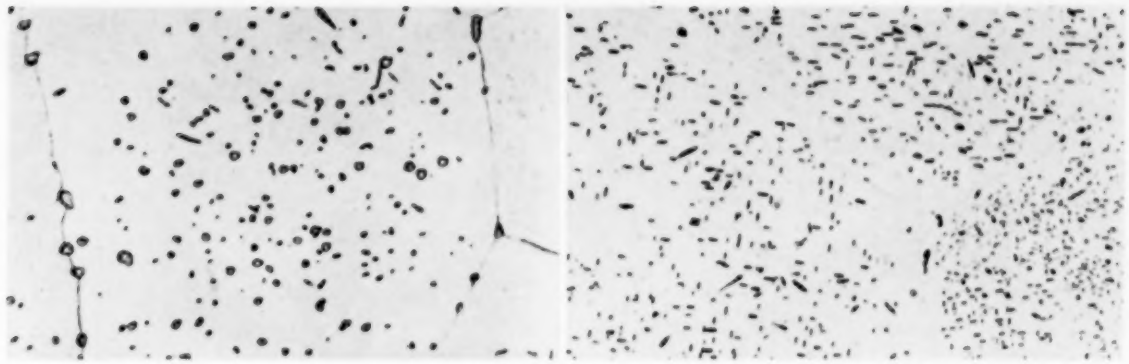

Fig. 6—Precipitate in Al-2 pct Cu alloys aged at 400°C. a) LEFT: Overaged for 960 min. Unstressed. b) RIGHT: Aged for 149 min under stress of 1700 psi. Keller's etch. X1000. Reduced approximately 10 pct for reproduction.

adapted by Dorn[9] to creep, although it was originally proposed for correlation of tensile properties by Zener and Hollomon.[10] This function, Z, may be written

$$Z = \dot{\epsilon}_s e^{\Delta H/RT} \qquad [2]$$

where ΔH is a constant, an experimental activation energy for creep which is closely akin to the activation energy for self diffusion, and the other terms are as before.

Both Eqs. 1 and 2 were used in an effort to compare the creep behavior of aging and nonaging Al-2 pct Cu alloys. However, since these expressions are equivalent,* the same results were found regardless of which parameter was used. The actual values of the constants in each case were calculated from the experimental data. Thus, the values of C from Eq. 1 that were found to fit the creep data for the single-phase and two-phase alloys are 12 and 17, respectively. Similarly, ΔH's of 48,000 and 58,000 cal per mole were found to fit the data best in Eq. 2. That this latter constant should have different values is logical, because in one case we have creep in a solid solution, undisturbed by aging effects, while in the other case aging exerts its complex influence on the creep process. Dorn[9] was unable to correlate the creep data of age-hardenable alloys with his ΔH for dilute single-phase alloys, but this is understandable if a different process is controlling in aging alloys.

* This is shown readily by recasting the Larson-Miller parameter to the same form as the log $\dot{\epsilon}_s$ parameter. That is, by solving Eq. 1 for C, $C = \log t_r + P/T$ is obtained, and by taking logarithms of Eq. 2, $\log Z = \log \dot{\epsilon}_s + \Delta H/2.3RT$ is obtained.

Table II. Creep Data for Al-Cu Alloys

Composition, Wt Pct Cu	Testing Temperature, °C	Initial Creep Stress, Psi	Number of Specimens Used	Location on Equilibrium Diagram
1	300	2400	1	Two-phase
	300	2000	1	Two-phase
	300	1700	1	Two-phase
	419	200	1	Single-phase
	439	200	2	Single-phase
	457	200	1	Single-phase
2	200	7500	4	Two-phase
	200	7000	1	Two-phase
	200	6000	2	Two-phase
	300	2400	5	Two-phase
	300	2050	3	Two-phase
	300	1700	3	Two-phase
	400	1700	5	Two-phase
	400	1235	4	Two-phase
	400	700	4	Two-phase
	430	1000	1	Single-phase
	460	353	1	Single-phase
	460	251	1	Single-phase
	460	201	1	Single-phase
	500	362	1	Single-phase
	500	202	1	Single-phase
	500	140	1	Single-phase
	540	206	1	Single-phase
	540	140	1	Single-phase
	540	86	1	Single-phase
3	300	3200	4	Two-phase
	300	2800	1	Two-phase
	300	2400	3	Two-phase
4	300	4000	1	Two-phase
	300	3200	1	Two-phase
	300	2800	1	Two-phase

The experimental results are presented in Fig. 4 but, for the sake of brevity, only in terms of the Larson-Miller parameter. The curves for the 2 pct Cu alloys are representative of creep in single-phase alloys ($C = 12$) and in two-phase aging alloys ($C = 17$). The tensile points appearing at the highest stresses are obtained from crept single-phase and two-phase specimens. They help to delineate the course of the curves, as does the combined creep[4,5] and tensile[4,10] curve for high-purity aluminum.

The qualitative nature of the high-stress portions of these curves precludes any quantitative calculations, but some observations can be drawn. In general the single-phase alloys are weaker* (i.e., have a higher minimum creep rate) over most of the stress range. For a constant temperature, the inequality given in the footnote predicts that the minimum creep rates tend to become equal at the higher stresses as the two curves tend to converge. At still higher stresses, an inversion in the minimum creep rate occurs and the single-phase alloys become stronger than the two-phase alloys. For a temperature of 500°K, the minimum creep rates become equal at 10,000 psi, and at higher stresses the two-phase alloys are weaker than the single-phase alloys. Depending on the temperature chosen, this inversion in creep strengths will occur at some higher or lower stress.

* When $|(P_{C=12})' - (P_{C=17})| \geq 5T$. The meaning of this inequality can be understood readily in the case of a constant temperature. Then, $5T$ is also constant and is equivalent to a constant distance on the parameter scale. As the two curves diverge more or converge less than this distance, the minimum creep rate for the single-phase alloy becomes more or less, respectively, than that for the two-phase alloy.

The prediction of an inversion in the minimum creep rate at the high-stress portion of the diagram is not at all unreasonable if an increased creep strength there can be attributed primarily to finer, more closely spaced particles. Gledt, Sherby, and Dorn[5] have demonstrated experimentally that this behavior is a fact at higher stresses. Consider a two-phase alloy in which the particles become increas-

Table III. Age-Hardening Data* for Unstressed Al-Cu Alloys

Composition, Wt Pct Cu	Average Initial Hardness†	Maximum Hardness at Reaction Temperatures, °C				Time, Min, to Maximum Hardness at Reaction Temperatures, °C			
		200	220	300	400	200	220	300	400
1	27.5	—	—	29	—	—	—	25	—
2	44.4	50.6	~50.3	~50	50.7	4100	1250	37	52
3	60.4	68	—	63	63.5	1100	—	16	3.7
4	81.6	81.7	—	76.6	74	1300	—	17	1.4

* Dphn obtained at room temperature with a 10-kg load.
† Alloys quenched from 540°C into water at room temperature.

ingly smaller and more finely dispersed. It is evident that the limiting case approaches that of a supersaturated solid solution, wherein the particles are now the solute atoms themselves. On the other hand, the equilibrium two-phase alloy possesses gross $CuAl_2$ particles and would have a lesser particle-strengthening increment than the *single-phase* alloy.

Another possibility is suggested by the Al-2 pct Cu curves of Fig. 4. A slight convergence of the two-phase and single-phase curves can be noted as the stresses decrease (below 1700 psi) or as the temperature increases. A trend of this type implies an inversion in relative strengths similar to that already noted at the higher stress levels. This prediction is given some element of confirmation by various reports[10-13] showing that, under appropriate conditions, single-phase alloys have greater creep strength than two-phase alloys. To illustrate the effect of even this slight convergence, minimum creep rates have been calculated for stresses between 800 and 1700 psi and are plotted in Fig. 5. Fig. 5A shows this inversion in minimum creep rates as the temperatures increase, while in Fig. 5B the same result is obtained with decreasing stresses.

To summarize, a comparison of minimum creep rates in single-phase and aging two-phase alloys *of the same composition* has been attempted. The results indicate that the two-phase alloys are generally stronger, but that at high and low stresses, single-phase alloys may have the lower creep rate. Experimental investigations tend to confirm this predicted behavior. Furthermore, the same trends are seen in Fig. 6 of the paper by Giedt et al.,[5] but for alloys of different compositions and in terms of the Z-parameter. Thus, it appears that new applications of the parametric plot are feasible, especially if the rather artificial restriction of constancy of C (or ΔH) is removed.

At higher temperatures the two-phase alloys should overage quickly under stress and the creep properties should approach those of an alloy overaged before creep. To test this conclusion, a specimen was aged for four days at 300°C and then was crept under a stress of 2400 psi at 300°C. The change in position because of prior overaging is indicated by the arrow in Fig. 4. It is obvious that this prediction was not confirmed. Recourse to the microstructures of the alloys aged before creep and aged during creep revealed a great disparity in the size, shape, number, and spacing of the precipitates. An example of the difference is given in Fig. 6. The relatively large coalesced particles in the overaged alloy apparently contribute little toward strengthening the matrix, unlike the small, platelike, and finely dispersed particles in the alloy aged during creep. In fact, at an assigned temperature of 500°K, the minimum creep rates of the overaged alloy and of the single-phase alloy should be approximately equal.

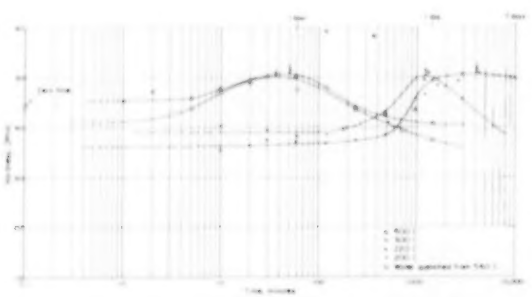

Fig. 7—Age hardening in unstressed Al-2 pct Cu alloys.

Age Hardening Curves—The primary function of the hardness measurements was to indicate the degree of age hardening that occurred during creep. However, it was also necessary to establish the hardness vs time curves in unstressed alloys, since they could serve most readily as a basis for comparison. In addition to the anticipated uses, interesting correlations were also developed between the hardness number and total creep strain.

The age-hardening curves for unstressed alloys of Al-2 pct Cu are shown in Fig. 7. The estimated times to maximum hardness have been indicated by small arrows. A consideration of all the data for all alloys reveals that the times decrease with increasing temperatures, but at a certain critical temperature the trend is reversed. The maximum hardnesses also follow the same pattern. These apparently inconsistent data have been rationalized on the basis of a kinetic analysis of the age-hardening curves, which has been reported in more detail elsewhere.[7] Briefly, this analysis shows that the maximum hardness attained during isothermal aging decreases to a minimum with increasing reaction temperature, then rises again. This temperature, at which the maximum hardness is the least, is also that at which the rate of reaction is the fastest.

The more important age-hardening data are listed in Table III for ready reference. The average hardnesses of quenched specimens, when plotted vs composition, were seen to lie above the data from other investigations.[7,9] The higher quenching temperature or differences in alloy purity may account for the systematic displacement of the curve.

Hardness data from the stressed creep specimens and from the unstressed alloys are compared in Fig. 8. For alloys stressed at 1700 psi, the hardness maximum is reached first in the gage section, and

then later in the shoulders. This order is not seen in the results for the alloys stressed at 1235 and 790 psi, although additional data for the earlier times would clarify this point. It does appear, however, that the hardness peak in the stressed samples is shifted to shorter times as the prior creep stress is increased.

An interesting correlation ensues if the hardnesses are considered, not in relation to the *time* of stressing during creep, but rather in relation to the total creep strain. A comparison is made in Fig. 9 by plotting the three shoulder hardness curves of Fig. 8 vs creep *time*, Fig. 9A, and then again vs total creep *strain*, Fig. 9B. Two radically different groups of curves result. In Fig. 9A there is no obvious relationship between stress, time, or hardness. However, in Fig. 9B, three distinct curves have sorted themselves out of the same data. The hardness levels decrease directly with the stress, while hardness peaks appear at essentially the same total creep strain of about 1.4 pct. Furthermore, through a fortuitous scatter in the individual creep curves, it can be seen that the contribution of aging time to the hardness is negligible compared to that from the strain. Qualitatively, the same results were obtained with the gage section hardnesses as with the shoulder hardnesses. However, the greater scatter in the gage-section hardnesses (presumably because of the greater surface distortion) prevented the relationship from being shown as clearly.

The results depicted in Fig. 9 suggest that the shoulder strain is directly related to the total creep strain. Such a relationship is not unlikely, since the stress in the shoulders should be about one third that in the gage section. It would also appear that there are two major contributions to the hardness—that of the age-hardening process and that of the structural deformation. The correlation presented in Fig. 9B indicates that the structural deformation plays the decisive role. The complex interplay of stress and strain on the age-hardening process makes it difficult to analyze the available data in more detail.

The relative importance of the structural deformation is also emphasized by the hardness data obtained from specimens crept into the tertiary stage. There is an abrupt drop in hardness that bears little connection with the age-hardening curve for the unstressed alloys. However, reference to the creep curves shows that the hardness breaks occur during

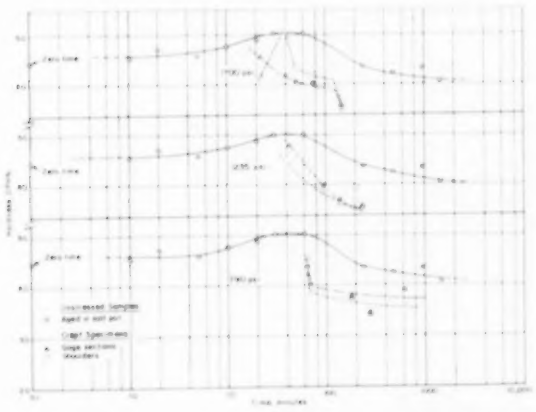

Fig. 8—Hardness vs time in stressed and unstressed Al-2 pct Cu alloys aged at 400°C.

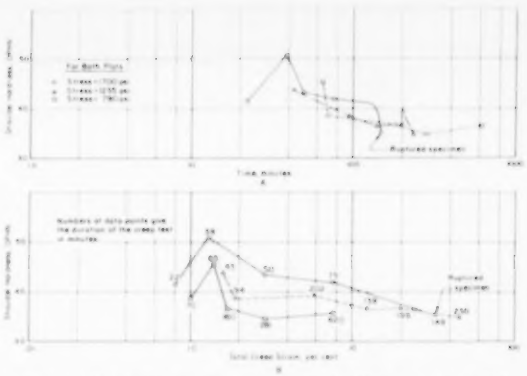

Fig. 9—Hardness at the specimen shoulders vs the total creep strain or creep time for Al-2 pct Cu alloys aged during creep at 400°C.

tertiary creep, and that the hardness falls off gradually as a function of total creep strain.

Tensile Tests—A typical series of stress-strain curves are presented in Fig. 10A. Al-2 pct Cu alloys were crept to the strains indicated in the figure, and were then tensile tested at room temperature. The effect of prior creep strain on the tensile flow stress is depicted in Fig. 10B. The similarity of these alloy flow stress curves to those established by Dorn et al.[5] with prestrained, crept, and tensile tested high-purity aluminum would indicate that the age-hardening contribution to the flow stress is negligible compared with the effects of structural deformation.

The effect of composition on the tensile flow stress of the Al-Cu alloys crept at 300°C is depicted in Fig. 11. The data were obtained from curves such as in Fig. 10B by plotting the flow stress at a creep strain of 1 pct against the composition. If the available data are drawn in three groups according to the original creep stresses, then the increase in tensile flow stress is roughly equal to the difference in creep stresses.

Table IV. X-Ray Diffraction Examination of Al-2 pct Cu Alloys Aged and/or Stressed at 1700 Psi and 400°C

Creep Strain, Pct	Aging or Creep Time, Min	Type of X-Ray Pattern	Size of Spots, Mm	Length of Areas, Mm	Grains Per Mm*
0	1470	Spot	1.2	—	—
0.80	22	Spot	2	—	3.04
1.29	39	Spot	3	—	3.02
2.89	50	Spot	6	—	2.66
7.58	75	Debye arc	—	15	2.73
33.0	149	Debye arc	—	Very long	2.26

* Grain sizes were measured after the creep runs. The average initial grain size was 5 grains per mm.

Fig. 12 reveals the effect of creep stress on the flow stress of 2 pct Cu alloys crept at 300° and 400°C. The effect of prior creep stress on the flow stress at 400°C is slight, but becomes appreciable at 300°C. The data available for 200°C are not shown, but suggest an even more pronounced effect—the increase in tensile strength is about double the increase in creep stress. Dorn,[5] among others, has shown that, under constant stress, a constant substructure results at equal creep strains, regardless of the temperature. A different substructure is obtained at a different creep stress. Since the tensile comparisons are made here at the same creep strain, it follows that the observed effects are attributable

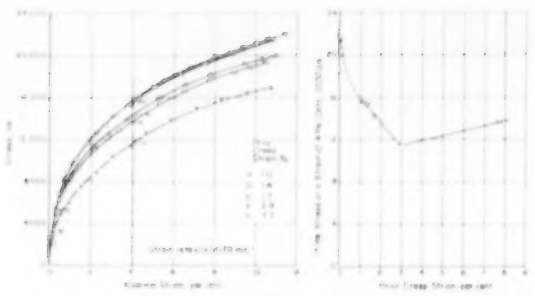

Fig. 10—Derivation of flow stress vs creep strain curve from stress strain curves. A) LEFT: Room temperature stress-strain curves of precrept Al-2 pct Cu alloys. Creep stress equals 790 psi, creep temperature, 400°C. B) RIGHT: Tensile flow stress, $\sigma_{f,\ \epsilon_{cr}}$, as a function of prior creep strain. Data from Fig. 10a.

primarily to the substructures inherited from the creep stresses.

X-Ray Investigation—The X-ray technique adopted in this investigation has been utilized previously with pure metals and single-phase alloys to determine the effects of deformation on the crystalline lattice. However, in the problem under consideration here, aging effects are superimposed on those due to deformation alone. The results of the X-ray investigation of the 2 pct Cu alloys crept at 1700 psi and 400°C are summarized in Table IV.

Very diffuse reflections were detected fanning out to one side of the sharp spots obtained from the overaged unstressed sample. These diffuse reflections probably result from residual θ' platelets, since they are quite persistent, see Fig. 6A. Some unresolved reflections also occurred outside the α solid solution (420) circles from specimens crept for 75 and 149 min. At these times the amount of θ' is greatest, see Fig. 7C of ref. 24, so diffraction effects could be expected from the precipitate. From the results obtained here, it seems likely that the deformational process proceeds in much the same sequence as observed in pure aluminum.[7] Moreover, when comparisons with pure aluminum are made at equal strains, it appears that the structural changes are accelerated in the age-hardening alloys.

Resume and Conclusions

A study of the creep behavior of high purity, polycrystalline alloys of aluminum with copper was conducted at temperatures that included both the single- and two-phase regions of the equilibrium diagram. Alloys tested within the two-phase field were initially in the quenched, single-phase condition so that aging could start simultaneously with the application of the creep load. Different specimens were crept to successive points along the creep curve, thus enabling a detailed examination to be made of the changes brought about by stress during aging.

Microscopic observations confirmed the occurrence of the same mechanisms of deformation and the same sequence of deformation markings with temperature as recorded for pure aluminum. The *light phenomenon* was found to occur as greatly enlarged grain-boundary regions in which a new precipitate had assumed orientations different from those in contiguous grains. The appearance of the precipitate induced under stress differed greatly from that of the precipitate originating in unstressed alloys. Whereas the former consisted almost entirely of finely dispersed, sharp platelets, the latter was composed mainly of widely spaced, spherical particles. X-ray photograms indicated that the sequence of deformational changes is the same in Al-Cu alloys as in pure aluminum. However, the process seems to be accelerated somewhat in the alloys.

The compositional dependence of the minimum creep rate at 300°C revealed a marked increase in creep strength at compositions just inside the two-phase boundary. This temperature and composition range corresponds to the region of the phase diagram where the rate of age hardening undergoes a relative retardation.

The effects of aging on the minimum creep rate were studied with Al-2 pct Cu alloys. Two curves resulted when the stress was plotted against a combined function of temperature and minimum creep rate (i.e., the Larson-Miller or the Zener parameter). One curve represented creep of two-phase aging alloys, while the other resulted from creep tests at temperatures within the single-phase region. An extrapolation of the latter curve into the two-phase field enabled comparisons to be made with the first curve. Thus, the difference between the hypothetical single-phase curve and the experimental two-phase curve was ascribed solely to the effects of aging on creep.

The following predictions were made on the basis of the comparison of the two curves. At intermediate stresses, the two-phase alloys were stronger than their single-phase counterparts, and precipitation resulted in a strengthening action. However, an inversion in relative strengths occurred at the higher and lower stresses, and the single-phase alloys assumed a greater (calculated) creep strength.

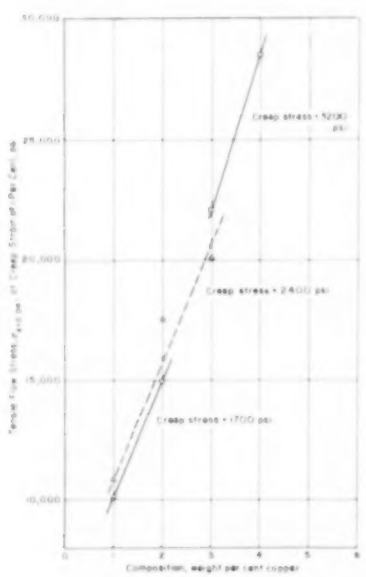

Fig. 11—Effect of composition on the tensile flow stress of Al-Cu alloys precrept to 1 pct strain at 300°C.

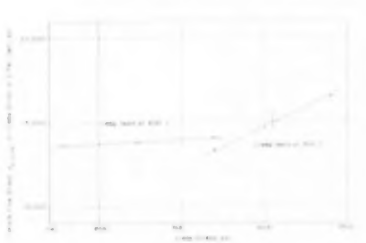

Fig. 12—Effect of creep stress on the tensile flow stress of Al-2 pct Cu alloys precrept to 2 pct strain at 300° and 400°C.

Similar inversions in the creep strength have been reported by other investigators.

Hardness changes in alloys aged under stress suggested that the time to maximum hardness was decreased by increased stress. When the hardnesses were plotted vs creep strain, and not aging times, a direct dependence of hardness level on creep stress ensued. The maxima in the hardness vs strain curves appeared at the same value of the strain.

The room-temperature tensile flow stress increased linearly with prior creep stress or composition, but passed through a minimum with creep strain. For a fixed composition, the greater the creep stress, the higher the flow stress, while the lower the creep temperature, the greater the increase in flow stress.

Acknowledgments

The author wishes to record a special note of thanks to R. D. Smith for his untiring efforts during the entire experimental program. The interest and encouragement shown by L. L. Marsh and G. K. Manning were greatly appreciated. This work was performed under Contract No. NAw-6413 for the National Advisory Committee for Aeronautics.

References

[1] J. Glen: *Journal* Iron and Steel Institute, 1948, vol. 158, p. 37.
[2] A. H. Cottrell: *Creep and Fracture of Metals at High Temperatures*, p. 141. Her Majesty's Stationery Office, London, 1956.
[3] W. A. Wood and W. A. Rachinger: *Journal* Institute of Metals, 1949-1950, vol. 76, p. 237.
[4] I. S. Servi and N. J. Grant: *AIME Trans.*, 1951, vol. 191, p. 909; Journal of Metals, October 1951.
[5] O. D. Sherby and J. E. Dorn: *AIME Trans.*, 1952, vol. 194, p. 959; Journal of Metals, September 1952.
[6] W. H. Giedt, O. D. Sherby, and J. E. Dorn: *ASME Trans.*, 1955, vol. 77, p. 57.
[7] E. E. Underwood, L. L. Marsh, and G. K. Manning: Creep of *Aluminum-Copper Alloys During Age Hardening*. Battelle Memorial Institute Final Report to NACA, 1956.
[8] F. R. Larson and J. Miller: *ASME Trans.*, 1952, vol. 74, p. 765.
[9] S. F. Reiter and W. R. Hibbard, Jr.: *AIME Trans.*, 1955, vol. 203, p. 655; Journal of Metals, May 1955.
[10] J. D. Nisbet and W. R. Hibbard, Jr.: *AIME Trans.*, 1953, vol. 197, p. 1149; Journal of Metals, November 1953.
[11] G. J. Heimerl: NACA TN 3195, 1954.
[12] C. Zener and J. H. Hollomon: *ASM Trans.*, 1944, vol. 33, p. 163.
[13] O. D. Sherby, R. L. Ott, and J. E. Dorn: *AIME Trans.*, 1954, vol. 200, p. 71; Journal of Metals, January 1954.
[14] R. P. Carreker, Jr. and W. R. Hibbard, Jr.: WADC Technical Report No. 55-113, 1955.
[15] O. D. Sherby, R. A. Anderson, and J. E. Dorn: *AIME Trans.*, 1951, vol. 191, p. 643; Journal of Metals, August 1951.
[16] I. I. Kornilov, R. S. Mints, and S. D. Onoprienko: *Doklady Akademii Nauk* SSSR, 1953, vol. 88, p. 683.
[17] I. I. Kornilov: *Creep and Fracture of Metals at High Temperatures*, p. 215. Her Majesty's Stationery Office, London, 1956.
[18] W. Peter and W. A. Fischer: *Archiv fur das Eisenhüttenwesen*, 1949, vol. 19, p. 161.
[19] W. Holtmann: *Mitteilungen des Kohle-und Eisenforschung*, 1941, vol. 3, p. 1.
[20] M. L. V. Gayler: *Journal* Institute of Metals, 1940, vol. 66, p. 67.
[21] H. K. Hardy: *Journal* Institute of Metals, 1951, vol. 79, p. 321.
[22] O. D. Sherby, A. Goldberg, and J. E. Dorn: *ASM Trans.*, 1954, vol. 46, p. 681.
[23] O. D. Sherby and J. E. Dorn: *AIME Trans.*, 1953, vol. 197, p. 324; Journal of Metals, February 1953.
[24] E. E. Underwood: *AIME Trans.*, 1956, vol. 206, p. 1411; Journal of Metals, October 1956.

Discussion of this paper sent (2 copies) to AIME by Dec. 1, 1957 will appear in AIME *Transactions* Vol. 212, 1958, and in Journal of Metals, April 1958.

Technical Note

Investigation of the Nickel-Rich Portion of the System Ni-Zr

by Emma Smith and R. W. Guard

INVESTIGATION of the nickel-rich end of the Ni-Zr system has been prompted by an interest in the effect of small amounts of zirconium in high temperature alloys. Hansen[1] presents a hypothetical diagram based on the work of Allibone and Sykes,[2] who investigated the system up to 44 atomic pct (55 wt pct) Zr by metallographic means. Since the alloys they used were melted in Alundum crucibles they were probably contaminated with appreciable amounts of aluminum. They found two compounds which they called Ni_2Zr and Ni_3Zr.

Hayes, Roberson, and Paasche[3] identified a compound NiZr (50 atomic pct Zr) with a melting point of 1470°C. Such a high melting compound is not compatible with the observation of Allibone and Sykes[2] that a eutectic is formed near 50 atomic pct.

The alloys containing up to 60 atomic pct Zr were melted in an inert atmosphere in a nonconsumable electrode arc furnace. Analysis of most of the alloys indicated negligible loss of zirconium. The alloys were examined in the as-cast condition and also after annealing for 6 hr at 1175°C (or 1000°C for the alloys between 25 atomic pct and 45 atomic pct). Metallographic specimens were etched using mixtures of HF-HNO_3-H_2O or acetic acid-HNO_3-H_2O. The specimens for the solidus determinations were wrapped in molybdenum foil and sealed in evacuated quartz tubes. Specimens to be heated above 1300°C were enclosed in zirconia tubes inside the quartz to prevent reaction with molybdenum. The solidus determinations were carried out by heating the specimens at various temperatures for a few minutes and then examining the interior structure metallographically to determine at what temperature melting began.

The 150 mesh powders for X-ray analysis were annealed in an evacuated quartz tube for 2 hr at 540°C to remove cold work. Alloys with 22.5 atomic pct Zr and 44.4 atomic pct Zr required annealing at 700°C for complete recovery. The grains of both of these alloys were soft and rather ductile. Both Debye-Scherrer film patterns and spectrometer traces were made for each alloy using filtered copper radiation.

E. SMITH is associated with the Metals Research Laboratory, Carnegie Institute of Technology, Pittsburgh. R. W. GUARD, Junior Member AIME, is associated with Alloy Studies Research, General Electric Co., Schenectady.

TN 385E. Manuscript, June 12, 1956.

Results and Discussion

The presence of a substantial amount of second phase in an alloy with 1.1 atomic pct Zr indicated that the solid solubility of zirconium in nickel is somewhat less than 1 atomic pct. The a_o value for the face-centered-cubic matrix in the same alloy was equal to that of pure nickel, so that the solubility must be very small. This observation is as expected from the large atom size difference.

Annealed specimens of alloys with 15.0, 16.7, 22.5, 28.6, 44.4, and 50.4 atomic pct Zr showed microstructures that were essentially single phase. When

combined with the information on the microstructures of the other alloys, these data indicate that there are five compounds in this half of the system. Based on lever rule calculations and X-ray data the compounds have tentatively been identified as Ni_8Zr (16.67 atomic pct Zr), Ni_7Zr_2 (22.22 atomic pct Zr), Ni_5Zr_2 (28.57 atomic pct Zr), Ni_5Zr_3 (44.44 atomic pct Zr), and NiZr (50 atomic pct Zr).

Microstructural observations indicate that alloys with 5.2 atomic pct Zr and 10.1 atomic pct Zr lie on opposite sides of the eutectic between Ni_8Zr and nickel. Measurements of the relative amounts of eutectic in the two alloys place the eutectic at 9.7 atomic pct Zr. The as-cast structures of alloys with 16.7 atomic pct Zr and 44.4 atomic pct Zr show a structure typical of alloys freezing through a peritectic reaction. A second eutectic is observed in alloys with 33.4 atomic pct Zr and 40.8 atomic pct Zr. From the relative amounts in each the eutectic point is calculated to be 37 atomic pct Zr.

The results of these microstructural and X-ray observations coupled with the determinations of peritectic and eutectic temperatures give the phase diagram shown in Fig. 1. This diagram is different from that of Hansen[1] and contains neither the Ni_2Zr or Ni_3Zr found by Allibone and Sykes,[2] although the compositions of Ni_7Zr_2 and Ni_5Zr_3 are close to the compounds Ni_3Zr and Ni_2Zr, respectively. Although Hayes, Roberson, and Paasche[3] found that NiZr had a melting point of 1470°C, the writers find one of only 1350°C. It was not possible to resolve this difference.

Structure of Ni_8Zr

The first compound on the nickel-rich end of the system is Ni_8Zr. The d-values were obtained from both film and spectrometer methods and it was found that the compound was face-centered-cubic with $a_o = 6.71$A. Intensity calculations verified that the structure was isomorphous with Ni_8U and Cu_8U previously determined by Baenziger, Rundle, Snow, and Wilson.[4] This structure, containing four atoms Ni, at $(\frac{1}{4},\frac{1}{4},\frac{1}{4})$, and 16 Ni_{II} at $(x,x,x;x,x,x;$ per unit cell, has four zirconium at (0,0,0), four $x,x,x;x,x,x;)$, where $x = 0.625 \pm 0.005$, see Fig. 2. In this structure the distances between Ni_{II} atoms and zirconium atoms or other Ni_{II} atoms are slightly less than the sum of the respective radii, while the distances between Ni_I atoms and other atoms are slightly larger than the sum of the radii. It is possible to explain this discrepancy by assuming that the Ni_{II} atoms have given some of their electrons to Ni_I atoms. The d-values, together with the observed and calculated intensities, are given in Table I.

The structures of the other compounds appear to be complex and were not determined. For this reason the formulae given previously for these compounds are not definite.

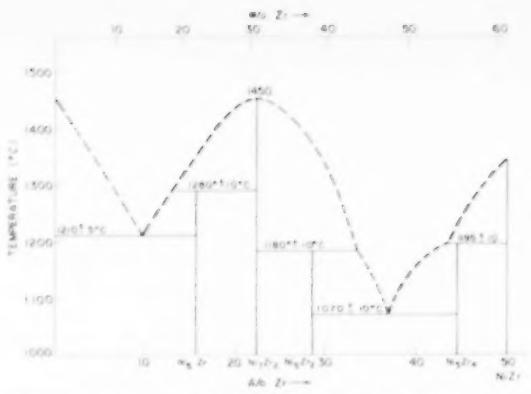

Fig. 1—Tentative constitution diagram for the system Ni-Zr up to 50 atomic pct Zr showing the positions of the compounds and solidus temperatures.

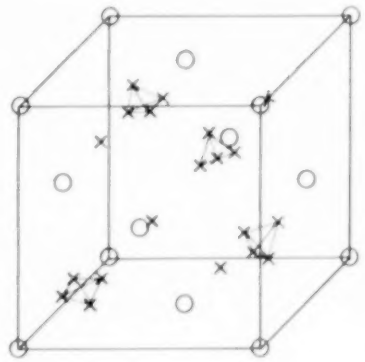

Fig. 2—Crystal structure of the compound Ni_8Zr unit cell having a face-centered-cubic structure with $a_o = 6.71$Å. Circle refers to zirconium; and cross, nickel.

Table I. X Ray Powder Data for Ni_8Zr*

$d_{obs.}$	$d_{calc.}$	hkl	$I_{obs.}$	Relative $I_{calc.}$	
3.854	3.874	111	W†	0.58	
3.346	3.355	200	W	0.38	
2.358	2.370	220	MS	7.96	
2.024	2.027	311	S	22.19	
1.928	1.937	222	MS	7.19	
1.670	1.678	400	W	0.45	
1.531	1.539	331	W	0.11	
1.494	1.500	420	W	0.14	
1.364	1.372	422	M	2.49	
1.287	1.291	333	MS	1.54	6.16
		511		4.62	
1.183	1.186	440	MS	5.26	
1.131	1.134	531	W	0.08	
1.116	1.118	600	W	0.01	0.07
		422		0.06	
1.080	1.081	620	M	1.18	
1.021	1.023	533	M	2.51	
1.010	1.011	622	M	2.76	
	0.970	444	A	0.12	
0.9583	0.9600	711	W	0.03	0.06
		551		0.03	
0.9297	0.9305	640	W	0.05	
0.8959	0.8967	642	M	2.27	
0.8724	0.8735	731	MS	5.38	8.07
		553		2.69	
0.8379	0.8387	800	M	2.32	
0.8195	0.8197	733	W	0.05	
0.8143	0.8137	820	W	0.08	0.16
		644		0.08	
0.7902	0.7908	822	M	2.52	3.78
		660		1.26	
0.7752	0.7748	751	S	23.86	27.84
		555		3.98	

* Cylindrical camera, film to specimen, 5 cm, filtered copper radiation.
† W means weak; M, medium; S, strong; and A, absent.

Acknowledgments

The authors wish to acknowledge the assistance of W. L. Roth in determining the structure of the compound Ni_7Zr; W. A. Roman, Dorothy Kontoleon, and Jean H. Tomlinson in the metallographic work; Rose Kimura and Ann Cooper in obtaining the X-ray powder data; and E. A. Smith in performing many of the high temperature heat treatments.

References

[1] M. Hansen: *Der Aufbau der zweistofflegerungen*, p. 969. J. Springer, Berlin, 1936.
[2] T. E. Allibone and C. Sykes: The Alloys of Zirconium I. *Journal* Institute of Metals, 1928, vol. 39, p. 179.
[3] E. T. Hayes, A. H. Roberson, and O. G. Paasche: The Zr-Ni Phase Diagram. *ASM Trans.*, 1953, vol. 45, p. 893.
[4] N. C. Baenziger, R. E. Rundle, A. I. Snow, and A. S. Wilson: Compounds of Uranium with the Transition Metals of the First Long Period. *Acta Crystallographica*, 1950, vol. 3, pp. 34-40.

Transformation Kinetics and Mechanical Properties Of Zr-Mo Alloys

Alloys containing 1.3, 3.3, 5.4, and 7.5 pct Mo were prepared using high purity molybdenum and sponge zirconium. Time-temperature-transformation curves were established for these alloys based on the resistivity vs time of anneal curves of isothermally quenched rods. Tensile and impact bars of each alloy were heat treated by isothermal quench techniques as well as by quench and reheat treatments. These bars were then machined, tested, and the properties compared. Optimum properties could be developed in the 1.3 pct Mo alloy using the isothermal quench technique. The 3.3, 5.4, and 7.5 pct Mo alloys exhibited a brittle behavior irrespective of type of heat treatment. An ω or transition phase in the $\beta \rightarrow \alpha$ transformation was discovered which undoubtedly accounts for most of the brittleness observed. The ω phase has been tentatively indexed as tetragonal, $c/a = 1.45$. Mechanical properties of unalloyed sponge zirconium are presented for comparison.

by R. F. Domagala, D. W. Levinson, and D. J. McPherson

SOME of the results of a program designed to study the kinetics of transformation and related mechanical properties of prototype Zr-*X* binary alloys systematically are presented here. The object of this program was to provide a sound basis for a scientific approach to the realization of optimum properties in binary zirconium alloys. Alloys of Zr-Mo (eutectoid), Zr-Sn (peritectoid), and Zr-Ti (α and β isomorphous) were prepared and studied. The data herein are confined to a presentation of the results of studying the eutectoid prototype alloys.

The Zr-Mo phase diagram has been determined.[1] A definitive metallographic study of isothermally annealed samples prepared from high purity elements served to position a sluggish eutectoid reaction, $\beta \rightarrow \alpha + ZrMo_2$, at 780°C. The compositions of the phases involved in this reaction are: β, 7.5 ±1 pct Mo; α, <0.18 pct Mo; and $ZrMo_2$, 67.8 pct Mo. Inasmuch as a lower purity sponge zirconium was used in this work boundary placements were reinvestigated with the less pure alloys.

R. F. DOMAGALA, Junior Member AIME, D. W. LEVINSON, and D. J. MCPHERSON, Member AIME, are Research Metallurgist, Supervisor, Nonferrous Research Section, and Assistant Manager, Metals Research Dept., respectively, Armour Research Foundation of Illinois Institute of Technology, Chicago.

TP 4495E. Manuscript, Sept. 6, 1956.

Materials and Procedures

Hafnium-free sponge zirconium was used to prepare all ingots. The arc melted hardness of a small button of this zirconium was found to be Vpn 168. Chemical analyses conducted at Armour Research Foundation are shown in Table I.

High purity molybdenum sheet was used as the alloy addition. A typical analysis is shown in Table I. Several 200-g Zr-50 pct Mo alloys were made by arc melting. Crushed granules of this material were used to ensure ingot homogeneity.

Alloy ingots were prepared by double melting techniques. First, three 5-lb ingots of each alloy composition were arc melted in a nonconsumable electrode arc furnace. After melting, the ingots were ground to remove surface defects. A subse-

Table I. Summary of Chemical Analyses

Material	Analysis					
	O, Pct	N, Pct	H, Ppm	C, Pct	Fe, Pct	Other, Pct
Zr (as-received)	0.131†	0.02	49†	0.023	0.042	
Zr (melted and forged)	0.124	0.02	65			
Mo (sheet)	0.045			0.015	0.005	Co + Ni = 0.02
						Mo
Zr-1 pct Mo*		0.02				1.3
Zr-3 pct Mo*	0.078		65			3.3
Zr-5 pct Mo*	0.105		62			5.4
Zr-7 pct Mo*	0.126	0.01	86			7.5

* Analysis on doubly melted and forged rod
† Analysis on 100 g arc melted ingot.

quent forging operation was performed to convert the ingots into 1 in. diam rods. The forged rods were centerless ground to eliminate surface contamination. The bars were then threaded and tapped to permit joining and remelting of each composition into a single ingot by consumable electrode melting techniques. Open anvils were employed for all forging operations; ingots were preheated in an electric furnace. Furnace temperatures employed during forging ranged from 1040°C for sponge zirconium to a maximum of 1315°C for the Zr-5 pct Mo alloy.

After the second melting operation, the large ingot of each composition was forged to 1 in. diam. The rod was then cut into lengths to produce, on subsequent forging, an equal number of tensile and impact blanks and a sufficient number of transformation study specimens. For *TTT* chart work, rods were forged to ⅜ in. diam and ground to 3/16 in.; for tensile bars a ⅜ in. diam rod was formed; for impact specimens the stock was forged in ⅜ in. sq.

TTT charts were determined principally by resistometric techniques. It has been demonstrated with titanium alloys[5,6] that decomposition of the β phase is associated with a significant change in resistivity. By following these changes in a plot of resistivity vs time of anneal for specimens isothermally quenched from the β field, a *TTT* diagram can be constructed. Such evaluation of resistivity data must initially be verified by metallographic checks. A *TTT* chart may then be constructed more rapidly and often more accurately than by metallographic means alone. This is true since it is usually difficult to position the completion of a reaction by metallography, and it is sometimes impossible to interpret structures developed on annealing at low temperatures.

The procedure followed in this phase of work was as follows:

1) Hold alloy rods (⅜ in. x 3½ to 4 in.) in β field (975° to 1000°C) for 15 to 30 min.

2) Isothermally quench specimen to some lower temperature, hold for a given length of time, and then rapidly water quench.

3) Measure resistivity, using standard current-potential method after removing slightly contaminated surface layer.

4) Remove small slice of rod from one end and submit for metallographic study.

5) Return rod to *beta-izing* furnace and proceed again from No. 1, but continually lengthen time at the transformation temperature.

When specimens for the kinetics study had to be isothermally transformed at rather high temperatures and/or for long periods of time these rods were sealed in evacuated Vycor bulbs for treatment. Tensile and impact blanks were heat treated after transformation kinetics data were determined.

Standard ¼ in. shoulder type tensile and *V*-notch Charpy impact specimens were machined from heat treated blanks, ⅝ in. round and ⅝ in. square, respectively.

A Debye-Scherrer powder camera was used for the X-ray work performed in this program. A molybdenum target and a ZrO_2 filter were used. The operating voltage was 50 kv at 15 ma. Exposure times were 24 hr. The powder specimen, passed through a 200 mesh screen, was placed in a glass capillary at the center of a 14 cm diam camera.

For metallographic study button heads of tested tensile bars were rough polished down to 0000 grit silicon carbide paper. The samples were then electropolished. A solution containing 59 pct methyl alcohol, 35 pct butyl cellusolve, and 6 pct perchloric acid was used. Current densities of ~1 amp per sq in. were maintained for 30 sec. Finally, the samples were etched with a solution of 10 to 20 pct HNO_3 and 10 to 20 pct HF in glycerine.

Results and Discussion

Pure zirconium, as well as zirconium alloys with small alloy additions, may transform, on quenching, from the high temperature β phase (body-centered-cubic) to the low temperature α phase(hexagonal-close-packed) with extreme rapidity. In zirconium alloys, when a needle-like martensitic configuration occurs, the term α' is used to describe the transformation structure. With increasing alloy content the high temperature β phase may finally be retained on quenching from above the $\beta/\alpha + \beta$ boundary. When such retained β structures are subsequently reheated or transformed by step-quenching below the $\beta/\alpha + \beta$ boundary, equilibrium phases are formed which may be α or α plus another phase (compound and/or β).

In view of the impurity content of sponge zirconium and its possible influence on mechanical properties, a heat treatment vs property study for unalloyed sponge zirconium was made. Tensile and impact properties were obtained for material processed in an identical manner to the alloy ingots. A sponge zirconium ingot was prepared by melting in the nonconsumable electrode furnace. The ingot was forged directly into stock for tensile and impact blanks.

Chemical analyses of the forged rod are shown in Table I. Mechanical property data for the sponge zirconium are shown in Table II. Some variation in tensile properties, impact strength, and hardness was observed. A generally ductile condition was

preserved, however, regardless of treatment. The 900°C level at which some of the specimens were treated represents a point in the $\alpha + \beta$ field for sponge zirconium. The $\alpha \rightarrow \beta$ transformation temperature for pure zirconium is given as ~865°C. A metallographic study of slices of the forged rods which were annealed at temperatures between 700°

Table II. Mechanical Property Data for Sponge Zirconium

Treatment	Ultimate Tensile Strength, Psi	Elongation, Pct	Reduction in Area, Pct	Impact Strength, Ft-Lb	Vpn, 20 Kg
1025°C, ½ hr → WQ	109,000	13	40	11.5	282
1025°C, ½ hr → AC	100,000	17	41	3.5	204
1025°C, ½ hr → FC	74,000	12	21	4.5	161
1025°C, ½ hr → WQ 900°C, 1 hr → WQ	101,000	14	36	6.0	230
1025°C, ½ hr → 900°C, 1 hr → WQ	84,800	18	48	12.5	216
1025°C, ½ hr → WQ 750°C, 1000 min → WQ	73,700	17	32	9.0	172
1025°C, ½ hr → 750°C, 1000 min → WQ	79,400	18	35	—	186
Forged at 900°C from ⅝ → ½ in. 900°C, 1 hr → AC	79,400	16	40	2.0	199

and 1025°C showed the transformation *range* to extend from ~975° to ~800°C.

The microstructural appearance of the tensile specimens varied from a martensitic (α') type structure to a coarse α configuration, depending on the annealing treatment. The α' structure provided the strongest condition.

Zr-Mo alloys nominally containing 1, 3, 5, and 7 pct Mo based on sponge zirconium were prepared and tested. Analytical data are given in Table I. Time-temperature-transformation curves were drawn for these alloys. Resistivity curves for isothermally quenched rods were used as the principal tool for *TTT* chart construction. Due to fineness of most of the phases formed during the isothermal transformations, and because of the presence of a fine dispersion of the unidentified impurity phase, the resistivity data proved more reliable than metallography in establishing initiation as well as completion of decomposition. Much impurity phase was observed in most zirconium and zirconium alloy structures. Metallographic interpretation of structures was very difficult because of it, especially so in cases where intimate transformation configurations occurred.

Annealing treatments were conducted with small portions of the four Zr-Mo alloys and portions of a 15 pct Mo (hypereutectoid) button ingot to position the eutectoid point for the sponge base alloys. A placement of the eutectoid point at ~6 to 7 pct Mo and 850°C was made although it must be appreciated that a three phase $\alpha + \beta + ZrMo_2$ field exists (because impurities are present) and the eutectoid figure given is a simplification of a more complex situation.

Typical resistivity curves are shown in Fig. 1. The complete set of curves for all alloys may be found in refs. 4 and 5. A decrease in resistivity accompanied the initial rejection of α. The formation of eutectoid also was accompanied by a decided drop in resistivity. When an incubation period preceded the formation of eutectoid, a plateau was observed in the resistivity vs time curves. It was not always possible to corroborate the interpretation of the resistivity data accurately by metallography because

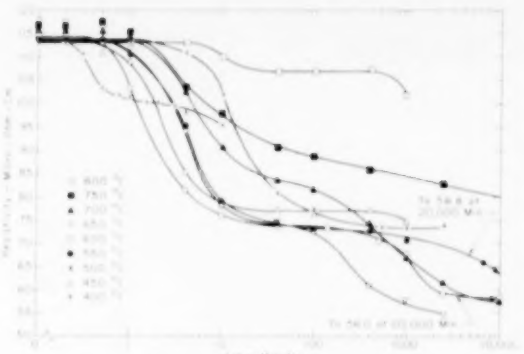

Fig. 1—Resistivity data for Zr-5.4 pct Mo alloy.

of the fineness of the decomposition products. At temperatures from 650°C and up it was possible to confirm the initial drop in resistance as coinciding with the formation of discrete α particles. The second drop in the curve occurred when a more complex microstructure (eutectoid decomposition) developed.

Combined techniques were used to establish the M_s temperature for the 1.3 pct Mo composition. The method is essentially a modification of the Greninger-Troiano technique for steel. Resistivity rods were quenched from 1000°C to incremental temperatures between 400° and 575°C, held for 10 sec, and then up-quenched to 600°C, held for 1 min, and water quenched. Small slices were submitted for metallographic study and the resistance of each rod was accurately measured. The resistivity vs temperature plot showed a discontinuity between 525° and 550°C. From this plot, the M_s temperature was presumed to lie within the discontinuity and was positioned at ~535°C. A metallographic study of slices of these resistivity bars was conducted. Specimens initially quenched to 550°C and higher were

Table III. Mechanical Property Data for Zr-1.3 Pct Mo Alloy

Treatment*	Ultimate Tensile Strength, Psi	Elongation, Pct	Reduction in Area, Pct	Impact Strength, Ft-Lb	Vpn, 20 Kg
1000°C, ½ hr → WQ	140,000	1	0	1.5	372
1000°C, ½ hr → AC	116,000	12	34	4.0	246
1000°C, ½ hr → FC	94,100	8	10	5.0	199
1000°C, ½ hr → OQ	102,000	Broke in 3 pieces		1.5	382
A + 800°C, 5 min	133,000	Broke in 3 pieces		1.0	316
A + 800°C, 20 min	141,500	4	4	1.5	277
A + 800°C, 180 min	135,000	5	6	1.5	279
A + 700°C, 5 min	132,000	12	29	4.0	282
A + 700°C, 20 min	128,000	8	15	2.5	288
A + 700°C, 180 min	118,000	16	28	4.0	249
A + 700°C, 2500 min	92,300	17	39	7.0	190
A + 600°C, 5 min	148,000	6	16	3.0	309
A + 600°C, 20 min	149,000	7	22	2.5	301
A + 600°C, 180 min	138,000	11	23	4.0	294
A + 600°C, 1500 min	106,000	17	40	6.0	209
A + 500°C, 5 min	176,000	3	0	2.0	347
A + 500°C, 20 min	164,000	4	9	2.0	340
A + 500°C, 180 min	170,000	6	0	2.5	344
B + 800°C, 5 min	92,800	Broke in 3 pieces		2.0	322
B + 800°C, 180 min	113,000	3	3	2.5	253
B + 700°C, 2500 min	101,000	7	12	4.5	232
B + 600°C, 5 min	161,000	0	0	3.0	353
B + 600°C, 180 min	114,000	1	0	4.0	274
B + 600°C, 1500 min	94,700	0	0	5.0	262
B + 500°C, 180 min	168,000	0	0	2.0	346

* *A* treatment consists of 1000°C, ½ to ¾ hr, isothermally quenched to temperature, held for indicated time, and water quenched. *B* treatment consists of 1000°C, ½ hr → WQ; reheated to temperature; held for indicated time; and water quenched.

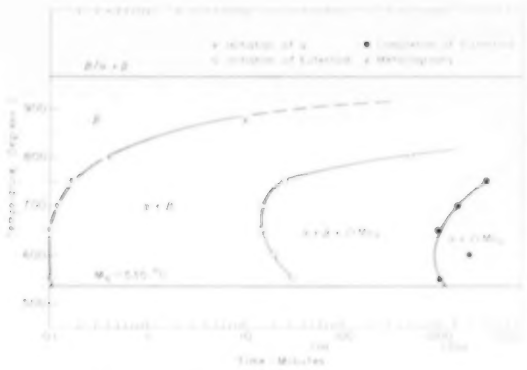

Fig. 2—*TTT* chart for Zr-1.3 pct Mo alloy.

relatively free of α' needles while those which were quenched to 525°C and below were predominantly α'. The *TTT* charts for the four alloys are shown in Figs. 2 to 5.

Chronologically, an identification of the ω (transition) phase in the $\beta \rightarrow \alpha$ transformation was made late in the work. Before this fact was established a heat treatment vs property study was initiated. Using the transformation curves as a guide, mechanical test blanks of the four alloys were heat treated by isothermal quench techniques to various stages of transformation, machined, and tested. Other blanks were subjected to quench (from β) and reheat treatments and varied cools from β so that the properties developed by the different methods could be compared.

Table IV. Mechanical Property Data for Zr-3.3 Pct Mo Alloy

Treatment*	Ultimate Tensile Strength, Psi	Elongation, Pct	Reduction in Area, Pct	Impact Strength, Ft-Lb	Vpn, 20 Kg
975°C, ½ hr → WQ	55,600†	0	0	0.5	353
A + 800°C, 5 min	122,600†	0	0	—	390
A + 800°C, 180 min	52,600†	0	0	—	320
A + 700°C, 5 min	136,000	7	16	3	274
A + 700°C, 180 min	108,000	1	2	—	244
A + 650°C, 4200 min	93,500	13	17	—	265
A + 600°C, 5 min	139,000†	0	0	—	332
A + 600°C, 14 days					244‡
A + 600°C, 28 days					239‡
A + 500°C, 5 min	144,000	0	0	—	406
A + 500°C, 180 min	192,000	1	6	1.5	391
A + 500°C, 14 days					275‡
A + 500°C, 28 days					261‡
A + 400°C, 14 days					285‡
A + 400°C, 28 days					278‡
Forged at 875°C					
⅝ → ½ in.					
875°C, 1 hr → AC					
650°C, 24 hr → WQ	116,000	6	9	—	235

* *A* treatment consists of 975°C, ½ hr; isothermally quenched to temperature; held for indicated time; and water quenched.
† Tensile specimen broke outside gage mark and/or into several pieces.
‡ Hardness data only collected.

heat treatments and varied cools from β so that the properties developed by the different methods could be compared.

The mechanical property data for the 1.3 pct Mo alloy are shown in Table III. This alloy exhibited a brittle behavior when water quenched from the β field. The biggest improvement in relieving this condition was found on isothermally transforming at about the nose of the curve. In general, the isothermal quench technique proved superior to the quench and reheat treatments in relieving the brittle condition for this alloy. When a tensile blank was water quenched from β prior to being given the transformation anneal, very low ductility levels were attained. For example, a specimen isothermally quenched to 600°C and held for 1500 min provided a specimen with ultimate tensile strength of 106,000 psi, 17 pct elongation, and 40 pct reduction in area. When water quenched from the β field and subsequently reheated to 600°C for 1500 min, a tensile bar of this same alloy failed in a brittle manner. Microstructures of the 600°C, 1500 min samples are shown in Figs. 6 and 7. The former has coarse α while the latter is martensitic. Exceptions to this behavior were found when specimens were given prolonged anneals following the initial quench.

A correlation between hardness and strength was found for this alloy which is shown in Fig. 8.

Mechanical property data for the 3.3, 5.4, and 7.5 pct Mo alloys are summarized in Tables IV, V, and VI, respectively. The results shown represent only a portion of all data collected. For a complete record of all treatments and properties for these alloys see refs. 4 and 5. These alloys exhibited a brittle behavior for all but a very few conditions of heat treatment.

Table V. Mechanical Property Data for Zr-5.4 Pct Mo Alloy

Treatment*	Ultimate Tensile Strength, Psi	Elongation, Pct	Reduction in Area, Pct	Impact Strength, Ft-Lb	Vpn, 20 Kg
975°C, ½ hr → WQ				2.0	323
A + 800°C, 5 min	115,000†	0	0	1.0	326
A + 700°C, 180 min	115,000†	0	0	1.0	259
A + 650°C, 2500 min	115,000†	0	0	2.5	269
A + 650°C, 7 days	107,000	1	3	—	244
A + 600°C, 20 min	121,000	0	0	1.5	334
A + 600°C, 180 min	138,000†	0	0	2.0	325
A + 600°C, 7 days					256‡
A + 600°C, 14 days	126,000	2	3	—	254
A + 500°C, 5 min	94,500†	0	0	2.0	349
A + 500°C, 180 min	126,000†	0	0	2.0	372
A + 500°C, 7 days					379‡
A + 500°C, 14 days					364‡
A + 400°C, 5 min	85,900†	0	0	1.0	345
A + 400°C, 7 days					438‡
A + 400°C, 14 days					447‡

* *A* treatment consists of 975° to 1000°C, ½ to ¾ hr; isothermally quenched to temperature; held for indicated time; and water quenched.
† Tensile specimen broke outside gage mark and/or into several pieces.
‡ Hardness data only collected.

An increase in reaction rate below ~500°C was noted and is shown on the *TTT* charts for these alloys. Such behavior in the case of titanium alloys has been attributed to the formation of ω phase.[3,6] The ω is believed to be a transition phase interme-

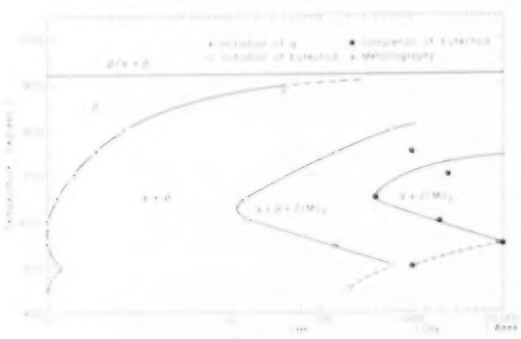

Fig. 3—*TTT* chart for Zr-3.3 pct Mo alloy.

diate in the transformation of β to α. It is found only in certain alloy compositions and forms over specific temperature ranges or cooling conditions. A very brittle condition is associated with the existence of this phase.[7,8]

The X-ray study performed to help identify the existence of ω phase in the Zr-Mo alloys was patterned after a similar program with titanium alloys.[9] The term ω and other nomenclature regarding the transition phase have been drawn from those already established for titanium alloys.

Table VI. Mechanical Property Data for Zr-7.5 Mo Alloy

Treatment*	Ultimate Tensile Strength, Psi	Elongation, Pct	Reduction in Area, Pct	Impact Strength, Ft-Lb	Vpn, 20 Kg
1000°C, ½ hr → WQ	135,000†	0	0	3.0	299
1000°C, ½ hr → AC	146,000†	0	0	1.5	307
1000°C, ¼ hr → FC	82,000†	0	0	2.0	349
A + 750°C, 30 min	110,000†	0	0	1.5	291
A + 700°C, 5 min	118,000†	0	0	1.5	299
A + 700°C, 180 min	123,000	0	0	1.5	282
A + 600°C, 30 min	157,000†	0	0	1.5	328
A + 650°C, 1000 min	108,000	0	0	1.0	265
A + 650°C, 5280 min	108,000	4	5	2.0	235
A + 550°C, 5 min	149,000†	0	0	1.5	302
A + 550°C, 180 min	160,500	0	0	1.5	361
A + 400°C, 5 min	126,000	0	0	1.5	405

* A treatment consists of 1000°C, ½ hr; isothermally quenched to temperature; held for indicated time; and water quenched.
† Tensile specimen broke outside gage mark and/or into several pieces.

From the water quenched impact bar of the 5.4 pct Mo alloy, a quantity of powder was prepared for study. This material was divided into five small Vycor bulbs which were evacuated and sealed. The bulbs were held at 1000°C for 5 min and water quenched without breaking the bulbs. One bulb was kept in this condition and others were reheated to 400°C for times from 2 min to one week and water quenched (bulb not broken) at the conclusion of the anneal. X-ray powder photograms were prepared.

The patterns were measured and the β-Zr (body-centered-cubic) lines identified and eliminated. A strong pattern of β-Zr was present, which seemed to diminish in intensity with increased annealing times at 400°C. The lines which remained in each pattern are shown in Table VII. A recurring set of lines is evident. Average d values were calculated for each line and an attempt was made to index the structure. Too few lines were present for a positive identification, but a rather good fit was made for a

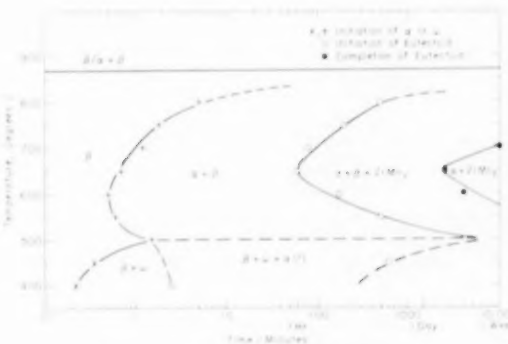

Fig. 4—*TTT* chart for Zr-5.4 pct Mo alloy.

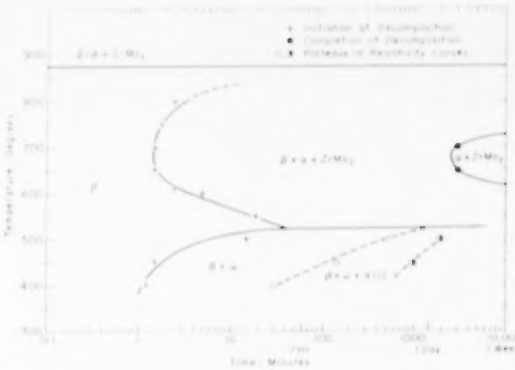

Fig. 5—*TTT* chart for Zr-7.5 pct Mo alloy.

tetragonal structure, $c/a = 1.45$, $a = 4.40$Å. In no pattern were any lines corresponding to a α-Zr (hexagonal-close-packed) observed.

It seems clear that there is a transition phase (tentatively tetragonal in structure) in the $\beta \rightarrow \alpha$ transformation in the Zr-5 pct Mo alloy. This transition phase undoubtedly accounts in part for the brittleness observed. Because of the wide scope of the project under which this work was performed, it was never intended to study this phenomenon exhaustively. It is hoped that some ground work has been laid for a definitive study of ω or transition phase in zirconium alloys.

A few tensile blanks of the 3.3 and 5.4 pct Mo alloys were given prolonged treatments aimed at producing less brittle conditions. The brittle condition generally persisted, however. In only a few cases was any ductility shown.

Table VII. Summary of d Values for Transition Phase (ω) Lines Observed in Zr-5.4 Pct Mo Alloy

1000°C, Water Quenched	400°C* 2 Min	1 Hr	1 Day	1 Week	Average	hkl†
3.118	3.196	3.062	3.211	3.181	3.154	110 or 002
2.320	2.297	2.313	2.309	2.313	2.309	112
2.202	—	2.204	2.206	2.204	2.204	200
1.978	1.97	1.939	1.974	1.974	1.967	210
1.908	—	—	—	—	1.908	211
1.641	—	1.631	—	—	1.636	004
1.569	1.578	1.564	1.572	1.573	1.571	220
1.337	1.335	1.336	1.332	1.337	1.335	302
—	—	—	—	1.166	1.166	313
1.068	1.070	1.067	1.066	1.068	1.068	006 or 411
—	—	—	1.030	—	1.030	106 or 331
0.981	0.979	0.982	0.981	0.985	0.982	403
0.877	—	0.878	0.877	—	0.877	226
0.911	0.816	0.815	0.809	0.814	0.813	521

* Treatment was 1000°C → WQ, then 400°C for times indicated and water quenched.
† *hkl* values assigned on a basis of a rather good fit to a tetragonal structure, $c/a = 1.45$.

Fig. 9 is a microstructure observed for the Zr-3.3 pct Mo alloy after 4280 min (71 hr) at 650°C. This represents a completely decomposed condition and is one of the few cases where any ductility was observed for this alloy.

Hardness data only were gathered for the 3.3 and 5.4 pct Mo alloys in several instances to note whether any softening would occur after prolonged heat treatments at low (400° to 600°C) temperatures.

For the 3.3 pct Mo alloy, very long annealing times of the order of one to two weeks at these tem-

Fig. 6—Micrograph of a Zr-1.3 pct Mo alloy; 1000°C, ¾ hr → 600°C, 1500 min → water quenched. Specimen has coarse α + $ZrMo_2$ structure. Compare with Fig. 7. X250. Reduced approximately 15 pct for reproduction.

Fig. 7—Microstructure of Zr-1.3 pct Mo alloy; 1000°C, ¾ hr → water quenched; 600°C, 1500 min → water quenched. Specimen has a tempered martensite structure. Compare with Fig. 6. X250. Reduced approximately 15 pct for reproduction.

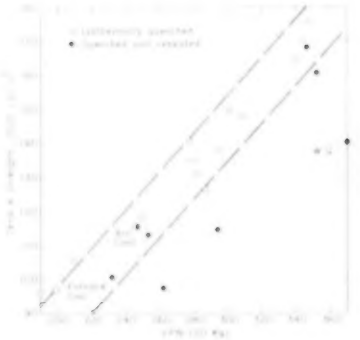

Fig. 8—Correlation between hardness and strength for Zr-1.3 pct Mo alloy.

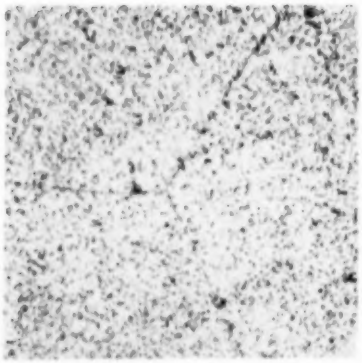

Fig. 9—Micrograph of Zr-3.3 pct Mo alloy; 975°C, ¾ hr → 650°C, 4280 min → water quenched. Specimen has a completely decomposed structure, α + $ZrMo_2$.

peratures would probably provide little improvement in ductility.

In the case of the 5.4 pct Mo composition, anneals at 400°C only served to make the alloy harder and presumably more brittle. Little change in hardness occurred after one to two weeks at 500°C. After one and two weeks at 600°C a significant hardness drop was found, and here some slight relief from the brittle condition might be anticipated.

It should be noted that no oxygen pickup was experienced in processing the ingots. Nevertheless, oxygen may have contributed to the brittle condition. Increasing amounts of $ZrMo_2$ probably was also a factor. It is impossible to distinguish the combined or overlapping effects of ω, oxygen, and $ZrMo_2$.

Summary

Time-temperature-transformation curves have been established for sponge base zirconium alloys containing 1.3, 3.3, 5.4, and 7.5 pct Mo. These prototype eutectoid alloys have *noses* corresponding to the initiation of transformation at about 600° to 650°C which are moved to longer times with increasing molybdenum contents. Resistivity as a function of transformation was the principal tool employed in this work.

Mechanical properties as a function of degree of transformation were determined for the alloys. Isothermal quench techniques provided optimum properties in the 1.3 pct Mo alloy. The other three alloys generally exhibited a brittle behavior irrespective of heat treatment. The brittle nature has been associated with the formation of ω or transition phase in the $\beta \rightarrow \alpha$ transformation. This transition phase has tentatively been indexed as tetragonal, $c/a = 1.45$.

Acknowledgments

The authors wish to thank the AEC, sponsors of this work under Contract No. AT(11-1)-315 *A Study of the Mechanisms of Heat Treatments of Zirconium Base Alloys*, for permission to publish this paper. Thanks are due to L. Murphy of the Metals Dept. metallographic section for the photomicroscopy and to H. L. Nurnberg for the resistivity work.

References

[1] R. F. Domagala, D. J. McPherson, and M. Hansen: Systems Zirconium-Molybdenum and Zirconium-Wolfram. *AIME Trans.*, 1953, vol. 197, p. 73; JOURNAL OF METALS, January 1953.

[2] D. J. DeLazaro and D. W. Levinson: Correlation Between Microstructure and Resistivity of Transforming Ti-Mn Alloys. *AIME Trans.*, 1954, vol. 200, p. 1089; JOURNAL OF METALS, September 1954.

[3] D. W. Levinson and W. Rostoker: Structural Changes of Commercial Titanium-Base Alloys on Heat Treatment. Contract No. WADC-TR-54-244, 1954.

[4] R. F. Domagala and D. J. McPherson: A Study of the Mechanisms of Heat Treatment of Zirconium-Base Alloys. USAEC Report No. 2, Summary (C00-207), 1955.

[5] R. F. Domagala and D. W. Levinson: A Study of the Mechanisms of Heat Treatment of Zirconium-Base Alloys. USAEC Report No. 3, Summary (C00-211), 1956.

[6] F. R. Brotzen, E. L. Harmon, Jr., and A. R. Troiano: Decomposition of Beta Titanium. *AIME Trans.*, 1955, vol. 203, p. 413; JOURNAL OF METALS, February 1955.

[7] P. D. Frost, W. M. Parris, L. L. Hirsch, J. R. Doig, and C. M. Schwartz: Isothermal Transformation in Titanium-Manganese Alloys. *ASM Trans.*, 1954, vol. 46, p. 1056.

[8] P. D. Frost, W. M. Parris, L. L. Hirsch, J. R. Doig, and C. M. Schwartz: Isothermal Transformation in Titanium-Chromium Alloys. *ASM Trans.*, 1954, vol. 46, p. 231.

[9] S. A. Spachner: Comparison of the Structure of the Omega Transition Phase in Three Titanium Alloys. *AIME Trans.* To be published.

Discussion of this paper sent (2 copies) to AIME by Jan. 1, 1958 will appear in AIME *Transactions* Vol. 212, 1958, and in JOURNAL OF METALS, April 1958.

Copper-Silica and Copper-Alumina Alloys Of High Temperature Interest

Utilizing relatively coarse copper powders and several sizes of silica and alumina powders, alloys containing up to 10 volume pct of oxide were made. The alloys were prepared by mechanical mixing of powders, followed by cold hydrostatic pressing, sintering, and hot extrusion. Measurements were made of room temperature tensile properties, recrystallization temperature, creep rupture properties from 250° to 450°C, and resistivity. In addition, metallographic studies were made of the resultant structures. Of particular interest was the stability of the structure with respect to temperature, time, and stress.

by Klaus M. Zwilsky and Nicholas J. Grant

EVER since the unusual high temperature creep resistance and structure stability of SAP (Sintered Aluminum Powder) and similar aluminum-alumina alloys were reported,[1,2] there has been a need to determine whether other metal-metal oxide (or other hard stable particle) alloys, not so ideal as the Al-Al_2O_3 system, would show similar high temperature strength and stability. Of the many possible methods of obtaining a metal-metal oxide alloy,[3] one that offers many practical and theoretical advantages is the simple mechanical blending of metal powders with hard stable particles, followed by pressing, sintering, and hot extruding.

With this purpose in mind copper powder and silica and alumina were selected for experimentation because these materials are readily available, cheap, reliable, and lend themselves to the simplest processing and testing.

Starting Materials—Two sizes of electrolytically deposited copper powders were used, a −200 mesh powder referred to as *A* powder in this investigation and a −325 mesh powder referred to as *C* powder. Silica was added in the form of *pure Potter's flint* from which a −10μ fraction had been separated. Alumina of the α variety was used in two size ranges. The first was a −10μ fraction separated from a coarser aggregate, the second a commercial product of 0.3μ average diam manufactured by Linde Air Products.

Preparation of Powders—Five-hundred gram batches of *A* copper with 1, 3, and 10 volume pct of each of the three oxides mentioned above were prepared, as well as *C* copper containing 1, 3, and 10 volume pct of −10μ silica. Powders were weighed out carefully and blended by ball milling in air for 24 hr. Since this treatment resulted in surface oxidation of the copper, the charge was hydrogen reduced at 260°C for 5 hr. The next step consisted of hydrostatically compacting the powder into a shape suitable for the required hot working. For this purpose a slug about 1½ in. in diam and 3½ in. in length was produced by placing the mixed powders into a rubber sleeve, holding in a perforated steel canister, and rubber stoppering at the ends; the assembly was then subjected to a hydrostatic pressure of 50,000 psi. The air was evacuated from the assembly prior to pressing in order to prevent

K. M. ZWILSKY and N. J. GRANT, Member AIME, are Research Assistant and Professor, respectively, Dept. of Metallurgy, Massachusetts Institute of Technology, Cambridge, Mass.

TP 4588E. Manuscript, Nov. 13, 1956.

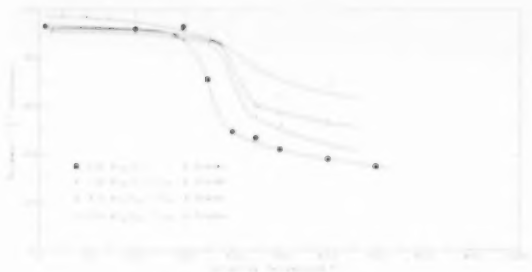

Fig. 1—Rockwell *E* hardness vs annealing temperature for —200 mesh copper containing 0 to 10 pct —10μ alumina, after 50 pct cold work and 1 hr annealing at indicated temperature.

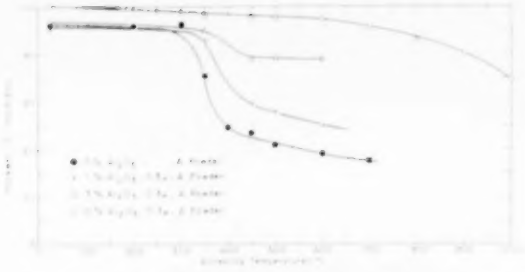

Fig. 2—Rockwell *E* hardness vs annealing temperature for —200 mesh copper containing 0 to 10 pct 0.3μ alumina, after 50 pct cold work and 1 hr annealing at indicated temperature.

gas entrapment inside the compact. This method gave a compact of considerable green strength, which could be handled readily. Sintering took place in purified hydrogen for 1 hr at 500° and for 2 hr at 1000°C. A shrinkage of 2 to 4 pct was observed during sintering and a theoretical density of about 90 pct was obtained. The compacts containing silica were then sheathed in copper, the void space was filled with fine Al_2O_3 and the container sealed by welding. The purpose of this was to prevent oxidation during the hot working treatment. After it was observed in early trials that oxidation during hot working occurred only at the surface, and to a much lesser degree than anticipated, a number of subsequent compacts containing alumina were hot worked in the *as-sintered* condition.

Table I. Mechanical Properties at Room Temperature for As Extruded and Annealed at 400°C Conditions

Material	Condition	Yield Strength, 0.2 Pct Offset, Psi	Ultimate Strength, Psi	Elongation, Pct	Reduction in Area, Pct
Pure copper	vacuum melt as cold worked	63,800	65,000	17	85
	400°C anneal	7,900	35,900	52	94
29A Si-1	as extruded	12,200	36,000	41	52
	400°C anneal	10,300	35,500	43	52
14A Si-3	as extruded	39,000	40,800	13	35
	400°C anneal	29,400	38,900	27	40
14A Si-10	as extruded	36,000	37,700	5	12
	400°C anneal	30,800	37,000	10	15
29A Al-1	as extruded	12,900	36,300	43	54
	400°C anneal	11,400	35,600	43	52
29A Al-3	as extruded	13,300	35,500	39	42
	400°C anneal	11,800	35,400	36	44
29A Al-10	as extruded	19,400	31,900	16	14
	400°C anneal	17,800	32,000	21	23
29A Al-1 fine	as extruded	15,900	35,500	43	53
	400°C anneal	11,600	35,300	44	54
29A Al-3 fine	as extruded	22,100	33,000	28	65
	400°C anneal	20,200	32,900	28	60
29A Al-10 fine	as extruded	30,200	39,300	15	7
	400°C anneal	30,000	39,000	15	29

Since maximum densification and a good dispersion of the oxide depend on the proper hot working of the material, the slugs were hot extruded at 760°C to a final diameter of 0.300 or 0.375 in. The optimum extrusion ratio was not known. Therefore, several reduction ratios were studied; namely, 14, 21, and 29 to 1. Sound extrusions were obtained in all instances, all with good surfaces.

Results

Densities—All of the extruded products except two had theoretical densities of 99 pct or greater. The two exceptions were for *A* copper plus 10 volume pct of —10μ alumina and *A* copper plus 10 volume pct of 0.3μ alumina. The former had a theoretical density of 96; the latter, 97.8 pct. Accuracy was within ±1 pct.

Recrystallization—Three-eighth in. samples were cut from the extruded rods and cold swaged 50 pct reduction in area. Rockwell *E* hardness was measured after each specimen had been annealed for 1 hr at various temperatures. Figs. 1 and 2 represent the results graphically. Fig. 1 shows the results for the alloys containing —10μ alumina additions, but is representative of the alloys containing —10μ silica additions to *A* and *C* copper. The 0 pct addition curve was obtained from measurements on ½ in. diam copper powder slugs, ⅜ in. in length, which had been compacted, sintered (but not extruded), cold worked, and annealed. It can be noted in Fig. 1 that 1 and 3 pct additions raise the recrystallization temperature about 50°C, while a 10 pct addition raises it by approximately 100°C. Of particular interest is the higher retained hardness after recrystallization which increases with increasing percentage of oxide. Fig. 2 presents the data for *A* copper and additions of 0.3μ alumina. It can be seen that a 10 pct addition prohibits recrystallization completely in terms of the usual hardness vs temperature curve, and only a slow softening is observed, becoming slightly more pronounced beyond 600°C. Even at 1000°C, 83° below the melting point of copper, considerable hardness is retained by this alloy.

Table II. Stress for 10, 100, and 1000 Hr Rupture Life and Interpolated Ductility Values at 250°, 350°, and 450°C

Material	10 Hr	Elongation, Pct	100 Hr	Elongation, Pct	1000 Hr	Elongation, Pct
			250°C			
Pure copper	18,000	38	13,000	40	9,000	—
21A Si-3	30,000	6	22,000	5	14,000	4
14C Si-3	25,000	9	19,000	6	11,000	2
14A Si-10	20,000	4	14,000	6	10,000	3
29A Al-3 fine	20,000	14	18,000	8	17,000	—
29A Al-10 fine	23,000	5	21,000	—	20,000	—
			350°C			
Pure copper	10,000	31	6,000	30	4,000	—
21A Si-3	11,000	3	6,000	4	4,000	—
14C Si-3	10,000	4	5,500	1	3,000	—
14A Si-10	7,500	6	4,800	5	3,000	—
29A Al-3 fine	15,000	14	13,500	—	12,000	—
29A Al-10 fine	19,000	4	18,000	4	17,000	4
			450°C			
29A Al-10 fine	13,500	2	12,000	1	11,000	—

Tensile Data—Threaded test bars having a 1 in. gage length by 0.160 in. diam were machined from the extruded bars. Tests were made in the *as-extruded* condition and after a 1 hr anneal in vacuum at 400°C. For comparison purposes tests were run

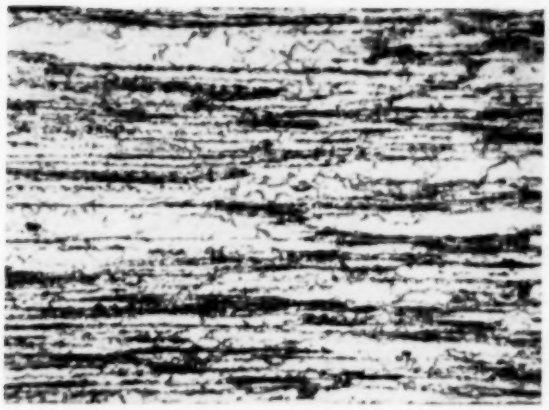

Fig. 3—Longitudinal section of —200 mesh copper plus 10 volume pct of 0.3μ alumina (29*A* Al-10 fine). Section *as-extruded*. Etched with $K_2Cr_2O_7$. X500. Reduced approximately 10 pct for reproduction.

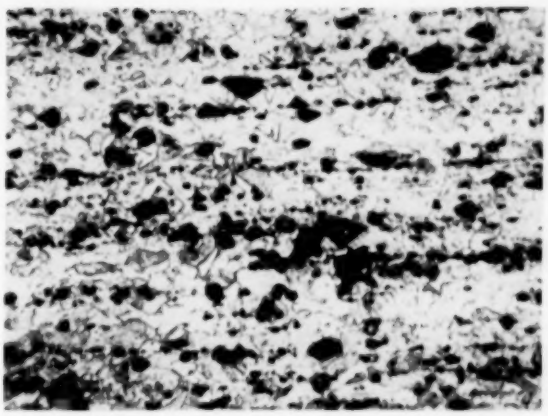

Fig. 4—Longitudinal section of —200 mesh copper plus 10 volume pct —10μ alumina (29*A* Al-10). Section *as-extruded*. Etched with $K_2Cr_2O_7$. X500. Reduced approximately 10 pct for reproduction.

on a vacuum melted copper alloy, which had been cold worked more than 50 pct reduction in area by swaging to the desired diameter. Table I summarizes the tensile data, giving yield strength (0.2 pct offset), ultimate strength, elongation, and reduction in area.

The most striking feature noted in Table I is that the maximum change with annealing is in the yield strength, not the tensile strength, along with a much smaller change in ductility. These powder products exhibit yield strengths after a 400°C anneal which are from 70 to 99 pct of the original *as-extruded* yield strength values. For the vacuum melted cold worked copper, however, the yield strength decreased to a value which is only about 23 pct of the original cold worked value after a 1 hr anneal at 250°C, and is less than one third that of the better metal-metal oxide products after a 1 hr anneal at 400°C. Similar to the SAP-type Al-Al_2O_3 products, this is a manifestation of extreme structure stability with respect to temperature.

The alloys with —10μ and 0.3μ alumina additions can be compared directly. It can be established that the finer oxide is the more effective one in achieving and retaining high yield strength values. A comparison of the microstructures shows that the fine oxide is dispersed more effectively for strengthening than the coarser oxide. Figs. 3 and 4 present longitudinal views of alloys with fine and coarse alumina additions.

It is difficult to compare directly the alloys with —10μ additions of silica and those with alumina since they have different extrusion ratios. The 3 and 10 volume pct alloys of the two oxides show a large difference in yield strength values, the silica giving a product two or three times as strong as the alumina, see Table I. It cannot be stated conclusively whether this difference is a function of the oxide chemistry, of the shape of the particular oxide added, of the hot working treatment, or of a difference in oxide dispersion.

Strength and ductility values for silica additions to *C* copper were very similar to those for the silica to *A* copper and therefore have not been included here. It should be pointed out, however, that in all of the extruded products tested rather good values of ductility were recorded, which is encouraging from an engineering point of view for any future application of these wrought powder alloy products, see Table I.

Stress Rupture Testing—Stress rupture tests of the constant load variety were run using the same type of specimen as was used for the tensile tests. Specimens were brought up to temperature and annealed for 1 hr at the test temperature prior to testing. Fig. 5 shows typical log stress-log rupture life data at 250° and 350°C for three alloys and also includes data for the vacuum melted cold-worked pure copper, which is shown for comparison purposes. Table II summarizes the creep rupture data by showing the stress necessary to produce rupture in 10, 100, and 1000 hr at several test temperatures along with interpolated ductility values. The oxide alloys in Fig. 5 include 21*A* Si-3, 14*C* Si-3, and 29*A* Al-10 fine.* It can be seen that at 250°C the 3 pct addition of —10μ silica (21*A* Si-3) is the most effective in increasing the stress for short rupture life values over that of pure copper. However, after about 50 hr there is an instability break in the log-log curve for each SiO_2 alloy which is associated with recrystallization, see Figs. 7 to 9. Beyond about 150 hr the 29*A* Al-10 fine alloy (0.3μ alumina) shows the best properties, exhibiting a flat stable curve to longer than 1000 hr.

* The numbers 21, 14, and 29 refer to the extrusion ratio. *A* refers to the —200 mesh copper powder. Si-3 or Al-10 refers to the type of oxide, silica, or alumina, and to the volume pct added, in this case 3 or 10 pct. It is understood that any oxide added was —10μ unless the word fine appears after the pct number, in which case the oxide added was 0.3μ in size.

At 350°C it will be noted that the two Cu-SiO_2 alloys, while stronger for short rupture lives,

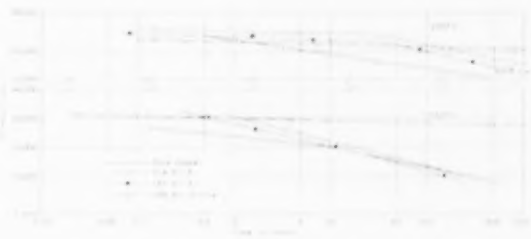

Fig. 5—Log stress vs log rupture life of pure copper and three alloys at 250° and 350°C.

Fig. 6—Log stress vs log rupture life of pure copper at 250° and 350°C and 29*A* Al-10 fine at 250°, 350°, and 450°C.

weaken rapidly and show no superiority over pure copper, which has recrystallized to a rather coarse grain size. The 29*A* Al-10 fine alloy remains stable, as indicated by the flat slope of the curve, out to beyond 1000 hr.

Since the alloy containing fine alumina exhibited such superior properties at 350°, tests were also run on this material at 450°C, and values are plotted in Fig. 6. It will be noted that alloy 29*A* Al-10 fine at 450° is stronger than pure copper at 350°C for rupture times greater than 0.1 hr, and is stronger at 450° than pure copper at 250°C for rupture times greater than about 200 hr. Even at 450°C, this alloy shows the same stable flat slope as at 250° and 350°C.

Table II shows the same striking superiority for the copper plus fine alumina alloys that has already been exhibited in Figs. 5 and 6. While the silica alloys give the best values at lower temperatures and shorter rupture lives, the fine alumina products can sustain twice the stress that pure copper can for a 1000 hr rupture life at 250°, and from three to four times the stress of pure copper for a 1000 hr rupture life at 350°C. It is interesting to observe that for the coarser silica additions the rupture life values decrease with increasing percentages of oxide as exemplified by the 21*A* Si-3 and 14*A* Si-10 products. At 250°C, for instance, the stress for a 100 hr rupture life for the 3 pct addition is 22,000 psi, while for the 10 pct addition it is 14,000 psi. For the products containing fine alumina, however, the reverse is indicated, the strength of the alloy increasing with increasing amounts of oxide added. These results may well be a function of the distribution of oxide in the matrix metal. Coarser oxides, differing in diameter from the metal powder by only five to ten times, appear to strengthen the matrix by local straining action. At the higher percentages of coarse oxide additions segregation will result in increased crack formation, thus weakening the metal. The finer oxides, on the other hand, varying in diameter from the metal powder by 100 to 200 times, seem to group themselves around the metal grains more ideally, which may be more effective in preventing recrystallization and grain growth than the more randomly dispersed coarser particles.

Fig. 7 shows a typical fracture for 29*A* Al-10 fine after testing at 450°C and 13,500 psi. Note the elongated fibrous appearing fracture which suggests that it is a transcrystalline failure. By comparison, Figs. 8 and 9 show both recrystallized structures and definite intercrystalline fractures, typical of all the other fractures noted at high temperatures or low stresses, that is, beyond the noted instability breaks in Fig. 5.

In line with the stable flat slopes noted in Figs. 5 and 6, these alloys showed large decreases in secondary creep rate over that of pure copper. Fig. 10 shows typical curves for several of the alloys at 350°C at 15,000 and 17,000 psi. Compared to pure copper, with a minimum creep rate of 100 pct per hr, alloy 29*A* Al-10 fine had a creep rate of 0.0086 pct per hr, an improvement of 11,000 times.

Resistivity—So far resistivity has only been measured for the silica containing alloys. Room temperature values indicated an increase of 6 to 24 pct over pure copper for 3 pct additions of silica, the particular value apparently depending on the extrusion ratio, and an increase of 30 pct over pure copper for a 10 pct addition of silica.

Modulus Measurements—Modulus measurements showed an increase of up to 3 million psi over pure

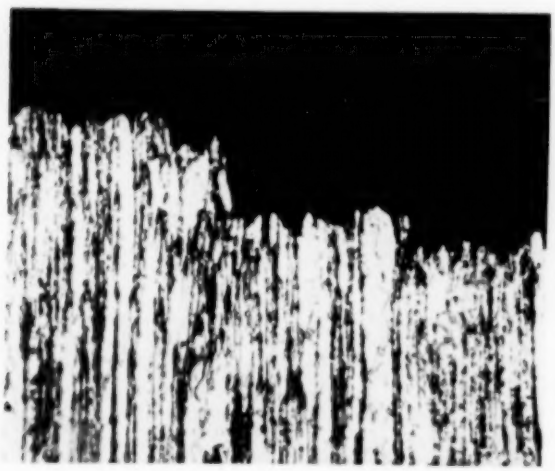

Fig. 7—Transcrystalline fracture of —200 mesh copper plus 10 pct 0.3μ alumina (29*A* Al-10 fine). Test temperature, 450°C; stress, 13,500 psi; life, 7.35 hr. Etched with $K_2Cr_2O_7$. X500. Reduced approximately 10 pct for reproduction.

Fig. 8—Intercrystalline fracture of vacuum melted cold-worked copper. Test temperature, 350°C; stress, 4900 psi; life, 342 hr. Etched with $K_2Cr_2O_7$. X500. Reduced approximately 10 pct for reproduction.

copper for 3 pct additions of -10μ silica or alumina. A decrease of up to 2 million psi was recorded for 10 pct additions of the -10μ oxides. Three and 10 pct additions of the 0.3μ alumina decreased the modulus from 16 million psi for pure copper to less than 12 million psi. One pct additions in all cases were mildly beneficial, increasing the modulus to 17.5 million psi.

Discussion and Summary

There is a significant increase in recrystallization temperature of the Cu-SiO_2 and Cu-Al_2O_3 alloys, the increase being larger with increasing amounts of oxide and with increasing fineness of oxide. In the best alloy produced in this program (29*A* Al-10 fine), there is no sign of recrystallization, as measured by the shape of the hardness vs temperature curve, up to about 80°C below the melting point of pure copper.

The increase in recrystallization temperature is also manifested in the retention of yield strength after an anneal of 1 hr at 400°C for these alloys. Cold worked pure copper, on the other hand, softens completely at about 200°C. Of interest is the change in yield strength of these alloys without a significant change in the ultimate tensile strength.

Probably the most important data are found in the creep rupture tests. Whereas most of the oxide containing alloys which were tested at 250°C showed the desirable flat slopes which indicate time-temperature-stress stability, see Fig. 5, the silica additions, which were of coarse size, did not sustain this slope out to long times and a break resulted in the curves, indicating a structure instability (probably recrystallization). The alloy with 0.3μ Al_2O_3 (29*A* Al-10 fine), on the other hand, showed the desired stability and strength up to 450°C and up to 1000 hr, see Fig. 6. The measured high recrystallization temperature, see Fig. 2, and the apparently transcrystalline fracture at 450°C both attest to the desirable properties. The flatness of slope noted in Fig. 6 over the entire test temperature range for this alloy clearly demonstrates that the mechanical mixing of metal and oxide powders,

Fig. 9—Intercrystalline fracture of —200 mesh copper plus 3 pct -10μ silica (14*A* Si-3). Test temperature, 250°C; stress, 12,000 psi; life, 2218 hr. Etched with $K_2Cr_2O_7$. X500. Reduced approximately 10 pct for reproduction.

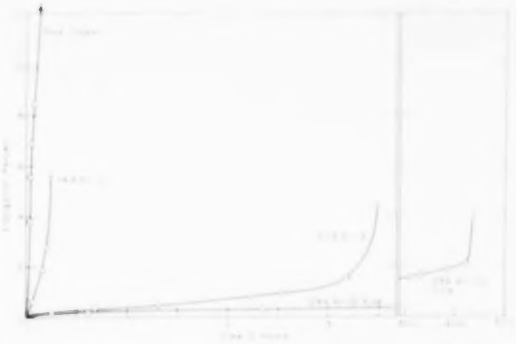

Fig. 10—Creep curves at 350°C and 15,000 psi; the curve for the 29*A* Al-10 fine is at 17,000 psi.

followed by compaction, sintering, and extrusion, can produce alloys with properties similar to those of the SAP-type Al-Al_2O_3 alloys.

The major problem encountered in this program was the inability in these early trials to attain uniform mixing of metal and oxide. This is clearly illustrated in Figs. 3, 4, and 7. Yet, in spite of this difficulty, alloys were produced which showed useful high temperature strength and unusual stability on exposure to temperature and stress for long periods of time.

The role of extrusion and the extrusion ratio could not be accurately determined either on the strength and ductility values or on the oxide distribution.

Whereas it has been postulated that a very fine metal powder must be used to achieve high temperature strength, the present work indicates that large increases in strength and stability can be achieved with relatively coarse metallic powders, such as —200 mesh copper.

The peculiar and unexplainable modulus of elasticity results must await more careful and extensive investigation to determine the role of the many variables involved on the elastic properties and behavior of the metal-metal oxide alloys.

Acknowledgments

The authors are very pleased to acknowledge the help of many who have contributed to this investigation of a new system of alloys, especially to Aeronautical Research Laboratory, Wright-Patterson Air Force Base, for support of this program, but also to Watertown Arsenal, Nuclear Metals Inc., and Oliver Preston. This paper is based on a portion of a thesis by K. M. Zwilsky, submitted to the Dept. of Metallurgy, Massachusetts Institute of Technology, in partial fulfillment of the requirements for the degree of Master of Science.

References

[1] R. Irman: Sintered Aluminum with High Strength at Elevated Temperatures. *Metallurgica*, 1952, vol. 46, No. 275, pp. 125-133.
[2] E. Gregory and N. J. Grant: High Temperature Strength of Wrought Aluminum Powder Products. *AIME Trans.*, 1954, vol. 200, pp. 247-252; Journal of Metals, February 1954.
[3] N. J. Grant and O. Preston: Dispersed Hard Particle Strengthening of Metals. *AIME Trans.*, 1957, vol. 209, pp. 349-360; Journal of Metals, March 1957.

Discussion of this paper sent (2 copies) to AIME by Jan. 1, 1958 will appear in AIME *Transactions* Vol. 212, 1958, and in Journal of Metals, April 1958.

Technical Note

Some Characteristics of the Martensite Transformation Of Cu-Al-Ni Alloys

by C. W. Chen

MARTENSITE transformations in β Cu-Al alloys have been studied by Greninger[1] and other investigators. According to Greninger, the parent phase β_1, an ordered body-centered-cubic structure obtained from β phase by suppressing the eutectoid decomposition, transforms into an ordered hexagonal-close-packed phase γ' in composition containing 12.9 to 14.7 pct Al. The M_s temperature decreases with increasing aluminum content; for the alloy containing 14.5 pct Al, for example, the $\beta_1 \rightarrow \gamma'$ transformation occurs below room temperature. More recently, Kurjumow[2] studied the transformation in β Cu-Al alloys with the addition of nickel. His report stimulated new interest in the subject due to the observation of completely reversible transformation without hysteresis in the transformation temperature ranging from 10° to −10°C. In the present paper some characteristics are described of the transformation of Cu-Al-Ni alloys that were partly studied by Kurjumow.

Experimental Procedure

High purity copper (99.999 pct) and aluminum (99.99 pct) and electrolytic nickel were used in the preparation, by the Bridgman technique, of single crystal specimens which contained aluminum and nickel of 14.5 and 0.5 to 3.0 pct, respectively. Polished surfaces were prepared mechanically. Specimens were then chemically etched to remove distorted material, homogenized at 1000°C for several hours, and quenched drastically to room temperature in a 10 pct NaOH bath to produce the parent phase β_1. The transformation was studied under a microscope and, in some cases, recorded by means of motion pictures. A device similar to that designed by Greninger and Mooradian[3] was used to cool and reheat the specimens.

Results and Discussion

When the specimens were cooled below room temperature, the β_1 to γ' transformation began at 10°C with the appearance of γ' crystals in relief, Fig. 1a. As the specimen temperature dropped further, the transformation continued, either by the growth of the γ' crystals, with the $\beta_1 - \gamma'$ interface moving into the β_1 phase, Fig. 1c and 1d, or by the formation of new γ' crystals, Fig. 1b. As a consequence of the former process, banded structure is observed as a common feature of the low temperature phase. According to the theory of the formation of martensite by Wechsler, Lieberman, and Read,[4] the bands of γ' phase are probably twin-related, as is the case in the diffusionless phase change of In-Tl alloys,[5] but this was not revealed by X-ray techniques. New γ' crystals, in needle form, often emerged suddenly across the γ' bands during the transformation. These acicular crystals then grew, both in length and in width, see Fig. 2a through 2d. The transformation on cooling is completed at about −35°C.

Upon heating, the reverse transformation started at −10°C, in a manner nearly opposite to the transformation on cooling, and completed at 35°C. There was no noticeable change in the transformation temperature when the nickel content was varied within the limits previously mentioned. Through control of the specimen temperature, the transformation can be started, stopped, or reversed at will. This phenomenon has frequently been observed in the martensite transformation of many nonferrous alloy systems. Other systems are Au-Cd[6] and In-Tl.[5] However, in the latter systems, the transformation is accomplished by single interface motion if the specimen composition is homogeneous and the temperature gradient in the specimen is uniform and sharp, whereas in the Cu-Al-Ni specimens, only multiple interface transformation is observed. The speed of the interface motion appears to be a function of the rate of temperature change and the temperature gradient across the specimen length. In one case, in which the temperature increased at the rate of 10°C per min and there was no temperature gradient along the specimen axis, the speed of the disappearance of a γ' plate was determined, by the study of the motion pictures made, to be 26 μ per sec.

Quench markings were observed on the polished surfaces of specimens. The markings were grouped into one or more sets of different orientations, and were parallel in each set. The γ' plates formed in subsequent transformation were parallel to the markings, indicating that the γ' plates and the quench markings had the same geometric relationship to the β_1 matrix. The quench markings on two intersecting surfaces of a specimen were therefore used in the determination of the habit plane of transformation, by the trace method suggested by Barrett.[7] Results obtained from five sets of markings in three specimens indicate that the habit plane is an irrational plane about 2° from one of the {221} planes. This is very close to the habit plane (3° from 221 planes) of β Cu-Al alloys containing more than 13.0 pct Al.[5]

The martensite transformation of Cu-Al-Ni alloys is reproducible. No sluggishness was found between consecutive transformation cycles, although a slight difference in the distribution pattern of the γ' plates was observed, compare Figs. 1d and 2d. The transformation can be strain-induced. This characteristic has been tested by a simple method. When a specimen was elastically strained slowly in a vise, γ' plates were gradually produced in the same fashion as during transformation on cooling. This test was done at room temperature, and thus above the M_s

C. W. CHEN, Member AIME, formerly with the School of Mines, Columbia University, is now with the Magnetics and Solid State Physics Dept., Research Laboratories, Westinghouse Electric Corp., Pittsburgh.

TN 396E. Manuscript, Feb. 30, 1956.

TRANSFORMATION ON COOLING

Fig. 1a —— 12.3 sec ——→ Fig. 1b —— 5.1 sec ——→ Fig. 1c —— 6.6 sec ——→ Fig. 1d

REVERSE TRANSFORMATION

Fig. 1h ←—— 6 sec —— Fig. 1g ←—— 5.1 sec —— Fig. 1f ←—— 16.1 sec —— Fig. 1e

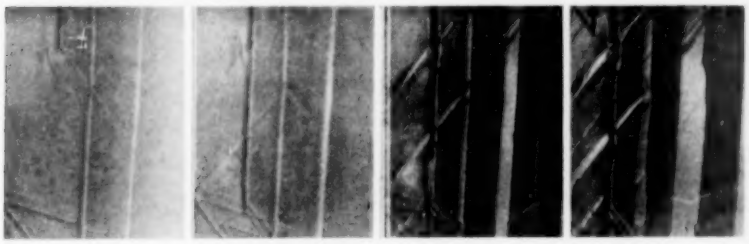

Sequence of martensite transformation on cooling and heating in a Cu-14.5 pct Al-1.5 pct Ni alloy. Crystals which appear bright in either band or needle form represent γ' phase; matrix in the dark background is the parent β_1 phase. Rate of cooling and heating: approximately 10°C per min. All micrographs are reproduced from 16 mm film taken at a magnification of X100 and an exposure speed of 8 frames per sec. Time between successive pictures is indicated above in seconds. X3.

TRANSFORMATION ON COOLING, NEXT CYCLE

Fig. 2a —— 3.1 sec ——→ Fig. 2b —— 6.9 sec ——→ Fig. 2c —— 14 sec ——→ Fig. 2d

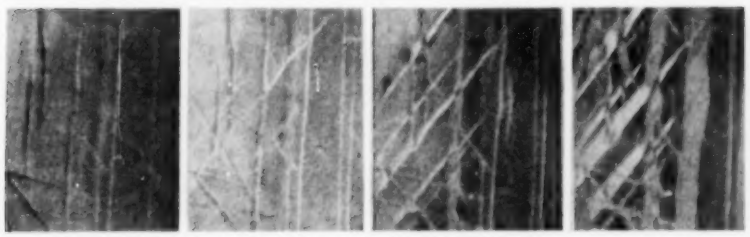

temperature for unstrained specimens. The induced γ' plates disappeared as soon as the strain was released. The strain-induced behavior of the transformation is very similar to that observed with β brass by Reynolds and Bever.[9]

Some observations are not in agreement with those of Kurjumow. For example, the temperature range for the transformation, as described above, was found to be larger in the present study than he indicated. In addition, a hysteresis of 25°C was observed in the transformation; but the complete reversibility of the transformation, as reported by Kurjumov in the sense that the reverse transformation takes place in regions where the transformation on cooling ceases was not observed in a careful study of the motion pictures of the transformation prepared in the present investigation. Not only did γ' plates other than those formed just before the cessation of transformation disappear earlier than the latter, but residual γ' plates which did not disappear even when the specimen had been heated to 100°C were observed. This incomplete reversibility was not affected by holding the specimen below M_s temperature for a period of time.

Acknowledgments

This work was supported by the Atomic Energy Commission under Contract No. AT (30-1)-904. The author wishes to thank T. A. Read for valuable suggestions and discussion.

References

[1] A. B. Greninger: *AIME Trans.*, 1939, vol. 133, p. 204; METALS TECHNOLOGY, February 1939.
[2] G. Kurjumow: *Report of the Academy of Science* USSR, 1949, vol. 66, No. 2.
[3] A. B. Greninger and V. G. Mooradian: *AIME Trans.*, 1938, vol. 128, p. 337.
[4] M. S. Wechsler, D. S. Lieberman, and T. A. Read: *AIME Trans.*, 1953, vol. 197, p. 1503; JOURNAL OF METALS, November 1953.
[5] M. W. Burkart and T. A. Read: *AIME Trans.*, 1953, vol. 197, p. 1516; JOURNAL OF METALS, November 1953.
[6] C. W. Chen and T. A. Read: To be published.
[7] C. S. Barrett: *Structure of Metals*, McGraw-Hill Pub. Co. New York, 1955.
[8] J. E. Reynolds, Jr. and M. B. Bever: *AIME Trans.*, 1952, vol. 194, p. 1065; JOURNAL OF METALS, October 1952.

Approximate Method for Calculations Using Concentration-Dependent Diffusion Coefficients

Standard methods are available for calculating the results of diffusion processes providing the diffusion coefficient is a constant. In fact, the diffusion coefficient changes radically with composition in most alloy systems and therefore the standard methods are not quantitatively applicable. It is shown that a correction can be made for the variation of the diffusion coefficient with concentration by employing a special coordinate transformation. Illustrative calculations for two types of variation of the diffusion coefficient with concentration show that the accuracy of this approximate method is of the order of 20 pct for large changes in the diffusion coefficient. The relation of the present method to that of Wagner is discussed.

by A. G. Guy, M. Golomb, and A. S. Yue

IN the course of a research on steady-state diffusion it became necessary to make diffusion calculations for a finite solid. This problem was found to be sufficiently different from the corresponding problem for the semi-infinite solid for an entirely new approach to be necessary in obtaining a useful solution. The assumption of an exponential variation of the diffusion coefficient with concentration[1] was no longer a practical necessity, so that the new solution offered the possibility of handling diffusion in semi-infinite solids for arbitrary variations of the diffusion coefficient with concentration.

In discussing the principle on which this method of calculation is based, it is convenient to consider the relatively simple problem of one dimensional diffusion into a matrix that initially contains none of the diffusing substance. The solution of the second Fick Law, $\frac{\partial C}{\partial t} = D_s \frac{\partial^2 C}{\partial x^2}$, for diffusion into a semi-infinite solid is[2]

$$\frac{C}{C_s} = 1 - \phi\left(\frac{x}{2\sqrt{D_s t}}\right) \qquad [1]$$

where C is the concentration of the diffusing substance at a depth x cm below the surface after diffusion has occurred for t seconds; C_s is the concentration of the diffusing substance at the surface of the matrix; D_s is the diffusion constant, expressed in sq cm per sec; and ϕ represents the Gauss error function.

The corresponding solution for diffusion into a finite solid of thickness, l, is conveniently written for the change in concentration, $C_{l/2}$, at a point midway through the matrix and for times, t, great enough for the following equation to be used[2]

$$\frac{C_{l/2}}{C_s} = \left(\frac{1}{2} - \frac{2}{\pi} e^{-\frac{\pi^2 D_s t}{l^2}}\right). \qquad [2]$$

In Eqs. 1 and 2 the diffusion coefficient is represented by the symbol D_s (rather than by D) to emphasize that these equations are valid only for *constant* values of D.

To understand how these equations can be modified to take account of actual variations of D, such as that shown in Fig. 1, first consider the fact that for a given time of diffusion the concentration at a given point is determined, not by the D value alone, but by the ratio $\frac{x}{\sqrt{D_s}}$ in Eq. 1 and by a similar ratio, $\frac{l}{\sqrt{D_s}}$, in Eq. 2. Even though in fact D varies, it is possible to keep this ratio constant by using a special coordinate system, x_s, that varies with D in the appropriate manner.

The necessary character of this special coordinate system can be easily visualized by imagining that

A. G. GUY, Member AIME, and M. GOLOMB are Professor of Metallurgical Engineering and Professor of Mathematics, respectively, Purdue University, Lafayette, Ind., A. S. YUE, formerly with Purdue University, is now with the Research Laboratory, Dow Chemical Co., Midland, Mich.

TP 4505E. Manuscript, July 18, 1956.

the region into which diffusion has occurred is divided into infinitesimal regions of thickness dx. At each instant the diffusion in each of these elementary regions will be determined by the ratio $\frac{dx}{\sqrt{D}}$, where D is the value of the diffusion coefficient for the concentration at the region being considered. Consider that in the fictitious x_o coordinate system corresponding infinitesimal regions are set up so that for every region dx, there is a corresponding region dx_o of such thickness that

$$\frac{dx}{\sqrt{D}} = \frac{dx_o}{\sqrt{D_o}} \qquad [3]$$

where D_o is a constant reference value of the diffusion coefficient, such as the value for diffusion in extremely dilute solution. Eq. 3 may now be solved for any value of x

$$x = \int^{x} dx = \int^{x_o} \sqrt{\frac{D}{D_o}}\, dx_o \qquad [4]$$

where the indicated integration is conveniently done graphically, as illustrated below.

The above method is only an approximate one, and it would be possible to show by a mathematical analysis to what degree it approximates the rigorous solution. However, a clearer picture of the usefulness of the method is given by typical examples of its application. Its use in determining a concentration-distribution curve for diffusion into a semi-infinite solid may be illustrated by a calculation for the diffusion of zinc into copper. The steps in the calculation are: 1) determining the curve of C vs (fictitious) x_o that would be produced if the diffusion coefficient were constant at D_o, the value characteristic of 0 pct Zn in copper; 2) using this curve in connection with the actual variation of D with concentration to find x as a function of x_o; and 3) converting the curve of step 1 from a plot of C vs x_o to a plot of C vs the actual distance coordinate, x. Note that x is conveniently replaced by the dimensionless quantity $\frac{x}{\sqrt{D_o t}}$ in the following example.

Consider the diffusion of zinc into copper at 855°C (1571°F) from a vapor that maintains a zinc concentration of 2.56 g per cu cm (30 wt pct) at the surface of the copper. If the reference (constant) D_o is chosen to be the value of D in a dilute solution of zinc in copper, then from Fig. 1

$$D_o = 1.0 \times 10^{-7} \text{ sq cm per sec.} \qquad [5]$$

Table 18-1 in ref. 3 can be used to obtain the data for the curve of C vs $\frac{x_o}{\sqrt{D_o t}}$. These data are tabulated in the first two columns of Table I.

The next step is to plot $\sqrt{\frac{D}{D_o}}$ vs $\frac{x_o}{\sqrt{D_o t}}$ as a means for evaluating the integral of Eq. 4. The values of D corresponding to the C values in Table I were found using Fig. 1. These are tabulated along with the $\sqrt{\frac{D}{D_o}}$ values in Table I. A series of $\frac{x}{\sqrt{D_o t}}$ values determined by graphical integration are listed in the last column.

Fig. 2 is a comparison of the concentration-distribution curve obtained by this approximate method with the one determined by Wagner's method. The latter curve is based on an exponential approximation to the diffusion data, shown by the dashed line in Fig. 1. The five points from a step by step calculation, described below, indicate that in the case being considered, Wagner's result is better in the high concentration region and the present method is better in the low concentration region.

Unlike the semi-infinite solid, for which there is essentially only one characteristic concentration-distribution curve, the finite solid has a number of concentration curves that may be of interest. Consider, for example, the diffusion of zinc into a thin copper specimen of thickness l at 855°C. Convenient boundary conditions are provided by maintaining zinc concentrations of 30 pct (2.56 g per cu cm) and 0 pct at the opposite faces of the specimen. Initially diffusion is of the semi-infinite type discussed above, but later the concentration-distribution curves are of the types shown in Fig. 3. These curves were calculated by a laborious step by step method[4] to provide a comparison for the results obtained by the present more convenient approximate method.

The problem of principal interest was the determination of the time, t_s, necessary to reach the steady-state concentration distribution. An analysis similar to that employed for the semi-infinite solid was used to determine the fictitious dimension, L_o, that would require the same time to reach the steady-state assuming a constant diffusion coefficient, D_o, as is required by the true dimension, l, for

Table I. Data Used in Obtaining a Concentration-Distribution Curve for the Diffusion of Zinc into a Semi-Infinite Copper Bar at 855°C (1571°F).

$\frac{x_o}{\sqrt{D_o t}}$	C, G per Cu Cm	$D \times 10^7$, Cm Sq per Sec	$\sqrt{\frac{D}{D_o}}$	$\frac{x}{\sqrt{D_o t}} = \int^{x_o} \sqrt{\frac{D}{D_o}}\, \frac{dx_o}{\sqrt{D_o t}}$
0	2.56	36.6	6.05	0
0.1	2.41	31.0	5.56	0.58
0.2	2.27	25.8	5.08	1.11
0.3	2.13	21.2	4.60	1.60
0.4	1.99	17.0	4.13	2.03
0.6	1.72	10.0	3.16	2.76
0.8	1.46	6.0	2.45	3.32
1.0	1.23	4.0	2.00	3.77
1.2	1.02	2.8	1.67	4.14
1.4	0.83	2.1	1.45	4.45
1.6	0.66	1.7	1.30	4.72
1.8	0.52	1.4	1.18	4.97
2.0	0.40	1.3	1.14	5.20
2.4	0.23	1.2	1.10	5.65
2.8	0.12	1.1	1.05	6.08
3.2	0.06	1.0	1.00	6.49
3.6	0.03	1.0	1.00	6.89
4.0	0.01	1.0	1.00	7.29
4.8	0.00	1.0	1.00	8.09

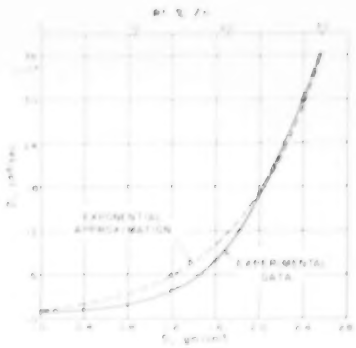

Fig. 1—Variation of the diffusion coefficient with concentration in the Cu-Zn system at 855°C (1571°F). The experimental data are replotted from Horne and Mehl.[2]

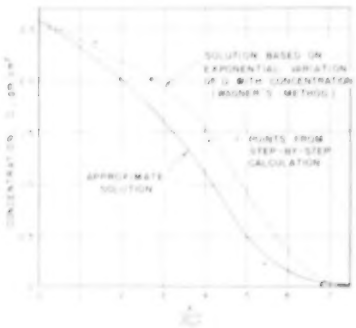

Fig. 2—Concentration-distribution curve obtained by the present approximate method. A curve obtained by Wagner's method and five points from a step by step calculation are shown for comparison.

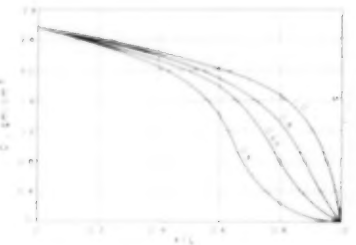

Fig. 3—Concentration-distribution curves at 0.5, 0.65, 0.8, and 1.0 t_s, where t_s is the time required for first reaching the steady-state condition.

the actual concentration-dependent diffusion coefficient, D. Using the dimension L, a calculation involving D_c was made according to Eq. 2 to determine t_s. The steps involved in this calculation were the following.

1) The curve of concentration vs distance that exists under steady-state conditions was determined from the known data on the variation of the diffusion coefficient with concentration.[2] Under steady-state conditions the flux, K, of zinc through the specimen is constant and, therefore, for the steady-state condition, the following equation holds.

$$\int^{C} dx = -\frac{1}{K}\int^{C} D\,dC \qquad [6]$$

Graphical integration of this equation gave the desired curve.

2) A plot was made of $\sqrt{\frac{D_c}{D}}$ vs $\frac{x}{l}$, and L was determined as the area under this curve, Eq. 4, expressed as a fraction of l. In the present example, $L = 0.278l$.

3) Since a suitable criterion of achievement of the steady-state condition is that the concentration at the midpoint of the specimen should have attained the steady-state value to within 1 pct, Eq. 2 was written

$$\frac{0.99}{2} = \frac{1}{2} - \frac{2}{\pi}\,e^{-\frac{\pi^2 D_c t_s}{(0.278l)^2}} \qquad [7]$$

For $D_c = 1 \times 10^{-7}$, this equation gave $t_s = (3.8 \times 10^{7})\,l^2$. The corresponding result calculated by the step by step method was $t_s = (4.3 \times 10^{7})\,l^2$.

A consideration of the approximations involved in the procedure used above showed that errors of opposite sign had largely cancelled one another. However, in most systems the curve of D vs concentration is analogous to the one considered here and similar cancellation would be expected to occur. As a more conclusive test of the general applicability of the method, it was applied in a case where the variation of D with concentration was radically different from that in the Cu-Zn system. The diffusion data used for this purpose were adapted from the results on the Cu-Au system quoted by Birchenall[6] in which the diffusion coefficient goes through a maximum. The time to reach the steady-state condition was calculated by the approximate method described in the section above and was found to be $(2.35 \times 10^{7})\,l^2$, while the step by step solution gave a value of $(2.0 \times 10^{7})\,l^2$. Again, the agreement between the two values was satisfactory, being within 20 pct.

Conclusions

The present approximate method permits a correction to be made for the variation of the diffusion coefficient with concentration, using equations that apply for a constant D value. Since D values typically vary by about a factor of ten, it is useful to be able to take this variation into account in a reasonably quantitative manner. In the case of the Cu-Zn system, which was used for the principal illustration here, the time to reach the steady-state condition was estimated to within about 20 pct by the present method, even though the diffusion coefficient varies thirty seven fold over the concentration range involved.

Concentration-distribution curves describing diffusion into a semi-infinite solid can also be obtained with comparable accuracy for actual variations of the diffusion coefficient with concentration. However, in those instances in which the variation of the diffusion coefficient is almost exponential, the latter calculation can be made more rigorously and more conveniently by Wagner's method.

Acknowledgment

This research was supported by the United States Air Force through the Air Force Office of Scientific Research of the Air Research and Development Command under Contract No. AF 18(600)1463.

References

[1] Carl Wagner: On the Solution of Diffusion Problems Involving Concentration-Dependent Diffusion Coefficients. *AIME Trans.*, 1952, vol. 194, p. 91; JOURNAL OF METALS, January 1952.

[2] G. T. Horne and R. F. Mehl: Mobilities in Diffusion in Alpha Brass. *AIME Trans.*, 1955, vol. 203, p. 88; JOURNAL OF METALS, January 1955.

[3] L. S. Darken and R. W. Gurry: Physical Chemistry of Metals, p. 443. McGraw-Hill Book Co. Inc. New York, 1953.

[4] R. M. Barrer: *Diffusion In and Through Solids*, p. 15. Cambridge University Press. Cambridge, 1951.

[5] A. G. Guy: Interstitial Diffusion. *ASM Trans.*, 1952, vol. 44, p. 382.

[6] C. E. Birchenall: Volume Diffusion—an Empirical Survey. *ASM Trans.*, 1951, vol. 43A, p. 122.

Discussion of this paper sent in 2 copies to AIME by Jan. 1, 1958 will appear in AIME *Transactions* Vol. 212, 1958, and in JOURNAL OF METALS, April 1958.

Diffusion of the Elements of the IB and IIB Subgroups in Silver

Data are given for the diffusion of the elements of the IB and IIB subgroups in single crystals of silver. With the exception of those for mercury in silver, the data indicate that the activation energies for diffusion of the atoms of a given subgroup in the same solvent are similar, but the frequency factors differ. From this, it is concluded that atomic size, provided solid solutions are formed, probably does not affect the activation energy. The relation of the present results to several of the more popular generalizations concerning diffusion is discussed.

by A. Sawatzky and F. E. Jaumot, Jr.

IT as long been recognized that there is a need for accurate systematic data on diffusion in solids. Originally, such data were needed to check existing theories but, more recently, it would appear that it could be used most advantageously as a guide to, or a check for, much needed extensions of the theory of diffusion. The awareness of the conditions which are important to experimental accuracy, the availability of the materials for accurate experiments, and the techniques have improved to the extent that it would now seem to an experimentalist that, unless extensions of the theory are made which take into account the fundamental parameters of the atoms, the electrons, and the lattice in some detail, the field of diffusion will rapidly become an empirical or semi-empirical field.

The present series of experiments was designed to provide accurate data on the diffusion of the elements of the IB and IIB subgroups in silver; that is, to provide data on the diffusion in silver of three face-centered-cubic elements with roughly similar chemical properties, but with different atomic or ionic sizes and, similarly, for three noncubic elements. The elements of these two subgroups have different valences, so that the data will not give any significant information on differences due to the crystal structure of the solute.

The present paper reports data on the diffusion of copper and mercury in single crystals of silver; the data for the other elements of the IB and IIB subgroups were reported previously by the authors[1,2] and by Tomizuka and Slifkin.[3]

Experiment

The general technique used was identical to that previously described[1,2] and will not be repeated here. In all cases, the sectioning technique and high specific activity isotopes* were used.

* Obtained from Oak Ridge National Laboratories.

The short half-life of Cu^{66} made decay corrections more important than for the other isotopes, and necessitated *around the clock* shifts while data were being taken. Each section was counted at least twice (as was true for all longer half-life isotopes) and a monitor was counted along with each sample.

Data for the diffusion of mercury in silver are presented at a greater number of temperatures than for the other solutes. This is a result of two circumstances. First, six (of 30) samples had to be discarded because of pitting or recrystallization which occurred during the diffusion runs, even though the samples had sustained high temperature prediffusion anneals. Either of these was a very rare phenomenon in the other experiments, and their occurrence in this case is considered in more detail below. Second, the curves of the logarithm of the activity of the sections vs the square of the penetration depth† were, in general, quite good, but frequently seemed to show one point to have high activity and the next point to have slightly low activity in terms of the best straight line. When this occurred, there was remarkable regularity of the high-low sequence. In any event, the results, as far as diffusion coefficients are concerned, were not affected by this *amalgam* effect. In fact, the mercury data had the highest internal consistency of any of the data.

† The diffusion coefficient is obtained from the slopes of these curves by a least-squares method.

Results

Diffusion of Copper in Silver—Diffusion runs were made at eight temperatures in the temperature range from 700° to 950°C, for times ranging from 5 to 45 hr. A linear curve of the logarithm of the activity vs the square of the penetration depth was obtained for all samples. Table I summarizes the results for individual samples and Fig. 1 gives a plot of the logarithm of the diffusion coefficients as

A. SAWATZKY is associated with The Franklin Institute Laboratories for Research & Development, Philadelphia. F. E. JAUMOT, JR., Member AIME, formerly with The Franklin Institute Laboratories for Research & Development, is now Director, Research and Engineering Semiconductors, Delco Radio Div., General Motors Corp., Kokomo, Ind.

TP 4591E. Manuscript, Nov. 7, 1956.

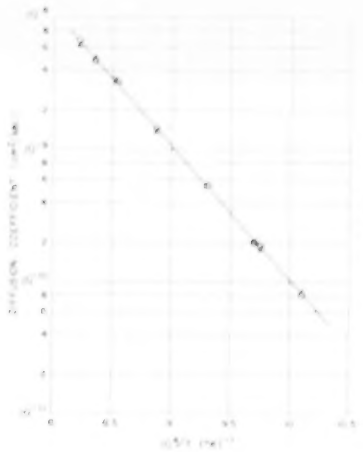

Fig. 1—Data for diffusion of copper in silver, plotted as log D vs $1/T$.

a function of the reciprocal of the absolute temperature.

The activation energy, Q, and the frequency factor, D_0, were obtained from a least-squares fit of the data of Fig. 1. With an estimated probable error of ±4 pct in D, ±2 pct in Q, and as much as 20 pct in D_0, the data may be represented by

$$D = 1.23 \exp(-46{,}100/RT) \text{ sq cm per sec.} \quad [1]$$

The accuracy of these data is not as good as that for zinc or mercury, probably due to the difficulties introduced by the short half-life of the copper isotope. The average difference in values of D obtained at a given temperature is slightly more than 2 pct, with by far the greatest contribution (6.3 pct) coming from the highest temperature data. The mean deviations from the values given by Eq. 1 are less than 2 pct, with a maximum deviation of about 4 pct.

Diffusion of Mercury in Silver—Diffusion runs were made at thirteen temperatures in the temperature range from 650° to 950°C, for times ranging from 6 to 360 hr. Only linear curves of lnC vs x^2 were obtained. Table II summarizes the data for the individual samples and Fig. 2 gives a plot of ln$D$ vs $1/T$.

A least-squares fit of the data in Fig. 2 indicates the data is well represented by

$$D = 0.079 \exp(-38{,}100/RT) \text{ sq cm per sec.} \quad [2]$$

The internal consistency (we hesitate to call it accuracy) of these data can only be described as remarkable and probably fortuitous. The average difference in the values of D obtained from different samples at the same temperature is 0.47 pct, with no difference being as great as 1 pct. The mean deviation of the individual points from the values calculated from Eq. 2 is less than 1 pct. In spite of the apparent accuracy of the data, no better than ±2 pct in D, ±0.5 pct in Q, and perhaps ±10 pct in D_0 is claimed.

Discussion

Fig. 3 and Table III summarize the recent experimental results for diffusion of elements of the IB and IIB subgroups in silver. Also included in the table are some previous results on similar systems. Finally, Table III gives the values of D_0 and Q calculated, using Zener's theory[7] and Nowick's method,[8] respectively. The calculated values are, in general, in good agreement with the recent data, the only real departures coming for the high atomic number solutes, gold and mercury.

The recent data support the now generally accepted idea that for solute diffusion in very dilute solutions, the values of D_0 and Q should not differ as greatly from those for self-diffusion as the older data indicated. On the other hand, there seems to be no doubt that the differences which are present are significant. Thus, LeClaire's suggestion[6] that the differences might vanish at very small concentrations of solute is probably unfounded.‡ Both of these points have been discussed in more detail elsewhere.[8]

‡ From the thickness of the plated layer and the penetration depth, a maximum concentration of the solutes of 5×10^{-4} is estimated, which is within the range of the purity of the single crystals of silver. The starting material was 99.99 pct Ag from Handy and Harman.

One of the main objectives of this series of experiments was to learn more of the effects of the ionic or atomic size and the valence of the solute on the frequency factor and activation energy. There is now reliable data available on three monovalent metals (subgroup IB) of different sizes and three divalent metals (subgroup IIB) of different sizes assuming, of course, the Hume-Rothery valences.

It is seen from Fig. 3 that the plots of ln$D$ vs $1/T$ for solutes of a given subgroup tend to group together and, with the exception of the curve for mercury, they are relatively parallel within subgroups.

Thus, the data indicate that, provided solid solutions are formed, the ionic size does not appreciably affect the activation energy for diffusion, but does affect the frequency factor (valence obviously has an appreciable effect). That is, the activation energies for diffusion of silver and gold in silver are identical, and that for copper in silver is not very different. A similar situation exists for zinc and cadmium in silver, but the difference in the activation energy for mercury from that for zinc and cadmium is too great to be within experimental error. This will be discussed in more detail below. On the other hand, the frequency factors vary in accordance with Zener's theory,[7] or roughly as the Debye temperature of the solutes. This would appear reasonable, since it is expected that the vibration frequency of the solute atom would partially control the jump frequency, and the heavier the atom the lower the vibration frequency.

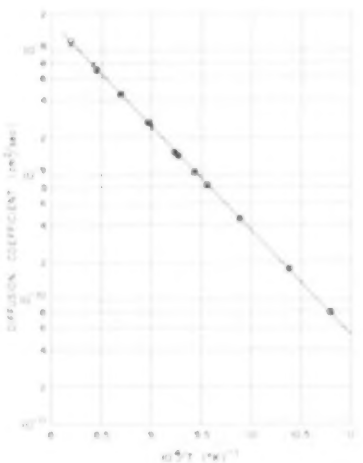

Fig. 2—Data for diffusion of mercury in silver, plotted as log D vs $1/T$.

That the activation energy is not appreciably affected by the size of the solute atom is not unreasonable from a physical point of view, but is much more tenuous on theoretical grounds. That is, it is likely, at these low concentrations, that the solute atom sees only a solvent lattice. Then, an adjacent vacancy (assuming vacancy diffusion) would tend further to reduce any effect of size so far as the energy barrier is concerned. There appear to be no good grounds for determining whether the fact that each of the solute atoms discussed here (except silver, of course) can have a smaller ionic or atomic radius‡ than the solvent atom plays an important role. It is believed that it would, on lattice strain considerations, and a similar study using copper or zinc as the solvent would be interesting.# Along these lines, however, the present data indicate that it makes no appreciable difference whether small concentrations of the solute expand or contract the lattice.

‡ All except gold have smaller ionic radii, and gold, as a pure metal, has a smaller atomic radius.

Although Mercer and Shuttleworth[6] have studied diffusion of various elements in copper (to be published), the authors do not consider it a truly similar study because of the quite different techniques used.

Lazarus[7] has given an atomistic treatment of solute diffusion in metals for cases of negligible chemical concentration gradients. Using a Thomas-Fermi approximation, he calculated the influence of impurity atoms on the Fermi electrons of the lattice. The results, applied to the data of Ref. 3, indicated that the screening terms are sufficient to explain the magnitude and direction of the observed deviation from self-diffusion in silver.

Table I. Summary of Data for Diffusion of Copper in Silver

Sample No.	Temperature, °C	Time, Sec x10⁻⁴	D, Sq Cm per Sec
1	944.5	1.80	6.334×10^{-9}
2	944.5	1.80	6.740×10^{-9}
3	925	2.19	4.922×10^{-9}
4	925	2.19	4.710×10^{-9}
5	899	3.06	3.371×10^{-9}
6	899	3.06	3.327×10^{-9}
7	854.5	3.99	1.395×10^{-9}
8	854.5	3.99	1.435×10^{-9}
9	804	7.56	5.429×10^{-10}
10	804	7.56	5.386×10^{-10}
11	758	9.39	2.039×10^{-10}
12	758	9.39	2.016×10^{-10}
13	752	11.84	1.838×10^{-10}
14	752	11.84	1.860×10^{-10}
15	716.5	16.05	8.354×10^{-11}
16	716.5	16.05	8.253×10^{-11}

Table II. Summary of Data for Diffusion of Mercury in Silver

Sample No.	Temperature, °C	Time, Sec x10⁻⁴	D, Sq Cm per Sec
1	947.5	2.34	1.188×10^{-8}
2	947.5	2.34	1.202×10^{-8}
3	916	3.06	7.690×10^{-9}
4	911	5.40	7.037×10^{-9}
5	911	5.40	7.026×10^{-9}
6	877.5	8.46	4.451×10^{-9}
7	877.5	8.46	4.411×10^{-9}
8	842	8.64	2.677×10^{-9}
9	842	8.64	2.652×10^{-9}
10	837	17.28	2.419×10^{-9}
11	809.5	14.67	1.528×10^{-9}
12	809.5	14.67	1.532×10^{-9}
13	805.5	25.92	1.472×10^{-9}
14	805.5	25.92	1.466×10^{-9}
15	787	35.82	1.075×10^{-9}
16	787	35.82	1.073×10^{-9}
17	773	17.01	8.349×10^{-10}
18	773	17.01	8.410×10^{-10}
19	738	70.38	4.484×10^{-10}
20	738	70.38	4.460×10^{-10}
21	690.5	104.59	1.760×10^{-10}
22	690.5	104.59	1.765×10^{-10}
23	653	129.78	7.923×10^{-11}
24	653	129.78	7.886×10^{-11}

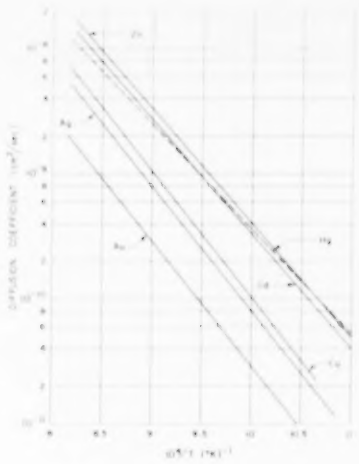

Fig. 3—Summary of results for diffusion of elements of the IB and IIB subgroups in silver.

Since the excess valence and the screening constant are the only variables of interest in the final expressions, Lazarus' treatment can be compared with experiment either by assuming an excess valence and a screening constant and computing D_0 and Q for the solute, or by using the Q obtained experimentally to determine a screening constant with which to calculate D_0.

The difficulty with this treatment is that it leads automatically to the same activation energy and same D_0 for solute and self-diffusion if solute and solvent have the same valence. Further, for the divalent elements which have the same activation energies, this treatment leads to the same value of D_0. Thus, for experiments of the present type, Lazarus' treatment has little meaning, because insufficient parameters are considered. Lazarus himself points out that the most questionable assumption he makes is that a solute atom may be represented as a solvent atom differing only in nuclear change and numbers of valence electrons.

It is tempting to explain both the diffusion results (low Q) for mercury and the tendency of the samples to pit and/or recrystallize during the diffusion anneal in terms of sensitivity to imperfections. The recrystallization and pitting could be explained logically on the basis of a high degree of segregation of mercury at dislocations, and the low activation energy could be explained by a significant contribution of dislocation diffusion to the low temperature data. However, without more direct data, these must remain only suggestions, particularly since it is difficult to imagine dislocation diffusion yielding data of such high internal consistency. Also, a valence effect can equally well be argued, in view of Lazarus' work, to account for the diffusion results.

Frequently, generalizations are found in the literature which describe the effects of various physical properties on diffusion rates. Three of the more popular ones were restated recently by Mercer and Shuttleworth[6] in connection with diffusion of various solutes in copper. These are:

1) Diffusion rates increase with increase of valence. This is the *only* generalization that appears to be more or less universally true.

Table III. Summary of Data for Diffusion of Group IB and Group IIB Elements in Single Crystals of Silver

	Recent Values*		Calculated†		Previous Work‡		
Solute	D_0, Sq Cm per Sec	Q, Kcal per Mole	D_0, Sq Cm per Sec	Q, Kcal per Mole	D_0, Sq Cm per Sec	Q, Kcal per Mole	Solute Concentration, Atomic Pct
Cu	1.23	46.1	1.66	45.7	5.9×10^{-5}	24.8	1
Ag	0.724	45.5	0.724§	44.9	0.895	45.9	0
Au	0.26	45.5	0.53	47	5.3×10^{-4}	29.8	0
					1.1×10^{-1}	26.6	18
Zn	0.54	41.7	0.54	41.7	4.4×10^{-4}	23.5	5
Cd	0.46	41.7	0.46	41.7	4.9×10^{-5}	22.35	2
					4.7×10^{-3}	31.3	0.5
Hg	0.079	38.1	0.15	39.5	—	—	—

* The values for silver and cadmium were taken from Ref. 1. The others were obtained in these laboratories.
† For the methods used, see Refs. 2 and 3.
‡ The constants involved in the theoretical expression for D_0 were adjusted so that the calculated and experimental values for self-diffusion in silver agreed.
§ These values were taken from Refs. 9 or 10. Since most of the older data were obtained with appreciable solute concentration, this information is given.

2) Diffusion rates increase with increase of size of solute. Mercer and Shuttleworth state that size appears to be more important than valence. The present experiments and those of Ref. 3 are in virtually uniform disagreement with this. Only mercury, at the lower temperatures, could be said to be in agreement.

3) The smaller the maximum solubility of the solute in the solvent, the greater the diffusion rate. The only comparison here is among copper, silver, and gold, for which the maximum solubilities in silver are 14, 100, and 100 atomic pct, respectively. At the higher temperatures, copper obeys the generalization, but at the lower temperatures it does not. The crossover of the curves for silver and copper occurs at about 260°C for copper and at about −90°C for gold. Of course, all of the group II elements have smaller solubilities in silver than silver and gold, but their higher rates are attributed to valence.

Finally, one of the more generally accepted concepts is that of a general direct correlation between Q and D_0. However, if the activation energies are similar for equivalent atoms in the same solvent, and the frequency factors are different, the validity of any general correlation must be questioned.

Acknowledgments

The authors would like to thank J. N. Bierly, J. Drew, R. L. Smith, and C. Varker for continued aid throughout this series of experiments. A. Sawatzky would like to express his appreciation to L. Muldawer of Temple University for his continued interest and encouragement. This work was supported by the U. S. Atomic Energy Commission. The paper is a portion of a thesis by A. Sawatzky submitted to Temple University in partial fulfillment of the requirements for the degree of Doctor of Philosophy.

References

1. A. Sawatzky and F. E. Jaumot, Jr.: *Physical Review*, 1955, vol. 100, p. 1627.
2. F. E. Jaumot, Jr. and A. Sawatzky: *Journal of Applied Physics*, 1956, vol. 27, No. 10, p. 1186.
3. C. T. Tomizuka and L. Slifkin: *Physical Review*, 1954, vol. 96, p. 610.
4. C. Zener: *Journal of Applied Physics*, 1951, vol. 22, p. 372.
5. A. Nowick: *Journal of Applied Physics*, 1951, vol. 22, p. 1182.
6. A. D. LeClaire: *Acta Metallurgica*, 1953, vol. 1, p. 438.
7. D. Lazarus: *Physical Review*, 1954, vol. 93, p. 973.
8. Mercer and Shuttleworth: To be published.
9. D. Kuhaschewski: *Trans. Faraday Soc.*, 1950, vol. 46, p. 713.
10. C. J. Smithells: *Metals Reference Book*, Butterworths, London, 1949.

Discussion of this paper sent (2 copies) to AIME by Jan. 1, 1958 will appear in AIME *Transactions* Vol. 212, 1958, and in JOURNAL OF METALS, April 1958.

Technical Note

Investigation Of Grain Boundary Phase In Stainless Steel

by C. C. Clark, J. R. Mihalisin, and K. G. Carroll

OBSERVATIONS made in this paper were for the purpose of exploring the anomalous behavior of a particular heat of Type 310 stainless steel. The alloy, of nominal composition 25 pct Cr, 20 pct Ni, was observed to form a grain boundary precipitate at exceedingly high rates. A sheet of this metal, 0.060 in. thick, after cooling in air from 2000°F showed the presence of the grain boundary material, whereas none was found after water-quenching from the same temperature. X-ray techniques were applied without success and, in view of the ex-

C. C. CLARK, J. R. MIHALISIN, Member AIME, and K. G. CARROLL are associated with Research Laboratory, International Nickel Co. Inc., Bayonne, N. J.

TN 401E. Manuscript, Nov. 23, 1956.

tremely small amount of embrittling phase, data were obtained through use of the electron microscope.

The electron micrographs shown in Figs. 1 and 2 reveal the striking difference in behavior between water-quenched and air-cooled specimens. Some of the thin, intergranular phase which adhered to the replica is evident in Fig. 2. In order to permit diffraction study of the phase, *extraction replicas* were prepared, in the manner reported by Fisher.[1] Relatively large amounts of the grain boundary phase were removed from the metal by this procedure. A typical example of the material is shown in Fig. 3, enlarged to 18,000 diam. In appearance the phase is quite similar to chromium carbides which were reported by Mahla and Nielsen[2] in the course of their work with bromine extractions from stainless steels. The two-dimensional nature of the carbide is apparent from Fig. 3. Visible thickness gradations suggest that the carbide is frequently thinner than 200A.

Selected area electron diffraction on the material of Fig. 3 yielded a spotty pattern which nevertheless permitted measurement of Debye-Sherrer rings. The interplanar spacings found are given in Table I and compared with X-ray diffraction data for chromium carbide and iron boro-carbide. The data establishes that the embrittling phase is structurally similar to

Fig. 1—Parlodion replica of Type 310 stainless steel sheet after water quenching from 2000°F. Germanium shadowed. Etched with electrolytic 10 pct chromic acid. X7500. Reduced approximately 50 pct for reproduction.

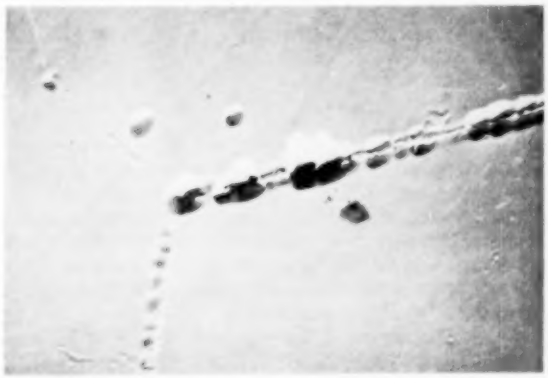

Fig. 2—Parlodion replica of Type 310 stainless steel sheet after air cooling from 2000°F. Replica prepared in the same manner as in Fig. 1. X7500. Reduced approximately 50 pct for reproduction.

Fig. 3—Parlodion extraction replica of air cooled steel, showing the structure of grain boundary material. Etched with hydrochloric-picric acid in methanol. X18,000. Reduced approximately 50 pct for reproduction.

the complex cubic chromium carbide, $Cr_{23}C_6$. It might well contain boron which is known to stabilize the related structure, $Fe_{23}(C,B)_6$.[3]

Chemical analysis of the steel indicated a boron concentration of about 0.001 pct by weight. Subsequent work on other heats of the steel indicated that the quantity of network phase formed during cooling is sensitive to the concentration of boron. Inasmuch as the network forms during the short time in which the steel cools through the temperature range of carbide formation, it is suggested that boron here behaves as a powerful catalyst to carbide formation. In view of the possibility of chromium substitution for iron in this structure, it may be that the first precipitate to form is the boro-carbide $(Cr,Fe)_{23}(B,C)_6$ which, in turn, nucleates $Cr_{23}C_6$, the carbide generally found in stainless steels.

Table I. Electron Diffraction Pattern, 100 Kv, Electrons, of Material shown in Fig. 3

Interplanar Spacing, *d*, A	Chromium Carbide, $Cr_{23}C_6$,[3] *d*, A*	Iron Boro-carbide, $Fe_{23}(B,C)_6$,[4] *d*, A*
		3.187 W
		3.055 W
2.67		2.644 W
2.42	2.389 MS	2.367 S
2.20	2.172 M	2.161 S
2.08	2.048 S	2.037 VS
1.91	1.882 M	1.872 S
1.82	1.800 M	1.792 S
		1.765 M
1.70	1.683 W	1.674 VW
		1.613 W
1.62	1.605 MW	1.595 MW
1.50		1.466 VW
1.36		1.325 W
1.31	1.291 M	1.284 W
1.26	1.255 MS	1.248 M
1.24	1.229 M	1.222 M
1.20		1.183 W
1.17	1.168 M	1.162 W
		1.111 W
1.09	1.086 S	1.082 M

* S stands for strong, M, medium; W, weak; and V, very.

References

1. R. M. Fisher: Special Publication No. 155, p. 49. ASTM, Philadelphia, 1953.
2. E. M. Mahla and N. A. Nielsen: Carbide Precipitation in Type 304 Stainless Steel—An Electron Microscope Study. *ASM Trans.*, 1951, vol. 43, pp. 290-313.
3. H. J. Goldschmidt: Interplanar Spacings of Carbides in Steels. *Metallurgica*, 1949, vol. 40, p. 103.
4. K. G. Carroll, L. S. Darken, E. W. Filer, and L. Zwell: A New Iron Boro-Carbide. *Nature*, 1954, vol. 174, p. 978.

Elastic Properties of Yttrium and Eleven Of the Rare Earth Elements

by J. F. Smith, C. E. Carlson, and F. H. Spedding

ELASTIC constants of yttrium and eleven of the rare earth elements have been measured. This has been accomplished by measuring the propagation velocities of ultrasonic pulses. The velocity measurements were made by noting the elapsed time between an applied pulse and the appearance of successive echoes. The pulse-echo technique has become relatively common, and the basis of the measurement is outlined in several standard tests, e.g., Heuter and Bolt.[1]

Two important assumptions are made when using this method for the determination of elastic moduli. First, the pulse is assumed to propagate as a plane wave. To justify this assumption, the cross section of the test specimen should be large compared to the wave length of the transmitted pulse. For these measurements on the rare earth elements the minimum cross section wave length ratio was about 20. A second assumption which must be made when using polycrystalline specimens is that the grains are sufficiently numerous and randomly oriented so that the specimen may be approximated as elastically isotopic. The grain size in the as-cast specimens which were used is believed to be sufficiently fine for this approximation, and the degree of preferred orientation is believed to be small. Supporting this viewpoint is the fact that elasticity measurements by the pulse-echo technique on as-cast specimens of other metals give results which are in satisfactory agreement with values obtained by other techniques. Hence, it is believed that the measured elasticity values for the rare earth elements are not apt to be seriously in error due to the assumption of elastic isotopy.

The apparatus used in this determination was a modified Sperry Reflectoscope with a precisely calibrated time base circuit. Piezoelectric transducers were used both to generate the pulse and to detect the echoes. X-cut quartz crystals were used for the longitudinal modes, and Y-cut quartz crystals were used for the shear modes. Frequencies of 2.25 and 5 megacycles per sec were employed. Most of the specimens were 2.5 to 5.0 cm in length.

Results

Table I is a tabulation of the measured propagation velocities of longitudinal waves and of shear waves, together with densities obtained by Spedding, Daane, and Herrmann[2] from lattice parameter measurements. The shear modulus, Poisson's ratio, and Young's modulus were calculated from the data in Table I through use of the following relationships:

$$\mu = \rho v_s^2 \qquad [1]$$

$$\sigma = \frac{2 - (v_s/v_l)^2}{2\,[1 - (v_s/v_l)^2]} \qquad [2]$$

and

$$Y = 2\mu\,(1 + \sigma) \qquad [3]$$

where μ is the shear modulus, Y is the Young's modulus, σ is Poisson's ratio, ρ is the density, v_l is the longitudinal wave velocity, and v_s is the shear wave velocity. The calculated quantities are shown in Table II.

Compressibility values can be computed from the relationship

$$\beta = \frac{3(1 - 2\sigma)}{Y} \qquad [4]$$

and the computed values may be compared with measured values obtained by Bridgman.[3] Table III lists the data for such a comparison. The agreement is satisfactory, being particularly good for neodymium and gadolinium, poor for samarium, and intermediate for the other elements. Some variation is expected since Bridgman's measurements are isothermal, whereas the present measurements are adiabatic. In addition there may be some effect due to small variations in purity. Though most of the rare earth metals measured by Bridgman and all of the metals used in the present measurements were prepared at this laboratory, minor purity variations might exist since the samples came from different lots. Also, any imperfections such as dislocations, vacancies, voids, grain boundaries, microcracks, etc., should contribute to the volume change of a com-

Table I. Measured Values for Sonic Velocities in Yttrium and Some of the Rare Earths

Element			Sonic Velocity x 10⁻⁵ Cm per Sec	
No.	Symbol	Density, G per Cu Cm	Longitudinal Wave	Shear Wave
39	Y	4.472	4.280 ± 0.021	2.420 ± 0.018
57	La	6.612	2.751 ± 0.006	1.501 ± 0.002
58	Ce	6.768	2.390 ± 0.020	1.332 ± 0.011
59	Pr	6.769	2.660 ± 0.011	1.476 ± 0.016
60	Nd	7.007	2.718 ± 0.006	1.438 ± 0.013
62	Sm	7.540	2.702 ± 0.004	1.292 ± 0.017
64	Gd	7.868	2.951 ± 0.003	1.682 ± 0.002
65	Tb	8.253	2.920 ± 0.009	1.661 ± 0.002
66	Dy	8.536	2.958 ± 0.006	1.724 ± 0.009
67	Ho	8.799	3.039 ± 0.011	1.742 ± 0.004
68	Er	9.058	3.082 ± 0.004	1.808 ± 0.006
70	Yb	6.959	1.820 ± 0.012	0.999 ± 0.001

J. F. SMITH, Member AIME, is with Ames Laboratory, Institute for Atomic Research, Iowa State College. C. E. CARLSON, formerly with Ames Laboratory, Iowa State College, is now with Pratt and Whitney Corp., East Hartford, Conn. F. H. SPEDDING is with Ames Laboratory, Institute for Atomic Research, Iowa State College, Ames, Iowa.

TP 4502E. Manuscript, Feb. 12, 1957.

pressed sample as determined by Bridgman, but these imperfections should affect only the attenuation of sonic waves and not the velocity through the crystal lattice.

Discussion

The compressibility is the reciprocal bulk modulus and is a measure of the interatomic forces resisting volume changes. The shear modulus is a measure of the interatomic forces resisting deformation of shape at constant volume. The compressibility and shear modulus thus give complementary information about the binding forces in solids. Compressibility and shear modulus as functions of atomic number are plotted in Figs. 1 and 2, respectively. In both plots there is an approximately linear increase in bond strength with atomic number. This could indicate a small contribution of the 4*f* electrons to the bonding but, more probably, it is due to an increasing strength of interaction between the core and the bonding electrons due to increasing nuclear charge.

From the graphs it can be seen that lanthanum (57), samarium (62), and ytterbium (70) deviate significantly from the linear trend in shear modulus, while cerium (58) and ytterbium (70) deviate appreciably from the linear trend in compressibility. These deviations seem to be correlated with crystal structure. Most of the rare earth elements crystallize at room temperature in the ordinary, double-layered hexagonal-closest-packed structure, but the elements noted above all crystallize in other structures. Cerium has been reported[1] to crystallize in both the hexagonal-closest-packed and face-centered-cubic structures, but the metal used in these measurements was the face-centered-cubic modification. Samarium crystallizes with a hexagonal

Table II. Elastic Moduli Calculated From Measured Sonic Velocities

Element No.	Element Symbol	Young's Modulus x 10⁻¹¹ Dynes per Sq Cm	Shear Modulus x 10⁻¹¹ Dynes per Sq Cm	Poisson's Ratio
39	Y	6.63	2.62	0.265
57	La	3.84	1.49	0.288
58	Ce	3.00	1.20	0.248
59	Pr	3.52	1.35	0.305
60	Nd	3.79	1.45	0.306
62	Sm	3.41	1.26	0.352
64	Gd	5.62	2.23	0.259
65	Tb	5.75	2.28	0.261
66	Dy	6.31	2.54	0.243
67	Ho	6.71	2.67	0.255
68	Er	7.33	2.96	0.238
70	Yb	1.78	0.70	0.284

structure which has peculiar layering[2] of close-packed planes. Ytterbium crystallizes with the face-centered-cubic structure. Europium, which was not

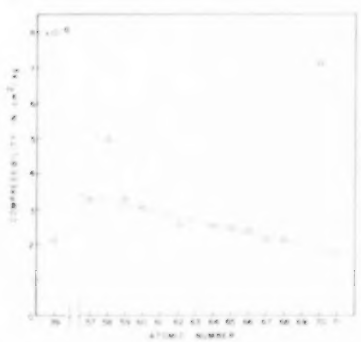

Fig. 1—Compressibility plotted against atomic number for the rare earth elements.

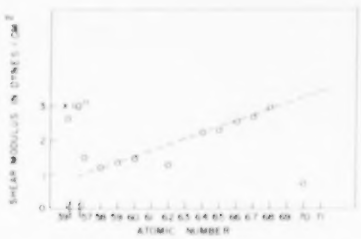

Fig. 2—Shear modulus plotted against atomic number for the rare earth elements.

measured, crystallizes with the body-centered-cubic structure. Ytterbium and europium would be expected to have abnormally weak bonding since chemical evidence indicates that these two elements tend to fill and half-fill, respectively, the 4*f* electronic states at the expense of the 5*d* and 6*s* states.

Lanthanum, praseodymium, and neodymium crystallize with a structure closely related to hexagonal-closest-packed. In this structure the basal planes are layered *ABACABAC* instead of the usual *ABABAB*; the unique lattice parameter and the unit cell are twice as large as the ordinary hexagonal-

Table III. Compressibility Values

Element No.	Element Symbol	Compressibility x 10⁶ Sq Cm per Kg: These Data, Adiabatic	Compressibility x 10⁶ Sq Cm per Kg: Bridgman, Isothermal
39	Y	2.09	—
57	La	3.24	3.9
58	Ce	4.95	4.7
59	Pr	3.28	3.7
60	Nd	3.02	3.0
62	Sm	2.56	3.5
64	Gd	2.52	2.5
65	Tb	2.45	—
66	Dy	2.39	2.6
67	Ho	2.14	2.5
68	Er	2.11	2.5
69	Tm	—	2.6
70	Yb	7.12	7.5
71	Lu	—	2.3

closest-packed structure. However, praseodymium and neodymium both follow the linear trends closely in compressibility and shear modulus. Hence, it may be that the high shear modulus of lanthanum is due to oxygen contamination. Oxygen removal from lanthanum is particularly difficult.

Yttrium (39) is shown in the plots because of its chemical similarity to the rare earths, even though it is not properly a member of the lanthanide series. The yttrium value projects on the compressibility trend at about element 68 and on the trend in shear modulus at about 66.5. The binding forces in yttrium might therefore be expected to be intermediate between rare earth elements 66 and 68.

Acknowledgments

The authors are indebted to J. E. Powell and his group for separating the pure rare earth oxides and to A. H. Daane and his group for preparing the metal specimens.

References

[1] T. F. Heuter and R. H. Bolt: *Sonics*, p. 323, John Wiley & Sons Inc., New York, 1955.

[2] F. H. Spedding, A. H. Daane, and K. W. Herrmann: *Acta Crystallographica*, 1956, vol. 9, p. 559.

[3] P. W. Bridgman: *Proceedings* Am. Academy of Arts and Sciences, 1954, vol. 83, p. 1.

[4] M. C. Udy: *Reactor Handbook*, 1955, vol. 3, chapter 1.16, p. 243, U. S. Atomic Energy Commission, Washington, D. C.

[5] A. H. Daane, R. E. Rundle, H. G. Smith, and F. H. Spedding: *Acta Crystallographica*, 1954, vol. 7, p. 532.

Discussion of this paper sent (2 copies) to AIME by Jan. 1, 1958 will appear in AIME *Transactions* Vol. 212, 1958, and in JOURNAL OF METALS, April 1958.

Mechanism of Precipitation in a Cu-2.5 Pct Fe Alloy

The precipitation process in a Cu-2.5 pct Fe alloy was studied experimentally by means of X-ray diffraction and hardness measurements and light and electron microscopic observations. It was concluded that γ-Fe and α-Fe precipitate simultaneously, γ-Fe dominating in the early stages. During later stages, the particles of γ-Fe dissolve, providing the copper lattice with iron atoms which diffuse to the more stable α-Fe particles. The α-Fe particles continue to grow until all evidence of the γ-Fe is gone.

by J. B. Newkirk

IN 1939 Bitter and Kaufmann[1] suggested that iron, precipitating from a copper-rich, Cu-Fe solid solution, appears initially as coherent particles of γ-Fe which transform to the body-centered-cubic form of iron when the alloy is cold worked. Since then there has been considerable discussion, supported only by indirect evidence, regarding the validity of the concept. For example, Reekie, Hutchison, and Hetherington[2] interpreted the changes in electrical resistance accompanying the aging of Cu-Fe specimens in terms of a coherent γ-Fe precipitate which transformed to the incoherent α-phase during long aging or cold working. Greninger[3] found that Cu-Fe alloys which had been water quenched from 1050° and then held at 650°C for 3 hr changed from weakly to strongly ferromagnetic as the aged wire was subsequently cold worked. He also found diffraction lines corresponding to body-centered-cubic iron in Debye-Scherrer patterns given by aged and worked specimens but lines corresponding to only one face-centered-cubic phase in specimens which had been aged but not worked. Knoppwost,[4] and later Cech and Turnbull,[5] found that aged Cu-Fe specimens showed a slight increase in ferromagnetism after they had been cooled in liquid nitrogen. Very recently Denney[6] followed the kinetics of the precipitation reaction as indicated by the saturation magnetization, hardness, and diffuse X-ray effects.

The experimental results reported by all of the authors mentioned above are readily explained in terms of the Bitter and Kaufmann concept. However, most of the evidence is indirect when used to define the structural changes involved. It was the aim of the present investigation to determine the mechanism of precipitation of iron from a Cu-Fe solid solution in the light of available published information and with additional new and more direct experimental data.

J. B. NEWKIRK, Member AIME, is associated with General Electric Research Laboratory, Schenectady.

TP 4486E. Manuscript, Sept. 19, 1956.

Experimental Method

At 1060°C copper will contain up to 3 atomic pct Fe in equilibrium solid solution.[7] The solvus slopes rapidly toward lower iron concentration, so that at 600°C only about 0.5 pct Fe remains in solution at equilibrium. Below the eutectoid temperature (850°C), the iron-rich phase in equilibrium with the copper-rich solid solution consists of body-centered-cubic α-Fe. Above 850°C the equilibrium iron-rich phase is face-centered-cubic γ-Fe.

The alloy to be studied was made by melting electrolytic iron and OFHC copper by induction under vacuum in an Alundum-lined crucible. The metal was held molten for about 5 min, after which time the power was turned off and the crucible was tipped about 70° to promote directional solidification. The resulting ingot, containing 2.5 wt pct Fe by analysis, was clean, large grained, and free of gross segregation. Slices $\frac{3}{8}$ in. thick were cut from the ingot, rolled to $\frac{1}{8}$ in. in thickness, homogenized in hydrogen at 1060°C for 24 hr and, finally, quenched in cold water. Specimens for all subsequent tests were made from these slices.

Squares measuring about 1 cm on a side were cut from the slices to make specimens for studying hardness and microstructure. Wires (0.020 in.) for the Debye-Scherrer survey were drawn from $\frac{1}{8}$ in. sq rods which had been cut from the homogenized slices. Large crystals for observing diffuse X-ray diffraction effects were prepared by mechanically

abrading slices to a thickness of 0.005 in. after the final aging treatment and then etching them in dilute HNO_3 to about 0.003 in. in thickness.

All specimens to be aged were first solution treated for 1 hr at 1060°±10°C in hydrogen under a layer of at least $^1/_8$ in. of alumina. After this treatment the ceramic boat holding the specimens was removed from the furnace and its contents were dumped into a vessel containing cold water at least 12 in. deep. The solution treated specimens were handled carefully thereafter to avoid distorting them mechanically.

The specimens were aged at 600° or 700°C in small Vycor vials containing argon gas at low pressure. The longest aging treatment was 3840 hr at 700°C.

Hardness measurements were made with a Kentrall hardness testing machine using the 1/16 in. ball and 60 kg load. Since the specimen grain size was large, the average of 12 impressions is reported here. Each aging condition was represented by an individual specimen. Debye-Scherrer photographs were made with a cylindrical camera of 10 cm diam using a rotating wire specimen. Filtered copper radiation (CuK_{α_1} = 1.5405A) was used throughout the survey. The microstructure was observed on polished sections which had been etched with a dilute aqueous solution of K_2CrO_4 and H_2SO_4 or a solution of H_2O_2, KOH, NH_4OH, and water. A few specimens were etched both chemically and, after repolishing, by cathodic bombardment with ionized krypton gas, using a technique described elsewhere.[5,6] Electron microscopy was done using a standard technique in which a collodion replica of the etched section was *shadowed* with chromium and examined in transmission with a Philips EM-100 microscope at an accelerating potential of 40 kv.

Table I. Debye-Scherrer Patterns Given by Heat Treated Cu-Fe Wires

Treatment	Pattern
1050°C, 1 hr water quench	Single face-centered-cubic. Resolved doublets.
600°C, 30 min air cooled *	Single face-centered-cubic. Resolved doublets. a_o = 3.615A.
600°C, 6 hr air cooled	Single face-centered-cubic. Faint diffuse sidebands on high angle side. See Fig. 2b.
600°C, 40 hr air cooled	Single face-centered-cubic. Resolved doublets. Diffuse sidebands on high angle side. a_o = 3.616A.
600°C, 90 hr air cooled	
600°C, 600 hr air cooled	Strong face-centered-cubic (a_o = 3.616A) plus weak face-centered-cubic (a_o = 3.590A) identically oriented. See Fig. 2c.
600°C, 600 hr air cooled. Cool in liquid N_2.	Same as immediately above.
600°C, 600 hr air cooled. Cool in liquid N_2. Bent repeatedly at 20°C.	Strong face-centered-cubic copper pattern. Doublets barely resolved. Faint body-centered-cubic (a_o = 2.864A) pattern. See Fig. 2f.
700°C, 24 hr, quench	Strong sharp face-centered-cubic (copper) plus weak face-centered-cubic (γ_2-Fe) plus trace of body-centered-cubic (a_o = 2.864A). Quench distorted.
700°C, 286 hr, air cooled	Strong sharp face-centered-cubic (copper) plus weak sharp face-centered-cubic (γ_2-Fe).
700°C, 819 hr, air cooled	Strong sharp face-centered-cubic (copper) plus very weak sharp face-centered-cubic (γ_2-Fe) plus very weak sharp body-centered-cubic (α-Fe). See Fig. 2d.
700°C, 3840 hr, air cooled	Strong face-centered-cubic (copper) plus weak body-centered-cubic (α-Fe). See Fig. 2e.

* This and all subsequently listed specimens were initially solution-treated 1 hr at 1060°C and water quenched.

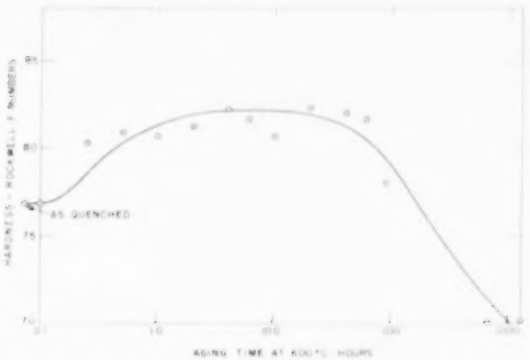

Fig. 1—After reaching a broad maximum of about Rockwell F82, the hardness gradually falls below that of the as quenched condition.

In an effort to observe diffuse X-ray scattering, thinned, partially precipitated crystals were glued to a small quartz rod and were mounted on the goniometer head of a 10 cm diam cylindrical camera. The specimen crystal was oriented so that a <110> direction was parallel to the vertical rotation axis of the goniometer. Stationary-crystal photographs were then made with the crystal in chosen positions. Unfiltered copper radiation was used to make these photographs.

Results

The results of the hardness tests using specimens aged at 600°C are given graphically in Fig. 1. Results of less complete surveys made with Cu-Fe specimens at other temperatures are also in qualitative agreement with normal age hardening behavior.

Table I summarizes Debye-Scherrer X-ray diffraction patterns given by Cu-Fe wire specimens. Six distinctly different conditions are present:

1) *Sharp coarse grained pattern corresponding to face-centered-cubic copper, with well-resolved back-reflection doublets.* See Fig. 2a. This is characteristic of the solution-treated condition prior to aging.

2) *Single coarse grained face-centered-cubic pattern, each spot of which has a diffuse sideband on the high angle side of the main line.* See Fig. 2b. This is found at relatively early stages of aging.

3) *Two coarse grained face-centered-cubic patterns of slightly different lattice parameters.* See Fig. 2c. Each spot on the intense pattern given by the copper matrix has a corresponding spot of much lower intensity on the second pattern. The corresponding spots are joined by a diffuse band. This is characteristic of intermediate stages of aging.

4) *Two coarse grained face-centered-cubic patterns as in condition 3, plus one weak body-centered-cubic pattern with continuous lines.* See Fig. 2d. This is characteristic of moderately long aging time at high temperature.

5) *One coarse grained face-centered-cubic (copper) pattern plus one fine grained body-centered-*

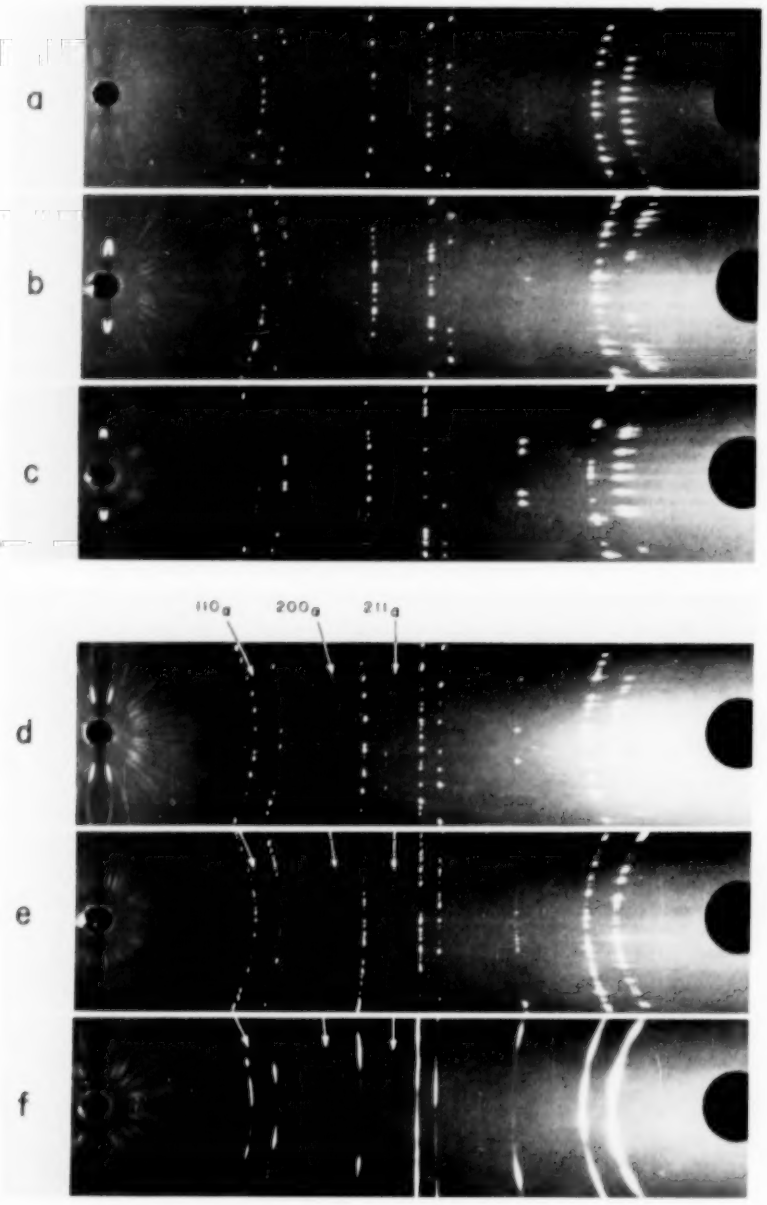

Fig. 2—Debye-Scherrer photographs given by Cu-Fe wires after the following heat treatments: a) 1060°C, 1 hr water quench (solution treatment); b) solution treated, aged 6 hr at 600°C, air cooled; c) solution treated, aged 600 hr at 600°C, air cooled; d) solution treated, aged 810 hr at 700°C, air cooled; e) solution treated, aged 3840 hr at 700°C, air cooled; and f) solution treated, aged 600 hr at 600°C, cooled in liquid N_2, plastically deformed by bending.

cubic (α-Fe) pattern. See Fig. 2e. This is characteristic of very late stages of aging.

6) *One fine grained face-centered-cubic and one fine grained body-centered-cubic pattern.* See Fig. 2f. This pattern is given by an aged specimen which had been cold worked after aging.

The diffuse X-ray scattering given by partially aged Cu-Fe single crystals in the transmission region could all be accounted for by thermal diffuse scattering and the usual Compton modified and air scattering. There was no evidence of streaks or other extra-Bragg scattering of the type sometimes given by partially ordered or precipitated[6] crystals in the transmission region of the diffraction spectrum. A crystal of annealed OFHC copper gave the same diffuse effects around low index Bragg spots as did any of the aged Cu-Fe single crystal X-ray specimens. Diffuse scattering associated with the iron precipitate was found around high angle Bragg spots. This is treated more fully in the Discussion.

Microscopic examination showed that solution treated and unaged specimens were composed of single phase copper solid solution. After aging 60 hr at 600°C, a fine precipitate, see Fig. 3, appeared throughout the grains and, in heavier concentration, at grain and incoherent twin boundaries. Precipitate particles did not form preferentially at coherent twin boundaries. At high magnification, see Fig. 4a, the fine particles appear to be pits randomly dispersed and roughly equiaxed in shape. Later in the aging process these particles are more clearly defined, Fig. 4b, and appear to have a characteristic substructure. At high magnification the surface of the etched section also occasionally showed definite ridges, the direction and height of which varied from grain to grain, Fig. 5.

Specimens which had been slowly cooled from the solution temperature to the aging temperature ultimately developed large particles which had no preferred morphology or orientation, Fig. 6a. These particles grew in size as aging progressed. On the other hand, specimens which had been quenched from the solution temperature and then reheated developed on long aging a clear Widmanstätten figure, as shown in Fig. 6b. During the late stages of aging, the fine particles of general precipitate near the grain boundaries and near the larger intragranular Widmanstätten particles apparently dissolve, as shown in Fig. 7.

Stereographic analysis of the Widmanstätten figure found in the microstructure of greatly overaged specimens shows that the precipitate particles could be explained by the presence of platelets parallel with {111} planes of a cubic (matrix) lattice. An example of this is shown in Fig. 8, which gives a stereographic analysis of the trace directions taken from Fig. 6b. This result is typical of many such analyses made with overaged Cu-Fe specimens. It was found by similar analysis that the Widmanstätten pattern in aged Cu-Co alloys[11] can also be accounted for by the presence of precipitate platelets parallel with {111} planes of a cubic lattice.

Discussion

The observed change of hardness with aging time is in qualitative agreement with the observation of Gordon and Cohen,[11] though the magnitude of the age hardening is not as pronounced. The curve in Fig. 1 is typical of age hardening alloys in that a maximum is reached after which the hardness falls below that of the original solid solution. No initial hardness decrease, which might be attributable to a decrease of iron in supersaturated solid solution, has been observed. Previous work,[6] in which an initial hardness decrease was found, is of doubtful significance since the hardness measurements were made on specimens which were approximately half the minimum recommended thickness[12] for material of this hardness.

Coherent γ Iron Precipitate—The Debye-Scherrer pattern, Fig. 2a, given by a solution treated and unaged wire shows that the specimen was coarse grained, chemically homogeneous, and free of gross strains. Patterns, Fig. 2b, containing face-centered-cubic lines with diffuse high angle side bands indicate the presence of: 1) lattice strains, 2) a coherent face-centered-cubic lattice with a lattice parameter less than that of the matrix, and 3) composition gradients or a combination of these. The high angle side bands ultimately become resolved, Fig. 2c, into distinct Debye-Scherrer spots which form a pattern corresponding to a face-centered-cubic lattice with $a_o = 3.590$A. It is proposed that this pattern is direct evidence for the existence of γ-iron as originally suggested by Bitter and Kaufmann.

The lattice parameter of the new phase is within 0.9 pct of that of the now depleted parent matrix at room temperature and furnishes a measurement by which the value of the lattice parameter of pure γ-Fe at room temperature may be estimated. According to the Fe-Cu equilibrium phase diagram,[7] the solubility of copper in γ-Fe at 700°C (the aging temperature for the specimen of Fig. 2c) is roughly 4 pct Cu. This much copper in solution would be expected to impose a Vegard expansion of 0.05 pct on the γ-Fe lattice. Subtracting this from the observed lattice parameter, a value of 3.588A is found for the parameter of pure γ-Fe at room temperature. Using this figure, the curve of a_o (γ-Fe) vs temperature, reported by Basinski et al.,[13] may be extended to room temperature, see Fig. 9. The data in Table I show that most of this face-centered iron does not transform spontaneously to α-Fe even when cooled to the temperature of liquid nitrogen.

Fig. 3—Microstructure of a specimen aged 60 hr at 600°C shows a uniform dispersion of a fine unresolvable precipitate. Potassium dicromate etch. X500. Reduced approximately 15 pct for reproduction.

Since the diffraction spots given by the new face-centered-cubic phase are sharp at intermediate stages of aging, the particles of this phase must be at least 1000A in minimum dimension. Also, since each Debye-Scherrer spot on the copper pattern is matched by a corresponding spot on the γ-Fe pattern, the two lattices must be oriented identically. It follows that, whereas each matrix Debye-Scherrer spot comes from a single copper crystal, many identically oriented precipitate crystals contribute to each of the γ-Fe spots.

The absence of precipitate-induced diffuse X-ray scattering in transmission Laue diagrams is probably due to the small difference in scattering powers of iron and copper and by the small difference in a_o of copper and γ-Fe, viz., 1.2 pct at room temperature. Thus, the diffuse figures which one might hope to see about reciprocal lattice points at early stages of aging and which are well known for some other systems are so slight in Cu-Fe alloys as to be obscured by thermal and other background scattering.

The particles seen in Fig. 4b are reminiscent of a precipitate reported by Westbrook[14] for the system Ni-Al, in which the precipitate and matrix are also both face-centered-cubic. Westbrook describes the form of the precipitate particles as *ogdoadically diced cubes* of Ni_3Al. Faced with the inability to deduce directly the form of the early γ-Fe precipitate by the available diffuse X-ray techniques, it can only be inferred, from the electron micrographs, that the γ-Fe particles are roughly equiaxed, as in the Al-Ag system.[15] In Cu-Fe precipitation there appears to be no well-defined transition structure other than the distorted face-centered-cubic lattice, part of which is held out of its equilibrium configuration by the coherency forces at the Cu/γ-Fe boundary. This is somewhat the same situation as occurs in the Cu-Ni-Fe system studied by Bradley,[16] and the similar Cu-Ni-Co[17] system, except that the

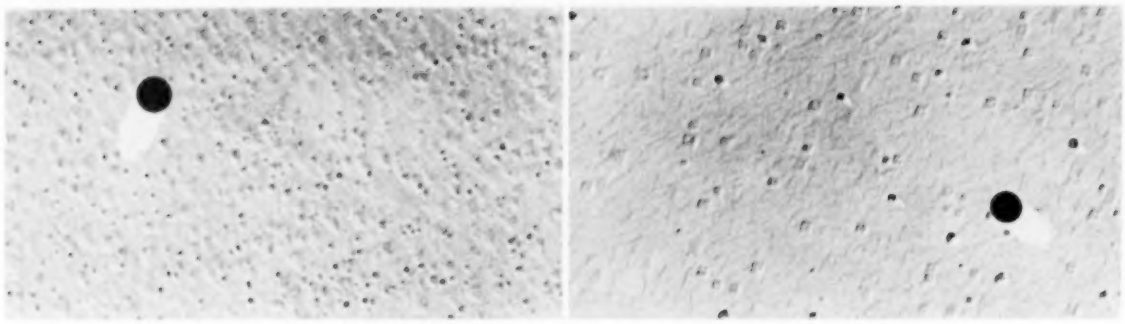

Fig. 4—By means of electron micrographs the precipitate particles can be resolved. Polystyrene spheres 25μ in diam are included for microscopy control. Potassium dichromate etch. a) LEFT: 60 hr at 600°C. b) RIGHT: 1300 hr at 600°C. X500. Reduced approximately 5 pct for reproduction.

amount of precipitate and the disregistry are much smaller in the case of Cu-Fe. This small amount of coherent precipitate in Cu-Fe alloys would account for the failure to observe any evidence of distortion in the matrix lattice. Such distortion is quite evident in partially aged Cu-Ni-Co alloys through X-ray diffraction effects, where the face-centered-cubic matrix decomposes into two face-centered-cubic lattices in approximately equal amounts.

The α Iron Precipitate—At very late stages of aging all X-ray evidence for the presence of the γ-Fe lattice is missing. Instead, definite lines which fit the diffraction spectrum of α-Fe can be seen, see Fig. 2e. Since each of these body-centered-cubic lines is of uniform intensity, the pattern proves the existence of small crystals of α-Fe in random orientation. The specimen which gave this pattern was thoroughly overaged, having been held for 160 days at 700°C. The specimen was very carefully handled to avoid distorting it before the X-ray picture was made. On the basis of these results it is believed that incoherent particles of randomly oriented α-Fe formed as a normal precipitation product at grain boundaries. Intragranular particles of α-Fe may have nucleated at lattice imperfections or they may have arisen through the transformation of some of the unstable γ-Fe particles to the α-Fe lattice, in which case a definite lattice orientation relation with respect to the matrix would be expected.*

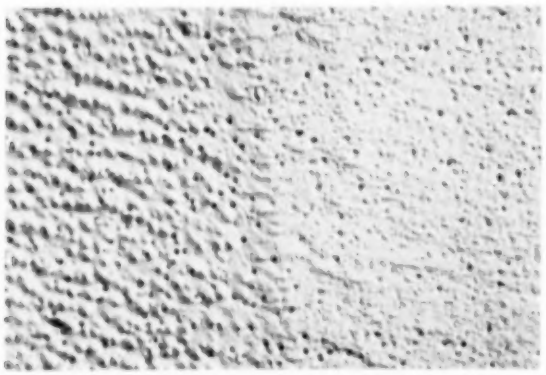

Fig. 5—Some grains are characterized by definite ridges made up of individual mounds on the specimen surface. This specimen was aged 90 hr at 600°C. Potassium dichromate etch. X20,000.

* An experiment outside the scope of the present work suggests itself here. It should be possible to determine experimentally the orientations of α-Fe which result from the transformation of γ-Fe precipitate in a single crystal of a Cu-Fe crystal. The Kurdjumov and Sachs[8] orientation relationship would probably be found.

Another source of α-Fe is obviously the coherent γ-Fe precipitate which transforms to the more stable body-centered-cubic lattice when it is cold worked. The Debye-Scherrer photograph in Fig. 2f contains a face-centered-cubic pattern and a body-centered-cubic pattern having lattice parameters corresponding, respectively, to copper and α-Fe. The specimen for this photograph was a wire which had been plastically deformed after aging. Before deformation this specimen gave the pattern shown in Fig. 2c, which pattern corresponds to the copper matrix plus γ-Fe only. It is evident therefore that the iron-rich precipitate has transformed from the original coherent face-centered-cubic γ phase to the noncoherent body-centered-cubic form, an expected consequence of the cold working.

Specimens at a moderately late stage of aging apparently contain three phases as shown by the three patterns in Fig. 2d. These phases are: a) the depleted copper matrix, and b) the particles of γ-Fe which are in the process of dissolving in favor of c) the growing particles of stable α-Fe.

No evidence has been found for the existence of a tetragonal body-centered-cubic form of iron, a recently reported structure.[7] The high angle 310 Debye-Scherrer line, which would show evident splitting at a c/a ratio as close to unity as 1.01, was always quite sharp.

The mechanism of precipitation has been studied in several systems in which the precipitate and the matrix are both face-centered-cubic and both have the same orientation when the original coherency is lost. These systems include Cu-Ag, Ag-Cu, Cu-Ni-Fe, Cu-Ni-Co, and Fe-Ni-Al.[9] Without exception the observed Widmanstätten structures have been satisfactorily explained on the basis of precipitate platelets which are parallel to {100} matrix planes. Thus, the platelets in overaged Cu-Fe might not be the coherent γ-Fe phase, but rather the α-Fe phase. This would be consistent with the gradual appearance of α-Fe lines in Debye-Scherrer patterns given by greatly overaged specimens and with the fact that the platelets are ferromagnetic, as observed by

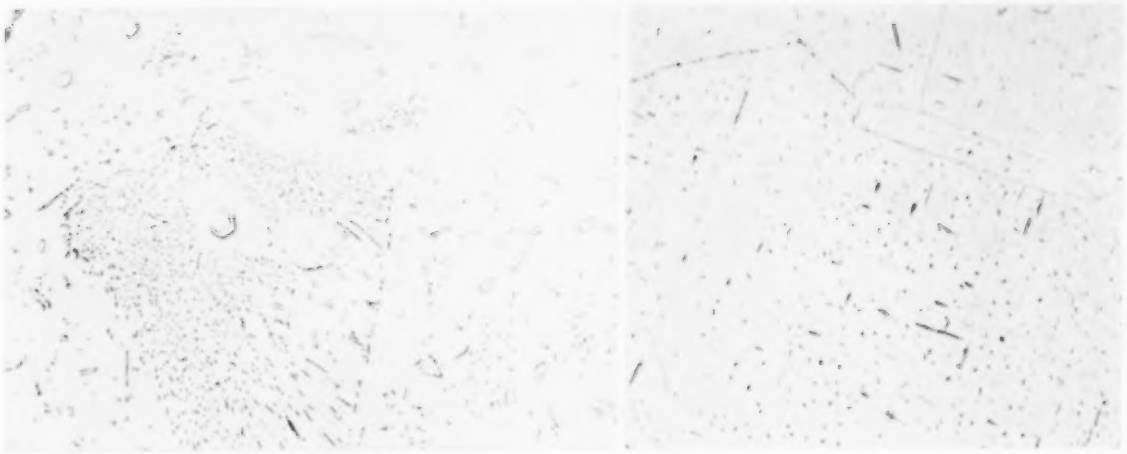

Fig. 6—Stable α-Fe precipitate a) LEFT: grows as equiaxed particles if the specimen is slowly cooled from the solution temperature to the aging temperature, or b) RIGHT: forms a Widmanstatten structure if the specimen is quenched and reheated to the aging temperature. Aged 3840 hr at 700°C. Potassium dichromate etch. a) Furnace cooled from 1060°C to aging temperature. b) Water quenched from 1060°C and reheated to aging temperature. X250. Reduced approximately 2 pct for reproduction.

Gordon and Cohen. The clear boundary between the Widmanstätten precipitate and the matrix, seen in Fig. 7, leaves no doubt that this is a true $\{111\}_{\alpha}$ habit of a single particle, and not a pseudohabit such as was reported at first for Ag-Cu alloys. (The latter structure, being unconfirmed, was later identified[4] as preferred precipitation of unresolved particles on $\{111\}_{\alpha}$ slip planes.) Perhaps the $\{111\}$ habit in overaged Cu-Fe alloys can be explained in terms of accelerated growth of the α-Fe particles in $\{111\}_{\alpha}$ slip planes. Thus, specimens which had been plastically strained by quenching prior to aging would develop $\{111\}$ Widmanstätten platelets, as observed, whereas those which had been slowly cooled to the aging temperature would not.

The absence of fine γ-Fe precipitate in the neighborhood of the α-Fe grain boundary and Widmanstätten particles can be clearly seen in Fig. 7. This effect indicates that the γ-Fe, though it is the first precipitate to form, is not the more stable. The α-Fe particles provide a low energy sink into which iron atoms from the less stable and therefore more soluble γ-Fe particles can diffuse. Thus, the γ-Fe will disappear completely if enough aging time is allowed. The precipitation sequence from the supersaturated solid solution to the final state, where α-Fe exists in equilibrium with the depleted copper matrix, is illustrated schematically in Fig. 10.

The continual increase of magnetic susceptibility of aged and unworked specimens, reported by Gordon and Cohen, is clearly explained in terms of the gradual triumph of the ferromagnetic α phase over the previously precipitated nonferromagnetic γ phase.

Fig. 7—At a late stage of precipitation, the finely dispersed γ-Fe particles dissolve and the massive particles of α-Fe grow. Quenched from 1060°C, aged 3840 hr at 700°C. Alkaline hydrogen peroxide etch. X500. Reduced approximately 20 pct for reproduction.

Fig. 8—Octahedral poles of a cubic lattice in standard 100 orientation can be made to lie on the trace normals of the Widmanstatten particles in Fig. 6a by a rotation of 44° about an axis in the specimen surface.

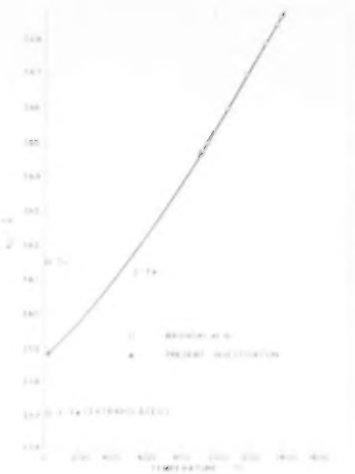

Fig. 9—The lattice parameter of γ-Fe varies nearly linearly with temperature down to 20°C.

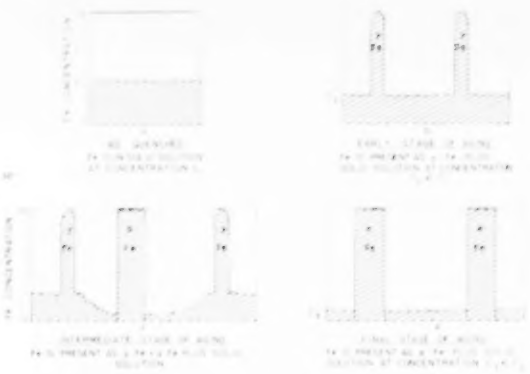

Fig. 10—At an early stage of aging, most of the precipitate is in the form of coherent γ-Fe. On continued aging, the persistent growth of the more stable incoherent α-Fe particles leads to the re-solution and ultimate disappearance of the γ-Fe particles.

The ridge-furrow structure found on the etched surface of partially aged specimens, Fig. 5, may be a manifestation of rows of edge dislocations, each of which has an atmosphere of impurity (iron) atoms about it. The structure is similar in appearance to that observed by Wilsdorf on Al-Cu alloys.[30]

Summary and Conclusions

X-ray diffraction patterns have shown that the decomposition of a supersaturated solid solution of iron in copper occurs by the simultaneous precipitation of discrete particles of γ and α-Fe. Depletion of the matrix first occurs by the copious precipitation of coherent γ-Fe. This stage is accompanied by moderate hardening of the alloy. Continued aging permits the growth of the less numerous α-Fe particles. This growth of α-Fe particles is accompanied by softening, further depletion of the matrix, and the re-solution of the γ-Fe particles.

Microscopic examination has shown that the γ-Fe particles occur as a general precipitate. According to X-ray evidence the orientation of the γ-Fe lattice is the same as that of the copper matrix with which it is coherent. The shape of the γ-Fe particles could not be determined by available X-ray techniques, although electron micrographs indicate that the particles are roughly equiaxed. The γ-Fe does not, in general, transform spontaneously to α-Fe, even when it is cooled as low as —196°C. However, if the specimen is plastically strained at room temperature, transformation to α-Fe occurs immediately.

At an intermediate stage of aging particles of α-Fe appear at grain boundaries and within grains. Grain boundary precipitate grows as equiaxed particles and with random lattice orientation. Intragranular particles of α-Fe, probably resulting from the transformation of a few of the γ-Fe particles, may have a definite lattice orientation with respect to the matrix, although this has not been demonstrated. The α-Fe particles are much less numerous than those of γ-Fe and produce little if any matrix hardening. Being more stable than the γ-Fe precipitate, the α-Fe particles grow continuously during aging, while the γ-Fe precipitate redissolves. The α-Fe particles are equiaxed in specimens which have been slowly cooled to the aging temperature. However, in specimens which have been plastically strained by quenching, a definite Widmanstätten figure is found which is explained by the presence of platelets parallel to {111} planes of the copper matrix. The more rapid growth of the intragranular α-Fe particles on $\{111\}_{Cu}$ planes may be accounted for by increased diffusion on these faulted slip planes.

Acknowledgments

Most of the experimental work described in this paper was performed by W. G. Martin. The light micrographs were prepared by Miss D. Kontoleon and the electron micrographs by A. S. Holik. The author is grateful to C. S. Barrett, D. Turnbull, and F. C. Frank for their valuable comments on the manuscript.

References

[1] F. Bitter and A. R. Kaufmann: *Physical Review*, 1939, vol. 56, pp. 1044-1051.
[2] J. Reekie, T. S. Hutchison, and F. E. Hetherington: *Proceedings* Physical Soc., 1953, vol. B66, pp. 1101-1112.
[3] C. S. Smith: *Physical Review*, 1940, vol. 57, p. 337.
[4] A. Knoppwost: *Ztsch. fur Electrochemie*, 1954, vol. 58, pp. 65-66.
[5] R. E. Cech and D. Turnbull: *AIME Trans.*, 1954, vol. 200, p. 45; Journal of Metals, January 1954.
[6] J. M. Denney: *Acta Metallurgica*, 1956, vol. 4, pp. 586-592.
[7] *Metals Handbook*, p. 1186. ASM, Cleveland, 1948.
[8] J. B. Newkirk: *ASM Trans.*, 1957, in press.
[9] J. B. Newkirk, R. Smoluchowski, A. H. Geisler, and D. L. Martin: *Acta Crystallographica*, 1951, vol. 4, pp. 507-512.
[10] A. H. Geisler: *Phase Transformations in Solids*, Chap. 13. John Wiley & Sons Inc., New York, 1951.
[11] R. B. Gordon and M. Cohen: *Age Hardening of Metals*, pp. 61-84. ASM, Cleveland, 1940.
[12] *Metals Handbook*, p. 97. ASM, Cleveland, 1948.
[13] Z. S. Basinski, W. Hume-Rothery, F. Ris, and A. L. Sutton: *Proceedings* Royal Soc., London, 1955, vol. 229, pp. 459 ff.
[14] J. H. Westbrook: Report No. 1453, 1956. General Electric Research Laboratory, Schenectady.
[15] A. Guinier: *Comptes rendus*, 1942, vol. 214, pp. 34-37.
[16] A. J. Bradley, W. F. Cox, and H. J. Goldschmidt: *Journal* Institute of Metals, 1941, vol. 67, pp. 189-201.
[17] A. H. Geisler and J. B. Newkirk: *AIME Trans.*, 1949, vol. 180, pp. 101-120; Journal of Metals, February 1949.
[18] G. Kurdjumow and G. Sachs: *Ztsch. fur Physik*, 1930, vol. 64, p. 325.
[19] M. L. V. Gayler and W. E. Carrington: *Journal* Institute of Metals, 1947, vol. 73, pp. 625-639.
[20] H. Wilsdorf and D. Kuhlmann-Wilsdorf: *Defects in Crystalline Solids*, pp. 175-186. Physical Soc., London, 1954.

Discussion of this paper sent (2 copies) to AIME by Jan. 1, 1958 will appear in AIME *Transactions* Vol. 212, 1958, and in Journal of Metals, April 1958.

Some Observations on 885°F Embrittlement

The hardening of several 24 to 30 pct Cr steels was studied at temperatures near 885°F. In alloys containing normal amounts of carbon, the temperature and time of preheat treatment affect the hardening, apparently because of destruction of potential hardening nuclei by carbide nucleation. This occurs to a lesser extent in decarburized alloys and does not occur at all if the carbon is stabilized by titanium or is sufficiently low. Nitrogen has an effect similar to that of carbon. Hardening does not occur in electrolytic chromium. Interference with the nucleation of the hardening constituent also affects the optimum hardening temperature. On the basis of one neutron diffraction run, long range ordering in any sizable amount does not appear to be a likely explanation for 885°F hardening. Thus, the evidence tends to substantiate the belief that 885°F hardening is the result of coherent precipitation of a chromium-rich phase, the nature of which is still not entirely clear.

by G. F. Tisinai and C. H. Samans

HARDENING and embrittlement of the ferritic chromium stainless steels at temperatures near 885°F have been known for a long time.[1] However, no satisfactory explanation has been given. Both ordering and precipitation hardening have been suggested. Fisher, Dulis, and Carroll[2] discovered a chromium-rich body-centered-cubic precipitate in embrittled alloys. Subsequently, Williams[3] and Wright[4] also have found evidence of this body-centered-cubic constituent. William's hardness, electrical resistance, and magnetic studies led to his proposal of a new constitutional diagram for the Fe-Cr alloys. The new feature of this diagram is the eutectoidal decomposition, below about 970°F, of the σ phase into two stable body-centered-cubic solid solutions, one rich in iron and the other rich in chromium. An observation of Heger[5] that the amount of σ phase has increased and the amount of chromium-rich body-centered-cubic phase decreased in the interval 5000 to 32,600 hr at 900°F, even though the alloy increased in hardness, casts some doubt on this diagram.

If precipitation hardening causes the embrittlement, the precipitate probably is always coherent with the matrix, since no evidence of overaging has been reported. It cannot be stated positively, however, that Fisher's body-centered-cubic constituent is the embrittling phase. According to Preston's data,[6] such a chromium-rich phase should have a parameter less than about 0.5 pct larger than that of the iron-rich matrix lattice. Moreover, the constitutional relationships whereby Fisher's constituent forms, and whether it is stable, metastable, or a transition phase, are not yet completely clear.

G. F. TISINAI and C. H. SAMANS, Members AIME, are Assistant Project Engineer and Associate Director, respectively, Materials Div., Engineering Research Dept., Standard Oil Co., Whiting, Ind.
TP 4468E. Manuscript, Sept. 18, 1956.

The recent studies of Wright[4] and of Lommel,[7] as well as the earlier studies of Becket[8] and of Hochmann,[9] have shown that 885°F hardening occurs in relatively pure Fe-Cr alloys. No evidence of its occurrence or absence in chromium itself has been reported. The rate of hardening in high purity alloys seems appreciably slower than that in alloys containing larger amounts of impurities (chiefly carbon and nitrogen). This may be due merely to the absence of hardening and straining effects from precipitated carbides and/or nitrides. These observations on high purity alloys make it seem unlikely that 885°F hardening is caused by a constituent containing other than iron and chromium atoms, e.g., carbides and/or nitrides.

Wright,[4] Lommel,[7] and Lena and Hawkes[10] demonstrated the accelerating effects of a finely dispersed precipitate of (probably) chromium nitride on the hardening reaction. This appears to be evidence that lattice straining increases the rate of nucleation of the hardening constituent.

Some new observations on 885°F hardening are reported here. They show an effect of preheat treatment that should contribute to a better understanding of the 885°F hardening phenomenon. They also clarify a discrepancy which exists in the literature. Some investigators have reported most rapid hardening at 885°, whereas others have reported it at 930°F. The present work also shows that 885°F hardening does not occur in electrolytic chromium, and that any long range ordering type of reaction affecting any sizeable part of the volume is unlikely.

Materials Studied

Table I shows the composition of the alloys used in this investigation. In these alloys carbon and nitrogen are present in roughly similar amounts. Presumably both elements precipitate, as carbides and/or nitrides, during the heat treatments given.

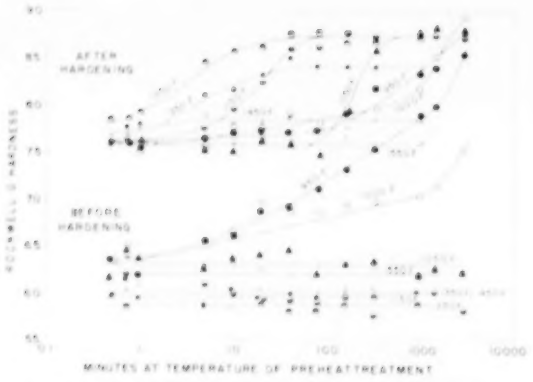

Fig. 1—Effect of time and temperature of preheat treatment on the hardness of a 30 pct Cr steel before (lower curves) and after (upper curves) a 24 hr hardening heat treatment at 885°F. Initial treatment was 1 hr at 1700°, furnace cool to 1550°F, hold 1 hr, water quench. Closed circle refers to 950°; open circle, 1000°; closed triangle, 1050°; open top circle, 1150°; closed top circle, 1250°, closed square, 1350°; open triangle, 1450°; and open square, 1550°F.

Although it is not possible, strictly, to separate the effects of these two, an effort has been made to do so wherever there was any evidence to present.

Types of Heat Treatments Used—Throughout this paper the effects of three general types of heat treatment will be discussed.

1) The initial treatment produces the base condition. When it was desired to have materials free of the effects of cold work and to have most of the carbides precipitated, the initial treatment consisted of 1 hr at 1700° followed by a furnace cool to 1550°F and a water quench. In experiments where the base condition desired was a treatment above 1550°F, that higher temperature treatment comprised the initial treatment.

2) The preheat treatment immediately precedes the final or hardening heat treatment. In some instances, the initial treatment and the preheat treatment are identical.

3) The hardening heat treatment is the final heat treatment given the specimens, generally for 24 hr at 885°F, although some treatments were given in a gradient furnace over a range of hardening temperatures.

Preheat Treatments in the Range 950° to 1550°F—The small specimens used here were given the initial 1700° to 1550°F heat treatment to produce a base condition. Individual samples then were held for varying times at preheat treatment temperatures in the range 950° to 1550°F and water quenched. All samples finally were given a hardening heat treatment of 24 hr at 885°F. Rockwell G (1/16 in., 150 kg, red) hardness readings were taken before and after the 885°F hardening treatment.

The hardness readings for the 30 pct Cr, low (0.04 pct) nitrogen alloy are plotted in Fig. 1 against the time of holding at the preheat treating temperature. Data for the material after preheat treatment but before the hardening heat treatment are given in the lower curves, and for the material after the additional 24 hr at 885°F hardening heat treatment in the upper curves. For simplicity, the intermediate data secured at the even 100° temperatures have been omitted. Results for the 24 pct Cr alloy were similar except that the hardness levels were about ten points lower. The treatments given to the commercial purity 27 pct Cr alloy were not so extensive as those given the other two alloys. However, the results secured showed clearly that it reacts in substantially the same way, but with intermediate hardnesses.

Effects of Time of Holding at 885°F—The influence of preheat treatments on the hardening at 885°F shown in Fig. 1 are maintained even after relatively long hardening periods at 885°F. Fig. 2 shows this for the commercial purity 27 pct Cr steel. These samples were given an initial treatment of 16 hr at 1700°F and water quenched. Preheat treatments of 1 hr at temperatures of 925° to 1700°F then were given, followed by a series of hardening treatments at 885°F. The greater hardening which resulted at 885°F because of a preheat treatment of 1 hr in the range 1150° to 1250°F has persisted even after 330 hr at 885°F.

Effect of Preheat Treatment on the Temperature of Maximum Hardening—Two samples of the commercial purity 27 pct Cr steel were given the initial 1700° to 1550°F heat treatment, then one sample was given an additional preheat treatment for 1 hr at 1200°F. Both samples were then held in a gradient furnace maintained between 835° and 1045°F to determine the optimum hardening temperature. Rockwell G hardness measurements were made on the hardened bars. The data are plotted in Fig. 3.

Effect of Preheat Treatments in the Range 200° to 950°F—These data were secured for the 30 pct Cr, low (0.04 pct) nitrogen alloy and for the 27 pct Cr, 0.67 pct Ti alloy. The purpose of the titanium addition was to tie up the carbon and nitrogen as a titanium carbonitride and thus to remove these elements from solid solution in the chromium ferrite. The hardness data are summarized in Fig. 4. One sample was given an initial heat treatment for 1 hr at 1600° and another an initial heat treatment for 1 hr at 2000°F. Water quenching was used following each heat treatment. Both then were held in a gradient furnace, which covered the range from 200° to 950°F, for times of 120, 360, or 720 hr. No significant differences in hardness were found between the 120 and 720 hr treatments except in the hardening range, viz., above about 525°F, where the differences were not more than about 5 points. Both samples were then given a final hardening treatment of 24 hr at 885°F.

Effect of Cold Rolling on the Rate of Hardening at 885°F—To determine if mechanical straining could increase the rate of 885°F hardening, samples of the commercial purity 27 pct Cr steel, which had been given an initial treatment of 2 hr at 1850°F, water quench, were cold rolled to varying reductions and then given a hardening heat treatment of 24 hr at 885°F. As shown in Fig. 5, as little as 6 pct reduction caused a decided increase in the amount of hardening produced by a subsequent heat treatment at 885°F.

Hardness Changes in Decarburized Materials—The 30 pct Cr, low (0.04 pct) nitrogen and the 24 pct Cr alloys were decarburized to a level of 0.02 pct C by an initial heat treatment in dry hydrogen at 2200°F. Although nitrogen analyses were not made on these specimens, other specimens, after a similar treatment, showed little change in the nitrogen content. Both these two decarburized alloys and the same alloys in their original (i.e., hot forged) condition were preheat treated for 16 hr in a gra-

dient furnace operating in the range from 1280° to 1940°F. Finally, the materials were given a hardening treatment for 24 hr and for 360 hr at 885°F. The Rockwell G hardness data for the 30 pct Cr alloy are shown in Fig. 6; the results for the 24 pct Cr alloy were comparable.

Effect of Nitrogen Level on 885°F Hardening— Two specimens each of the 30 pct Cr, 0.08 pct C, high (0.12 pct) nitrogen alloy and of the 30 pct Cr, 0.08 pct C, low (0.04 pct) nitrogen alloy were given the initial 1700° to 1550°F heat treatment. One specimen of each alloy was given a further heat treatment of 1 hr at 1200°F and water quenched. All four specimens then were positioned in a gradient furnace operating between 550° and 1300°F and given a hardening heat treatment of 120 hr. The Rockwell G hardness measurements, made along the gradient bar, are plotted against the corresponding temperatures in Fig. 7.

Hardness Changes in a High Purity Alloy— Comparable hardness data for the commercial purity 27 pct Cr alloy and for the high purity 35 pct Cr alloy are given in Table II.

In the commercial purity alloy the hardness increased markedly (ΔH=30 points) during preheat treating, as the preheat treating temperature was raised from 1200° to 1950°F. In the high purity alloy the change was much smaller (ΔH=6 points).

After the 885°F hardening heat treatment, the commercial purity alloy showed high hardnesses for those samples given the 1950° or 1200°F preheat treatments and lower hardnesses for the sample given the 1600°F preheat treatment. In the high purity material, the hardness was substantially independent of the temperature of preheat treatment.

Attempt to Embrittle Chromium at 885°F—To determine if 885°F embrittlement would occur in pure chromium, samples of high purity electrolytic chromium about 0.050 in. thick were sealed in evacuated Vycor tubes. One specimen was given an initial heat treatment of 1 hr at 1800°, followed by a furnace cool to 1550°F, where it was held for 1 hr and water quenched. A second specimen also was given this initial heat treatment plus an additional preheat treatment of 1 hr at 1200°F, followed by water quenching. Hardness measurements (Vickers pyramid with 1 kg load) were made both after the above heat treatments and after a final hardening heat treatment of 24 hr at 885°F.

The 1200° preheat treated sample had hardnesses substantially the same as those of the 1550°F heat treated sample. The samples given either treatment fell in the hardness range of 311 to 313 Vpn before the 885° hardening heat treatment and in the range of 251 to 257 Vpn after the 885°F treatment.

Neutron Diffraction Study of a Hardened Specimen—One sample of the commercial purity 27 pct Cr alloy also was examined by neutron diffraction.*

* Through the kindness of C. C. Shull and W. C. Koehler of the Oak Ridge National Laboratory, whose assistance and cooperation are gratefully acknowledged.

The neutron beam had a principal wave length of 1.315 angstrom units, with about 7 pct of a second order wave length of 0.6575 angstrom units.

This sample was in the form of about 8 cu cm of loosely packed filings which had been heat treated in three successive steps: a) 1 hr at 1550°F, water quench; b) 1 hr at 1200°F, water quench; and c) 168 hr at 885°F, water quench. This treatment should first precipitate most of the carbon as car-

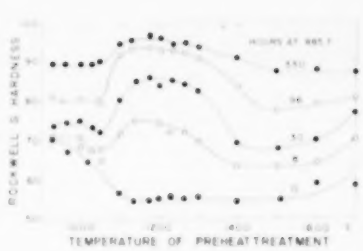

Fig. 2—Effect of time at 885°F on the hardness of a commercial purity 27 pct Cr steel after preheat treating for 1 hr at temperatures from 930° to 1700°F. The initial heat treatment was 16 hr at 1700°F followed by a water quench.

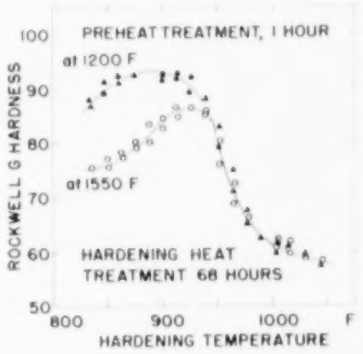

Fig. 3—Effect of hardening temperature on the hardness of a commercial purity 27 pct Cr steel which had been preheat treated for 1 hr at 1200° or 1550°F.

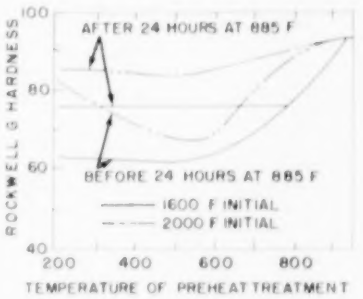

Fig. 4—Effect of preheat treatments of 720 hr at temperatures in the range from 200° to 950°F on the hardness of the 30 pct Cr, low nitrogen steel. The lower curves are for data taken before and the upper curves are for data taken after a 24 hr hardening heat treatment at 885°F. Initial treatment was a water quench following 1 hr either at 1600° or at 2000°F, as indicated.

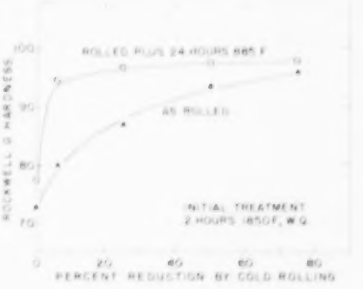

Fig. 5—Effect of cold rolling on the hardening of a commercial purity 27 pct Cr steel; lower curve, as rolled; upper curve, rolled plus a 24 hr heat treatment at 885°F. Before rolling, the material was water quenched following a 2 hr heat treatment at 1850°F.

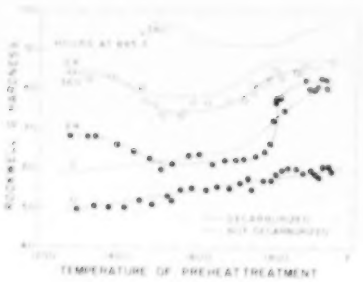

Fig. 6—Effect of decarburization of a 30 pct Cr, 0.08 pct C steel on its reaction to 885°F hardening treatments, after a 16 hr preheat treatment at various temperatures.

bides and then produce appreciable 885°F hardening for the time used.

The diffraction pattern showed no evidence of anything other than the body-centered-cubic reflections of the normal unit cell. This could indicate either a) that no superstructure was present, or b) that the technique was not sensitive enough to detect the presence of the superstructure.

Partial ordering or short range ordering would not be excluded by the data, so it only can be said that complete ordering appeared to be ruled out. However, more than likely a 20 to 40 pct degree of order would have been undetectable in the study. Thus, although the results are far from conclusive, it appears that the random substitution model should be preferred to an ordered model. The peaks secured were not sharp enough to furnish useful evidence on the possible existence of a chromium-rich constituent.

Discussion

According to modern nucleation theory,[11] in homogeneous chromium ferrite there will be chromium-rich clusters of various sizes. These clusters could serve as nucleating sites for the 885°F hardening constituent, if this is a chromium-rich constituent, as well as for chromium carbide and/or chromium nitride. The stable carbide, $(Cr, Fe)_{23}C_6$, contains about 68 pct Cr and 26.5 pct Fe[12]. The stable nitride, (Cr, Fe)$_2$N, extracted during the present study contained about 83.5 pct Cr and 4.5 pct Fe. Nucleation of chromium carbide and/or chromium nitride could use up chromium-rich clusters. Such *destroyed* clusters could not nucleate the 885°F hardening constituent. Hence, if carbides and/or nitrides are precipitated, the hardening produced by a constant hardening heat treatment will be decreased.

Carbon solubility in chromium ferrite increases with temperature. Above about 1600°F this was verified metallographically by observing the re-solution of carbides. Hardness increases with increasing amounts of carbon in solid solution were similar to those reported by Rickett and Kristufek[13] for ferrite.

Preheat treatments at 1550°F leave a limited amount of carbon in solid solution. In Fig. 1, the 1550°F preheat treated hardness is 62 Rockwell G. Much of this limited amount of carbon precipitates as carbide during the subsequent 24 hr hardening treatment at 885°F, so the hardness attained is only 76 Rockwell G. At temperatures of preheat treatment lower than 1550°F the limited amount of carbon dissolved at 1550°F tends to precipitate as carbide. The hardness therefore decreases, reaching a minimum of about 58 Rockwell G for the 1250°F preheat treatment. Since less carbon remains in solid solution after these lower temperature preheat treatments, fewer clusters are destroyed during the 885°F hardening heat treatment. After a constant 885°F hardening heat treatment, the hardness of samples given only short time lower temperature preheat treatments is a minimum (comparable to that of the 1550° preheat treated and 885°F hardened samples), but hardness then increases with increasing time of preheat treatment, to a maximum 88 Rockwell G. This is attributed to the restoration of the characteristic chromium-rich cluster distribution by chromium diffusion at the preheat treatment temperature. For temperatures below about 1250°F a plot of the logarithm of the time at preheat treating temperature required to regain the maximum hardness, Fig. 1, against the reciprocal of the preheat treating temperature (absolute) gives a straight line. The slope of this line gives an activation energy (Arrhenius) for the rate controlling step of 54 kcal per mole. This is in excellent agreement with the value of Campbell et al.[10] of 55.2 kcal per mole for diffusion of chromium in iron.

The different hardness levels illustrated in Fig. 1 after a 24 hr hardening time at 885°F are maintained for much longer hardening times. Fig. 2 shows this for times up to 330 hr. This indicates that the hardness differences result from differences in nucleation determined by the preheat treatment. For a constant hardening temperature the growth rate should be constant.

Hardness differences between the 1200° and 1550°F preheat treatments are found for hardening heat treatments below about 950°F, Fig. 3. At each hardening temperature the 1200°F preheat treated material hardens more and reaches its highest hardness at a lower temperature (885°F) than the 1550°F preheat treated material (930°F). It has been noted in the literature[14] that 885° hardening sometimes was greatest at 885° and sometimes at 930°F, but this has not been previously related to temperature of preheat treatment. Material with minimum cluster destruction during hardening (1200°F preheat treatment) hardens more than material which has partial cluster destruction during 885°F hardening (1550°F preheat treatment). With fewer hardening nuclei initially a more rapid growth (i.e., a higher temperature of hardening) is needed to reach maximum hardness in a constant time than is true with the normal number of nuclei. Above about 930°F the hardness is lower than maximum for material given either preheat treatment. This suggests that the smaller clusters will not become hardening nuclei at hardening temperatures above about 930°F.

Preheat treatments below the hardening range seem largely to precipitate carbon from solid solution, Fig. 4. The hardness after the pretreatment alone decreases slowly with increasing temperature of preheat treatment above 200°F (to 1250°F); this must be interpolated in the hardening range (525° to 1125°F). These hardnesses changed only slightly with time (up to 720 hr). It cannot be stated definitely whether the intermediate values between the carbon in solution and the carbides precipitated is the result of incomplete precipitation or of a balance between softening from carbon removal from solid solution and dispersion hardening from carbide precipitation. The hardening noted in Fig. 1 for preheat treatments in the range 1250° to 1050°F suggests the latter explanation.

These low preheat treatment temperatures had no effect on the hardening produced by the 24 hr

Table I. Materials Studied, Pct

Designation	Cr	C	N	Ni	Mn	Si	P	S
24 pct Cr	24.95	0.07	*	0.05	0.31	0.59	0.026	0.008
27 pct Cr, commercial purity	27.80	0.04	*	0.08	0.38	0.54	0.024	0.015
27 pct Cr, Ti†	26.96	0.02	*	0.01	0.62	0.82	0.010	0.020
30 pct Cr, low N_2	31.00	0.08	0.04	0.08	0.36	0.65	0.024	0.008
30 pct Cr, high N_2	30.40	0.08	0.12	0.20	0.52	0.51	0.012	0.009
35 pct Cr, high purity‡	34.75	0.010	0.002	nil	nil	nil	0.008	0.016

* Not determined; similar materials prepared in the same manner consistently have contained 0.04 to 0.06 pct N.
† With 0.67 pct Ti and 0.01 pct Mo.
‡ The authors are indebted to A. B. Kinzel, Union Carbide & Carbon Corp., for this material.

at 885°F treatment if there was only a small amount of carbon retained in solid solution during the initial heat treatment (1600°F initial heat treatment in Fig. 4). However, if there was appreciable carbon in solid solution (2000°F initial heat treatment in Fig. 4), the hardening produced by the 885°F treatment was appreciably higher. This is explained by an increase in nucleation of the hardening constituent because of the mechanical straining effects of the precipitated carbides. This is similar to the effect reported for chromium nitride by others.[8,9,10] Positive proof of such a straining from a well dispersed precipitate is difficult to secure. However, the data in Fig. 5 show that the basic concept is valid. The strain induced by a 6 pct reduction by cold rolling has raised the hardness level appreciably after the hardening heat treatment. This effect usually is attributed to an increased nucleation because of strain. It should be noted that the increased nucleation caused by straining more than compensated for the *destruction* of the chromium-rich clusters by carbide nucleation, Fig. 4.

If nucleation of carbides during the preheat treatment or hardening treatment has these effects on hardness level after hardening, marked differences should result from making the carbon ineffective or lowering it. To test this, 0.67 pct Ti was used to tie up most of the carbon (and nitrogen) as titanium carbonitride. No effect of preheat treatment was found in any temperature range, i.e., hardening after the 885°F heat treatment was independent of preheat treatment temperature.

A comparison of data for the material before and after decarburization, Fig. 6, shows a definite decrease in hardness level in the decarburized material before hardening. Temperature of preheat treatment still influences this to some extent, possibly an effect of nitrogen. After hardening for 24 or 360 hr at 885°F the same general differences in hardness level with preheat treatment are shown for both the original and the decarburized material. However, the hardness level for the latter is lower in each case. This decrease is related to the lower carbon content of the decarburized material. Less carbon is available either for solid solution hardening or for dispersion hardening from precipitated carbides. The minimum hardness, after 885°F hardening, is again found following preheat treatments in the range of about 1550° to 1750°F. Even in the decarburized material these particular heat treatments leave enough carbon in solid solution to interfere with nucleation of 885°F hardening by destroying chromium-rich clusters. However, there is not enough carbon in solution to dispersion harden the matrix by precipitation during the 885°F hardening heat treatment, and hence accelerate nucleation by strain, except following preheat treatments above about 1800°F. The nitrogen content of these two materials is the same, so the effects of precipitated nitrides will be comparable.

The data for the 35 pct Cr high-purity alloy also are in agreement with this picture. The electrolytic chromium does not harden because the hardening constituent forms only from an Fe-Cr solid solution. The softening observed is believed to be the result of precipitation from solid solution but it cannot be stated specifically what the precipitating constituents are.

The effects of nitrogen would be expected to be similar to those of carbon. However, this is not easy to establish, since it is difficult to make nitrogen-bearing material low enough in carbon to be sure all observed effects are due to nitrogen alone. In Fig. 7 there definitely is a difference in hardness (for heat treatments above 1100°F, for example) of about five to six points between the two alloys of different nitrogen content. The two alloys also show the effects from carbide precipitation already discussed. The 1200°F preheat treatment definitely lowers the initial hardness level (600°F hardening) about six points in each alloy, and yet permits maximum hardening in the low nitrogen alloy because of less interference with nucleation. It should be noted also that the maximum hardness for both the high and low nitrogen alloys preheat treated at 1200°F is the same. The increase in hardness of the low (0.04 pct) nitrogen alloy is appreciably greater, however, since it has a lower initial hardness. The data for the 0.04 pct N alloy are directly comparable with those given in Fig. 3. For the 0.12 pct N alloy, however, the straining caused by the precipitation of chromium nitrides increased nucleation of the 885°F hardening constituent to such an extent that the differences between the 1550° and 1200°F preheat treatments were eliminated; these two hardness curves are quite similar for hardening temperatures above about 700°F.

The present observations provide only limited clarification of some aspects of the complicated problem of 885°F hardening. Of the various possibilities they appear to strengthen the probability that the coherent precipitation of a chromium-rich constituent, the specific nature of which is still uncertain, is the correct explanation. The observed effects of carbon and nitrogen make it unlikely that this constituent is a carbide or nitride. Limited neutron diffraction data gave no evidence to substantiate ordering as a valid explanation.

Summary and Conclusions

1) On the basis of these observations on 24 to 30 pct Cr steels, the explanation of 885°F hardening as

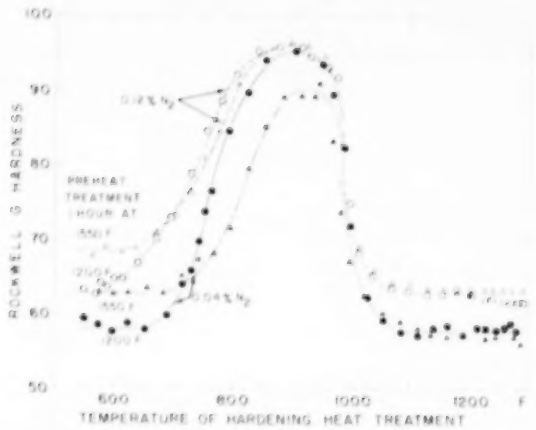

Fig. 7—Effect of hardening heat treatments of 120 hr at temperatures in the range from 550° to 1300°F on the hardness of two 30 pct Cr, 0.08 pct C steels containing, respectively, 0.12 pct and 0.04 pct N.

being caused by the coherent precipitation of a chromium-rich constituent seems to be strengthened considerably. The specific nature of this constituent has not been established here but, since its potential nuclei apparently can be destroyed by earlier nucleation of chromium carbide, its chromium-rich nature seems clear.

2) The data indicate a relatively rapid (within minutes) restoration of conditions in the solid solution favorable to 885°F hardening during preheat treatments at temperatures above about 1250°, but a much slower restoration at temperatures below 1250°F. The activation energy for this restoration process is in excellent agreement with that reported in the literature for chromium diffusion in iron.

3) For a constant hardening time, the hardness level after a 885°F hardening heat treatment can be increased by first straining the matrix, by cold work, or by precipitation of a sufficient amount of finely dispersed carbides and/or nitrides. This increased hardness is believed to be the result of an increased rate of nucleation of the hardening constituent. Also, the nucleation is more rapid the more closely the Fe-Cr matrix approaches the statistically homogeneous condition, with the consequent characteristic number and distribution of chromium-rich clusters.

4) Peak hardness is secured near 885° if the hardening nucleation is optimum, but it may occur as high as 930°F if there is interference with this nucleation. Prior or simultaneous nucleation of carbides is suggested as an interfering or competing process.

5) The probable effect of carbon in destroying the chromium-rich clusters, which are potential hardening nuclei, in the hardening range can be decreased to a low level, or eliminated, by a) precipitation of carbides at temperatures near about 1250°F before hardening, b) decreasing the carbon content of the alloy sufficiently, or c) using suitable added elements, such as titanium, to remove the carbon from solid solution. If titanium is used, however, a heat treatment first must be given which is suitable for precipitating the carbon as titanium carbonitride, e.g., near 1600°F.

Table II. Rockwell G Hardness of Commercial Purity and High Purity Ferritic Chromium Steels after Various Heat Treatments

Treatment	Commercial Purity 27.80 Pct Cr, 0.04 Pct C Steel		High Purity 34.75 Pct Cr, 0.010 Pct C, 0.002 Pct N Steel	
	Not Hardened	Hardened*	Not Hardened	Hardened*
1 hr at 1950°F, water quenched	87	88	57	84
1 hr at 1950°F, water quenched 1 hr at 1600°F, water quenched	60	72	54	82
1 hr at 1950°F, water quenched 1 hr at 1600°F, water quenched 1 hr at 1200°F, water quenched	57	84	51	83

* In each instance the final hardening heat treatment was 24 hr at 885°F.

6) The likelihood of 885°F hardening being an ordering reaction is small as judged by the result of a limited neutron diffraction study of a hardened commercial purity 27 pct Cr alloy. Although not completely conclusive it is believed that evidence of ordering to a degree of more than about 20 to 40 pct would have been found had it existed. No evidence of anything other than the random substitution solid solution was detected.

7) Heat treatment of electrolytic chromium at 885°F produced a softening rather than a hardening.

References

[1] J. J. Heger: Embrittlement at 885°F of the Ferritic Chromium-Iron Alloys. *Metal Progress*, 1951, vol. 60, No. 2, pp. 55-61.

[2] R. M. Fisher, E. J. Dulis, and K. G. Carroll: Identification of the Precipitate Accompanying 885°F Embrittlement in Chromium Steels. *AIME Trans.*, 1953, vol. 197, pp. 690-695; JOURNAL OF METALS, February 1953.

[3] R. O. Williams: An Investigation of the Nature of the Aging of Iron Chromium Alloys Around 500°C. Doctoral Dissertation, College of Engineering and Science, Dept. of Metallurgical Engineering, Carnegie Institute of Technology, 1955.

[4] W. V. Wright, Jr.: Precipitation Embrittlement Studies in Vacuum Melted Iron-Chromium Alloys. Doctoral Dissertation, California Institute of Technology, 1955.

[5] J. J. Heger: Discussion to Ref. 2. *AIME Trans.*, 1954, vol. 200, pp. 663-664; JOURNAL OF METALS, May 1954.

[6] G. D. Preston: X-Ray Examination of Chromium-Iron Alloys. *Journal* Iron and Steel Institute, 1931, vol. 124, pp. 139-145.

[7] J. M. Lommel: Some Aspects of 475°C Embrittlement. M.S. Dissertation, Illinois Institute of Technology, 1954.

[8] F. M. Becket: On the Allotropy of Stainless Steels. *AIME Trans.*, 1938, vol. 131, pp. 15-36; METALS TECHNOLOGY, June 1938.

[9] J. Hochmann: Influence of Melting under Vacuum on the Properties of 25% Chromium-Iron Alloys. *Revue de métallurgie*, 1950, vol. 48, pp. 734-758.

[10] A. J. Lena and M. F. Hawkes: 475°C (885°F) Embrittlement in Stainless Steels. *AIME Trans.*, 1954, vol. 200, pp. 607-615; JOURNAL OF METALS, May 1954.

[11] A. H. Cottrell: Theoretical Structural Metallurgy, Chap. 14, pp. 224-248. Longmans, Green & Co. Inc., New York, 1948.

[12] W. T. Tofaute, C. Küttner, and A. Büttinghaus: Das System Eisen-Chrom-Chrom Karbid Cr-Cr$_7$C$_3$-Zementit. *Archiv für das Eisenhüttenwesen*, 1936, vol. 9, pp. 606-616.

[13] I. E. Campbell, V. D. Barth, R. F. Hoeckelman, and B. W. Gonser: Salt Bath Chromizing. *Journal* Electrochemical Soc., 1949, vol. 96, No. 4, pp. 262-273.

[14] G. Bandel and W. T. Tofaute: Brittleness of Chromium-Rich Steels at Temperatures around 500°C. *Archiv für das Eisenhüttenwesen*, 1942, vol. 15, No. 7, pp. 307-319.

[15] R. L. Rickett and F. C. Kristufek: The Microstructure of Low Carbon Steel. *ASM Trans.*, 1949, vol. 41, pp. 1113-1141.

Discussion of this paper sent (2 copies) to AIME by Jan. 1, 1958 will appear in AIME *Transactions* Vol. 212, 1958, and in JOURNAL OF METALS, April 1958.

Phase Transformations in Hypoeutectoid Ti-Cr Alloys

The morphologies of proeutectoid α in a Ti-Cr alloy have been investigated in some detail and found to be basically similar to those previously observed in the proeutectoid ferrite reaction in plain carbon steels. The eutectoid reaction in hypoeutectoid Ti-Cr alloys was found to consist primarily in the precipitation of α and of $TiCr_2$ from β in non-lamellar form.

by H. I. Aaronson, W. B. Triplett, and G. M. Andes

ONLY limited studies have been made of proeutectoid α morphology in hypoeutectoid Ti-Cr alloys during previous investigations.[1-3] The nature of the eutectoid reaction, $\beta \rightarrow \alpha + TiCr_2$, has been considered in somewhat more detail.[1,2,4] Inasmuch as the proeutectoid ferrite reaction in plain carbon steels has recently been extensively investigated in this laboratory,[5-10] advantage has been taken of the opportunity to compare the morphologies developed in two rather different eutectoid systems in order to permit a preliminary estimate to be made of the degree of generality which may be ascribed to the various results obtained.

Experimental Procedure

The chemical analyses of the alloys used are given in Table I.

The 7.22 pct Cr alloy was prepared by the Battelle Memorial Institute from iodide titanium and high purity chromium. The initial ingot was made by arc melting a master alloy and iodide titanium. The resultant ingot was twice remelted by the consumable electrode technique. Upset forging at 950°C reduced the final ingot to ¾ in. sq bars.

The 10.94 pct Cr alloy was prepared by the Titanium Metals Corp. of America from sponge titanium and chromium of ordinary purity. This alloy was melted twice by the consumable electrode technique, forged at 1200° to a ¾ in. sq bar, and rolled at 815°C to a ½ in. round.

Specimens 1/4 in. x 1/4 in. x 1/16 in. were cut from the 7.22 pct Cr alloy; halves of disks 1/2 in. in diam and 1/16 in. thick served as specimens of the 10.94 pct Cr alloy. These specimens were individually encapsulated in Vycor. Each capsule was evacuated three times to a pressure of 2 to 6 x 10^{-5} mm Hg and flushed twice with a reduced pressure of argon prior to sealing. The inclusion of two small packets of zirconium chips permitted the capsules to be outgassed and internally gettered, without heating the specimen, prior to heat treatment.

The specimens were solution annealed for 40 min at 1000°C, isothermally reacted in deoxidized lead pots, and quenched in iced water. Most of the isothermal reaction treatments were carried out at 25° intervals between 725° and 550°C on specimens of the 7.22 pct Cr alloy and at 650°C on specimens of the 10.94 pct Cr alloy.

Results and Discussion

Morphologies of Proeutectoid α*—*Kinetics of the $\beta \rightarrow \alpha$ Reaction*: Fig. 1 shows the *TTT*-curves for the beginning of the proeutectoid α and the eutectoid reactions in the temperature range investigated in the 7.22 pct Cr alloy. The M_s temperature in this alloy is below 0°C. The curve for the beginning of the proeutectoid α reaction is in good agreement with that of Frost, Parris, Hirsch, Doig, and Schwartz[1] for a 7.54 pct Cr alloy, appears at considerably earlier reaction times than the corresponding curve presented by Rostoker[4] for a 7 pct Cr alloy, and lies athwart the curve of Spachner and co-workers[11] for an 8 pct Cr alloy. Differences in criteria for the beginning of the α reaction and the relatively high rate of this reaction at lower temperatures presumably account for some of these divergences and may also explain, in part, the apparent failure of an iodide-base 7.22 pct Cr alloy to react more slowly than sponge-base 7 to 8 pct Cr alloys.

Grain Boundary Allotriomorphs: Crystals of this morphology nucleate at and grow preferentially and more or less smoothly along the matrix grain boundaries.[6,7] Allotriomorphs are the first morphology to precipitate at most grain boundaries at reaction temperatures from 725°C, the highest temperature studied, at least through 575°C. Fig. 2 shows typical allotriomorphs, formed during an early stage of transformation at 725°C.

Grain boundary allotriomorphs are not the predominant morphology at late reaction times at any temperature studied. However, from 725° through

* This part of the investigation was performed entirely on the Ti-7.22 pct Cr alloy.

H. I. AARONSON, Junior Member AIME, W. B. TRIPLETT, and G. M. ANDES are Research Metallurgist, Assistant Research Metallurgist, and Junior Research Metallurgist, respectively, Metals Research Laboratory, Carnegie Institute of Technology, Pittsburgh.
TP 4498E. Manuscript, Oct. 31, 1956.

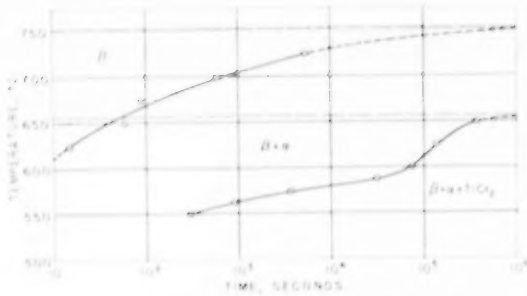

Fig. 1—777 diagram for iodide Ti 7.22 pct Cr alloy.

625°C, the lowest temperature at which rates of reaction are still slow enough to permit the beginning of the transformation to be investigated in some detail, allotriomorphs are initially the dominant morphology. The interval of reaction time during which allotriomorphs are the most important morphology and the amount of thickening which occurs during this stage of the transformation increase with increasing temperature.

The thickening of allotriomorphs at temperatures of 600°C and above is not halted when the proportion of α in the microstructure becomes constant, as indicated by comparison of Figs. 3 and 4. At temperatures below 600°C, the relatively early intervention of the eutectoid reaction and the small sizes of the α crystals tend to obscure thickening of this type.

A. *Widmanstatten Sideplates*: At Temperatures Above 600°C. Sideplates grow into the interiors of matrix grains from the region of the grain boundaries, usually from grain boundary allotriomorphs.[5-7] The α sideplates normally form in groups which are parallel to a common habit plane in the β grain into which they develop, as illustrated in Fig. 5. Sideplates develop into both of the bounding β grains from the allotriomorphs at some grain boundaries and into only one β grain from the allotriomorphs at other boundaries; at a few rows of allotriomorphs, sideplates do not form even at comparatively late stages in the transformation, Fig. 5. At most grain boundaries whose orientation is nearly constant, sideplates form parallel to only one, or occasionally two habit planes. As shown in Fig. 6, a marked change in the orientation of a grain boundary can change the habit plane of sideplates or even prevent completely the development of this morphology.

Sideplates are the dominant morphology after appreciable amounts of α have formed in virtually all of the β grains in specimens reacted at 725° and 700°C. From 675° through 625°C, there is an increasing tendency for intragranular plates to contribute the largest proportion of α, especially in β grains which are larger than average or in which one or more grain boundaries does not serve as a prolific source of sideplates.

Although some complexities are involved, the average spacing at early reaction times between sideplates associated in groups decreases with decreasing reaction temperature. The average width of sideplates, and apparently also the average width to length ratio, decrease in the temperature range 725° to 625°C.

A well formed sideplate has a needle-like cross section on a plane of polish which makes an appreciable angle with the broad faces of the plate. Many α plates formed at temperatures above 600°C, however, deviate sufficiently from this ideal shape to be termed *degenerate*. The evolution of variations of the basic sideplate shape does not occur at random. One or two basic motifs normally characterize an entire group of degenerate sideplates at a grain boundary whose orientation is approximately constant. The total number of different types of degeneracy appears to be limited. An individual type of degeneracy is often found repeatedly in a given specimen and in other specimens reacted for different times at the same temperature. Some types of degenerate sideplates appear at more than one reaction temperature, with the average number of crystals in a group of sideplates rapidly increasing and the size of the individual crystals rapidly decreasing as the temperature is reduced.

Figs. 7a and 7b are examples of two of the most common types of degenerate sideplates formed at 700° to 725°C. Figs. 7c and 7d show groups of degenerate sideplates, formed at 675°C, in which the basic motifs of the corresponding structures in Figs. 7a and 7b have been essentially reproduced in miniature. Further reductions in temperature result in the development of additional complexities of shape among groups of degenerate sideplates, though the types of structure shown in Figs. 7a and 7b continue to appear.

One source of degeneracy among sideplate structures is illustrated in Fig. 7b. The sideplates in this field are composed of short segments. Close examination of the individual segments, such as the one pointed out by the arrowhead, indicates that they are composed of individual *beads* of α, separated by α:α boundaries. Neither coincidence nor a nonrepresentative plane of polish appears to be a satisfactory explanation for these rows of *beads*. It is more probable that individual *beads* nucleated at the interphase boundaries of previously formed *beads*, despite the deterrent to the nucleation of chromium-poor α crystals which should be provided by regions of β enriched in chromium to nearly the maximum permitted by the phase diagram. The phenomenon of nucleation at the interphase boundaries of previously formed crystals of the same phase has been previously identified in the proeutectoid ferrite reaction in a plain carbon steel and was named *sympathetic nucleation*.[8]

When only a small proportion of the plates in a group of sideplates grows from grain boundary allotriomorphs or from a β grain boundary and the

Fig. 2—Typical grain boundary allotriomorphs of α, Ti-7.22 pct Cr. Solution annealed 40 min at 1000°C; reacted 25 min at 725°C. Etched in 60 pct glycerine, 20 pct HNO_3, 20 pct HF. X500.

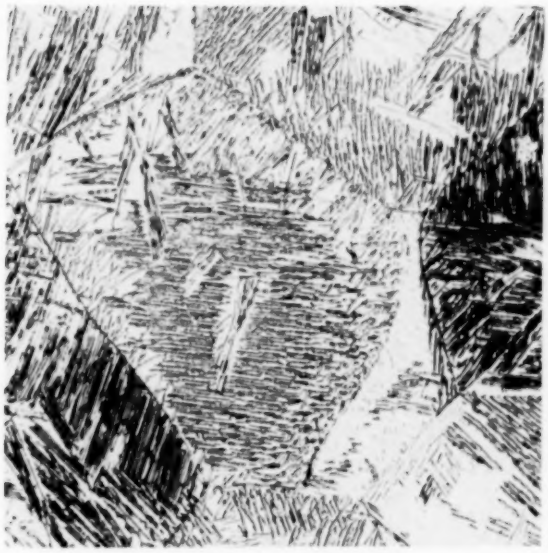

Fig. 3—General view of structure shortly after metastable equilibrium is attained at 675°C. Ti-7.22 pct Cr. Solution annealed 40 min at 1000°C; reacted 1 hr at 675°C. Etched in 60 pct glycerine, 20 pct HNO_3, 20 pct HF. X250. Enlarged approximately 10 pct for reproduction.

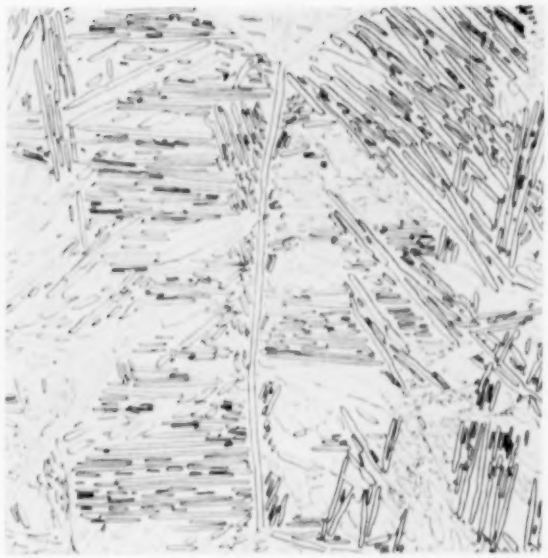

Fig. 4—General view of structure after prolonged reaction at 675°C. Ti-7.22 pct Cr. Solution annealed 40 min at 1000°C; reacted 7 days at 675°C. Etched in 60 pct glycerine, 20 pct HNO_3, 20 pct HF. X250. Enlarged approximately 10 pct for reproduction.

remainder are nucleated at the broad faces of plates previously formed, the resultant structure is termed a *sheaf of sideplates*.[9] Structures of this type first appear in significant numbers at 650° and are the dominant mode of sideplate formation at 625°C. Fig. 7e shows several sheaves of sideplates formed at 650°C. The observations that these sheaves often attain their maximum thickness at some distance from the grain boundary and that a number of the component plates of the sheaves are separately resolvable indicate that the sheaves are neither structures composed entirely of secondary sideplates nor intricately shaped single plates.

Fig. 7f shows a typical group of sheaves of sideplates formed at 625°C. The individual plates are now in contact over most of their lengths, but the boundaries between them are sufficiently revealed to indicate that each sheaf is composed of many thin plates of varying lengths.

The sideplate structures presented above developed during the early stages of the formation of α. With increasing reaction time, drastic changes occur in these structures.* These changes may be summarized as follows:

1) The average spacing between sideplates increases substantially, compare Figs. 3 and 4, despite the fact that the average plate thickness also becomes larger.

2) The rate of increase in the average intersideplate spacing, which was semiquantitatively assessed in terms of the ratio of the increase in spacing during a given interval of reaction time to the initial spacing, increases with decreasing temperature, passes through a maximum at 650°, and decreases at 625°C.

3) The perfection of shape of many sideplates increases noticeably with increasing isothermal reaction time, compare Figs. 7a through 7d and 8a.

4) The connections between sideplates and allotriomorphs, which are not too good even during the early stages of reaction, are almost completely severed at late reaction times, Fig. 8a.

Fig. 8b shows the separation of sideplates from allotriomorphs at an earlier stage than in Fig. 8a. Arrowhead *A* points out a sideplate whose base has been nearly dissolved, while arrowhead *B* indicates a sideplate which appears to have been disconnected from the allotriomorph from which it developed shortly before the termination of the isothermal reaction anneal. A protuberance remains in the interphase boundary of the allotriomorphic base layer on the side which faces the sideplate at arrowhead *B*, and at several other places along this boundary. At later reaction times, Fig. 8a, these protuberances largely disappear and the interphase boundaries of most allotriomorphs become smoothly shaped.

5) At very late reaction times, even well formed sideplates tend to break up into shorter segments, which then tend to become increasingly separated; the more degenerate groups of sideplates apparently tend to break up almost completely into irregularly disposed platelets and idiomorphs.

B. At Temperatures Between 600° and 550°C. An unexpected change in the morphology of sideplates occurs when the reaction temperature is reduced to 600°C. In addition to densely packed groups and sheaves of very thin sideplates, another type of sideplate, illustrated in Figs. 9a and 9b, begins to appear. These crystals develop as single plates, rather than as sheaves, etch darkly, are usually much longer and thicker than ordinary single sideplates in the same specimen, and are characterized by exceptional perfection and simplicity of shape. Although no X-ray studies were made of specimens reacted in the 600° to 550°C region, a careful investigation by Spachner et al.[9] of the crystal structure of the transformation products in a Ti-8 pct Cr alloy demonstrated that α is the only proeutectoid phase to form above 550°C. The *black*

* Van Thyne and Rostoker[6] have previously described these changes, in general fashion, as *coarsening* of the Widmanstätten structure.

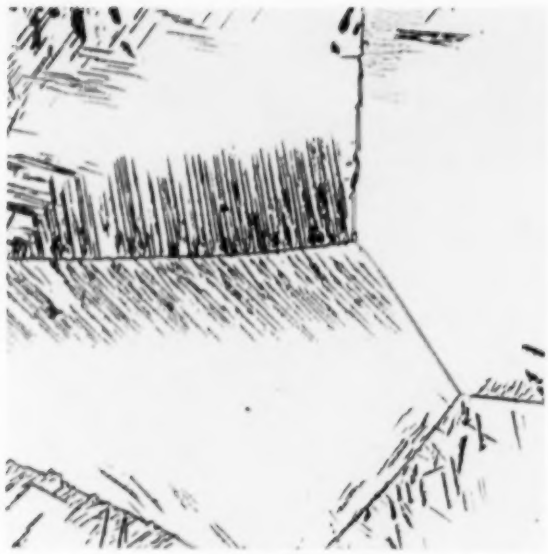

Fig. 5—Widmanstätten sideplates developed from allotriomorphs. Ti-7.22 pct Cr. Solution annealed 40 min at 1000°C; reacted 30 min at 700°C. Etched in 60 pct glycerine, 20 pct HNO_3, 20 pct HF. X250. Enlarged approximately 10 pct for reproduction.

Fig. 6—Effects of grain boundary orientation on sideplate morphology. Ti-7.22 pct Cr. Solution annealed 40 min at 1000°C; reacted 2 min at 650°C. Etched in 60 pct glycerine, 20 pct HNO_3, 20 pct HF. X500. Enlarged approximately 10 pct for reproduction.

plates are therefore presumed to be α. These crystals constitute a relatively small proportion of the sideplates formed at 600°C, Fig. 9a, are the dominant sideplate morphology at 575°C, Fig. 9b, and may be the only sideplate structure to develop at 550°C.

The ratio of black plates to normal α plates at a given grain boundary, the particular matrix habit plane(s) to which the black plates at a boundary are parallel, and the rate of nucleation of black plates exhibit the same types of orientation dependencies as do the sideplates of normal α formed at higher temperatures. Some of these effects are illustrated in Fig. 9b.

Fig. 10a shows sideplates and intragranular plates in a structure formed at 600°C. Both *black plates* and sheaves of normal α are present; the total amount of these structures constitutes nearly the metastable equilibrium proportion of α. Although the *black plates* are clearly visible, they are present in much smaller quantity than the sheaves of normal α. Fig. 10b, on the other hand, illustrating a typical structure at a much later reaction time at the same temperature, is dominated by crystals which appear to be thickened *black plates*. The average spacing between *black plates* does not appear to have changed significantly, but the sheaves of normal α have disappeared. Groups of small, rather well shaped cross-plates and occasional complex, light etching groups of crystals not much thinner than the main *black plates* have replaced the sheaves of normal α plates.

Similar changes in structure were found at 575°C. At this temperature, however, the smaller amount of normal α initially present quickly disappeared. Late reaction time structures at 550°C appeared to be composed entirely of thickened *black plates*, slightly thinner and noticeably shorter and more uniform in size than those developed at 600°C.

Intragranular Widmanstätten Plates: At Temperatures Above 600°C. Intragranular plates are the last α morphology to appear at reaction temperatures above 600°C. This morphology is present at all of the reaction temperatures studied, but its importance at late reaction times increases with decreasing temperature. Intragranular plates form a relatively small component of the microstructure at 725°, are prominent at 700° to 675°C, and become the dominant morphology at 625° to 600°C. The variations of β grain size within individual specimens were sufficient to demonstrate that an appreciable decrease in grain size will materially reduce the proportion of intragranular plates in the microstructure, especially at the higher reaction temperatures.

Intragranular plates appear as isolated single plates and grouped together in sheaves. Single plates appear most frequently at 725° and during the early stages of reaction at 700°C; sheaves are the dominant intragranular structure during later reaction times at 700°, and at all stages of α formation within β grains at lower temperatures through 625°C. Single plates, however, are still present in small numbers throughout this temperature range.

Fig. 11a shows part of a single intragranular plate formed at 700°C. Close inspection indicates that this plate was probably formed by the successive sympathetic nucleation of smaller plates at the edges of previously formed plates. Fig. 11b is a low magnification view of most of a β grain, in which a number of sheaves have developed. The almost complete absence of α plates in the comparatively large spaces between the sheaves and the relatively short lengths of the sideplates make it highly unlikely that most of the component plates of the sheaves, which are so close together that they are largely unresolved at this magnification, were formed by any mechanism other than sympathetic nucleation.

Both single plates and sheaves sometimes appear as components of larger groupings. Known as *Widmanstätten stars*,[5] these structures consist of two or more plates or sheaves, usually nucleated at a central locus, which are parallel to different matrix habit planes. Additional plates or sheaves of plates

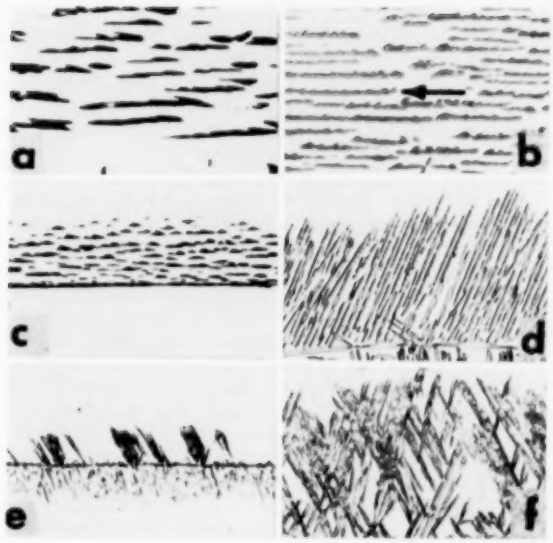

Fig. 7—Ti-7.22 pct Cr, solution annealed 40 min at 1000°C. a to d) Degenerate sideplates. e, f) Sheaves of sideplates. a) 725°C for 6 hr. X500. b) 700°C for 30 min. X250. c) 675°C for 15 min. X1000. d) 675°C for 30 min. X500. e) 650°C for 1 min. X1000. f) 625°C for 10 min. X1000. Etched in 60 pct glycerine, 20 pct HNO_3, 20 pct HF. Enlarged approximately 10 pct for reproduction.

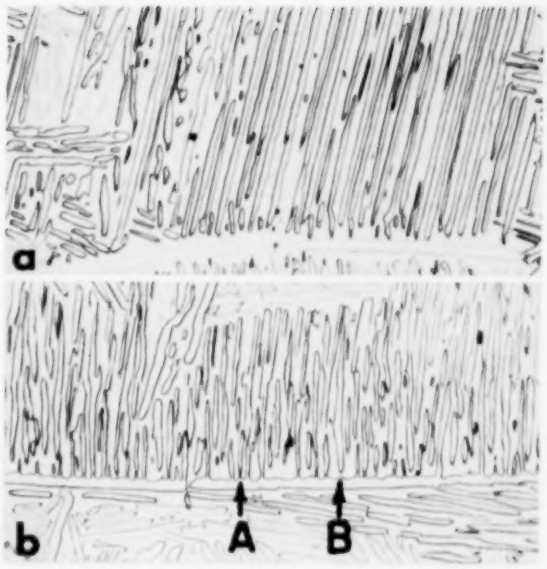

Fig. 8—Ti-7.22 pct Cr, solution annealed 40 min at 1000°C. a) Increased perfection of sideplates at late reaction time; reacted 15 days at 650°C. X500. b) Dissolution of junctions between sideplates and allotriomorphs; reacted 3 days at 650°C. X1000. Etched in 60 pct glycerine, 20 pct HNO_3, 20 pct HF. Enlarged approximately 10 pct for reproduction.

are often sympathetically nucleated, at their edges, against the broad faces and the edges of components of the star.

Fig. 11c, taken for convenience from a specimen reacted at 600°C, shows a complex Widmanstätten star composed largely of single plates. Fig. 11d shows a star of sheaves formed at 650°C. Both types of star appear in noticeable numbers at 650°C and below, but stars of sheaves are found with noticeably greater frequency than stars of single plates.

Ideally, a sheaf of intragranular plates should be composed of a number of well formed, parallel plates of approximately equal thickness, with lengths decreasing slowly from the center to the edges of the sheaf; the broad faces of adjacent plates should be in contact over most of their lengths. It is found experimentally, however, that deviations from this ideal morphology are the rule rather than the exception. As in the case of degenerate sideplates, the deviations are both systematic and repetitive.

Fig. 11e shows an example of one of the more common types of intragranular sheaf. Two comparatively thick outer plates, concave in shape and not well formed, enclose many very thin, closely packed, and highly degenerate plates. Fig. 11f shows an example of another frequently found type of intragranular sheaf. Close examination indicates that this structure is largely composed of numerous thin, short plates, intricately interconnected as a result of frequent sympathetic nucleation.

The effects of continued annealing at the temperature of isothermal reaction upon the structure of sheaves are largely similar to those previously listed for sideplates. The effects of reaction time on intragranular sheaves differ from the effects on sideplates in only one important respect: the rate of increase in the average interplate spacing in intragranular sheaves increases continuously with increasing temperature.

A. At Temperatures Between 600° and 550°C. Intragranular plates begin to form shortly after sideplates appear at 600° and 575°C and soon become the dominant morphology. At 550°C, however, the rapid formation of sideplates at subboundaries tends to obsecure, and reduce the importance of intragranular precipitation.

As in the case of sideplate structures, *black plates* begin to appear intragranularly at 600°C. At this temperature, they are intermixed with sheaves of normal α, Fig. 12a. A higher magnification view of a typical mixed structure is shown in Fig. 12b. The largest Widmanstätten star in this field appears to have developed by the sympathetic nucleation of sheaves of normal α about a central *black plate*. Other structures in this field, however, are apparently composed entirely of either *black plates* or normal α. Evidently intragranular precipitation at 600°C can be initiated by either type of plate.

At 575°C, *black plates* become the dominant, and almost the only, intragranular morphology. Unlike normal α, the *black plates* do not form sheaves. As illustrated in Fig. 12c, these plates tend to appear singly or in small, simple groupings, such as checks and triangles. Subboundaries in the β grains, as well as sympathetic nucleation, appear to play a role in the formation of these groupings.

The summary previously given of the behavior of sideplates at late reaction times in this temperature range is also applicable to intragranular plates.

Discussion: Although a detailed discussion of all of the individual features of the morphologies of proeutectoid α cannot be attempted here,* an insight into the origins of these structures may be obtained by comparison of the α morphologies with those of proeutectoid ferrite, as formed in plain carbon, hypoeutectoid steels. Outwardly, the two reactions differ in several basic aspects: the type of

* A more extensive discussion of these features has been provided in ref. 13.

solid solution involved, the crystal structures of the matrix and the precipitate phases, and the differences in the individual characteristics of the solvent and solute atoms. The morphologies of proeutectoid α and proeutectoid ferrite, however, have at least three important features in common: the Dube[1] morphological classification system is applicable to both precipitates, the orientation dependencies of α sideplates are the same as those of proeutectoid ferrite,[2] and sheaves of sideplates and intragranular sheaves develop at lower temperatures in both alloy systems.[3,10] These fundamental similarities suggest that the shapes of precipitate crystals may be largely controlled by general factors, rather than by the individual characteristics of particular alloy systems. It has been suggested that the structure of the sites at which precipitates nucleate and the migrational characteristics of the interphase boundaries which enclose them are the most important of these factors.[8,10]

There are, however, some differences between the α and the ferrite reactions which require discussion. The details of degenerate α sideplate and intragranular plate structures differ appreciably from those of degenerate ferrite sideplates[10] and intragranular sheaves.[3,10] This difference is perhaps to be expected. Degenerate plates are considered to result, in part, from the disruption of portions of the interfacial structure of the broad faces of plates by volume transformation strains, with the consequent alteration of the migrational characteristics of the affected areas.[10] The amount and distribution of these strains is controlled, for a crystal of a given shape, by the volume change associated with the individual reaction and the elastic constants (at a given reaction temperature) of the phases involved. Both of these factors vary markedly among different systems. The sites at which sympathetic nucleation, another source of degeneracy, will be most likely to occur should also be influenced by the local changes in interfacial structure and energy produced by transformation strains.

The *black plates* formed in Ti-Cr alloys have no counterpart in hypoeutectoid steels. This difference is both unexpected and unexplained.

Two additional differences between the α and the ferrite reactions appear to be more of degree than of kind. The amount of undercooling below the transus required to form large numbers of plates or sheaves of plates is much less in Ti-7.22 pct Cr than in hypoeutectoid steels.[5-7,9] Grain boundary allotriomorphs are thus not the dominant α morphology at late reaction times even at temperatures near the transus; in hypoeutectoid steels,[5-7] allotriomorphs are the dominant, and often almost the only, ferrite morphology present over an appreciable range of undercooling.

The changes which take place in the α plate morphologies at late reaction times might also occur in ferrite plates formed in plain carbon steels if these morphologies developed more readily at temperatures above the eutectoid or if pearlite did not form so rapidly at temperatures below the eutectoid. The nature of the changes previously listed strongly indicates that the minimization of interphase interfacial free energy is the driving force for these changes. High energy interfaces, such as the edges of plates, irregularities in the broad faces of plates, and the junctions between sideplates and allotriomorphs will thus tend to be dissolved, with the more sharply curved interfaces being attacked more rapidly. Simultaneously, the low energy interfaces, such as the dislocation facets in the broad faces of plates,[7] will tend to increase in area and to migrate normal to themselves into the surrounding β.

The rate at which the intersideplate spacing increases should rise with increasing degeneracy of

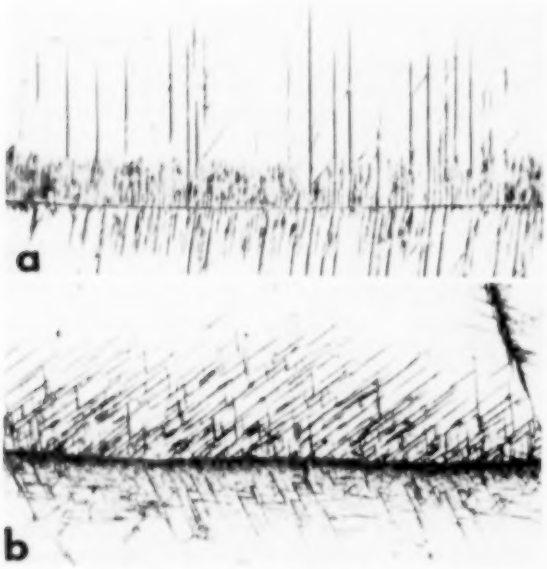

Fig. 9—Ti-7.22 pct Cr, solution annealed 40 min at 1000°C. a) Sheaves of normal α and *black plates*, reacted 3 min at 600°C. X1000. b) Different proportions of *black plates* and normal α on opposite sides of grain boundary; reacted 1 min at 575°C. X500. Etched in 60 pct glycerine, 20 pct HNO_3, 20 pct HF. Enlarged approximately 10 pct for reproduction.

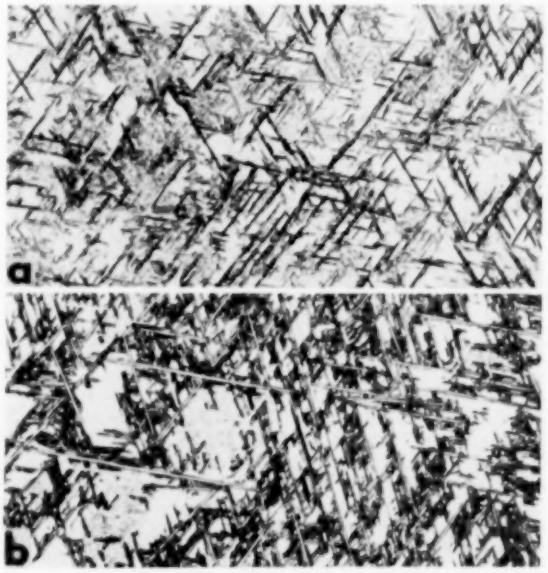

Fig. 10—Ti-7.22 pct Cr, solution annealed 40 min at 1000°C. a) *Black plates* and normal α at a comparatively early reaction time; reacted 7 min at 600°C. b) *Black plates*, appreciably thickened, become the dominant structure; reacted for 3 days at 600°C. Etched in 60 pct glycerine, 20 pct HNO_3, 20 pct HF. X500. Enlarged approximately 10 pct for reproduction.

the sideplates, decreasing plate thickness, decreasing initial interplate spacing, and increasing diffusivities of titanium and chromium atoms. In the temperature range between 725° and 625°C, all of these factors but the diffusivities become more favorable with decreasing temperature. The maximum in the rate of increase of the interplate spacing which is accordingly to be expected was found experimentally at about 650°C. The continuous rise in the rate of increase of the interplate spacing of intragranular sheaves with increasing temperature is presumably due to the circumstance that the initial interplate spacing in sheaves does not vary markedly with temperature.

The Eutectoid Reaction—*Mechanism*: The mechanism of the eutectoid reaction was studied in specimens of iodide Ti-7.22 pct Cr reacted in the range between 650° and 550°C and in specimens of sponge Ti-10.94 pct Cr reacted at 650°C. The latter alloy was employed because its higher chromium and oxygen contents accelerate the eutectoid reaction[1,6,10] sufficiently to permit virtually the full course of this reaction to be followed conveniently at 650°C, a temperature at which the size of the $TiCr_2$ crystals is relatively large. No important differences were found in the nature of the eutectoid reaction in the two alloys.

The eutectoid reaction begins with the precipitation of $TiCr_2$ crystals at α allotriomorphs, Fig. 13a. The $TiCr_2$ crystals are readily identified by the high etching rates of their interphase boundaries. An extended study was made of the locations of $TiCr_2$ crystals formed at the earliest stages of reaction. As illustrated in Fig. 13a, most of these crystals are found at the following locations: 1) almost entirely in β at α:β boundaries; 2) about equally in α and β at α:β boundaries; and 3) almost entirely in α at α:β boundaries. Few crystals were found wholly and deeply imbedded within α. It will shortly be shown that appreciable numbers of $TiCr_2$ crystals do not appear in the initially unblemished areas of proeutectoid α at a later stage in the transformation. The simplest and perhaps the most probable conclusion which may be drawn from this evidence is that the eutectoid reaction begins with the precipitation of $TiCr_2$ in β at α:β boundaries, with an unknown, though presumably small, amount of $TiCr_2$ precipitating in α. (Structures No. 2 and 3, above, are thus considered to be the result of displacement of the α:β boundaries with respect to stationary $TiCr_2$ crystals.)

The next step in the eutectoid reaction is either 1) the nucleation of new α crystals at β:$TiCr_2$ boundaries; or 2) the resumption of the migration of the β: proeutectoid α boundaries into β, Fig. 13b. The evidence available is insufficient to permit a decision to be made as to the operative mechanism. In either case, the α formed as a result of the prior nucleation of $TiCr_2$ will be termed *eutectoid* α. As shown in Fig. 13b, further precipitation of $TiCr_2$ occurs preferentially at β:eutectoid α boundaries and results in the formation of additional eutectoid α. The composite structure thus advances into the untransformed β by the successive precipitation of $TiCr_2$ and of α from β.

Fig. 13b indicates that the growth of eutectoid α is roughly isotropic, in marked contrast to that of proeutectoid α. As indicated in Fig. 14a, however, the steric interference of proeutectoid α often markedly affects the morphology of eutectoid α.

Fig. 14b shows that the rates of the eutectoid reaction can vary appreciably at different grain boundaries.

The structures shown in Figs. 13b and 14a suggest that eutectoid α may absorb, in some way, the previously formed proeutectoid α, as previously sug-

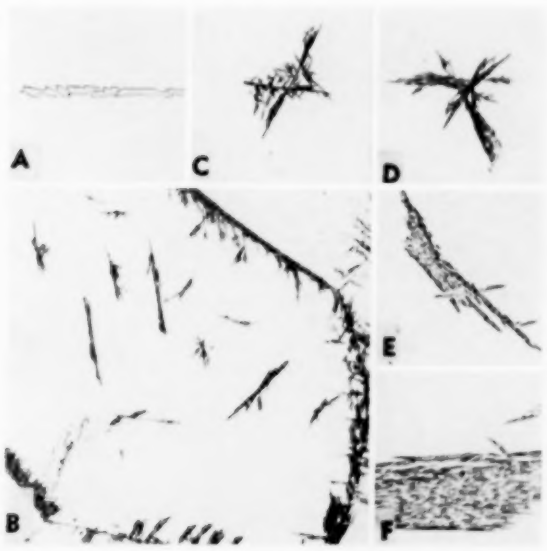

Fig. 11—Ti-7.22 pct Cr, solution annealed 40 min at 1000°C. a) Segmented intragranular plate; reacted 4 hr at 700°C. X500. b) Intragranular sheaves; reacted 7 min at 650°C. X250. c) *Star* of single plates; reacted 7 min at 600°C. X1000. d) *Star* of sheaves; reacted 10 min at 650°C. X500. e) Complex intragranular sheaf; reacted 10 min at 650°C. X1000. f) Another type of complex intragranular sheaf; reacted 30 min at 650°C. X1000.

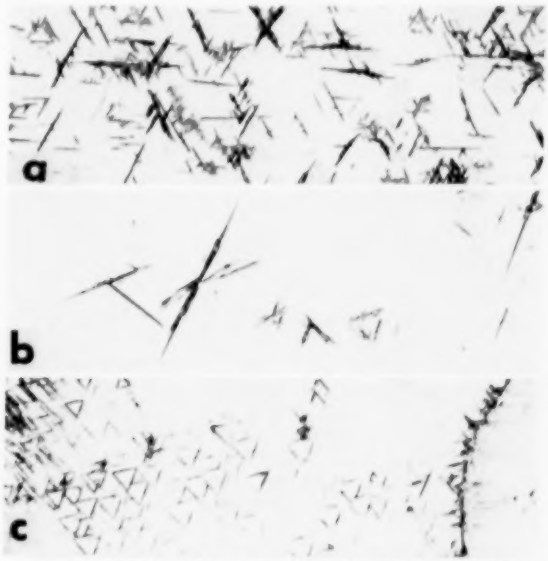

Fig. 12—Ti-7.22 pct Cr, solution annealed 40 min at 1000°C. a) Mixed intragranular *black plates* and sheaves of normal α; reacted 3 min at 600°C. X500. b) Widmanstätten *star* formed about a *black plate*, and structures composed entirely of either *black plates* or normal α; reacted 3 min at 600°C. X1000. c) Configurations of intragranular *black plates*; reacted 10 sec at 575°C. X500. Etched in 60 pct glycerine, 20 pct HNO_3, 20 pct HF. Enlarged approximately 15 pct for reproduction.

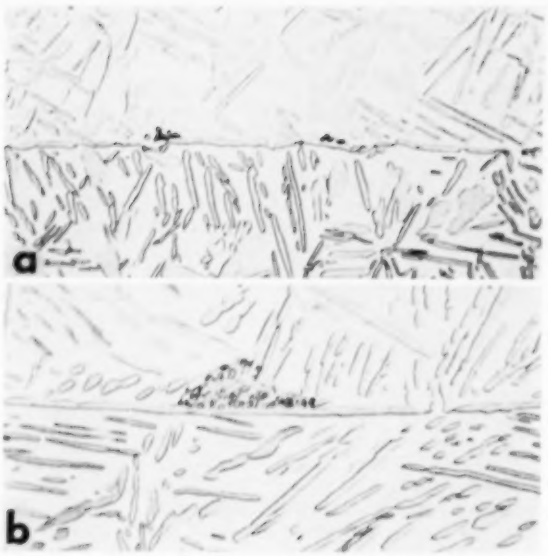

Fig. 13—Ti-10.94 pct Cr, solution annealed 40 min at 1000°C. a) Precipitation of $TiCr_2$ largely in β at interphase boundaries of α allotriomorphs; reacted 12 hr at 650°C. b) Formation of $TiCr_2$ primarily in association with eutectoid α; reacted 1 day at 650°C. Etched lightly in 60 pct glycerine, 20 pct HNO_3, 20 pct HF. X1000. Enlarged approximately 15 pct for reproduction.

gested by Frost et al.[1] and Rostoker.[4] Fig. 15, however, indicates that proeutectoid α is probably not absorbed, but merely engulfed. The sizes of the individual $TiCr_2$ crystals and the mean free α path in the eutectoid α are much reduced in consequence of the lower reaction temperature (600°C), permitting the preservation of the thickened *black plates* and allotriomorphs, which comprise most of the proeutectoid component of this structure, to be readily established.

Intragranularly, the eutectoid reaction begins much later than at the grain boundaries. Comparison of Figs. 13a and 16a and of Figs. 13b and 16b indicates, however, that the basic mechanism is the same.

At late reaction times, the continued growth of eutectoid structures nucleated intragranularly and at grain boundary allotriomorphs slowly transforms the remaining β. In the 10.94 pct Cr alloy, the reaction is more than 95 pct complete after 29 days of reaction at 650°C.

Kinetics: The initial stage of the eutectoid reaction, the precipitation of $TiCr_2$ at α allotriomorphs, develops so slowly, especially at temperatures near the eutectoid, that the selection of a reproducible criterion for the *beginning* of the reaction necessarily involves the use of a somewhat later stage in the transformation. The initial appearance of a scattering of closely packed rows of $TiCr_2$ crystals was found to be suitable for this purpose. Fig. 1 shows the *TTT*-curve obtained on this basis for the 7.22 pct Cr alloy.

In view of the unexpected change in the shape of this curve which occurs at 600°C, additional series of specimens were reacted at 562° and 587°C. As shown in Fig. 1, the results of these heat treatments are consistent with those previously performed.

Discussion: Frost et al.[1] have shown that the formation of $TiCr_2$ is accompanied by a decrease in the chromium content of the untransformed β, indicating that $TiCr_2$ precipitates from β. Rostoker[4] has suggested that impurity elements may convert nominally binary Ti-Cr alloys into polycomponent systems and that $TiCr_2$ may precipitate from α as the composition of the α changes in conjunction with displacement of the three-phase field $\alpha + \beta + TiCr_2$. The results of the present investigation are in agreement with those of Frost and co-workers.

The markedly higher rates of nucleation of $TiCr_2$ at the interphase boundaries of grain boundary allotriomorphs, as compared with those at the boundaries of sideplates and intragranular plates, are readily explained on the basis of the different proportion of high interfacial free energy facets in these boundaries. Inasmuch as allotriomorphs are compelled to follow the paths of the grain boundaries, the proportion of high energy facets in the boundaries of allotriomorphs will tend to be considerably greater than in sideplates or in intragranular plates. Since heterogeneous nucleation theory predicts that the rate of nucleation will increase very rapidly as the energy of the nucleation site is increased,[10] the observed dependence of the nucleation rates of $TiCr_2$ upon α morphology is consistent with theory.

Summary

The morphologies and mechanisms of the proeutectoid α and eutectoid reactions have been investigated in an iodide Ti-7.22 pct Cr alloy in the temperature range between 725° and 550°C; supplementary studies were performed on the eutectoid reaction in specimens of a sponge Ti-10.94 pct Cr alloy reacted at 650°C.

The morphological classification scheme devised by Dube[11] for the proeutectoid ferrite reaction in plain carbon steels was found to be applicable to the morphologies of proeutectoid α. Many of the characteristics of the individual α morphologies

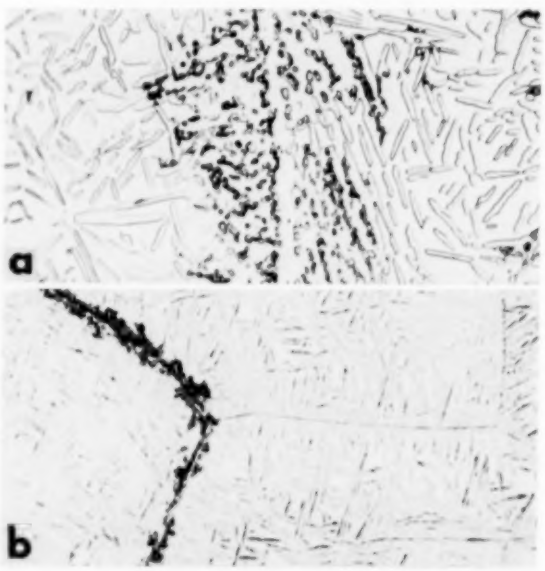

Fig. 14—Ti-10.94 pct Cr, solution annealed 40 min at 1000°C. a) Steric interference of proeutectoid α with growth of eutectoid α; reacted 2 days at 650°C. X1000. b) Illustration of the marked difference in rates of the eutectoid reaction at different grain boundaries; reacted 8 hr at 650°C. X250. Etched lightly in 60 pct glycerine, 20 pct HNO_3, 20 pct HF. Enlarged approximately 15 pct for reproduction.

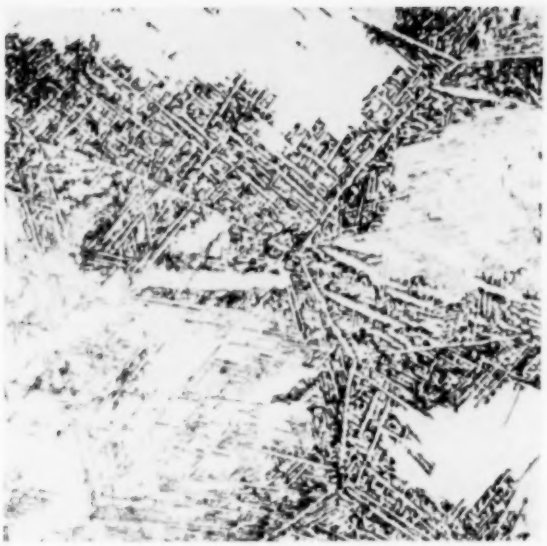

Fig. 15—Ti-7.22 pct Cr, solution annealed 40 min at 1000°C. Evidence for the failure of eutectoid α to absorb proeutectoid α; reacted 5 days at 600°C. Etched lightly in 60 pct glycerine, 20 pct HNO_3, 20 pct HF. X500. Enlarged approximately 10 pct for reproduction.

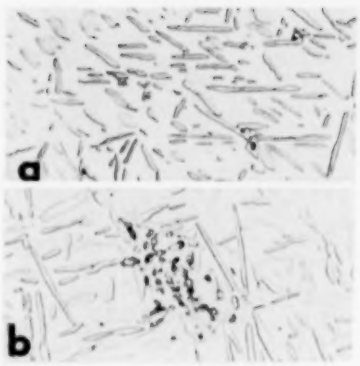

Fig. 16—Ti-10.94 pct Cr, solution annealed 40 min at 1000°C. a) Nucleation sites of $TiCr_2$ formed at intragranular α plates; reacted 3 days at 650°C. X500. b) Formation of eutectoid nodule intragranularly; reacted 2 days at 650°C. X1000. Etched lightly in 60 pct glycerine, 20 pct HNO_3, 20 pct HF. Enlarged approximately 10 pct for reproduction.

were observed to be the same as those of ferrite. These observations provide evidence to show that the shape of a precipitate crystal may be controlled primarily by generally operative factors rather than by the particular characteristics of an individual alloy system.

The following are some of the more important characteristics of the various α morphologies:

1) Grain boundary allotriomorphs are present at all reaction temperatures studied but are never the dominant morphology at late reaction times. The α allotriomorphs continue to thicken even after the metastable equilibrium proportion of α has formed.

2) Widmanstätten sideplates are the dominant morphology at late reaction times between 725° and 675°C. The crystals are often degenerate in shape, but the description of the degeneracy evolved tends to remain constant at a grain boundary whose orientation is approximately constant. Sideplates often appear in sheaves at 625° and 600°C. At 600°C and lower temperatures, a new type of α sideplate—long, slender, nearly perfect in shape, and initially dark etching—increasingly replaces the type of sideplate formed at higher temperatures.

3) Intragranular plates are dominant at late reaction times at 650° to 550°C. These plates also appear frequently in sheaves. The sheaves are often characteristically degenerate. *Black plates* also begin to replace normal α plates intragranularly at 600°C.

The following sequence describes the mechanism of the eutectoid reaction at all of the reaction temperatures studied:

1) $TiCr_2$ crystals nucleate initially at α allotriomorphs, later at α plates. It was deduced that most of these crystals nucleate in β at α:β boundaries.

2) The growth of α is resumed (or new α crystals nucleate) and the $TiCr_2$ crystals originally formed are engulfed.

3) $TiCr_2$ crystals then nucleate preferentially at the interphase boundaries of the newly formed α, resulting in further growth of the α crystals.

Table I. Compositions of Titanium Alloys, Pct

Cr	O	N	H	C
7.22	0.0403	0.010	0.0067	0.019
10.94	0.302	0.030	—	—

Acknowledgments

This investigation was initiated and largely performed under the sponsorship of the Aeronautical Research Laboratory, Wright Air Development Center, and completed with the support of the Office of Naval Research. The authors express their appreciation to both of these agencies, to J. G. Kura and the Battelle Memorial Institute for advice and the preparation of the 7.22 pct Cr alloy, to S. A. Herres and the Titanium Metals Corp. of America for the gift of the 10.94 pct Cr alloy, and to W. A. Peifer and the Allegheny Ludlum Steel Corp. for the chemical analyses of the latter alloy. Appreciation is also expressed to E. T. Kennedy, E. J. Pasierb, and H. V. Nelly for much assistance in the laboratory and to C. Wells and W. Rostoker (Armour Research Foundation) for valuable discussions.

References

[1] P. D. Frost, W. M. Parris, L. L. Hirsch, J. R. Doig, and C. M. Schwartz: Isothermal Transformation of Titanium-Chromium Alloys. *ASM Trans.*, 1954, vol. 46, p. 231.

[2] M. K. McQuillan: A Redetermination and Interpretation of the Titanium-Rich Region of the Titanium-Chromium System. *Journal* Institute of Metals, 1953-1954, vol. 82, p. 433.

[3] W. Rostoker, D. J. McPherson, and M. Hansen: Structural Changes of Commercial Titanium and Titanium-Base Alloys on Heat Treatment. WADC Technical Report No. 53-62, 1953.

[4] W. Rostoker: Discussion to Ref. 1. *ASM Trans.*, 1954, vol. 46, p. 251.

[5] C. A. Dube: Ph.D. Thesis, Carnegie Institute of Technology, 1948.

[6] R. F. Mehl: The Decomposition of Austenite by Nucleation and Growth Processes. *Journal* Iron and Steel Institute, 1948, vol. 159, p. 113.

[7] R. F. Mehl and C. A. Dube: The Eutectoid Reaction. *Phase Transformations in Solids*, p. 545. John Wiley & Sons Inc. New York, 1951.

[8] H. I. Aaronson: Effects of Nucleation Site Upon Precipitate Morphology. *Symposium on the Mechanism of Phase Transformations in Metals*, p. 47. The Institute of Metals. London, 1955.

[9] H. I. Aaronson and C. Wells: Sympathetic Nucleation of Ferrite. *AIME Trans.*, 1956, vol. 206, p. 1216; JOURNAL OF METALS, October 1956.

[10] H. I. Aaronson: Unpublished research.

[11] S. A. Spachner, R. F. Domagala, A. W. Goldenstein, and W. Rostoker: Structural Changes in Commercial Titanium and Titanium-Base Alloys on Heat Treatment. WADC Technical Report No. 55-352, 1956.

[12] R. J. Van Thyne and W. Rostoker: Discussion to Ref. 2. *Journal*, Institute of Metals, 1953-1954, vol. 82, p. 648.

[13] H. I. Aaronson, G. M. Andes, W. B. Triplett, and C. Wells: Phase Transformations in Hypoeutectoid Titanium-Chromium Alloys. WADC Technical Report No. 56-469, 1956.

[14] R. J. Van Thyne, H. D. Kessler, and M. Hansen: The Systems Titanium-Chromium and Titanium-Iron. *ASM Trans.*, 1952, vol. 44, p. 974.

[15] J. H. Hollomon and D. Turnbull: Nucleation. *Progress in Metal Physics*, vol. 4, p. 333. Interscience Publishers. New York, 1953.

Discussion of this paper sent (2 copies) to AIME by Jan. 1, 1958 will appear in AIME *Transactions* Vol. 212, 1958, and in JOURNAL OF METALS, April 1958.

The Uranium-Silicon Epsilon Phase

The properties of the U-Si ε phase have been investigated, with emphasis on the means of obtaining material resistant to corrosion in water. Evidence is presented that the corrosion resistance depends on the absence of phases other than ε and that the desired ε phase has a silicon content in the range of 3.9 to 4.0 wt pct, rather than the 3.78 wt pct of stoichiometric U_3Si. It was necessary to develop an analytical method to overcome the apparently low silicon content found in this system under certain conditions. Attempts to fabricate this alloy were devoted primarily to coextrusion with Zircaloy-2. Extrusion constants are reported.

by S. Isserow

RECENTLY, a description of the wartime work in this laboratory on the U-Si phase diagram was published.[1] This diagram was available earlier in the open literature,[2] as were Zachariasen's crystal structure identifications for the compounds in the system.[3] The uranium end of the phase diagram is shown in Fig. 1. The most recent work on this system has emphasized the peritectoid ε phase, of particular interest for a number of reasons. The early work provided evidence of this phase's resistance to corrosion in water and of its slight ductility. Further information on these properties has been obtained here. Work elsewhere[4] has provided evidence of stability under irradiation. This body-centered-tetragonal phase is relatively isotropic compared to the more usually applied α or γ uranium phases. Unlike the other compounds in this system, it contains no Si-Si covalent bonds.[5] In addition, consideration on the basis of Pauling's concepts leads to the conclusion that in the ε phase, uranium has a higher valence than in any of the other phases.

Definition of the composition of the ε phase has been of prime concern in the study of this alloy. Evidence is presented below that its silicon content is slightly higher than that of stoichiometric U_3Si, the composition frequently assigned this phase on the basis of Zachariasen's identification. This work on the composition required careful attention to the method of dissolving the alloy for analysis, since apparently low silicon contents could be found under certain conditions, see Appendix.

Preparation: Melting, Casting, and Heat Treatment—Almost all the samples were from castings with a diameter of 1¾ or 2 in. and about 1 ft long, weighing 10 to 15 lb. The U-Si charge was melted by heating to about 1650°C in an induction heated vacuum furnace. Beryllia crucibles were used at first, but were replaced by zirconia-washed graphite as the technique of keeping the carbon content low enough (about 500 ppm) was mastered. The alloy was bottom-poured at about 1650°C into graphite molds. A few small buttons, weighing no more than 50 g, were prepared in a small arc melting unit.[6]

Since cast material has a preponderance of uranium and U_3Si_2, heat treatment is necessary to obtain the ε phase by the solid-solid peritectoid reaction. Once obtained, the ε phase is stable to room temperature, obviating the need for special attention to the method of cooling after epsilonization, see Fig. 1. It was found desirable to epsilonize at 800°C for a week. For some purposes, in which residual uranium and/or U_3Si_2 are tolerable, shorter periods may be adequate. The temperature of 800°C is not critical, since essentially the same results were obtained from 785° to 825°C. Further departure from this epsilonization range is inadvisable.

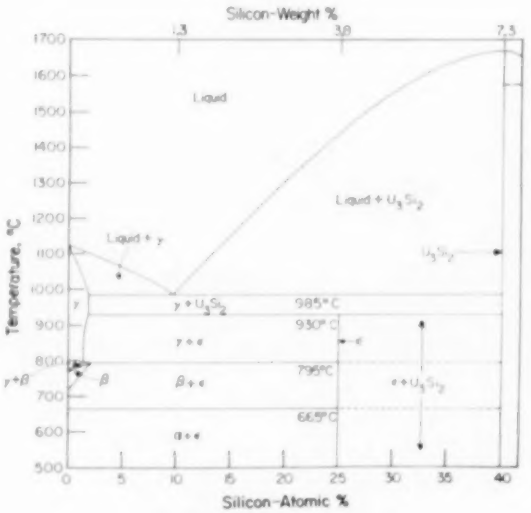

Fig. 1—U-Si phase diagram.

S. ISSEROW is associated with Nuclear Metals Inc., Cambridge, Mass.

TP 4578E. Manuscript, Sept. 28, 1956.

Attempts to find means of promoting epsilonization were unsuccessful. They were based on the presumed facilitation of the solid-solid reaction by grain refinement. Extrusion of the casting before heat treatment or extrusion as an intermediate stage between two heat treatments did not improve the product of the final heat treatment. Deliberate de-epsilonization did not generate fine uranium and U_3Si_2 for more complete reaction in the final epsilonization. The uranium agglomerated, as it does during epsilonization in the eutectic zones of cast material.

Since the formation of ϵ by the peritectoid reaction involves a volume decrease, application of pressure would be expected to promote epsilonization. No experimental data are available on such attempts.

Composition and Corrosion Resistance—When adequately heat treated, material of suitable composition withstands attack by high temperature water. In this work the test medium was degassed distilled water at 500°F (680 psi) or 650°F (2200 psi). Uniform attack at rates of about 50 and 1000 mg per sq cm per month respectively were observed. (In several tests in 750°F steam at 1500 psi, the alloy crumbled as a result of severe attack.) Unalloyed uranium is attacked at a rate of about 1000 mg per sq cm per month by boiling distilled water (212°F).

The crucial problem is the establishment of the existence range of the ϵ phase. The narrowness of this range justifies the use of a vertical line in the usual phase diagram, but evidence was obtained that the silicon content is higher than that of stoichiometric U_3Si. This narrow range makes it difficult to achieve completely epsilonized material. Even at the required composition, small but significant amounts of free uranium and U_3Si_2 are likely to be retained near each other, Fig. 2, because of the small concentration gradient in the ϵ separating these two phases.

The establishment of the silicon content of ϵ was made difficult by two factors. First, cast alloys may have composition variations as high as 0.3 wt pct Si so that, after epsilonization, even a sample shorter than 1 in. can show considerable variation in corrosion resistance from one end to the other. This variation makes it difficult to use the analyses of portions of a billet to determine the composition of a sample of known metallography or corrosion resistance from that billet. The more subtle second difficulty can be overcome by modification of the analytical procedure, see Appendix. Unless the alloy is epsilonized or oxidized before solution in acid for analysis, silicon contents low by several tenths of a percent are likely to be observed. When not in the ϵ phase, the alloy can evolve volatile silanes during direct solution in acid.

The definition of the composition of ϵ was advanced by the establishment of the relation between the alloy's metallographic purity and its corrosion resistance. The expectation that residual uranium

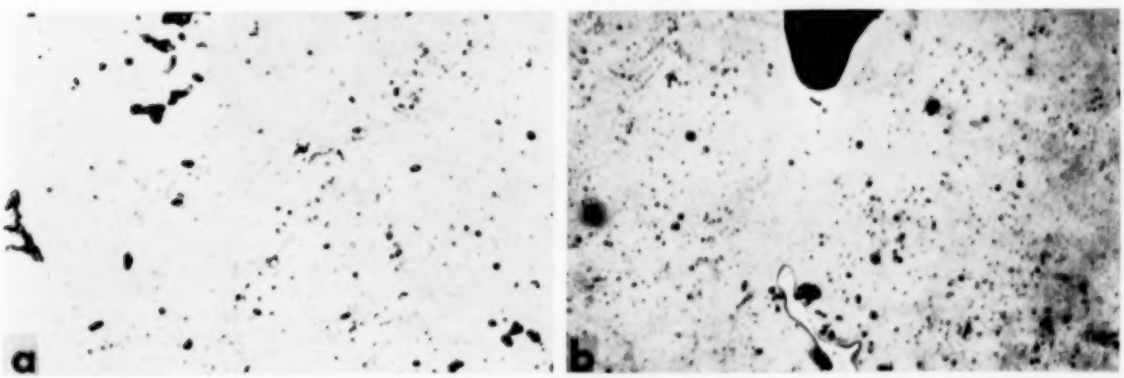

Fig. 2—U-Si alloy UA148 (3.9 wt pct Si) heat treated seven days at 800°C. Electropolished in 10:1 acetic acid/perchloric acid. Bright light, ϵ matrix, light phase U_3Si_2, dark phase -U. a) X100 b) X500. Enlarged approximately 15 pct for reproduction.

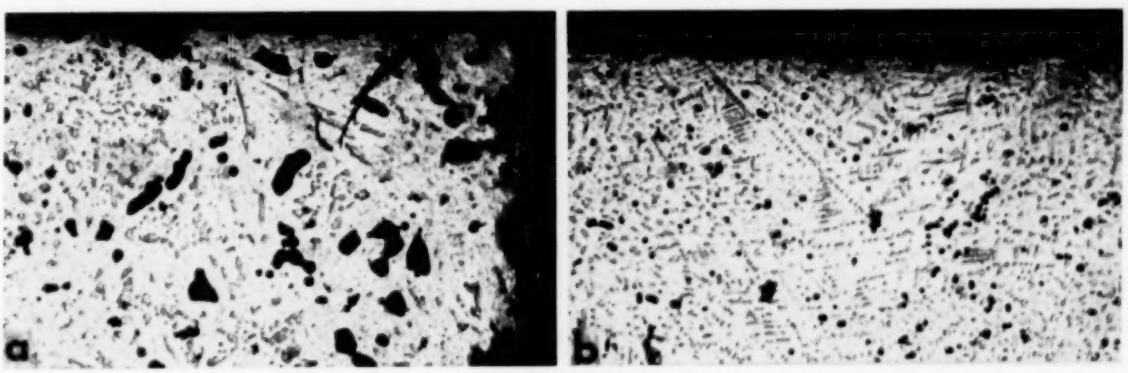

Fig. 3—Effect of non-ϵ phases (U, U_3Si_2) on corrosion of alloy in 500°F water for 100 days. a) X500 b) X50. Enlarged approximately 15 pct for reproduction.

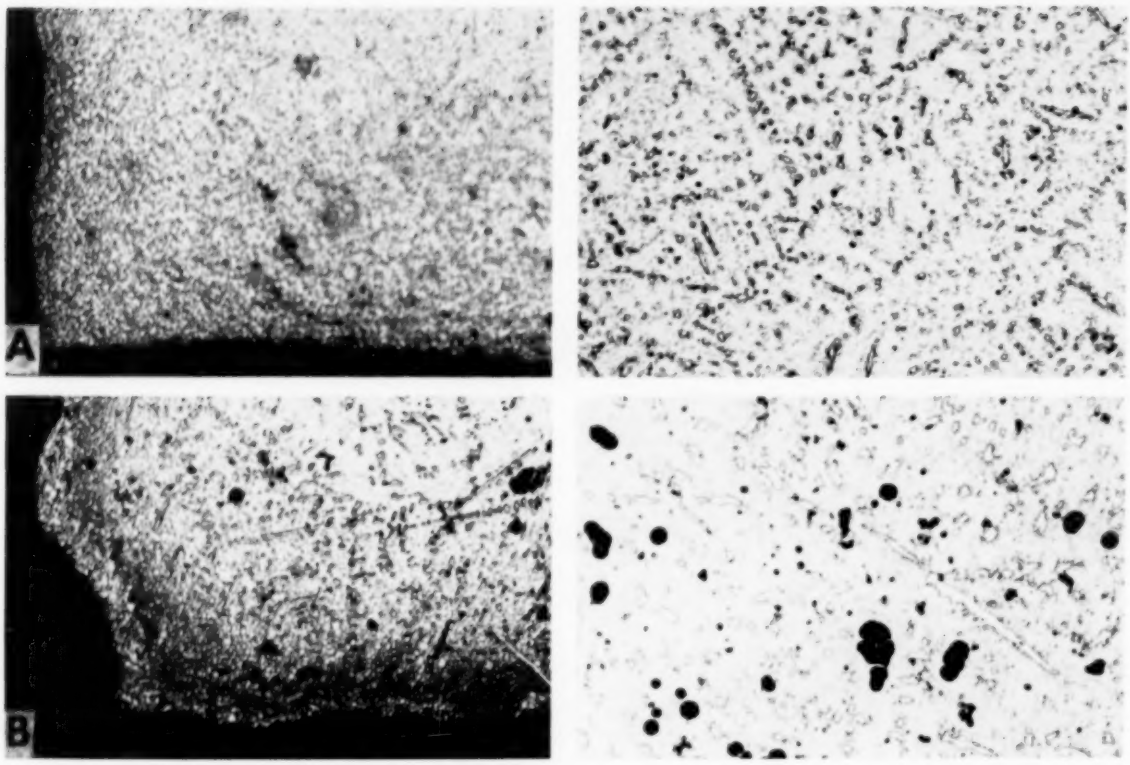

Fig. 4—Effect of non-ε phases (U, U_3Si_2) on corrosion of ε alloy in 650°F water for about 40 days. a) LEFT: Corner. X50. RIGHT: Center. X100. b) LEFT: Corner. X50 RIGHT: Center. X100. Enlarged approximately 15 pct for reproduction.

or U_3Si_2, both having inferior resistance, would impair the corrosion resistance of the ε was borne out by examination of samples of known corrosion history. Figs. 3 and 4 provide examples of 500° and 650°F samples, respectively, which show the sensitivity of the alloy's corrosion resistance to retained uranium and U_3Si_2, especially when these non-ε phases are coarse.

With the method of analysis modified to overcome low silicon values previously obtained for non-ε material, it was possible to evaluate the composition of about 50 billets as it affected the metallography and corrosion resistance of samples from these billets. This evaluation was supplemented by the analysis of a number of samples after corrosion resistance had been established. For this application it was necessary, in some cases, to crop samples of non-uniform corrosion resistance to isolate the portion having good corrosion resistance and confirm its behavior before analysis. This evaluation led to the establishment of the range of 3.9 to 4.0 wt pct Si for the ε phase. The silicon content is thus significantly higher than for stoichiometric U_3Si. Support for this high silicon content was obtained by analysis of a metallographically pure ε sample. A section of an arc-melted button had been found to have a concentration gradient which left a band of pure ε sandwiched between zones containing an excess of uranium or U_3Si, respectively, Fig. 5. Metallographic examinations of the other faces of the button permitted a survey of this band and the isolation of a 120 mg sample for analysis. This sample was found to contain 3.97 wt pct Si. (The carbon content of the button was 85 ppm, whereas the range of carbon content of the cast material is about 500 ppm.)

Physical and Mechanical Properties—The earlier work[1] provided information on such properties as density, hardness, compressive strength, and thermal conductivity. In spite of the advance in the technology of preparation, further investigation of these properties was not undertaken. The results of some exploratory tests are recorded here.

Tensile tests of an extruded and machined rod gave about 100,000 psi as the ultimate strength and a proportional limit of about 60,000 psi. The values obtained after annealing were about 60 pct of these

Fig. 5—Section of arc-melted U-Si button, heat treated 7 days at 800°C. Clear section isolated and found to contain 3.97 wt pct Si. X50.

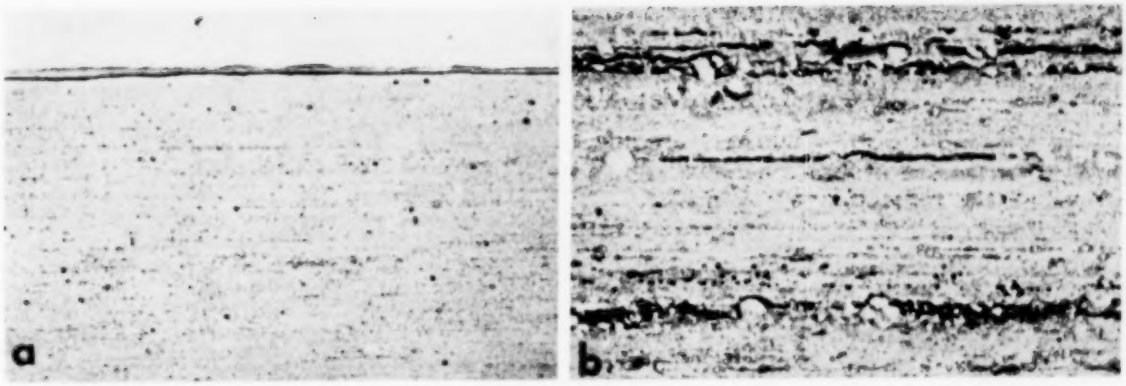

Fig. 6—Longitudinal section of coextruded rod 8355 from billet UA148, see Fig. 2. a) Near edge (clad on left) b) Near center. X100. Enlarged approximately 15 pct for reproduction.

values. The total elongation was about 1 pct. The elastic modulus was near 22,500,000 psi.

The following overall coefficients of expansion from room temperature to the specified temperatures were obtained in the course of the investigation of dilatometry as a means of detecting free uranium: $\alpha \times 10^6$—12, 300°C; 14, 600°C; and 16, 800°C. The linear expansion on de-epsilonization is about 1.7 pct.

The electrical resistivity of ϵ was found to be 55 microhm-cm at room temperature.

Considerable effort was devoted to the development of techniques for the extrusion of the ϵ alloy, notably coextrusion with Zircaloy-2. Temperatures above 1560°F were not considered because of possible peritectoid decomposition. At 1500° or 1560°F, the extrusion constant K^* is about 45,000 psi. In the range of 1400° to 1450°F, this constant is increased to about 55,000 psi. Further reduction of the temperature causes a sharper increase in the constant: at 1350°F, it exceeds 70,000 psi.

* $P = K \ln R$ where P is the pressure, determined from the force over the initial area, and R is the ratio of the initial to the final cross sectional area.

In the course of extrusion, uranium retained in the alloy generates stringers. These stringers are more likely to be observed near the axis of the rod than at the edges, Fig. 6. They provide a corrosion path when the specimen is tested in such a way that the axial region is exposed to the corrosive medium, e.g., rods with flat ends. This attack can lead to splitting of the rods in spite of the excellent resistance of the cylindrical surface.

Coextrusion with zirconium or its alloys can lead to interaction between the U-Si alloy core and the zirconium of the cladding. The formation of intermediate layers is illustrated in Fig. 6a.

It is well to recall that the alloy can be machined fairly readily either before or after epsilonization.

Appendix—Analytical Method: Elimination Of Sensitivity To Phases Present

After the alloy is dissolved in nitric acid to which hydrofluoric acid is added, silicon is determined colorimetrically by reduction of the silicomolybdate complex. The reliability of the colorimetric method was checked against the gravimetric method in which SiO_2 is determined by weight difference upon volatilization with HF.

As an outgrowth of the analyses of samples of established corrosion resistance, it was found that lower results were obtained for alloys consisting of uranium and U_3Si, than for alloys in which ϵ predominated. This sensitivity of apparent silicon content was first demonstrated by comparison of three small adjoining pieces from several castings, only the middle piece being epsilonized before analysis. Confirmation of the effect of the phases was obtained in analyses of sets of three adjoining samples, all of which had been epsilonized together, with the middle sample then being deliberately de-epsilonized at 950°C.

It was then established that this sensitivity to the phases is eliminated by atmospheric oxidation at 500°C before dissolution in acid. In analyses of sets of three samples with the central piece in a different phase from the outside pieces, this prior oxidation eliminated the differences between ϵ and non-ϵ material. For epsilonized material, the same results were obtained with or without atmospheric oxidation before solution in acid. Losses of silicon on direct solution of non-ϵ material are attributed to volatilization of silanes. The ignition of such volatilized silanes is observed when these alloys are dissolved in other mineral acids.

Acknowledgments

This investigation was performed under Contract No. AT(30-1)-1565 with the Atomic Energy Commission. Metallographic and chemical analyses were performed under the supervision of Miss H. P. Roth and Mr. E. B. Read, respectively. Special mention should be made of Miss Phyllis Hicks, who performed the many analyses necessary to establish the existence range of the silicon phase and to eliminate the sensitivity to the phases present.

References

[1] A. Kaufmann, B. Cuility, and G. Bitsianes: Uranium-Silicon Alloys. *AIME Trans.*, 1957, vol. 209, p. 23; JOURNAL OF METALS, January 1957.

[2] J. J. Katz and E. Rabinowitch: *The Chemistry of Uranium*, vol. 5, Div. VIII, National Nuclear Energy Series, p. 227, McGraw-Hill Book Co. New York, 1951.

[3] W. H. Zachariasen: *Acta Crystallographica*, 1949, vol. 2, p. 94.

[4] S. H. Paine and J. H. Kittel: Irradiation Effects in Uranium and Its Alloys. *Proceedings* International Conference on the Peaceful Uses of Atomic Energy, Geneva, 1955, vol. 7, p. 445.

[5] J. F. Kuchta and S. Isserow: Construction and Operation of a Laboratory Scale Arc Melting Unit. Report No. NMI-1142. U. S. Atomic Energy Commission. Washington, D. C., 1956.

Discussion of this paper sent (2 copies) to AIME by Jan. 1, 1958 will appear in AIME *Transactions* Vol. 212, 1958, and in JOURNAL OF METALS, April 1958.

Misfit Strain Energy in the Au-Cu System

Misfit strain energy has been calculated for the AuCu lattice from interatomic distances and the Morse function; the calculations give results of the same order of magnitude as calculations from elasticity theory. It is shown that electronic rearrangements occur during uniaxial tension, greatly reducing the strain energy from that calculated by ordinary methods. The theory of Pauling is applied and the electronic rearrangements derived from this theory reduce the strain energy to small values. This is not true, however, in other lattices. An explanation is advanced as to why Au-Cu alloys form more exothermically than Au-Ag alloys.

by Ralph Hultgren

IN solid solutions atoms of differing sizes occupy the same crystalline lattice, requiring that some of them be compressed and others expanded. The energy involved has been called *misfit strain energy* and is an important concept of crystal chemistry.

If the atomic sizes and elastic constants of interatomic bonds are known, the misfit energy may be calculated,[1] provided certain simplifying assumptions are allowable. Usually, isotropic crystals are assumed and interatomic distances are taken to be the statistical average determined from X-ray diffraction. Such calculations yield values of the misfit energy of the order of 1 or 2 kcal per atom in alloys such as Au-Cu at compositions of 50 atomic pct.

However, evidence has accumulated in recent times that atoms change their sizes with composition of alloys, implying electronic rearrangement of the bonds. The size changes have been found particularly by application of the X-ray method developed by Warren, Averbach, and Roberts.[2] Thus, Averbach, Flinn, and Cohen[3] determined radii in Au-Cu alloys. Oriani[4] showed that these new radii led to a calculated misfit energy in disordered AuCu, which was decreased from the values calculated by the usual theory more than twenty-fold, to only 80 cal per g atom. Thermodynamic calculations from the phase diagram[5] also show misfit energy to be no more than a few hundred calories per g atom in this alloy.

The question of what electronic rearrangements are possible therefore becomes compelling in estimating misfit energy. In the following pages the results of certain calculations on the AuCu tetragonal superlattice are submitted. Conclusions drawn from these should be applicable in large degree to disordered solid solutions.

As in all ordered states, bonding distances in the superlattice are individually known, rather than being merely average distances as found from lattice constants of disordered states. Moreover, only the Au-Au and Cu-Cu distances are strained; the elastic constants of these are known in the elementary state. In the usual calculation it is necessary to assume elastic constants for Au-Cu bonds. Misfit energy has thus been calculable without the need of many simplifying assumptions usually made.

R. HULTGREN, Member AIME, is Professor of Metallurgy, University of California, Berkeley, Calif. Contribution No. 2125 from the Gates and Crellin Laboratories of Chemistry, California Institute of Technology, Pasadena, Calif.

TP 4488E. Manuscript, Sept. 10, 1956.

It is still assumed that equilibrium bond lengths and elastic properties of the bonds are the same in the alloy as in the pure metals. As previously discussed, this is probably not correct. Also assumed is that the bonds are not affected by strain of neighboring bonds. A calculation of Young's modulus from compressibility data shows this to be far from true; extensive electronic rearrangements take place. It would seem that misfit energy cannot be calculated from elasticity data for the elements. The usual methods may, however, give an upper limit which is often much higher than the true value.

The question of electronic rearrangement is, of course, a complex one. Pauling's theory gives a simple, approximate treatment of the relation between type of bond and bond distance. This has been applied with some success to the Au-Cu system, as will be shown in a later section.

Misfit Energy in Au-Cu Alloys

Hume-Rothery and Raynor[6] discuss the Au-Cu system as a type example of strain energy. The gold atom is 12.8 pct larger in diameter than the copper atom, near the size factor limit beyond which solid solubility is severely restricted. They therefore consider the misfit energy to be large, a conclusion for which they believe they find evidence in the phase diagram. Gold and copper are completely miscible in the solid state, but the alloy has a minimum melting point at an intermediate composition. From this Hume-Rothery and Raynor conclude that the strain energy is nearly large enough to prevent miscibility; the phase diagram tends toward a eutectic type. In Ag-Cu, which has almost identical size relationships, solid miscibility is quite limited; whereas in Au-Ag, where atomic sizes are nearly the same, there is complete miscibility without a minimum in the melting point. From their arguments the heat of formation of Au-Cu would be expected to be endothermic or only slightly exothermic, that of Ag-Cu to be endothermic, and that of Au-Ag to be exothermic. Deviations from Vegard's law of additivity of atomic radii support these conclusions, since Au-Cu and Ag-Cu both have pronounced positive deviations, and Au-Ag has a negative deviation.

Nevertheless, Au-Cu alloys form exothermically; indeed, considerably more exothermically than Au-Ag, Table I. Hence, strain energy must be much less important in this case than Hume-Rothery and Raynor have supposed.

Calculation of Misfit Energy Assuming No Change in Bond Type

The AuCu superlattice is derived from the disordered face-centered-cubic solid solution by ordering the gold and copper atoms respectively on alternate planes parallel to the cube face, Fig. 1. The structure thereby becomes tetragonal with the c axis a few percent shorter than the other two. It is required by geometry that

$$d_{Au\text{-}Au} = d_{Cu\text{-}Cu} = \tfrac{1}{2}\sqrt{2}\,a$$

whereas the distance $d_{Au\text{-}Cu}$ may assume any value by adjusting the length of the c-axis. Hence, bonds between unlike atoms may take equilibrium lengths and be strain-free. For experimental bond distances, see Table II.

The misfit energy of the superlattice would be calculable from the elastic constants of the bonds in elementary gold and copper if the bonds did not change their nature during alloying. As mentioned earlier, this assumption is not warranted, but the calculation should give an upper limit of the misfit energy.

Elastic strains experimentally realizable amount at most to a few tenths of a percent, so that calculations from experimental elastic constants involve a large extrapolation. In gas molecules the interatomic distance vs energy relationship has been found to obey with surprising accuracy an empirical function proposed by Morse.[7] This function has been used in the following form

$$E = -D[{}_e{}^{-2a(d-d_0)} - 2{}_e{}^{-a(d-d_0)}] \qquad [1]$$

from which the force can be derived by differentiation

$$F = \frac{dE}{dd} = 2aD[{}_e{}^{-2a(d-d_0)} - {}_e{}^{-a(d-d_0)}] \qquad [2]$$

where E equals energy of strained bond; D, energy of unstrained bond; d, bond distance, strained bond; d_0, bond distance, unstrained bond; a, constant depending on elastic properties; and F, force in strained bond.

Of the above quantities, D can be evaluated from the energy of sublimation to monatomic gas. Waser and Pauling[8] have tabulated force constants k and k' for bonds in most metallic elements from compressibility data. The force constants may be defined as follows

$$E - D = \frac{k}{2}(d - d_0)^2 + \frac{k'}{3}(d - d_0)^3.$$

Expanding the Morse function in series and taking the first few terms gives the following expression valid for small values of $d - d_0$

$$E - D = D[a^2(d - d_0)^2 + a^3(d - d_0)^3]$$

from which a can be evaluated for a typical $d - d_0$ such as 0.02A, where the Morse curve fits the compressibility data exactly, fitting approximately at other distances. Values of a calculated in this manner are tabulated in Table III.

Bond energies are shown in Fig. 2 on p. 1243 as a function of interatomic distances. The distance at which the tensile stress of copper equals the compressive stress of gold should be the distance of static balance in the lattice. This is found to be 2.794A, surprisingly close to the experimental distance, 2.800A. At this point the strain energy of copper amounts to 7.73 pct of the total energy; for gold it is 2.2 pct. Considering that Au-Au and Cu-Cu bonds each constitute one sixth of the total

Table I. Heats of Formation of Binary Alloys of Gold, Silver, and Copper

Alloy Composition, Atomic Pct			Heat of Formation, Cal per G Atom	Source of Data
Au	Ag	Cu		
50	50		−1100	White et al.[14]
50		50 (disordered)	−1230	Orr,[16] Oriani[15]
50		50 (ordered)	−2150	Orr[16]
	89	11	+600	Orr[16] (1956)

Table II. Interatomic Distances in Au-Cu Alloys

Substance	Interatomic Distances, A					Atomic Volume, Cubic A
	Au-Au	Cu-Cu	Au-Cu	Average		
Au	2.884			2.720	16.962	14.387
Cu		2.556			11.812	
AuCu (ordered)	2.800	2.800	2.705	2.737		14.449
AuCu (disordered)				2.740		14.453

Table III. Morse Exponent a for Certain Elements

Element	kx10^{-5} Dyne per Cm	k'x10^{-13} Dyne per Sq Cm	ax10^{-8} Cm^{-1}	D, Kcal per G Atom	Dx10^{12} Erg per Bond
Au	51.9	−500	1.54	85.0	0.981
Cu	36.9	−210	1.37	81.1	0.938
Fe	72.26*	−118*	1.465*	97.9	1.696*
Co	48.4	400	1.37	102.0	1.18
Ni	48.9	−450	1.37	101.75	1.175
Pd	54.1	−450	1.52	93.0	1.075
Pt	80.0	−1100	1.55	121.6	1.405

* Values per bond of D and k are large for iron because its coordination number is 8 instead of 12 as in the other elements. However, a is less dependent on coordination number as shown by the approximate agreement of values for iron with those of the neighboring elements cobalt and nickel. Actually, the results listed in Table IV are not very sensitive to values of a and, for these calculations, the value of a for iron was taken to be 1.37, in agreement with the values for cobalt and nickel.

Table IV. Calculated and Experimental Bond Distances in AuCu-Type Superlattices

Substance	a_0	c_0	Bond Distances				Calculated Misfit Energy
			A-B		A-A and B-B		
			Experimental	Additivity	Experimental	Predicted	
AuCu	3.9592	3.6772	2.705	2.720	2.800	2.794	1350
FePt	3.863	3.759	2.695	2.650	2.732	2.707	1280
CoPt	3.826	3.646	2.642	2.643	2.705	2.703	1190
NiPt	3.8227	3.589	2.622	2.633	2.703	2.701	1360
FePd	3.856	3.727	2.681	2.638	2.726	2.672	790
AlTi	4.006	4.070	2.856	2.892	2.833	2.902	40

Table V. Calculated and Observed Values of Young's Modulus Along c Axis

Element	E, Dyne per Sq Cm	
	Calculated	Observed
Au	2.62x10^{12}	0.429x10^{12}
Cu	2.02x10^{12}	0.67x10^{12}

Table VI. Bond Distances in Au-Cu Superlattices

Bond	Distances, A			
	AuCu Structure		AuCu$_3$ Structure	
	Calculated	Experimental	Calculated	Experimental
Au-Au	2.809	2.800	—	—
Cu-Cu	2.773	2.800	2.614	2.651
Au-Cu	2.701	2.705	2.679	2.651

number, this amounts to 1350 cal per g atom. This is somewhat smaller than the value of 1870 cal per g atom calculated for disordered AuCu, by Averbach, Flinn, and Cohen[5] from elasticity theory, but an ordered state should have a smaller strain energy.

Five other superlattices of this structure were found for which there are sufficient experimental data to make the calculation. Results are shown in Table IV. In two cases excellent agreement is found; in three cases deviations are rather large. In FePt and FePd distances are larger than predicted; in AlTi, smaller.

It is of interest to examine the bond distances, *A-B*, between unlike atoms in these superlattices, since these distances are not affected by geometric constraints. Usually it is felt that stronger bonds lead to shorter interatomic distances; for example, in nearly all intermetallic compounds bond distances are shorter than the sum of the atomic radii. Thus short bond distances may go with exothermic heats of formation.

Thermodynamic data are available for two of the pairs in Table IV. AuCu, as shown in Table I, forms exothermically and the deviation from additivity of radii is negative. It is noteworthy that consideration of Vegard's law leads to wrong conclusions in this case; disordered AuCu has a considerable positive deviation from Vegard's law. Oriani (1953) found that disordered CoPt formed endothermically, $\Delta H_f = +1000$ cal per g atom. The ordered alloy consequently should form with approximately zero heat effect, which fact coincides with the nearly additive interatomic distance.

However, as will be discussed later, changes in radius of atoms during alloying may occur in a complex way, so that a simple relationship between interatomic distance and heat of formation will hardly be expected in all cases.

Strain and Electronic Rearrangement

That electronic rearrangements occur in bonds as they are strained can be shown from the relationship of Young's modulus to the elastic constants of hydrostatic compression. During hydrostatic compression of cubic crystals, all bonds are equally shortened and the tendency for rearrangement of bonding electrons may be negligible. The elastic constants for compression may therefore be taken as properties of bonds in their unaltered state. In uniaxial tension some bonds are shortened and some lengthened. The LeChatelier principle predicts that changes in bonds brought about by strain will be such as to weaken the stretched bonds and strengthen the compressed ones. Hence, Young's modulus calculated from compressibility data should be greater than experimental values, if there has been electronic rearrangement. Young's modulus on a cubic axis can be calculated from compressibility data alone. Gunnar Bergman* of the California Institute of Technology has kindly calculated Young's modulus and finds for the c direction of face-centered-cubic metals that Young's Modulus $= \frac{8}{3}\frac{a^4D}{a_c}$ where a_c is the edge of the unit cell and the other letters have the same significance as previously.

* Dr. Bergman has also found that for bonds in which electronic rearrangements such as those postulated by Pauling occur during straining, the Cauchy relations will not be fulfilled, a fact which is experimentally observed. The nonfulfillment of the Cauchy relations has previously been an objection to considering metallic lattices as being held together by bonds between atomic nearest neighbors. *Acta Metallurgica*, to be published.

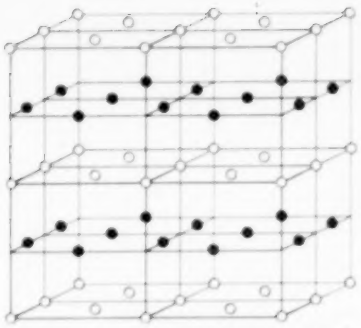

Fig. 1—Crystal structure of AuCu. Closed circles represent gold; open circles, copper.

As seen in Table V, gold and copper have experimental values far below the calculated ones, indicating considerable change has occurred in the bonds. Diamond, on the other hand, has covalent bonds that are the best possible sp^3 bonds, and electronic rearrangement would not be expected during deformation. Hence, much closer agreement should be expected between Young's modulus as determined experimentally and as calculated above. Unfortunately, diamond has an open structure in which extensive bending of bonds may occur, so that it is not possible to make the above calculation without data on resistance to bending of the bonds. It can be shown, however, that the calculated value in diamond will not greatly exceed the experimental value, in agreement with the picture here presented.

It thus appears that bonds do change during straining. The effect is so large that the usual calculation of misfit energy from the theory of elasticity yields results which are not even approximately correct; they are much too large. The effect of atomic size on alloy formation can be predicted only when much more is known of the kinds of electronic rearrangement which occur on straining.

The only theory which simply relates type of bond with bond length is that of Pauling. A straightforward application of this theory to the Au-Cu system gives bond distances which greatly reduce the strain energy. However, the theory is shown to be incomplete since it fails to predict the unusual behavior of FePd, FePt, and AlTi.

Pauling's Theory

Electronic rearrangements that reduce strain energy are a feature of the theory of Pauling.[6] An electron transfer may be part of the electronic rearrangement. The principle of electroneutrality[6] favors a transfer from the more electronegative atom to the more electropositive one, in this case from gold to copper. This direction of transfer is also favored by the size factor, since it will reduce the size of the gold atom and increase that of copper.

According to Pauling, both gold and copper are hyperelectronic; they both have too many electrons to develop the full valence of 6 found in transition metals adjacent to them. Loss of an electron by gold therefore increases its valence. Moreover, the *d* character of the bond is increased, strengthening it and decreasing the atomic radius. Gain of an electron by copper has the opposite effect.

Transfer of about ½ electron from gold to copper will give good agreement with the facts, as will be shown later. This will result in bond numbers that are simple fractions, which has been observed to give best agreement in other cases, presumably because resonance is favored by such bond numbers. This amount of electron transfer is reasonable since the electronegativity of gold (2.5) differs from that

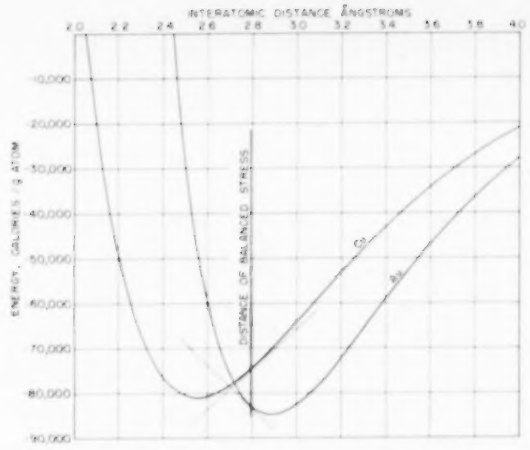

Fig. 2—Energy vs interatomic distance in gold and in copper.

of copper (1.8) by an amount that predicts that the bond will be 11 pct ionic. Thus, four bonds would give each gold a charge of —0.44 and each copper, +0.44. A transfer of ½ electron would approximately neutralize these charges, achieving electroneutrality.

Such a transfer increases the valence of gold to 6, decreasing its single bond radius from 1.339A to 1.314A. The valence of copper decreases to 5 and its single bond radius increases from 1.176A to 1.206A.

Hexavalent gold can form bonds with its 12 neighbors with $n = \frac{1}{2}$. Copper would then use four of its five valences in bonding with its eight gold neighbors, leaving a single valence with $n = \frac{1}{4}$ for its four copper neighbors. The bond distances for unstrained bonds may be calculated from the formula

$$D_n = D_1 - 0.60 \log n$$

where D_1 is the sum of the single bond radii of the elements concerned. Results of the calculation are given in Table VI.

For the superlattice $AuCu_3$ similar considerations would lead to a transfer of ¾ electron from the gold, each copper receiving ¼ electron. Gold would then have a valence of 6 and a single bond radius of 1.307A, while copper would have a valence of 5¼ and a single bond radius of 1.191A. Bond distances would be those shown in Table VI.

The agreement in Table VI is remarkably good. The Au-Cu bond in AuCu is practically strain-free, as expected. The other bonds have most of their strain removed; only about 100 cal per g atom remains. In $AuCu_3$, strains have been reduced to about 300 cal per g atom. These results were attained by simple and natural assumptions in the Pauling theory.

However, for the other lattices of Table IV, Pauling's theory does not lead to a similar release of strain. The transition metals involved, except nickel, would change neither their valence nor their radius appreciably on electron transfer. Two interpretations are possible. The estimated strain energy may remain in the alloy. In this case, thermodynamic measurements should show heats of formation that are less negative than in AuCu; unfortunately, these measurements are not yet available. The second possibility is that forces are involved that are not accounted for by any existing theory. Certainly this is true at least to some extent; Fe-Pd and Fe-Pt distances are unaccountably large and Al-Ti distances unaccountably small.

The question as to why Au-Ag alloys are less exothermic than Au-Cu alloys may have an intriguing explanation. Silver has nearly the same electronegativity as copper and might be expected to attract gold equally well. The size of the silver atom is nearly equal to that of the gold atom, so that misfit energy should be absent. As seen in this paper, the size difference of gold and copper is overcome by a transfer of electrons, which is approximately the amount predicted by the difference of electronegativity in order to produce electrical neutrality. Such a transfer cannot occur in Au-Ag without producing differences in size with consequent misfit energy. This may produce a less stable bond, accounting for the difference in heats of formation.

Electronic rearrangements are probably common in alloys, so common that the ordinary calculation of misfit energy from elasticity data may not be correct even as to order of magnitude.

Acknowledgments

The author is indebted to Linus Pauling for advice and encouragement in this work. He thanks Gunnar Bergman for calculating the uniaxial elastic constants from the constants for compressibility. This work has been sponsored by the Office of Ordnance Research, U. S. Army.

References

[1] A. W. Lawson: *Journal of Chemical Physics*, 1947, vol. 15, p. 831.
[2] B. E. Warren, B. L. Averbach, and B. W. Roberts: *Journal of Applied Physics*, 1951, vol. 22, p. 1493.
[3] B. L. Averbach, P. A. Flinn, and M. Cohen: *Acta Metallurgica*, 1954, vol. 2, p. 92.
[4] R. A. Oriani: Research Laboratory Report No. RL-1175. General Electric Co. Schenectady, 1954.
[5] R. A. Oriani: *Acta Metallurgica*, 1956, vol. 4, pp. 15-25. C. Wagner: *Acta Metallurgica*, 1954, vol. 2, pp. 242-249.
[6] W. Hume-Rothery and G. V. Raynor: *The Structure of Metals and Alloys*. Institute of Metals, London, 1954.
[7] P. M. Morse: *Physical Review*, 1929, vol. 34, p. 57.
[8] J. Waser and L. Pauling: *Journal of Chemical Physics*, 1950, vol. 18, pp. 747-753.
[9] L. Pauling: *Physical Review*, 1938, vol. 54, p. 899.
[10] L. Pauling: *Journal ACS*, 1947, vol. 69, pp. 542-553.
[11] L. Pauling: *Proceedings* Royal Soc., London, 1949, vol. 196A, p. 343.
[12] L. Pauling: *Proceedings* National Academy of Science, 1950, vol. 36, pp. 533-538.
[13] L. Pauling: *Journal* Chemical Soc., 1948, vol. 15, p. 1461.
[14] J. L. White, R. L. Orr, and R. R. Hultgren: *Acta Metallurgica*, to be published.
[15] R. A. Oriani: *Acta Metallurgica*, 1954, vol. 2, p. 608.
[16] R. L. Orr: Unpublished data, 1956.

Discussion of this paper sent (2 copies) to AIME by Dec. 1, 1957 will appear in AIME *Transactions* Vol. 212, 1958, and in JOURNAL OF METALS, April 1958.

Technical Note

Temperature Dependence of the Tensile Properties of Vanadium

by J. W. Pugh

J. W. PUGH, Member AIME, formerly with Research Laboratory, General Electric Co., is now associated with the Lamp Wire and Phospors Dept., General Electric Co., Cleveland.

TN 424E. Manuscript, Jan. 30, 1957.

VANADIUM has only recently received consideration with respect to structural applications.[1,2] It would appear likely to find service where its high electrical resistance and constant temperature

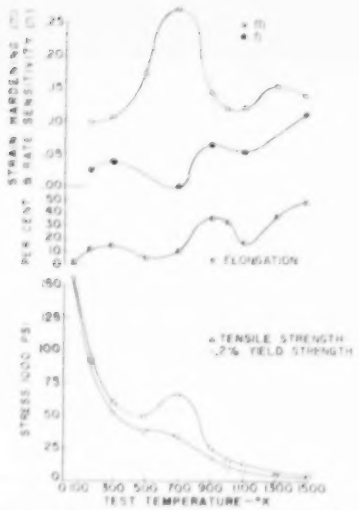

Fig. 1—Tensile parameters vs temperature for the 1273°K annealing treatment.

coefficient of resistance are advantageous. In addition, there are applications for vanadium which exploit its resistance to attack by corrosive chemicals. The relatively high melting point, 2173° ±25°K (1900° ±25°C),[1] suggests good structural strength at high temperature. Detailed information about temperature dependence of strength has been lacking, although some data between room temperature and 1200°K are available.[2] In this report, an analysis is made of the tensile properties of sheet metal for constant strain rate and at temperatures between 78° and 1500°K.

Arc melted ingots were cast in a rotating hearth furnace described previously by Keeler.[3] These ingots were scalped and hot rolled in mild steel *sandwich jackets* at 1073°K (800°C). Billets were removed from the jackets and cold rolled from 0.200 to 0.020 in. with an intermediate vacuum anneal (1073°K, ½ hr) at 0.100 in. thick. Chemical analysis of the rolled sheet indicated the impurity content shown in Table I. The temperature required to produce complete recrystallization for a ½ hr annealing treatment was approximately 1200°K (927°C).

Tensile test specimens were cut from the sheet parallel to the rolling direction. These were tested as cold rolled and as recrystallized at 1273°K (1000°C) for 1 hr. The grain size for the recrystallized metal was 0.03 mm. An Instron testing machine was used at a nominal strain rate of 0.09 in. per in. per min and at temperatures from 78° to 1500°K. In order to determine the effect of strain rate on flow stress, the rate was changed momentarily to 0.009 during each test. Data were plotted autographically. Elevated temperature tests were made in vacuum, and temperatures were recorded by means of a Pt—Pt-Rh thermocouple positioned at the middle of the gage length. A description of the test equipment can be found elsewhere.[4] Evaluation was made in terms of ultimate tensile strength, 0.2 pct yield strength, strain hardening, and rate sensitivity of the flow stress.

Logarithmic plots of true stress-strain were quite straight so that hardening could be evaluated in terms of the slope, n, of these logarithmic curves.

$$n = \left.\frac{\partial \log \sigma}{\partial \log \epsilon}\right|_{\dot{\epsilon},\, T}$$

where n is called the strain hardening exponent, σ is the flow stress, and ϵ is the strain.

Table I. Chemical Analysis of the Rolled Sheet

Element	Wt Pct Present
O	0.057
N	0.07
H	0.0004
C	0.09
W	<0.02
Fe	<0.005
Si	<0.005

Table II. Data for Cold Rolled Specimens

Test Temperature, °K	0.2 Pct Yield Strength, Psi	Tensile Strength, Psi	Elongation, Pct	Strain Hardening, M	Rate Sensitivity, N
300	102,770	105,000	0.8	—	—
500	87,680	88,400	0.2	—	0.021
700	77,880	80,150	0.9	0.013	0.030
1000	33,330	40,580	4.5	0.029	0.051
1300	4,710	8,480	46.3	0.043	0.071

A similar relationship is used to evaluate rate sensitivity.

$$n = \left.\frac{\log \dfrac{\sigma_1}{\sigma_2}}{\log \dfrac{\dot{\epsilon}_1}{\dot{\epsilon}_2}}\right|_{\epsilon,\, T}$$

where n is called the strain rate sensitivity; σ_1 is the flow stress at the faster rate; σ_2 is the flow stress at the slower rate; $\dot{\epsilon}_1$ is the faster rate, 0.09; and $\dot{\epsilon}_2$ is the slower rate, 0.009. There are no data to indicate that the logarithmic relationships between strain rate and stress for vanadium should be linear. In view of the temperature dependence of stress, they may be presumed not to be linear. Hence, the values for n are not expected to apply to rates other than those listed above.

Table II lists data for the cold rolled specimens, and Fig. 1 shows the tensile parameters vs temperature for the conditions resulting from the 1273°K (1000°C) annealing treatment. Fractures were observed to be transgranular at all temperatures.

Vanadium has a temperature dependence of tensile properties which is characteristic of body-centered-cubic metals. There are several features of this dependence. For example, strength is exceedingly dependent on temperature in the low temperature range. Below 300°K strength rises very rapidly as temperature is diminished. Yield points and discontinuous yielding, observed at low and intermediate temperature, respectively, indicated strain aging behavior. Other strain aging indicators are the minima in strain rate sensitivity and elongation, and the maxima in strain hardening and strength relationships at about 700°K. Similar temperature dependences have been observed for iron and steel,[7,8] molybdenum,[9] and tantalum.[10]

References

[1] J. L. Everhart: Titanium, Zirconium, Molybdenum, Tungsten, Tantalum, Columbium, Vanadium, Hafnium as Engineering Materials. *Materials and Methods*, 1951, vol. 39, p. 89.

[2] A. R. Gardner: Fitting Your Product to the Atomic Age, Part II. *Dun's Review and Modern Industry*, 1955, vol. 66, p. 39.

[3] H. K. Adenstedt, J. R. Pequignot, and J. M. Raymer: The Titanium-Vanadium System. *ASM Trans.*, 1952, vol. 44, p. 990.

[4] W. Rostoker, A. S. Yamamoto, and R. E. Riley: The Mechanical Properties of Vanadium-Base Alloys. *ASM Trans.*, 1956, vol. 48, p. 569.

[5] J. H. Keeler: The Tensile Characteristics of Unalloyed Zirconium at Low and Moderate Temperatures. *ASM Trans.*, 1955, vol. 47, p. 157.

[6] J. W. Pugh: How to Test Refractory Metals. *Steel*, 1955, vol. 137, No. 16, p. 114.

[7] J. L. Everhard et al.: Mechanical Properties of Metals and Alloys. Circular C 447, p. 265. National Bureau of Standards. Washington, D. C., 1943.

[8] G. W. Geil and N. L. Carwile: Tensile Properties of Ingot Iron at Low Temperatures. *Journal of Research* National Bureau of Standards, 1950, vol. 45, p. 129.

[9] J. W. Pugh: The Tensile Properties of Molybdenum at Elevated Temperatures. *ASM Trans.*, 1955, vol. 47, p. 984.

[10] J. W. Pugh: The Tensile Properties of Tantalum. *ASM Trans.*, 1956, vol. 48, p. 677.

Sand Cast Magnesium-Rare Earth Metal-Zirconium Alloys

Addition of zirconium to cast magnesium-rare earth metal alloys results in a marked degree of grain refinement and a significant improvement in strength and ductility at temperatures up to 400°F. The strength properties and creep resistance of Mg-didymium-Zr alloys are markedly superior to those of Mg-Mischmetal-Zr alloys. Results of studies on alloys containing various proportions of Mischmetal and didymium, and cerium and didymium, are also presented. In general, both in Ce-didymium and Mischmetal-didymium alloys the strength properties increase with increasing didymium content.

by T. E. Leontis and D. H. Feisel

MAGNESIUM alloys containing rare earth metals have received considerable attention during the past several years because of the need for light alloys having high strength and creep resistance at elevated temperatures. Although much of the work reported earlier has dealt with alloys containing Mischmetal, it has been shown in two previous papers[1,2] that distinctly different effects are produced by various rare earth metals and rare earth metal mixtures on the properties of magnesium. For example, much higher strengths are obtained in magnesium alloys containing didymium (essentially neodymium plus praseodymium) than in alloys made with Mischmetal, which contains all the rare earth metals in the proportions in which they occur naturally in the monazite ore.

Mg-rare earth metal alloys are characterized by a relatively coarse grain size, which greatly impairs castability. The addition of zirconium as a second alloying ingredient has been shown[3-5] to refine the grain size, which also produces a distinct improvement in the strength properties. Certain Mg-Mischmetal-Zr and Mg-Mischmetal-Zn-Zr alloy compositions which are currently being produced commercially have been discussed in detail by Nelson and Strieter,[6,7] who also present some information on a Mg-low Ce-Mischmetal-Zr alloy, and by Nelson.[8] A patent issued to Jessup, Emley, and Fisher[9] emphasizes the superiority of Mg-didymium-Zn-Zr alloys over the corresponding alloys made with Mischmetal.

The purpose of this paper is to present the results of an extensive investigation concerned with the effect of increasing amounts of zirconium on magnesium sand casting alloys containing several different rare earth metal mixtures in varying amounts. The effect of the addition of zinc to some of these alloys is also being reported.

T. E. LEONTIS, Member AIME, is associated with Metallurgical Laboratory, Magnesium Dept., The Dow Chemical Co., Midland, Mich. D. H. FEISEL, Student Member AIME, formerly with Dow Chemical Co., is now Dow Chemical Co. Graduate Fellow, Carnegie Institute of Technology, Pittsburgh.

TP 4475E. Manuscript, Sept. 12, 1956.

Preparation and Testing of Alloys

The alloys studied in this investigation were prepared in small laboratory melts according to the melting procedures described by Nelson[10] as the *Crucible Method*. Electrolytic magnesium having the composition shown in Table I was used as the starting material. The rare earth metal alloying ingredients used in preparing these alloys were essentially of the compositions listed in Table II. Some of the didymium-containing alloys were prepared using a Mg-didymium hardener. The rare earth metal content of this hardener analyzed 1.2 pct Ce, 10.4 pct Pr, 80.8 pct Nd, and 7.6 pct La. The zirconium was added in one of three forms: 1) as sponge zirconium obtained from the Bureau of Mines; 2) as a fused salt consisting of 50 pct $ZrCl_4$ and 50 pct alkali chlorides from which the zirconium is reduced by the magnesium; or 3) as a Mg-Zr hardener. The alloying procedures and melt hand-

Table I. Typical Analysis of Electrolytic Magnesium by Spectrographic Method, Pct

Al	Ca	Cu	Fe	Mn	Ni	Pb	Si	Sn	Zn
<0.01	<0.01	<0.01	0.03	0.05-0.10	<0.001	<0.001	<0.01	<0.001	<0.01

Table II. Chemical Analyses of Rare Earth Metals

Producer's Designation of Material	Total Rare Earths, Pct	Ce, Pct	Nd, Pct	Pr, Pct	Th, Pct	La, Pct	Fe, Pct	Si, Pct	Cr, Pct	Other Impurities, Pct
Mischmetal	97.8	50.6	18.2	6.4	nil	22.6	0.59	0.16	0.03	1.42
Cerium-free Mischmetal	94.5	0.2	35.2	12.2	0.9	46.0	3.24	0.20	0.31	1.79
Didymium	89.8	0.8	72.3	7.9	nil	8.8	7.05	0.56	0.75	2.84
Cerium	94.8	92.2	0.9	0.3	nil	1.4	2.37	0.02	0.50	2.21

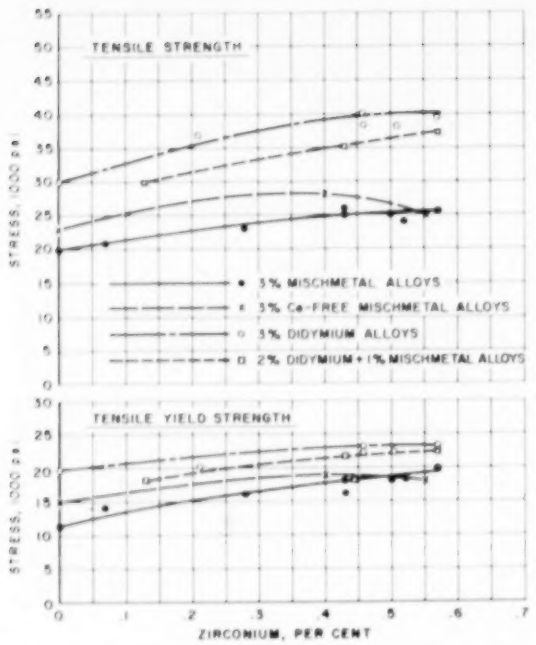

Fig. 1—Tensile strength and tensile yield strength at 70°F of Mg-3 pct rare earth metal-Zr alloys in the *T6* condition.

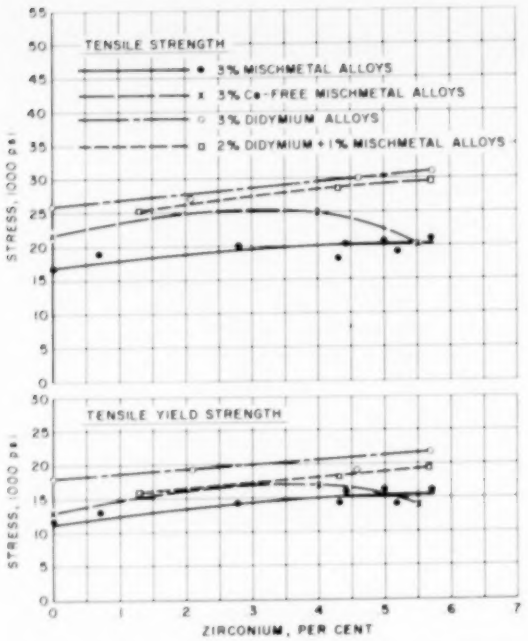

Fig. 2—Tensile strength and tensile yield strength at 400°F of Mg-3 pct rare earth metal-Zr alloys in the *T6* condition.

ling techniques for alloy compositions of this type are discussed in detail by Nelson and Strieter.[9,10]

The alloys were cast into sand molds using a four-bar pattern to produce test bars of 6½ in. length with a reduced section 2½ in. long and ½ in. diam. The test bars were tested without machining the surface of the reduced section.

All alloys were tested in various conditions of heat treatment. The following ASTM designations are used throughout the paper to indicate the different conditions: *T5*, aged at 400°F for 16 hr; *T4*, solution heat treated; and *T6*, solution heat treated and aged at 400°F for 16 hr. Differences in the solidus temperatures of the various alloys necessitated the use of different solution heat treating temperatures as shown in Table III. The heat treating conditions listed are adequate for effecting maximum solution of the alloying elements and coalescence of the undissolved compound without causing a significant increase in the grain size.

The methods of tension and creep testing have been described in detail in earlier papers.[11,12] The creep characteristics of each alloy are described by the following three parameters obtained by interpolation of log stress vs log extension plots of the original data: 1) creep limit based on 0.1 pct creep extension in 100 hr, 2) creep limit based on 0.2 pct total extension in 100 hr, and 3) creep limit based on 0.5 pct total extension in 100 hr. The total extension includes both the creep extension and the initial extension resulting from application of the load. Creep rates are not reported since they bear little significance when derived from tests of 100-hr duration.

Table III. Solution Heat Treating Temperatures*

Alloy Addition to Mg-Zr Base Alloy	Solution Heat Treating Temperature, °F
½ to 2 pct Mischmetal	1050
1 to 3 pct Cerium-free Mischmetal	1050
1 to 2 pct Didymium	1050
3 to 6 pct Didymium	1000
2 to 3 pct Didymium + 1 to 1.5 pct Mischmetal	1025
2 to 4 pct Didymium + 2 pct Zn	925
2 to 4 pct Didymium + 4 pct Zn	900

* Solution heat treating time of 16 hr for all alloys.

Discussion of Results

Tensile Properties—As indicated earlier, the most significant effect of zirconium on sand cast Mg-rare earth metal alloys is the reduction in the grain size. Binary Mg-rare earth metal alloys are characterized by a rather coarse equiaxed grain structure. Addition of between 0.10 and 0.30 pct Zr reduces the grain size to between 0.002 and 0.005 in., while increasing the zirconium content to between 0.4 and 0.6 pct further reduces the grain size to between 0.001 and 0.002 in. In general, the presence of rare earth metals decreases the maximum amount of zirconium soluble in magnesium from 0.7 pct to a value in the range of 0.5 to 0.6 pct. When zirconium contents are indicated, they are given as *acid soluble*. This serves to distinguish these values from the small amount of unalloyed zirconium which does not dissolve when the analytical sample is subjected to the action of a dilute solution of hydrochloric acid. The *acid insoluble* zirconium did not exceed a few hundredths of 1 pct in any alloy.

All the Mg-rare earth metal-Zr alloys are benefited by a solution heat treatment prior to the aging treatment. Both the ductility and strength are higher in the *T6* condition than in the *T5* condition at all testing temperatures. For this reason, only properties of these alloys in the *T6* condition are being reported.

The enhancement of the tensile properties of Mg-3 pct rare earth metal alloys by the addition of zirconium is clearly shown in Figs. 1 to 3. Zirconium

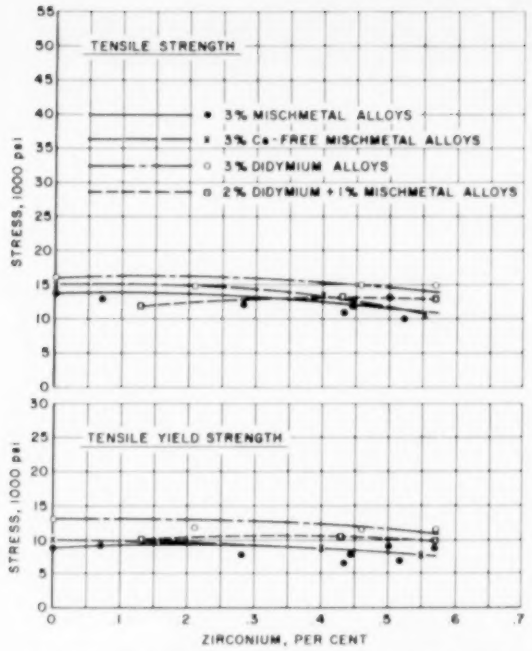

Fig. 3—Tensile strength and tensile yield strength at 600°F of Mg-3 pct rare earth metal-Zr alloys in the *T6* condition.

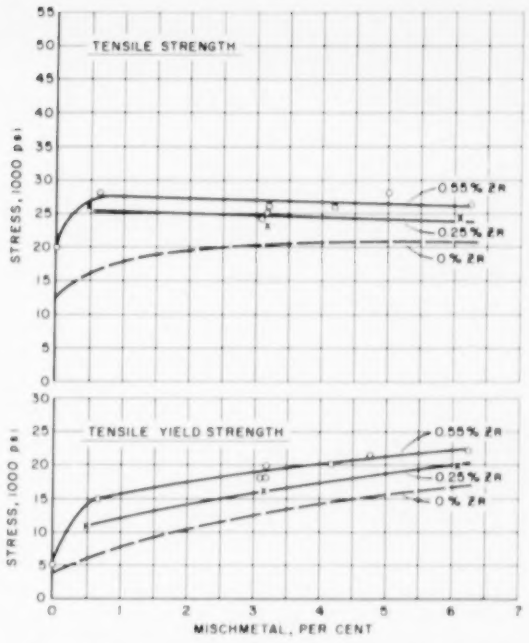

Fig. 4—Tensile strength and tensile yield strength at 70°F of Mg-Mischmetal-Zr alloys in the *T6* condition.

content affects tensile properties in a similar way at both higher and lower levels of rare earth metal content. As a general statement, it can be said that for all rare earth-containing alloys, the strength properties up to 500°F increase with increasing amounts of zirconium. At 600°F, however, zirconium content has no significant effect on the properties of these alloys. The effect of zirconium on the ductility of the alloys is shown by the data in Table IV. These data show that zirconium increases the ductility of alloys containing up to 3 to 4 pct rare earth metals, whereas this property is not improved in alloys of 5 to 6 pct rare earth metal content.

Figs. 1 to 3 also show that significant differences exist among the various rare earth metals in their effect on the strength properties, as in the case of zirconium-free alloys.[3]

Alloys containing cerium-free Mischmetal + zirconium are superior to Mg-Mischmetal-Zr alloys, but the outstanding properties are exhibited by Mg-didymium-Zr alloys.

The effects of Mischmetal content, zirconium content, and testing temperature on the tensile properties of the Mg-Mischmetal-Zr alloys in the *T6* condition are shown by the curves in Figs. 4 to 6. The curves of Mg-Mischmetal alloys (0 pct Zr) are reproduced from a preceding publication.[1] Elongation values for these alloys are to be found in Table IV. The curves in Fig. 6 emphasize a previous statement that at 600°F zirconium content has no significant effect on the properties of the Mg-rare earth metal alloys. In fact, the values for Mg-Mischmetal-Zr alloys fall quite closely to the curve for Mg-Mischmetal alloys.

The tensile properties of Mg-didymium-Zr alloys at 70°, 400°, and 600°F are shown by the curves in Fig. 7. Curves for Mg-didymium alloys are reproduced from a preceding publication[1] for comparison. Elongation values are given in Table IV. Above

Table IV. Elongation of Alloys at Room and Elevated Temperatures

Alloy No.	Rare Earth, Pct	Zirconium, Pct	Percentage of Elongation in 2 In. 70°F	400°F	600°F
		Magnesium			
	0	0	6	38	81
		Mg-Mischmetal-Zr Alloys, T6 Condition			
1	0.40	0	8	24	52
2	0.49	0.21	8	20	59
3	0.66	0.55	8	21	54
4	2.50	0	2	8	33
5	3.23	0	1	5	24
6	3.39	0.07	2	12	34
7	3.19	0.28	3	13	70
8	2.85	0.43	4	16	58
9	3.61	0.44	3	10	55
10	3.19	0.50	3	9	49
11	3.11	0.52	3	12	54
12	3.21	0.57	3	13	52
13	4.20	0.51	4	12	53
14	4.76	0.56	3	2	49
15	6.33	0	1	7	12
16	6.12	0.36	0.5	2	38
17	6.22	0.53	0.5	3	58
		Mg-Cerium-Free Mischmetal-Zr Alloys, T6 Condition			
18	3.66	0	2	14	41
19	3.17	0.40	2	11	58
20	2.95	0.55	2	12	51
		Mg-Didymium-Zr Alloys, T6 Condition			
21	1.0	0	5	17	34
22	1.04	0.69	9	20	52
23	2.0	0	4	14	32
24	1.98	0.61	7	16	51
25	3.0	0	3	11	30
26	3.49	0.21	2	10	37
27	2.98	0.46	7	10	50
28	3.76	0.51	6	14	37
29	3.39	0.57	6	14	43
30	4.47	0.23	3	12	22
31	4.47	0.54	4	11	41
32	5.5	0	1	3	28
33	5.53	0.53	—	4	38
		Mg-Ce-Didymium-Zr Alloys, T6 Condition			
	Cerium, Pct / Didymium, Pct				
34	0.75 / 2.41	0.57	5	15	57
35	1.13 / 2.04	0.64	5	14	45
36	2.25 / 1.08	0.60	5	13	64
37	2.78 / 0	0.23	4	13	50
		Mg-Didymium-Mischmetal-Zr Alloys, T6 Condition			
	Didymium, Pct / Mischmetal, Pct				
38	1.8 / 1.8	0.45	4	14	55
39	1.6 / 1.6	0.41	5	14	50
40	2.0 / 1.0	0.13	3	12	66
41	2.0 / 1.0	0.43	4	14	56
42	2.0 / 1.0	0.57	6	15	57
43	3.2 / 1.6	0.48	2	4	50

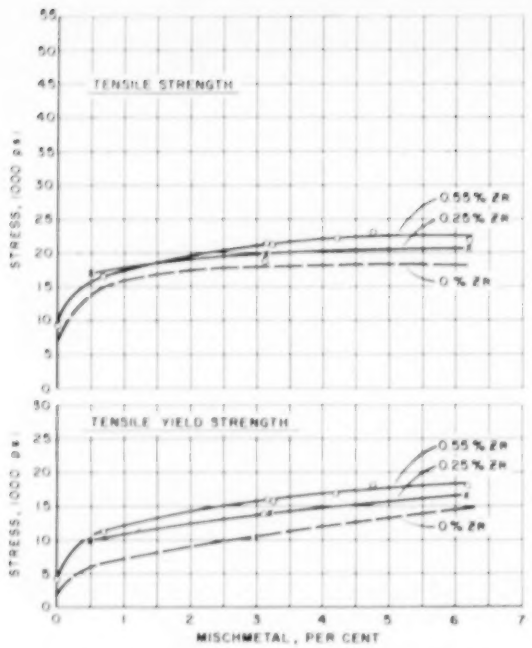

Fig. 5—Tensile strength and tensile yield strength at 400°F of Mg-Mischmetal-Zr alloys in the *T6* condition.

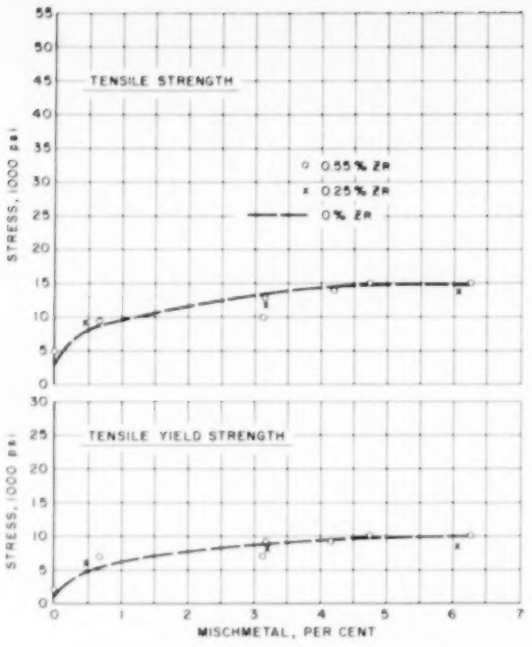

Fig. 6—Tensile strength and tensile yield strength at 600°F of Mg-Mischmetal-Zr alloys in the *T6* condition.

the 3 pct didymium level, tensile strength decreases with increasing didymium content. The effect of zirconium additions to Mg-didymium alloys is most pronounced on the tensile strength at room temperature. Attention is called particularly to the excellent combination of strength and ductility at room temperature of the alloy containing 3 pct didymium + 0.5 pct Zr. The superiority of these alloys over all other Mg-rare earth-Zr alloys persists at all temperatures investigated.

In addition to studying Mg-didymium-Zr alloys, the properties of alloys containing mixtures of didymium and pure cerium and of didymium and Mischmetal were also determined. The results of tensile tests on such alloys are shown in Figs. 8 and 9 and Table IV. It can be seen from these data that replacement of the didymium by increasing amounts of either pure cerium or Mischmetal, while maintaining the same total rare earth metal content, results in a progressive decrease in the strength properties. The Mg-pure Ce-Zr alloy used in this comparison is somewhat low in zirconium content. However, at the level of 3 pct rare earth metal content, magnesium alloys containing pure cerium are quite similar to Mg-Mischmetal alloys. Reference to the properties of a Mg + 3 pct Mischmetal + 0.5 pct Zr alloy will confirm the trends established by the Mg-Ce-didymium-Zr alloys.

The curves in Fig. 8 show that an alloy whose rare earth metal content is composed of two parts didymium and one part Mischmetal is only slightly inferior in tensile properties to the corresponding alloy containing only didymium. This alloy has been

Table V. Tensile Properties of Mg-Didymium-Zn-Zr Alloys

Alloy No.	Rare Earth Metals, Pct	Zn, Pct	Zirconium, Pct, Acid Soluble	70°F Percentage of Elongation in 2 In.	70°F Tensile Yield Strength in 1000 Psi	70°F Tensile Strength in 1000 Psi	100°F Percentage of Elongation in 2 In.	100°F Tensile Yield Strength in 1000 Psi	100°F Tensile Strength in 1000 Psi	600°F Percentage of Elongation in 2 In.	600°F Tensile Yield Strength in 1000 Psi	600°F Tensile Strength in 1000 Psi
										Properties in the *T5* Condition		
			Alloys Containing Didymium									
24	1.98		0.61	6	19	33	16	14	23	53	8	11
44	2.13	1.81	0.69	8	15	28	25	11	21	38	8	13
45	2.09	3.68	0.76	2	20	28	26	13	20	39	10	12
29	3.39		0.57	3	21	31	11	17	27	48	8	12
46	3.92	1.93	0.58	2	16	22	19	11	24	44	8	15
47	4.01	3.82	0.63	4	17	27	25	12	22	42	8	13
			Alloys Containing Mischmetal									
48	2.82	2.99	0.69	3	17	22	11	11	21	50	8	12
										Properties in the *T6* Condition		
			Alloys Containing Didymium									
24	1.98		0.61	7	18	36	16	17	25	51	12	14
44	2.13	1.81	0.69	10	15	32	31	11	21	50	8	12
45	2.09	3.68	0.76	12	16	34	39	10	15	70	7	8
29	3.39		0.57	6	23	39	14	22	31	43	12	15
46	3.92	1.93	0.58	3	16	25	20	12	24	61	9	12
47	4.01	3.82	0.63	7	16	30	27	11	20	52	8	10

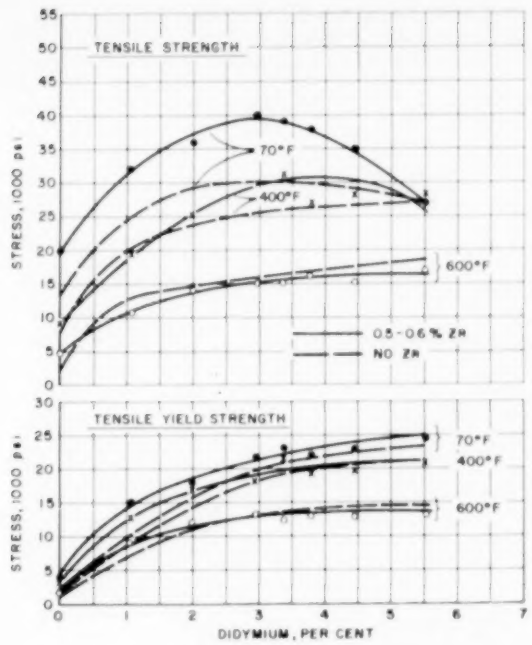

Fig. 7—Tensile strength and tensile yield strength at 70°, 400°, and 600°F of Mg-didymium-Zr alloys in the *T6* condition.

studied in considerably more detail and the effect of zirconium content on its properties has already been shown in Figs. 1, 2, and 3. Although the strength properties of this alloy in separately-cast test bars are slightly lower than those of the corresponding Mg-didymium-Zr alloy, bar sections from a simulated production casting of both compositions exhibit nearly equivalent tensile properties in the *T6* condition. Replacement of a portion of the didymium by Mischmetal offers the possibility of a lower cost alloy and in addition conserves the less abundant rare earth metals.

From the standpoint of porosity tendency it has been found beneficial to add zinc to Mg-Mischmetal-Zr alloys. This has resulted in a commercial alloy containing 3 pct Mischmetal, 3 pct zinc, and 0.5 pct minimum Zr (ASTM designation *EZ33A*).[55] The results of tensile tests on a series of alloys containing didymium and zinc are given in Table V together with the properties of *EZ33A* alloy. It has been found that a solution heat treatment prior to aging does not enhance the properties of Mg-Mischmetal-Zn-Zr alloys. To illustrate these effects for Mg-didymium-Zn-Zr alloys, data for both the *T5* and *T6* tempers are included in Table V. It can be clearly seen that the Mg-didymium-Zn-Zr alloys behave in the same way with respect to heat treatment. On the other hand, Mg-didymium-Zr alloys are markedly benefited by a solution heat treatment. And what is more important is that Mg-didymium-Zr alloys in the *T6* temper exhibit

Table VI. Creep Limits of Mg-Rare Earth Metal-Zr Alloys

Alloy No.	Rare Earth, Pct	Zirconium, Pct	100-Hr Creep Limits, 1000 Psi					
			400°F			600°F		
			0.1 Pct Creep Extension	0.2 Pct Total Extension	0.5 Pct Total Extension	0.1 Pct Creep Extension	0.2 Pct Total Extension	0.5 Pct Total Extension
					T6 Condition			
			Mg-Cerium-free Mischmetal-Zr Alloys					
18	3.09	0	11.8	9.6	12.7	1.4	1.7	2.1
19	3.17	0.40	9.4	8.7	11.2	1.2	1.3	1.5
20	4.98	0.32	10.8	9.8	12.4	1.1	1.4	1.7
			Mg-Didymium-Zr Alloys					
21	1.0	0	8.5	7.2	9.5	1.9	2.1	2.6
22	1.04	0.60	10.8	9.8	12.0	1.6	1.8	2.1
23	2.0	0	11.5	9.0	12.5	1.2	2.0	2.8
24	1.98	0.61	12.0	10.0	14.6	1.1	1.3	1.8
25	3.0	0	13.2	10.0	14.5	1.0	1.4	1.7
27	2.98	0.46	11.2	9.2	15.0	1.2	1.4	1.6
32	5.5	0	14.5	10.0	16.8	1.0	1.4	2.4
33	5.53	0.53	11.1	9.2	14.3	1.9	1.0	1.4
			Mg-Didymium-Ce-Zr Alloys					
	Cerium, Pct / Didymium, Pct							
34	0.75 / 2.41	0.57	11.0	10.0	13.0	1.1	1.2	1.4
35	1.13 / 2.04	0.64	9.5	8.4	12.4	0.8	0.9	1.2
36	2.25 / 1.08	0.60	8.3	7.9	11.0	1.1	1.3	1.6
37	2.78 / 0	0.23	8.5	7.6	8.8	1.8	2.0	2.3
			Mg-Didymium-Mischmetal-Zr Alloys					
	Didymium, Pct / Mischmetal, Pct							
40	2.0 / 1.0	0.13	9.6	8.5	11.5	0.7	0.9	1.2
42	2.0 / 1.0	0.57	9.4	8.5	11.7	0.8	0.9	1.2
43	3.2 / 1.6	0.48	8.3	7.6	10.5	0.7	0.9	1.1
			Mg-Didymium-Zn-Zr Alloys					
	Didymium, Pct / Zinc, Pct				*T5* Condition			
24	1.98 / —	0.61	8.6	8.3	10.2	0.8	0.9	1.1
44	2.13 / 1.81	0.69	8.6	8.0	9.9	1.1	1.4	1.7
45	2.09 / 3.68	0.76	7.8	7.2	10.0	0.6	0.7	1.0
46	3.92 / 1.93	0.58	10.0	8.1	10.0	0.9	1.4	1.7
47	4.61 / 3.82	0.63	9.8	8.6	11.0	1.0	1.4	1.7
					T6 Condition			
44	2.13 / 1.81	0.69	8.5	8.0	10.4	1.0	1.2	1.7
45	2.09 / 3.68	0.76	6.1	6.1	8.0	0.5	0.6	0.8
46	3.92 / 1.93	0.58	8.6	7.6	10.8	1.2	1.4	1.8
47	4.61 / 3.82	0.63	9.2	8.8	10.3	1.0	1.2	1.5
			Mg-Mischmetal-Zn-Zr Alloy					
	Mischmetal, Pct / Zinc, Pct				*T5* Condition			
48	2.82 / 2.99	0.69	9.0	8.0	10.1	1.0	1.2	1.5

Table VII. Comparison of Principal Sand Cast Magnesium Alloys for Elevated Temperature Service

Nominal Composition, Pct				Commercial Designation	Temper	Tensile Properties										Stress for 0.2 Pct Total Extension in 100 Hr		
						Room Temperature			400°F			600°F						
Mischmetal	Didymium	Thorium	Zinc	Zirconium		Percentage of Elongation in 2 In.	Tensile Yield Strength in 1000 Psi	Tensile Strength in 1000 Psi	Percentage of Elongation in 2 In.	Tensile Yield Strength in 1000 Psi	Tensile Strength in 1000 Psi	Percentage of Elongation in 2 In.	Tensile Yield Strength in 1000 Psi	Tensile Strength in 1000 Psi	400°F	500°F	600°F
2				0.5	T6		16	23	13	12	20	70	6.6	13	7.7	5.5	2.5
4				0.5	T6		16	25	14	13	20	58	6.6	13	8.0	5.6	2.5
4				0.5	T6*		18	25	10	11	21	50	6.6	13	8.0	5.6	2.5
	3			0.5	T6*		17	22	11	10	21	52	6.6	13	8.0	5.6	2.5
	3		2	0.5	T6*		16	22	11	10	21	52	6.6	13	8.0	5.6	2.5
		3		0.5	T6†		16	21	11	10	21	52	6.6	13	8.0	5.6	2.5
		3	2	0.5	T6†		18	29	11	10	21	52	6.6	13	8.0	5.6	2.5
		2.5		0.5	T6†		16	26	13	11	24	58	6.6	13	8.0	5.6	2.5
		2.5		0.5	T6†		18	26	14	11	24	58	6.6	13	8.0	5.6	2.5
							21	40	12	20	30	52	6.6	13	8.0	5.6	2.5
2				0.5	T6				30	33	38	70	6.6	13	7.7	5.5	2.5
4				0.5	T6				31	33	38	58	6.6	13	8.0	5.6	2.5
4				0.5	T6*				28	33	38	50	6.6	13	8.0	5.6	2.5
	3			0.5	T6*				28	33	38	52	6.6	13	8.0	5.6	2.5
	3		2	0.5	T6*				28	33	38	52	6.6	13	8.0	5.6	2.5
		3		0.5	T6†				28	33	38	52	6.6	13	8.0	5.6	2.5
		3	2	0.5	T6†				28	33	38	52	6.6	13	8.0	5.6	2.5
		2.5		0.5	T6†				30	33	38	70	6.6	13	7.7	5.5	2.5
		2.5		0.5	T6†				31	33	38	58	6.6	13	8.0	5.6	2.5

* Aged 420°F, 5 hr.
† Aged 600°F, 16 hr.

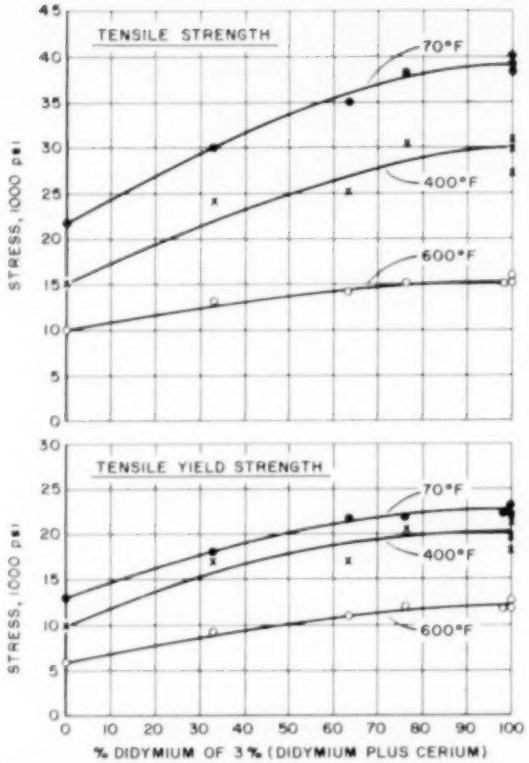

Fig. 8—Tensile strength and tensile yield strength at 70°, 400°, and 600°F of Mg-3 pct (didymium + cerium) — 0.5 pct Zr alloys in the T6 condition.

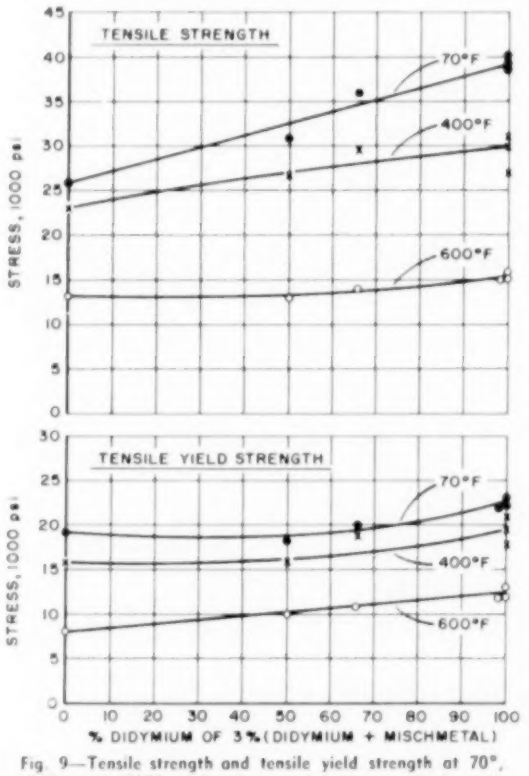

Fig. 9—Tensile strength and tensile yield strength at 70°, 400°, and 600°F of Mg-3 pct (didymium + Mischmetal) — 0.5 pct Zr alloys in the T6 condition.

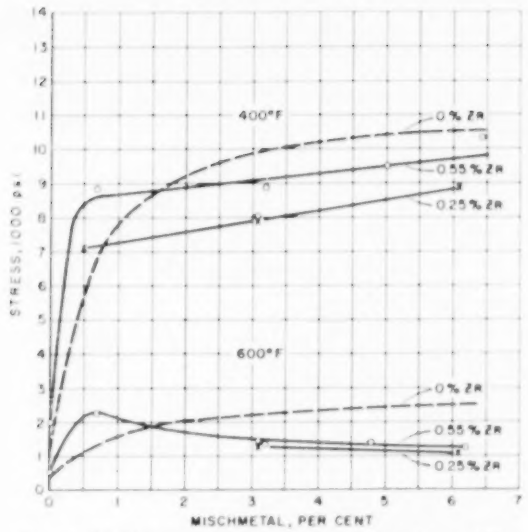

Fig. 10—Limiting stress for 0.1 pct creep extension in 100 hr of Mg-Mischmetal-Zr alloys in the *T6* condition.

markedly higher strength properties at all temperatures than the corresponding alloys containing zinc.

Creep Resistance—The effects of zirconium content on the creep properties of the Mg-Mischmetal-Zr alloys at 400° and 600°F are shown by the curves in Figs. 10 to 12. At all levels of Mischmetal content except approximately 0.5 pct, there is a downward trend in the creep limits with increasing zirconium content. Percentagewise, the decrease is much greater at 600° than at 400°F. There appears to be a minimum of the creep resistance of the Mischmetal alloys at about 0.25 pct Zr. These effects may be a result of the opposing effects on creep resistance of grain refinement and strengthening resulting from the addition of zirconium. At the level of 0.5 pct Mischmetal, the creep resistance is definitely improved by the addition of zirconium. In fact, at 600°F, the creep resistance of the Mg + 0.66 pct Mischmetal + 0.55 pct Zr is the highest of any of the zirconium-containing alloys investigated. The creep resistance of this alloy at 400°F is comparable to that of the commercial alloys *EK30A-T6* (Mg + 3.4 pct Mischmetal + 0.3 pct Zr) and *EK41A-T6* (Mg + 4 pct Mischmetal + 0.6 pct Zr), and at the same time has a good combination of strength and ductility at room temperature. It appears that more work is needed in the lower Mischmetal range. There are possibilities for an alloy cheaper and more castable than the higher Mischmetal-containing *EK30A* and *EK41A*. The *T5* condition creep limits were obtained but are not reported. The creep limits of the Mg-Mischmetal-Zr alloys in the *T5* and *T6* conditions do not differ significantly.

The creep limits of other Mg-rare earth metal-Zr alloys and the Mg-didymium-Zn-Zr alloys are presented in Table VI. The Mg + 3 pct cerium-free Mischmetal + 0.40 pct Zr alloy shows a distinct superiority in creep resistance at 400° over the corresponding alloy containing Mischmetal, but at 600°F the two compositions are equivalent. The results confirm those of Nelson and Strieter,[7] who tested an alloy made with low-cerium Mischmetal in which the cerium amounted to about 3 to 4 pct of the total rare earth metal content. Significantly, higher creep resistance at 400°F is exhibited by Mg-didymium-Zr alloys, a result which confirms the findings on Mg-didymium alloys.[1] At 600°F, however, these alloys show no advantage in creep resistance over the corresponding alloys containing Mischmetal. The Mg-Ce-didymium-Zr alloy shows a definite downward trend in creep resistance with increasing cerium content. The Mg-didymium-Mischmetal-Zr alloys have creep resistance at 400°F superior to those of corresponding alloys made with Mischmetal but inferior to that of the alloys containing only didymium; at 600°F the alloys are about equivalent. Addition of zinc to Mg-didymium-Zr alloys is detrimental to the creep resistance of these alloys.

Summary

The results presented in this paper clearly show that the grain refinement of Mg-rare earth metal alloys resulting from the addition of zirconium is

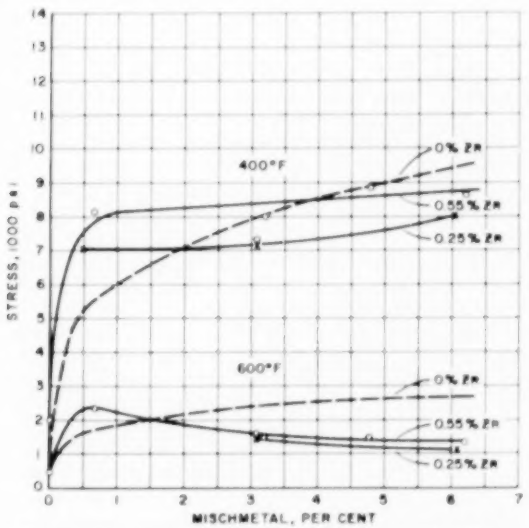

Fig. 11—Limiting stress for 0.2 pct total extension in 100 hr of Mg-Mischmetal-Zr alloys in the *T6* condition.

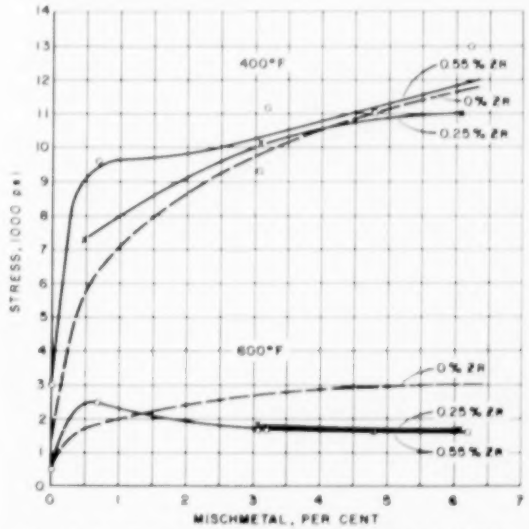

Fig. 12—Limiting stress for 0.5 pct total extension in 100 hr of Mg-Mischmetal-Zr alloys in the *T6* condition.

accompanied by a significant improvement in strength and ductility at temperatures up to 400°F. Creep resistance is impaired slightly at 400° and more drastically at 600°F by the addition of zirconium.

Table VII is presented in order to afford a quick comparison of some of the experimental alloys discussed in this paper with commercial Mg-rare earth metal alloys (*EK30A*, *EK41A*, and *EZ33A*) used at elevated temperatures. Data are included in this table at 500°F in order to give a more complete picture of the effect of temperature. Also, properties of two important magnesium alloys containing thorium (*HK31A* and *HZ32A*) are presented. These alloys are discussed in much more detail elsewhere.[14,15] In general, alloys *EK30A-T6*, *EK41A-T5*, *EK41A-T6*, and *EZ33A-T5* are essentially equivalent both in static properties and creep resistance, with *EK41A-T6* showing some superiority. The Mg-didymium-Zr alloys exhibit the highest strength and ductility and show some superiority in creep resistance at 400°F. The alloy containing 2 pct didymium appears to have some advantage in creep resistance at 500°F. The outstanding characteristic of the alloys containing thorium is the high creep resistance at 500° and 600°F, which is even more pronounced when evaluated in tests of longer duration than 100 hr.

References

[1] T. E. Leontis: *AIME Trans.*, 1949, vol. 185, p. 968; JOURNAL OF METALS, December 1949.
[2] T. E. Leontis: *AIME Trans.*, 1951, vol. 191, p. 987; JOURNAL OF METALS, November 1951.
[3] K. E. Nelson and F. P. Strieter: *Trans.* Amer. Foundrymen's Soc., 1951, vol. 59, p. 532.
[4] K. E. Nelson and F. P. Strieter: *Trans.* Amer. Foundrymen's Soc., 1950, vol. 58, p. 400.
[5] A. J. Murphy and R. J. M. Payne: *Journal* Institute of Metals, 1946, vol. 73, p. 105.
[6] C. J. P. Ball: *Metal Industry*, London, 1949, vol. 75, p. 152.
[7] J. W. Meier and M. M. Martinson: *Trans.* Canadian Institute of Mining and Metallurgy, 1950.
[8] K. E. Nelson: *Proceedings* ASTM, 1954, vol. 54, p. 1081.
[9] A. C. Jessup, E. F. Emley, and P. A. Fisher: U. S. Patent No. 2,549,955, April 1951.
[10] C. E. Nelson: *AIME Trans.*, 1944, vol. 159, p. 392; METALS TECHNOLOGY, August 1944.
[11] T. E. Leontis and J. P. Murphy: *AIME Trans.*, 1946, vol. 166, p. 295; METALS TECHNOLOGY, April 1946.
[12] A. A. Moore and J. C. McDonald: *Proceedings* ASTM, 1946, vol. 46, p. 970.
[13] T. E. Leontis: *AIME Trans.*, 1952, vol. 194, p. 633; JOURNAL OF METALS, June 1952.
[14] K. E. Nelson: *AIME Trans.*, 1953, vol. 197, p. 1493; JOURNAL OF METALS, November 1953.
[15] C. J. P. Ball, A. C. Jessup, P. A. Fisher, D. J. Whitehead, and J. B. Wilson: *AIME Trans.*, 1953, vol. 197, p. 924; JOURNAL OF METALS, July 1953.
[16] K. E. Nelson: *Trans.* Amer. Foundrymen's Soc., 1953, vol. 61, p. 315.
[17] K. E. Nelson: *Trans.* Amer. Foundrymen's Soc., 1955, vol. 63, p. 596.

Discussion of this paper sent (2 copies) to AIME by Dec. 1, 1957 will appear in AIME *Transactions* Vol. 212, 1958, and in JOURNAL OF METALS, April 1958.

Grain Boundary Deformation in Fine-Grained Electrolytic Magnesium

by S. L. Couling and C. S. Roberts

PLASTIC strain in polycrystalline metal as a result of bulk movement of one grain with respect to another along grain boundaries is not new. Rosenhain and Humphrey observed such effects shortly after the turn of the century.[1] Since then, observations of grain boundary deformation have been made on several metals.[2-4] In recent years, intensive studies of the deformation at grain boundaries have been performed on polycrystalline metal and bicrystals.[5-13] Aluminum or its alloys have been used in these latter studies. The subjects of controversy at present appear to be not whether grain boundary deformation exists, but 1) how quantitatively important it can be in polycrystalline metal, and 2) what its detailed mechanism is. Some investigators have concluded that such deformation is minor in importance while others have concluded that it is a major consideration. Some have concluded that it involves shear of one grain over another at the interface while others have concluded that it operates by crystallographic deformation within the grains near the boundary. A categorical statement for electrolytic magnesium cannot be made on either of these points. When polycrystalline magnesium is deformed in creep under conditions of high strain rate and low temperature, grain boundary deformation is relatively slight.[14] Under these conditions, much deformation occurs within the grains and boundary contours change to a higher-energy jagged form. The result is shown in Fig. 1, where boundary jaggedness is pronounced upon polishing and etching after a plastic strain of approximately 6 pct at 300°F and 3000 psi. No migration of the boundaries has been detected in this process. When the same metal is deformed the same amount at 600°F and 300 psi, resulting in a much lower strain rate, the boundaries migrate toward a lower energy configuration, where

S. L. COULING is associated with the Metallurgical Laboratory, Dow Chemical Co., Midland, Mich. C. S. ROBERTS, Junior Member AIME, formerly with Dow Chemical Co., is now with Shockley Semiconductor Laboratory, Mountain View, Calif.

TP 4580E. Manuscript, Sept. 5, 1956.

their smoothness equals or exceeds that of the original aggregate. Such a result is shown in Fig. 2.

This paper presents quantitative evidence on this second process, which involves *migration* of boundaries in conjunction with shear of one grain with respect to the other. The results show that under conditions of high temperature and low strain rate boundary deformation is by far the major strain contributor. In the limiting case it appears that all the deformation would be localized at the boundaries.

Experimental Procedure

Completely recrystallized extruded electrolytic magnesium was used in the investigation. This material was identical with respect to purity, extrusion conditions, and preferred orientation to that used in earlier work by one of the authors.[18] Creep specimens with a ½ in. wide gage section were machined from ⅛ x 1¼ in. cross section flat stock. The average grain diameter was about 0.003 in. with some minor variation between specimens. Specimens were tested at 600°F under stresses of 750, 500, 400, and 300 psi; additional tests at 500° and 650°F were made with respective stresses adjusted so as to have approximately the same strain rate as in the 600°F, 500 psi test.

Grain boundary displacements were measured by a grid technique. Electropolished samples were ruled with lines transverse to the stress axis using a sharp razor blade and then reelectropolished for 30 sec. Metallographic examination with the aperture diaphragm stopped down to the limit showed the lines to be almost hairbreadth. Measurements were made at X1000 with a calibrated filar eyepiece. An idealized sketch of a gridded area after grain boundary deformation has occurred is shown in Fig. 3. The exact method of obtaining the strain localized at grain boundaries (ϵ_{gb}) from measurements of individual boundary displacements (X) and boundary angles (θ) is presented in the Appendix. Providing a sufficient number of boundary shears are measured to determine the average boundary shear, $\overline{x}$, within narrow limits, the grid technique used in this investigation should give an accurate figure for ϵ_{gb}. It is assumed, of course, that surface measurements are representative of the interior of the metal and that the grid lines do not influence in any way the behavior of boundaries they happen to cross. Concerning this latter point, no interaction between grid lines and boundaries was ever noted. In an effort to obtain as accurate as possible a figure for $\overline{x}$, at least 500 boundary shears were measured in every specimen. Between 2 and 4 pct of these individual displacements were negative; the algebraic sum of positive and negative displacements was used in computing x. Negative shears were most often observed on boundaries of low θ and most likely resulted from grain rotation.

Measurements of grain boundary migration were obtained by traversing in a longitudinal or transverse direction and measuring at X1500 with a filar eyepiece the apparent distances through which boundaries had migrated. The angle that each boundary made with the stress axis was measured with a protractor eyepiece. Careful metallographic examination of grain boundary deformation was made and micrographs of representative areas after various amounts of creep obtained.

Measurements of overall creep extension, ϵ_T, made by Martens extensometer readings were compared with those calculated from direct measurements of grid line spacings before and after creep. These latter measurements were made using the calibrated stage of a metallograph. Where slight differences were observed between the two measurements, an average value was arbitrarily taken for ϵ_T.

Boundary Deformation

A representative picture showing grain boundary deformation is presented in Fig. 4. The smooth cyclic nature of the boundary deformation process is evident; boundary shears alternate with migrations of the respective boundaries to new positions. Metallographic examination of all specimens showed that the amount of basal slip present was a function of the test conditions, an increasing occurrence of basal slip being noted with increasing stress (temperature constant) or decreasing temperature (strain rate constant). Almost no basal slip could be detected in the sample stressed at 600°F, 300 psi. Examination of representative areas in several specimens after ~3 pct and again after ~6 pct creep showed that the total shear at any one boundary had roughly doubled between the 3 and 6 pct creep levels while the total boundary migration (although larger after 6 than 3 pct) had not increased proportionately. The distance between successive boundary steps was observed to decrease with continued cycling until individual displacements were no longer resolvable.

Relative movements of grains perpendicular to the specimen surface were examined metallographically at high magnification. It was noted that the direction of boundary migration was always *downhill*, i.e., into the receding grain. No correlation could be observed between the direction in which a particular boundary tended to migrate and curvature of the boundary.

The data are collected in Tables I and II so as to show the effects of *time* and *temperature* on the amount of boundary contributed strain. Higher temperatures (time constant) or longer times (temperature constant) to the same total strain lead to increased contributions from grain boundary deformation. Values of ϵ_{gb}/ϵ_T range from 0.67 to 0.93. These values are considerably higher than those reported by other investigators making similar determinations for pure aluminum and aluminum alloys. In McLean's[20,21] work, a test temperature of only 200°C was used and the grain size of his material was six times larger than that used in the present work. In the work of Fazan et al.,[22] the grain size was of the order of 50 times larger than that used here. Since large contributions from boundary deformation are favored by small grain size, high temperature, and low strain rate, it is not surprising that higher contributions were determined in the present case.

Boundary Migration

Measurements of boundary migrations were made in four of the six specimens. The procedure followed was to traverse 66 consecutive boundaries in both the longitudinal and transverse directions, measuring apparent migration and angle for each boundary encountered. Average apparent migration in each 10° angular increment of θ could then be calculated. Actually, such measurements and calculations would not give true migration values because some contribution from boundary shearing would be present in the measurements. The true migration

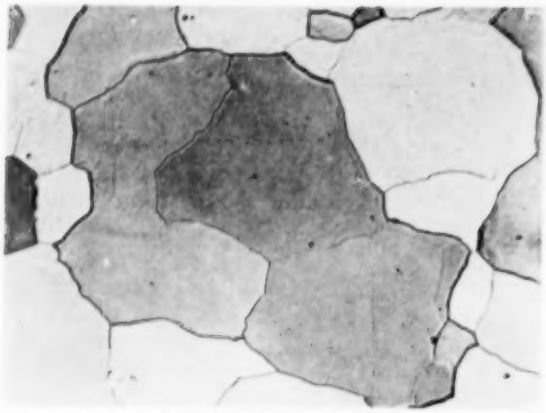

Fig. 1—6 pct creep at 300°F and 3000 psi. Repolished and etched after deformation. X500. Reduced approximately 20 pct for reproduction.

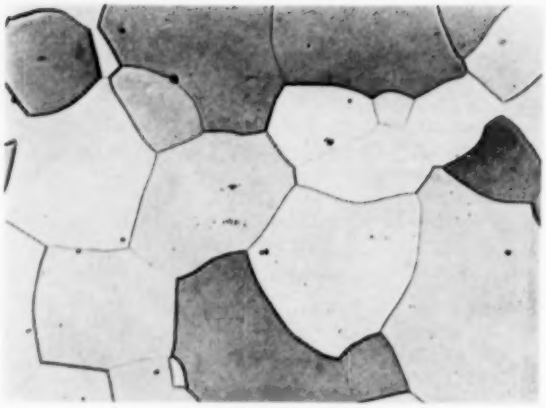

Fig. 2—6 pct creep at 600°F and 300 psi. Repolished and etched after deformation. X500. Reduced approximately 20 pct for reproduction.

in an angular increment should be the apparent migration minus the product of the average shear in that increment multiplied by sine θ. Because only 132 boundaries per specimen were measured, the data showed fairly wide scatter. However, the following general trends were apparent:

1) After 3 pct creep, boundaries perpendicular to the stress axis ($\theta = 90°$) had migrated through a distance which was 1.5 to 2.5 times as great as the distance through which they had sheared. Boundaries parallel to the axis ($\theta = 0°$) had migrated about half as much as the $\theta = 90°$ boundaries. For intermediate angle boundaries, a linear relationship between these two extremes appeared to obtain.

2) After 6 pct creep, the amount of shearing on the $\theta = 90°$ boundaries had doubled, but the amount of migration did not increase proportionately, the result being that the migration to shearing ratio was now between 1.0 and 2.0. Boundaries with $\theta = 0$ had not changed as much in their migration rate, so they had now migrated 0.75 to 1.0 times as much as the $\theta = 90°$ boundaries. Again, an approximately linear relationship obtained for intermediate angles.

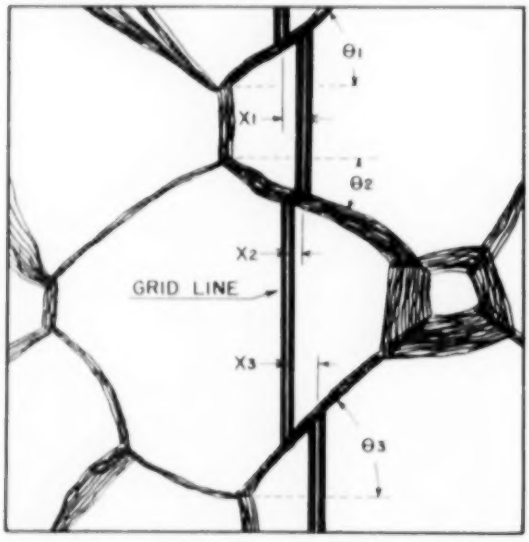

Fig. 3—Grain boundary displacements and boundary angles.

Discussion

The results indicate that the high-temperature boundary deformation process consists of cyclic boundary shearing and migration. A structural model for such a process is presented. Consider that, like deformation within grains, grain boundary shear may be elastic, anelastic, or plastic. The first two have been observed in the studies of Kê[35,36] and discussed comprehensively by Zener.[37] The static modulus of an aggregate involves anelastic behavior of the boundaries because of stress relaxation across them. The anelastic strain approaches a finite limit because of stress concentration at boundary edges. The dynamic modulus involves elastic behavior of the boundaries because the period of oscillation is so much less than the relaxation time. It is suggested here that plastic boundary behavior occurs in static creep when a thermally activated phenomenon, boundary migration, relieves the blocking stress concentration at grain edges and allows the anelastic boundary shears to be *captured*. This concept is analogous to the anelastic dislocation movement between barriers within a grain becoming plastic strain by the thermal activation of the dislocations over the barriers.

Suppose that a shear stress is applied to boundary *A-B* in Fig. 5. As this stress is relaxed by anelastic strain, stress concentrations will build up in grains *C* and *D* at the triple points. Now let migration of the *B-C*, *A-C*, *B-D*, and *A-D* boundaries operate. Since the shear has slightly increased the total boundary area, migration is driven by the lowering of interfacial energy as well as by the lowering of elastic strain energy. When the local stress concentration is adequately relieved by the sweeping grain boundaries, the original boundary can shear again. Boundary *A-B* may also migrate to relieve stress concentrated by shear on *B-C*, *A-C*, *A-D*, or *B-D* and so on in a complex fashion throughout the entire aggregate.

The maximum anelastic displacement which can occur on a favorably oriented boundary during one cycle may be calculated with the help of an expression developed by Kê.[35] If s is the shear stress acting on the boundary; Gu the unrelaxed shear modulus; d, the average grain diameter; and $\Delta X'$ the displacement that occurs during relaxation time τ, then $\Delta X'/d = s/Gu$. Now $\Delta X'$ represents all but one eth of the maximum possible displacement, ΔX, so that

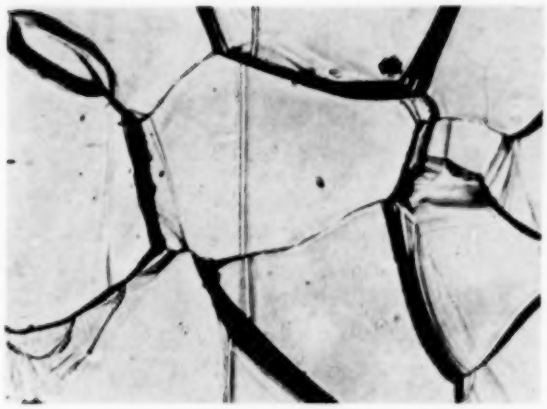

Fig 4—6 pct creep at 600°F and 400 psi X500. Reduced approximately 20 pct for reproduction.

$\Delta X = \left(\frac{e}{e-1}\right)\Delta X' = 1.58\,\frac{sd}{Gu}$. For a test stress of 300 psi, a $\theta = 90°$ boundary (boundary trace perpendicular to the stress axis) lies, on the average, at 45° to the surface, and the resolved shear stress is 150 psi. Taking $d = 0.003$ in. and Gu (600°F) $= 2.0 \times 10^6$ psi, $\Delta X = 3.6 \times 10^{-7}$ in. Resolved on the surface, this would correspond to a displacement in the direction of the stress axis of 2.5×10^{-7} in. From Fig. 6, after 3.45 pct creep, boundaries with $\theta = 90°$ in the 600°F, 300 psi specimen showed an average shear of 6.3×10^{-6} in.; and after 5.61 pct creep, a shear of 11.0×10^{-6} in. These measured shears, therefore, correspond to about 250 and 440 cycles, respectively, each of the cycles contributing a displacement of 2.5×10^{-7} in. Metallographic examination at high magnification has disclosed that these figures are quite reasonable. In some boundaries, individual steps are not resolvable but in others, more than 100 steps can be distinguished along with an unresolvable region.

It has been proposed several times[18,19,21,28] that deformation localized at grain boundaries is caused by the stress concentrations resulting from deformation in the interior of adjoining grains. In the case of electrolytic magnesium, this concept may be valid for low temperature creep (conditions similar to those of Fig. 1) but it is invalid for the conditions of high temperature-low strain rate investigated here, where it was observed that grain boundary deformation became more pronounced as strain within the grains decreased. In a like manner, the results also contradict the suggestion that dislocation movement on slip planes is the cause of boundary migration.[29]

Summary

High temperature grain boundary deformation in a simple polycrystalline magnesium aggregate is a two-stage process involving alternate boundary shearing and migration. Increasing test temperatures and decreasing strain rates favor larger contribution to the overall strain from boundary deformation. In the limiting case, it appears that all the deformation would be localized at the boundaries. A mechanism which explains the observations is the alternation of anelastic boundary shears with the *capture* of these shears when the boundaries migrate to new positions. Repetition leads to cyclic process. The number of cycles necessary to produce the measured shear on a simple boundary has been calculated and found to agree qualitatively with metallographic observation.

Table I. Effect of Time on Grain Boundary Deformation of Electrolytic Magnesium

Test Conditions	ϵ_T, Pct	t, Hr	$\bar{x}$, In.	$\bar{\bar{x}}$, In.	N	ϵ_{GB}, Pct	ϵ_{GB}/ϵ_T
600°F, 500 psi	3.39	119	3.53×10^{-4}	5.12×10^{-4}	540	2.77	0.81
600°F, 400 psi	2.71	214	3.63	5.22	460	2.40	0.89
600°F, 300 psi	3.45	672	4.12	5.97	540	3.23	0.93
600°F, 750 psi	5.80	122	6.54	9.48	410	3.89	0.67
600°F, 500 psi	6.14	237	6.46	9.37	525	4.92	0.80
600°F, 400 psi	5.88	573	6.98	10.12	450	4.55	0.78
600°F, 300 psi	5.61	1149	6.35	9.20	525	4.83	0.86

* ϵ_T equals total creep strain, t, creep testing time; $\bar{x}$, average grain boundary displacement, $\sum_{i=1}^{n} x_i/n$; $\bar{\bar{x}}$, corrected displacement, $F\bar{x}$, where $F = 1.45$, see Appendix; N, number of grain boundaries intercepted in a 1 in. longitudinal traverse; ϵ_{GB}, strain contributed by grain boundary deformation, $N\bar{\bar{x}} \times 100$ pct; and ϵ_{GB}/ϵ_T, fraction of the total strain caused by grain boundary deformation.

Table II. Effect of Temperature on Grain Boundary Deformation of Electrolytic Magnesium

Test Conditions	ϵ_T, Pct	t, Hr	$\bar{x}$, In.	$\bar{\bar{x}}$, In.	N	ϵ_{GB}, Pct	ϵ_{GB}/ϵ_T
500°F, 1100 psi	3.24	120	3.01×10^{-4}	4.37×10^{-4}	540	2.36	0.73
600°F, 500 psi	3.39	119	3.53	5.12	540	2.77	0.81
650°F, 375 psi	3.20	98	3.51	5.09	540	2.75	0.86
500°F, 1100 psi	6.16	267	5.68	8.25	525	4.33	0.70
600°F, 500 psi	6.14	237	6.46	9.37	525	4.92	0.80
650°F, 375 psi	6.36	259	6.72	9.74	525	5.12	0.81

* ϵ_T equals total creep strain, t, creep testing time; $\bar{x}$, average grain boundary displacement, $\sum_{i=1}^{n} x_i/n$; $\bar{\bar{x}}$, corrected displacement, $F\bar{x}$, where $F = 1.45$, see Appendix; N, number of grain boundaries intercepted in a 1 in. longitudinal traverse; ϵ_{GB}, strain contributed by grain boundary deformation, $N\bar{\bar{x}} \times 100$ pct; and ϵ_{GB}/ϵ_T, fraction of the total strain caused by grain boundary deformation.

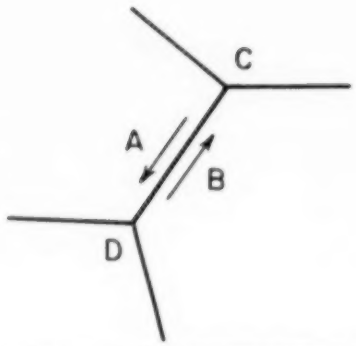

Fig. 5—As the shear stress applied to boundary A-B is relaxed by anelastic strain, stress concentrations build up at the triple points.

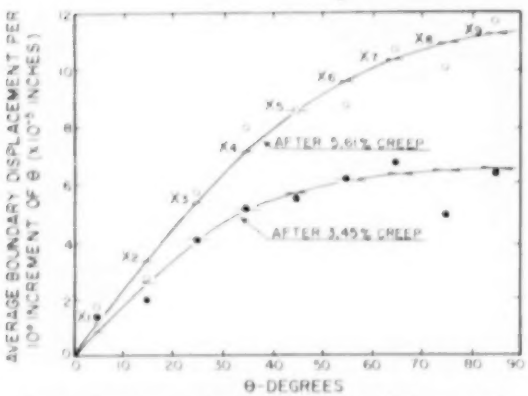

Fig. 6—Boundary displacement vs θ after 3.45 pct creep and after 5.61 pct creep in 600°F, 300 psi specimen.

Appendix Calculation of ϵ_{ss} From Boundary Displacement Measurements

Fazan, Sherby, and Dorn[28] have calculated ϵ_{ss} by measuring individual boundary displacements (X) in a direction parallel to the stress axis, averaging the displacements to get $\bar{x}$, and multiplying this figure by the number of grain boundaries (N) intercepted by a transverse of unit distance in the longitudinal direction. The value of ϵ_{ss} so obtained is only correct if boundary displacement is independent of the angle which the trace of the boundary makes with the stress axis or if all boundaries make the same angle with the stress axis. In the present work it was found that there was a large dependence of boundary shear on trace angle; boundaries almost parallel to the axis made little or no contribution while those perpendicular evidenced maximum shears. It was therefore necessary to calculate a correction factor, F, which could be applied to values of ϵ_{ss} obtained simply by measurements of N and $\bar{x}$. This was accomplished in the following manner:

a) A specimen was creep tested to 3.45 pct and later to 5.61 pct at 600°F, 300 psi. After each creep increment, values of boundary displacement, x, and angle, θ, which the respective boundaries made with the stress axis were measured for at least 550 grain boundaries.

b) Average boundary displacement $\bar{x} = \frac{\sum_{i=1}^{n} X_i}{n}$ was determined for each case.

c) The average boundary displacement in each 10° angular increment of θ was calculated for both cases, plotted on a graph, and a smooth curve drawn through the graphed points to give $\bar{x}_1$, $\bar{x}_2$, $---\bar{x}_n$, as shown in Fig. 6.

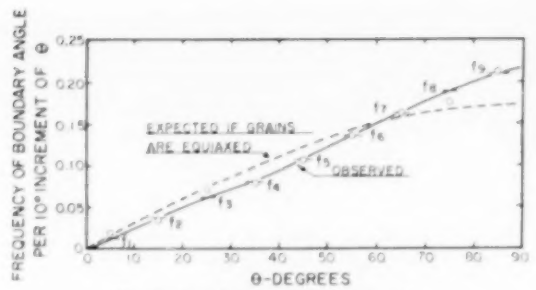

Fig. 7—Boundary angle frequency vs θ.

d) Boundary angles were measured on a longitudinal traverse. A normalized plot of frequency of occurrence of boundary angle in each 10° angular increment of θ was made and a smooth curve drawn through the graph points to give f_1, f_2, $---f_n$, as shown in Fig. 7. (This step would be unnecessary if the grains were symmetrical, since the curve would have the shape of a normalized sine wave. However, in the electrolytic magnesium used in this work the grains were slightly elliptical in shape with the major axis of the ellipse in the transverse direction; as a result, the shape of the curve is more like that shown in Fig. 7.)

e) The corrected average boundary displacement, $\bar{\bar{x}}$, for both cases was then obtained as the sum $\sum_{i=1}^{n} \bar{x}_i f_i$, where $\bar{x}_1$, $\bar{x}_2$, $---\bar{x}_n$ and f_1, f_2, $---f_n$ are as shown in Figs. 6 and 7, respectively.

f) The correction factor, F, is the $\bar{\bar{x}}/\bar{x}$ for each case. The calculated values of F were 1.43 (3.45 pct creep) and 1.47 (5.61 pct creep). An average, $F = 1.45$, was applied to measurements in which only $\bar{x}$ was obtained. The validity of such a procedure is believed to be reasonably good, since the specimens were all of uniform grain geometry.

References

[1] W. Rosenhain and J. Humphrey: *Proceedings* Royal Soc., London, 1909, vol. 83, p. 200.
[2] D. Hanson and M. A. Wheeler: *Journal* Institute of Metals, 1931, vol. 45, p. 229.
[3] G. R. Wilms and W. A. Wood: *Journal* Institute of Metals, 1949, vol. 75, p. 693.
[4] C. H. M. Jenkins and G. A. Mellor: *Journal* Iron and Steel Institute, 1935, vol. 132, p. 179.
[5] A. H. Cottrell and V. Aytekin: *Journal* Institute of Metals, 1950, vol. 77, p. 389.
[6] J. A. Ramsey: *Journal* Institute of Metals, 1951, vol. 80, p. 167.
[7] W. Betteridge and A. W. Franklin: *Journal* Institute of Metals, 1951, vol. 80, p. 147.
[8] R. C. Gifkins: *Nature*, 1952, vol. 169, p. 238.
[9] J. W. Suiter and W. A. Wood: *Journal* Institute of Metals, 1952, vol. 81, p. 181.
[10] I. S. Servi and N. J. Grant: *AIME Trans.*, 1951, vol. 191, p. 909; Journal of Metals, October 1951.
[11] I. S. Servi and N. J. Grant: *AIME Trans.*, 1951, vol. 191, p. 917; Journal of Metals, October 1951.
[12] C. S. Roberts: *AIME Trans.*, 1953, vol. 197, p. 732; Journal of Metals, May 1953.
[13] C. S. Roberts: *AIME Trans.*, 1953, vol. 197, p. 1121; Journal of Metals, September 1953.
[14] H. C. Chang and N. J. Grant: *AIME Trans.*, 1952, vol. 194, p. 619; Journal of Metals, June 1952.
[15] H. C. Chang and N. J. Grant: *AIME Trans.*, 1953, vol. 197, p. 305; Journal of Metals, February 1953.
[16] D. McLean: *Journal* Institute of Metals, 1951, vol. 80, p. 507.
[17] D. McLean: *Journal* Institute of Metals, 1952, vol. 81, p. 133.
[18] D. McLean: *Journal* Institute of Metals, 1952, vol. 81, p. 287.
[19] D. McLean: *Journal* Institute of Metals, 1952, vol. 81, p. 293.
[20] D. McLean: *Nature*, 1953, vol. 172, p. 300.
[21] D. McLean and M. H. Farmer: *Journal* Institute of Metals, 1954-1955, vol. 83, p. 1.
[22] B. Fazan, O. D. Sherby, and J. E. Dorn: *AIME Trans.*, 1954, vol. 200, p. 919; Journal of Metals, August 1954.
[23] F. N. Rhines, W. E. Bond, and M. A. Kissel: *ASM Trans.*, 1956, vol. 48, p. 919.
[24] F. Weinberg: *Acta Metallurgica*, 1954, vol. 2, p. 889.
[25] T. S. Ke: *Physical Review*, 1947, vol. 71, p. 533.
[26] T. S. Ke: *Physical Review*, 1947, vol. 72, p. 41.
[27] C. Zener: Elasticity and Anelasticity of Metals, pp. 147-159. University of Chicago, Chicago, 1948.
[28] C. Zener: *Physical Review*, 1941, vol. 60, p. 906.

Discussion of this paper sent (2 copies) to AIME by Dec. 1, 1957 will appear in AIME *Transactions* Vol. 212, 1958, and in Journal of Metals, April 1958.

Nature of the Ni-Cr System

It is shown that chromium-rich nickel alloys precipitate rapidly on cooling in more than one fashion. The solubility of nickel in chromium increases rapidly with temperature. No support was found for the recently proposed version of the Ni-Cr diagram.

by Robin O. Williams

AN investigation has been made of the Ni-Cr system for the purpose of elucidating certain points, namely the nature of aging in both terminal solid solutions and the nature of the phase diagram. Information pertaining to solubilities and precipitation has been obtained.

Experimentation

Five alloys, Table I, were arc melted in a cold copper crucible using electrolytic chromium and carbonyl nickel, both dry hydrogen treated. These 100 g buttons were homogenized 24 hr at 1300°C in dry hydrogen and air cooled. Powders were prepared by filing or pulverizing and subsequent heat treatment was done in vacuum or helium using titanium chips as a getter.

Powder of −80 mesh was filed from the 60 pct Ni alloy quenched from 1000°C and was sealed in silica under vacuum using a 250°C outgassing. After aging as indicated in Table II the lattice parameters were measured on the quenched samples using the standard $\cos^2\theta$ extrapolation. These parameters are considered accurate to roughly 0.0001A. In all cases chromium lines of 2.8812 ± 0.0005A at 30°C were found.

Drastic quenching from sufficiently high temperatures produced very sharp body-centered-cubic lines in the first four alloys without indications of transformations. Temperatures to 1250°C were used. Solid samples less than 1/16 in. thick were quenched in water without transformation and the powders could be adequately quenched in small helium filled thin wall silica tubing using a water quench.

For those powder samples which were quenched from the two phase field the relative intensity of the body-centered-cubic lines and the face-centered-cubic lines were estimated and extrapolated to give the indicated solubility data in Fig. 1. The data for the two higher alloys were somewhat limited, the plotted points being the lowest temperature where no nickel phase was found.

Neither filing, abrading, pulverizing, nor cooling to −190°C produced any new diffraction lines for solid samples quenched from the single phase region, nor did the character of the body-centered-cubic lines change. Single phase body-centered-cubic powders likewise did not change on cooling to −190°C. Also, samples which had some precipitation due to inadequate quenching showed no additional changes under these conditions.

R. O. WILLIAMS, Junior Member AIME, formerly with General Electric Research Laboratory, is now associated with Cincinnati Milling Machine Co., Cincinnati.

TP 4621E. Manuscript, June 25, 1956.

The first change apparent by X-ray diffraction form samples quenched almost fast enough to prevent precipitation was the diffuseness of the body-centered-cubic lines, particularly on the low angle side. For slower cooling rates the diffuse face-centered-cubic lines appeared. Work on the large grained castings showed profuse streaking through some of the Laue spots while oscillating patterns showed broad body-centered-cubic and face-centered-cubic lines as well as some new lines. For the 23.6 pct Ni alloy the new lines corresponded to 2.16, 1.96, and 1.86A and were more similar in character to the face-centered-cubic lines than the body-centered-cubic lines. Samples which were air cooled gave only face-centered-cubic and body-centered-cubic lines which were still broad. One pattern indicated that face-centered-cubic (111) plane was parallel to a body-centered-cubic (110) plane.

For those samples which were examined by light microscopy there were details which were not resolved. However, varied and beautiful structures were obtained. Fig. 2 is of an alloy quenched in a helium filled silica tube from the single phase region and shows particles associated apparently with dislocations which are arranged in low angle boundaries. Finer, general precipitation has also taken place within the grains. Figs. 3 to 5 show the variety of structures produced in these alloys on continuous cooling. It appears that there are four distinct modes of precipitation as evidenced by these figures. Annealing these structures at higher temperatures in the two phase field gives structures as shown in Fig. 6, which shows nickel plates in the chromium matrix which reprecipitated nickel on a much finer scale of the final quench. Lower annealing temperatures and shorter times naturally give finer plates of the nickel-rich phase.

Samples of the first four alloys were annealed for appreciable times between 900° and 1250°C and gave structures like Fig. 6. The relative amounts of the two phases were measured and extrapolated to give solubility data as indicated in Fig. 1. The point at 1250°C was deduced from data of Oxx.[1] These and most of the other samples were checked for ferromagnetism but none was apparent. In fact, it appeared that the magnetic susceptibilities were not more than three times that for paramagnetic chromium.

Discussion

In Fig. 1 it is seen that the solubility of nickel in chromium can be represented by a slightly curved line on the usual log X vs $1/T$ plot. These data are believed to be accurate to roughly 5 to 10°. There is only fair agreement with the data of Taylor and

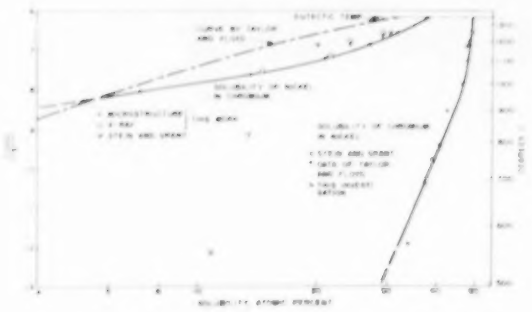

Fig. 1—Solubility of nickel in chromium and chromium in nickel.

Floyd,[3] but this is not surprising because of the relative insensitiveness of the lattice parameter to composition and the possibility of some precipitation effecting their results. There is fair agreement with the high temperature results of Stein and Grant,[2] but no agreement at all at low temperatures. Their highest point, which agrees so well, is considered by them to be the solubility of nickel in a new, high temperature phase.

The present data agree on the solubility of chromium very well with the earlier results[3] except for their point at 900°C which deviates from the line in Fig. 1 by an amount appreciably greater than their apparent experimental error. A possible reason for this is not known. In any case, the present representation is considered more likely to be correct than their curve having an inflexion point (log X vs $1/T$ plot), since the basis for an inflexion has not been established. The curve is drawn slightly under the point at 570°C, since 34 days at this temperature is relatively short. These results demonstrate that the aging in these alloys at about 500°C is not due to precipitation.

Because of the difference in crystal structures complete miscibility in this system is not possible and it is necessary for the log X vs $1/T$ curves to curve upward at high temperatures, as shown. However, the rapidly increasing solubility of nickel in chromium is not consistent with a *regular* system (Raoult's law) unless it is supposed that the free energy of body-centered nickel is decreasing rapidly with increasing temperatures. The straight line portions of these solubility curves correspond to 29,000 and 1,900 cal per mol for the chromium and the nickel phases, respectively. Fig. 7 shows the solubility curves replotted exactly on regular coordinates and demonstrates the significant point that solubilities which are concave upward are not abnormal but actually can represent the normal exponential type of solubility.

Table I. Alloys Investigated

	Alloy No.				
	1	2	3	4	5
Wt Pct Ni	16.0	23.6	26.4	31.9	60
Atomic Pct Ni	14.4	21.5	24.1	29.4	57

Table II. Solubility of Chromium in Nickel as Indicated by Lattice Parameters

Temperature, °C	Time, Days	Lattice Parameter, at 25°C, A	Composition Using Data of Taylor and Floyd[3]
700	17	3.5734	40.6 atomic pct
690	10	3.5693	37.2 (average)
	20	3.5691	
	34	3.5694	
565	34	3.5644	33.8

These experiments clearly demonstrated that the precipitation of nickel from supersaturated chromium takes place very rapidly and only small samples can be quenched fast enough to prevent this. This high rate is the result of at least three factors; 1) the rapidly decreasing solubility, 2) the possibility of good atomic matching between the two phases, and 3) the large amount of heat released. The fact that a transition structure can form may also be significant. The microstructures suggest that precipitation can occur in many fashions, including nucleation at dislocations and grain boundaries as well as homogeneously. This precipitation process must have complicated most or all the previous studies of chromium-rich nickel alloys.

X-ray diffraction and microstructure established that the relation between the matrix and precipitate was as follows: body-centered-cubic (110) (habit plane) || face-centered-cubic (111) and body-centered-cubic [111] || face-centered-cubic [110].

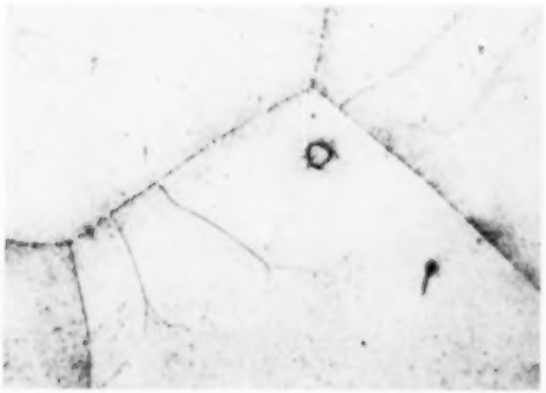

Fig. 2—Microstructure of a 23.6 pct Ni-Cr alloy quenched from 1250°C, showing precipitation along low angle boundaries. Electrolytic etch with 5 pct H_2SO_4. X500. Reduced approximately 15 pct for reproduction.

Fig. 3—Microstructure of a 23.6 pct Ni-Cr alloy as-cast, showing two modes of precipitation. Gelman's etch. X1000. Reduced approximately 15 pct for reproduction.

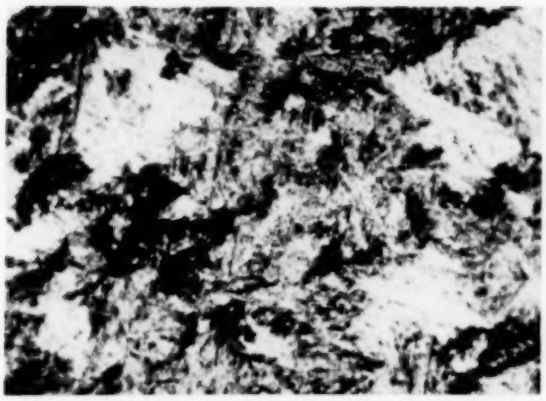

Fig. 4—Microstructure of a 23.6 pct Ni-Cr alloy air cooled from 1300°C, showing precipitation. Electrolytic etch in 5 pct H_2SO_4. X1500. Reduced approximately 15 pct for reproduction.

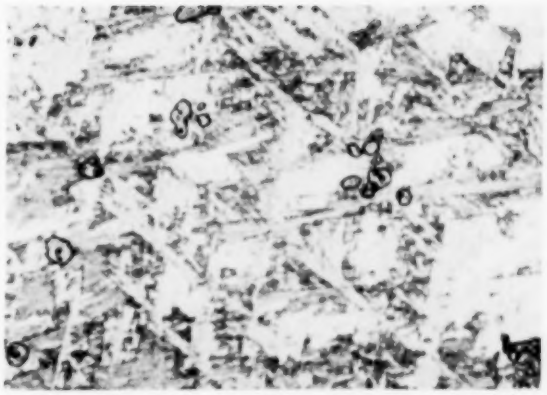

Fig. 5—Microstructure of a 26.4 pct Ni-Cr alloy air cooled from 1300°C. Electrolytic etch with acetic and nitric acids. X500. Reduced approximately 15 pct for reproduction.

Such a relationship is expected on the basis of reactions in other systems and it is found that fair atomic matching can exist on this plane. It is possible to account for the extra lines by means of a close-packed-hexagonal lattice with $a_0 = 2.50$ A and $c_0 = 3.92$ A, making the c/a ratio 4 pct under ideal. The three new lines index as (10.0), (00.2), and (10.1), respectively. The atomic arrangement and spacing of the basil plane are identical with the face-centered-cubic (111) plane. It may be that the lines from the body-centered-cubic, face-centered-cubic, and close-packed-hexagonal phases would explain the results of Blake and Lord,[4] but details of their work are lacking.

It is important to note that structures as in Fig. 6 result from growth during annealing of previously precipitated alloys and are not a primary result of transformation.

These results have failed to add substance to the recently proposed version of the Ni-Cr system.[2,5] If there is really a high temperature phase in chromium,[5,6] and there has been no positive evidence, then the eutectoid (or peritectic) reaction occurs above 1250°C. It is evident that most of the effects which have been attributed to this reaction are really the result of the precipitation observed here. Likewise, the anomolous thermal results reported by Jenkins et al.,[2] were caused by this precipitation, as were the reports of diffuse X-ray lines.[5,6]

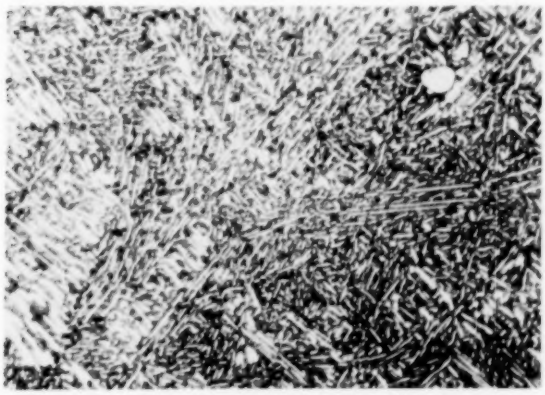

Fig. 6—Microstructure of a 26.4 pct Ni-Cr alloy air cooled from 1300°C and held 6 hr at 1100°C and quenched. White plates are the nickel phase. Electrolytic etch with 5 pct H_2SO_4. X500. Reduced approximately 15 pct for reproduction.

The qualitative observations on mechanical properties made during this study agree with earlier work.[1,2] Alloys 1, 2, and 3 were very hard and brittle in the as-cast or air cooled condition, whereas alloy 4 would not pulverize as air cooled, but could be filed. Alloys 1 and 2 could be filed when sufficiently well quenched.

Summary and Conclusions

1) New values have been reported for the terminal solid solubilities in the Ni-Cr system. The solubility

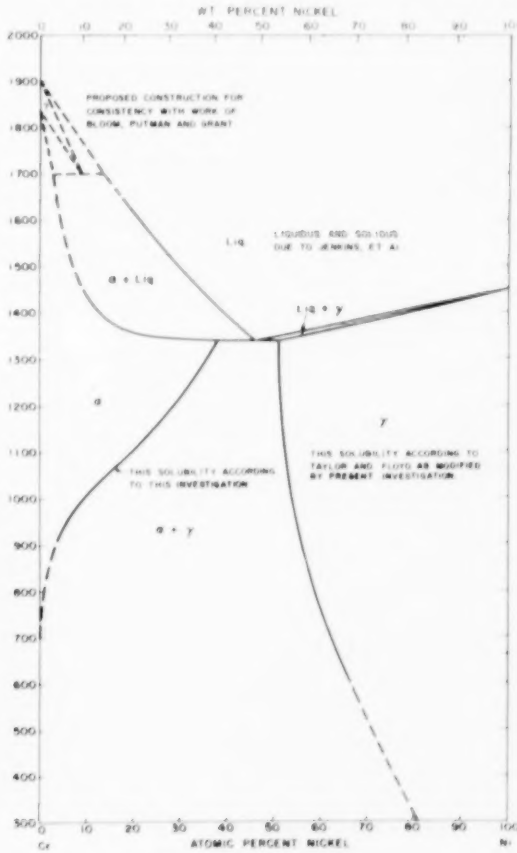

Fig. 7—Phase diagram of the Ni-Cr system.

of nickel in chromium decreases very rapidly with decreasing temperatures. The solubility of chromium in nickel is in fair agreement with Taylor and Floyd's results.[2] The aging in nickel-rich alloys at about 500°C is not attributable to precipitation of chromium.

2) The chromium-rich alloys are characterized by very rapid precipitation during cooling which can be prevented only by very effective quenching. This rapid precipitation results from the rapidly decreasing solubility, the large heat release, and good atomic matching between phases.

3) X-rays and microstructures show that there are several modes (perhaps four) of precipitation. The (110) is the habit plane in the matrix and is parallel to the (111) of the precipitate. Diffuseness of X-ray lines indicate coherency and/or large strains in most cases. In some cases, close-packed-hexagonal lines have been found where the basil plane is identical with the (111) of the face-centered-cubic precipitate.

4) The evidence showed that neither mechanical stress, low temperatures, nor both could produce transformations in these supersaturated chromium alloys. The very high hardness and brittleness found in these alloys are the result of precipitation. No magnetic structures were found.

5) No evidence has been found to support a recently proposed version of the Ni-Cr diagram.[5,6] If a eutectoid reaction (or peritectoid) reaction exists its temperature is above 1250°C.

6) The present knowledge of the Ni-Cr system is very incomplete.

Acknowledgments

The author wishes to acknowledge the assistance by R. E. Lewinski in doing the X-ray diffraction, and by D. Kontoleon, W. Roman, and D. Broecker, who did the metallography. He also has had several discussions with Gordon Oxx concerning this system.

References

[1] G. Oxx: Personal communique.
[2] A. Taylor and R. W. Floyd: *Journal* Institute of Metals, 1951-1952, vol. 80, p. 577.
[3] C. Stein and N. J. Grant: *AIME Trans.*, 1955, vol. 203, p. 127; JOURNAL OF METALS, January 1955.
[4] F. C. Blake and J. O. Lord: *Physical Review*, 1930, vol. 35, p. 660.
[5] D. Bloom and N. J. Grant: *AIME Trans.*, 1951, vol. 191, p. 1009; JOURNAL OF METALS, November 1951.
[6] D. S. Bloom, J. W. Putman, and N. J. Grant: *AIME Trans.*, 1952, vol. 194, p. 626; JOURNAL OF METALS, June 1952.
[7] C. H. M. Jenkins, E. H. Bucknall, C. R. Austin, and G. A. Mellor: *Journal* Iron and Steel Institute, 1937, vol. 136, p. 187.
[8] E. R. Jette, V. H. Nordstrom, B. Queneau, and F. Foote: *AIME Trans.*, 1934, vol. 111, p. 361.

Discussion of this paper sent (2 copies) to AIME by Dec. 1, 1957 will appear in AIME *Transactions* Vol. 212, 1958, and in JOURNAL OF METALS, April 1958.

Effect of Heat Treatment on the Hardness and Microstructure of U-Ti Alloys

The hardness and microstructure of U-Ti alloys may be varied over wide ranges by suitable heat treatment. Quench-temper or isothermal treatments were particularly effective. The overall response to heat treatment was dependent upon the phases present during solution treatment. Results are interpreted in terms of the phase diagram.

by David L. Douglass and Lyle L. Marsh, Jr.

CORRELATION was made between the heat treatment and hardness of three U-Ti alloys ranging in composition from 8.5 to 50 atomic pct Ti. The following important observations were made:

1) A direct quench of γ U-Ti solid solution resulted in the formation of a hard martensitic phase in low-titanium alloys.

2) Subsequent tempering initially increased the hardness by the precipitation of a fine dispersion of U_2Ti; further precipitation of U_2Ti with tempering time eventually resulted in softening.

3) High-hardness levels were obtained also by isothermal transformation of an 8.5 atomic pct Ti alloy at 400° and 500°C.

4) The crystal structure of the phases present at the solution-treating temperature (one region in the phase diagram excepted) and the temperature within a given phase region affected the hardness of both quenched and isothermally transformed alloys.

D. L. DOUGLASS and L. L. MARSH, JR., Junior Members AIME, are Principal Metallurgist and Assistant Division Chief, respectively, Metallurgical Engineering Div., Battelle Memorial Institute, Columbus, Ohio.

TP 4602E. Manuscript, Oct. 10, 1956.

Introduction

It has been known since 1887 that the mechanical properties of metals were dependent upon their microstructure. Sorby pointed out in that year that annealed gray iron castings were softer than chilled iron castings by virtue of the graphite which had replaced hard cementite in the microstructure. Over the years, interest has increased in the effect of microstructure on the mechanical properties of metals, and now high-strength levels may be achieved by bringing about the dispersion of a second phase or by other microstructural adjustments. The nature of a second phase in an alloy strongly influences the properties. For example, the size, shape, amount, and distribution of a second phase plays a very important role in the ultimate properties of an alloy. Microstructural control is achieved by heat treatments. Hence, any alloy system of potential use should be understood in terms of its response to heat treatment and the resultant effects upon the properties.

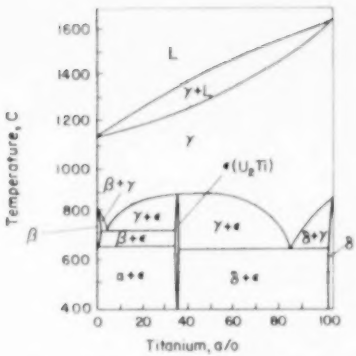

Fig. 1—U-Ti phase diagram.

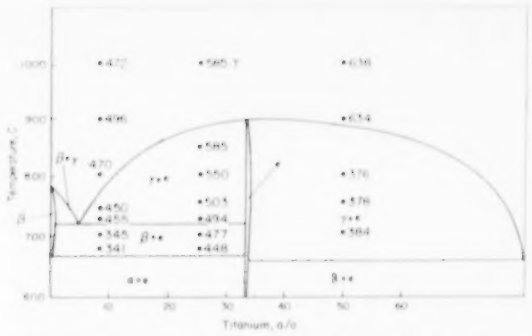

Fig. 2—Effect of quenching from various equilibrium phase fields on hardness of U-Ti alloys. Hardness values are shown at the location of the solution treatment.

U-Ti alloys are heat treatable and have been examined for their response to the three basic types of heat treatments, i. e., varied cooling rates through a phase change, interrupted quench (isothermal transformation through a phase change), and tempering (decomposition of a metastable structure). The results of this study have given an insight into the behavior of the system and have shown that a wide variety of structures and properties may be achieved by heat treatment.

Constitution of U-Ti Alloys

The high-temperature phases of uranium and titanium form a continuous series of body-centered-cubic solid solutions. A eutectoid exists between γ uranium and the compound U_2Ti at 723°C and 4 atomic pct Ti. The solubility of titanium in β uranium is about 1½ atomic pct at the eutectoid temperature. The compound exists over a narrow composition range and forms by the decomposition of γ-solid solution. The solubility of titanium in α uranium is very small. No reliable values have been reported. The phase diagram as proposed by A. G. Knapton[1] is shown in Fig. 1.

Experimental Procedures

Preparation of Alloys—Fifty-lb ingots of alloys containing 8.5, 25.5, and 50 atomic pct Ti were double arc-melted in water-cooled copper crucibles. Derby uranium and iodide titanium were used as charge materials. The ingots were forged at 1000° and rolled at 600°C to strips 4 in. wide and 0.150 in. thick.

Heat Treatments—Slow-cooled alloys were obtained by the following procedure. Specimens were sealed in Vycor tubes under an argon atmosphere, solution-treated 5 hr at 1000°C, and furnace-cooled at 5°C per hr.

Samples were air-cooled in Vycor tubes after solution treatment at 1000°C for 5 hr.

Quenched samples were obtained by plunging the alloys (in Vycor tubes) into water after solution treatment at 1000°C for 5 hr, and immediately smashing the tubes. Two other series of samples were quenched from 750° to 850°C. Small specimens were transformed isothermally by suspending them on Nichrome wire in a lead bath at the solution-treating temperature for 1 hr. Then they were removed and immersed in a second lead bath at the desired isothermal treatment temperature. After the desired time had elapsed, the specimens were quenched in water at room temperature. Both baths were covered by powdered charcoal. No visible attack by the lead baths was apparent.

Metallography—Specimens were mounted cold in Epon resin in order to prevent any further phase changes or tempering due to warm mounting in Bakelite. After the specimens had been ground and polished, they were etched either electrolytically with a 1:8 mixture of CrO_3: acetic acid or chemically with an etchant consisting of 196 g oxalic acid, 3 g $Fe(NO_3)_3$, and 4 cu cm HF per liter of water.

Hot-Hardness Tests—Hot-hardness was measured by means of a vacuum hot-hardness machine.[2] The machine consists essentially of a dead-weight mechanism with a sapphire-tipped indenter (136° pyramid tip) surrounded by a furnace in a vacuum

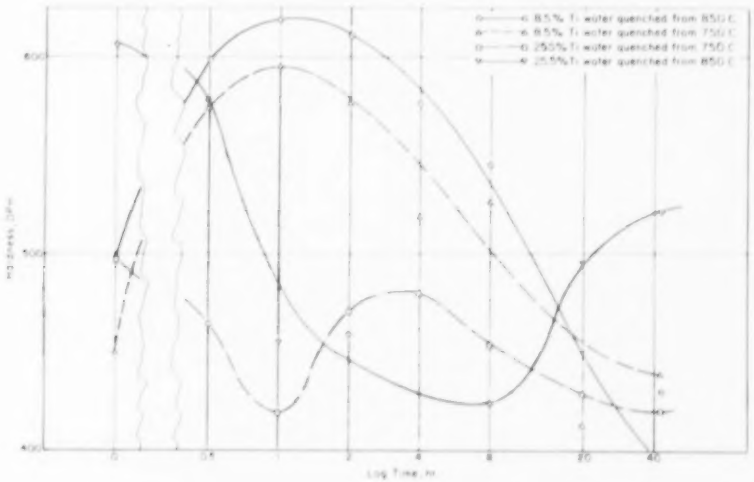

Fig. 3—The hardness of quenched and tempered U-Ti alloys as a function of time at a tempering temperature of 500°C.

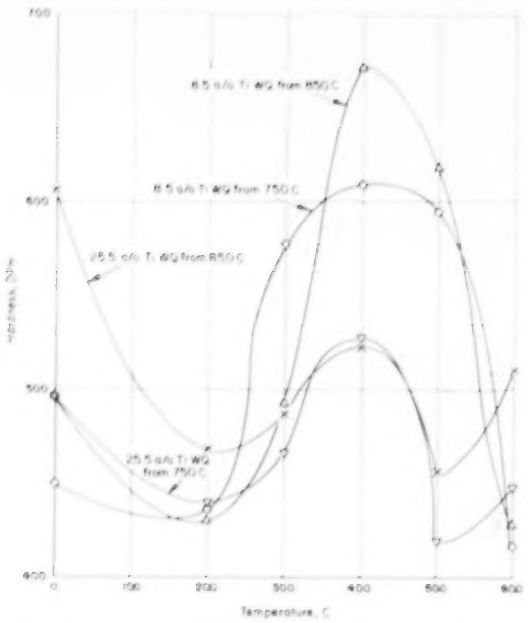

Fig. 4—The hardness of quenched and tempered U-Ti alloys as a function of tempering temperature for 1 hr.

chamber. The specimen and indenter were heated to the desired temperature, whereupon the load was applied for 15 sec. Three or four readings were taken at each temperature.

Experimental Results

Effect of Cooling Rate on Hardness—Slow-cooled specimens were considerably softer than were either quenched or air-cooled specimens. However, among the slow-cooled specimens, there were no marked changes in hardness as a result of adding titanium. It may be possible that any differences might have been masked by oxygen contamination during heat treating. An increase in cooling rate obtained by air cooling resulted in an increased hardness for all three alloys. The U-50 atomic pct Ti alloy increased in hardness from 341 Vhn to 575. The most drastic cooling rate, obtained by a direct water quench, increased the hardness of the 50 atomic pct alloy to 638 Vhn. The 8.5 atomic pct alloy increased in hardness from the value obtained by air cooling. The 25.5 atomic pct alloy showed a marked increase in hardness in the quenched condition compared with the air-cooled condition. Data for hardnesses as affected by cooling rate are listed in Table I. All alloys except the U-8.5 atomic pct Ti shattered upon quenching from 1000°C. However, it was still possible to obtain hardness readings on the larger pieces. The fracturing was caused by the large volume change associated with the formation of U_2Ti. This phenomenon will be covered subsequently in greater detail.

Table I. Hardness of U-Ti Alloys as Affected by Cooling Rates from 1000°C

Titanium Content (Balance Uranium), Atomic Pct	Hardness, Dph			
	As Rolled	Slow Cooled	Air Cooled	Quenched
8.5	395	345	401	472
25.5	470	304	449	585
50.0	535	341	575	638

Table II. As-Quenched Hardness Data for Material Used in Tempering Studies

Titanium Content, Atomic Pct	Solution Treating Temperature, °C			
	750°		850°	
	Phases	Hardness, Dph	Phases	Hardness, Dph
0	β	225	γ	258
8.5	$\gamma + \beta$	450	γ	496
25.5	$\gamma + \beta$	496	$\gamma + \beta$	585

Effect of Quenching from Various Equilibrium Phase Fields on Hardness—The hardnesses of quenched alloys solution treated in various regions

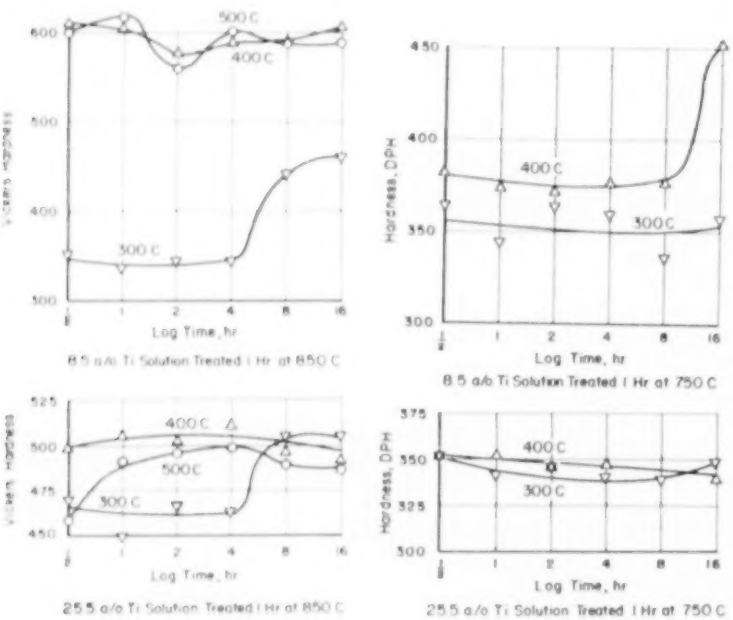
500 C
400 C
300 C
Log Time, hr
8.5 a/o Ti Solution Treated 1 Hr at 850 C
8.5 a/o Ti Solution Treated 1 Hr at 750 C
25.5 a/o Ti Solution Treated 1 Hr at 850 C
25.5 a/o Ti Solution Treated 1 Hr at 750 C

Fig. 5—Effect of isothermal transformation on hardness of U-Ti alloys. Hardness readings were taken on samples quenched to room temperature after isothermal transformation.

of the phase diagram are shown in Fig. 2. The room-temperature hardnesses are shown for each composition at the temperature of solution treating. The following observations were made.

8.5 Atomic Pct Ti Alloy:

1) Quenching from the $\gamma + \epsilon$ field produced a harder structure than quenching from the $\beta + \epsilon$ region.

2) There was little difference in hardness between alloys quenched from the γ region and those quenched from the $\gamma + \epsilon$ region.

25.5 Atomic Pct Ti Alloy:

1) As the quenching temperature was increased in the $\gamma + \epsilon$ field, the hardness increased. The same effect was observed on quenching from the $\beta + \epsilon$ field.

2) Quenching from above the $\gamma + \epsilon/\beta + \epsilon$ transus resulted in greater hardness than was obtained by quenching from below the transus. A similar result was also observed in the 8.5 atomic pct alloy.

50 Atomic Pct Ti Alloy:

1) Quenching from the γ region produced a very hard structure, but all samples shattered upon quenching.

2) The hardness of samples quenched from the $\gamma + \epsilon$ region appeared to be independent of quenching temperature and compared in hardness with the slow-cooled alloys. This region was the only one investigated in which temperature had no effect on the as-quenched hardness.

Effect of Quench and Temper Treatments on Hardness—Samples of biscuit uranium, U-8.5 atomic pct Ti, and U-25.5 atomic pct Ti were solution treated 1 hr at 750° and 850°C, and water quenched. Tempering treatments were then performed at 200°, 300°, 400°, 500°, and 600°C for times ranging from ½ to 40 hr. The hardness is shown as a function of tempering time at 500°C in Fig. 3. The effect of tempering temperature on the hardness is shown in Fig. 4 for times of 1 hr.

The hardness of an 8.5 atomic pct alloy tempered at 500°C increased to a maximum after 1 hr of tempering and then decreased rapidly. This was true for samples quenched from either 750° or from 850°C. The 25.5 atomic pct alloy quenched from 750°C started to soften immediately, reached a minimum hardness at 1 hr, and then hardened to a maximum at 4 hr, followed by further softening. The 25.5 atomic pct alloy quenched from 850°C followed the same pattern as the sample quenched from 750°C, except that the minimum hardness occurred at 8 hr, and the maximum value had not been reached after 40 hr.

The tempering temperature had a pronounced effect which was essentially the same for both alloys. A minimum hardness occurred at 200° for all cases, after which a maximum occurred at 400°C for all the samples. Both 25.5 atomic pct samples (quenched from 750° and 850°C) exhibited a secondary minimum at 500°C.

Hardness data for as-quenched samples are shown in Table II. It may be seen that hardness of the quenched structures increased with alloy content.

Effect of Isothermal Transformation on Hardness—Alloys containing 8.5 and 25.5 atomic pct Ti were solution treated for 1 hr at 750° and 850°C, and isothermally transformed at 300°, 400°, and 500°C for times ranging from ½ to 18 hr. All data are shown in Fig. 5.

Elevated-Temperature Hardness—Hot-hardness tests showed a decrease in hardness with increasing temperature for all alloys. The softening rate, expressed as log hardness/°C, and the ultimate hardness for the 25.5 atomic pct Ti alloy were less and greater, respectively, than for the 8.5 atomic pct alloy. Under a given set of test conditions, the quenched 8.5 atomic pct Ti alloy had a lower softening rate than for any other heat treatment investigated. Quenching of the 25.5 atomic pct alloy had little effect upon changes in hot hardness for the test conditions employed. Hot-hardness data are shown in Fig. 6.

Mechanical Properties—Tensile data were obtained for the U-8.5 atomic pct and 25.5 atomic pct alloys in the vacuum-annealed condition (10 hr at 800°C in vacuum and furnace-cooled), and for the 50 atomic pct alloy in the as-rolled condition. Heat treatments of machined tensile bars resulted in

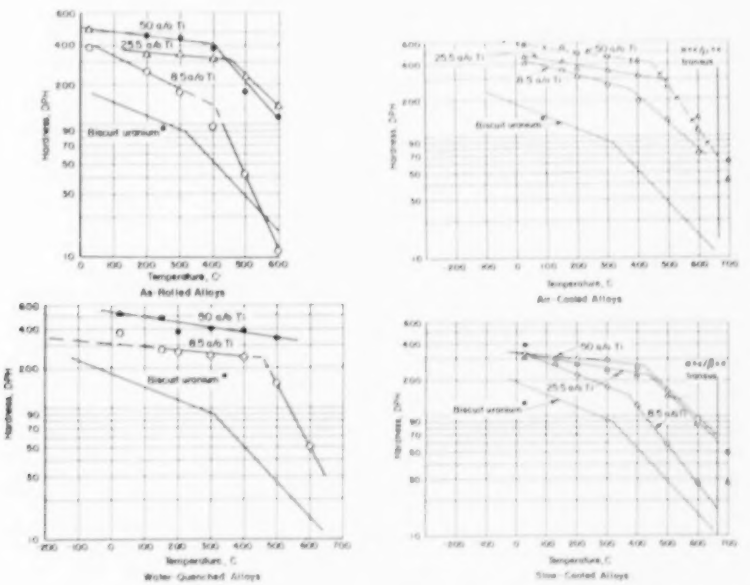

Fig. 6—Log hardness vs temperature plots of hot-hardness data for U-Ti alloys. Asterisked biscuit uranium is induction melted and hot-rolled.

Fig. 7—Microstructure of slow-cooled U-Ti alloys. a) U-8.5 atomic pct Ti slow cooled 1000°C at 5°C per hr. White needles: α uranium. Fine dispersion: U_2Ti. b) U-25.5 atomic pct Ti slow cooled from 1000°C at 5°C per hr. White equiaxed phase: U_2Ti. Matrix: α uranium. c) U-50 atomic pct Ti slow cooled from 1000°C at 5°C per hr. White particles: U_2Ti. Matrix: α titanium. X500. Reduced approximately 30 pct for reproduction.

Fig. 8—Microstructures of quenched U-Ti alloys. a) U-8.5 atomic pct Ti water quenched from 1000°C. Martensitic α uranium. X500. b) U-25.5 atomic pct Ti water quenched from 1000°C. Undissolved U_2Ti particles. U_2Ti precipitate at grain boundaries in retained γ matrix. X500. c) U-50 atomic pct Ti water quenched from 1000°C. U_2Ti network at grain boundaries and fine compound precipitate in grains. X100. Reduced approximately 25 pct for reproduction.

severe growth and warping for all alloys. The 25.5 atomic pct alloy was too brittle to be machined in the as-rolled condition, but was readily machined after vacuum annealing. The 50 atomic pct alloy failed in the grips with a brittle fracture on each of two samples tested. No yield strength or ultimate strength values were obtained. However, reliable values of the modulus of elasticity were obtained. The tensile data and room-temperature hardnesses of the tensile bars are listed in Table III.

Discussion

The hardness changes incurred by varied cooling rates from the γ region can be rationalized in terms of microstructures. Fully annealed uranium generally has a hardness of less than 200 Vhn. The solubility of titanium in α uranium is essentially 0; therefore, the hardness of annealed Derby uranium may be taken as the hardness of the α phase as a first approximation in the U-Ti alloy system. Microhardness measurements of the compound, U_2Ti, showed a Knoop hardness of about 800. The U-8.5 atomic pct Ti alloy showed a very fine precipitate in the slow-cooled condition, whereas the 25.5 atomic pct alloy consisted of large equiaxed particles of compound in an α matrix as shown in Fig. 7. The 50 atomic pct alloy had a dispersed compound phase intermediate in size to the other alloys. However, the amount of compound appears to be much greater than in either the 8.5 or 25.5 atomic pct Ti alloys. The hardness results are anomalous, inasmuch as the hardness should be a function of the amount of second phase if the shape and size are held constant. Microhardness measurements of the α phase were made with difficulty. The distance between the U_2Ti particles was too small to permit the entire indentation of the Knoop indenter to fall within the α phase alone, even with the lightest available load. Values ranged from 398 to 642 Knoop. Although the values are unreliable, it is believed that some of the α-phase hardness may be attributed to oxygen contamination.

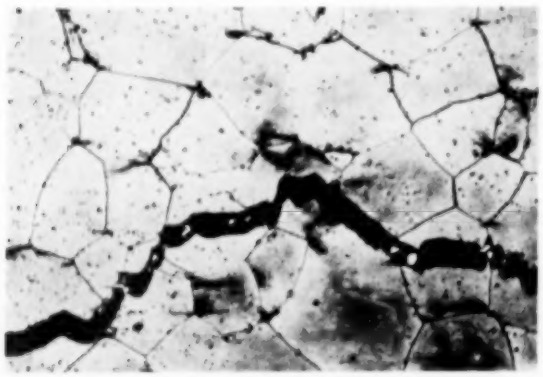

Fig. 9—Strain markings at grain junctions in vicinity of crack in a quenched U-25.5 atomic pct Ti alloy. X100. Reduced approximately 30 pct for reproduction.

Rapid cooling of the 8.5 atomic pct alloy resulted in a martensitic α uranium, having the titanium content of the parent γ phase. In the 25.5 and 50 atomic pct alloys rapid cooling retarded the decomposition of γ to equilibrium α and compound. Microstructures of quenched alloys are shown in Fig. 8. The martensitic structure obtained in the 8.5 atomic pct sample appeared to be similar to martensites observed in steels. The 25.5 atomic pct alloy contained some undissolved compound. A fine precipitate formed at some of the prior γ grain boundaries in the quenched structure. No precipitate was visible within the grains at X500. The 50 atomic pct alloy was the hardest of the quenched samples. A

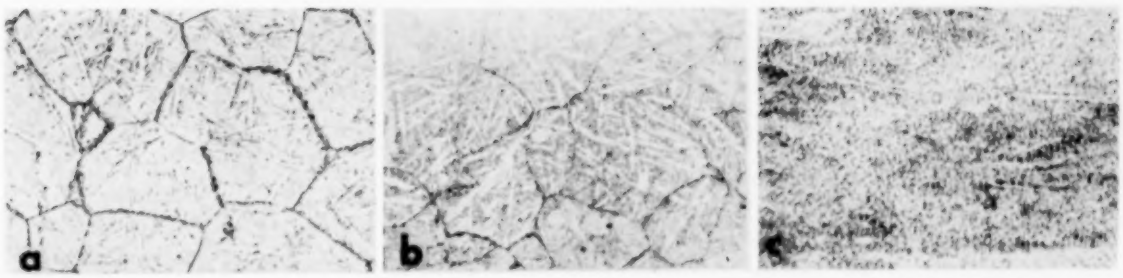

Fig 10—Microstructures of a U-8.5 atomic pct Ti alloy quenched from various equilibrium regions of the phase diagram. a) Water quenched from 900°C (γ region). b) Water quenched from 750°C (γ and ϵ region). c) Water quenched from 700°C (β and ϵ region). X100. Enlarged approximately 5 pct for reproduction.

nearly continuous grain-boundary network of compound was present, and a fine precipitate of compound was also distributed throughout the grains.

Precipitation of the compound caused severe lattice strains in both the 25.5 and 50 atomic pct alloys. It is thought that the 25.5 atomic pct sample had a submicroscopic precipitate and was comparable to an age-hardenable alloy at some intermediate stage of aging. The volume change associated with the decomposition of γ into the stochiometric composition of U_2Ti (33 atomic pct Ti) was calculated to be 15.8 pct expansion. This large volume change, coupled with the dissimilarity in crystal structures, was sufficient to cause severe lattice strains during quenching. The stresses associated with the volume change were sufficient to raise the yield stress to some value approaching or equal to the fracture stress. Stress relief can occur if relaxation takes place in the grain or at the grain boundary. When relaxation cannot occur, for example, at the junction of three grains, a crack will form and failure takes place. An example of this can be seen in Fig. 9, where quenching of the U-25.5 atomic pct Ti alloy from 900°C caused failure. Strain markings can be seen at the junctions of grains adjacent to the crack.

The effect of crystal structure of the alloy at the solution-treating temperature (one region of the phase diagram excepted) strongly influenced the hardness of the quenched alloys. Alloys containing 8.5 atomic pct Ti transform martensitically when quenched from temperatures above 723°C, the eutectoid temperature. The equilibrium phases above 723°C are either γ or $\gamma + \epsilon$. The high-titanium content of the γ phase (8.5 atomic pct) causes a distortion of the normally titanium-free α lattice as the martensite forms. The titanium atoms have insufficient time to diffuse out of the shearing planes and are entrapped in the α lattice. If solution treatment is performed in the $\gamma + \epsilon$ region instead of in the γ region, the γ composition will be less than 8.5 atomic pct Ti, and the α formed by quenching will have a correspondingly lower titanium content. Hence, the degree of supersaturation is lower, and the hardness is lower. Some ϵ will be present during solution treatment in the two-phase field and will be observed in the quenched alloy. The compound exists either as a precipitate or as a grain-boundary network and results in an overall hardness equal to or greater than the structure consisting of 100 pct 8.5 atomic pct Ti martensite.

Quenching the 8.5 atomic pct alloy from the $\beta + \epsilon$ region caused a softer final structure than obtained by quenching from other regions. The structure consisted of finely dispersed U_2Ti in a matrix of equilibrium α. The α in this structure was undistorted, as evidenced by the sharp lines on the X-ray diffraction pattern. The sharpness was attributed to the low titanium content of the β phase from which the α formed. Microstructures of alloys containing 8.5 atomic pct Ti quenched from the three regions are shown in Fig. 10.

Quenching of the U-25.5 atomic pct Ti alloy from various temperatures within the $\gamma + \epsilon$ field resulted in higher hardness as the quenching temperature was increased. The titanium content of the γ phase in the $\gamma + \epsilon$ field increases with increasing temperature. As the titanium content increased, the γ formed a distorted, supersaturated α upon quenching. As the temperature increased, more and more titanium was retained in the α formed during the quench, and the distortion due to a higher degree of supersaturation increased. Thus, the increase in hardness is explained. Alloys quenched from the $\beta + \epsilon$ field contained about 70 pct by volume of the hard U_2Ti phase, which accounted for the high hardness. Microstructures of this alloy quenched from the two regions are shown in Fig. 11.

The only region in the phase diagram from which quenching produced little change in hardness with respect to the solution-treating temperature was the $\gamma + \epsilon$ region on the titanium side of the compound. This behavior is to be expected in view of the small differences in the amount of U_2Ti present at the solution-treating temperatures and of the small variation in titanium content of the γ phase. A representative microstructure may be seen in Fig. 12.

Time of tempering had two effects on the U-8.5 atomic pct Ti alloy. Martensitic α initially rejected a fine dispersion of U_2Ti which caused considerable hardening up to times of 1 hr. Additional time at temperature softened the alloys by virtue of increased precipitation of compound and a corresponding decrease in the supersaturation of α martensite. This behavior is analogous to *aging* and

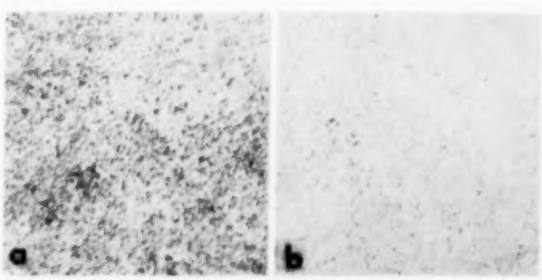

Fig. 11—Microstructures of a U-25.5 atomic pct Ti alloy quenched from various equilibrium regions of the phase diagram. a) Water quenched from 850°C (γ and ϵ region). b) Water quenched from 700°C (β and ϵ region). X100. Reduced approximately 20 pct for reproduction.

Table III. Mechanical Properties of U-Ti Alloys at Room Temperature

Titanium Content, Atomic Pct	Alloy Condition	Modulus of Elasticity, 10^6 Psi	Yield Strength, Psi	Ultimate Strength, Psi	Elongation, Pct	Reduction of Area, Pct	Hardness, Dph
8.5	Vacuum annealed	28.2	84,100	153,000	3.9	4.5	393
25.5	Vacuum annealed	29.4	73,900	97,900	0.5	0.26	376
25.5	Vacuum annealed	28.7	76,900	99,500	—	0.11	376
50.0	As-rolled	26.4	—	*	—	—	535
50.0	As-rolled	24.7	—	*	—	—	535

* Failed by brittle fracture in grip

overaging with respect to hardness changes. Fig. 13 shows small compound particles in a martensitic α matrix for an 8.5 atomic pct Ti alloy solution treated for 1 hr at 850°, water quenched, and tempered 1 hr at 300°C. Increased tempering temperature increased the amount of precipitation for a given time at temperature, Fig. 13b. Additional time at temperature, 500°C, shown in Fig. 13d, increased the thickness of the grain-boundary precipitate. Finally, at 600°C, the compound rejection and breakdown of the martensitic α was essentially completed within 1 hr.

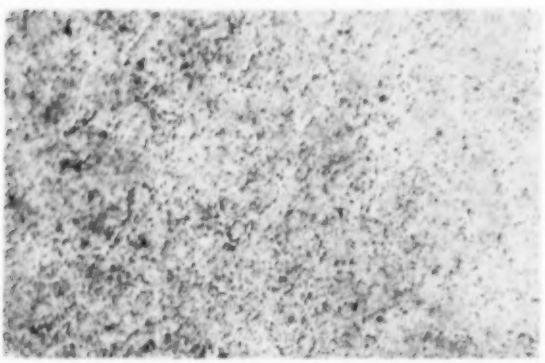

Fig. 12—Microstructure of a U-50 atomic pct Ti alloy water quenched from 700°C. X500. Reduced approximately 20 pct for reproduction.

The 25.5 atomic pct Ti alloy showed a minimum hardness followed by an increase for samples quenched from both 750° and 850°C and tempered at 500°C as a function of time. The minimum in the hardness-time curve appeared to be due to stress relief. No apparent microstructural change was observed in this alloy for treatments ranging from ½ to 8 hr at 500°C. A 20-hr tempering treatment changed the microstructure which is shown in Fig. 14. The longer treatment caused coalescence of the dispersed phase and, possibly, the transformation of a small amount of retained γ which was undetected by X-ray diffraction.

No analysis was attempted on the isothermal transformation hardness data. In order to account for the observations accurately, additional data, such as M_s temperatures and X-ray lattice constant determinations, would be required. It is apparent, however, that a wide variety of hardness levels may be obtained by suitable heat treatment of a given alloy.

Hot-hardness data are plotted as log hardness vs temperature. The semilog scale method of plotting was suggested by Westbrook.[3] This plot enables the determination of certain constants for a functional hardness-temperature relation proposed by Shishokin.[4] Unfortunately, these data are not susceptible to an analysis as proposed by Westbrook. In all but the slow-cooled alloys, the material is in a

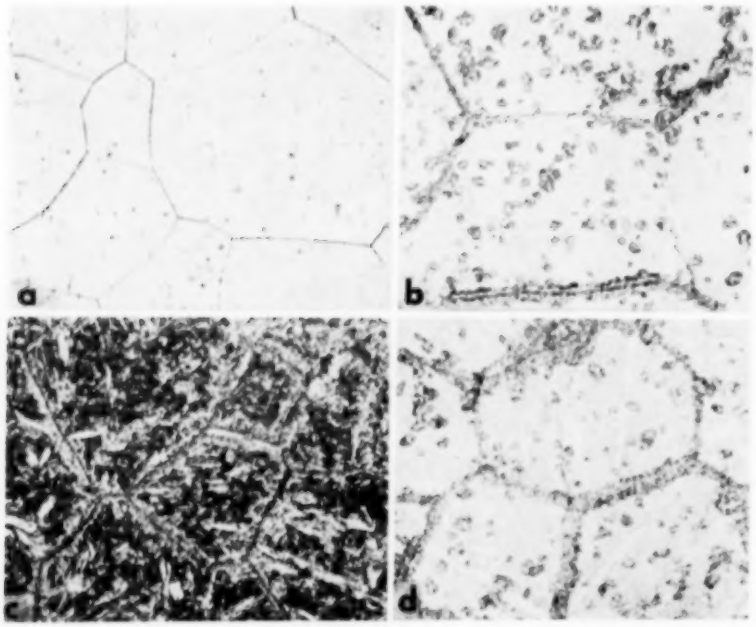

Fig. 13—Effect of temperature and time of tempering on the microstructure of a U-8.5 atomic pct Ti alloy. Solution treated 1 hr at 850°C, quenched and tempered as indicated. a) 1 hr at 300°C, b) 1 hr at 500°C, c) 1 hr at 600°C, and d) 4 hr at 500°C. X250. Reduced approximately 10 pct for reproduction.

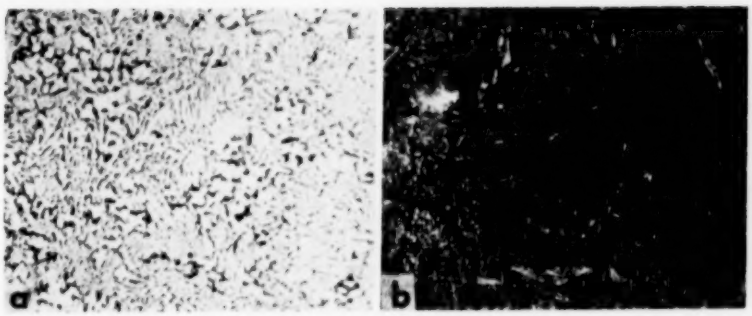

Fig. 14—Effect of tempering time on the microstructure of a U-25.5 atomic pct Ti alloy. Samples solution treated 1 hr at 850°C, quenched and tempered at 500°C for the indicated time. a) 2 hr at 500°C. X1000. b) 20 hr at 500°C. X250. Reduced approximately 10 pct for reproduction.

metastable condition and will undergo radical changes with time and temperature. Any variations in the time-temperature cycle of the test would have resulted in other values. The data are included so that a short-time comparison may be made between the heat-treated alloys and pure uranium. A more complete analysis would require the effect of time necessary to heat to temperature, and a time study of hardness at temperature. It may be concluded that the alloys and heat treatments produced more superior elevated-temperature strength and hardness characteristics than the pure uranium and equilibrium alloy structures.

The mechanical properties of the U-8.5 atomic pct Ti alloy in the vacuum-annealed condition are superior in every respect to those of the 25.5 atomic pct Ti alloy in the same condition. It is very likely that uranium alloys containing small amounts of titanium may be heat treated to high strengths and moderate values of ductility. The 50 atomic pct alloy appeared very sensitive to scratches or local stress raisers. The lower modulus values for this alloy may be attributed to the titanium-rich matrix instead of the uranium-rich matrix.

Conclusions

The hardness of U-Ti alloys is very sensitive to heat treatment. High hardnesses may be obtained by either isothermal transformation or by quenching and tempering.

Low-titanium alloys transformed martensitically upon quenching and exhibited high hardness. Quenching of the 25.5 and 50 atomic pct alloys from the γ region resulted in shattering due to the large volume change associated with the formation of U_2Ti. Quenching of these alloys from regions where U_2Ti was a stable phase produced a high hardness for the 25.5 atomic pct alloy, but eliminated shattering and produced softer structures for the 50 atomic pct alloy.

Tempering of an 8.5 atomic pct alloy as a function of time initially produced hardening due to a fine dispersion of compound, followed by *overaging* and softening. A maximum hardness as a function of temperature was achieved at 400°C (1 hr treatments).

Acknowledgment

This work was performed under AEC Contract No. W-7405-eng-92.

References

[1] A. G. Knapton: The System Uranium-Titanium. *Journal* Institute of Metals, 1954, vol. 83, p. 497.

[2] W. Chubb: Contribution of Crystal Structure to the Hardness of Metals. *AIME Trans.*, 1955, vol. 203, pp. 189-192; JOURNAL OF METALS, January 1955.

[3] J. H. Westbrook: Temperature Dependence of the Hardness of Pure Metals. *ASM Trans.*, 1953, vol. 45, p. 221.

[4] V. P. Shishokin: The Hardness and Fluidity of Metals at Different Temperatures. *Ztsch. fur anoganische Chemie*, 1930, vol. 189, p. 263.

Discussion of this paper sent (2 copies) to AIME by Dec. 1, 1957 will appear in AIME *Transactions* Vol. 212, 1958, and in JOURNAL OF METALS, April 1958.

Technical Note

Growth of Iron Alloy Single Crystals from the Melt

by R. C. Hall

DEVELOPED to grow single crystals of alloys of high hardness and high melting points is a simple but effective apparatus described in this note. Growth from the melt, that is, by the Bridgman technique,[1-3] may be applied to metals or alloys which are physically hard as long as no phase transformation occurs on cooling to room temperature. The present apparatus was employed to grow single crystals of the ferromagnetic Al-Fe alloys above 1 wt pct Al and the Si-Fe alloys above 3 wt pct Si.

R. C. HALL, Junior Member AIME, is associated with Magnetic Materials Development Section, Westinghouse Electric Corp., East Pittsburgh, Pa.

TN 413E. Manuscript, Jan. 16, 1957.

Single Crystal Growth

In a simple form, the method for growth of single crystals from the melt requires a molten metal charge in a pointed crucible which is slowly lowered through a heated zone into a colder zone. Solidification starts at the bottom point and continues up the charge as the crucible is lowered through the heated zone. If a single crystal nucleates at the bottom, one crystal may grow throughout the charge under ideal conditions of slow growth.[4,5] The presently developed method of growth was designed so that the chances that more than one crystal would grow were small.

The single crystals were grown by the apparatus illustrated in Fig. 1. The charge was in the form

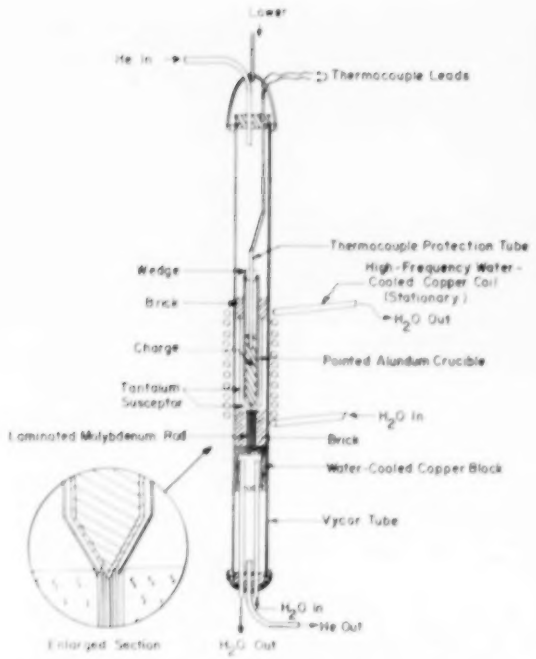

Fig. 1—Sketch of the furnace for growth of single crystals from the melt.

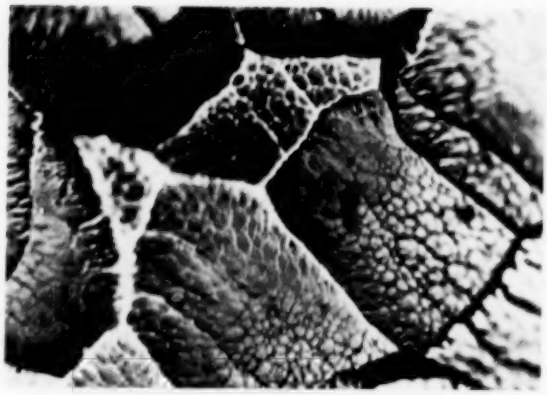

Fig. 2—Micrograph of a heavily etched surface of a single crystal of 3 pct Al-Fe. X1450. Reduced approximately 30 pct for reproduction.

of a round bar with one end pointed and the other end square. The pointed end was machined to fit the contour of the pointed-bottom Alundum crucible. The square end of the charge had a hole drilled in it to receive, from the top of the crucible, a Pt—Pt-10 pct Rh thermocouple and thermocouple protection tube. Thus, the temperature of one end of the bar could be determined at all times. The furnace assembly, consisting of the 2¼ in. ID Vycor tube and contents, was supplied with power by a high-frequency (10 kc) water-cooled copper coil. A tantalum susceptor, surrounding the crucible, picked up the high-frequency power and radiated heat to the crucible and charge. Thus, the melt was maintained placid.

To obtain the proper temperature distribution in the melt or charge, the tantalum susceptor was pointed just as the Alundum crucible was. The very point of the susceptor was removed to permit a ¼ in. diam rod to be freely inserted. This rod was made of smaller molybdenum rods which were 0.05 in. sq and 3 in. long. This form of laminated rod was chosen in order to reduce the heat that would have been generated through induced eddy currents if a solid rod had been used. The composite rod was drilled at the top end to receive the pointed crucible and was inserted in a water-cooled copper block at the lower end in order to extract heat. This rod supported the crucible and extracted a sufficient amount of heat from the bottom of the crucible so that, with the aid of the pointed susceptor, the proper heat distribution was maintained and single crystals could be grown.

The mechanics of growing crystals may be briefly described. After flushing the Vycor tube with helium, the charge was heated to 100° to 200°C above its melting point to be certain that it was entirely molten. Then the power input was slightly lowered until the thermocouple indicated the melt to be 20° to 40° above the solidification temperature. Past this point in the heating cycle the power setting was not changed. The entire Vycor tube assembly was lowered at a rate of 1/4 to 1/3 in. per hr through the heating coil. Lowering of the melt through this coil generally resulted in a single crystal starting to grow at the point. Continued lowering permitted this crystal to grow upward, often to the bottom of the thermocouple protection tube.

Nature of Single Crystals

The degree of perfection of the crystals made by this method was not always identical. Low angle boundaries were occasionally produced, although crystals could be grown without evidence of them. Furthermore, the single crystals as grown from the melt showed a distinct cellular structure when heavily etched.* Each main cell had a finer structure as seen in Fig. 2 for an alloy of 3 wt pct Al in iron. The photographed surface is approximately a (110) crystallographic plane with the angle between the direction of growth and the (110) plane (or surface viewed) about 5 degrees.

* The etchant was a solution of 25 pct nitric acid, 5 pct hydrochloric acid, and balance water.

In the Al-Fe alloys above 12 wt pct Al, segregation of the aluminum was observed. For instance, a difference in composition of about 1 pct Al was produced in a distance of 2 in. at nominally 15 pct Al.

The orientations (crystallographic direction parallel to the growth direction) of several single crystals of Al-Fe and of Si-Fe were found to be quite randomly distributed throughout the unit stereographic triangle.

Acknowledgment

This work was partially supported by the Wright Air Development Center, Air Force Contract No. AF 33(616)-309.

References

[1] A. U. Seybolt and J. E. Burke: *Procedures in Experimental Metallurgy*. John Wiley & Sons Inc. New York, 1953.
[2] E. Schmid and I. W. Boas: *Plasticity of Crystals*. F. A. Hughes and Co. Ltd. London, 1950.
[3] J. G. Walker, H. J. Williams, and R. M. Bozorth: Growing and Processing of Single Crystals of Magnetic Metals. *Review of Scientific Instruments*, 1949, vol. 20, No. 12, p. 947.
[4] B. Chalmers: Crystal Growth and Crystal Boundary Techniques. *Modern Research Techniques in Physical Metallurgy*, p. 170. ASM, Cleveland, 1953.
[5] B. Chalmers: The Preparation of Single Crystals and Bicrystals by the Controlled Solidification of Molten Metals. *Canadian Journal of Physics*, 1953, vol. 31, p. 132.

CsCl-Type Ordered Structures in Binary Alloys of Transition Elements

X-ray diffraction results indicate that in the VFe alloy, the body-centered-cubic disordered structure can be almost completely retained by quenching from 1250°C. On annealing at 600°C, the disordered body-centered-cubic structure transforms into a CsCl-type ordered structure before practically any of the stable σ phase is formed. The increasing stability of the CsCl-type ordered structure from CrFe to VFe to TiFe indicates that the *A-B* bond increases in strength, as compared with the *A-A* and *B-B* bonds. This is accompanied by increasing brittleness, increasing lattice contraction, and the disappearance of ferromagnetism. It is probable that the increasingly strong *A-B* bond results from a quasi-ionic bond component due to electron transfer.

by T. V. Philip and Paul A. Beck

IN a previous note[1] it was pointed out that the available information suggests a distinct correlation between the occurrence of the CsCl-type ordered structures formed in equi-atomic binary alloys of transition elements and the location of the components in the periodic table. A definite increase in the bond strength between unlike atoms, as compared with that between like atoms, is indicated when, in binary alloys of iron group elements, the other component is changed from chromium to vanadium or tantalum, to titanium. Laves and Wallbaum,[2] reported a CsCl-type ordered structure for the stable intermediate phase at the equi-atomic composition in the Ti-Fe system (and also in the Ti-Ru and Ti-Os systems). On the other hand, Tagaya, Nenno, and Nishiyama[3] found no ordering of this kind in the body-centered-cubic solid solutions in the Cr-Fe system. It was concluded[1] that the occurrence of a CsCl-type ordered phase of intermediate stability may be expected in the V-Fe system. Preliminary results were described,[4] suggesting that at least some degree of order does exist in the equi-atomic alloy VFe, annealed at 1200°C and quenched in cold water. Using CrK radiation, at least one weak superlattice line was found in the X-ray diffraction pattern which could be indexed as $(100)_s$ and which disappeared, as expected, when FeK radiation was used.

It was found more recently that the impurity phase (presumably VN), previously giving rise to additional X-ray diffraction lines and thus preventing definite indentification of the (111) superlattice line,[4] can be eliminated by preparing the alloy by arc melting in a helium atmosphere. The alloy specimen melted in this manner had clean surfaces and showed very littte, if any, nitride phase in the microstructure after annealing in vacuum at 1250°C and quenching. The relative intensity of the $(100)_s$ superlattice line with CrK radiation was greatly increased and, in addition, a fairly strong $(111)_s$ superlattice line and even a detectable $(210)_s$ superlattice line was obtained, when the powder produced by filing from the 1250°C annealed and quenched specimen was reannealed in vacuum at 625°C for 1 hr. By using a cellulose acetate film as a filter in front of the photographic film in order to absorb the soft radiation resulting from air fluorescence, the background intensity could be reduced considerably in relation to the intensity of the diffraction lines. All three superlattice lines, $(100)_s$, $(111)_s$, and $(210)_s$, disappeared, as expected, when a radiation other than CrK_α was used.[4] For the powder reannealed at 625°C, the strongest lines of the σ pattern also appeared weakly, indicating that during annealing at 625°C a small amount of transformation took place from the body-centered-cubic to the σ phase. However, since all superlattice lines to be expected in the θ angle range used were actually very clearly present, it was evident that the high temperature body-centered-cubic phase had transformed into a CsCl-type ordered structure before much σ phase could form. Reannealing filings for 1 hr at 700°C resulted in complete transformation into the σ phase. After 1 hr at 650°C the transformation into σ was not quite complete, the strongest body-centered-cubic diffraction lines were still present, although fairly weak, and only the $(100)_s$ superlattice line was detectable (extremely weak).

These findings not only confirm the previous conclusions[4] as to the existence of a CsCl-type ordered structure in the Fe-V system, but they also indicate that this metastable ordered structure forms at about 600°C preceding the formation of the stable σ phase, while at 1250°C the disordered body-centered-cubic phase is stable. The faint $(100)_s$ superlattice line previously observed in specimens quenched from 1200°C was probably due to the fact that the quenching of the powder in an evacuated fused quartz capsule was not fast enough to prevent completely the ordering reaction on cooling.

The present results conform with the suggestion that the *A-B* bond, in relation to the *A-A* and *B-B* bonds, increases in strength from CrFe to VFe to TiFe. It is, therefore, of interest to compare the measured values of the average atomic diameter for these three alloys with the corresponding average atomic diameters calculated from the atomic radii of the elements concerned. Assuming *A-B* contacts

T. V. PHILIP, Junior Member AIME, formerly at the University of Illinois, is now Staff Metallurgist, Research and Development Laboratory, Crucible Steel Co. of America, Pittsburgh. P. A. BECK, Member AIME, is Research Professor of Physical Metallurgy, College of Engineering, University of Illinois, Urbana, Ill.

TP 4509E. Manuscript, Dec. 26, 1956.

in a CsCl-type structure, it follows that the measured average atomic diameter is $r_A + r_B = a_o \frac{\sqrt{3}}{2}$. The a_o for VFe and for TiFe were determined experimentally, by using a symmetrical back reflection focusing precision camera with CrK and CuK radiation, respectively. The a_o value for CrFe has been calculated from data published by Nishiyama.[3] The a_o values, the corresponding $r_A + r_B$ values, and the average atomic diameters $R_A + R_B$ calculated from the atomic radii for coordination number = 8, according to Laves,[4] are shown in Table I. It is interesting that for CrFe the average atomic diameter calculated from the lattice parameter is in complete agreement with the sum of the atomic radii according to Laves, but that for VFe the value calculated from the lattice parameter is low, and for TiFe it is even lower. That the observed lattice contraction increased with increasing stability of the ordered structures, as indicated by the temperature range of stability, is quite reasonable. Both the increasing bond strength and the increasing contraction may well be due to an increasing ionic bond component resulting from electron transfer, as suggested previously.[1] It may be noted that the a_o for VFe was observed to decrease upon ordering by about 0.0018A, a value near the estimated experimental error. In line with the above reasoning a decrease in a_o might be expected when the number of V-Fe nearest neighbors increases, as in ordering. The fact that the change is so slight may be attributed to the presence of a considerable degree of short range order in the specimen quenched from 1250°C, even though it shows little, if any, long range order. The extent of electron transfer may be expected to depend on the number of V-Fe nearest neighbors, hence on short range order.

In this connection, it is interesting to compare the three CsCl-type ordered structures TiFe, TiCo, and TiNi,[5*] for which lattice parameter values have been published by Duwez and Taylor.[5] In the present work, lattice parameters have been redetermined for the three equi-atomic alloys by using a symmetrical back reflection focusing type precision camera and CuK radiation. By linear extrapolation of the lattice parameter vs $\cos^2\theta$ plot to $\theta = 90°$, the a_o values listed in Table I have been obtained. These values, except the one for TiNi, are in fairly good agreement with those published by Duwez and Taylor, and the two investigations are certainly in agreement on a significant point. The lattice parameter of TiFe is smaller than that of TiNi in spite of the fact that, in accordance with the usual atomic radii of these elements,[4] the reverse should be the case. From the data in Table I, it may be seen that this reversal is a result of the fact that the lattice contraction in FeTi is much larger than that in TiNi, TiCo being in-between. On the basis of the above observations regarding CrFe, VFe, and TiFe, these data may be interpreted to signify that the A-B bond in TiFe is stronger than that in TiCo, and this in turn is stronger than that in TiNi. While consideration of the data for CrFe, VFe, and TiFe indicates increasing attractive forces between transition element atoms with increasing separation in the periodic table, as would normally be expected, the reverse appears to be true for the series TiFe, TiCo, and TiNi.

* Duwez and Taylor,[5] using CuK radiation, could not find any superlattice lines for TiFe, TiCo, and TiNi. In the present work with CrK radiation superlattice lines were again not definitely detectable, even when the annealing temperature was decreased from 1200° (TiFe, TiCo) and 1000° (TiNi) to 600°C. This, however, may be a result of too small a difference between the atomic scattering power of the components, and it does not prove the absence of ordering.

Table I. Measured Average Atomic Diameter $r_A + r_B$ and Average Diameter $R_A + R_B$ Calculated from *Metallic Radii* for Coordination Number = 8, Laves,[4] for Transition Element Alloys

Alloy	a_o in A	$r_A + r_B$ in A	$R_A + R_B$ in A	Contraction in A, $(R_A + R_B) - (r_A + r_B)$
CrFe	2.875[3]	2.49	2.49	0.00
VFe (ordered)	2.910 ±0.001	2.52	2.57	0.05
TiFe	2.976 ±0.001	2.58	2.66	0.08
TiCo	2.991 ±0.001	2.59	2.65	0.06
TiNi	3.015 ±0.001	2.61	2.64	0.03
TiRe	3.104 ±0.001	2.69	2.76	0.07

It is very likely that these conditions result from electronic interactions of the various transition element atoms with each other. Certain conclusions as to the nature of these interactions may be inferred from the magnetic properties. Preliminary studies indicate that VFe is strongly ferromagnetic at room temperature, while TiFe, TiCo, and TiNi do not become ferromagnetic even at 78°K. Since the Fe-Fe distances in VFe and in TiFe differ only by about 2 pct, it is not very probable that the lack of ferromagnetism or low Curie temperature in TiFe is due to the insufficiency of the exchange forces resulting from the large Fe-Fe distances in the alloy as compared with those in iron. It appears more likely that electron transfer between the iron atoms and the surrounding titanium atoms reduces the atomic moment of iron by decreasing the number of d-electrons with unopposed spin. This suggestion could be tested by means of neutron diffraction. In agreement with the assumption of a quasi-ionic bond in TiFe, due to electron transfer, this alloy shows considerable hardness and brittleness. TiNi is noticeably softer and less brittle.

In view of the apparently increasing A-B bond strength from TiNi to TiCo to TiFe, one may wonder as to the cause of the reported absence of a CsCl-type ordered structure in TiMn.[6] In order to investigate further the alloying behavior of manganese group elements with titanium, an alloy of the composition TiRe was prepared. The X-ray diffraction patterns indicated a body-centered-cubic structure, with any superlattice lines, in spite of the great difference in the atomic scattering factor of titanium and rhenium for CrK radiation. The body-centered-cubic pattern, without superlattice lines, was observed after annealing at 1200°C and quenching to room temperature, and also after reannealing for 1 hr at 700° or for a week at 600°C. If a CsCl-type ordered structure occurs at this composition, it can be stable only below 600°C.* This observation, together with the reported absence of a CsCl-type ordered structure in the Ti-Mn system, appears to indicate that the A-B bond in equi-atomic alloys of

* An alloy of the composition Ti_2Re was found to be also body-centered-cubic, with $a_o = 3.199 \pm 0.001$A, when annealed for three days at 1200°C and quenched. With $a_o = 3.282$A for β-Ti at room temperature,[7] there is a nearly linear decrease in the a_o for the body-centered-cubic phase with increasing rhenium content, suggesting that a continuous body-centered-cubic solid solution field extends from β-Ti to nearly TiRe. An alloy of the composition Ti_3Re_5, when quenched from 1200°C, also showed strong body-centered-cubic diffraction lines, but its lattice parameter was the same as that of TiRe. The X-ray patterns for both TiRe and Ti_3Re_5 had, in addition to the strong body-centered-cubic diffraction lines, some weak lines, suggesting the presence of a small amount of a second phase. Microscopic examination indicated a somewhat larger amount of a very finely dispersed precipitate in the Ti_3Re_5 alloy than in the specimen corresponding to the composition TiRe. The body-centered-cubic solid solution appears to extend at 1200°C to a composition slightly higher in titanium than TiRe.

titanium with manganese group elements is much weaker than with iron group elements. However, the observed contraction of 0.07A of the average atomic diameter for TiRe, Table I, is not readily interpreted in the light of the foregoing discussion.

Summary

There is very clear indication of decreasing *A-B* bond strength, both from the temperature range of the stability of the CsCl-type structure and from its lattice parameter, as a shift is made from titanium to vanadium to chromium in equi-atomic alloys with iron. VFe has an order-disorder transformation in the temperature range between 600° and 1250°C. Evidence for CsCl-type ordering has been previously found[2] in alloys of vanadium group elements with ruthenium in the iron group. A particularly strong tendency to form CsCl-type ordered structures is found in the alloys of titanium with the iron group elements. Titanium also forms such structures with cobalt and nickel but, if the lattice contraction is accepted as an indicator, the bond strength is decreasing from TiFe to TiCo to TiNi. The two manganese group elements so far studied in this respect have no tendency to form CsCl-type ordered structures with titanium. TiRe is body-centered-cubic (with a small amount of second phase), with no long-range order as quenched from the temperature range between 600° and 1200°C.

Acknowledgment

This work was supported by the Office of Ordnance Research, U. S. Army, Contract No. DA-11-022-ORD-1175.

References

[1] J. B. Darby, Jr., O. P. Arora, and P. A. Beck: Occurrence of CsCl-Type Ordered Structures in Certain Binary Systems of Transition Elements. *AIME Trans.*, 1956, vol. 206, p. 148; Journal of Metals, February 1956.

[2] F. Laves and H. J. Wallbaum: Zur Kristallchemie von Titan-Legierungen. *Naturwissenschaften*, 1939, vol. 27, p. 674.

[3] M. Tagaya, S. Nenno, and S. Nishiyama: On the Fe-Cr Superlattice. *Memoirs* Institute of Scientific and Industrial Research, Japan, 1952, vol. 9, p. 76.

[4] F. Laves: Crystal Structure and Atomic Size, *Theory of Alloy Phases*, pp. 124-198. ASM, Cleveland, 1955.

[5] P. Duwez and J. L. Taylor: The Structure of Intermediate Phases in Alloys of Titanium with Iron, Cobalt and Nickel. *AIME Trans.*, 1950, vol. 188, p. 1175; Journal of Metals, September 1950.

[6] D. J. Maykuth, H. R. Ogden, and R. I. Jaffee: Titanium-Manganese System. *AIME Trans.*, 1953, vol. 197, p. 225; Journal of Metals, February 1953.

[7] P. Greenfield and P. A. Beck: Intermediate Phases in Binary Systems of Certain Transition Elements. *AIME Trans.*, 1956, vol. 206, p. 265; Journal of Metals, February 1956.

[8] B. W. Levinger: Lattice Parameter of Beta Titanium at Room Temperature. *AIME Trans.*, 1953, vol. 197, p. 195; Journal of Metals, February 1953.

Discussion of this paper sent (2 copies) to AIME by Dec. 1, 1957 will appear in AIME *Transactions* Vol. 212, 1958, and in Journal of Metals, April 1958.

Notch Tensile Properties of Selected Titanium Alloys

Selected α, α-β, and β titanium alloys have been tested in the notch-tension test. The base alloys were variously contaminated with carbon, nitrogen, and/or oxygen, and the notch sensitivity of the resultant materials was determined in the temperature interval $-320° \leq T \leq 75°$F. From these results contamination limits to produce embrittlement at the testing temperatures examined have been established.

by E. P. Klier and N. J. Feola

NOTCH properties of titanium materials have been extensively investigated in the impact test.[1-5] For the most part the impact strength measured suggests a ductile-brittle transition that lies at relatively high temperatures, thus indicating a possible notch sensitive condition at ambient temperatures. Recently it has been shown[6] that the impact strength for unalloyed titanium, as for aluminum alloys, may be a nonsensitive index of notch sensitivity as provided by the notch strength as measured in the notch tensile test.

The notch strength for unalloyed titanium was found to depend on the nitrogen and carbon contamination levels. In the present work the levels to which oxygen, nitrogen, and carbon contaminants can be tolerated without leading to excessive em-

[6] The impact strength of titanium materials on an exhaustive scale has been determined and reported in restricted circulation reports for the standard Charpy *V*-notch specimen. The results so obtained are in essential agreement with the results reported for the microspecimen generally used in the referenced studies.

E. P. KLIER, Member AIME, is Professor of Metallurgy, Syracuse University, Syracuse, N. Y. N. J. FEOLA is Assistant Project Engineer, Development Metallurgy Div., Curtiss-Wright Corp., Wood Ridge, N. J.

TP 4504E. Manuscript, July 30, 1956.

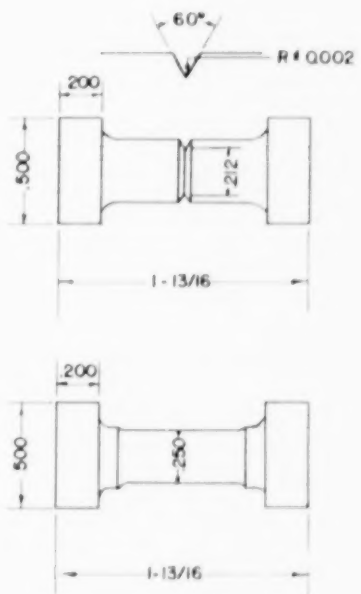

Fig. 1—Notched and smooth tensile specimens.

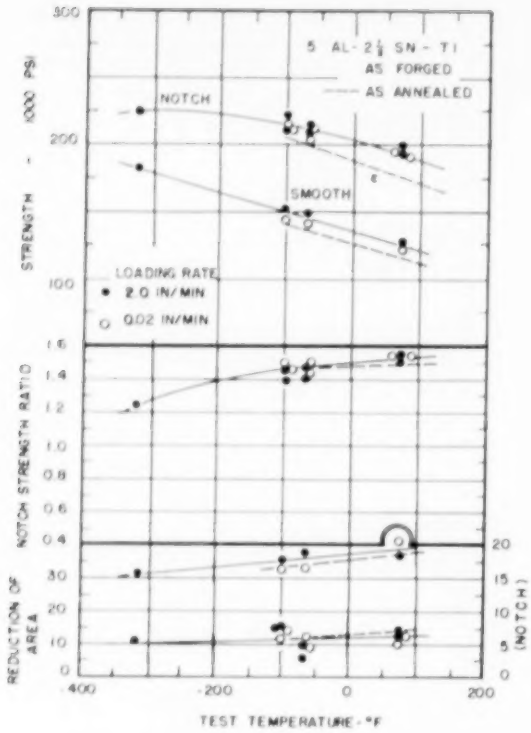

Fig. 2—Tensile and notch tensile properties of a 5 pct Al-2½ pct Sn-Ti as forged alloy as a function of test temperature. Specimen was 0.3 in. diam, with 50 pct notch; radius, ≤ 0.002 in.

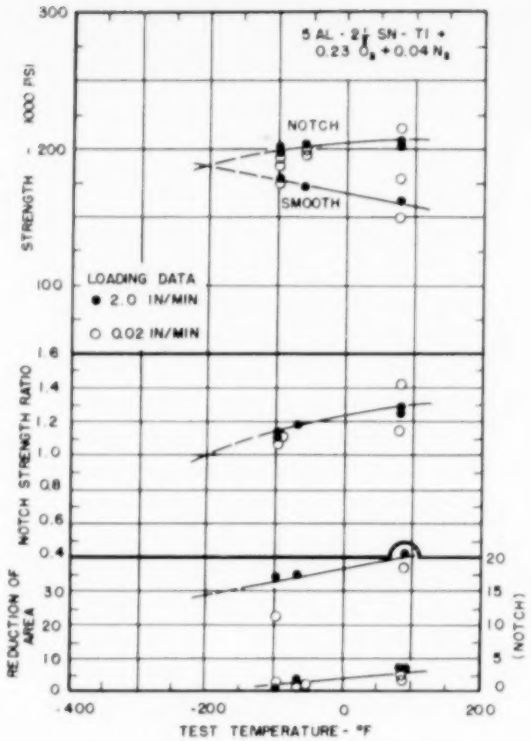

Fig. 3—Tensile and notch tensile properties of a 5 pct Al-2½ pct Sn-0.23 pct O_2-0.04 pct N_2-Ti alloy as a function of test temperature. Specimen was 0.3 in. diam, with 50 pct notch; radius, ≤ 0.002 in.

brittlement as determined in the notch tension test in selected alloy titanium are reported.

Experimental Procedure

Materials—It was considered probable that notch sensitivity in alloy titanium would be dependent on the phase relations in the respective alloys, and on the alloy content for a given type of phase condition. For this reason two α, one β, and three α-β type alloys were prepared. The base compositions of these alloys are presented in Table I.

Melting and Forging—Melting was completed in an inert atmosphere consumable electrode copper crucible arc furnace.[7] Sponge titanium and alloy additions were pressed into 2 x 2 x 10 in. compacts which were welded together to form suitable electrodes. Approximately 30 lb ingots were melted and these were forged either to ½ or 1 in. sq bar stock. The 1 in. sq stock was contaminated, remelted, and forged to ½ in. square bar. This stock was, in general, annealed and then used for specimen preparation.

Table I. Base Compositions of the Titanium Alloys

Nominal Pct	By Analysis, Pct
2½ pct Sn-5 pct Al-Ti	2.42 pct Sn; 5.70 pct Al; 0.02 pct C; 0.015 pct N; 0.052 pct O; 0.0033 pct H
6 pct Al-Ti	5.58 pct Al; 0.02 pct C; 0.018 pct N; 0.095 pct O; 0.011 pct H
3 pct Mo-7 pct Al-Ti	2.4 pct Mo; 6.2 pct Al; 0.01 pct C; 0.008 pct N; 0.081 pct O; 0.014 pct H
4 pct Al-4 pct Mn-Ti	4.5 pct Al; 4.6 pct Mn; 0.015 pct C; 0.008 pct N; 0.10 pct O; 0.0016 pct H
8 pct Mn-Ti	8.3 pct Mn; 0.025 pct C; 0.025 pct N; 0.228 pct O; 0.028 pct H
15 pct Cr-Ti	15 pct Cr; 0.02 pct C; 0.017 pct N; 0.0183 pct H

Contamination and Analyses—The 1 in. sq bar was contaminated in suitable lengths, by the addition of measured contaminants in a weld bead along the bar. Three to five lb ingots were then melted and processed. Following forging to ½ in. sq bar, analyses were made for carbon and nitrogen and, in selected instances, for oxygen and hydrogen.

The carbon and alloy analyses were determined by Kimman and Wheeler, Syracuse, N. Y. The oxygen and hydrogen analyses were determined by the National Research Corp., Cambridge, Mass. The nitrogen analyses were determined by a microkjehldahlometric-colorimetric procedure at Syracuse University. Compositions of the contaminated materials are presented in Table II.

Specimens and Testing Procedure—Specimens according to Fig. 1 were prepared from the ½ in. sq bar. The notches were machined with a suitably sharpened cutting tool. The dimensions of the specimens were measured on an optical comparator and a notch root radius of 0.002 in. or less was consistently obtained. Two notched and one smooth specimen were tested at 75°, −65°, −100°, and −320°F. For each of the three highest temperatures, specimens were tested at two loading rates. The fast loading rate led to failure of notched specimens within 3 to 6 sec. The slow loading rate was adjusted to give failure after a time about 100 times that for the fast test. Specimens were loaded to fracture in concentric loading fixtures,[8] one of which was adapted for testing in a liquid environment at low temperatures. All materials were examined metallographically after electropolishing.

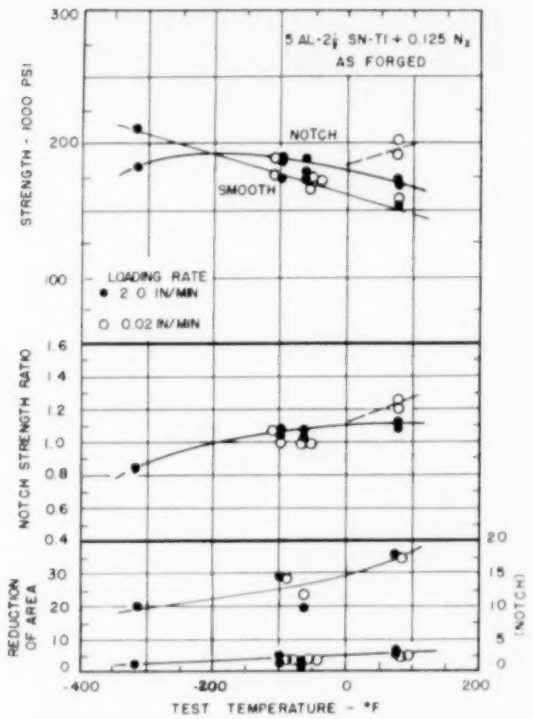

Fig. 4—Tensile and notch tensile properties of a 5 pct Al-2½ pct Sn-0.125 pct N_2-Ti alloy as forged as a function of test temperature. Specimen was 0.3 in. diam, with 50 pct notch; radius, ≤ 0.002 in.

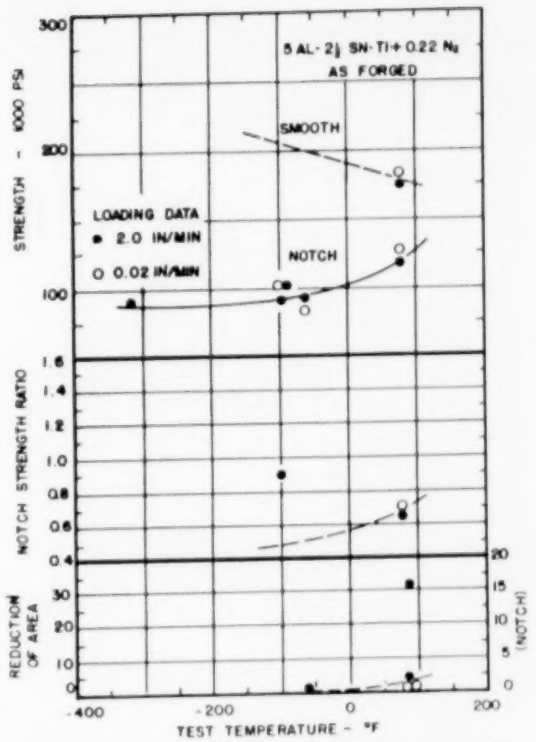

Fig. 5—Tensile and notch tensile properties of a 5 pct Al-2½ pct Sn-0.22 pct N_2-Ti as forged alloy as a function of test temperature. Specimen was 0.3 in. diam, with 50 pct notch; radius, ≤ 0.002 in.

Representation of the Test Data—Typical tensile and notch strength data are plotted against testing temperature to illustrate characteristic trends. Ductile-brittle transitional behavior, however, is best determined in the notch tensile test by examination of the notch strength ratio. Thus, for the specimens given in Fig. 1, the notch strength (defined as the maximum nominal stress under the notch) divided by the tensile strength gives a value of from 1.5 to 1.7 for a fully ductile material. As notch sensitivity sets in, this ratio is reduced and in the present work a value of 1.0 is set as the lower limit of the ductile range. Values of contamination with carbon, nitrogen, and oxygen which give a notch strength ratio of 1 at the several test temperatures are therefore plotted. Additional illustrative curves are presented.

Experimental Results

The α Alloys—The results obtained for the various titanium alloys form analogous sets. Relatively detailed results for the 5 pct Al-2½ pct Sn-Ti alloy only, therefore, will be presented.

The microstructure of this alloy is essentially α phase and the distribution of the microconstituents is that usually observed. The precipitate structure has not been identified but is considered to be made up of the compounds of oxygen, nitrogen, and carbon with titanium.

The tensile and notch strength data for the base alloy are presented in Fig. 2. The tensile strength (75°F) is 125,000 psi and increases linearly with reduction in temperature to a value of 180,000 psi at −320°F. The notch strength (75°F) is 195,000 psi and increases at a decreasing rate with reduction in temperature to a value of 225,000 psi at −320°F. Thus at −320°F this alloy is still notch tough, or the ductile-brittle transition temperature lies at less than −320°F.

If the oxygen content is raised to 0.23 pct, the alloy remains notch tough in the temperature interval 75°F to −100°F, Fig. 3, while the tensile strength (75°F) is raised to about 150,000 psi. A comparable nitrogen content, however, leads to extreme embrittlement, Figs. 4 and 5.

With the addition of nitrogen the tensile strength is raised at a relatively high rate. For the alloy containing 0.125 pct N_2 it is also indicated that the notch strength is velocity sensitive, Fig. 4, although for the alloy examined the effect may be due in some measure to the hydrogen present. As illustrated in this figure, it is nearly characteristic that while

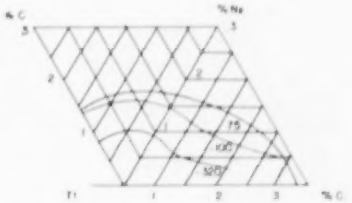

Fig. 6—Interstitial compositions which give a notch strength ratio equal to 1 at the indicated temperatures for the 5 pct Al-2½ pct Sn-Ti alloy.

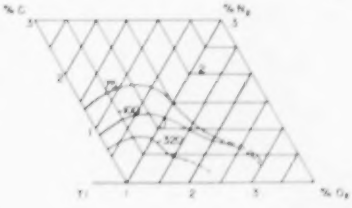

Fig. 7—Interstitial compositions which give a notch strength ratio equal to 1 at the indicated temperatures for the 6 pct Al-Ti alloy.

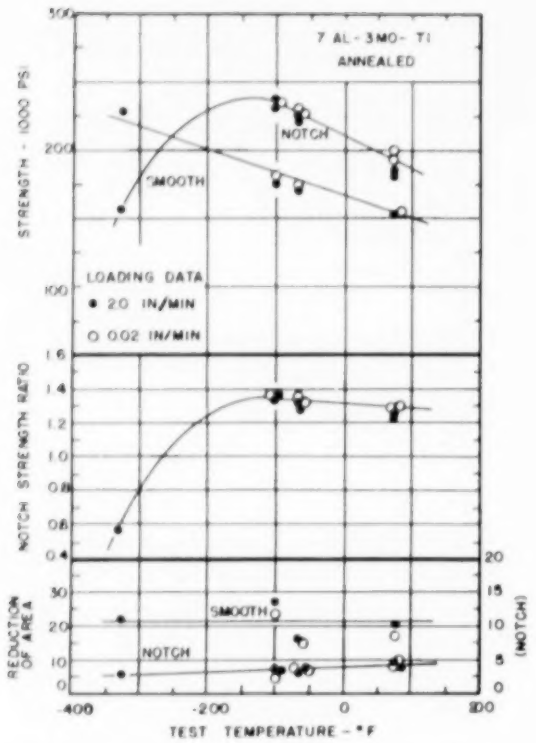

Fig. 8—Tensile and notch properties of a 7 pct Al-3 pct Mo-Ti as annealed alloy as a function of test temperature. Specimen was 0.3 in. diam, with 50 pct notch; radius, ≦ 0.002 in.

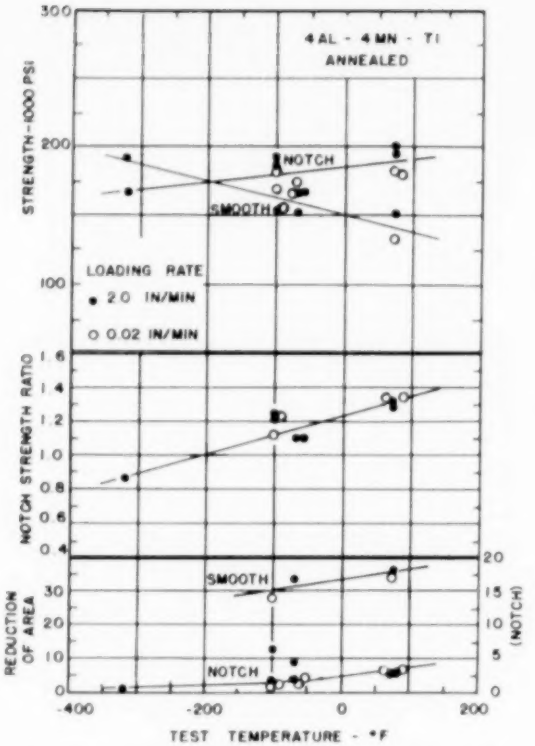

Fig. 10—Tensile and notch tensile properties of a 4 pct Al-4 pct Mn-Ti annealed alloy as a function of test temperature. Specimen was 0.3 in. diam, with 50 pct notch; radius, ≦ 0.002 in.

the tensile strength curve may be raised the notch strength curve remains only slightly displaced until a critical condition is obtained, at which point it is abruptly lowered. The consequence of this is that as the tensile strength is raised the curve of the notch strength ratio is gradually lowered to a value of about 1 and then seemingly discontinuously is lowered further to a value of about 0.7. The transition temperature is then moved abruptly from a temperature considerably less than −100°F to a temperature greater than 100°F, see Figs. 4 and 5. Where possible, the compositions at which the tensile and notch strengths are equal were established at each testing temperature. The data so obtained were plotted in Fig. 6 and establish the ductility limits, i.e., as given by a notch strength ratio of 1, as imposed by the interstitial contaminants. The results for the 6 pct Al-Ti alloy were very similar, as is indicated in Fig. 7.

The α-β Alloys—The two α alloys discussed in the preceding section are essentially non-heat treatable. The α-β alloys, on the other hand, are subject to structural changes through heat treatment. In order to minimize property changes due to structural changes the different contaminated bars were annealed together according to annealing procedures now in use in commercial practice.

The tensile properties of the uncontaminated 7 pct Al-3 pct Mo-Ti alloy are presented in Fig. 8. The tensile strength, which is 155,000 psi at 75°F, increases linearly with temperature decrease to 230,000 psi at −320°F. The notch strength, which also increases linearly with temperature decrease to −100°F, drops to 160,000 psi at −320°F. Thus, a ductile-brittle transition in the test exists in the temperature interval $-320° < T < -100°F$. This transition temperature is elevated as the carbon, nitrogen, and/or oxygen contents are allowed to change. Ductility limits which determine a notch strength ratio of 1 are given in Fig. 9 at testing temperatures of interest.

The tensile properties measured for the 4 pct Al-4 pct Mn alloy are presented in Fig. 10. The tensile strength is 140,000 psi and increases linearly with reduction in temperature to 190,000 psi at −320°F. The notch strength, on the other hand, decreases at a low rate with temperature decrease from 190,000 psi at 75°F to 170,000 psi at −320°F. The ductile-

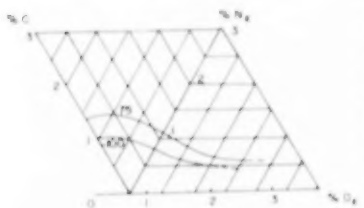

Fig. 9—Interstitial compositions which give a notch strength ratio equal to 1 at the indicated temperatures for the 7 pct Al-3 pct Mo-Ti alloy.

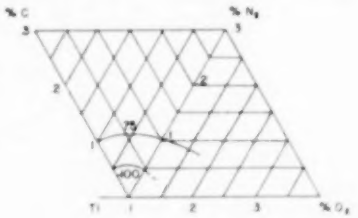

Fig. 11—Interstitial compositions which give a notch strength ratio equal to 1 at the indicated temperatures for the 4 pct Al-4 pct Mn-Ti alloy.

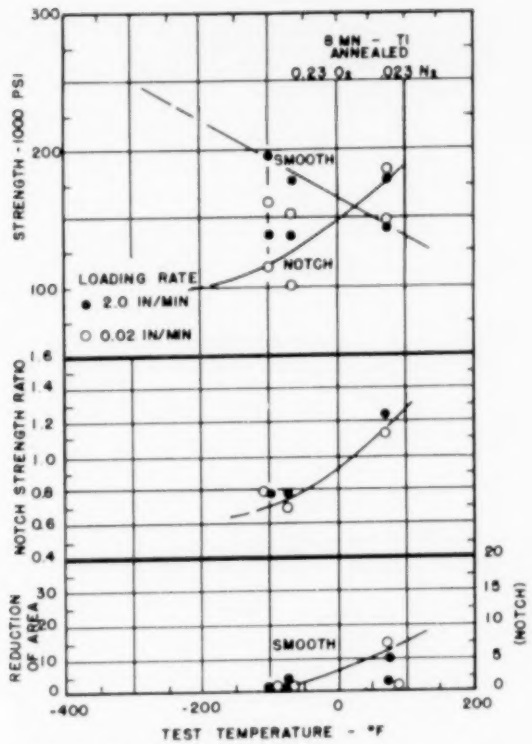

Fig. 12—Tensile and notch tensile properties of a 8 pct Mn-Ti annealed alloy as a function of test temperature. Specimen was 0.3 in. diam, with 50 pct notch; radius, ≤ 0.002 in.

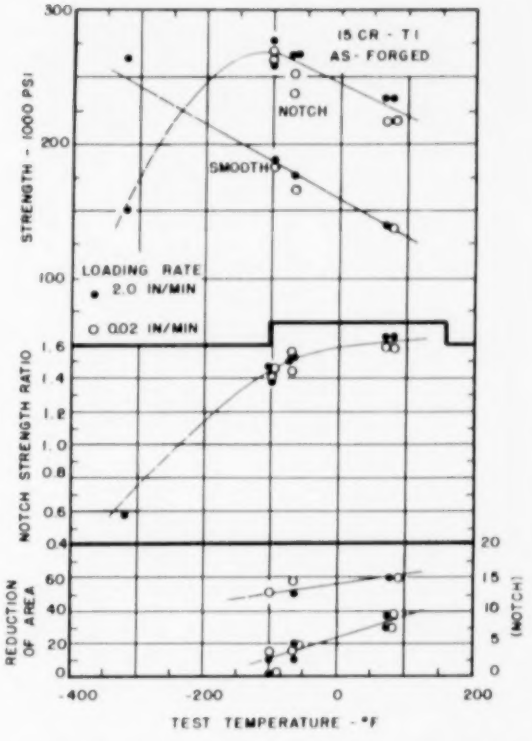

Fig. 13—Tensile and notch tensile properties of 15 pct Cr-Ti as forged alloy as a function of test temperature. Specimen was 0.3 in. diam, with 50 pct notch; radius, ≤ 0.002 in.

brittle transition for this material also lies in the interval $-320° < T < -100°F$.

Contamination limits of carbon and nitrogen in the 4 pct Al-4 pct Mn alloys producing a notch strength ratio of 1 are illustrated in Fig. 11.

The tensile properties of the 8 pct Mn alloy are presented in Fig. 12. The contaminant level in this alloy before contaminant addition was sufficiently high to cause extreme embrittlement.

The β Alloy—The β-phase titanium alloy selected for study contained 15 pct Cr, and could be retained as β phase at 75°F only by relatively fast cooling through the transformation range. During slow cooling a pearlitic structure is formed. Relatively little testing was completed on this alloy because of this indicated structural instability. The tensile properties of the β structure are presented in Fig 13. From 75°F to −100°F this alloy is evaluated as notch tough, while a ductile-brittle transition lies at less than −100°F. If the 15 pct Cr alloy is allowed to transform to a pearlitic structure, as by annealing, it becomes extremely notch sensitive.

Discussion and Conclusions

The notch tensile test has, in the past, been developed in the course of notch sensitivity studies on high strength steels.[4] It is a test of primary significance for steels as the strength level exceeds a limit of about 200,000 psi, Fig. 14. In this figure similar limiting tensile strengths for the test are indicated for both aluminum and titanium base materials.

In Fig. 14 the notch strength vs tensile strength data for all titanium alloys studied in this investigation are summarized. It is evident that as the tensile strength passes through the 130,000 to 150,000 psi

Table II. Chemical Analyses of the Titanium Alloys Invesitgated

Alloy	Pct C	Pct N	Pct O	H, Ppm
5 pct Al-2½ pct Sn-Ti	0.02	0.015	0.052	33
	0.065	0.025	0.097	57
	0.02	0.125	0.116	220
	0.01	0.220	—	—
	0.02	0.04	0.230	74
	0.105	0.155	—	—
	0.04	0.235	0.056	—
	0.03	0.155	0.214	97
6 pct Al-Ti	0.02	0.108	0.095	110
	0.065	0.06	0.104	150
	0.22	0.025	0.12	180
	0.02	0.116	0.12	145
	0.01	0.201	0.125	115
	0.02	0.686	0.242	171
	0.15	—	0.111	120
7 pct Al-3 pct Mo-Ti	0.01	0.008	0.081	169
	0.08	0.066	—	—
	0.155	0.0372	—	—
	0.12	0.056	0.117	130
	0.025	0.105	—	—
	0.105	0.205	0.124	120
	*	0.039	—	—
	0.16	0.056	—	—
	0.02	0.087	0.26	38
4 pct Al-4 pct Mn-Ti	0.15	0.008	0.097	16
	—	—	—	—
	0.09	0.04	—	—
	0.17	0.072	—	—
	0.02	0.18	0.179	73
	0.02	0.26	—	—
	0.015	0.09	0.129	24
	0.18	—	0.130	82
	0.03	0.09	0.150	69
	—	0.025	—	—
	0.015	—	0.117	100
	0.015	—	—	—

* Nominal 0.2 pct C too brittle to machine.

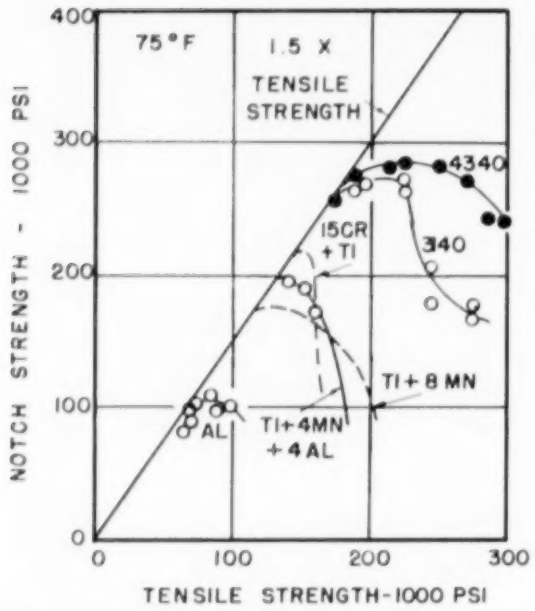

Fig. 14—Notch sensitivity vs tensile strength of high strength alloys; sharply notched 0.3 in. diam specimens. Alloys 4 pct Mn-4 pct Al-Ti; 7 pct Al-3 pct Mo-Ti; 6 pct Al-Ti; and 5 pct Al-2½ pct Sn-Ti have similar notch strength vs tensile strength curves, so only one curve was presented.

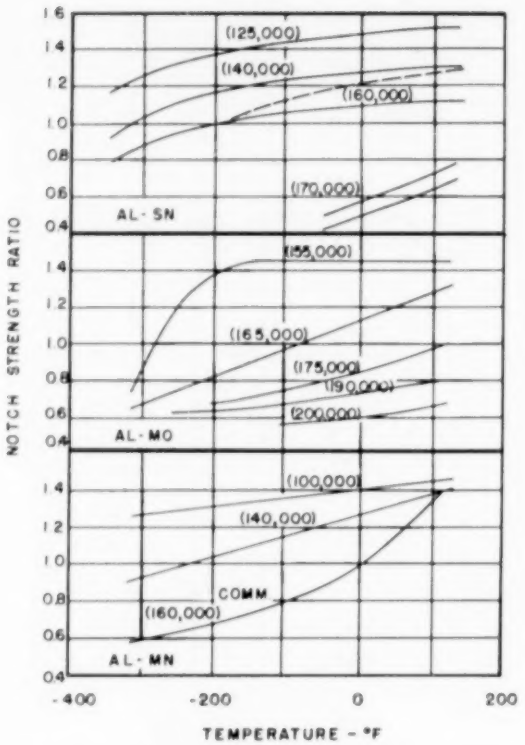

Fig. 15—Notch strength ratio vs testing temperature for selected titanium alloys at the indicated tensile strengths. Note that the tensile strengths are obtained through the addition of carbon, nitrogen, and/or oxygen.

interval the notch tensile test becomes a sensitive test of notch embrittlement. It is important to note in the examination of these data that the tensile strength changes have resulted from contamination effects and the properties obtained may not be the optimum properties obtainable by suitable structures control through heat treatment. However, it may be concluded from this figure that as the tensile strength of a titanium alloy exceeds 150,000 psi, notch sensitivity may well be encountered.

For a material that undergoes a ductile-brittle transition this phenomenon is usually found to be temperature dependent and in the notch tensile test the notch strength ratio plays a role similar to the impact strength in indicating this transition with temperature change. Characteristic data are presented in Fig. 15 for consideration of the ductile-brittle transition with testing temperature changes for selected alloys.

It has already been pointed out that the transition temperature defined in terms of a notch strength ratio of 1 shifts abruptly from very low to very high temperatures, and the manner in which this shifting is accomplished is given in Fig. 15. From these curves it is seen that tensile strengths at from 150,000 to 160,000 psi are potentially embrittling for some alloys. It is also indicated, however, that by both alloy and metallographic structures control this limit may potentially be increased. In this respect titanium alloys analogous to the superior ultra high strength steels would appear to be possible, see Fig. 14.

The limits to which the interstitial contaminants, oxygen, carbon, and nitrogen, can be tolerated for certain of the alloy systems can be fairly well established. For systems in which the relative volumes of α and β phase can be altered and consequently for which the partitioning of the interstitial contaminants can be altered some question may be raised as to the maximum contamination limits that may be tolerated. Indeed, if full ductility as signified by a notch strength ratio of 1.5 is required, it appears that no increase in interstitial contamination over the base level in the sponge is admissible for any but the α-phase alloys, if these alloys are to be given the conventional heat treatment. The possibility does exist, however, that by suitable heat treatment alloys containing maximum levels of interstitial contamination may be rendered suitably notch tough for service applications.

Summary

1) Six alloys of titanium have been prepared and contaminated variously with carbon, nitrogen, and oxygen. The respective materials were then examined in the tensile and notch-tensile tests at temperatures from 75°F to −320°F.

2) As the carbon, nitrogen, and/or oxygen contents of the various alloys were allowed to increase either singly or in combination, notch sensitivity was induced at a contaminant level which depended on the alloy and testing temperature. Possible contamination limits vary for the different alloys.

3) Notch sensitivity in the various titanium alloys in the notch-tensile test has been observed to depend on the strength level, with the critical strength level falling in the 140,000 to 160,000 psi range. For those alloys which have good low temperature toughness the transition temperature in the notch-tensile test is also dependent on the tensile strength.

Acknowledgments

The work reported in this paper was completed under USAF Contract No. AF 33(616)-2281, which was administered under the direction of the Materials Laboratory, Directorate of Research, Wright Air Development Center with Lt. H. Burte as project engineer.

References

[1] S. Abkowitz, J. J. Burke, and R. H. Hiltz, Jr.: *Titanium in Industry*, reference to L. D. Jaffee, D. Van Nostrand Co. Inc. New York, 1955.

[2] R. I. Jaffee, F. C. Holden, and H. R. Ogden: Mechanical Properties of Alpha Titanium as Affected by Structure and Composition. *AIME Trans.*, 1954, vol. 200, pp. 1282-1290; JOURNAL OF METALS, November 1954.

[3] H. R. Ogden, F. C. Holden, and R. I. Jaffee: Effect of Alpha Solutes on the Heat-Treatment Response of Ti-Mn Alloys. *AIME Trans.*, 1955, vol. 203, pp. 105-112; JOURNAL OF METALS, January 1955.

[4] E. P. Klier and N. Feola: The Effects of Carbon and Nitrogen Contamination on the Notch Tensile Properties of Titanium. ASTM. To be published.

[5] W. W. Stephens, N. L. Gilbert, and R. A. Beall: Consumable-Electrode Arc Melting of Zirconium Metal. *ASM Trans.*, 1953, vol. 45, pp. 862-871.

[6] G. Sachs, J. D. Lubahn, and L. J. Ebert: Notch Bar Tensile Test Characteristics of Heat Treated Low Alloy Steels. *ASM Trans.*, 1944, vol. 33, pp. 340-391.

[7] E. P. Klier, V. Weiss, and G. Sachs: A Stepped Austenitizing Treatment for 4340 Steel. *AIME Trans.*, 1957, vol. 209, pp. 424-425; JOURNAL OF METALS, April 1957.

Discussion of this paper sent (2 copies) to AIME by Dec. 1, 1957 will appear in AIME *Transactions* Vol. 212, 1958, and in JOURNAL OF METALS, April 1958.

Technical Note

Cylindrical Carbide Particles

by J. H. Westbrook

IT is always of interest to document the origin of real microstructures which closely approach various idealized morphologies. Such instances constitute excellent bases for experimental studies of the effect of microstructure on properties. Typical examples include the eutectoid steels (lamellae) used by many investigators and the two phase Cu-Cr alloys (spheres) recently employed by Hibbard and Hart.[1] The present note describes a structure with cylindrical particles.

In a study of certain alloys in the Cr-C system, an alloy was arc melted whose composition was very close to the αCr-$Cr_{23}C_6$ eutectic (3.2 wt pct C, according to the latest phase diagram published by Bloom and Grant[2]). The alloy was not analyzed but previous experience with the melting technique employed indicates good correspondence between intended and analyzed compositions with negligible tungsten contamination from the electrode.

The phases present in the alloy were identified by X-ray powder patterns as α chromium and $Cr_{23}C_6$. Typical micrographs, presented in Fig. 1, show unmistakable evidence of the cylindrical geometry of the carbide phase. The eutectic grains are randomly oriented and, consequently, only a few show the true fibrous nature of the carbide particles, most being cut so as to show slightly elliptical cross sections. Within any particular grain, remarkable uniformity is to be observed with respect to the size, shape, spacing, and orientation of the carbide particles. Length to diameter ratios have been estimated from the micrographs to be at least 250:1, with diameters of about 1μ.

This alloy may be of further interest from different viewpoints. On the one hand, it might be used to check the applicability of the equations derived by Fullman[5] for computing true particle dimensions of cylindrical particles from opaque random sections. On the other hand, it might be possible to extract the carbide particles from this alloy and repack them in a ductile matrix to form a synthetic structure of the type discussed by Metcalfe et al.[4] With the large l:d ratio and the small diameter of the carbide fibers, it is likely that the interdefect distance in each fiber is sufficiently great to permit realization of a large fraction of the presumed high strength of the carbide.

J. H. WESTBROOK, Junior Member AIME, is associated with Research Laboratory, General Electric Co., Schenectady.

TN 417E. Manuscript, Jan. 23, 1957.

References

[1] W. R. Hibbard, Jr. and E. W. Hart: Dispersion Hardening of Copper-Chromium Alloys. *AIME Trans.*, 1955, vol. 203, p. 200; JOURNAL OF METALS, January 1955.

[2] D. S. Bloom and N. J. Grant: The System Chromium-Carbon. *AIME Trans.*, 1950, vol. 188, p. 41; JOURNAL OF METALS, January 1950.

[3] R. L. Fullman: Measurement of Approximately Cylindrical Particles in Opaque Samples. *AIME Trans.*, 1953, vol. 197, p. 1267; JOURNAL OF METALS, September 1953.

[4] A. G. Metcalfe, C. H. Sump, and W. C. Troy: Fiber Metallurgy. *Metal Progress*, 1955, vol. 67, p. 81.

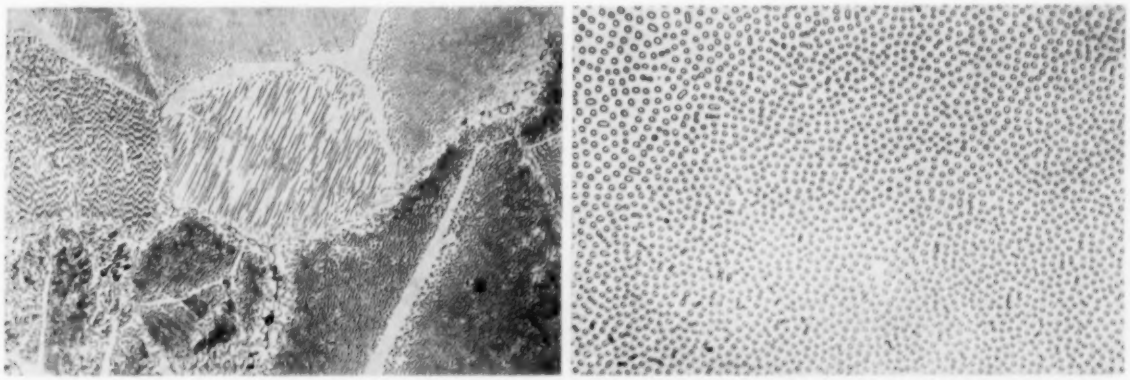

Fig. 1—Typical microstructures of the αCr-$Cr_{23}C_6$ eutectic showing the cylindricity of the carbide phase. Both, NaOH electrolytic etch. LEFT: X100. RIGHT: X1000. Reduced approximately 15 pct for reproduction.

Distribution of Boron in Gamma Iron Grains

The distribution of boron in γ iron grains as a function of temperature is studied, employing three experimental techniques: a) grain growth in high purity Fe-C and Fe-C-B alloys, b) X-ray parameter measurements on Fe-B alloys as a function of temperature, and c) the metallographic test for the boron constituent. It is concluded that boron undergoes positive adsorption to γ iron grain boundaries and that the temperature coefficient of adsorption is positive.

by R. M. Goldhoff and J. W. Spretnak

IN connection with establishing the mechanism by which boron enhances the hardenability of heat treatable steels, this research work has been undertaken. Spretnak and Speiser[1,2] indicated the need for studying high temperature effects in boron steels and, chief among these, the possible nonhomogeneous distribution of boron in γ iron grains. The occurrence of this effect may be of significance in explaining the mechanism of enhancement of hardenability by boron as well as in explaining some of the observed characteristics of boron steel behavior. Primarily, then, this work was undertaken a) to establish whether or not boron is adsorbed in γ solid solutions, b) to determine the nature of any such adsorption effects, i.e., whether it is positive or negative as well as its temperature coefficient, and c) to establish the magnitude of any such effect.

While past literature on this specific subject is rather sparse, a number of authors have postulated that the observed temporary loss of hardenability as well as the occurrence of the characteristic boron constituent in these steels is due to the nonuniform distribution of boron in austenite.[3-6]

Experimental Techniques

Attempts to obtain direct evidence of grain boundary effects in boron steels have been unsuccessful, both by using the technique of Chalmers[7] in which small concentrations of solute made radioactive by irradiation are detected by autoradiographic means, and by means of studying cleavage fractures with the electron microscope.[8]

The present study attempts the design of experiments to measure the effect of boron on properties which might be subject to variation because of grain boundary effects. A study of the theoretical aspects of grain growth indicates that such studies may be pertinent. Another valid type of experiment involves the measurement in polycrystalline materials of properties whose values depend on the bulk of the grain, being negligibly influenced by grain boundaries. One such property is the lattice parameter measured by X-ray diffraction. The value of the lattice parameter reflects the average conditions which obtain over a relatively large number of atoms in a fixed crystalline lattice, and is therefore mainly dependent on bulk grain material. Measurement of lattice parameter variation over the austenite range of temperature in iron with and without boron should give evidence of concentration variations in the bulk grain material if adsorption effects are significant.

Finally, use is made of the Grange and Garvey[9] metallographic test for boron in which a characteristic boron constituent can be developed in austenite grain boundaries. The very occurrence of this phenomenon suggests grain boundary enrichment of boron and a study of the occurrence of this constituent and its varation with austenitizing temperature should help to detect grain boundary effects.

Materials

One lb ingots of pure iron, an Fe-B alloy, an Fe-C alloy, and an Fe-C-B alloy were prepared. The melting technique included an initial melting of electrolytic iron under vacuum followed by remelting under hydrogen and, finally, by melting under argon with the addition of alloying elements. Each ingot was surface machined between meltings. A quantitative spectrographic analysis was obtained on the pure ingot and, in addition, oxygen, nitrogen, and carbon were determined by the vacuum fusion method. The results of these analyses are given in Table I. Semiquantitative spectrographic analyses were performed on the alloy ingots, while quantitative determinations of the alloy additions were obtained. These analyses are shown in Table II.

The cast ingots were subjected to the following sequence of fabrication treatments: forging to 5/8 in. bars, swaging to 0.300 in. rounds, drawing to 0.025 and 0.010 in. wire. Portions of each ingot were retained in the swaged condition for experimental use.

For certain portions of the work typical commercial steels were used. These materials were supplied by the Republic Steel Corp., Canton, Ohio, and correspond to AISI 8640 and AISI 86B40 compositions.

R. M. GOLDHOFF, formerly Graduate Student, Dept. of Metallurgical Engineering, Ohio State University, is now Metallurgist, Large Steam Turbine Div., General Electric Co., Schenectady. J. W. SPRETNAK, Member AIME, is Professor of Metallurgical Engineering, Ohio State University, Columbus, Ohio.

TP 4624E. Manuscript, Sept. 12, 1955.

Both materials were taken from the same base heat, the boron being added to a portion of the heat as Grainal No. 79. The composition and treatment of these materials are shown in Table III.

Grain Growth Studies

Many excellent reviews of boundary migration and grain growth theory appear in the literature.[9-11] The mathematical treatment of grain growth varies in complexity, but it is customary to treat the results of isothermal grain growth studies in accordance with a relationship of the form

$$D = kt^n \qquad [1]$$

where D equals average grain diameter; t equals time of anneal; and k and n are constants.

In theory the value of n in the above equation should be 0.5, but for metals its value in general is less. Fullman[12] has studied the factors which may influence n and has included the effects of inclusions, changes in grain boundary free energy, adsorption of impurities at grain boundaries, orientation, polygonization, and strain. A study of these effects in detail[12] shows that even though the adsorption of solute atoms at the grain boundaries does not appear to alter the surface energy significantly and thereby influence the grain growth exponent, such an occurrence can still have a substantial effect on grain boundary mobility, which tends to decrease n by a large relative amount. This provides a basis for studying the isothermal grain growth chacteristics of the Fe-C and Fe-C-B alloys described previously.

Specimens of each alloy were heat etched in a highly purified hydrogen atmosphere using a system analogous to that described by Miller and Day.[13] Isothermal grain growth curves were obtained at temperatures of 1750°, 1850°, and 1900°F for times ranging from 15 min to 4 hr. The average grain size analysis was based on the grain count as obtained from six photographic fields of about 100 grains taken from each specimen. By using the following equation, the average grain size is then determined,[14]

$$D = \frac{1.075}{M}\sqrt{\frac{A}{N}}$$

where D equals average grain diameter; M magnification; A, area of field; and N, the average number of grains in the field.

According to the equation $D = kt^n$, a plot of log D vs log t should give a straight line with slope n and intercept log k, based on the assumption that the initial grain size is negligible in comparison to grain sizes encountered on annealing and likewise that the time for recrystallization is negligible in comparison to the annealing times used. These assumptions appear valid for the data presented here.

Figs. 1 and 2 show the data plotted according to the above scheme and the results are reasonably good straight lines. It is apparent that the slope of the curves increases continuously for the Fe-C alloy over the range of temperatures studied, whereas it decreases continuously for the Fe-C-B alloy studied.

In order to refine the data, a least squares analysis was performed and the best equations to fit each set of data points were determined. A tabulation of these data is given in Table IV. Further, the equations of the straight lines of Figs. 1 and 2 have been differentiated to obtain rates of grain growth. These values are tabulated in Table V.

While the increase of n with temperature is probably chiefly a thermal effect, the decrease of n with temperature in the case of the boron alloy would seem to indicate a deterring mechanism for grain boundary migration. Examination of the data shows that at a given grain size and temperature the rate of growth of the Fe-C-B alloy is greater than that of the Fe-C alloy, yet with increasing temperature at this same grain size the comparable rate of grain growth increase is less in the Fe-C-B alloy. Again, if we differentiate Eq. 1

$$\frac{dD}{dt} = Knt^{(n-1)} \qquad [2]$$

and apply the data of Table V at unit time Table VI can be drawn up.

From Table VI it appears that there is a different temperature dependency of grain growth for the two alloys. The reason for the higher growth rate of the Fe-C-B alloy at 1750° and 1850°F is not clear, but it could be associated with some nitrogen compound in the Fe-C alloy. In any event it seems plausible that the observed behavior could be attributed to grain boundary adsorption of boron in the Fe-C-B alloy as the temperature increases.

X-ray Diffraction Studies

The basic concepts underlying the X-ray diffraction studies of γ iron have been briefly considered in a previous section. Several preliminary tests on the iron and Fe-B alloys indicated that boron does have a measurable effect on the lattice parameter of iron. Further tests were then carried out in the hope that detectable variations of comparative ther-

Table I. Quantitative Spectrographic and Vacuum Fusion Analyses of High Purity Iron

Element	Wt Pct
Mn	0.005
Si	0.01
Cu	0.0005
Ni	<0.005
Cr	<0.01
V	<0.01
Mo	<0.005
Al	<0.001
Sn	<0.001
B	<0.0005
Co	<0.01
Ca	<0.0005
C*	0.0072
O*	0.0023
N*	0.0080

* Carbon, oxygen, and nitrogen were determined by vacuum fusion analysis.

Table II. Semiquantitative Spectrographic Analyses of Iron Alloys

Alloy	Fe-B	Fe-C	Fe-C-B
Major, >10 pct	Fe	Fe	Fe
Low, 0.1 to 1 pct	None	None	None
Very low, 0.01 to 0.1 pct	None	None	None
Very low trace, 0.005 to 0.05 pct	Si	Si, Al	None
Trace, <0.01 pct	Mn Ti	B Bi	Cu As
	Cu As	Mn Ti	Ni Sb
	Ni Sb	Cu As	Cr Pb
	Cr Al	Ni Sb	V Sn
	V Pb	Cr Pb	Mo Zr
	Mo Sn	V Sn	Co Zn
	Co Zr	Mo Zr	Bi
	Bi Zn	Co Zn	Ti
Boron*	0.0053		0.0021
Carbon†		0.39	0.29

* Boron analyses were done spectrographically.
† Carbon analyses were done by a combustion method.

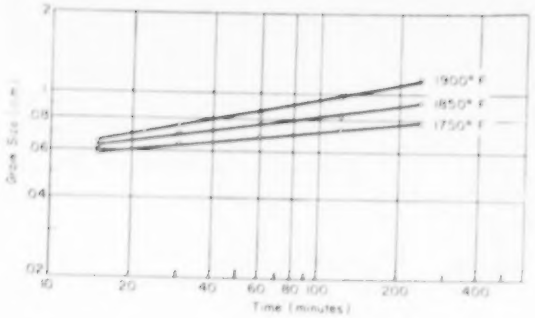

Fig. 1—Isothermal grain growth characteristics of high purity Fe-0.3 pct C alloy.

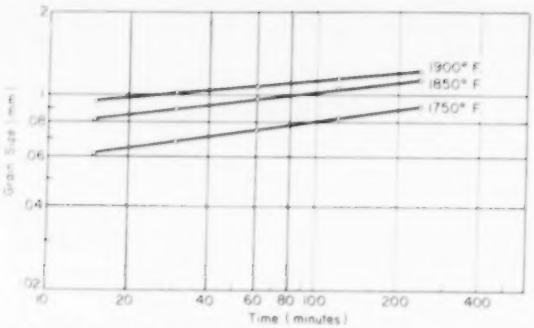

Fig. 2—Isothermal grain growth characteristics of high purity Fe-0.29 pct C-0.0021 pct B alloy.

mal expansion values might be interpreted in the light of concentration variations that might be induced by adsorption effects.

The materials used in this study were 0.010 in. wires of each of the high purity materials prepared for this work. Diffraction patterns were obtained on each of these fully annealed materials at room temperature. A 114 mm Norelco powder type camera was used for this work. The camera was thermostatted and cobalt radiation without filtering was used. Experimental accuracy was estimated to be 0.0001A using the extrapolation method of Nelson and Riley[16] in determining the parameters. Lattice parameters corrected to 20°C, as determined by this means, are shown in Table VII. Both boron containing alloys show a parameter contraction with reference to pure iron whereas the plain carbon alloy shows neither expansion nor contraction. On the basis of the patterns obtained it is felt that the parameter differences are significant, and that this may indicate some effective solubility of boron in iron at room temperature.

The high-temperature vacuum camera used in this work was capable of producing temperatures ranging from 900° to 1200°C and power input stabilization maintains the temperature to within ±2°C. Pressures of the order of 2×10^{-5} mm Hg were maintained at temperature. For accuracy of measurement and ease of handling the 0.010 in. wires were found satisfactory for use in the experiment. Initial tests on the fully annealed high purity wires showed that some critical reflections were absent due to grain growth and that the diffraction lines were too spotty to insure the needed accuracy. For this reason all the determinations could not be made on one specimen so that the values shown at each temperature represent different specimens from the same length of wire. The problems were further obviated by using cold drawn specimens which recrystallized in the camera during the heating up period. Only the pure iron and Fe-B alloy were used and again the Nelson-Riley method was used in measuring lattice parameters. Previous work using pure nickel at about 1000°C indicated that the camera gave results accurate to within 0.0005A in this temperature range. Fig. 3 presents the data obtained for the thermal expansion of the alloys studied. A check with some recent work by Basinski et al.[18] on lattice parameters in γ iron shows fair agreement at the higher temperatures but fairly large differences at the lower temperatures. Camera, characteristics, alloy purity, and differences in technique may well account for this, but for purposes of this study it is really the comparison rather than the absolute values which is important. Perhaps the greatest concern is whether or not the boron is retained in the specimen wires at these high temperatures. Unfortunately, this is very difficult to check since neither analysis nor the metallographic test can be applied under these conditions. However, the vacuums obtained, as cited before, would appear to be sufficient for assuming the retention of boron.

A preconceived notion of the expected behavior of the thermal expansion of the Fe-B alloy was developed as shown in Fig. 4a. This was based on the assumption that boron would be in interstitial solid solution in γ iron. As a result, an expansion of the lattice was expected. Further, if the boron were randomly distributed in the γ iron over the temperature range of the test, the thermal expansion curve of the Fe-B alloy could be expected to be parallel to the curve for pure iron. The occurrence of adsorption would be indicated if the thermal expansion curve of the alloy approached that for pure iron as shown in the figure. The observed behavior plotted in Fig. 3 has been redrawn schematically in Fig. 4b for comparison purposes. Obviously the addition of boron to pure iron causes a contraction of the lattice. The thermal expansion curve for the alloy is divided into two sections, *a* and *b*, in Fig. 4b. The portion of the curve marked *a* is better understood by reference to the Fe-Fe$_2$B equilibrium diagram of McBride, Spretnak, and Speiser.[17] In this diagram, at a 0.005 pct B concentration, a two phase field exists between 906° and about 1025°C. Above

Table III. Analysis of Republic Steel Corp. Heat No. E38720*

	C	Mn	P	S	Si	Ni	Cr	Mo	B
E38720, Ladle	0.39	0.85	0.015	0.019	0.31	0.53	0.48	0.23	—
3A, No. 79 Grainal	0.395	0.89	Not		0.31	0.54	0.46	0.25	0.0013
5A, Base	0.396	0.88	reanalyzed		0.31	0.54	0.47	0.25	0.0000

* Heat had base analysis of AISI 8740; special ingot treated with Grainal No. 79. 5A represents base analysis; 3A represents base plus 4 lb per ton of Grainal No. 79.

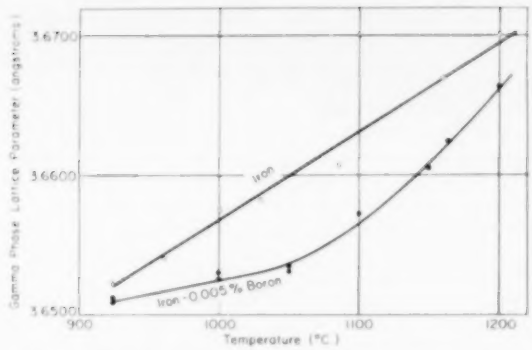

Fig. 3—The γ phase lattice parameter of pure iron and an Fe-0.005 pct B alloy.

1025°C all the boron is in solution in austenite. The observed constant slope portion of the thermal expansion curve for the Fe-B alloy must then represent the solution of Fe_2B. Along the portion of the curve marked *b*, the tendency is for the lattice parameter of the alloy to converge to that for pure iron. This behavior can be plausibly explained by concentration variations within the grains as previously surmised, i.e., the positive adsorption of boron in austenite, increasing with increasing temperature.

The lattice contractions observed when boron is added to iron indicate that boron atoms occupy substitutional sites in both the α and γ phases. There have been several publications which support the idea that boron is substitutional in α iron.[17-20] On the other hand, recent internal friction studies[21,22] on Fe-B alloys in the α range have disclosed a peak attributed to boron, in addition to peaks for carbon and nitrogen. Because of low concentrations of boron involved, it is concluded by these investigators that only interstitial boron atoms could give rise to such an internal friction peak. As for γ iron, on the basis of diffusion data showing boron and carbon to have comparable diffusion rates in austenite,[23,24] it had been assumed previously by the writers that boron forms an interstitial solid solution in γ iron. However, the X-ray parameters obtained in this work show a definite contraction of the lattice, pointing to a substitutional solid solution. Calculations[17] involving the dependency of solubility on the energy required to introduce a boron atom into either an interstitial or substitutional position seem to support the interstitial solid solution, although not decisively. These calculations neglect chemical interaction, which probably contributes to the restriction of the solubility of boron.

In considering the atomic radii of boron and iron, the radius ratio puts boron about midway between the values favorable for substitutional solutions and the interstitial solutions and suggests that boron is slightly more comfortable in a substitutional site. This leads to an interesting possibility of boron atoms occupying both types of sites, with the larger fraction in substitutional sites and a smaller fraction in interstitial sites at any particular instant (the proportions may be altered in α iron because of the smaller interstitial hole in this phase). Thus, diffusion could involve three types of jumps: a) substitutional-substitutional, b) interstitial-interstitial, and c) substitutional-interstitial. Since most of the atoms are expected to be substitutional, a contraction of the lattice parameter would be expected. Such a situation, admittedly unusual, could resolve the conflicting evidence on damping capacity, diffusivity, and lattice parameters.

Metallographic Studies

Grange and Garvey[7] have discussed a unique metallographic test for boron. Whenever addition of a small percentage of boron results in increased hardenability a characteristic constituent can be formed in the microstructure which cannot be found in steels not containing boron. Grange and Garvey obtained this constituent by heating in the vicinity of 2000°F and rapidly cooling to a subcritical temperature where ferrite forms at the austenite grain boundaries on holding. The authors speculated that boron atoms were concentrated at the grain boundaries at the high austenitizing temperature and precipitation of the constituent occurs on rapidly cooling to the subcritical transformation temperature. Under these circumstances it appears that a study of the variation of boron constituent with austenitizing temperature might be a sensitive means of establishing the possible occurrence of surface adsorption of boron in austenite.

The material used in this study was a portion of a commercial heat of AISI 86B40 steel supplied by the Republic Steel Corp. The analysis of this steel appeared in a previous section. Because of the extreme sensitivity of these steels to deboronization, the specimens were nickel plated before treatment in an argon atmosphere. Salt baths were used in subcritical transformation phase of the heat treatment cycle.

It was necessary to make a preliminary study of the temperature and time of holding in the subcritical transformation range in order to obtain optimum conditions for developing the boron constituent. Using an austenitizing temperature of 2000°F it was determined that a subcritical transformation temperature of 1200°F produced the desired ferrite network for developing the constituent. If transformation temperatures were lowered to a point where the proeutectoid ferrite was acicular in nature, the constituent was undiscernable. A study of the effect of holding times at 1200°F revealed that boron constituent was present in the first pro-

Table IV. Equations for the Isothermal Grain Growth of an Fe-0.3 Pct C Alloy and an Fe-0.29 Pct C-0.0021 Pct B Alloy at Various Temperatures

Alloy	Temperature, °F	Equation
Fe-0.3 pct C	1750	$D = 0.046t^{0.50}$
Fe-0.3 pct C	1850	$D = 0.043t^{0.50}$
Fe-0.3 pct C	1900	$D = 0.036t^{0.50}$
Fe-0.29 pct C-0.0021 pct B	1750	$D = 0.042t^{0.50}$
Fe-0.29 pct C-0.0021 pct B	1850	$D = 0.061t^{0.50}$
Fe-0.29 pct C-0.0021 pct B	1900	$D = 0.076t^{0.50}$

Table V. Equations for the Rate of Isothermal Grain Growth of an Fe-0.3 Pct C Alloy and an Fe-0.29 Pct C-0.0021 Pct B Alloy at Various Temperatures

Alloy	Temperature, °F	Equation
Fe-0.3 pct C	1750	$dD/dt = 0.0045t^{-0.50}$
Fe-0.3 pct C	1850	$dD/dt = 0.0060t^{-0.50}$
Fe-0.3 pct C	1900	$dD/dt = 0.0076t^{-0.50}$
Fe-0.29 pct C-0.0021 pct B	1750	$dD/dt = 0.0059t^{-0.50}$
Fe-0.29 pct C-0.0021 pct B	1850	$dD/dt = 0.0067t^{-0.50}$
Fe-0.29 pct C-0.0021 pct B	1900	$dD/dt = 0.0066t^{-0.50}$

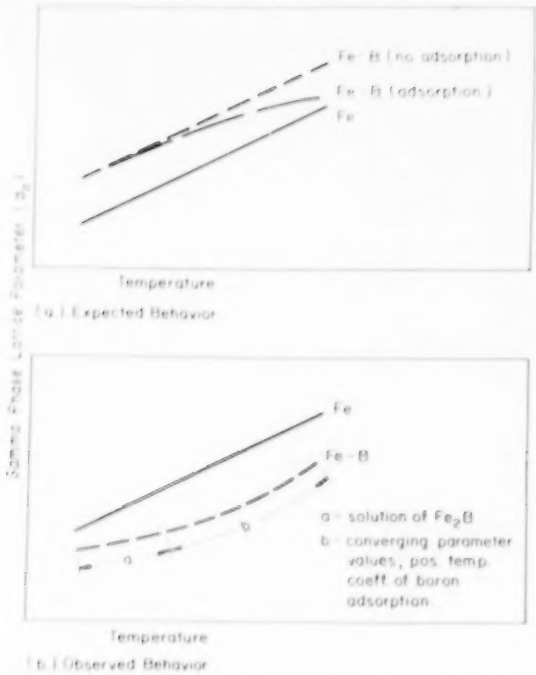

Fig. 4—Schematic representation of the effect of boron on the expected and observed behavior of the thermal expansion of pure iron.

eutectoid ferrite to form. The amount of constituent increased with time of holding until the proeutectoid ferrite transformation was complete. Beyond this time, which appeared to be about ½ hr at this temperature, no change of the amount or disposition of the constituent was noted. Further study showed that the coarsening temperature for this steel was about 1800°F. Detection of the boron constituent using austenitizing temperatures below this figure was very difficult. Undoubtedly, grain size is of importance in increasing the boron concentration at the grain boundaries.

The experiment consisted of heat treating specimens in increments of 100° from 1800° to 2200°F for 10 min, quenching into a constant temperature salt bath at 1200°F, and holding for 1 hr before removal and cooling in an air blast. Each specimen so treated was sectioned, polished, etched with picral, and viewed under the microscope at magnifications from X1000 to X1500. A typical microstructure obtained by heating at 2000°F is shown in Fig. 5.

The evaluation of the relative amount of boron constituent developed in the grain boundaries at the various temperatures involved the measurement of grain size, the average particle size of the constituent, and the relative amounts of grain boundary area covered by the constituent in each of the specimens. Grain size determinations were made by comparison with ASTM charts. The size and boundary coverage of the boron particles were determined microscopically at X1250 with the aid of a filar eyepiece and an oil immersion objective lens. Particle size was estimated by the measuring of diameters of approximately 500 particles in randomly distributed patches of constituent throughout the specimens. To estimate the grain boundary coverage, an average of 50 randomly chosen fields per specimen were evaluated. The results of these measurements are shown in Table VIII along with the calculated volume fraction of boron constituent at each temperature. This volume fraction was calculated according to

$$F = \frac{F_{ca} D_p}{D_a}$$

where F equals volume fraction of boron constituent; F_{ca}, fraction of grain boundary covered by boron constituent; D_p, particle diameter; and D_a, grain diameter.

From the results of the semiquantitative measurements made, it appears that twice as much boron constituent is present in the specimen heat treated at 2200° as is present in the specimen heat treated at 1800°F. The obvious interpretation of these data is that boron must be concentrating at grain boundaries in increasing amounts with increasing temperatures.

During the course of this work, several attempts were made to develop the boron constituent in high purity Fe-B alloys as well as high purity Fe-C-B alloys. In each case the alloy without carbon failed to develop the constituent. This appears to correlate with the data obtained by Darken et al.[27,28] on the phase equilibra in the ternary Fe-C-B system. This work establishes the presence of boro-cementite at temperatures in the austenite range of this system. Boron apparently substitutes in part for carbon in this compound. It is probable, then, that the observed boron constituent is a boro-cementite compound.

Summary and Discussion

Taken together, the results of studies involving grain-growth characteristics, lattice parameters, and metallography indicate the following:

1) Boron is adsorbed in γ iron.

2) The nature of the adsorption is that a) it is positive, i.e., boron atoms tend to segregate at the γ grain boundaries, and b) it has a positive temperature coefficient, i.e., boron atoms segregate to the γ grain boundaries in increasing amounts with increasing temperature.

Table VI. Temperature Dependency of Grain Growth Rate for Fe-C and Fe-C-B Alloys

Fe-C			Fe-C-B		
Temperature, °F	$\frac{dD}{dt}$	Pct of Increase	Temperature, °F	$\frac{dD}{dt}$	Pct of Increase
1750	0.00446		1750	0.00588	
		35.0			12.4
1850	0.00602		1850	0.00671	
		25.6			2.7
1900	0.00756		1900	0.00653	

Table VII. Lattice Parameters of Pure Iron and Some Iron Alloys at 20°C*

Alloy	Parameter, Corrected to 20°C
Fe	2.8665
Fe-0.005 pct B	2.8662
Fe-0.30 pct C	2.8665
Fe-0.29 pct C-0.0021 pct B	2.8664

* Unfiltered cobalt radiation, thermostatted camera.

3) A semiquantitative microscopic analysis of the boron constituent in AISI 86B40 indicates that about twice as much constituent is present in the γ grain boundaries at 2200° as is present at 1800°F.

4) From a study of the variation of lattice parameters in both α and γ iron, with and without boron, it appears that the boron atom forms a substitutional solid solution in both of these phases. However, recent diffusion data and anelasticity studies also point to the existence of interstitial solutions involving boron in iron.

It is well established that boron in hardenable steels acts to delay the start of the decomposition of austenite. The normal concentrations of boron in the bulk of the grain seem to have no deterring influence after the transformation is initiated. This behavior suggests a critically enhanced concentration at the grain boundaries. Such an enrichment of boron atoms can be brought about by a positive temperature coefficient of interfacial adsorption, as demonstrated by the research being reported.

The idea of a positive temperature coefficient of adsorption is often rejected on the basis of behavior of gas adsorption in catalysis. The heat of such adsorption is generally exothermic and, according to the Le Chatelier principle, increasing the temperature will reduce the degree of adsorption, yielding a negative temperature coefficient. However, Taylor and Glasstone[25] point out that heats of adsorption from solutions, and also the amounts of adsorption, are complicated by the participation of the solvent and are correspondingly difficult to interpret. In this particular case of solid solution interfacial adsorption, several factors can change with temperature, such as the chemical interaction between solute and solvent, the magnitude of the interfacial energy, the effect of the solute on the interfacial energy, and the strain energy effect resulting from the distortion induced by the solute atoms. It is reasonable then that the temperature coefficient cannot be predicted a priori. The authors[1,2] have pointed out previously that the temperature coefficient of adsorption in solid solutions must be determined experimentally because of the limitations in the present state of our knowledge.

Acknowledgments

This research was supported by the Aeronautical Research Laboratory, Wright Air Development Center, under Contract No. AF18(600)-94, with J. W. Poynter as project engineer. This paper is based on a portion of a thesis by R. M. Goldhoff submitted in partial fulfillment of the requirements for the degree of Doctor of Philosophy to Ohio State University. Professor R. Speiser contributed valuable discussions in certain phases of the work.

References

[1] J. W. Spretnak and R. Speiser: A Critical Evaluation of the Boron Hardenability Effect in Steel. Technical Report No. 1, Contract No. AF 18(600)-94, The Ohio State University Research Foundation, 1952.

Table VIII. Statistical Analysis of the Boron Constituent Formed in Specimen of AISI 86B40 Steel under Conditions of Varying Heat Treatment

Temperature of Austenitic Treatment, °F	Average Particle Diam, Mm	Average Grain Diam, Mm	Fraction of Grain Boundary Covered	Boron Constituent, Volume Fraction
1800	0.00035	0.051	0.23	0.0016
1900	0.00035	0.072	0.37	0.0018
2000	0.00034	0.101	0.75	0.0025
2100	0.00036	0.101	0.81	0.0029
2200	0.00036	0.122	0.95	0.0028

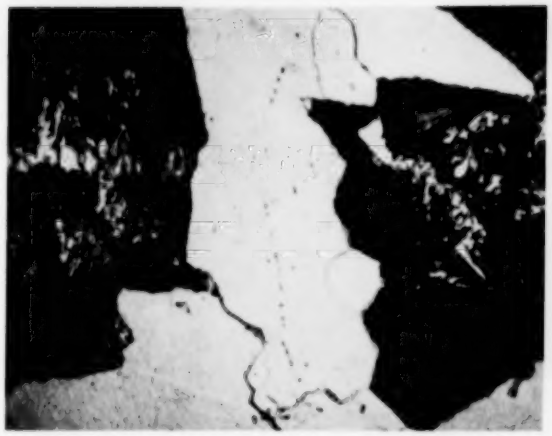

Fig. 5—Boron constituent developed at prior austenite grain boundary. Heat treatment: austenitized 10 min at 1800°, quenched to 1200°F and held 1 hr, cooled to room temperature in air blast. Picral etch. X1250. Reduced approximately 30 pct for reproduction.

[1] J. W. Spretnak and R. Speiser: Annual Summary Report, 1952, Contract No. AF 18(600)-94, The Ohio State University Research Foundation, 1953.
[3] R. A. Grange and T. M. Garvey: Factors Affecting the Hardenability of Boron-Treated Steels. *ASM Trans.*, 1946, vol. 37, p. 136.
[4] J. W. Spretnak and R. Speiser: Grain and Grain Boundary Compositions; Mechanism of Temper Brittleness. *ASM Trans.*, 1951, vol. 43, p. 734-747.
[5] C. R. Simcoe, A. R. Elsea, and G. K. Manning: Study of the Effect of Boron on the Decomposition of Austenite. *AIME Trans.*, 1955, vol. 203, pp. 193-200; JOURNAL OF METALS, January 1955.
[6] A. M. Adair, J. W. Spretnak, and R. Speiser: Effect of Boron on the Relative Interfacial Tension of Gamma Iron. *AIME Trans.*, 1955, vol. 203, pp. 353-354; JOURNAL OF METALS, February 1955.
[7] M. T. Stewart, R. Thomas, K. Wauchope, W. C. Winegard, and B. Chalmers: New Segregation Phenomena in Metals. *Physical Review*, 1951, vol. 83, p. 657.
[8] C. R. Simcoe, A. R. Elsea, and G. K. Manning: An Investigation of the Mechanism by which Boron Increases the Hardenability of Steel. Battelle Memorial Institute Report, 1953.
[9] D. Harker and E. R. Parker: Grain Shape and Grain Growth. *ASM Trans.*, 1945, vol. 34, p. 193.
[10] P. A. Beck, J. C. Kremer, L. J. Demer, and M. L. Holzworth: Grain Growth in High Purity Aluminum. *AIME Trans.*, 1948, vol. 175, pp. 372-394; METALS TECHNOLOGY, September 1947.
[11] J. E. Burke: Some Factors Affecting the Rate of Grain Growth in Metals. *AIME Trans.*, 1949, vol. 180, pp. 73-91; JOURNAL OF METALS, February 1949.
[12] R. L. Fullman: Boundary Migration During Grain Growth. *Metal Interfaces*, pp. 179-205. ASM, Cleveland, 1952.
[13] O. O. Miller and M. J. Day: Heat Etching as a General Method for Revealing the Austenite Grain Size of Steels. *ASM Trans.*, 1942, vol. 30, pp. 541-568.
[14] F. J. Dunkerley, F. Pledger, V. Damiano, and J. Fulton: Grain Growth and Recrystallization Characteristics of Zirconium. *AIME Trans.*, 1951, vol. 191, pp. 1003-1008; JOURNAL OF METALS, November 1951.
[15] J. B. Nelson and D. P. Riley: An Experimental Investigation of Extrapolation Methods in the Derivation of Accurate Unit Cell Dimensions of Crystals. *Proceedings* Physical Soc., London, 1945, vol. 57, p. 160.
[16] Z. S. Basinski, W. Hume-Rothery, and A. L. Sutton: The Lattice Expansion of Iron. *Proceedings* Royal Soc., London, 1955, vol. A229, p. 459.
[17] C. C. McBride, J. W. Spretnak, and R. Speiser: A Study of the Fe-Fe$_2$B System. Technical Report No. 2, Contract No. AF 18(600)-94, The Ohio State University Research Foundation, 1953.
[18] F. Wever and A. Mueller: Concerning the Binary Iron-Boron System and the Structure of Iron-Boride. *Ztsch. für anorg. allgem. Chemie*, 1930, vol. 192, p. 317.
[19] M. E. Nicholson: Factors Influencing Hardenability in Steel with Particular Reference to the Influence of Boron. Seventh Quarterly Progress Report, Contract No. AF 18(600)-12, The University of Chicago, 1953.
[20] P. E. Busby and C. Wells: Diffusion of Boron in Alpha Iron. *AIME Trans.*, 1954, vol. 200, p. 972; JOURNAL OF METALS, September 1954.
[21] W. R. Thomas and G. M. Leak: Condition of Boron in Alpha Iron. *Nature*, 1955, vol. 176, p. 29.
[22] R. R. Hasiguti and G. Kamoshita: Internal Friction of Alpha-Iron Due to Boron Atoms. *Journal* Physical Soc. of Japan, 1954, vol. 9, p. 646.
[23] T. G. Diggs, C. R. Irish, and N. L. Carwile: Effect of Boron on the Hardenability of High-Purity Alloys and Commercial Steels. *Journal of Research*, National Bureau of Standards, 1948, vol. 41, pp. 545-574.
[24] P. E. Busby, M. E. Warga, and C. Wells: Diffusion and Solubility of Boron in Iron and Steel. *AIME Trans.*, 1953, vol. 197, p. 1463; JOURNAL OF METALS, November 1953.
[25] K. G. Carroll, L. S. Darken, E. W. Filer, and L. Zewell: A New Iron Boro-Carbide. *Nature*, 1954, vol. 174, p. 978.
[26] L. S. Darken: Private communication.
[27] H. S. Taylor and S. Glasstone: *A Treatise on Physical Chemistry*, 1951, vol. 2, p. 610.

Discussion of this paper sent (2 copies) to AIME by Dec. 1, 1957 will appear in AIME *Transactions* Vol. 212, 1958, and in JOURNAL OF METALS, April 1958.

Technical Note

Crystallographic Angles for Manganese Bismuthide

by W. J. Romanow

RECENT papers by Williams, Sherwood, and Boothby,[1] Seybolt et al.,[2] Heikes,[3] and Roberts[4] attest to the increasing importance of the hexagonal ferromagnetic compound MnBi. Since the magnetic properties of MnBi crystals are highly anisotropic, it is useful and necessary to have appropriate aids for determining their orientations—a (00·1) standard stereographic projection and a corresponding table of crystallographic angles for this structure. The tables of crystallographic angles for the hexagonal system available in the literature[5] are computed for c/a ratios greater than that of MnBi and cannot satisfactorily be used to find the crystallographic angles of MnBi.

A table of angles between the crystallographic planes $(HK \cdot L)$ and $(hk \cdot l)$ was calculated for MnBi from the formula[6]

$$\phi = \arccos \frac{Hh + Kk + \frac{1}{2}(Hk + hK) + \frac{3}{4}(a/c)^2 Ll}{\sqrt{(H^2 + K^2 + HK + \frac{3}{4}(a/c)^2 L^2)(h^2 + k^2 + hk + \frac{3}{4}(a/c)^2 l^2)}}$$

on an IBM Type 650 Magnetic Drum Data Processing machine. The lattice constants used are listed in Table I and are those determined by Willis and Rooksby[7] at 20°C. More recently published values obtained by both X-ray and neutron diffraction[3,4] show no difference from these significant to the calculation.

From the crystallographic angles between the basal plane (00·1) and the general plane $(hk \cdot l)$ in Table I, an (00·1) standard stereographic projection was made for MnBi which is shown in Fig. 1.

W. J. ROMANOW is associated with the Bell Telephone Laboratories Inc., Murray Hill, N. J.

TN 395E. Manuscript, Oct. 10, 1956.

Table I. Angles Between the Crystallographic Planes of Manganese Bismuthide*

$HK \cdot L$	$hk \cdot l$	ϕ
00·1	10·8	11.64
	10·7	13.25
	10·6	15.36
	10·5	18.24
	10·4	22.39
	20·7	25.21
	10·3	28.78
	20·5	33.39
	10·2	39.48
	20·3	47.69
	10·1	58.75
	20·1	73.12
	10·0	90.00
	21·2	65.36
	21·1	77.08
	21·0	90.00
	11·8	19.63
	11·6	25.44
	11·4	35.51
	11·2	54.98
	11·0	90.00
	12·2	65.36
	12·1	77.08
	12·0	90.00
10·0	21·0	19.11
	11·0	30.00
	12·0	40.89
	01·0	60.00
11·0	12·0	10.89
	12·0	60.00

* a_o = 4.286A, c_o = 6.116A, and c/a = 1.427.

Acknowledgments

The author wishes to thank R. G. Treuting and J. N. Hobstetter for their technical assistance, and Miss D. P. Booth for programing the IBM machine for the calculations. He appreciates the opportunity to read the paper of B. W. Roberts of General Electric Co. prior to its publication.

References

[1] H. J. Williams, R. C. Sherwood, and O. L. Boothby: *Bulletin* Amer. Physical Soc., 1956, vol. 1, p. 132.
[2] A. U. Seybolt, H. Hansen, B. W. Roberts, and P. Yurcisin: *AIME Trans.*, 1956, vol. 206, p. 605; JOURNAL OF METALS, May 1956.
[3] R. R. Heikes: *Physical Review*, 1955, vol. 99, p. 446.
[4] B. W. Roberts: A Neutron Diffraction Study of the Structures of Manganese Bismuthide, *Physical Review*, 1956, vol. 104, p. 607.
[5] A. Taylor and S. Leber: *AIME Trans.*, 1954, vol. 200, p. 190; JOURNAL OF METALS, February 1954.
[6] C. S. Barrett: *Structure of Metals*, 2nd Ed., p. 635. McGraw-Hill Book Co. New York and London, 1952.
[7] B. T. M. Willis and H. P. Rooksby: *Proceedings* Physical Soc., London, 1954, vol. 67B, p. 290.

Fig. 1—Standard (00.1) stereographic projection for MnBi; c/a = 1.427.

Some Internal Friction Studies in Columbium

Carbon has been found to diffuse in columbium at a slightly more rapid rate than nitrogen. At 1 cps, that internal friction peak which arises from the stress-induced ordering of carbon in columbium is found at 268°C while the nitrogen peak occurs at 285°C. The diffusion coefficients are: $D = 0.0046 \exp(-33{,}300/RT)$ for carbon in columbium and $D = 0.0072 \exp(-34{,}800/RT)$ for nitrogen in columbium. The carbon peak in columbium is very unstable, the height declining rapidly with time in contrast to the nitrogen peak. The ratio of the height of the nitrogen peak to the concentration of nitrogen in solid solution (expressed in wt pct) was found to be 0.33, in good agreement with previous work. The internal friction in high purity columbium was found to be a sensitive function of the strain amplitude at which the damping was measured.

by R. W. Powers and Margaret V. Doyle

INTERNAL friction measurements, carried out as functions of temperature, have been used extensively to obtain data on the mobility of interstitial impurities in the Group V metals, vanadium, columbium, and tantalum. For a given frequency of vibration, the internal friction peaks at a temperature which depends principally on the particular metal and interstitial impurity. Relaxation times and corresponding activation energies are determined from a knowledge of such peak temperatures for various vibration frequencies. These experimentally determined relaxation times are related to the average jump frequencies of the interstitial impurity atoms using the model of Snoek[1] and can be related to macroscopic diffusion coefficients as shown by Polder.[2]

In these Group V elements, the impurity whose diffusion rate has been the hardest to pin down by the internal friction technique has been carbon. The experimental difficulties associated with carbon in these metals were not evident in the earliest investigation carried out by Ke on tantalum.[3] The carbon peak was thought to occur near 140°C at 1 cps on the basis of the enhancement of the height of this peak measured on specimens which had been coated with colloidal carbon and heated in vacuo at 1200°C. Presumably on the basis of similar evidence, Wert identified a peak also near 140°C at 1 cps in columbium with the diffusion of carbon in that element.[4]

Later, the difficulties of admitting carbon into these metals without simultaneously introducing oxygen were pointed out by Ang and Wert[5] and by Marx, Baker, and Sivertsen.[6] The latter suggested that the peaks attributed to carbon in tantalum and columbium might arise from the presence of traces of oxygen, adventitiously absorbed during the carburization. Such suspicion was confirmed, at least in tantalum, when it was found possible to prepare C-Ta specimens without contamination by oxygen. Specimens so prepared, although high in carbon content, gave no evidence of a damping peak near 140°C.[7]

Recently, the authors were able to show that carbon diffuses in tantalum at a rate only slightly slower than that for nitrogen.[8] At 1 cps, the carbon peak lies at 349°C, only a few degrees above the nitrogen peak at 341°C. However, the two could be distinguished by a different stability with respect to aging at 400°C and by a different dependence of peak height on solute concentration. On the basis of this experience with tantalum, it appeared worthwhile to search also for a carbon peak in columbium in the vicinity of the nitrogen peak.[9]

[9] The nitrogen peak in columbium has been investigated by Ang,[5] Ang and Wert,[4] and Marx, Baker, and Sivertsen.[6]

In this report, the location of the carbon peak in columbium is made known and its position relative to the nitrogen peak is compared with the authors' previous findings in tantalum. In addition, a second source of internal friction seen only in specimens of very high purity is discussed.

Columbium was obtained from the Fansteel Metallurgical Corp. as either 30 or 40 mil diam stock. The manufacturer gives the following analysis as typical of this material: 99.4 pct minimum Cb, 0.10 pct maximum C, 0.5 pct Ta, 0.04 pct Ti, 0.02 pct maximum Si, and 0.01 pct maximum Fe. Wires 13 in. long were degassed near 2200°C for 4 to 16 hr in an ultimate vacuum better than 2.10^{-6} mm Hg in an apparatus described previously.[7] This treatment reduced the oxygen and nitrogen damping peaks observed in the as-received material to less than 0.0001 in Q^{-1} above background. The latter value varied somewhat from specimen to specimen in the range 0.0004 to 0.0008, depending chiefly on the wire diameter and the frequency of vibration. The high temperature evacuation left the specimen in a rather soft condition, the Vhn being reduced to 40 from a value near 121 in the as-received condition. The grain size was about the diameter of the specimen. After outgassing, specimens were loaded with carbon by absorption of such hydrocarbons as methane or ethylene. Carbon was also added to a few specimens by heating them at

R. W. POWERS and M. V. DOYLE are associated with the Research Laboratory, General Electric Co., Schenectady.

TP 4601E. Manuscript, Feb. 15, 1957.

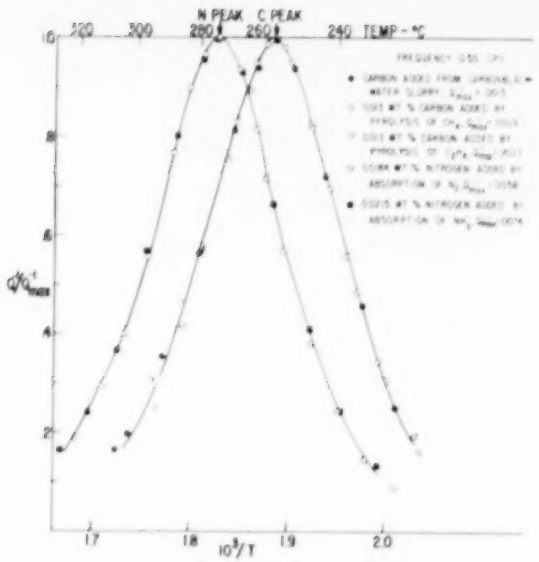

Fig. 1—Carbon and nitrogen internal friction peaks in columbium.

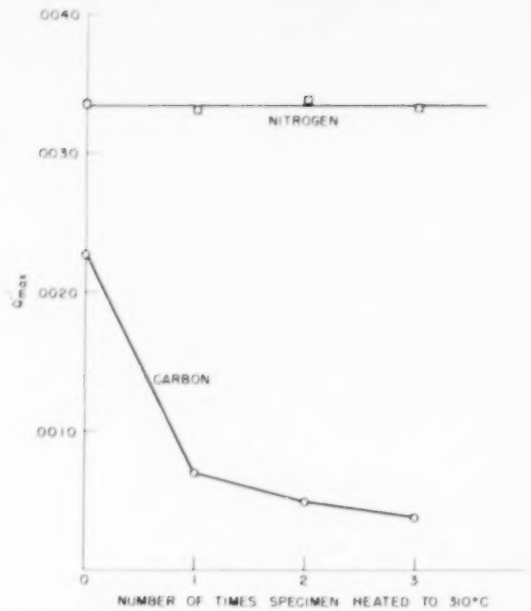

Fig. 2—Difference in stability between the nitrogen and the carbon peak in columbium with respect to aging at 310°C.

2000°C in vacuum following application of a carbon black-water slurry to their surfaces. Carbon solutions prepared in this manner were subject to almost no contamination by oxygen. The oxygen peak in no case exceeded 0.0003 in Q^{-1}. The very high carburization temperatures used were suggested by the experiments of Mrs. M. R. Andrews, who found many years ago that the absorption of oxygen by tantalum decreases rapidly with increasing temperature.[10] The situation in columbium is presumably similar. The presence of carbon in columbium produces a damping peak near one previously reported to arise from the diffusion of nitrogen. Consequently, for purposes of comparison, the internal friction was studied also in columbium specimens to which nitrogen was added by the absorption of either molecular nitrogen or ammonia.

The internal friction measurements were made in a torsion pendulum of the sort popularized by Ke.[11]

Identification of the Carbon Peak in Columbium—In Fig. 1, plots are shown of internal friction vs reciprocal temperature for various columbium specimens, which had been evacuated and then charged with carbon or nitrogen as designated in the figure. For purposes of critical intercomparison, the various curves have been normalized to unity at the peak. The background damping has been subtracted from the observed damping in each case. Note that in columbium, carbon diffuses at a somewhat more rapid rate than does nitrogen. At 0.55 cps, the carbon peak is located at 258°C while the nitrogen peak is found at 275°C. This is the inverse of that found previously in tantalum. In the latter, carbon diffuses at a slightly slower rate than does nitrogen. Moreover, in the specimens charged with carbon, either no peak or one not larger than 0.0003 was found near 140°C. This observation demonstrates that the previous association of the 140° peak in columbium with carbon was incorrect, and that the 140° peak was caused by absorbed oxygen.

Aging of C-Cb Solid Solutions—The height of the carbon peak in columbium was found to decline with time. This aging process, which proceeds considerably more rapidly than in C-Ta solutions, undoubtedly contributed to the initial delay in identifying the peak and made the characterization rather difficult. This effect is presumed to arise from the precipitation of columbium carbide. It is illustrated in Fig. 2, where for a specimen loaded with 0.01 wt pct C, the damping peak height was remeasured between successive heatings of the pendulum furn-

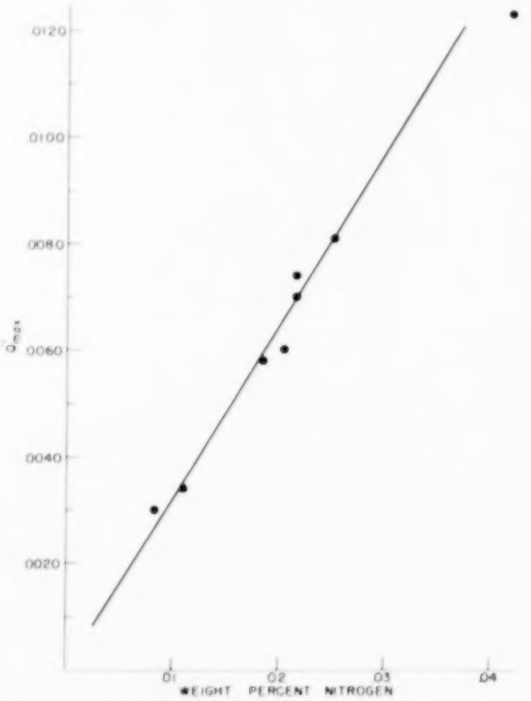

Fig. 3—Height of N-Cb damping peak as a function of nitrogen concentration.

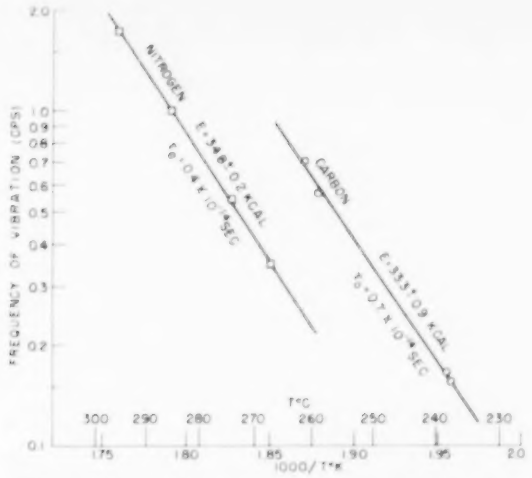

Fig. 4—Determination of the activation energies for the diffusion of carbon and nitrogen in columbium.

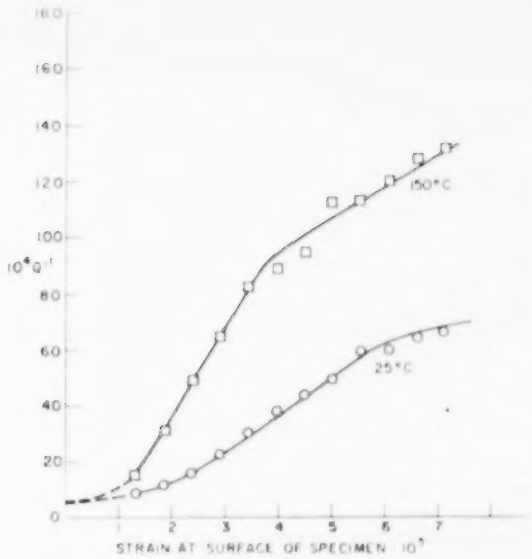

Fig. 5—Strain amplitude dependence of internal friction in pure columbium.

ace to 310°C. The peak damping is plotted against the number of times the specimen had been heated to 310°C. The instability of carbon solutions should be contrasted with that of nitrogen solutions. No aging of the peak, in a specimen containing 0.01 wt pct N, was expected from the work of Ang and Wert.[7] None was found, as shown also in Fig. 2.

Peak Heights as Functions of Solute Concentration—Attempts were made to establish the relationship between the height of the carbon peak and the carbon concentration. They were not successful because of the rapid aging of carbon solutions as discussed above. The height of the carbon peak for a given carbon concentration varied considerably from specimen to specimen and appeared to depend critically on the rapidity of quench. In general, higher peak heights were observed in those specimens prepared with methane, as compared with those prepared from ethylene. It is assumed that this is due to the greater amount of hydrogen associated with a given quantity of carbon in methane. The greater amount of hydrogen gives rise to a more rapid quench and thus provides for higher degrees of supersaturation.

The height of the nitrogen peak in columbium as a function of nitrogen concentration was determined, however. The data are reproduced in Fig. 3. A linear relationship, as predicted by Snoek's theory,[1] was noted with a peak height to wt pct N ratio of 0.33. For most other systems in which this ratio has been measured, such as for carbon and nitrogen peaks in iron and oxygen and nitrogen peaks in tantalum, a value near 1 has been observed.[8-10,12] The present value of 0.33 confirms very well, however, the result of Ang and Wert,[7] who obtained an average value of 0.34 from three determinations. The agreement is particularly satisfying since the methods used for determining nitrogen concentration were so disparate. The method used here is essentially a measurement of the volume of gas absorbed by a specimen of known mass, whereas Ang and Wert had a determination made of the amount of nitrogen extracted.

Diffusion Constants for Carbon and Nitrogen in Columbium—Some time ago, Polder,[9] and later Wert and Zener,[12] showed that the diffusion coefficient for an interstitial impurity in a body-centered-cubic metal is related to the relaxation time for the stress-induced ordering of interstitial impurity atoms through the expression $D = a^2/36\tau$. Here D is the diffusion coefficient; a, the lattice parameter; and τ, the relaxation time. At the temperature at which the internal friction peaks, $\tau = \frac{1}{2}\pi f$, where f is the frequency of the applied stress. Since relaxation times involving diffusional processes can usually be expressed as functions of temperature in the form $\tau = \tau_0 \exp(E/RT)$, the parameters τ_0 and E, the activation energy, can be obtained from plots of logarithm of applied frequency vs reciprocal peak temperature. Such information for both carbon and nitrogen in columbium are tabulated in Table I and are presented graphically in Fig. 4. The diffusion coefficients are found to be $D = 0.0046 \exp(-33{,}300/RT)$ for carbon in columbium and $D = 0.0072 \exp(-34{,}800/RT)$ for nitrogen in columbium. The error limits given in the figure are for the 50 pct confidence limit, appropriate correction having been given for the small sample size.

Because of the rapid aging of the carbon peak, it was not possible to determine the constants for the diffusion of carbon in columbium with the accustomed precision. Even though the constants for nitrogen in columbium have been measured previously and have been collated by Marx, Baker, and Sivertsen,[11] it would appear that the earlier measurements were made with specimens containing nitrogen at high concentration. It is now known that, as a result of interactions between the impurity

Table I. Experimental Data Used in Determining Diffusion Coefficients in Columbium

Specimen Containing 0.018 Wt Pct N		Specimen Containing 0.014 Wt Pct C	
Applied Frequency, Cps	Peak Temperature, °C	Applied Frequency, Cps	Peak Temperature, °C
0.349	267.3	0.155	237.5
0.542	274.4	0.165	238.3
1.005	285.5	0.568	259.3
1.728	295.3	0.710	261.6

atoms themselves, the activation energy is somewhat higher when measured on specimens containing impurities at high concentration in comparison to that for specimens containing low concentrations.[18] It was for this reason that it was considered worthwhile to repeat the measurement.

Internal Friction in Pure Columbium—In all the specimens into which carbon or nitrogen was added, the damping was strictly independent of the strain amplitude, at least up to strains of 10^{-4}. However, for those specimens which were merely evacuated at 2200°C and into which no impurity was back added, the damping proved to be a sensitive function of the strain amplitude, as shown in Fig. 5. It seems best to describe this physical situation as a second mode of mechanical energy absorption which becomes important when the impurity concentration is reduced. The strain amplitude dependence was found to increase with temperature up to those temperatures at which oxygen is absorbed. For columbium specimens in a pendulum through which high purity argon is flowing, this temperature is near 225°C. This absorbed oxygen irreversibly represses the strain amplitude dependent damping. For the most carefully evacuated specimens, the damping is strain amplitude dependent down to amplitudes of at least 10^{-6}. For less completely evacuated specimens or for those which have absorbed very small amounts of impurity, there appears to be a range of strain in which the damping is independent of amplitude. Above a critical amplitude, however, the damping increases rapidly with strain. It was observed that internal friction of this sort is very sensitive to small amounts of plastic deformation, increasing by a factor of 10 or more on application of plastic strain or 10^{-4}. It appears to be independent of frequency.

Internal friction with the characteristics described above has been observed many times previously in various classes of solids.[6,17] It is usually interpreted as arising from the motion of dislocation segments.[17-19] Very possibly, because of the greater binding energies of impurity atoms for dislocations in body-centered-cubic metals, somewhat higher degrees of purity are needed to observe this phenomenon with these metals. The authors' observations have been briefly described to make the point that the onset of this second source of energy absorption imposes a lower limit to the concentration at which investigations relating to the diffusion of impurities in body-centered-cubic metals may be carried out using the internal friction technique. This limit appears to occur in the neighborhood of 10^{-4} to 10^{-3} wt pct impurity.

References

[1] J. L. Snoek: *Physica*, 1941, vol. 8, p. 711.
[2] D. Polder: *Philips Research Reports*, 1946, vol. 1, p. 5.
[3] T. S. Kê: *Physical Review*, 1948, vol. 74, p. 9.
[4] C. A. Wert: *Journal of Applied Physics*, 1950, vol. 21, p. 1196.
[5] C. Y. Ang and C. A. Wert: *AIME Trans.*, 1953, vol. 197, p. 1032; JOURNAL OF METALS, August 1953.
[6] J. W. Marx, G. S. Baker, and J. H. Sivertsen: *Acta Metallurgica*, 1953, vol. 1, p. 193.
[7] R. W. Powers: *Acta Metallurgica*, 1955, vol. 3, p. 135.
[8] R. W. Powers and M. V. Doyle: *Journal of Applied Physics*, 1957, vol. 28, p. 225.
[9] C. Y. Ang: *Acta Metallurgica*, 1953, vol. 1, p. 123.
[10] M. R. Andrews: *Journal* Amer. Chemical Soc., 1932, vol. 54, p. 1845.
[11] T. S. Kê: *AIME Trans.*, 1948, vol. 176, p. 448; METALS TECHNOLOGY, June 1948.
[12] C. A. Wert and C. Zener: *Physical Review*, 1949, vol. 76, p. 1169.
[13] R. W. Powers and M. V. Doyle: *Acta Metallurgica*, 1956, vol. 4, p. 233.
[14] L. J. Dijkstra: *Philips Research Reports*, 1947, vol. 2, p. 357.
[15] J. D. Fast and M. B. Verrijp: *Journal* Iron and Steel Institute, 1955, vol. 180, p. 337.
[16] A. L. Kimball and D. E. Lovell: *Physical Review*, 1927, vol. 30, p. 948.
[17] T. A. Read: *Physical Review*, 1940, vol. 58, p. 371.
[18] A. S. Nowick: *Progress in Metal Physics*, 1953, vol. 4, Interscience Publishers, New York.
[19] A. Granato and K. Lücke: *Journal of Applied Physics*, 1956, vol. 27, p. 583.

Discussion of this paper sent (2 copies) to AIME by Dec. 1, 1957 will appear in AIME *Transactions* Vol. 212, 1958, and in JOURNAL OF METALS, April 1958.

Discussion — Iron & Steel Division*

Hydrogen in Steelmaking Slags 1288
J. H. Walsh, J. Chipman, T. B. King, and N. J. Grant

Self-Diffusion of Iron in Molten Iron-Carbon Alloys 1291
L. Yang, M. T. Simnad, and G. Derge

*TP 4638C

Hydrogen in Steelmaking Slags

by J. H. Walsh, J. Chipman, T. B. King, and N. J. Grant

JOURNAL OF METALS, November 1956, *AIME Trans.*, vol. 206, pp. 1568-1576.

P. Herasymenko *(New York University, New York)*—The authors' experiments on equilibria between water vapor and liquid synthetic slags represent a valuable contribution to our knowledge of the nature of liquid slags. They can be regarded as a proof of ionic splitting of water molecules dissolved in slags. The assumption that water dissolved in slag was completely ionized was made in my report on hydrogen equilibria in steelmaking as early as 1940[1]. In that paper, the first systematic data were given on the content of ionized hydrogen in acid and basic open-hearth slags. The paper probably escaped the notice of the authors, although they mention the articles published later by other investigators who reported erratic and

unreliable measurements of hydrogen content in industrial slags. In our experiments, the slag samples were taken as follows: Slag was cast into a water-cooled iron tube closed at one end; the upper end was provided with a ground joint, so that the tube could be tightly sealed by a cap immediately after casting the sample. Water vapor which evolved from the slag sample during solidification was determined by gas analysis of the air above the sample. The amount of water collected from the air above the sample in the sealed tube was usually smaller than 5 pct of the total hydrogen content of the sample.

The solid slag sample was afterwards quickly transferred from the sealed iron tube into a quartz tube and heated in vacuo at 950 - 1000°C for three hours. Water vapor extracted from slag samples passed through a heated bed of ferromanganese lumps and was converted to hydrogen gas, which was then determined by gas analysis. The weighing of samples was carried out after vacuum extraction. It was found to be essential that slag samples should not be exposed to moist air for a time longer than 2 min, because basic slags absorbed water from the air. Acid slags were not hygroscopic when present in lumps of about ¼ in. size. The average content of hydrogen in acid open-hearth slags determined on a large number of samples was found to be (H) = 12.2 ± 2.0 ppm. The average value reported by the authors is practically the same as ours (12.7 ± 2.1 ppm). This excellent agreement shows that our extraction method was equally as reliable as that described by the authors. Evidently, the diffusion rate of hydrogen ions in slag samples at 950°C was high enough for complete extraction of water from lumps of ¼ in. size in 3 hr.

There is, however, a surprising lack of agreement in the results for the average content of hydrogen in basic slags. The authors report for basic slags the average hydrogen content (H) = 33 ppm, whereas our average value was (H) = 11 ppm, i.e., practically the same as in acid slags. Such a large discrepancy cannot be due to difference in the extraction methods. Basic slags are very hygroscopic, and can easily absorb 20 or more ppm of hydrogen during cooling in air and storing, or even during weighing prior to vacuum extraction. It is not certain if these sources of error were eliminated in the authors' experiments. Further experimental work is necessary to develop reliable analyses of hydrogen in basic slags.

The authors did not consider the possibility of slag-metal equilibria for hydrogen, apparently for the following reasons. They equilibrated acid open-hearth slags with a steam-nitrogen atmosphere at $p_{H_2O} = 0.25$ atm, and found the solubility of (oxidized) hydrogen in slags equal to 33 ppm. Therefore, according to the authors, the solubility of hydrogen in acid slags should be given by the equation:

$$(\text{H ppm}) = 73 \cdot p_{H_2O}^{1/2} \qquad [1]$$

Acid open-hearth slags contained an average of 12.7 ppm; therefore, the activity of water vapor for these slags calculated from Equation 1 should be equal to $p_{H_2O} = 0.03$ atm.

Acid open-hearth steel as made in the United States contains on the average [H] = 3 ppm and [O] = 0.010 – 0.015 pct. Using the thermodynamic data on equilibria:

$$H_2(g) + \tfrac{1}{2}\,O_2(g) = H_2O(g)$$
$$O = \tfrac{1}{2}\,O_2(g)$$

and

$$\overline{H} = \tfrac{1}{2}\,H_2(g)$$

we find that the activity of water vapor in steel is about $p_{H_2O} = 6 \times 10^{-4} - 10^{-3}$ atm, i.e. 30 to 50 times lower than the water vapor activity of the acid slag calculated above. Thus, according to the authors, the activity gradient for water vapor at the slag-metal interface should be very high, and the distance from equilibrium very large.

However, the above reasoning is not convincing. Let us consider the starting point of the above train of thought. In reporting that an acid slag equilibrated with water vapor at 0.25 atm. pressure dissolved 33 ppm hydrogen, the authors tacitly assumed that the slag after this equilibration remained practically the same as the original slag from the open hearth furnace or, at least, that any change in the composition did not affect the hydrogen solubility. However, the oxygen potential of water vapor at 0.25 atm. pressure is so high, that a slag—which, for instance, had the initial composition 19.5 pct FeO, 0.5 pct Fe_2O_3, 20 pct MnO, 4 pct CaO and 56 pct SiO_2—will change its nature so profoundly as to lose any resemblance with the original acid open-hearth slag. Practically all ferrous ions will be oxidized to ferric ions, and solid silica will precipitate from the slag, which was originally saturated with silica. The amount of the remaining liquid phase may be considerably reduced. Therefore, there is no justification in using the *solubility* of hydrogen obtained in such experiments for the calculation of the activity of water vapor in an acid open-hearth slag of entirely different composition. The true solubility of water vapor in slag could be obtained only under a ($H_2 + H_2O$) atmosphere having the ratio of p_{H_2O} to p_{H_2} such that the composition of slag remained the same as it was in the open-hearth furnace. Until such data are available, the authors' conclusion—that hydrogen distribution between slag and metal should be very far from equilibrium—cannot be regarded as proven.

Steelmaking slags always contain suspended droplets of liquid steel—sometimes a few percent of the slag weight. A very high activity of water vapor in slag cannot be maintained in the presence of finely dispersed steel globules. Therefore it is reasonable to assume that the actual activity of water vapor of slags is much lower than that assumed by the authors, and should be near to equilibrium with steel. My own studies on hydrogen contents of the open-hearth furnace slags and steel strongly support the conclusion that hydrogen content of liquid steel is determined by oxidation reduction equilibria such as:

$$2\,H^+ + O^{=} = 2\,\overline{H} + \overline{O}$$
$$2\,H^+ + Fe = 2\,\overline{H} + Fe^{++}$$
$$2\,H^+ + Mn = 2\,\overline{H} + Mn^{++}$$

which are, of course, interdependent. The last equilibrium is the most convenient one—for practical reasons—for the description of hydrogen distribution between slag and metal.

From numerous analyses of steel and slag in the acid open-hearth furnace the equilibrium constant

$$k_H^{Mn} = \frac{[\text{pct H}]^2\,(\text{pct MnO})}{(\text{pct H})^2\,[\text{pct Mn}]} \qquad [2]$$

was calculated. In acid slags the weight percentages of (H) and (MnO) are proportional to ionic concentrations of H^+ and Mn^{++} ions. The value of the constant in Eq. 2 was found to be

$$k_H^{Mn} = 9.7 \text{ at } 1600^\circ\text{C}.$$

This constant decreased with temperature, but the effect of temperature was not determined sufficiently accurately. Fig. 17 shows the content of hydrogen in acid steel as a function of pct Mn and pct MnO at 1600°C and at (H) = 12×10^{-4} pct (12 ppm).

The diagram can be used to explain why different hydrogen contents in steel are observed in different methods of acid steelmaking. In Europe, acid steel is often made with a high content of manganese in the charge, so that the content of manganese during refining varies within the range 0.40 to 0.65 pct Mn. In one method which I described in detail elsewhere,[6] the metal contained about 0.50 pct Mn and the slag around 33 pct MnO at the end of the boil. The observed aver-

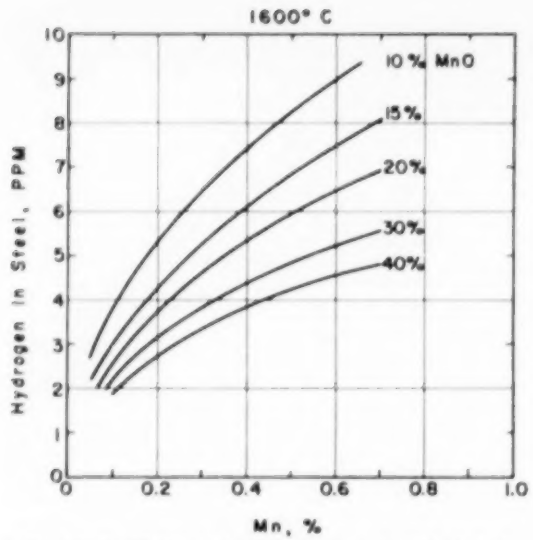

Fig. 17—Equilibrium contents of Hydrogen in acid steel at various contents of Mn (in steel) and MnO (in slag).

age content of hydrogen was 4.5 ± 0.3 ppm. This agrees well with Fig. 17 which predicts 4.6 ppm at 1600°C.

In the American practice,[5] the average residual manganese content is around 0.1 pct and the average content of MnO in acid slag is about 20 pct. According to Fig. 17, the hydrogen content of such steel should be about 2.5 ppm. Carney et al.[28] found a slightly higher value of 3.1 ppm. (average of three heats), and the authors found similar values. Sims et al.[29] reported values ranging from 1.4 to 2.8 ppm. The agreement between the predicted and observed values can be regarded as good, considering the possibility of deviations from the average analyses of slag and metal assumed above, and deviations from equilibria.

The chemistry of basic slags is more involved than that of acid slags. The activity coefficients of basic slag constituents vary considerably with slag composition and are largely unknown. Therefore, only qualitative deductions can be made with respect to the hydrogen equilibria in basic open-hearth furnaces. Let us consider the following reactions leading to the slag-metal distribution of hydrogen and manganese in basic steelmaking:

$$2\,\underline{H} + O = 2\,H^+ + O^= \qquad [3]$$

$$\underline{Mn} + O = Mn^{++} + O^= \qquad [4]$$

It follows that

$$[H] = k_H'' \cdot (H^+) \cdot \left(\frac{(O^=)}{[O]}\right)^{1/2} \qquad [3a]$$

and

$$[Mn] = k_{Mn}'' \cdot (Mn^{++}) \cdot \frac{(O^=)}{[O]}. \qquad [4a]$$

These equations indicate that the contents of hydrogen and manganese in basic steel should increase with increasing content of $O^=$ ions (i.e. with increasing basicity), when other factors are kept constant. The observations illustrated in Fig. 18 confirm this conclusion. In the course of the heats shown in these examples the slag basicity strongly increased with time during the second half of refining, due to gradual solution of lime which was present in excess at the start of refining, and both hydrogen and manganese in steel also increased by reduction from the slag. Accurate determinations of hydrogen in basic slags are required to develop a quantitative theory of hydrogen equilibria in basic open-hearth furnaces. A possible effect of carbon on the activity coefficient of hydrogen in steel also has to be investigated for a complete description of equilibria.

Agitation of the bath of carbon monoxide during the boil facilitates the establishment of equilibria but is inefficient to influence the direction in which these equilibria are displaced by changes of slag and metal composition, or by temperature variations. Of course, the bubbles of carbon monoxide do transfer some hydrogen from steel to the furnace atmosphere but this loss is rapidly compensated by the oxidation-reduction reactions at the slag-metal interface. The establishment of slag-metal hydrogen equilibria should be more rapid than those of, say, manganese or sulfur reactions (and the latter are known to reach equilibria quite easily): the diffusion rate of small hydrogen atoms and ions is certainly higher than that of the larger manganese or sulfur atoms.

A knowledge of the oxidation-reduction equilibria appears to be more important for the control of hydrogen in steel than reliance on the elusive kinetics of the so-called flushing action of the boil.

J. H. Walsh, J. Chipman, T. B. King, and N. J. Grant *(authors' reply)*—The authors wish to thank Dr. Herasymenko for drawing their attention to his 1940 paper[30] and regret having overlooked this contribution.

One of the points at issue is whether our method of sampling and analysis for basic open hearth slags is reliable. These slags were sampled in several different ways involving different rates of cooling but no appre-

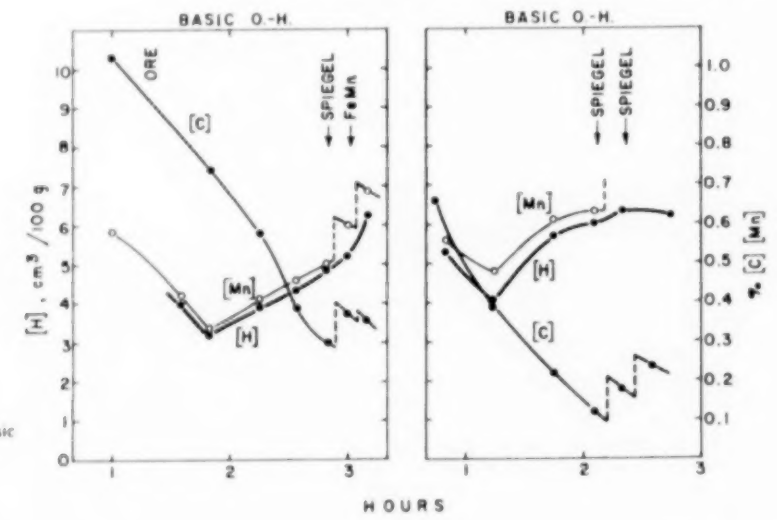

Fig. 18—Logs of two basic open hearth heats.

ciable differences in the analyzed hydrogen content was found. We agree that basic slags can pick up moisture from the air, especially those slags which contain undissolved lime, but feel that our own sampling procedure avoids this. Slag samples were stored in a desiccator to prevent pick-up of surface moisture and a freshly-broken piece was always used for analysis.

We do not agree that the correspondence between our results and those of Dr. Herasymenko for acid slags represents a proof that his extraction method is reliable. In this connection we would refer Dr. Herasymenko to a recent paper by S. Sawa.[25] Sawa's results suggest that only part of the water is removed from basic slags by vacuum extraction at temperatures as low as 950°C, and that temperatures above the melting point are necessary to remove all the water in times as short as three hours.

A second question concerns whether slag-metal equilibrium with respect to hydrogen is reached in open-hearth furnaces. The authors do not share Dr. Herasymenko's faith in equilibrium constants derived from operating data. It is known however that a steady-state distribution of manganese between slag and metal is reached in basic open-hearth furnaces in a relatively short period, say 40 minutes, after a major addition has been made. Darken,[26] has suggested that the rate of approach to manganese equilibrium is governed by transport of manganese in the metal to the metal-slag interface. The rate-controlling factor in the transfer of hydrogen from slag to metal is by no means so simple, though it is certainly not likely to be the transport of hydrogen in the metal. Hydrogen is present in the gas phase as water vapor, in the slag as hydrogen or hydroxyl ions, in the metal as protons or hydrogen atoms, and in the boil gases as gaseous hydrogen. That the boil gases do remove considerable quantities of hydrogen is quite clearly confirmed by the work of Kalling and Rudberg.[27] Epstein, Chipman, and Grant[28] have shown that, to account for experimental observations the furnace atmosphere must supply comparable quantities of hydrogen to the metal through the slag. For slag-metal equilibrium to be attained with respect to hydrogen one would have to postulate that the relevant slag-metal reaction is very much faster than the slag-atmosphere or metal-boil gas reactions. Such a possibility seems very unlikely. Slag-metal equilibrium with respect to manganese is an entirely different case since only the slag-metal reaction takes place. If we continually added manganese to the metal we would not expect equilibrium to be maintained. In the open-hearth furnace, while the boil is proceeding, one would logically expect the activity of water vapor in the slag to be intermediate between that in the metal and that in the furnace atmosphere. This is exactly what our results show.

Dr. Herasymenko's objection to such a conclusion is that the experiments in which furnace slags were equilibrated in the laboratory with atmospheres containing water vapor may not have been properly conducted and that the equilibrium solubility of hydrogen may be much higher.

If we assume for the moment that an acid slag containing 12.7 ppm hydrogen is indeed in equilibrium with the metal, for which $p_{H_2O} = 10^{-3}$ atm, then the solubility equation is approximately, using Dr. Herasymenko's figures,

$$(\text{H ppm}) = 400 \cdot p_{H_2O}^{1/2}.$$

For $p_{H_2O} = 0.25$ the solubility of hydrogen would then be 200 ppm. It is quite inconceivable that the experimental values of 30 to 40 ppm are so seriously in error. Recent experiments[29] suggest that the oxygen pressure has no appreciable influence on the solubility of hydrogen in iron-silicate slags or in basic open-hearth slags.

[25] P. Herasymenko and P. Dombrowski: Archiv fur das Eisenhuttenwesen, 1940, vol. 14, p. 109.
[26] P. Herasymenko: *Journal of the Iron and Steel Institute*, 1947, vol. 157, p. 515.
[27] G. R. Fitterer: *Trans. ASM*, 1945, vol. 34, p. 1.
[28] D. C. Carney, J. Chipman, and N. J. Grant: Electric Furnace Steel Proceedings, 1948, *AIME*, vol. 6, p. 34; *Trans. AIME*, 1950, vol. 176, p. 397.
[29] C. E. Sims, G. A. Moore, and D. W. Williams: *AIME*, Techn. Publ. No. 234, *Metals Technology*, Feb. 1948.
[25] P. Herasymenko and P. Dombrowski: Archiv fur das Eisenhuttenwesen, 1940, vol. 14, p. 109.
[25] S. Sawa: *Journal of the Iron and Steel Institute of Japan*, Aug. 1956, vol. 42, No. 8, p. 638.
[26] L. S. Darken: *Basic Open Hearth Steelmaking*, *AIME*, New York, 1951.
[27] B. Kalling and N. Rudberg: Jernkontorets Annaler, 1938, vol. 122, p. 91.
[28] H. Epstein, J. Chipman, and N. J. Grant: JOURNAL OF METALS, April 1957; *AIME Trans.*, vol. 206, p. 601.
[29] J. M. Uys: Unpublished results, M.I.T., 1956.

Self-Diffusion of Iron in Molten Iron-Carbon Alloys

by L. Yang, M. T. Simnad, and G. Derge

JOURNAL OF METALS, November 1956, *AIME Trans.*, vol. 206, pp. 1577-1588.

James Lommel and Bruce Chalmers *(Harvard University, Cambridge, Mass.)*—Comparison of the values of physical constants whose accuracies are unknown can lead one into drawing unwarranted conclusions. The standard deviation or probable error of an empirical constant is just as much a part of it as its value since no physical measurement can be made with absolute accuracy. The authors have presented the values of diffusion constants for the self-diffusion of iron in liquid iron-carbon alloys without including an estimate of their accuracy. A statistical analysis of the accuracy of these experiments would indicate the reliability of the diffusion data and whether there is a real difference in the activation energy and D_o for the two different carbon-content alloys.

It is obvious from Fig. 4 of the paper, a plot of log D vs $1/T$, that there was a considerable spread in the values of D at a fixed temperature. There were many possible sources of error: insufficient counting time of radioactive samples, uncertainty in the length of the capillary diffusion sample, the time of the run, etc. Random errors in these quantities can give rise to a spread in the values obtained for D. Statistical analysis of the effects of errors in these quantities on the values obtained for D would show if they are the only ones responsible for the observed spread in the values of D. Errors introduced by convective mixing in the diffusion capillary would be suspected if the spread in D values could not be adequately explained on the basis of errors in the above quantities.

The data given in Table I were analysed by the method of least squares to obtain the best straight line in a plot of log D vs $1/T$ for each carbon content. It was assumed that the random errors in D were much greater than those in $1/T$ and the errors in the latter were neglected. The values calculated for Q, the activation energy, and log D_o are given below, along with their standard deviations. These standard deviations were obtained by calculating the mean square deviation of the observed values of log D from the least squares straight line and using the appropriate multiplying factor following the technique described by Davies.[30]

Least Squares values for Q and log D_o for self-diffusion of Fe in Fe-C alloys:

Pct C	Q, cal per mole	Log D_o	D_o, sq cm per sec
4.6	11,180 ± 3,610	−3 + .490 ± .504	3.1x/3.2 10^{-3}
2.5	16,070 ± 5,130	2 + .068 ± .216	1.17x/1.64 10^{-3}

To test if there was an effect of carbon content on the diffusion coefficient and activation energy for dif-

fusion the t distribution was used to see if there was a significant difference in the values of Q, and log D_o, for the two carbon content alloys. The statistical hypothesis is that there is no difference in Q, and log D_o, for the two alloys. It was found that the experimentally obtained difference in the two values of Q could be expected once every two times this experiment was repeated. In the case of log D_o, as large a difference in the two values as that obtained experimentally could be expected in 30 pct of the experiments. These probabilities are not large enough to reject the hypothesis that there is not a significant difference in the values of Q, and log D_o, for the two alloys.

Because of the large scatter in the values of D, the authors have not substantiated their claim that the carbon content of a liquid iron-carbon alloy influences the diffusivity of iron and the activation energy associated with it.

L. Yang, M. T. Simnad, and G. Derge *(authors' reply)*—The careful analysis of our data by the discussers is appreciated by the authors. We wish to point out that in the text no strong claim is made for the significance of the apparent small change in activation energy of diffusion with carbon content. However, we cannot agree that the data do not show a dependence of diffusivity on composition. The following additional analysis of our data is offered.

The random error involved in our experimental measurement is estimated to be about ± 5 pct which would cause a scattering of about ± 10 pct in the D values. This is approximately the degree of scattering in our experimental D values. Although we are by no means certain that the errors due to convection and the deviations from the boundary conditions are completely eliminated, we think we have minimized them by discarding uncontrolled samples as identified by our autoradiographic and sectioning methods.

Assuming that the relationship $D = D_o \exp(-\Delta H/RT)$ holds, and that the errors in log D are normally distributed about $1/T$, we obtained the following equations for a 50 pct confidence limit by using the methods described by Hald[20].

$$D = (3.09 \pm 0.10) \times 10^{-1} \exp[(-11200 \pm 3500)/RT]$$
for carbon = 4.6 pct

$$D = (1.23 \pm 0.02) \times 10^{-2} \exp[(-16200 \pm 4950)/RT]$$
for carbon = 2.5 pct

Subsequent t-tests show that the two values of activation energy are significantly different only at the 50 pct level. However, the same test also shows that the two lines (therefore the log D_o values) are significantly different at the 95 pct level. This substantiates that the self-diffusion coefficient of iron in the 4.6 pct C melt is higher than that in the 2.5 pct C melt.

We certainly agree that the small observed difference in activation energy does not have statistical significance. However, the possibility of such a difference should not be overlooked, since it can be correlated with other types of evidence. Calculations based on viscosity data of Wimmer and Theilmann[21] indicates that the values of activation energy for viscous flow are about 12, 16 and 17 kcals per mole for melts containing 4, 3 and 2.5 pct C respectively. It is interesting to see that their change with carbon content is similar to that observed for self-diffusion.

[19] O. L. Davies: *Statistical Methods in Research and Production*, Oliver and Boyd, London, 1947, pp. 118-167.

[20] Hald: *Statistical Theory with Engineering Applications*, John Wiley & Sons, New York, 1952, Ch. 18.

[21] Wimmer and Theilmann: *Stahl und Eisen*, 1947, vol. 47, p. 389.

Discussion — Extractive Metallurgy Division*

Selective Sulfation for Cadmium Recovery at Josephtown Smelter 1292
R. E. Lund and D. E. Warnes

Basal Plane Development in Electrodeposited Hexagonal-Close-Packed Metals: Zinc, Titanium, and Zirconium 1293
W. R. Opie

The Vapor Pressure of Liquid Copper and Activities in Liquid Iron-Copper Alloys 1293
J. P. Morris and G. R. Zellars

*TP4639D

Selective Sulfation for Cadmium Recovery at Josephtown Smelter

by R. E. Lund and D. E. Warnes

JOURNAL OF METALS, April 1957, *AIME Trans.*, vol. 206, pp. 608-611.

H. G. Haemers *(Ghent University, Belgium)*—The authors claimed "the results of their work indicate that the metals can be arranged in a sulfation series similar in its application for selective sulfation tot the electromotive series for displacement of metals from solution".

The series as stated in decreasing order for tendency of SO_3 give up, is the same as that stated by free energy diagrams. Indeed, the degree of stability of a sulfate is measured by the free energy of sulfate formation out of the corresponding metal oxide and SO_3. The more negative the value of the free energy $(-DG)$ the greater the stability of the sulfate.

As a second consequence this statement results in a relative aptitude for capture of SO_3 by each metal oxide when brought in contact with the sulfate of other metals. Let M_1 and M_2 be the two metals, and $-DG_1$ and $-DG_2$ their free energy values at temperature T. Both sulfates are stable at temperature T if $-DG_1 < O$ and $-DG_2 < O$.

In case where $-DG_1 < -DG_2$ the stability of M_1SO_4 is greater than that of M_2SO_4, and when M.O (oxide of

M_2O is brought in contact with M_2SO_4 the equilibrium-reaction proceeds to formation M_2SO_4 and MO, thus forming the most stable component.

$$M_2O + M_2SO_4 \rightarrow M_2SO_4 + MO$$

The free energy diagram of sulfation gives up the series: $Fe_2(SO_4)_3$ — $Al_2(SO_4)_3$ — $CuSO_4$ — $ZnSO_4$ — $FeSO_4$ — $CdSO_4$ — $PbSO_4$ where the authors found the following order: $FeSO_4$ — $Fe_2(SO_4)_3$ — $Al_2(SO_4)_3$ — $CuSO_4$ — $ZnSO_4$ — $CdSO_4$ — $PbSO_4$.

The fact that $FeSO_4$ is situated at top of the series as stated by the authors, is probably due to the following facts: a)—oxidizing character of the oven atmosphere; b)—the influence of the humidity in the oven gases.

As the $-DG$ of the reaction $2\ FeO + O_2 \rightarrow 2\ Fe_2O_3$ is negative, it seems that Fe_2O_3 is more stable than FeO; i. e., the formation of a higher oxide of iron out of FeO is very probable. This explains why the authors state the order $FeSO_4$ — $Fe_2(SO_4)_3$ when it is known that $FeSO_4$ is more stable than $Fe_2(SO_4)_3$. In the oxidizing medium the iron will be converted to the ferric-state, thus becoming a very active sulfation agent.

Basal Plane Development in Electrodeposited Hexagonal-Close-Packed Metals: Zinc, Titanium, and Zirconium

by W. R. Opie

JOURNAL OF METALS, September 1956, *AIME Trans.*, vol. 206, pp. 1192-1194

R. Weil *(Stevens Institute of Technology, Hoboken, N. J.)* **and H. J. Read** *(Pennsylvania State University, University Park, Pa.)*—It is interesting that Mr. Opie found essentially the same structural types in the surfaces of thick deposits as we[1] observed in thin ones. We also noted the same relationship between microstructure and brightness. The surfaces of bright deposits can consist of either fine nodules (a structure which Mr. Opie called mammillar) or aligned platelets, which may be coarser. This relationship is probably the reason why it has not been possible to establish a correlation between brightness and the degree of preferred orientation[2] or between brightness and grain size[3]. It is well known that such correlations have been widely postulated in the electroplating industry.

In a comprehensive investigation of the structure of electrodeposits, based largely on electron microscopy, we[1] found that many nodular and acicular structures consist of platelets, the basal planes of which are oriented almost perpendicular to the surface of the deposit.

It is hoped that Mr. Opie's work will encourage more research in the metallurgy of electrodeposits, especially in view of progress which has been made in explaining some structural features of vapor deposits by the dislocation theory. In this connection, it may be of interest that we observed evidence of growth by screw dislocations in a very thin nickel deposit which was stripped from the basis metal, examined directly in the electron microscope, and the structure of which is shown in Fig. 15.

[1] R. Weil and H. J. Read: *Metal Finishing*, Nov. 1954, p. 60, Dec. 1955, p. 60; Jan. 1956, p. 51.
[2] W. H. Smith, J. H. Keeler, and J. H. Read: *Plating*, 1949, vol. 36, p. 355.
[3] H. J. Read and R. Weil: *Plating*, 1950, vol. 37, p. 1257.

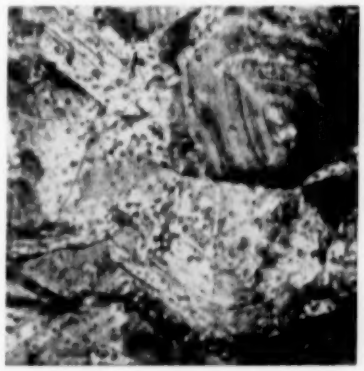

Fig. 15—Microstructure of electrodeposited nickel showing evidence of growth by screw dislocation. X500.

The Vapor Pressure of Liquid Copper and Activities in Liquid Iron-Copper Alloys

by J. P. Morris and G. R. Zellars

JOURNAL OF METALS, August 1956, *AIME Trans.*, vol. 206, pp. 1086-1091

F. C. Langenburg *(Crucible Steel Company, Pittsburgh)*—The authors are to be congratulated for a fine research. Their experimental techniques are good, and the data on the activity of copper in liquid iron is important in view of a rising residual copper level in steelmaking.

Two related investigations which are as yet unpublished should be mentioned now for a comparison with the present authors work. Koros and Chipman[1] have determined the activity coefficient of copper in liquid iron at 1600°C. They measured the distribution of copper between liquid silver and iron at 1600°C. From this data and the activity of copper in silver, obtained from the Ag-Cu phase diagram, the activity coefficient of copper up to three atom percent in iron was found. The value of the activity coefficient of copper at infinite dilution with pure liquid copper as the standard state was 8.0. Langenberg[2] has also determined the activity coefficient of copper in liquid iron. The distribution of copper between pure iron and lead was measured at 1600°C. The activity of copper in lead was determined from the Cu-Pb phase diagram. Utilizing the heat of mixing in copper-lead alloys, and the experimental distribution data, a value for the activity coefficient of copper at infinite dilution in iron of 8.8 was obtained.

The authors' experimental techniques should be applicable to determining the activities of other residual elements in iron. It it suggested that research on the activity of tin in iron, and perhaps nickel, would be most useful.

[1] P. J. Koros and J. Chipman: *Activity Coefficient of Copper in Liquid Fe, Fe-C, and Fe-C-Si Alloys at 1600°C*. Submitted to AIME.
[2] F. C. Langenberg: *The Activity Coefficient of Copper in Liquid Iron at 1600°C*. Submitted to AIME.

Discussion — Institute of Metals Division*

Action of Vibration on Solidifying Aluminum Alloys 1295
P. D. Southgate

Constant Strain Rate Bend Tests on Hydrogen-Embrittled High Strength Steels 1296
W. Beck, E. P. Klier, and G. Sachs

Creep of Polycrystalline Nickel 1297
J. Weertman and P. Shahinian

Creep of Single Crystals and Polycrystals of Aluminum, Lead, and Tin 1299
C. D. Wiseman, O. D. Sherby, and J. E. Dorn

Delayed Yielding in a Substitutional Solid Solution Alloy 1301
L. A. Sheppard and J. E. Dorn

Effect of Orientation on the Plastic Deformation of Aluminum Single Crystals and Bicrystals 1302
R. S. Davis, R. L. Fleischer, J. D. Livingston, and Bruce Chalmers

Effect of Rolling Procedure on the Kinetics of Recrystallization of Cold-Rolled Copper 1303
J. T. Michalak and W. R. Hibbard, Jr.

Effect of Temperature on the Flow Stress and Strain Hardening Coefficient of Magnesium Single Crystals 1303
H. Conrad and W. D. Robertson

Embrittlement of Ti-Al Alloys in the 6 to 10 Pct Al Range 1304
F. A. Crossley and W. R. Carew

Etch Pits and Dislocations in Zinc Monocrystals 1305
J. J. Gilman

Flaking of Heavy Alloy Steel Sections 1306
C. R. Garr and A. R. Troiano

Grain Boundary Displacement vs Grain Deformation as the Rate Determining Factor in Creep 1308
J. A. Martin, M. Herman, and N. Brown

Internal Friction and Grain Boundary Viscosity of Copper and of Binary Copper Solid Solutions 1309
L. Rotherham and S. Pearson

Magnetic Method for the Measurement of Precipitate Particle Sizes in a Cu-Co Alloy 1309
J. J. Becker

Nucleation of Voids in Metals During Diffusion and Creep 1310
R. Resnick and L. Seigle

On the Nature of Embrittlement Occurring While Tempering a Ni-Cr Alloy Steel 1310
G. Bhat and J. E. Libsch

Some Properties of Certain High-Conductivity Copper-Base Alloys 1311
Webster Hodge

Strain Induced Transformation in Beta Brass 1312
T. B. Massalski and C. S. Barrett

Strength of Silver Brazed Joints in Mild Steel 1312
M. G. Moffatt and J. Wulff

Studies on Diffusion in Molten Metals 1314
K. Niwa, M. Shimoji, S. Kado, Y. Watanabe, and T. Yokokawa

The Martensite Transformation in the Iron-Nickel System 1314
Larry Kaufman and Morris Cohen

Upper Nose Temper Embrittlement of a Ni-Cr Steel 1316
L. D. Jaffee and D. C. Buffum

*TP4640E

Action of Vibration on Solidifying Aluminum Alloys

by P. D. Southgate

JOURNAL OF METALS, April 1957, *AIME Trans.*, vol. 209, pp. 514-517

A. N. Turner *(Aluminium Laboratories Ltd., Banbury, Oxon, England)*—It should not be assumed from the information given by Southgate that the application of ultrasonic energy to solidifying melts of aluminum-based alloys will necessarily decrease segregation tendency. Fig. 6 refers to experiments carried out in 1947 at Aluminium Laboratories Limited, Banbury, in a manner very similar to that described, using a 120 watt 26 kc generator operating on 20 lb melts cooling slowly in plumbago crucibles. Chemical analyses were made at standard positions from the top and bottom of a number of aluminum-copper and aluminum-silicon alloy melts; the difference in analysis between the top and bottom is plotted as a function of melt analysis in Fig. 6a for aluminum-copper alloys and in Fig. 6b for aluminum-silicon alloys, both for ultrasonically treated and for *blank* melts. It may be seen that in the case of aluminum-copper alloys, a tendency towards gravity segregation apparent in normally solidified melts was greatly increased by the application of ultrasonics; there was no tendency towards segregation in alloys containing less than 8 pct Cu or at the eutectic composition. In the case of Al-Si alloys, no segregation tendency was shown in normally solidified hypo-eutectic alloys, but ultrasonic agitation caused a separation of primary aluminum solid solution dendrites towards the bottom of the crucible, leaving a silicon-rich portion at the top; again there was no tendency towards segregation at the eutectic composition, but marked segregation of primary silicon occurred in the hypereutectic range.

A number of papers have been published recently reporting the influence of vibration, sonic and ultrasonic, on the metallurgical structure of metal melts, but few of these have referred to treatment on a large scale. The following notes concerning the use of ultrasonic vibrations during semi-continuous casting may therefore be of interest. A 1500 watt 26 kc generator was used and experiments carried out on 5 in. diam billets, and ingots of 20 x 6 in. cross-section. Under no conditions was it found to be possible to get grain refinement of commercial-purity aluminum, Al-1.25 pct Mn, or Al-12 pct Si, although this had been accomplished when these alloys were solidified statically in crucibles. It was, however, found to be possible to refine intermetallic phases greatly in cases where these appeared

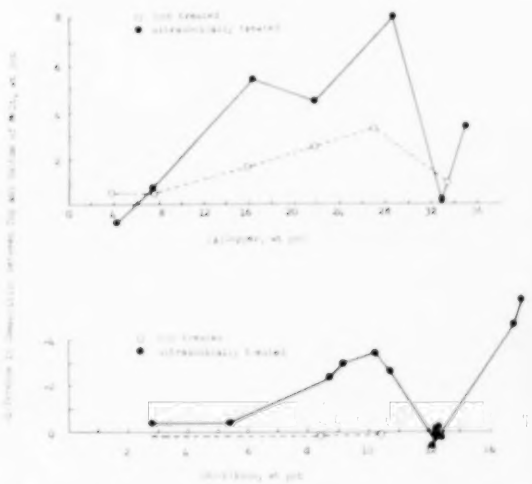

Fig. 6—Influence of ultrasonic vibration on tendency towards segregation of (A) aluminum-copper alloys, and (B) aluminum-silicon alloys.

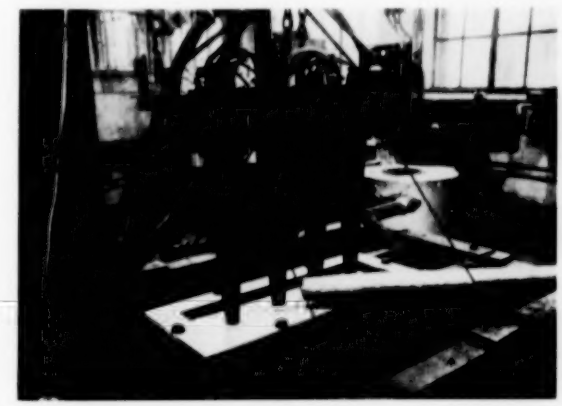

Fig. 7—Treatment of semi-continuously cast ingots of 20 x 6 in. cross-section.

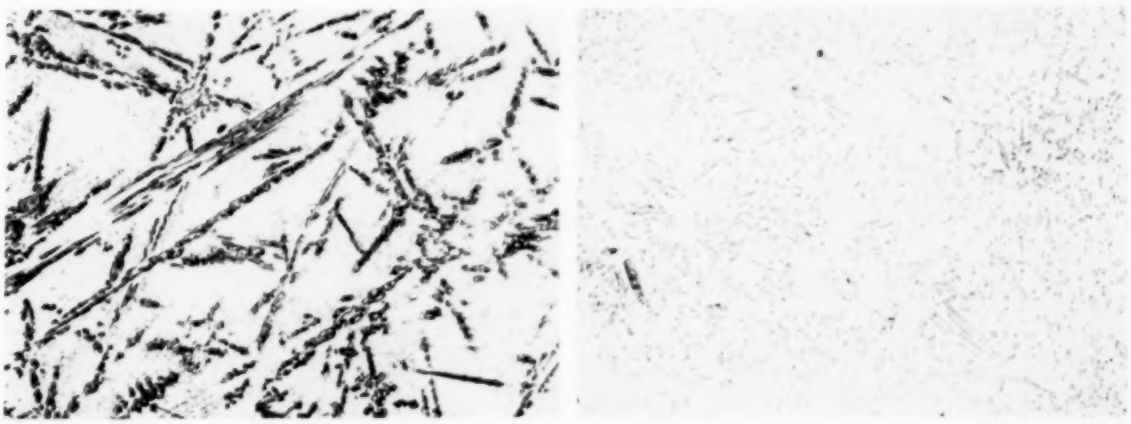

Fig. 8—Break-up of primary $MnAl_6$ produced by ultrasonic treatment of a semi-continuously cast ingot of 20 x 6 in. cross-section of an Al-4 pct Mn alloy. Left: untreated; right: treated. X20.

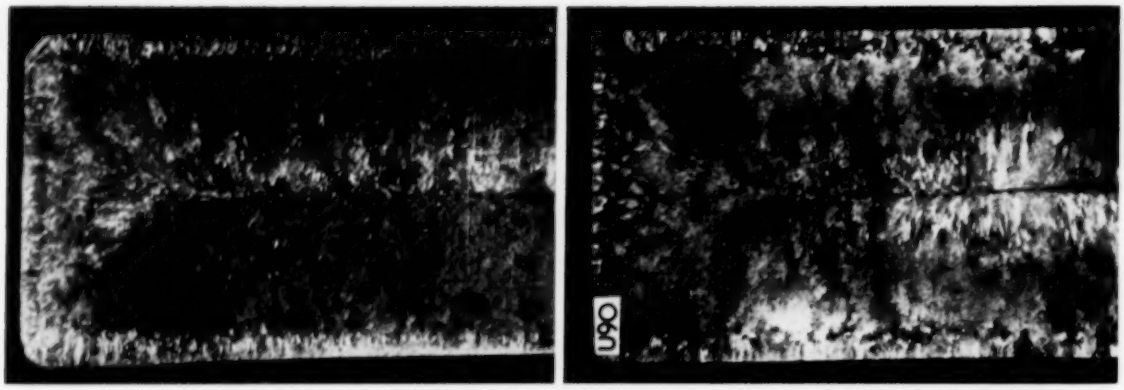

Fig. 9—Treatment of Al-4 pct Mn alloy showing break-up of primaries but lack of grain refinement. Left: untreated; right: treated. X½.

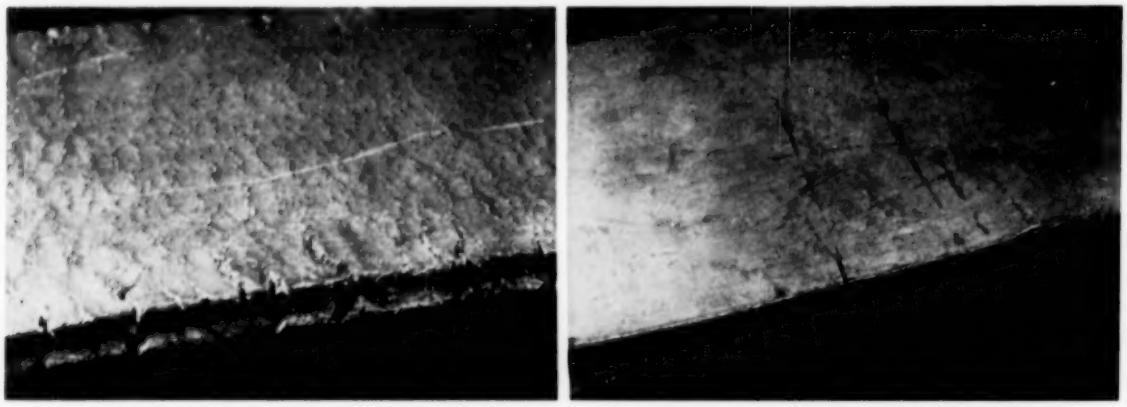

Fig. 10—Effect of ultrasonic treatment on rolling characteristics of a transverse section of a 20 x 6 in. semi-continuously cast ingot in an Al-4 pct Mn alloy. Slab hot rolled from 2 to 1 in. Left: untreated; right: treated. X½.

as primaries. The experimental set-up in the case of the 20 x 6 in. ingots is shown in Fig. 7; an electrical energy of 350 watts was applied to each transducer, and the probe tips were heated to a dull red heat before use and immersed to a depth of about ⅛ in. in the molten metal pool. The degree of primary break-up can be seen from Fig. 8, while the lack of grain refinement is shown in Fig. 9.

The effect on the rolling characteristics of the alloy may be seen from Fig. 10 which illustrates the condition of hot mill slab of 1 in. thickness, rolled from 2 in. thick transverse slices cut from 20 x 6 in. ingots. Deep crazing along the $MnAl_4$ needles was obtained in the normally cast alloy; perfectly satisfactory slab was obtained from the ultrasonically heated ingot, which could be rolled further to thin sheet.

Constant Strain Rate Bend Tests on Hydrogen-Embrittled High Strength Steels

by W. Beck, E. P. Klier, and G. Sachs

JOURNAL OF METALS, October 1956, *AIME Trans.*, 1956, vol. 206, pp. 1263-1268.

J. H. Maker and W. R. Johnson *(Wallace Barnes Company, Bristol, Conn.)*—The phenomenon of delayed fracture at stresses well below the fracture stress is a subject of much concern in high strength steels, particularly when the parts are plated. However, this problem is not new to the spring industry, which has been using highly stressed components at very high hardness levels for many years. We are happy to see this study and others on the subject which throw light on the explanations for the occasional service failure in plated springs stressed at supposedly safe levels. Several years ago we undertook to study the phenomenon of embrittlement due to plating by means of a test similar to that described by the authors; actually the test is one very old to the makers of flat high carbon strip for springs.

Our test is somewhat different, since we normally must deal with a range of stock thicknesses. The measure of ductility is the parameter of stock thickness divided by the jaw gap at which fracture occurred. This distance is known as the *break distance* and the test as the *break test*. A chart of experimentally determined values for high carbon spring steel strip, continuously hardened, is given in the graph. Specimen length in this test is unimportant, at least in the range of thicknesses tested, provided sufficient length is present to form a U shape considerably before fracture. One important consideration is that the

width-thickness ratio be at least 10, or lack of lateral constraint will result in an apparently higher ductility.

The break test has been found to be a consistent and workable test for investigating hydrogen embrittlement, both of plated and unplated specimens. It is important to note that valid results can be obtained merely with a bench vise and a 6 in. decimal scale. Using this test, we noticed that plated specimens of high hardness held in jaws at distances somewhat larger than the break distance often fractured after an hour or so. This knowledge was used in developing routine lock-up tests on troublesome springs. In general, if there are no faliures in the test, which is conducted at stresses higher than the anticipated service stress, it has so far proved to be a safe indication that the springs would not fail in service.

It was also found that the effect of slow strain rates could be approximated by a stepping procedure, increasing the deflection after fixed holding intervals until fracture occured. We are intrigued with the concept of the relation of *break distance* at fracture to percent elongation, but with one qualification. This test is quite sensitive to surface conditions such as carburization, decarburization, roughness, grain boundary oxidation, and residual stresses. Even careful grinding, while it removes the surface layers, may introduce non-uniform residual stresses. Have the authors checked their grinding procedure by stress relieving after grinding at a temperature lower than the original tempering temperature?

W. Beck, E. P. Klier, and G. Sachs *(authors' reply)*—The authors have been aware of the use of the *break test* used in the spring industry from the publications by Noble[10] and by Eakin & Lownie.[11] However, Bastien & Azou[12] appear to be the first who showed that hydrgen embrittlement greatly depends upon the rate or the duration of load application. It is interesting to note that now attention is being paid to this factor, but apparently, no reliable standard procedure has yet been developed for springs.

Regarding such effects as decarburization, surface roughness, residual stresses, etc., it may be stated that very careful grinding with flood cooling is used at Syracuse University in order to insure reproducible values of hardness, tensile strength, fatigue strength, notch strength, etc., of high-hardness steels. This procedure removes decarburization and produces consistent surface roughness, and state of residual stress. The

Fig. 12—Normal break test curves for 90 — 1.05 pct carbon steel continuously hardened. Width-thickness ratio 10:1 or more.

break test also yields consistent results with unembrittled strip specimens.

Unfortunately, however, this technique still fails to result in good conformance of hydrogen-embrittlement data. Stress-relieving cannot be applied as it reduces the hydrogen content.

[10] H. J. Noble: Hydrogen Embrittlement, *Iron Age*, Nov. 27, 1941, vol. 148, p. 45.

[11] C. T. Eakin & H. W. Lownie: Reducing Embrittlement in Electroplating, *Iron Age*, Nov. 21, 1946, vol. 158, p. 69.

[12] P. Bastien & P. Azou: Effect of Magnitude and Rate of Straining on the Segregation of Hydrogen in Iron and Steel, *Comptes Rendus*, 1951, vol. 232, p. 69.

Creep of Polycrystalline Nickel

by J. Weertman and P. Shahinian

JOURNAL OF METALS, October 1956, *AIME Trans.*, vol. 206, pp. 1223-1226.

J. D. Meakin *(Leeds University, Leeds, England)*—In their paper the authors have sought to confirm a creep law of the form

$$d\epsilon/dt = A(\text{stress})^n \exp(-Q/kT) \qquad [2]$$

Their Fig. 2 shows the experimental justification for such a law. A close examination of the graph however indicates that at each temperature a power law of different index should be used. The line shown only applies to the results obtained at 1100°C to any reasonable extent and from the points shown it appears that as the temperature rises the power applicable should decrease (see values at 600° and 900°C in particular). It is possible to fit a power law to a "sinh" curve over considerable ranges under certain conditions as shown by Feltham.[13] In order to test the applicability of such a law to the creep results on nickel each series of tests at a particular temperature were plotted assuming a law of the form

$$d\epsilon/dt = \dot{\epsilon} \sinh(q\sigma^2/kT). \qquad [3]$$

It was found that within the apparent experimental scatter this law was obeyed, q being a stress independent constant, characteristic of the temperature of test.

As shown by Diehl et al.[14] the process of climb by dislocations in face centered cubic metals to explain creep must be rejected on energetic considerations. In order to explain observed creep rates and slip line formation at high temperatures Mott[15] concludes that the rate controlling mechanism is the movement of screw dislocations containing jogs. This theory is successfully applied by Feltham[16] to the creep of lead. The creep rate should then depend on stress according to a law of the form

$$d\epsilon/dt = \nu(b/d)\exp(-W/kT)\sinh(\lambda b^3\sigma/kT) \qquad [4]$$

where λ is the separation of jogs, b the Burgess vector, and d the separation of active planes. Clearly q would be expected to vary with temperature.

From an analysis of published work by Tyte on lead and tin, and work on copper, which it is hoped to publish in the near future, an exponential variation of q

with temperature of general validity seems to apply. From Weertman's results on nickel, values of q were determined varying from 0.7×10^{-7} °K (dynes per sq cm)$^{-1}$ at 400°C to 7.7×10^{-7} at 1100°C, and obeying an exponential variation with temperature. (The result at 400°C is rather indeterminate.)

On attempting to correlate all the creep results using a law of the form

$$d\epsilon/dt = A \exp(-Q/kT) \sinh(q\sigma/kT) \quad Q = 65 \text{ kcals.} \quad [5]$$

reasonable agreement is obtained except for the results at 400°C and 600°C (Fig. 4).

Work by Sherby and his co-workers[29] on aluminum and copper have indicated that the activation energy for creep is only equal to that for self diffusion above a temperature of about $0.5T_m$ K°. The results on nickel cover a temperature range of about 0.4-0.8 T_m with $0.5\ T_m = 590$°C. Below $0.5\ T_m$ it is expected that an activation energy of about 2/3 that for self diffusion should apply, and using this value good correlation is obtained for the results at 400°C and 600°C. Further support for the use of a reduced activation energy has been obtained by Dr. Weertman himself and Dr. Breen[30] on the creep of tin, in which they find a reduction in the activation energy for creep of one half below 130°C.

A point of interest is the divergence of the curves (Fig. 4) from the law predicted by Eq. [5] at low stresses. Although the results are too few for accurate estimation of the point of divergence, the tensile stress is of order 10×10^7 dynes per sq cm at 1100°C and 25×10^7 dynes per sq cm at 800°C. In Friedel's[31] paper on hardening in face centered cubic metals he estimates that the termination of linear hardening should occur when $(\tau_1/T) = 7 \times 10^7$ cgs. This gives the critical tensile stress ($= 2\tau_1$) at 1000°C of about 15×10^7 dynes per sq cm, which is of the order found for the divergence of the author's results. It is suggested that it may be due to the mode of hardening changing as the stress falls below τ_1, creep being considered a dynamic equilibrium between hardening and recovery. Work on copper in these laboratories which it is hoped to publish in the near future shows striking parallels with the results for nickel, especially in relation to the variation of q with temperature.

[28] P. Feltham: *Journal of Applied Physics*, 1955, vol. 6, p. 26.
[29] J. Diehl, S. Mader, and A. Seeger: *Zeit. Metallkunde*, 1955, vol. 46, p. 650.
[30] N. F. Mott: *Symposium on Creep and Fracture of Metals at High Temperatures*, H.M.S.O. 1956.
[31] P. Feltham: *Proceedings, Phys. Soc. B.*, (in the press).
[32] O. D. Sherby, J. L. Lytton, J. E. Dorn: Minerals Research Laboratory Report 46, Univ. of California, Berkeley.
[33] J. Weertman, J. E. Breen: *Journal of Applied Physics*, 1956, vol. 27, p. 1189.
[34] J. Friedel: *Philosophical Mag.*, 1955, vol. 46, p. 1169.

J. Weertman and P. Shahinian *(authors' reply)*—Mr. Meakin questions the nature of the stress dependence of the creep rate. At low stresses we believe it to be a power law; he believes it to be a temperature-modified hyperbolic sine law. Since our data appear to fit both laws it is desirable to examine the question of how great a stress range must be covered before it can be conclusively shown which law is obeyed. (Since the "sinh" law contains a term q which it is argued depends very sensitively on the temperature, only tests carried out at some fixed temperature can be considered.) A simple calculation shows what the stress range must be. Thus let the creep power law be

$$K = C\sigma^n \quad [6]$$

where K is the creep rate, σ is the stress, C and n are constants; let the sinh law be

$$K^* = C^* \sinh(q\sigma/kT) \quad [7]$$

where K^* is the creep rate and C^* is another constant. Eqs. 6 and 7 define two curves of creep rate versus stress. By adjusting the values of C and C^* these curves can be made tangent to each other at any stress σ_0. On setting $K = K^*$ and $dK/d\sigma = dK^*/d\sigma$ at

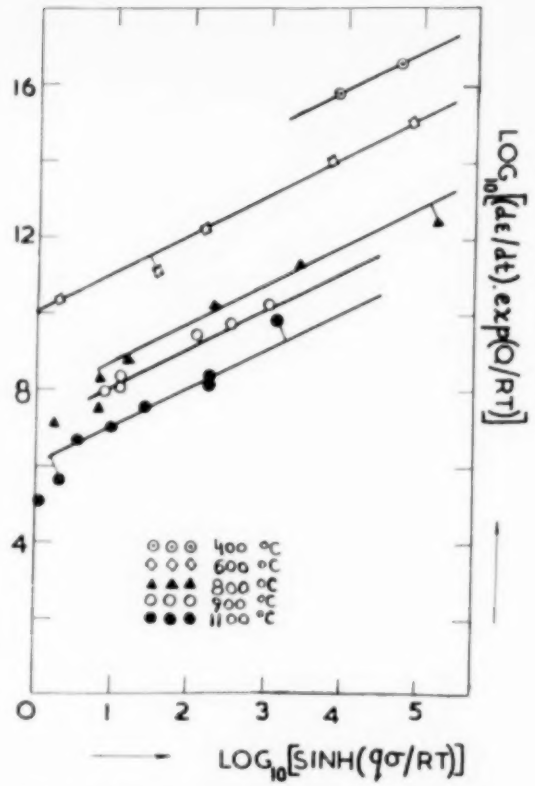

Fig. 4—Illustrates the divergence of the curves from the law predicted by Eq. 4 at low stresses.

the stress σ_0 and solving for C and C^* we obtain the relationship

$$\frac{K^*}{K} = \left(\frac{\sigma_0}{\sigma}\right)^n \left(\frac{\sinh n\,\sigma/\sigma_0}{\sinh n}\right) \quad [8]$$

Over the stress range where $K^*K = 1$, a power law and a sinh law can explain creep data equally well. Only at stresses where K^*/K departs significantly from 1 is it possible to decide between a power law and a sinh law. We believe that when K^*/K becomes greater than 2 or 3 it is possible to decide from experimental data. Thus from Eq. 7 it can be seen that a stress range of greater than about 6 must be covered to decide between a power law and a sinh law.

The greatest stress range we covered at any one temperature with our nickel data was about 8. However, other data exist which cover an even wider stress range. Fig. 5 shows results obtained by H. Laks.[35] At 853°K a stress range of 20 was covered. A hyperbolic sine curve has been fitted to the 853°K points as shown. It can be seen that the fit is, at best, fair. On the other hand the fit to a power law is good.

Mr. Meakin remarks that our nickel data taken at different temperatures have different power indices. We believe that to within the scatter of the experimental data they have the same index up to stresses where the creep curve bends up.

Mr. Meakin states that a drop in the activation energy is expected below $0.5T_m$. However, all the tin data reported in the paper to which he refers were taken at temperatures above $0.58T_m$ and the fall in the activation energy occurs at $0.8T_m$. The tin results have been discussed more extensively by one of us in later papers.[33,34]

We shall now discuss the temperature dependence of q appearing in the sinh law. It is stated that when the rate controlling mechanism is the movement of screw

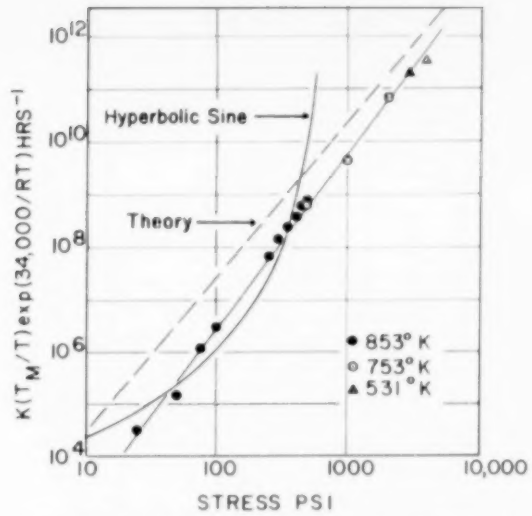

Fig. 5—Data of H. Laks[25] on aluminum containing 3.1 pct Mg. Double log plot of temperature compensated creep rate versus stress. T_m = melting point of Al. Theoretical curve calculated from analysis given in reference 26, assuming Cottrell-Jaswon microcreep is the rate-controlling mechanism. The theoretical curve was calculated using a diffusion coefficient of Mg in Al of (13.2 sq cm per sec) exp $(-34{,}000/RT)$.

dislocations containing jogs that "clearly q would be expected to vary with temperature." We do not think this temperature dependence is so obvious. If jogs are put into screw dislocations by intersection with other dislocations their separation will be determined by the spacing of the dislocation forest. Their separation cannot depend on temperature and q will not depend on temperature.

If the jogs in the screw dislocations are thermal jogs it is quite true that their initial separation will depend on temperature. However, before it can be concluded that q will also depend on temperature it is necessary to examine what happens to these jogs upon application of a stress. Fig. 6 shows a screw dislocation containing jogs immediately after application of a stress. The points A, B, C, and D represent jogs hindering the motion of the screw dislocation. As pointed out by Friedel[27] such jogs will undergo *sideways* motion

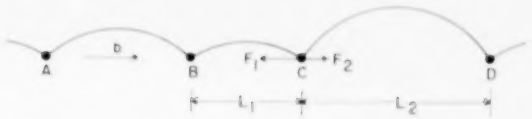

Fig. 6—Screw dislocation containing jogs immediately after application of stress. The arrow b represents the Burgers vector.

Fig. 7—Screw dislocation containing jogs some time after application of stress.

(i.e., motion parallel to the dislocation line) after application of a stress. Since a jog in a screw dislocation is a segment of pure edge dislocation it can move by conservative motion parallel to the Burgers vector. When a dislocation line is bowed out into loops such as is shown in Fig. 6 there will in general be a net force on a jog parallel to the Burgers vector. The force exerted by the smaller loops is greater than the force exerted by the larger loops. Thus in Fig. 6 the force F_1 is greater than F_2 because L_1 is smaller than L_2. Jogs will therefore move in a direction such that small loops will get smaller and large loops larger. In Fig. 6 a jog will move even when $L_1 = L_2$ since this is a position of unstable equilibrium. When two jogs meet they will either annihilate each other or form a larger jog, depending on their signs. Eventually the configuration given in Fig. 7 will be reached. In this situation the force on any jog in the direction of the Burgers vector is zero because the dislocation line meets a jog at an angle of 90° to the Burgers vector.

We strongly emphasize that the spacing between the jogs in Fig. 7 does not depend on the temperature but only on the stress. Therefore, there is no reason to expect a temperature dependence in q for even thermal jogs.

[25] J. E. Dorn: *Symposium on Creep and Fracture of Metals at High Temperatures*, National Physical Laboratory (Her Majesty's Stationery Office, 1956) p. 89.
[26] J. Weertman and J. E. Breen: *Journal of Applied Physics*, 1956, vol. 27, p. 1189.
[27] J. Weertman: *Journal of Applied Physics*, 1957, vol. 28, p. 196.
[28] J. Friedel: Private conversation.
[29] J. Weertman: *Journal of Applied Physics*, Oct. 1957 (To be published).

Creep of Single Crystals and Polycrystals of Aluminum, Lead, and Tin

by C. D. Wiseman, O. D. Sherby, and J. E. Dorn

JOURNAL OF METALS, January 1957, *AIME Trans.*, vol. 209, pp. 57-59.

F. Haeszner and M. Krause *(University of Gottingen, Gottingen, Germany)*—In the following we are submitting some results of our own investigations on the determination of activity energy of the creep of high purity aluminum which we carried out at Goettingen in the years 1954-1956. An extensive publication is being prepared. The investigations were made on polycrystals and single crystals of high purity aluminum, like those of Wiseman, Sherby and Dorn, and, on principle, with the same experimental technique, the same method of evaluation, and the same range of creep rate. Unlike Wiseman, Sherby and Dorn, however, the polycrystals were hard drawn, and the temperature range was between 290° and 320°K. We thought it worthwhile to communicate our findings and to suggest a discussion of our conclusions.

We investigated wires of high purity aluminum (99.989 pct Al) in two extremely different initial conditions: 1) hard drawn polycrystals (120 mm; 0.8 mm) 2) single crystals tempered at 550°C (2 single crystals prepared by the strain-anneal technique, 1.5 m length, 1.5 mm separated into samples of 60 mm). The crystals were in a continuous laminar flow of paraffin oil. The bath temperature was kept constant by thermostats at ±0.05°. By changing over to a second oil flow kept at a different temperature, the temperature could be raised or lowered, within less than a minute. The reading accuracy of the strain indicator magnifying approximately 4000 times was about $\Delta l = \pm 1 \times 10^{-4}$ of sample length. The creep curves were plotted point by point. For the computation of the creep rate of polycrystals immediately at the point of temperature change, the

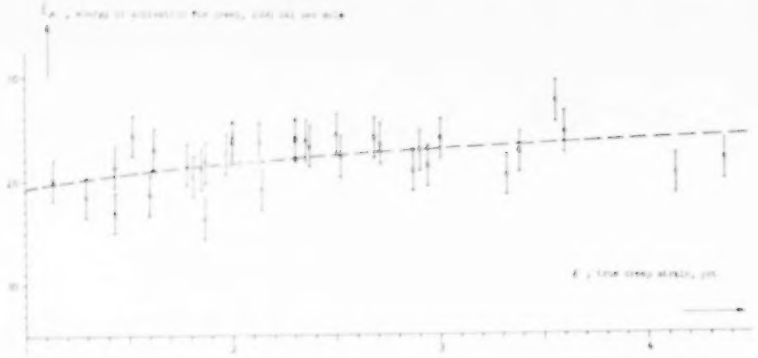

Fig. 3—Energy of activation for creep of pure aluminum (hard, polycrystalline), as a function of creep strain.

curve equations were determined from 12 to 14 measuring points by means of the method of least squares. The creep curves of single crystals were evaluated graphically. The error in values of activation energy for polycrystals were max. ± 2000 cal per mole for single crystals ± 4000 cal per mole.

a) Results for polycrystals—Fig. 3 shows the activation energy values obtained in dependence on the plastic deformation of the samples in the range of 1 to 4.5 pct (rupture strain about 1 pct). The maximum error limit is indicated. The values show a systematic increase with strain. In relation to the work of deformation this increase is comparable with that given by Carraker[11] for recrystallized platinum.

b) Results for single crystals—The activation-energy values determined for single crystals can be comprised in four groups, viz. shear strain of approximately 3 pct, 9 pct, 14 pct and 40 pct. Mean values of these groups of activation energy are plotted in Fig. 4 in dependence on the shear strain. As is seen, the values decrease distinctly with increasing shear strain. The drawn curve in this figure shows the theoretical values of activation-energy for cross-slip of screw-dislocations, obtained from the contribution of A. Seeger[12] when the shear stress τ_0 in the cross-slip system is computed from tensile stress σ at the single crystals by means of the graphical representation given in the paper by Diehl, Krause, Staubwasser and Offenhauser.[13] Fig. 4 shows that with increasing shear strain the activation energies measured more and more approach the theoretical values of the activation energy of the cross-slip of screw-dislocations.

During the plastic deformation we have a whole series of processes: Production and motion of dislocations (partly along with the migration of vacancies and interstitial atoms), reactions between dislocations, and finally even decrease of high-energy arrangements of lattice imperfections. The amount of individual processes during creep will depend on the initial structure of the sample (polycrystals hard, polycrystals soft, single crystals tempered), as well as on the degree of structural changes during creep.

If Wiseman, Sherby and Dorn have found the same activation energy for polycrystals and single crystals at higher temperatures, we are inclined to think that this indicates that in their case the different structure dependent individual processes have less importance for the deformation than a common control process. The diffusion, we think, may be such a control process. Then the activation energy found is mainly that of self-diffusion.

In this respect information might be obtained by experiments in which, with equal samples, activation energies of creep will have to be measured at low temperatures, at which diffusion is of no great importance, as well as at higher temperatures at which the diffusion actually is of influence. It might be expected, then, that at low temperatures the activation energy will be structure-dependent whereas at high temperatures it will be constant and be approximately of the value of self-diffusion. To what extent structural changes during creep affect the activation energy may be recognized particularly well at low-temperature creep experiments on single crystals of different orientations (for example a <111> or a <100> crystal — multiple slip — or a crystal from the middle of the orientation triangle —simple slip—).

Finally we will point out that the value E_i obtained by means of the relation

$$E_i = \frac{T_1 T_2}{T_2 - T_1} \ln \frac{\dot{\epsilon}_2}{\dot{\epsilon}_1}$$

and the corresponding technique of experimentation with abrupt temperature changes need not necessarily have the meaning of a physically real activation energy of single process. In the case of complex structural changes in the sample, it might repre ent a value composed of several activation energies, and merely having the meaning of a constant with which temperature dependence of the rate of creep in a limited stress and temperature interval can be described.

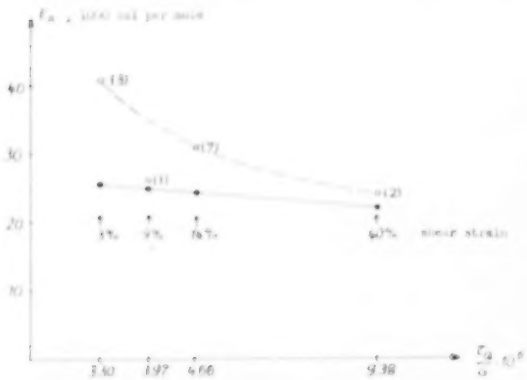

Fig. 4—Activation energies measured on single crystals compared with theoretical values of the cross-slip of screw-dislocation. Dots indicate theoretical values; open circles indicate mean values of measured activation energies, number of averaged values being given in parentheses. τ_0 is the shearing stress in the cross-system, G is the shearing modulus.

[11] R. Carraker: *Journal of Applied Physics*, 1950, vol. 21, p. 1289.
[12] A. Seeger: *Handb. der Physik*, vol. VIII, part I, Fig. 127.
[13] Diehl, Krause, Staubwasser, and Offenhauser: *Z. f. Metallkde.*, 1954, vol. 45, p. 490.

C. D. Wiseman, O. D. Sherby, and J. E. Dorn *(authors' reply)*—The authors are appreciative of the comments made by Haeszner and Krause relative to their data on the activation energies for creep of Al. Recently Sherby, Lytton and Dorn[11] have reported the apparent activation energies for creep of annealed polycrystal-

line aluminum over the range of temperatures from 78°K to 850°K. These data clearly reveal that the activation energy between 240°K and about 375°K was 28,000 cal per mole, in good agreement with the estimated activation energy for cross-slip. A series of activation energies for strains ranging from 0.07 to 0.27 were obtained by cycling the temperature from 264° to 273°K. Under these conditions, which do not differ appreciably from those used by Haeszner and Krause, the activation energy was found to be 28,000 cal per mole for the entire range of strains. A review of Fig. 3 equally suggests insensitivity of the activation energy for creep in this temperature range to strain. Their average activation energy, however, is about 24,000 cal per mole as compared with the 28,000 cal per mole value obtained by Sherby, Lytton and Dorn. It is possible that this minor discrepancy can be attributed to the fact that Haeszner and Krause used severely cold worked aluminum whereas Sherby, Lytton and Dorn used annealed stock.

Activation energies for creep of single Al crystals oriented for simple shear on the (111) planes in the [101] direction have been determined by Lytton, Shepard and Dorn[15] over the entire range of temperatures from 78° to 890°K. These results are distinctly different from those quoted by Haeszner and Krause for their single crystal test. Over the range from 78° to 400°K the unique activation energy of 3400 cal per mole was obtained over wide ranges of stress and strain. The mechanism was associated with the Peierls energy, which is estimated to have an activation energy of 3600 cal per mole. On the other hand if the crystals were severely bent they gave the same activation energies as those obtained for polycrystalline Al. Y. A. Rocher[16] determined the activation energies for single Al crystals favorably oriented for simple shear on the (010) planes in the [101] direction. Only (111) slip was observed. The activation energies, however, agreed well with those for the polycrystalline aluminum specimen at the same temperature. Consequently accurate activation energies for creep of single Al crystals require extreme care in the preparation, handling and method of testing. It is not possible at present to rationalize the high values at low strains reported in their Fig. 4 for the activation energies for aluminum single crystals by Haeszner and Krause.

In agreement with Haeszner and Krause it has been found[15] that the abrupt change in temperature technique applied in the low and intermediate temperature range yields *apparent* activation energies which represent weighted sums of the activation energies of the individual processes which are contributing to the deformation.

[15] Sherby, Lytton, and Dorn: *Acta Metallurgica*, 1957, vol. 5, pp. 219-227.
[15] Lytton, Shepard, and Dorn: *Institute of Engineering Research Report*, Series 103, Issue No. 1, University of California, Berkeley, April 9, 1957.
[16] Y. A. Rocher: Master's thesis, University of California, Berkeley, June 1957.

Delayed Yielding in a Substitutional Solid Solution Alloy

by L. A. Shepard and J. E. Dorn

JOURNAL OF METALS, October 1956, *AIME Trans.*, vol. 206, pp. 1229-1235

H. C. Rogers *(General Electric Company, Schenectady)*—I would like to comment on the authors' interesting paper, hoping that I have correctly ascertained their experimental technique from the details reported. The authors, apparently in an effort to eliminate the influence of gripping on Lüders' band nucleation, have resorted to the use of tensile specimens which have been strained and aged. This might well have produced a spurious effect which may have led to some erroneous deductions and interpretations of the experimental results of the paper.

The question raised is the following: Is the prenucleation strain homogeneous (i.e., occurring at least in favorably oriented grains along the entire gage length) or is it actually a localized creep? Since the authors did not examine the specimens during the deformation, one cannot say with certainty which of the above proposals is more likely. The reason for raising this question will be apparent from the discussion and description of some of our own experiments which follow.

First, it is somewhat surprising that the rate of band propagation in a specimen in which the band was nucleated by indentation (i.e., local deformation) was identical to that in which the band was nucleated by homogeneous prenucleation creep, which strains the entire gage length. For the latter specimen, the Lüders' bands would be propagating into plastically strained material while in the indented specimen the bands would be propagating into material which has previously been strained only elastically.

Secondly, unpublished work here indicates that in the case of steel tensile specimens with a similar strain history, the plastic deformation which occurs before band propagation is localized at the fillets. If one prestrains a filleted specimen the gage length yields inhomogeneously at first and then deforms homogeneously with strain hardening. As the gage length strain hardens the fillets begin to deform also, the amount of deformation decreasing as the fillet cross-section increases. After aging, retesting such a specimen in tension produces a load-elongation curve such as that shown in Fig. 13, which is plotted with the elastic limit of 320 lb as the coordinate zero. It will be seen that there is a considerable amount of plastic deformation prior to the region of approximately constant lower yield load, and that this latter region itself, in this case, actually consists of two different levels. A microscopic examination at intervals during a tensile test of such a specimen indicates that in region (1) of the load elongation curve the specimen is undergoing heavy deformation locally in the fillets. The fillets were prestrained less than the gage length prior to aging, and yielding was found to start at the boundary between the unprestrained and lightly strained and aged portions of the fillet. As this deformation proceeds, a Lüders' band is suddenly nucleated without a load drop at the deforming region at one fillet and proceeds to grow along the gage length of the specimen under approximately constant load (region (2)). At region (3) another band is nucleated in the center of the specimen gage length where the cross-section of the original specimen was machined slightly smaller. The load in region (3) drops because three band fronts rather than one are propagating. They can move more slowly than one and still provide the rate of extension imposed on them by the tensile machine. This slower propagation rate can be accomplished with a lower load.

The authors have also used strain-aged tensile specimens; it is highly likely, therefore, that they also may be producing relatively high local deformations in the fillets before Lüders' band propagation. Since they have dead-weight loaded their specimens, they will initially be carrying out a creep test on the fillet region only, before Lüders' band propagation begins. The rate

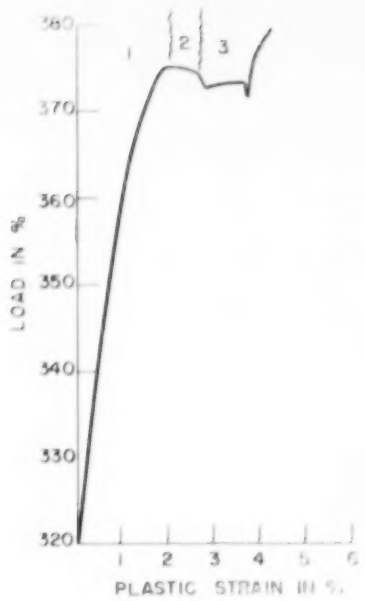

Fig. 13—The initial yield portion of the load elongation curve of strain-aged rimmed steel.

of strain decreases as the deformed region strain hardens under the constant load. When the local stress reaches a critical value, a band is nucleated in this region. This occurs at different times since the creep rate varies with different stresses. If this indeed occurs then it is not surprising that the Lüders' bands are nucleated at approximately the same measured strain (one does not know the stress or strain distribution too well in the fillet, but the loads do not vary markedly and hence the strain to critical stress would not vary markedly) nor that the time for the nucleation of the first band obeys the stress-temperature relationship characteristics of creep since this is what is being measured.

In view of our observations it seems imperative that the authors demonstrate conclusively that this creep in the fillets does or does not occur in their tests. Also, an explanation of why the band propagation rate in the indented and unindented specimens are identical would be appreciated.

L. E. Shepard and J. E. Dorn *(authors' reply)*—A.—All strains reported were measured across the central 2 in. of the specimen gage section, and not between the shoulders of the specimen as he may have supposed. It is therefore reasonable to assume that the prenucleation strain was homogeneous. Certainly it did not represent localized strain arising in the fillet region of the specimen.

B.—It will be noted in Table II of the paper that in the majority of cases, yielding began with the spreading of two band fronts within the gage section. If the yielding conditions suggested by Dr. Rogers were correct, this would require that Lüders' bands be initiated simultaneously at both fillets of the specimen so as to reach the measured gage section at the same moment, a rather unlikely situation.

Two factors lead us to the belief that the first and succeeding bands nucleated within the measured gage section. The first is that, as was noted, two band fronts began moving in most cases at the delay time, indicating the nucleation and growth of one band. The second is that the second and following bands which must have nucleated in regions that had not as yet yielded, and therefore, within the gage section, were found to obey the same time laws for nucleation as the first band. This factor, though not specifically discussed in the report, is an evident requirement, following from the congruency of the curves in Figs. 6 and 7 of the paper.

C.—It does not appear peculiar that the rate of band propagation in the indented specimen was the same as that resulting from homogeneous prenucleation creep when it is considered that the total prenucleation creep is of the order of 0.09 pct and that the major resistance to deformation must result from the approximately 10 pct prestrain to which the specimen was subjected prior to aging.

Effect of Orientation on the Plastic Deformation of Aluminum Single Crystals and Bicrystals

by R. S. Davis, R. L. Fleischer, J. D. Livingston, and Bruce Chalmers

JOURNAL OF METALS, January 1957, *AIME Trans.*, vol. 209, pp. 136-140

K. T. Aust *(General Electric Company, Schenectady)*—I would like to report on some previously unpublished data obtained by N. K. Chen and myself, which deal with some effects of grain boundaries on the plastic behavior of aluminum (99.997 pct purity) during room-temperature deformation. Fig. 11 shows the tensile stress - tensile strain curves of one single crystal, and two isoaxial bicrystals with misorientations of 60° and 140° about the specimen axis depicted in the unit stereographic triangle. The preparation of the specimens and the stress-strain determinations were carried out as previously described.[1] The specimens had rectangular dimensions, approximately 3 mm by 6 mm, and about 7-½ cm long. The specimen axis orientation in relation to the direction of stress is identical for the single crystal and the crystals comprising the bicrystal specimens, and lies between specimen axis orientations 1 and 2 studied by the authors.

It is evident that an appreciable grain boundary effect exists here also, at least in the early stages of

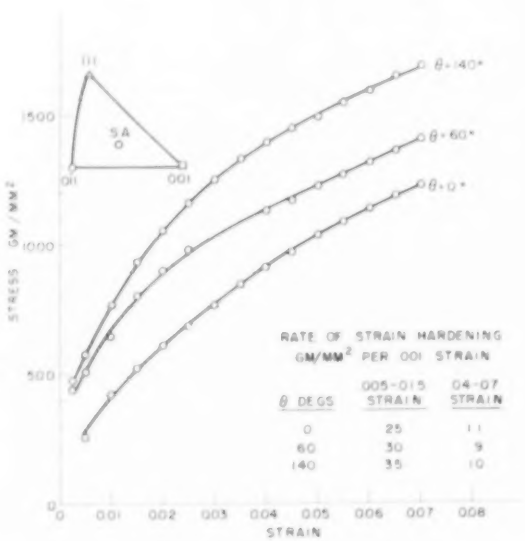

Fig. 11—Tensile stress—tensile strain curves of one single crystal and two isoaxial bicrystals with misorientations of 60° and 140°.

deformation. The rate of strain hardening increased with increased misorientation in the deformation range from about 0.005 to 0.02 strain. However, the rate of strain hardening was similar for the three specimens after greater deformation, that is, from approximately 0.04 to 0.07 strain. Metallographic observations revealed a single set of slip lines which correspond to the most highly stressed {111} plane in the single crystal and bicrystals. Additional slip markings corresponding to possible cross-slip were observed near the grain boundary of the bicrystals.

The above observations indicate that for specimens of the present size and shape, and for the case of only one slip plane operating in the single crystal, the 60° and 140° boundaries have raised the level of the stress-strain curves. This is in general agreement with the findings of the authors for orientations 1, 2 and 3. This effect of the grain boundary has apparently originated in the early stages of plastic deformation, as shown by the similar strain-hardening characteristics of the three specimens after larger deformation.

This work was sponsored at the Johns Hopkins University, Baltimore, Maryland, by the Office of Ordnance Research (Contract No. DA-36-034-ORD-1153 RD).

Effect of Rolling Procedure on the Kinetics of Recrystallization of Cold-Rolled Copper

by J. T. Michalak and W. R. Hibbard, Jr.

JOURNAL OF METALS, January 1957, *AIME Trans.*, vol. 209, pp. 101-106.

Paul A. Beck *(University of Illinois, Urbana, Illinois)*—As pointed out by the authors, the texture of straight-rolled copper obtained by them, Fig. 2, is very similar to that previously obtained[12] by quantitative methods. The authors use the indices erroneously given by us[12] for the ideal orientation of the deformation texture components. Instead of (123) [121], it is more appropriate to use the simplified indices (123) [412].

In addition to the photographic texture determination for cross-rolled copper by Brick and Williamson[13], to which the authors do refer, more recently quantitative determination has been made of the texture of cross-rolled and of cross-rolled and annealed copper[14]. The lack of resolution inherent in the photographic method prevented the earlier investigators from identifying the orientations present in cross-rolled and annealed copper. However, the octahedral pole figure they published was fairly consistent with the more recent quantitative results[14], and both investigations, particularly the quantitative pole figures, clearly show a rather surprisingly sharp development of each of the eight texture components. The reduction of area in cross-rolling for Brick and Williamson's specimen was 99 pct and for the more recent quantitative texture work it was 96.5 pct. I wonder whether the authors could explain the conspicuous lack of sharpness in the texture of their copper specimen cross-rolled 96.4 pct and annealed at approximately the same temperature that has been used in the previous quantitative texture work. Since the amount of deformation and the annealing treatment were both quite similar, the pronounced difference in the textures is rather surprising.

[12] Hsun Hu, P. R. Sperry, and Paul A. Beck: Rolling Textures in Face-Centered Cubic Metals, *Trans. AIME*, 1952, vol. 194, p. 76.
[13] R. M. Brick and M. A. Williamson: *Trans. AIME*, 1941, vol. 143, p. 84.
[14] A. Merlini and Paul A. Beck: Study of the Origin of the Cube Texture, *Acta Metallurgica*, 1953, vol. 1, p. 598.

J. T. Michalak and W. R. Hibbard, Jr. *(authors' reply)*—We would like to thank Dr. Beck for calling our attention to the corrected indices and his paper with Dr. Merlini on cross rolled copper. It is not possible for us to explain the difference between his sharper recrystallized texture and our dull one. However, certain differences are apparent—a) Their copper recrystallized after five minutes at 250°C. (Their Fig. 1) Ours required almost 6 hr at 250°C. b) Their copper had an as-rolled hardness of 105 Vhn and an as-recrystallized hardness of about 56 Vhn. (Also their Fig. 1) Ours had an as-rolled hardness of 97 and as-recrystallized of 51.5.

These results suggest a significant difference in purity and in strain hardening rate, i.e. there are differences in the material and possibly how they were rolled.

Finally, the low density areas of the pole figures of the different investigations are similar—it is the high density areas which are very different.

Effect of Temperature on the Flow Stress and Strain Hardening Coefficient of Magnesium Single Crystals

by H. Conrad and W. D. Robertson

JOURNAL OF METALS, April 1957, *AIME Trans.*, vol. 209, pp. 503-512.

W. F. Sheely, E. D. Levine, and R. R. Nash *(Rensselaer Polytechnic Institute, Troy, New York)*—In their study of the basal slip of unalloyed magnesium single crystals, the authors empirically derived the relation:

$$\dot{\gamma} = C \exp.\ (-\Delta H/RT) \exp.\ B(\tau - \tau_0(0) - h\gamma) \quad [15]$$

where

$C = 4.5 \times 10^{-12}$ per min.
$\Delta H = 10.3$ kcal per mol
$R =$ the gas constant
$T =$ temperature
$B = 0.65$ mm³ per gm
$\tau =$ applied stress
$\tau_0 =$ an internal stress
$h =$ strain hardening coefficient
$\gamma =$ strain

As the authors point out, this result varies with most theories of low temperature plasticity which are based on specific dislocation models in that the derived relations contain a stress term in the activation energy. The general form of many of the equations predicted by these theories is:

$$\dot{\gamma} = C \exp.\ -([\Delta H - g(\tau)V]/RT) \quad [16]$$

where $g(\tau)$ is some function of the applied stress.

One could test the validity of either point of view by determining the sensitivity of the stress required to maintain flow at a given rate to changes in strain

rate and comparing the result to the mode of response predicted by [15] and [16].

From Eq. [15], if it may be assumed that a strain rate change can be effected with only negligible accumulation of plastic flow during the change, the following equation for flow stress change may be derived:

$$\Delta\tau = 3.5 \log_{10} \frac{\dot{\gamma}_2}{\dot{\gamma}_1} \qquad [17]$$

where

$$\Delta\tau = \tau_2 - \tau_1$$

From Eq. [16], making the commonly used assumption that $g(\tau)$ is a linear function of stress, the corresponding equation for flow stress sensitivity would be:

$$\Delta\tau = KT \log_{10} \frac{\dot{\gamma}_2}{\dot{\gamma}_1} \qquad [18]$$

where

K = a constant
T = temperature

The writers performed a series of strain rate changes on a magnesium single crystal stressed in shear and deforming by basal slip. Experiments were done on an Instron testing machine at room temperature and in two cold baths. Strain rates were changed by factors of ten and one thousand. The resulting flow stress changes, $\Delta\tau$, as a function of $\log_{10} \dot{\gamma}_2/\dot{\gamma}_1$ are illustrated in the accompanying figure. Also shown in the figure is the curve of Eq. [17].

The following observations were made:

(a) The magnitude of the stress change resulting from a particular strain rate change was independent of whether the change was an increase or a decrease.

(b) No regular change in $\Delta\tau$ as a function of temperature was detected.

(c) The relation of $\Delta\tau$ to $\dot{\gamma}_2/\dot{\gamma}_1$ fitted equation [17].

These results give quantitative support to the authors' equation.

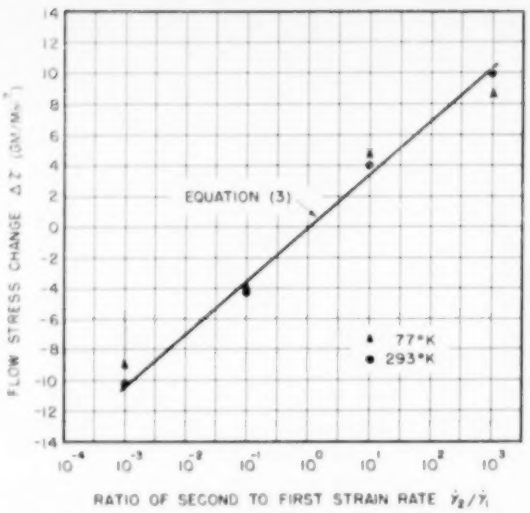

Fig. 15—Change of flow stress resulting from strain rate change.

Hans Conrad and W. D. Robertson *(authors' reply)*—It was indeed gratifying to hear of the results obtained by Sheely, Levine, and Nash. Their data offers further proof that the constant B is independent of temperature, and consequently that the activation energy for plastic flow of magnesium crystals at low temperatures is independent of stress and strain, in disagreement with the requirements of present theories of deformation.[1,2]

Of special interest is the fact that the value of B derived from their data is equal to that obtained in our tests, even though the crystals were grown under different conditions and the tests were of a different nature. The physical significance of B is not known at present, however, additional tests are in progress with the aim of evaluating this.

Embrittlement of Ti-Al Alloys in the 6 to 10 Pct Al Range

by F. A. Crossley and W. R. Carew

JOURNAL OF METALS, January 1957, *AIME Trans.*, vol. 209, pp. 43-46.

A. Klibanoff, C. D. Dickinson, and S. Abkowitz *(Mallory Sharon Titanium Corp., Niles, Ohio)*—We wish to compliment the authors on their fine work. Titanium alloys in this high aluminum range are certainly of interest, and the authors' work is an important contribution to understanding the problems involved in alloys of this type.

We are concerned that others might extrapolate the data of Crossley and Carew for binary Ti-Al alloys to more complex Ti-Al alloys and reach erroneous conclusions. From the data of Crossley and Carew, the prospect of developing thermally stable titanium alloys in the 8 to 10 pct Al range seems poor. We have studied this system and have information which presents a more promising picture for the use of the higher aluminum content in the titanium alloys. The mechanical properties of Ti-8Al and Ti-8Al-2Cb-1Ta in several conditions of heat treatment are compared in Table I.

The properties of both alloys (melted using 120 Bhn sponge) air cooled from soaking temperature are similar. The 8Al binary was embrittled by furnace cooling from 1700°F while the Ti-8Al-2Cb-1Ta alloy retained its ductility when subjected to similar treatments.

We have since tested both alloys after subjection to the embrittling treatment suggested by Messrs. Crossley and Carew. The results appear in Table II.

The Ti-8Al binary was embrittled by this treatment; however, this heat treatment had little effect on the tensile ductility of Ti-8Al-2Cb-1Ta. We have subjected the Ti-8Al-2Cb-1Ta alloy to more severe conditions of temperature, stress, and time (1000°F-10,000 psi-300

Table I. Mechanical Properties of Ti-8Al and Ti-8Al-2Cb-1Ta Sheet*

Heat Treatment	Ti-8Al Mechanical Properties			Ti-8Al-2Cb-1Ta Mechanical Properties		
	UTS, Ksi	YS, 0.2 Pct Off., Ksi	Elong. in 2 In., Pct	UTS, Ksi	YS, 0.2 Pct Off., Ksi	Elong. in 2 In., Pct
1650°F-1/3 hr-air cool	119	113	13.5	127	120	16
1650°F-1/3 hr-furnace cool to 900°F, air cool				127	123	14.3
1700°F-1 hr-furnace cool to 900°F, air cool	114	109	5.5			
1750°F-1/3 hr-furnace cool to 900°F, air cool				127	122	13.5

* All values are averages of six tests.

hr). After this treatment, the room temperature mechanical properties were:

UTS, Ksi	Elong. in 1 In., Pct	R.A., Pct
153	13.0	26.3

Our results for the 8Al binary sheet are in good agreement with those of Crossley and Carew for 8Al bar and strongly indicate that an embrittling reaction takes place in the suggested temperature range. The addition of tantalum and columbium to 8 pct Al produces an alloy whose behavior is markedly different.

We would, therefore, like to point out that the severe instability which occurs in the Ti-8 to 10 aluminum binary alloys does not necessarily occur in certain complex Ti-Al alloys.

F. A. Crossley and W. F. Carew *(authors' reply)*—The authors have some experience, although limited, with high aluminum, ternary alloys of the type represented by the Ti-8Al-2Cb-1Ta alloy. This experience supports the findings presented in the discussion. It is considered that tensile testing below room temperature, e.g., 0°C, gives a more critical evaluation of instability due to the mechanism discussed above.

Table II. Tests After Embrittlement

Alloy	Heat Treatment	Mechanical Properties			
		UTS, Ksi	YS, 0.2 Pct Off., Ksi	Elong., Pct	R.A., Pct
Ti-8Al (Sheet)	1650°F-1.3 hr, air cool; 1020°F-48 hr, air cool	127	123	4.5, in 2 in.	—
Ti-8Al-2Cb-1Ta (Bar)	1650°F-1 hr, air cool; 1020°F-48 hr, air-cool	148	146	12.0, in 1 in.	27.3

Etch Pits and Dislocations in Zinc Monocrystals

by J. J. Gilman

JOURNAL OF METALS, August 1956, *AIME Trans.*, vol. 206, pp. 998-1004.

G. Wyon and P. Lacombe *(Centre de Recherches Metallurgiques Ecole des Mines, Paris)*—We have been very interested by J. J. Gilman's work on etch pits in zinc crystals. We were impressed by the fact that the etch technique has given valuable results only after an impurity such as cadmium is added to pure zinc and especially that aging of the Zn-Cd solid solution is necessary in order to obtain etch pits along small angle boundaries.

We wish to compare these results with our experiments on etch figures in refined aluminum of varying degrees of purity.[15-18] We pointed out the influence of iron content and heat treatments (quenching and aging) on the number and the distribution of etch-pits. We have shown, in particular, that for a given heat treatment and a crystal of determined orientation, the density of etch-pits is the higher, the more impure the metal. In most cases, the number of pits counted on a crystalline matrix is much lower than the theoretical number of present dislocations: the difference is higher, the purer the metal.

These results have led us to relate the possibility of etch pits formation to the existence of an association between impurities and dislocations. As Dr. Gilman remarked, this interaction also plays a role in the case of etch-pits on zinc with 0.1 pct Cd.

By considering that for metal crystals the presence of dislocations is a neccesary but not sufficient condition for formation of etch figures, we may explain some apparently contradictory, or simply unexpected, facts.

1) *Density of etch pits.* We have remarked that Al samples quenched from 630°C present a higher density of etch pits if the cooling rate is low (air cooling) than if it is high (water cooling to 0°C). A priori, there are more dislocations locked in the crystal during the fast quench, but the cooling time being very short, the necessary diffusion of the impurities to the dislocations cannot come about with a sufficient speed: this explains the low density of etch pits observed.[17,18]

2) *Study of Polygonization.* We have shown[15-17] that the micrographic detection of polygonization in Al crystals through etch-pits is possible only after heat treatment:

a. If the cooling rate after a heat treatment is high (water quenching to 0°C), etch figures will appear along the subboundaries only if the temperature of the heat treatment has not been too high. Above the limit of solubility of iron, the association of this element with dislocations becomes very loose because of *evaporation* of the Cottrell atmospheres. Since diffusion of impurities towards dislocations cannot happen during quenching, for a high cooling rate, the subboundaries are visible only if the associations with dislocations are not loosened by the heat treatment.

b. For a temperature of treatment higher than the limit of solubility of the least soluble impurity, the micrographic perception of polygonization is possible with etch-pits only if the cooling rate after the treatment is low enough. This critical rate is lower, the purer the metal, which agrees with the hypothesis of a necessary diffusion of impurities towards dislocations.

There have been many discussions about the detection of polygonization on lightly cold-worked and heat-treated aluminium. The refined X-ray methods used by some authors[20] show that polygonization appears for very low heat treatment temperatures (from 200°C, or at room temperature). Micrography, on the contrary, shows the fragmentation in subgrains only for high treatment temperatures (between 450° and 600°C according to the purity of the metal). This led us to call *macromosais* the polygonization which may be revealed through etch-pits, and thus corresponds to a new distribution of dislocations happening during anneals above the solubility limit of the least soluble impurity. *Low temperature polygonization* cannot be revealed through etch-pits with refined aluminum where the iron impurity seems to play a leading role.

3) *Study of slip lines.* Wanting to reveal slip lines through etch-figures, we have seen[21] that it was impossible in the case of aluminum to obtain alignment of figures along these lines after repolishing. However, we could note the presence of alignment if the deformed samples had afterwards undergone an aging treatment. It seems to us that the only difference with the Zn-Cd alloys investigated by J. J. Gilman is that aging to aluminum-iron alloys happens only at a temperature distinctly higher than room temperature, where polygonization processes may interfere. Has Dr. Gilman systematically investigated the influence of aging time (at room temperature) on the number of etch-pits along the slip lines? These observations and those about the density of etch figures on polygonization subboundaries versus aging time could probably give more precise data about the diffusion coefficient of cadmium in a zinc lattice. Could Dr. Gilman explain why he chooses cadmium to obtain good etching? Has he observed a change in the density of etch-pits on the crystal matrix with different heat treatments (quench-aging) which would support the hypothesis of the association of dislocations and impurities? This would show that, as in aluminum, the number of etch-pits cannot be bound by a one to one relation to the

number of dislocations in the crystals." Experiments about polygonization would be also interesting. Would it be possible with Zn-0.1 pct Cd to make the subboundaries vanish micrographically through a quench from the temperature of complete solubility of cadmium? After quenching, is aging at room temperature sufficient to show the subboundaries through etch-pits? Is polygonization micrographically perceptible at temperatures lower than the temperature of complete solubility of cadmium (even after very long aging at room temperature)?

In conclusion, it seems more and more probable that impurities play an essential role in the appearance of etch-pits, and we agree perfectly with Dr. Gilman on this point. It may even be asked if etch-pits would still be possible in an extremely pure metal. Unluckily, in the case of aluminum, it is very difficult to eliminate the last traces of iron. Would not zinc be more favorable in this respect, since the impurities might easily be eliminated?

J. J. Gilman *(author's reply)*—At the time that I was preparing my manuscript on etching in zinc, I was not aware of the very interesting results of G. Wyon and P. Lacombe on etch-pitting in aluminum. They have looked into the role impurities played in much more detail than I did. I was primarily interested in obtaining some idea of dislocation distributions in zinc after various mechanical treatments and did not concern myself with the mechanism of the etching procedure. None of my observations are in contradiction with those of Wyon and Lacombe. On the contrary, I fully support their conclusions.

The discussors ask why cadmium was chosen as the impurity to give good etching. The answer is that the cadmium alloys were prepared for another purpose and their etching characteristics were discovered only after a chain of more or less accidental circumstances. Other impurities might be just as effective as cadmium. Air cooling from high temperatures is sufficient to suppress the etching effect. After such a mild quench, an aging period of about one week at room temperature is needed to restore good etching. As stated in the paper, it has not yet been possible to etch high purity zinc. Unfortunately, I do not have sufficiently detailed information to answer the many other questions of the discussors. I regret this as they are good questions.

[11] G. Wyon et J. M. Marchin: Comptes Rendus Acad. Sc. Paris, 1954, vol. 238, p. 2429.
[12] G. Wyon et P. Lacombe: Congres du Centenaire de l' Aluminium, 1954, Paris Tome 1, p. 289.
[13] G. Wyon et P. Lacombe: Report of the Conference *Defects in crystalline solids*, Bristol, 1953, The Phys. Soc. London, p. 18.
[14] G. Wyon, J. M. Marchin et P. Lacombe: Journees Metallurgiques de Paris, Oct. 1955, in press.
[15] F. A. Bilby and A. R. Entwisle: Acta Met. 1956, vol. 4, p. 257.
[16] H. Lambot, Z. Vassamillett, and J. Dejace: Acta Met. 1955, vol. 3, p. 157.
[17] G. Wyon et J. M. Marchin: Phil. Mag. 1955, vol. 46, p. 1119.

Flaking of Heavy Alloy Steel Sections

by C. R. Garr and A. R. Troiano

JOURNAL OF METALS, April 1957, *AIME Trans.*, vol. 209, pp. 445-449

S. L. Hoyt *(Battelle Memorial Institute, Columbus)*—This paper has just now come to hand but I should like to congratulate the authors for bringing out the individual, though related, effects of hydrogen and the transformation of austenite. Thus it appears that there is a close similarity between flaking in forgings and the underbead cracking that is observed in welds of hardenable steels.

As a wartime project, Messrs. Sims, Banta, and I studied the latter effect[1] and found that a susceptible steel would not crack if the austenite were completely transformed at an elevated temperature at which hydrogen diffuses readily. On the other hand, if the weld were cooled to room temperature, the remanent austenite would gradually transform and precipitate its dissolved hydrogen and initiate a crack. Later work by Messrs. Mallett and Rieppel showed quite clearly just what were the factors which were necessary to produce cracking. From the work of the authors, it would appear that the two mechanisms of flaking and underbead cracking are essentially the same.

[1] S. L. Hoyt, C. E. Sims, and H. M. Banta: Metallurgical Factors of Underbead Cracking, *Trans. AIME*, 1945, vol. 162, p. 326.

J. Hewitt *(United Steel Companies Ltd., Rotherham, England)*—The authors have stated that a delicate balance exists between hydrogen embrittlement and stress required for flaking, but do not appear to have taken into account the variation in hydrogen level after heat treatment of the different blocks. Since the treatments have removed varying quantities from each block we have calculated* the distributions in the blocks after each cycle—Fig. 6. The picture is then altered and the role of transformation stresses is questioned. The hydrogen content now appears to determine whether or not the billets had cracked *after* 36 days, regardless of structure. Our experience has shown that a reduction of the stresses arising from rapid cooling, either transformation or thermal, does not necessarily prevent cracking, but only delays it at these relatively high hydrogen levels. We would have fully anticipated cracking on further standing in blocks numbered 5 and 9 and would ask if these blocks were examined for cracks immediately prior to re-cycling?

If the other blocks are still available it would be of some interest to re-examine the samples found crack-free during the earlier examination.

We would also suggest that the blooms be examined microscopically for very small cracks since such cracks appear under certain conditions and may not be revealed by macro techniques. It would also be of interest to show the extent of the cracks on the same graphs as the calculated distribution curves since we have found in two cases, on different sections, that the levels at which cracking appeared to start were identical.

From the calculations made earlier we would have estimated the original hydrogen content at approximately 12 ml per 100 gm and wonder if the authors have actual results on the ½ in. round cast samples? We would expect difficulty in obtaining good samples of liquid steel at this level of hydrogen and would place more reliance on hydrogen determinations on samples taken from the center of a forging (before it had time to crack) and after such a treatment that hydrogen would only have been lost from the outer portions of the forging.

To illustrate the delay in cracking the following results may be of interest. We have examined recently the cracking of a cast of 0.30 pct C, 1½ pct Mn steel. Two 9 in. square billets were taken after rolling, one was air cooled and the other slowly cooled from 650°C. The hydrogen distribution across the two blooms was essentially similar with a maximum, in the center of the billet, of 5.8 ml per 100 gm. The air cooled billet cracked on the 6th day after reaching room tempera-

* The method of calculation of hydrogen distribution in large masses of low alloy steel is based on a method outlined by Sykes, Burton and Gegg and further developed by J. D. Hobson. It has been subsequently checked on a large number of low alloy steel forgings of various compositions by both Hobson and ourselves. This work will be published shortly.

Table III. Flaking of High Hydrogen 4340

Code	Treatment	Percentage Flaked, No. of Samples 6 In. Diam	9 In. Diam	13 In. Diam
Hydrogen: cu cm per 100 gm		3.2	4.8	9.7*
A	Air cooled after forging	100 (2)	100 (2)	100 (2)
D	Air cooled to 700°F, held in 600°F furnace for 24 hr, and air cooled	50 (2)†	100 (2)	100 (2)
E	Same as (D) but held 24 hr	0 (2)	100 (2)	100 (2)
C	Equalized at 1250°F, cooled 30°F per hr to 1150°F, held at 1150°F for 48 hr, and air cooled	0 (2)	0 (2)	100 (2)
B	Same as (C) but after 48 hr at 1150°F, cooled 30°F per hr to 600°F, held at 600°F for 24 hr, and air cooled	0 (2)	0 (2)	50 (4)†

* The 5.39 hydrogen result was discounted because it was between nos. 3 and 11 in the ingot and because it should approach no. 3 and exceed no. 11.
† Flaked rounds from top 1/3 of ingot

ture, the slowly cooled billet did not crack until the 82nd day after reaching room temperature.

Some typical work on a 28 in. square forging is shown in Fig. 7. The forging is 0.36 pct C, 0.66 pct Mn, 2.67 pct Ni, 0.68 pct Cr, 0.54 pct Mo steel, with a tempered bainite microstructure, and illustrates some of the points raised above.

The attention of the authors is also drawn to the recent work by Barker and Wainwright[6] who showed that many cracks were formed in Ni - Cr - Mo steels after a treatment such that transformation stresses were completely absent and thermal stresses considerably reduced.

[6] *Nature*, 16th June, 1956.

E. Houdremont *(Essen, Germany)*—It has been known for about 20 years[4] that the interaction of hydrogen and stresses is the cause of flaking but, according to our experience, it is not necessary that these stresses have to be transformation stresses.

The following results show very clearly that flakes can be produced without transformation stresses:[7] 1. A wholly ferritic steel with 4 pct Si charged with hydrogen can show flakes. 2. A ball bearing chromium steel transforms easily enough in the perlitic range so, that the transformation can be performed between 650° and 600° if you keep the steel for a certain time in a furnace at this temperature. Nevertheless you can produce flakes by cooling them down in air, oil or water afterwards to room temperature. 3. If you charge a wholly transformed steel with high pressure hydrogen at 550° below the transformation temperature you can get flakes on subsequent cooling and the number of flakes increase with the rate of cooling. In this experiment no transformation occurs. 4. The direction of stress is the main point and not the transformation stresses has been shown by changing the direction of flakes by applying external stresses. The flakes are perpendicular to the applied stress (See Fig. 1206, page 1383 of Reference 6). In accordance with this the direction of flakes in forged pieces mostly corresponds to the direction of cooling stresses. The relation between an applied external stress and hydrogen content is also shown by the fact that a steel which contains not enough hydrogen to form flakes on cooling may form flakes during the tensile test.

So we would be in agreement if we state that hydrogen and stress are the cause of flakes and that transformation stresses may be also a kind of stress which promotes flakes formation.

[4] E. Houdremont: *Handbuch der Sonderstahlkunde*, 3rd Edition, Berlin, 1956, pp. 1375-1390.

[7] E. Houdremont and H. Schrader: *Techn. Mitt. Krupp, Forschungsber.*, 1941, vol. 4, pp. 67-98; *Stahl und Eisen*, 1941, vol. 61, pp. 649-653.

W. Wilson *(A. Finkl & Sons, Chicago)*—Dr. Troiano and his associates are to be congratulated for another

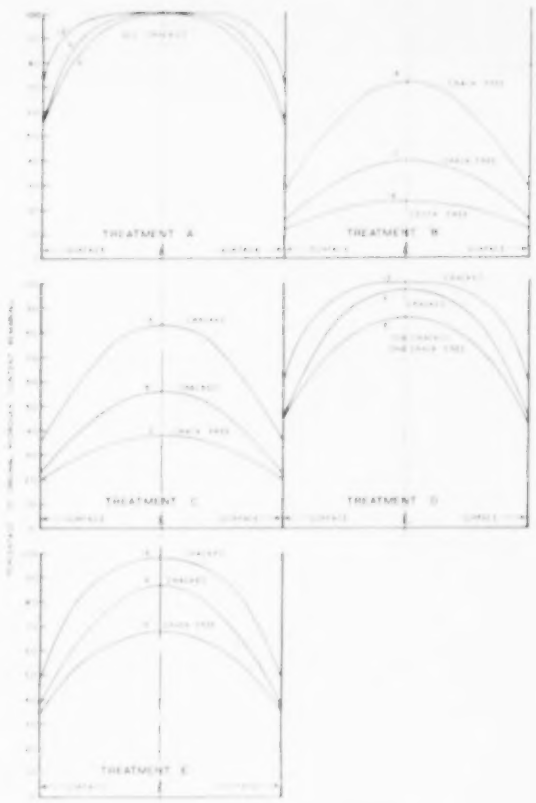

Fig. 6—Calculated hydrogen distributions.

paper reducing some of the apparent idiosyncrasies of flaking to scientific principles. I have taken the liberty of re-arranging the data in Tables I and II as shown in Table III. The treatments in Table I were ranked - my opinion - as to the probability of flaking (A - most likely, B - least likely). For each size and treatment in Table II, the percentage of flaked samples and number of samples are shown in Table III.

Two broken lines are used to bracket the treatments and sizes or hydrogen contents which gave 100 pct flaked and 0 pct flaked. Where 50 pct was observed, the flaked samples were from the top 1/3 of the ingot. This observation on ingot location suggests that positive segregation is important only in borderline cases.

The two, flake free, 13 in. diam samples were halved after 6 to 9 mo of storage and normalized. These samples with less than one-half of the original hydrogen were found to be flaked after one month. This finding agrees with the original results which show that normalizing with 3.2 cu cm H_2 or more yields flakes.

The two 9 in. diam samples did not flake upon similar treatment. Probably the hydrogen content of these was less than 2.4 cu cm per 100 gms. This observation leads to the conclusion that normalizing becomes permissible at some hydrogen content less than 3.2 cu cm per 100 gms.

In making these comparisons, I have assumed that the hydrogen content and treatment are closely correlated and that the only mass effect in these treatments is the retention of hydrogen. These assumptions are not rigorously established by the results and I am sure the authors will wish to comment upon them.

In addition to the presented data, I would like to know the equalization (transformation) times at 1250°F and the method of determining the forging temperatures.

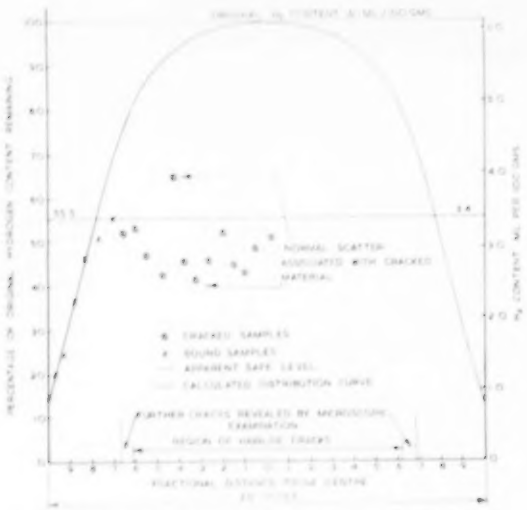

Fig. 7—Hairline cracking on 28 in. sq blocks of 2½ pct Ni, Cr, Mo, steel.

In the bainitic cycles, an air cool is followed by a direct transfer to the final temperature. However, the pearlitic cycles consist of equalizing at 1250°F, slow cooling to 1150°F, and then holding at 1150°F. Why do the authors prefer the more complex pearlitic cycle?

I wonder if the authors would be willing to hazard their opinion as to when in the processing of the 6 and 9 in. diam samples the bulk of the hydrogen was lost.

C. R. Garr and A. R. Troiano *(authors' reply)*—Mr. Wilson's comments are appreciated. To be sure, positive segregation is important in borderline cases; but we like to feel that most flaking represents borderline cases. In other instances, the borderline element may be introduced by cooling stresses, etc. We believe that it may be dangerous to generalize that normalizing becomes permissible at some hydrogen content below 3.2 cu cm per 100 gm. Too many other factors may influence the increment of stress necessary for flaking.

Of course the mass effect observed will not only affect the retention of hydrogen but may also have considerable influence on the thermal macrostresses.

We regret that the information on equalization times and forging temperature is not available. However, standard mill practice was followed in both cases.

The authors' have no preference for a complex pearlitic cycle. A number of different cycles were tried in an effort to evaluate the variables that contribute to flaking. Unfortunately, insufficient material was available to try all the cycles that appeared to be of interest. One cycle, in particular, of interest would have involved holding near Ms for essentially complete transformation to bainite, followed by holding in the pearlite range near 1250°F and slow cooling from this temperature.

We feel that the major portion of the hydrogen was lost during and after the transformation of the austenite, and before cooling to room temperature.

Of course, there are no serious areas of disagreement with Dr. Houdremont's analysis as presented in this discussion. Reference is again made to the last paragraph of the paper where in it is stated, "The results of this investigation indicate that transformation stresses play a major role in the flaking of heavy steel sections and that the influence of hydrogen is primarily through its action as an embrittling agent. However, it should be appreciated that any stress in the presence of hydrogen, regardless of its origin, could be sufficient to cause ruptures which may be considered flakes from a generalized point of view, although it is felt that the conventional flake patterns familiar to the industry are largely the result of transformation stress where other stresses, such as cooling, residual, externally applied, etc., may be contributory."

We find it somewhat difficult to follow the discussion by Hewitt. Of course, we can not be certain that in all cases a time delay of more than 36 days may not have indicated the presence of flakes. However, for the specific cases of blocks 5 and 9, it is certain that flakes had not appeared 6 to 9 mo later, since they were re-examined at this time (see text, last paragraph before section on Results and Discussion).

Reference is made to recent work by Barker and Wainwright, in which the intent was to show that flakes could be produced without transformation and the stresses that go with it. It is not clear how these authors know they have not had transformation in the nickel steels and *residual* stresses not low, and how can one rationalize insufficient stress to crack their carbon steel, but sufficient to crack the stronger, more ductile nickel steels?

We look forward to examining the new method of calculating hydrogen distribution in large masses, presumably to be published soon.

We definitely agree with Sam Hoyt that the mechanism of underhead cracking and flaking are much the same.

Grain Boundary Displacement vs Grain Deformation as the Rate Determining Factor in Creep

by J. A. Martin, M. Herman, and N. Brown

JOURNAL OF METALS, January 1957, *AIME Trans.*, vol. 209, pp. 78-81.

Frederick N. Rhines *(Carnegie Institute of Technology, Pittsburgh)*—It is unusual and very gratifying, in a field as controversial as that of creep, to find such extensive agreement as exists between the results on β-brass, now presented by Martin, Herman, and Brown and those on aluminum, which Bond, Kissel, and I presented last Fall. In particular, I am pleased to observe that these authors have concluded, as we did, that "the grain boundary displacement is a byproduct of grain deformation." We agree also that "the ratio of grain boundary displacement to overall strain is independent of temperature, if the temperature is high enough to produce mobile boundaries." Moreover, the essentially identical behavior of our aluminum bicrystals and the polycrystalline β-brass, currently under discussion, demonstrates more conclusively than could any argument, the error in Grant's contention of last Fall that the single crystal results are not applicable to polycrystalline materials. I should like to point out once more, that much of the disagreement amongst the observers of grain boundary displacement has arisen from the fact that flow takes place in a complex manner within a layer of metal of finite thickness, so that the lateral displacement of the grain boundary cannot be measured between reference points that lie upon the axis of extension of the specimen. The present authors have measured the displacement in a direction that is effectively parallel to the plane of the grain boundary. This gives a true measure of displacement and acounts, I think, for the agreement between the β-brass and aluminum results.

Norman Brown *(author's reply)*—We would like to thank Dr. Rhines for his discussion. Also, Mclean, with polycrystalline aluminum, has recently demonstrated that above 350°C the ratio of grain boundary displacement to overall strain remains constant.

Internal Friction and Grain Boundary Viscosity of Copper and of Binary Copper Solid Solutions

by L. Rotherham and S. Pearson

JOURNAL OF METALS, August 1956, *AIME Trans.*, vol. 206, pp. 881-892

H. H. Bleakney *(Dept. of Mines and Technical Surveys, Ottawa, Ontario, Canada)*—The writer of this discussion did not read very far before being brought up sharply by what appeared to him to be a rather surprising observation. That was the implication in the title of the paper that the alleged viscosity of grain boundaries is an established fact. It is true that Ke's evidence for the occurrence of viscous flow at metal grain boundaries was widely accepted, and was not seriously challenged for many years. It is also true that this paper was written in 1954 before critical examination had disclosed the unreliability of Ke's conclusions.[51,52] Nevertheless, even before 1954 enough evidence had been presented[53,54,55,56,57] to arouse suspicion of the validity of the viscous grain boundary hypothesis. In any event in view of references 1 and 2 the authors might well have considered modifying their statement between submission and publication.

This paper contributes a very useful addition to the evidence that the internal friction peak, noted by Ke in aluminum, is characteristic of all polycrystalline metals of high purity; and by noting some of the factors which affect the peak, it brings an explanation for the phenomenon a little nearer. All those who have conducted these tests must have been impressed, as the writer was, by the rather startling drop in internal friction at temperatures slightly higher than that of the peak. Since the work of Rhines, Bond, and Kissel[57] has shown that the viscous grain boundary hypothesis is untenable, some other explanation for this phenomenon must be sought. It is not unlikely that when that answer is found it will prove to illuminate an area of metal behavior much wider than that occupied by internal friction alone.

It is to be hoped, therefore, that the authors will continue to add their contributions to this end.

[51] H. H. Bleakney and J. Can. *Technology*, 1955, vol. 33, p. 56.
[52] F. N. Rhines, W. E. Bond, and M. A. Kissel: *Trans. ASM*, 1956, vol. 48, p. 919.
[53] Bruce Chalmers: Crystal Boundaries, *Prog. in Met. Phys.*, 1949, vol. 1, p. 148. Butterworths Scientific Publications, London.
[54] K. T. Aust and Bruce Chalmers: Energies and Structures of Grain Boundaries, *Metal Interfaces, ASM*, Cleveland, 1952, p. 159.
[55] A. S. Nowick: Stress Relaxation across Interfaces, *Metal Interfaces, ASM*, Cleveland, 1952, p. 266.
[56] C. Wert: The Metallurgical Use of Anelasticity, Modern Research Techniques in Physical Metallurgy, *ASM Trans.*, 1953, vol. 45A, pp. 229 and 248.
[57] W. Betteridge: *Journal* Institute of Metals, 1953, vol. 82, no. 4, p. 155.

L. Rotherham and S. Pearson *(authors' reply)*—I think that Dr. Bleakney's comments should be regarded as non-controversial. Much of the earlier work on this subject was given theoretical explanations which have since appeared inadequate, but a whole series of experimental facts have been uncovered which have proved strange and difficult to interpret. I think our work must be mainly considered in this light.

Magnetic Method for the Measurement of Precipitate Particle Sizes in a Cu-Co Alloy

by J. J. Becker

JOURNAL OF METALS, January 1957, *AIME Trans.*, vol. 209, pp. 59-63

John Cahn *(General Electric Company, Schenectady)*—Dr. Becker's elegant method for measuring precipitate particle sizes in Cu-Co alloys in this submicroscopic range should stimulate a great deal of work in which the particle size is an important variable. I would, therefore, like to suggest an alternate way of relating the measurements to the particle size distribution. This method is not dependent on an assumed distribution curve, but otherwise depends on the same physical assumptions postulated by Dr. Becker.

Let us consider the number of particles $n(V)dV$ per unit volume which have volumes between V and $V + dV$. Then $n(V)$ is related to Dr. Becker's $f(V)$ as follows:

$$Vn(V) = V_v f(V) \qquad [21]$$

where V_v is the total particle volume in a unit volume of specimen. The observed saturation magnetization, i.e., the magnetic moment per unit volume of specimen, is then

$$I_b = I_s V_v = I_s \int_0^\infty Vn(V)dV \qquad [22]$$

where I_s is the saturation magnetization per unit volume of pure cobalt.

From Eq. 12 for the initial volume susceptibility we obtain

$$\chi = \lim_{H \to 0} I/H = I_s/H_i = \frac{I_s}{3KT} \int_0^\infty V^2 n(V)dv \qquad [23]$$

Similarly from Eq. 15 for the high field magnetization

$$\frac{I}{I_s} = I - \frac{H_b}{H} = 1 - \frac{kT}{I_s H} \int_0^\infty \frac{f(V)}{V} dv$$
$$= 1 - \frac{kt}{I_s H V_v} \int_0^\infty n(V)dv \qquad [24]$$

or

$$I = I_s - \frac{Nkt}{H} \qquad [25]$$

and

$$H_b = \frac{Nkt}{V_v I_s} \qquad [26]$$

where N is $\int_0^\infty n(V)dV$, the total number of cobalt particles per unit volume of specimen. In other words the high field thermal reduction in magnetization depends only on the total number of particles, not on their size.

Therefore, from experimentally determined values of I_s, χ and H_b, one can obtain the total number of cobalt particles per unit volume of specimen,

$$N = \frac{I_s H_b}{kT}, \qquad [27]$$

the fraction of specimen volume occupied by the particles

$$V_v = \frac{I_b}{I_s}, \qquad [28]$$

their average volume

$$\frac{1}{N} \int_0^\infty Vn(V)dv = \bar{V} = \frac{V_v}{N} = \frac{kT}{I_s H_b}, \qquad [29]$$

their root mean square volume

$$(\bar{V^2})^{1/2} = \left[\frac{\int_0^\infty V^2 n(V)dV}{N} \right]^{1/2} = \frac{kT}{I_s} \left[\frac{3\chi}{I_s H_b} \right]^{1/2}, \qquad [30]$$

and the root mean square deviation from their average volume

$$(\Delta V^2)^{1/2} = \left[(\bar{V^2}) - \bar{V}^2 \right]^{1/2} = \frac{kT}{I_s H_b} \left[\frac{3\chi H_b}{I_s} - 1 \right]^{1/2}$$
$$= \frac{kT}{I_s H_b} \left[\frac{3H_b}{H_i} - 1 \right]^{1/2} \qquad [31]$$

without any further assumptions about their volume distribution function.

Nucleation of Voids in Metals During Diffusion and Creep

by R. Resnick and L. Seigle

JOURNAL OF METALS, January 1957, *AIME Trans.*, vol. 209, pp. 87-94

L.M.T. Hopkin *(National Physical Laboratory, Middlesex, England)*—The authors have shown, conclusively, in their paper that the presence of oxide particles promotes the formation of holes in brass during dezincification in vacuo. However, there are other factors which may be important particularly in creep where, according to current ideas, grain boundary holes and cracks are formed by the precipitation of excess vacancies in much the same way as holes are formed during dezincification of brass in vacuo.

Of these other factors one is stress. Balluffi and Seigle[1] and, more recently, the present writer[2,3] showed that during dezincification of brass in vacuo holes at grain boundaries occurred only in the presence of stress whether it be internal or due to an applied force. In the absence of stress, the holes were randomly distributed. Under the conditions used by the present writer, holes and cracks occurred preferentially at grain boundaries only in the simultaneous presence of stress and an excess of vacancies produced during dezincification; in the absence of either of these conditions no grain boundary cracking occurred. It seems likely, therefore, that most grain boundary holes are not nucleated on oxide particles.

It has been shown also by the present writer[2,3] that in the simultaneous presence of stress and an excess of vacancies produced by dezincification of brass in vacuo the addition of 0.2 pct Sb, which is in solid solution in brass, markedly increased the preferential formation of grain boundary cracks and holes. This effect of antimony was also observed after holding the molten antimonial brass at 1000°C in a graphite pot in an atmosphere of oxygen-free nitrogen when any zinc oxide present should have been chemically reduced. Soluble impurities behaving in the same way as antimony may have been removed, together with oxide particles, by the zone-refining treatment used by Resnick and Seigle. Their observation, therefore, that zone-refined commercial brass contained far fewer intergranular cracks during creep than the as-received material may have been due not only to the removal of oxide particles but also to the removal of soluble impurities. It may be that some soluble impurities enhance the effect of any grain boundary nuclei, including oxide particles, by lowering surface energy and promoting the precipitation of vacancies.

[1] R. W. Balluffi and L. L. Seigle: *Acta Met.*, 1955, vol. 1, 170.
[2] L. M. T. Hopkin: *Journal Institute of Metals*, 1957.
[3] L. M. T. Hopkin. To be published.

R. Resnick and L. Seigle *(author's reply)*—The authors wish to thank Dr. Hopkin for his interesting discussion. With regard to his first point, it is agreed that both a stress and an excess of vacancies are required to produce voids at the grain boundaries. However, the evidence presented does not eliminate the need for a nucleating site. The diminished cracking in the creep specimens, prepared from brass purified by one pass through a Bridgman furnace, indicates that heterogeneous nucleating sites are necessary in addition to the other conditions.

The effect of antimony in increasing the porosity is most interesting. The authors did not infer that oxide particles were the only source of nucleating sites for voids in brass. The results obtained in the dezincification of brass, prepared from zone purified copper which did not possess a significant concentration of oxygen, suggests that other impurities can act in the same way as zinc oxide. It is possible that the antimony modifies the inclusion surface in such a manner as to make nucleation more efficient.

On the Nature of Embrittlement Occurring while Tempering a Ni-Cr Alloy Steel

by G. Bhat and J. E. Libsch

JOURNAL OF METALS, January 1957, *AIME Trans.*, vol. 209, pp. 20-22

D. McLean *(National Physical Laboratory, Middlesex, England)*—A possible explanation of these interesting results seems to be that two segregating elements are involved: a slow diffusing element, presumably substitutional, that segregates in the upper temperature region, and a fast diffusing element, presumably interstitial, that segregates in the low temperature region. Preliminary embrittlement in the low temperature region would then have little effect on subsequent embrittlement in the high temperature region; this is the result shown in Fig. 2. On the other hand, preliminary embrittlement in the high temperature region, by occupying the sites to which segregating atoms go with slow moving atoms, would retard any new segregation on heating in the low temperature region; this is the result shown in Fig. 3.

Whether this explanation is right or wrong, the authors' work, and the related paper by L. D. Jaffe and D. C. Buffum in the same issue of Journal of Metals (p.8), by helping to show that the two ranges of embrittlement have different causes, assist in bringing to the fore the important but neglected problem of the interaction, in solid solution, of different elements.

G. Bhat and J. E. Libsch *(authors' reply)*—The authors wish to thank Dr. D. McLean for an intriguing explanation of embrittlement in steels. Dr. McLean is one of the early proponents of the segregation mechanism. The authors are in agreement with Dr. McLean's suggestion that two segregating elements might be involved. This question was raised during the oral discusion which followed the formal presentation of our paper.

Although it is difficult, at this time, to decide on the elements responsible for the high temperature (above 1100°F) and the low temperature (850-1000°F) embrittlement, the authors wish to put forth a mechanism somewhat contrary to that offered by Dr. McLean.

It is pertinent to follow the embrittlement mechanism from the austenitizing stage where presumably all alloying elements are in solid solution in austenite. It appears quite likely that the low temperature embrittlement is *inherited* from the austenitizing treatment. The iron lattice at the grain boundaries is in a distorted state. Consequently, atoms nearer to the grain boundary could be in a state of tension or compression. The energy of the system as a whole should be reduced if alloy atoms (of size different from that of iron) during austenitizing, occupy the grain boundary sites.

The austenite transformation may be considered a diffusionless process. When the quenched steel is

tempered, the first element that starts diffusing appreciably is carbon and possibly other interstitial elements. A fast diffusing element, therefore, is least likely to segregate.

During the early stages of tempering there may be a concentration of certain types of atoms at the grain boundaries. It should be borne in mind that substitutional alloy atoms are slow to diffuse at low temperatures. This situation may cause a temporary change in the physical property of the grain boundary material which may be responsible for embrittlement at 850-1000°F. This embrittlement decreases with considerable length of time at this temperature which might be due to a homogenization of the composition between the grain interior and the grain boundary material. On the other hand, when the tempering temperature is raised, these elements start diffusing more readily, thus moving away from the grain boundaries. It is also likely that these alloy atoms combine with carbon to form stable alloy carbides as explained by Hultgren[6]. This could account for the decrement of embrittlement in specimens tempered at 1000-1100°F.

At temperatures above 1100°F, the delineation of ferrite grains becomes progressively complete. During this stage an increasing amount of carbon and probably other interstitial elements having low solubility in ferrite separate and they either segregate or more probably precipitate at the *freshly* formed ferrite grain boundaries. The fracture in specimens embrittled in the range 1100°F up to the lower critical temperature of the steel is intercrystalline through the ferrite grain boundaries. The irreversible nature of high temuerature embrittlement seems to be due to a continual growth of ferrite grains which could also cause an increase in embrittlement.

[6] A. Hultgren: *Isothermal Transformation of Austenite and Partitioning of Alloying Elements in Low Alloy Steels*, Kungl. Svenska Vetenskademiens Handlinger, FJARDE Serien Ban 4 N:03, 1953.

Some Properties of Certain High-Conductivity Copper-Base Alloys

by Webster Hodge

JOURNAL OF METALS, April 1957, *AIME Trans.*, vol. 209, pp. 408-412.

L. L. France and A. W. Cochardt *(Westinghouse Electric Corp., Pittsburgh)*—We would like to congratulate the author on a very interesting paper and would like to ask the following questions:

1) What causes the unusual decrease (Fig. 2) in hardness upon aging the zirconium alloy that had previously been solution annealed below 1500°F (815°C)? For example, upon aging at 800°F (425°C) the hardness decreases from about 69 to 65 R_B after a previous solution anneal at 1300°F (705°C).

2) Why is the reverse effect observed on other samples (Table II)? For example, upon aging at 800°F (425°C) the hardness increases from 56 R_F (sample 1) to 58 R_F (sample 4) after a previous solution anneal at 1300°F (705°C).

3) Why would the addition of the first 0.12 pct Zr have little effect on the softening temperature of copper? Usually, the first amount of solute has the largest effect on the softening temperature of the solvent metal. Could it be that the 0.12 pct Zr does not go in solution, but combines with oxygen to form zirconium oxide, and could the dark phase in the microstructure in Fig. 3 be zirconium oxide?

4) Is it possible to expect zirconium in solid solution to cause such a small decrease in conductivity? Might this minor change be due to most of the zirconium being present as zirconium oxide acting as a dispersion hardener similar as the aluminum oxide in SAP-type alloys?

Webster Hodge *(author's reply)*—We wish to thank Messrs. France and Cochardt for the interest they have shown in this paper. With reference to the numbered questions that they have presented, we believe the following to be true explanations:

1. The decrease in hardness shown by aging a 0.25 pct zirconium alloy at 800°F after solution annealing at 1300°F is probably caused by a deficiency of zirconium in solution after a solution anneal at 1300°F. It will be noted in Fig. 2 that the resistance to softening increased in a linear manner over a limited range as the solution annealing temperature was increased to 1500°F. We assume that at each higher solution temperature more zirconium went into solution in the alloy. At the lower temperatures not enough zirconium was in solution to resist softening when the alloy was reheated to 800°F. Normal aging curves for annealed 0.22 pct and 1 pct Zr-Cu alloys are shown in Fig. 8. All of these alloys had an excess of zirconium available since we believe the maximum solid solubility of zirconium in copper is 0.15 pct. It is of interest to note that the 0.22 pct Zr alloy was melted in a graphite crucible under a carbon monoxide atmosphere and cast in that atmosphere. The 1 pct alloy was arc melted in a water-cooled copper crucible with a tungsten-tipped electrode under an argon-helium atmosphere. Nevertheless, results of the aging tests on the two alloys are practically identical.

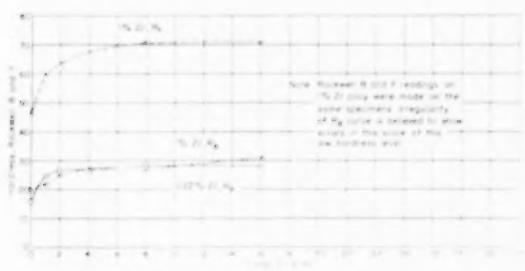

Fig. 8—Hardness of Cu-Zr alloys, solution annealed at 1740°F and aged at 840°F.

2. The reverse effect mentioned in Question 2 and noted in Table 2, Sample 4 is readily understood. Whereas the specimens shown in Figure 2 have been cold rolled 60 pct before aging, Specimen 4 in Table 2 had been solution annealed and not cold rolled. The only effect possible on this latter alloy was age hardening since it was completely soft to start with. It will be noted that Specimen 3 in Table 2 had been cold worked and also had softened.

3. "Why would the addition of the first 0.12 pct Zr have little effect on the softening temperature of copper?" is a good question. We have to admit an error on our original observations. We have done a great deal of work more recently on alloys of much lower zirconium content and found that with as little as 0.02 pct of Zr appreciable hardening is obtained. Since the alloys with less than 0.15 pct Zr are single phase, and the aging effects are completely erased by reannealing, we can only conclude that the effects reported are not caused by zirconium oxide but are caused solely by zirconium in solution. It should be noted that the work with low-zirconium alloys has shown that these alloys too can be softened by annealing and rehardened by aging in the same manner as the higher zirconium alloys.

4. "Is it possible to expect zirconium in solid solution to cause a small decrease in conductivity?". We can only answer yes. The zirconium in our alloys is not acting essentially as zirconium oxide in dispersion.

Strain Induced Transformation in Beta Brass

by T. B. Massalski and C. S. Barrett

JOURNAL OF METALS, April 1957, *AIME Trans.*, vol. 209, pp. 455-461.

G. Wasserman *(Institut fur Metallkunde, Clausthal-Zellerfeld, Germany)*—Having recently been concerned with the martensitic transformation in β-brass, we have read the paper by Massalski and Barrett with special interest. In our own experiments on cooled single crystals of β-brass with 60 pct Cu, it was found that transformation begins after a deformation whose magnitude depends upon the orientation. The final state of the transformation is a martensite single crystal with a body-centered-tetragonal structure (α_1). This structure can also be described with the help of a face-centered-tetragonal cell. In the interface between the β-crystal and the martensite crystal there is another phase, which we have called α_2, whose structure however has not yet been determined.

A greater degree of deformation can be achieved during drawing of multi-crystalline material than during elongation of single crystals. At degrees of deformation of about 70 pct the α_1-phase begins to transform itself to face-centered-cubic α-brass. This transition may be considered the result of the disappearance of the overstructure produced by the deformation.

Full details of our experimental results are given in *Zeitschrift für Metallkunde*, No. 6, June 1957.

A. R. Bailey *(Imperial College of Science & Technology, London)*—The most significant aspect of this interesting work is that some kind of transformation is induced by strain in alloys generally considered as coming in the single-phase β' region at room temperature. However, as the transformation apparently is only temporary it cannot be accepted yet that pure β' alloys of this type are unstable, especially in view of the authors' suggestion on p. 459 that the effect arises as part of the deformation process in an ordered structure.

It appears to the writer that critical determinations would be to ascertain whether: 1) Similar transformation occurs in very slowly cooled alloys which become pure β' at room temperature or in the β' of slowly-cooled α-β' alloys; 2) the tendency to transform persists after the first transformation product has disappeared.

The formation of transformation product, either by cooling or strain induction is not surprising in any of the authors' other alloys, because in these precipitation has been suppressed by quenching so that a metastable condition is obtained. The fact that pure β-brass age-softens after quenching also indicates some degree of instability, and it is possible that this is connected with the transformation observed.

With regard to metallographic detection of the transformation product, would the authors specify the strength of the dichromate used for etching, and state whether other common etching solutions have been found to reveal the new constituent.

T. B. Massalski and C. S. Barrett *(author's reply)*—No additional experiments are needed to answer the question as to whether the β' phase in a slowly cooled $\alpha + \beta'$ alloy could be induced to transform by cold work. This phase would have a composition in the range between our alloys number 4 and 6; consequently the behavior should be like that of our quenched alloys 4, 5, and 6, each of which underwent a strain induced transformation when cold worked. It should be remembered that a high degree of order is reached in the β' phase even during quenching, and slow cooling would merely be expected to remove some of the boundaries between quite well ordered domains. This removal presumably would have an influence on the progress of the transformation, since it does seem to account for the softening that is observed; that is, dislocations would move more freely both in plastic flow and perhaps also in martensite formation if domain boundaries were fewer. Since there is no evidence that any transformation product forms in the composition range above 37 wt pct on quenching to room temperature, there is no basis for attributing age-softening of quenched alloys in this range to the formation or reversion of a transformation product.

Further information on the etching characteristics of the martensitic product is as follows. Best results were obtained with a 2 pct solution of potassium dichromate. We did not make tests of many other reagents, but we did have success in revealing the phase with at least two others. One was the common ammonium hydroxide-hydrogen peroxide etchant, and the other consisted of 20g CrO_3, 25g HNO_3, 25g H_2SO_4, 3.7g NH_4Cl, 1900 ml H_2O. Improved results were obtained by electropolishing first, using approximately 6 volts and a bath consisting of 250 cu cm H_3PO_4, 125 cu cm H_2O, 95 cu cm carbitol, 5 cu cm HF.

In reply to Dr. Wassermann's discussion, we regret that his paper has not yet been received here. Since his experiments are on single crystals rather than polycrystalline samples and filings, it is possible that single crystals exhibit some different structural characteristics than polycrystalline samples; or it may be that the diffraction data, which is none too extensive, can be interpreted in more than one way. Our interpretation is based on diffraction patterns of the type we have reproduced, including patterns in which, by suitable choice of alloy content, we have suppressed the pattern of the body-centered cubic phase that normally accompanies the new phase in the binary alloys.

Strength of Silver Brazed Joints in Mild Steel

by M. G. Moffatt and J. Wulff

JOURNAL OF METALS, April 1957, *AIME Trans.*, vol. 209, pp. 442-445.

K. M. Weigert *(Curtiss-Wright Corp., Quehanna, Pa.)*—The authors contributed experimental data to the interesting problem of brazed joint tensile strength as a function of joint thickness and diameter.

All data with clearance below .005 in. and more than 0.2 in. diam confirmed what had been found previously: The tensile values converge towards a constant value, independent of the diameter, somewhat below the UTS of the parent metal for extremely small clearances.

Table II. Tabulation of Constants

t	.005	.01	.02	.04	1
c	24	12	6	4	75
T_U	55,000	52,000	50,000	46,000	35,000
D_C	—	—	.002	.013	30

In Fig. 5 a separation of the old and new data is shown by replotting the authors Table I, also separating the influence of clearance and diameter variations by plotting the tensile strength as a function of the diameter D for various clearances t. For the new data of clearances at 0.01, 0.02 and 0.04 in. and for diameters between 0.1 and 0.5 in. an analytical expression was found to satisfy the experimental data and to allow an extrapolation to higher clearances and lower diameters as follows:

$$T_U = (T_H - T_L)\ (1 - e^{D_L - D}) + T_L$$

where:

T_U = Ultimate tensile strength (UTS) in psi.
T_H = Upper joint strength (extrapolated from the experimental data)

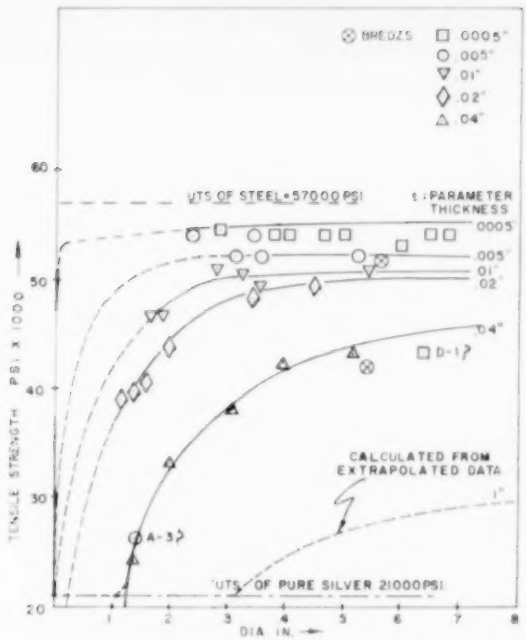

Fig. 5—Strength of silver brazed joints in mild steel.

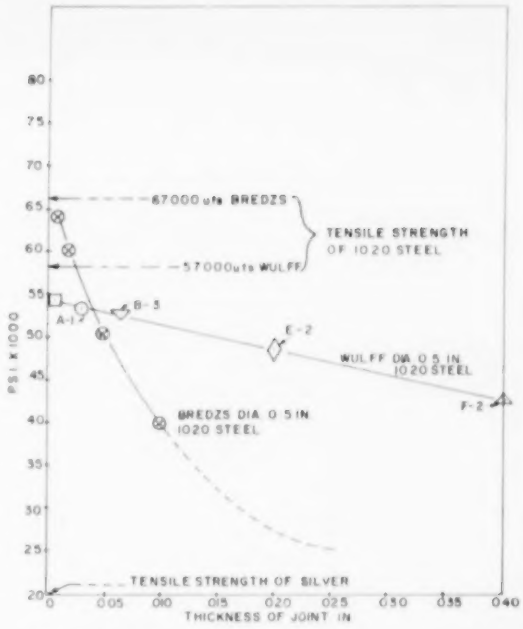

Fig. 6—Tensile strength of brazed joints. Specimen numbers from Table I.

T_L = 21,000 (UTS of silver)
t = joint clearance, in.
c = joint clearance parameter $c = c(t)$
D = Diameter of specimen
D_L = Diameter of lowest joint strength

The curve for t = 0.1 was calculated, for lack of experiments, from extrapolated data.

Fig. 6 shows the increase of strength with decreasing joint thickness as found by N. Bredzs and J. Wulff. For a diameter of 0.5 in. Bredzs finds a higher brazing strength value at small clearances, corresponding to a higher ultimate tensile strength of his 1020 steel. For larger joint clearances the data between the two authors differ as Wulff finds higher values.

A possible explanation for the discrepancies of data was offered by Mr. N. Bredzs in a private communication. He used short times in direction heating whereas the authors applied a furnace brazing method.

No mention is made of a recent paper of Bredzs and Schwartzbart,[5] where extremely thin and also extremely thick joints were investigated.

[5] N. Bredzs and H. Schwartzbart: *Triaxial Tension Testing and the Brittle Fracture Strength of Metals*, The Welding Journal, Research Supplement, December 1956, pp. 610s-615s.

T. H. Crane *(Kinetics Corp., Hingham, Mass.)*—Any technical paper that supplies solid design data to the industrial metallurgist is to be received with gratitude by all interested parties. The discussion of brazing by Moffatt and Wulff is one of those papers that supplies data on a field of assembly that appears to be undergoing a rebirth and it is very timely.

There are several points that are not quite clear that bear directly on the formation of the joint in the brazing process. The first and most obvious point is the reasoning behind the very high temperature used. Pure silver has a listed melting point of 960.8°C (38th Edition, Handbook of Chemistry and Physics). The heating rate used by Moffatt and Wulff calculates, on a straight line basis, to 2.18°C per min. From this data it appears that the silver was liquid for about 35 min. This allows ample time for the undesirable side effects of diffusion to enter into the problem. It is hard to estimate the rate at which flow into small joint clearances takes place, but 35 min does appear to be a very long period above the liquidus. The rule of thumb used by commercial furnace brazing firms is to keep the cycle as short as possible. It is usual to make several test runs at shorter and shorter cycle times until there is only enough time to allow full wetting of the joint area to take place.

The second question is brought up by the writers position as metallurgist for a vacuum brazing contractor. The data in Table I of the original paper indicates that four samples broke during the machining operation. All of these samples were within a braze joint thickness to indicate a tensile strength in excess of 38,000 lb per sq in. This would, in itself, indicate some tendency towards brittleness of the joints. An additional six samples were flawed in the joint area. The exact form of these flaws is not indicated but from the statement that is made in the Discussion and Conclusions of the original paper "With steel or base material of low ductility * * * * and freedom from gas pockets are achieved * * * * to approach the ultimate strength of the base material"; it would appear that the flaws were of the gas pocket type. The only answer to the problem of gas pockets is to obtain pressures of 1μ or less during the time that the braze material is liquid.

The best brazing of this base alloy, 1020 steel, could be done in the following manner, based on the paper of Moffatt and Wulff and the experience of the writer of this discussion. The joint thickness should be in the vicinity of 0.001 in. or as low as 0.0005 in. if possible. The brazing cycle would be heat to 900°C in a purified hydrogen atmosphere and then evacuate to 1μ or lower pressure. After the pressure is lowered the heat input would continue to a temperature of 1050°C. A short hold period of 5 min or less at this temperature followed by cooling at the natural rate of the vacuum furnace to a temperature well below the solidus, say 900°C before force cooling by helium.

The writer wishes to offer the use of the vacuum furnace brazing equipment of his corporation to Drs. Moffatt and Wulff so that they might perform any comparison tests along the lines indicated in this discussion that they might desire.

Studies on Diffusion in Molten Metals

by K. Niwa, M. Shimoji, S. Kado, Y. Watanabe, and T. Yokokawa

JOURNAL OF METALS, January 1957, *AIME Trans.*, vol. 209, pp. 96-101

R. E. Grace *(Purdue University, Lafayette, Ind.)*—Professors Niwa and Shimoji and Messrs. Kado, Watanabe and Yokokawa have done an excellent job in showing that variety of experimental techniques can be used with success in measuring diffusivities in liquid metal systems. It is surprising to see how smooth the concentration-penetration profiles are as listed in Table I and Fig. 4. I would like to know whether these measuring techniques yielded diffusion data with every run, or whether a large fraction of the experiments had to be discarded. Also, did the authors correct for or estimate the volume changes attendant in their methods due to contraction of their samples during solidification? Such contractions result in uncertainties of X in the solutions of the diffusion equations.

Finally, it is surprising to see their results on Pb-Bi alloys show that the chemical diffusivity of Bi only changes from 6×10^{-5} sq cm per sec at $N_{Bi} = 0.1$ to 9×10^{-5} sq cm per sec at $N_{Bi} = 0.8$. In further experiments performed by the discusser,[20] incremental studies in the ranges 53 to 58 pct Bi and 56 to 60 pct Bi were made. In the case of the runs made near $N_{Bi} = 0.5$ at 427°C the diffusion coefficient of bismuth was 10^{-5} sq cm per sec, about 5 times faster than was previously reported.[20] Since the concentration interval was minimized in these experiments, the D value reported herein should be closer to the true chemical diffusivity of Bi near the Pb-Bi eutectic.

The capillary reservoir technique was used in all of the above experiments. While there is some ambiguity about volume changes during diffusion arising from density changes within the capillary (a constant volume system) it should be emphasized that the capillary reservoir technique minimizes convection and is very simple to use.

[20] R. E. Grace and G. Derge: Diffusion in Liquid Pb-Bi Alloys, *AIME Trans.*, 1955, vol. 203, p. 839.

K. Niwa, M. Shimoji, S. Kado, Y. Watanabe, and T. Yokokawa *(authors' reply)*—1) In the diffusion, the concentration penetration profile shows an error integral curve. For Example

$$c = c_0 [1 - \text{erf}\ (x/2\sqrt{Dt})] \qquad [2]$$

is employed for the data in Table I. Thus putting

$$\xi = x/2\sqrt{Dt},$$

c/c_0 corresponds to ξ through Eq. (2). Then, the graphical representation of χ as a function of ξ should be a straight line. Let the observed data in each ξ be plotted against the corresponding χ. If the data satisfies the error integral curve, a straight line will be obtained. When some points scatter, the most reasonable curve is to be used. The smoothing curve corresponds to the straight line.

2) As mentioned in the paper, the data always give the negative results, when pure metal is filled in the upper part of the tube in the second method. Except doubtful results which show no concentration gradient, most data have been used.

3) We have not any correction for volume change due to solidification. Qualitatively this correction may give the errors at most of 20 to 30 pct to the results. These errors are the same order as in the accuracy of the authors's experimental technique.

4) Professor Grace's careful examination of Pb-Bi is very interesting, since the diffusion coefficient is 10^{-5} sq cm per sec near $N_{Bi} = 0.5$ at 427°C. It will be necessary to investigate this abnormal result from experimental and theoretical viewpoints.

The Martensite Transformation in the Iron-Nickel System

by Larry Kaufman and Morris Cohen

JOURNAL OF METALS, October 1956, *AIME Trans.*, vol. 206, pp. 1393-1401.

A. G. Haynes *(Mond Nickel Company, Birmingham, England)*—In recent years, martensite formation ranges have been determined for a variety of nickel-containing steels, and it is interesting to compare the data accumulated with those presented in this most interesting paper by Kaufman and Cohen.

In Table VI are listed the M_s temperatures of a series of steels containing 28 — 31 pct Ni.[28] These values are considerably lower than those obtained by Kaufman and Cohen. It is gratifying to note, however, that excellent agreement is obtained if correction is made for the effects of carbon and manganese. The corrections were made in accordance with the factors given in the following empirical formula proposed recently[27] for the calculation of M_s temperatures of low alloy steels —

$$M_s(°C) = 561 - 474C - 33Mn - 17Ni - 17Cr - 21Mo \qquad [42]$$

This formula was based on data accumulated for a wide variety of steels containing 0 to 5 pct Ni and therefore was certainly not intended to be used for steels of very high nickel content. On the other hand, it is surprising that the M_s temperatures calculated using this equation are not in good accord with the values indicated by Kaufman and Cohen for steels of low nickel content.

The data presented in Table VII have been collected together from the literature[29-31] in an attempt to explain the discrepancies. Again the experimentally determined M_s temperatures have been corrected for the effects of elements other than nickel, using the equation indicated above. The values listed for the upper limits of bainite formation (B_s or A'') were similarly corrected, using the equation given below —

$$B_s(°C) = 830 - 270C - 90Mn - 37Ni - 70Cr - 83Mo \qquad [43]$$

These corrected values have been plotted against nickel content in Fig. 12. In this diagram the experimental results of Kaufman and Cohen are represented by a full line. The corrected M_s temperatures taken from the literature are shown by crosses, and the corrected B_s temperatures by circles. The disposition of the various experimental points suggests that the M_s temperatures of the iron-nickel alloys of lower nickel

contents were not observed under the experimental conditions adopted by Kaufman and Cohen, due to the onset of transformation to bainite.

If it be assumed that the M_s temperatures of iron-nickel alloys containing up to 25 pct Ni vary in accordance with Eq. 42, then reference to Fig. 10 of the paper suggests that the constant free energy difference of approximately 270 cal per mole is required for martensite formation in alloys having nickel contents within this range. This constant value is in good accord with that obtained from the study of iron-carbon alloys.[32]

[25] C. A. Clark: unpublished work, The Mond Nickel Co. Ltd., Birmingham, England.
[27] W. Steven and A. G. Haynes: The Temperature of Formation of Martensite and Bainite in Low-Alloy Steels, *Journal of the Iron and Steel Institute*, vol. 183, 1956, pp. 349-359.
[28] G. R. Brophy and A. J. Miller: The Metallography and Heat-Treatment of 8 and 10 Pct Nickel Steel, *ASM Trans.*, 1949, vol. 41, pp. 1185-1201.
[29] *Transformation Characteristics of Nickel Steels*: The Mond Nickel Co. Ltd., London, 1952.
[30] J. P. Sheehan, C. A. Julien, and A. R. Troiano: The Transformation Characteristics of Ten Selected Nickel Steels, *ASM Trans.*, 1949, vol. 41, pp. 1165-1181.
[31] *Atlas of Isothermal Transformation Diagrams*, United States Steel, 1951.
[32] M. Cohen, E. S. Machlin, and V. G. Paranjpe: Thermodynamics of the Martensite Transformation, Thermodynamics in Physical Metallurgy, *ASM*, 1950.

L. Kaufman and M. Cohen *(authors' reply)*—Dr. Haynes has offered an ingenious explanation for the effect of nickel on the driving force at the start of the cooling transformation. This driving force increases rapidly with nickel concentration up to about 25 atom pct Ni, and then tends to level off (Fig. 11). If the product formed in the low-nickel range were bainite instead of martensite, the above dependence on nickel could be rationalized.

However, there is a serious question as to whether the transformation product in the low-nickel alloys is bainite instead of martensite. Although the bainitic reaction may be displacive in nature, a diffusion process must be involved; otherwise the bainitic and martensitic transformations would be indistinguishable from each other. In steels, carbon is the controlling element in this diffusion process. For the iron-nickel alloys, one cannot expect nickel to play the role of carbon in view of the extremely low diffusion rate characteristic of substitutional elements in the temperature range under consideration.

Unfortunately, a real test of the insuppressibility of the transformation in the low-nickel alloys has not been made, although this reaction is known to be insensitive to the rate of cooling. On the other hand, such information is available for the analogous iron-manganese alloys which are very similar in thermodynamic and transformation characteristics. Troiano and Maguire[33] have shown that the M_s temperature for a wide range of iron-manganese alloys is insensitive to cooling rates between 1°C per sec and 6000°C per sec. These M_s temperatures were checked by Jones and Pumphrey[34] using a cooling rate of 2°C per min. Consequently, there can be little doubt about the martensitic nature of the cooling reaction in this system. Yet, when Dr. Haynes' equations for M_s and B_s are used, the experimental values of M_s lie closer to the calculated values of B_s than they do to the calculated values of M_s, at least for manganese contents up to about 5 wt pct, and this is what Dr. Haynes finds for the iron-nickel system. However, the reaction is insuppressible over the entire range of manganese contents, which raises considerable doubt as to the validity of the bainite hypothesis.

Moreover, in the iron-manganese alloys, Dr. Haynes' equations indicate that above approximately 5 wt pct manganese, the calculated B_s falls below the calculated M_s. It is hard to imagine the physical meaning of this situation; most likely the equations are not applicable over the entire range of compositions.

Even though it is doubtful that a bainitic transformation is at play in the iron-nickel alloys under study here, it might be worthwhile to try variations in cooling rate in an effort to determine whether some other type of reaction may be involved in the low-nickel alloys.

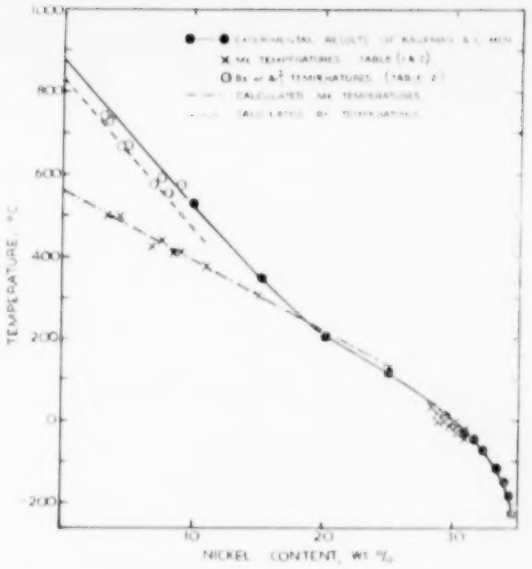

Fig. 12—The effect of nickel on M_s and B_s temperatures.

[33] A. R. Troiano and F. T. Maguire: A Study of the Iron-Rich Iron-Manganese Alloys, *ASM Trans.*, 1943, vol. 31, p. 340.
[34] F. W. Jones and W. I. Pumphrey: Free Energy and Metastable States in the Iron-Nickel and Iron-Manganese Systems, *Journal Iron and Steel Institute*, 1949, vol. 163, p. 121.

Table VI. Comparison of M_s Temperatures of Nickel-Containing Steels and Iron-Nickel Alloys

Chemical Composition, Wt Pct			Experimentally Determined M_s, °C	Experimentally Determined M_s, Corrected for Effects of C and Mn, °C	M_s Values Derived from the Experimental Results of Kaufman and Cohen
Ni	C	Mn			
28.3	0.20	0.43	−74	+35	+38
28.7	0.16	0.58	−79	+16	+26
28.9	0.13	0.53	−81	−2	+22
29.4	0.14	0.49	−82	0	+10
29.7	0.17	0.56	−116	−17	2
29.9	0.10	0.48	−69	−6	−2
29.9	0.15	0.41	−85	−1	2
30.0	0.13	0.53	−100	−21	−4
30.6	0.18	0.52	−124	−22	−22
30.7	0.16	0.47	−129	−38	−25

Table VII. Calculated and Experimentally Determined M_s and B_s or A_s'' Temperatures of Nickel Steels

Chemical Composition, Wt Pct			Calculated M_s, °C	Experimentally Determined* M_s, °C	Calculated B_s, °C	Experimentally Determined* B_s or A_s'', °C	Reference
Ni	C	Mn					
3.04	0.11	0.48	—	—	718	740	28
3.45	0.40	0.62	502	497	702	730	29
4.23	0.35	0.44	489	498	673	665	29
4.92	0.12	0.48	—	—	648	668	28
7.01	0.08	0.50	442	420	570	576	28
7.42	0.10	0.48	—	—	555	592	28
7.61	0.29	0.15	431	438	—	—	30
7.93	0.09	0.35	—	—	536	548	28
8.5	0.09	0.49	417	402	—	—	28
8.94	0.08	0.49	409	414	500	c 570	31
11.0	0.10	0.50	374	367	—	—	28
15.0	0.10	0.50	306	302	—	—	28

* Corrected for solute elements other than nickel, in accordance with factors given in Eq. 42 and 43.

A. E. Powers *(General Electric Company, Schenectady)*—It is noticed that the authors have applied corrections to the transition temperatures of specimens possessing hardness values other than 24 R$_c$. The basis for these corrections is obtained from previous work[28] in which transition temperatures were found to decrease with decreasing hardness upon tempering martensitic structures to a hardness values of not less than 24 R$_c$. For softer structures than 24 R$_c$, the transition temperatures were found to progress upward in the reverse manner. It is difficult to understand why the same correction factors that are applied to structures harder than 24 R$_c$ should be applied to structures softer than the 24 R$_c$. If the authors are to be consistant in applying correction factors for varying hardness values then their correction factors should vary from one hardness range to another. This will, of course, eliminate the appearance of *upper-nose* embrittlement in their isothermal embrittlement diagrams and it would not appear to be a realistic manner in handling the phenomenon. I believe that it would be best to accept the fact that steels possess inherent transition-temperature values that are dependent on the state of tempering and to avoid applying dubious correction factors to specimens not tempered to a uniform hardness value.

The authors claimed a retrogression phenomenon on the basis of one experiment in which heating to 500°C for 100 min after aging for 48 hr at 475°C has lowered the transition temperature by 15°C. It would be interesting to see if this result can be duplicated.

Reversibility in upper-nose embrittlement has been suggested on the basis of one instance in which the transition temperature was reduced 15°C by heating one hour at 675°C after aging 48 hr at 650°C. The authors were not able to duplicate this behavior in a repeat experiment. Perhaps the issue of retrogression or the lack of it should not be pressed further until more positive data has been accumulated.

The concept of an equilibrium of embrittlement at temperatures between 500 and 560°C has been doubted by the authors on the basis that they have observed a reduction in transition temperature upon aging beyond 10 hr at 550°C. The claim is made that this behavior indicated overaging in an age-hardening system, with the result that the solid-solution segregation theory is ruled out. Their conclusions are based on one point (10 hr at 550°F) that is about 5°C higher in transition temperature than it should be if the iso-embrittlement curve were horizontal. This point is located on the steep portion of the transition- temperature-vs-aging temperature curve where a 5°C error in specimen aging temperature can lead to a 5°C alteration in equilibrium transition temperature. It is suggested that this equilibrium portion of the diagram be investigated more thoroughly to determine whether the iso-embrittlement lines are horizontal or not.

The claim that no ferrite grain growth was observed during tempering seems to be contrary to the findings of Fisher and Boyce[29] and to Hyam and J. Nutting.[30] Fisher and Boyce found that increasing the tempering time from 1 hr to 18 hr at 1250°F, increased the ferrite grain size of AISI 1060 steel from ASTM No. 15 to No. 13.5. The data of Hyam and Nutting show the same tempering treatments on a 0.7 pct C steel to increase ferrite grain size from about ASTM No. 18 to about No. 16. In both of these investigations the electron microscope was found necessary to observe the ferrite grain size. One may question whether optical microscopic observations at 800 diameters is sufficient to observe ferrite grains, which for a grain size of No. 15 have a mean diameter of about 2μ.

Several proposals have been made to relate, quantitatively, grain size to fracture stress, with accompanying implications for relating grain size with fracture transition temperatures,[31-34] but the most promising theory is that of J. J. Gilman[35] who, in working with crack propagation during crystalline cleavage rather than with crack nucleation, has shown that in addition to the static Griffith criterion, $\sigma_g = \sqrt{\frac{2\,E\,\omega}{\pi\,l}}$, a minimum crack velocity is required for the maintenance of brittle fracture through a crystal. The crack velocity will build up as the crack is progressing catastrophically through the crystal and will progress across the grain boundary to the next grain only if energy losses at the grain boundary do not lower the velocity below the critical velocity. The larger the grain size, the more the crack velocity can build up before the grain boundary is encountered, and the more likely will brittle fracture proceed entirely through the crystalline aggregate.

[28] D. C. Buffum and L. D. Jaffe: Effect of Hardness on Temper Brittleness, *Trans AIME*, 1951, vol. 191, p. 540.
[29] R. M. Fisher and J. F. Boyce: Discussion to paper by Baeyertz, Craig, and Bumps, Effect of Ferrite Grain Structure upon Impact Properties of 0.80 Pct Carbon Spherodite, *Trans AIME*, 1951, vol. 191, p. 1064-1065.
[30] E. D. Hyam and J. Nutting: The Tempering of Plain Carbon Steel, *Journal of the Iron and Steel Institute*, Oct. 1956, vol. 184, p. 148-165.
[31] N. J. Petch: The Cleavage Strength of Polycrystals, *Journal of the Iron and Steel Institute*, May, 1953, vol. 174, p. 25-28.
[32] J. R. Low: The Relation of Microstructure to Brittle Fracture, ASM Symposium, *Relation of Properties to Microstructure*, 1953, p. 163-179.
[33] J. J. Gilman: Propagation of Cleavage Cracks in Crystals, *Journal of Applied Physics*, Nov. 1956, vol. 27, p. 1262-1269.

L. D. Jaffe and D. C. Buffum *(authors' reply)*—As was pointed out in the reference cited by Dr. Powers,[28] the increase in transition temperature observed in a structure softer than 24 R$_c$ was due to upper-nose embrittlement developing during the 4-hr temper at 675°C. This is proved in the present paper (Table III). Accordingly, there is no evidence that the curve of transition temperature vs hardness for *unembrittled* structures is not linear, and corrections were therefore made on the assumption of linearity (on a Brinell scale). We are inclined to agree with Dr. Powers that where upper-nose embrittlement alone is being studied, corrections for hardness are not needed, but when interrelations of upper- and lower-nose embrittlement are of concern, we feel that they are needed. Otherwise, for example, it may be erroneously concluded that upper-nose treatments reduce subsequent lower-nose embrittlement, whereas they in truth may only be reducing the hardness. In any case, uncorrected as well as corrected transition temperature data are given throughout this paper; Dr. Powers and other readers have available whichever they prefer.

We agree that the evidence of lower-nose retrogression and of upper-nose reversibility is merely suggestive and not conclusive; this was mentioned in the paper. We, too, would like to see further work on these questions.

We agree, also, that our own evidence of overaging in the lower-nose region, at 550°C, is not in itself conclusive. It is, however, confirmed by the data of Vidal[36] and of Bhat and Libsch[37].

Dr. Powers is correct in stating that there are better methods of measuring ferrite grain size than the one we used. It may be that ferrite grain growth occurred even though we did not observe any.

Appreciation is gratefully acknowledged to the following organizations whose support has helped to make possible AIME's extensive publications program of metallurgical research:

Aerojet-General Corp.
Allis-Chalmers Mfg. Co.
Aluminum Co. of America
American Brake Shoe Co.
American Cast Iron Pipe Co.
American Iron & Steel Institute
American Metal Co. Ltd.
American Metallurgical Products Co.
American Smelting & Refining Co.
American Zinc, Lead & Smelting Co.
Anaconda Co.
Apex Smelting Co.
Arnold Engineering Co.
Atomic Energy of Canada, Ltd.
Avco Manufacturing Corp.
Battelle Memorial Institute
Bridgeport Brass Co.
Budd Co.
Bunker Hill Co.
Calumet & Hecla, Inc.
Cerro de Pasco Corp.
Clevite Corp.
Climax Molybdenum Co.
Consolidated Coppermines Corp.
Consolidated Mining & Smelting Co. of Canada Ltd.
Copper Range Co.
Cornell Aeronautical Laboratory Inc.
Crane Co.
Cyprus Mines Corp.
Detroit Testing Laboratory Inc.
Dow Chemical Co.
Driver-Harris Co.
Wilbur B. Driver Co.
Eagle-Picher Co.
Eaton Mfg. Co.
Electro Metallurgical Co., Div. of Union Carbide & Carbon Corp.
Engineering Foundation
Esso Research and Engineering Co.
Ford Motor Co.
Freeport Sulphur Co.
General Electric Co.
General Motors Corp.
Handy & Harman
E. F. Houghton & Co.
Howe Sound Co.
Hudson Bay Mining & Smelting Co. Ltd.
International Nickel Co. Inc.
Janney Cylinder Co.
Kennecott Copper Corp.
Leeds & Northrup Co.
Magma Copper Co.
Mallinckrodt Chemical Works
P. R. Mallory & Co., Inc.
Mallory-Sharon Titanium Corp.
Metal Hydrides, Inc.
Miami Copper Co.
Molybdenum Corp. of America
Mueller Brass Co.
National Lead Co.
New Jersey Zinc Co.
Newmont Mining Corp.
Noranda Mines, Ltd.
Olin Mathieson Chemical Corp.
Owens-Corning Fiberglas Corp.
Owens-Illinois Co.
Phelps Dodge Corp.
Quigley Co. Inc.
Raytheon Mfg. Co.
Rem-Cru Titanium Inc.
Revere Copper & Brass Inc.
Reynolds Metals Co.
Richfield Oil Corp.
Scovill Mfg. Co.
Alfred P. Sloan Foundation, Inc.
Southwestern Engineering Co.
Steel Improvement & Forge Co.
St. Joseph Lead Co.
Superior Tube Co.
Texas Gulf Sulphur Co.
Thompson Products Inc.
Titanium Metals Corp. of America
U. S. Smelting, Refining & Mining Co.
Vanadium Corp. of America
S. K. Wellman Co.

FOURTH VOLUME

ON

NUCLEAR METALLURGY

All the Papers at a Symposium
on Uranium and Uranium Dioxide
Conducted by

INSTITUTE OF METALS DIVISION

THE METALLURGICAL SOCIETY

AMERICAN INSTITUTE OF

MINING, METALLURGICAL, AND PETROLEUM ENGINEERS, INC.

November 6, 1957

(AIME IMD Fall Meeting, Morrison Hotel, Chicago, Illinois)

Development of Casting Techniques for Uranium and Uranium Alloys	by G. E. Jaynes, D. T. Doll, and J. M. Taub
Uranium Ingot Production at Atomic Energy Commission Feed Materials Production Centers	by B. J. Buntz
Induction Melting of Uranium Base Alloys	by N. J. Carson, Jr.
Melting and Casting of Uranium, Zirconium, Niobium Alloys	by J. E. Baird and N. J. Carson, Jr.
Centrifugal Casting of U-Zr Alloy Rods	by A. B. Shuck
Injection Casting of Uranium-Fissium Alloy Pins	by F. L. Yaggee, J. E. Ayer, and H. F. Jelinek
Arc Melting of Uranium-Rich Alloys	by W. H. Britton and W. V. Haynes
Press Forging of Dingot Uranium	by J. A. Fellows and H. J. Schaffer
Rolling of Uranium	by G. S. Hanks, J. M. Taub, and D. T. Doll
Extrusion of Uranium	by P. Loewenstein
Cold Working of Uranium	by J. M. Taub, D. T. Doll, and G. S. Hanks
Fusion Welding of Uranium	by E. L. Brundige, D. T. Doll, G. S. Hanks, and J. M. Taub
Powder Metallurgy of Uranium and Uranium Alloys	by J. L. Zambrow
Various Methods of Preparing Uranium Dioxide for Fuel Element Use	by G. W. Tompkin, D. E. Rhodes, and C. M. Henderson
Fabrication of Bulk Form Uranium Dioxide for Use as Nuclear Reactor Fuel	by J. Glatter
Fabrication of High-Density Uranium Dioxide Fuel Components for the First Pressurized Water Reactor Core	by T. J. Burke, J. Glatter, H. R. Hoge, and B. E. Schaner

Price: $7.00
(AIME Members: $5.00)

AIME, 29 W. 39th St., New York 18, N. Y.

Please send me a copy of Nuclear Metallurgy (Vol. 4).
Enclosed is Check ☐; Money Order ☐ for $ .....
(AIME members may be billed.)

Name .....

Address .....

City and Zone ..... State .....

Nonmember Foreign Order, Add 50¢ for Mailing.

Purchase your copy at the Registration Desk, Morrison Hotel, Chicago, during the IMD Fall Meeting, or use the form at the left to order by mail. (Mail Orders will be filled after Nov. 7, 1957.)

Volumes 1, 2, and 3 of Nuclear Metallurgy will also be available at the Registration Desk, or can be ordered by mail. They are priced at $3.75 (AIME members: $2.50.)